2004

# Analysis of water masses distribution and circulation in the White Sea, Russia

Latche, Laurent

# ANALYSIS OF WATER MASSES DISTRIBUTION AND CIRCULATION IN THE WHITE SEA, RUSSIA.

by

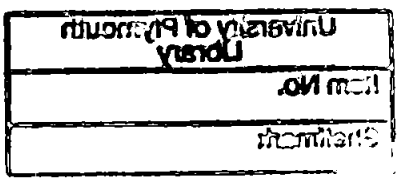


**LAURENT LATCHÉ**

A thesis submitted to the University of Plymouth

In partial fulfilment for the degree of

**DOCTOR OF PHILOSOPHY**

School of Earth, Ocean and Environmental Sciences

Faculty of Science

March 2004

# ANALYSIS OF WATER MASSES DISTRIBUTION AND CIRCULATION IN THE WHITE SEA, RUSSIA.

by Laurent Latché

## ABSTRACT

The White Sea is a semi-enclosed sea, which consists of several bays and estuaries connected to the open ocean through the narrow and shallow Gorlo Strait. Several studies have been carried out in the region during the last decade in order to investigate the potential threat of anthropogenic pollutants. However, the temporal and spatial resolution of such experiments has been inadequate to resolve issues such as the dispersion and propagation of environmentally hazardous substances.

The present investigation uses *in-situ* measurements of temperature and salinity gathered at high spatio-temporal resolution for the first time, as part of the INTAS project "Mesoscale physical and biogeochemical processes in coastal waters of the Russian Arctic" and of a number of Russian national and EU research projects. The study focuses on the formation, evolution and spatial distribution of fine-scale thermohaline structures. The mixing processes were thoroughly studied in the southwest area of the Gorlo Strait, where present water masses have an important contribution in the dynamics of the White Sea including water-exchange and deep-water renewal. Satellite images were used to estimate the mesoscale circulation and the contribution of freshwater inputs to the formation and distribution of the water mass structure. Smaller scale mixing processes were also investigated using a statistical method of fine structure-inhomogeneity analysis in order to assess the intensities of the diapycnal and isopycnal modes of small-scale mixing.

The results showed i) the intrusion of mixed layers into the White Sea initially formed in the Gorlo area due to tidal mixing of the saline Barents Sea waters and the White Sea waters. The mixed layers were traced across the whole section, in the vicinity of an active boundary layer in a form of a domed structure, which separates from stagnant deep-water masses of the White Sea. ii) The formation of shelf-edge dense water was revealed in Kandalaksha Bay suggesting cascading phenomena. iii) A detailed study of the mixing processes in Gorlo revealed four interacting water masses: the Gorlo Strait Water (GSW), the White Sea Surface Water (WSSW), the Dvina Bay Water, and the White Sea Intermediate Water. Mesoscale "lens" of WSSW was observed in the near-surface layer associated with a thermal front, which resulted in the formation of an intrusion of the GSW into the White Sea Basin, facilitated by the Terskii Coastal Current and the cyclonic Dvina Bay gyre. iv) The spatial distribution of temperature and salinity fluctuations within the water masses revealed the intensity of mixing and demonstrated the thermohaline transformation of the Gorlo Strait Waters during its mesoscale displacement at the intermediate depths across the northern part of the White Sea.

The findings of this study therefore provide a better understanding of the deep water renewal mechanisms in the White Sea. The classical concepts suggest that the saline waters of the Barents Sea enter the White Sea and sink at the entrance carrying with them all potential pollutants. The present study supports the hypothesis that the Barents Sea water is transformed at the Gorlo Strait and subsequently is propagated in the form of mixed layers across the White Sea until they reach the shelf of Kandalaksha Bay, where they finally sink.

# CONTENTS

# LIST OF FIGURES

# LIST OF TABLES

## ACKNOWLEDGMENTS

I would like to take this opportunity to express my gratitude to all the people who have given me support and assistance in producing this thesis. Primarily, I would like to acknowledge the support and encouragement offered throughout my study by my two supervisors: Prof. G. Shapiro and Dr. Ken George. I am grateful for their guidance and advice offered during the various aspects of the study, which kept me going throughout the last 3 and half years; for their encouragement especially during the final stages of the writing up.

I would like to thank the following people, without whom the completion of the thesis would have been impossible:

The IMS within the University of Plymouth for supporting the studentship and the trip to the conferences; many thanks to Prof. D. Huntley, and also to Lyn Stott, Marie Sleeman, Jo and Rita for administering my studentship.

Prof. G. Shapiro and Dr. A. Pantiulin for collecting the CTD data in the White Sea during the oceanographic campaigns of June 2000 and May-June 2001; for providing the CTD data from campaign 1991. Dr. T. Smith from PML for providing the SST imagery of the White Sea. Dr. Kevin Horsburgh for his expertise and discussion on the study. Dr. M. Emelianov for providing his code for the software used in analysing the fine structure inhomogeneities and Sebastien Villeneuve (ISITV, France) for his assistance in the data processing.

I am also very grateful to Ron Hill, Graig Douglas and Christ Hatton for managing and solving technical problems along with my PhD.

Many thanks to Dr. G. Glegg and to Pr. Alexei Nikrasov, who organised the expedition on the catamaran Centaurus II in the Gulf of Finland, and with whom I spent a great time in Saint Petersburg along with the sailing crew. Thank you Alexei for sharing materials and exchanging ideas about the study.

On a more personal note, my time in Plymouth was made very enjoyable by my very close friends. Many thanks to Jon and Becks (more windsurfing sessions are coming along!), Debbie, Cécilia and Ismael, John, Riqui and Olivia, Didier, Anna, Emily, Jos and Duncan, Martin, Nigel, Vladimir, Hugh and Vicky, Asha, Tophe, Marcos and Caina. Thank you all, and to those I haven't individually mentioned, who have given me both advice and support. Again thank you!

*à ma grande famille que j'aime!*

*à Michel, Cathy, Céline, Stéphanie, Fabrice, Emmanuelle, Noémie et Marília, eu amo você!*

## AUTHOR'S DECLARATION

At no time during the registration for the degree of Doctor of Philosophy has the author been registered for any other University award. This study was financed with the aid of a studentship from the University of Plymouth. Relevant scientific seminars and conferences were regularly attended at which work was often presented; external institutions were visited for consultation purposes.

**Relevant publications**:

Latché, L., Shapiro, G.I., and Pantiulin, A.N., 2002. Thermohaline Intrusion in the White Sea in June 2000. In Geophysical Research Abstracts, 03437, 127th General Assembly of the European Geophysical Society , Nice, France.

Lukashin, V. N, Kosobokova K.N., Shevchenko V.P., Shapiro G.I., Pantulin A.N., Pertzova N.M., Savenko A.V., Deev M.G., Kljuvitkin A.A., Novigatsky A.N., Prego R., Latché L., (2003). Results of multi-disciplinary oceanographic observations in the White Sea, June 2000. Oceanology, том 43, №2, с. 237-253.

Shapiro G.I., Latché L., Pantiulin A.N. 2003. Mixing processes in the Gorlo Strait of the White Sea. Oceanology, том 43, №1, с. 26-31. In Geophysical Research Abstracts, Vol. 5, 14781, EGS-AGU-EUG Joint Assembly, Nice, France, 06-11 April 2003.

**Conferences attended**:

XXVII General Assembly of the EGS, Nice, France, 2002. (Latché L.; Shapiro G.I; Pantiulin A.N).

Challenger Conference for Marine Science, Plymouth, 2002. (Latché, L.; Shapiro, G.I; Pantiulin, A.N).

XXVIII General Assembly of the EGS, Nice, France, 2003. (Shapiro G.I., Latché L., Pantiulin A.N., 2003).

**External Institution contacts**:

Moscow State University

Russian State Hydrometeorological Institute (St. Petersburg)

Plymouth Marine laboratory (PML; UK)

Signed: .....

Date:.....18....June 2004

# Chapter 1: Introduction

## 1.1. Background

The White Sea is a semi-enclosed sea located in the far north of Russia, next to the Arctic Circle. Semi-enclosed seas are partially closed systems, which consequently have relatively slow exchange rates with the open ocean, and their unique exchange properties can lead to effects that are of special interest for biogeochemical, ecological, and fisheries oceanography studies. The circulation in semi-enclosed seas is influenced by variable bottom topography, atmospheric forcing, river runoff, and tides to varying degrees.

The properties of water masses in semi-enclosed seas are influenced by mesoscale variability, including eddies and fronts. Various types of water motion and biogeochemical processes have been studied intensively over the recent decades in many semi-enclosed seas (e.g. South China, Japan, Mediterranean, Baltic and Irish Seas). However the White Sea is an exception, usually the data are sparse, incomplete, and old.

## 1.2. Motivation

Understanding oceanographic regimes is becoming increasingly important with the growing anthropogenic influence in semi-enclosed seas. Some regions are already experiencing significant anthropogenic impacts: for example the environmental problems in the Black Sea and the North and Baltic Sea regions are well known. Disposal of radioactive wastes north of the White Sea (Pfirman *et al.*, 1995) and in the Sea of Japan is also of serious concern. Scientifically and practically, the study of semi-enclosed seas is timely. Recent rapid advances in ocean and related sciences and associated technologies serve to focus research issues and to make feasible definitive studies. The main motivation for this study is to apply the techniques and knowledge from better studied regions, for example the European shelf seas, to understand the water mass distribution and circulation in the White Sea. While some work has been done in the region of the White Sea in the past years, it was generally not systematic,

and this resulted in very few interdisciplinary studies. This work was originated as a contribution of two multi-disciplinary projects named: EU-INTAS-97-1881[1]: "Mesoscale physical and biogeochemical processes in coastal waters of the White Sea"; and EU-INTAS-99-1600[2]: "Dense water overflows off continental shelves" funded by EU-INTAS programme.

## 1.3. Objectives

The specific objectives of this study are to:

- identify mesoscale and fine thermohaline structure of water masses in the Northern part of the White Sea
- quantify the inter-annual variability of the thermohaline structure of water masses
- get a better understanding of the physical processes, which control mixing of water masses in the Gorlo Strait and the formation of quasi-homogeneous layers across the White Sea
- estimate mesoscale circulation patterns in the White Sea from satellite imagery
- analyse the isopycnal and diapycnal transformation of the Gorlo Strait Water as it enters the White Sea Basin.

## 1.4. Approach

The project compares and analyses data from in situ observational campaigns carried out in 1991, 2000, 2001 and satellite imagery. The collation of the observational data in the White Sea includes (i) *in-situ* data obtained through co-operation with EU-INTAS and Russian national projects, (ii) remote sensing data acquired from AVISO (Sea Level Anomaly) and from PML (Sea Surface Temperature), and (iii) scientific publications.

[1] See project details at web site: http://www.intas.be/CallsCat/project_det.asp?call_id=971&project=1881
[2] See project details at web site: http://www.intas.be/CallsCat/project_det_new2.asp?call_id=991&project=1600

## 1.5. Wider dissemination

The results of this study will help understanding fine and mesoscale structure of water masses, mixing processes, diffusion of pollutants, estimate primary biology production, and to control long-term water quality in order to provide helpful scientific background for coastal zone management.

## 1.6. Outline of thesis

Following this introductory chapter, the **Chapter 2** provides a comprehensive literature review of the dynamics of different types of semi-enclosed seas, followed by an overview of physical processes, such as e.g. cascading phenomena and fine thermohaline structure and mixing. Finally the recent development of the physical oceanography of the White Sea is reviewed. Then, **Chapter 3** describes the data collection and processing. The in situ observation is complemented by satellite observations such as Sea Surface Temperature images and Sea Level Anomaly maps. **Chapter 4** provides a detailed analysis of the extent and structure of water masses including an analysis of step-like structure in the vertical profiles in summer 2000. In **Chapter 5**, the interannual variability of the water mass structure is investigated by comparison of data from 1991, 2000 and 2001 field campaigns. In **Chapter 6** a comprehensive analysis of a 3D water mass structure and mixing process are studied in the west region of the Gorlo Strait during survey 2000. **Chapter 7** validates the use of satellite data and estimates the mesoscale circulation of the White Sea in summer 2000. This study enables to analyse in particular the extent of the circulation of the modified Gorlo Strait Waters in the Basin of the White Sea. In **Chapter 8** the parameters and characteristics of small scale mixing are studied by analysing inhomogeneities in the fine structure of water masses. Finally **Chapter 9** integrates the results from the previous chapters, and gives recommendations for future research.

# Chapter 2: Literature Review

## 2.1. Introduction

The White Sea is a semi-enclosed sea where little work has been completed and is barely known within the European scientific community. The present study is focused on improving understanding of the processes that drive the formation and circulation of water masses in the White Sea. These processes consist of a wide range of phenomena including waves, tides, fronts, vertical velocities, horizontal currents, eddies, stratification, water mass and ice formations and transformations, turbulence and mixing (formation of fine mixed layers, microstructures). These phenomena can occur (or not) with varying strength in various semi-enclosed seas. They can be different or similar in regard to the mix of phenomena that are present, which can range from a simple linear superposition of effects to intense nonlinear interactions (e.g. straits enhance nonlinear interactions). Hence the literature review in this chapter is divided into three sections covering (i) an overview of the forcing mechanisms influencing the circulation of semi-enclosed seas (e.g. the Mediterranean Sea; the Baltic and the North Seas, the Irish Sea; the Okhotsk and Japan Seas; the Black Sea; the Red and Arabian Seas), (ii) specific processes relevant to the White Sea (well observed in the open and coastal oceans) responsible for the formation and distribution of mixed layers (fine structure) and deep-water renewal (cascading), and finally (iii) an up-to-date descriptive physical oceanography of the White Sea, which shows the importance of the present study .

## 2.2. Overview of processes in semi-enclosed seas

Semi-enclosed seas can be forced both locally and remotely by oceanic, atmospheric, bottom and terrestrial interactions. Their circulations are influenced through the inflow of fresh or saline water through narrow straits.

Strong air-sea interaction and mixing in the Mediterranean (Bethoux *et al.*, 1994; Bergamasco and Gacic, 1996), the Red and Arabian Seas (Morcos, 1970; Edwards,

1987; Eshel *et al.*, 1994; Hunter, 1986), result in the formation of water masses that can be traced well beyond these regions and often right across ocean Basins. Despite the regions having different physical characteristics, they are all affected by wind forcing (Furnes, 1980; Prell and Van Campo, 1986) and air-sea interactions, and there is much seasonal and interannual variability (Garrett, 1994; Prell, 1984; Prell and Kutzback, 1987; Damm *et al.*, 1994).

At high latitudes, a unique feature of the shelves of the polar boundary is the importance of buoyancy forcing on the coastal circulation relative to mid-latitude shelves (Aagaard and Carmack, 1989; Gow and Tucker, 1990). This difference is the result of high rates of freshwater input to the sea, and the nonlinearity represented by the equation of state of seawater. The nonlinearity means that since the upper-layer temperatures at high latitudes are relatively low, the relative effect of changes of salinity on density are much greater than similar changes in salinity at higher temperatures. In addition to the introduction of fresh water, the salinity (density) can also be altered by brine rejection and ice melting over the shelves (Royer, 1981 and 1982). Although the seasonal changes in surface buoyancy are similar over the polar shelves (Ohtani and Azumaya 1995), the resulting vertical density structures differ, even across a given shelf. These differences depend on the initial vertical density structure, water depth, shelf width, freshwater input, wind and tidal mixing, advection and ice distributions. For example in the Sea of Okhotsk, the ice forms in early November and extends through the winter until approximately 60-75% of the sea is ice covered (Yasuoka, 1967 and 1968). This extensive ice cover may be due to a layer of low-salinity water created during the summer months, mainly by river outflow. Estimates of the total fresh water supply for the Sea of Okhotsk indicate that 55% is due to river outflow and 37% is from the Amur River alone (Pices Working Group 1, 1995). This shallow low-salinity layer of water is separated from the deeper water by a sharp pycnocline. During the late fall and early winter, atmospheric cooling lowers the surface water temperature. This cold water sinks and warm water replaces it at the surface. However, the depth to which the water sinks is limited by the depth of the shallow pycnocline. Therefore, the upper layer of water cools rapidly allowing ice to form (Watanabe, 1963). Area of high ice production, as a result generates area of large salt flux into the sea and dense water formation. The importance of the dense water formation (Kitani, 1973a) contributes here to the creation of Okhotsk Intermediate Water (Kitani, 1973b; Watanabe and Wakatsuchi, 1998).

Tides are often the most important forcing component in flow circulation which is the case for example in the North Sea (Hill *et al.*, 1993; Huntley, 1980; Otto *et al.*, 1990). Elsewhere amongst other semi-enclosed seas, tidal effects are moderate or weak (see table 2.I). In some regions, strong tidal currents and associated mixing are a significant control on summer stratification (Simpson and Bowers, 1981), and tidal fronts form between regions of stratified and well mixed waters ($h/u^3$ fronts, where $h$ is the water depth and $u$ is the amplitude of the tidal current; Simpson, 1997). Tidal conditions in the North Sea are perhaps the best known. In the western and southern parts, tidal currents are dominant. Tidal energy, entering the North Sea from the north and through the English Channel in the south, results in strong tidal mixing and tidal mixing fronts ($h/u^3$ fronts) in water depths of 20-50m. These tidal fronts include a baroclinic jet (velocities up to 0.15 $ms^{-1}$ have been observed) and a weaker secondary circulation perpendicular to the front. In the south, tidal residual currents are also important. A similar baroclinic jet-like flow (located above the strongest near-bed density gradients at a depth consistent with the base of the thermocline) was also observed in the St. George Channel of the Irish Sea (Horsburgh *et al.*, 1998). Hill *et al.* (1997) have reported the recirculation of part of the Scottish coastal current around an intrusion of dense, saline Atlantic water in the Hebrides and Brown *et al.* (1999) have identified density-driven circulation paths in the North Sea. A feature common to all these flows is the existence of strong density gradients near the seabed, which control for example the western Irish Sea gyre (Horsburgh *et al.*, 2000).

An excess of precipitation and runoff over evaporation is also important in many of the semi-enclosed seas (Bergström and Carlsson, 1994; Gustafsson and Stigebrandt, 1996), with the exception of the Mediterranean, the Red and Arabian Seas, where a small freshwater input and an excess of evaporation leads to the formation of saline waters (Ovchinnikov, 1984; Malanotte-Rizzoli, 1991; Shapiro and Meschanov, 1991).

Flow over shallow sills, either at the entrance to the region via Straits (Bryden and Kinder, 1992; Bryden *et al.*, 1994; Candela, 1991) or between Basins, and the associated mixing often set the conditions within individual Basins (Georgopoulos *et al.*, 1989; Kõuts and Omstedt, 1993; Krauss and Brüge, 1991; Kinder and Parilla, 1987; Lacombe and Richez, 1982).

Some coastal phenomena, such as tides and storm surges (North Sea), which have long been recognized as of significant societal importance, are quite well understood generally. For example the Baltic and North Seas are one of the most extensively

studied areas of the world coastal ocean. Tides, surface winds, air-sea heat and freshwater fluxes and coastal freshwater input are all important in the Baltic-North Sea region. Others, such as cross-shelf transport with water exchange (Zore-Armanda, 1969; Prell and Van Campo 1986), water mass formation (MEDOC Group, 1970; Ovchinnikov, 1984; Shapiro and Meschanov, 1991; Shapiro *et al.*, 1996) including cascading phenomena, or small-scale mixing (revealed in the fine thermohaline structures), are processes which remain poorly understood at best or remain to be identified, but are now recognized to be of substantial practical importance. Cascading phenomena and fine thermohaline structure are therefore reviewed in this chapter in the following sections.

| Semi-enclosed seas | Ocean influence | Tidal forcing | Seasonal variability | Freshwater influence | Flow over sills | Anthropogenic influence |
|---|---|---|---|---|---|---|
| | | | | | | |
| Sea of Okhotsk | moderate | weak | moderate | moderate | moderate | weak |
| Sea of Japan | weak | weak | moderate | moderate | moderate | moderate |
| Baltic Sea | weak | weak | moderate | strong | strong | strong |
| North Sea | moderate | strong | moderate | moderate | moderate/weak | strong |
| Mediterranean Sea | moderate | weak | moderate/ strong | concentration | strong | strong |
| Black Sea | weak | weak | moderate | strong | moderate | strong |
| White Sea | weak | moderate | moderate | strong | strong | moderate |
| Irish Sea | strong | strong | moderate | weak | moderate | strong |
| Arabian seas | moderate | moderate | moderate | concentration | moderate | moderate |

Table 2.I: Summary of the physical characteristics and the strength of a number of factors in each semi-enclosed sea (Church *et al.*, 1998).

## 2.3. Cascading phenomena

Cascading phenomena are expected to occur in the northern part of the White Sea as inferred by scientists who lead the EU-INTAS-1600 campaign. Cooper and Vaux (1949) first introduced the term of "cascading" (see figure 2.1), whereas Nansen (1912) had first introduced the idea of exchange between oceanic and deep waters. A complete definition of the term cascading was raised by Whitehead (1987): Cascade occur when dense water formed on continental shelf spills over the shelf edge and descends the continental slope as a gravity current under influence of friction, entrainment and rotation. Cascading may be regarded as a special form of downwelling. A review and a simple physical approach done by Huthnance (1995), is that it occurs when shallow waters on the shelf are cooled in winter to lowers temperatures and greater density than the adjacent waters over the slope. The density is enhanced if the cooling forms ice, expelling salt into the water below, and then there is a tendency for the dense water to form a distinct bottom layer.

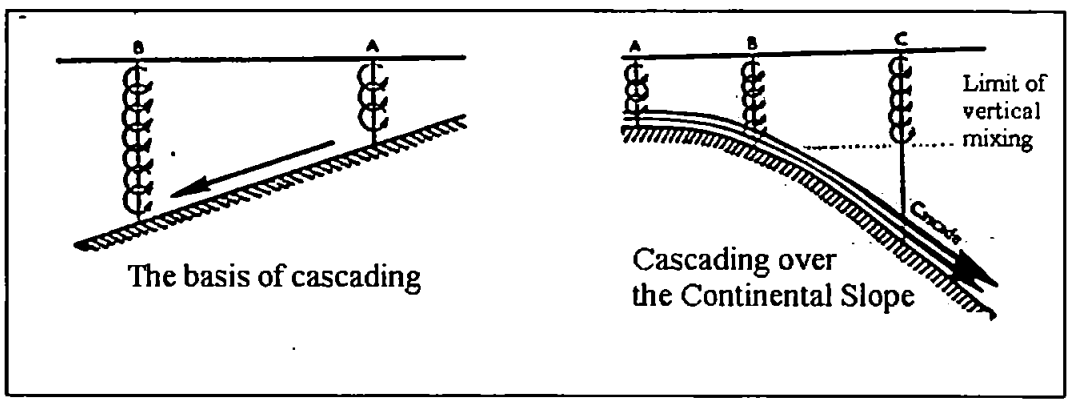


Figure 2.1: Schematic representation of cascading (Cooper and Vaux, 1949) during winter at stations A, B, C of same water properties. (Left) Sufficient vertical mixing with same loss of heat through the surface at A and B result in colder and heavier water at A, which tends to cascade downhill along the bottom. (Right) Same scenario with a cascade current established from A to B approaching the edge of the slope and cascade further down as a heavy relatively cold blanket of water until it reaches the density of the neighbouring ocean water.

Cascades are of interest in downslope transport and represents an irreversible mechanism for ocean-shelf exchange (Huthnance, 1995), an export of carbon and suspended matters from continental shelves to deep ocean. Hence, cascade phenomena are traced worldwide (Ivanov *et al.*, 2003). The dynamics of dense water cascades at the Hebridean shelf edge, west of the British Isles, were modelled (Shapiro and Hill, 1997),

and correspond to the observations (see figure 2.2). Some observations were also compared with satellite observations on the northern Okhotsk shelves (Gladyshev *et al.*, 2000).

Also, these processes juxtaposing ocean to shelf waters like up/downwelling may be important contributors to shelf-sea heat flux, leading to ventilation of intermediate water and of deep water renewal.

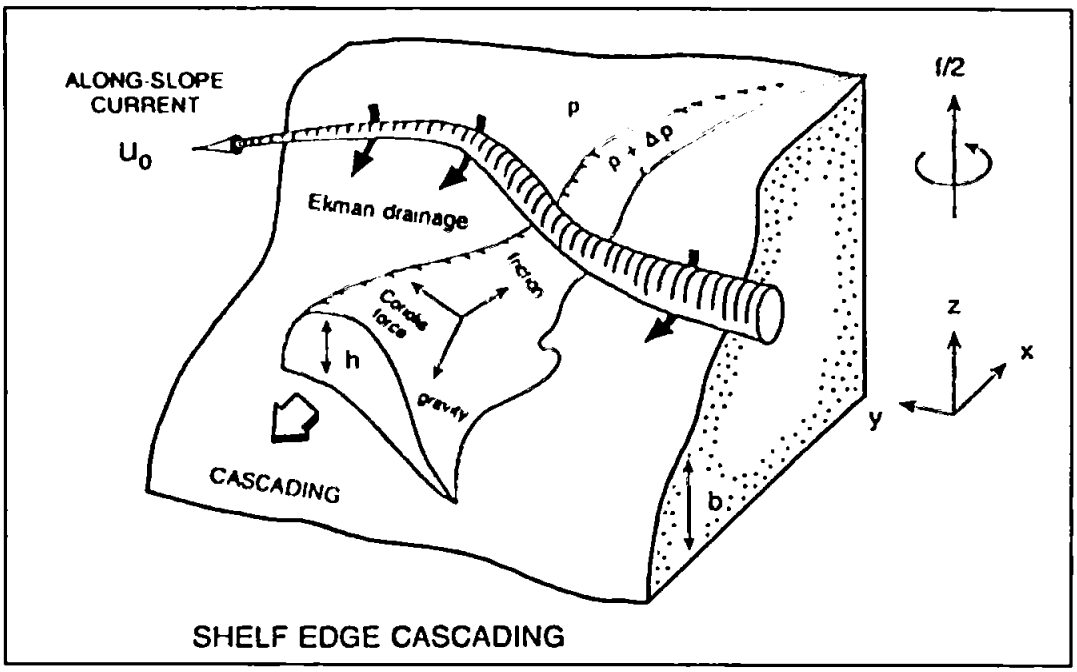


Figure 2.2: Schematic of Cascading and current-forced Ekman drainage on a continental slope (source: Shapiro and Hill, 1997).

In polar seas, shelf edge cascade are often associated with extreme climatic condition such as occur on Arctic and Antarctic shelves where winter brine release due to ice growth raises shelf water densities (Gill, 1973; Foster and Carmack, 1976; Melling and Lewis, 1982; Quadfasel *et al.*, 1988). The presence of strong pycnocline in these Polar Regions limits considerably the depth of convection shielding the deep water from atmospheric forcing. The mechanism of cascading thus results in the decisive role of the salinity, mainly determined by either small seasonal water temperature variation or large seasonal salinity variation due to ice freezing cycle.

Outside polar seas, cascade is associated with semi-enclosed, shallow gulfs subject to arid continental climates where shelf water densities are raised due to an excess of

salinity by summer evaporation followed by intense winter cooling. This was observed in southern Australia and off the Spencer Gulf (Lennon *et al.*, 1987), the Gulf of California (Lavin *et al.*, 1995) and in the Adriatic Sea. Winter cooling and evaporation over the northern Adriatic provides a source of cold and dense (but relatively fresh) water that has been seen following isobaths southwards and sinking down canyons (Zoccolotti and Salusti, 1987; Bignami *et al.*, 1990). These relatively dense water productions in the Adriatic Sea have been modelled confirming the downwelling-favourable effect of the cold Bora wind during winter (Bergamasco and Gačić, 1996). Further east, the Mediterranean water entering the Black Sea has about twice the salinity of the ambient shelf waters. Hence it forms a thin (2-3m) bottom layer which cools to the ambient temperature, subsequently sinking along the continental slope (Őzsoy *et al.*, 1993) until forming a neutrally buoyant plume off-shelf (Oguz and Rozman, 1991). In the eastern USA near 32□N, Li *et al.* (1986) related some downwelling on the Georgia Shelf to also downwelling-favourable winds, usually occurred when the Gulf Stream was close to the Shelf and probably assisted by winter cooling.

The Bass Strait cascade (SE Australia) may be the best-documented (Tomczak, 1985, 1987), comprising water of higher temperature and salinity than the adjacent Tasman Sea and manifesting two winter sources at the northern side of the strait. Luick and Tomczak (1994) showed a front and along slope current across the eastern entrance of the Bass Strait; however winter-cooled water from the shallow strait was liable to transgress down the slope in various places. Much of it forms a northward undercurrent along the slope at 300-400m during winter, extending to 500km from the sources. The east Australian Current was observed to include packets of cascaded water.

Although Cascading is sensitive to hydrographic conditions and degree of winter cooling in any one year (Huthnance, 1995), fragment of historical evidence point to the possibility that intermittent winter cascading occurs in the northwest European waters that are subject to relatively mild temperate climate (see figure 2.3). This is observed in the Celtic Sea (Cooper and Vaux, 1949) and the Malin-Hebrides Shelves (Hill *et al.*, 1998). Recent observations of cascading worldwide are reported in Ivanov *et al.* (2003), and the physical mechanisms of dense water cascades are discussed in Shapiro *et al.* (2004).

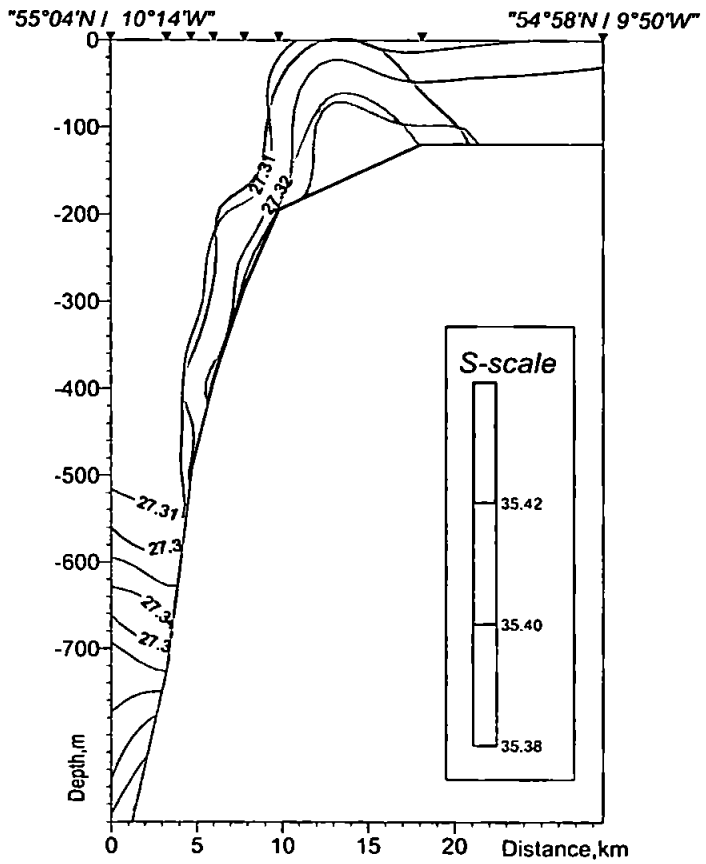


Figure 2.3: Potential density (solid lines) and salinity (shaded areas) across the edge of the Malin Shelf in February 1996 (Shapiro *et al.*, 2004).

## 2.4. Fine thermohaline structure

Small-scale processes involved in stratification, oceanic microstructure and mixing need much details and attention. In recent years accurate instruments that can provide continuous profiles of temperature and salinity in the ocean have become available. The fine-scale features that are observed in the CTD profiles have come to be known as oceanic microstructure, fine structure, often called 'step-like' structure or 'staircase'. The first observations of fine thermohaline structure in the vertical profiles were reported by Stommel and Fedorov (1967). The observation of such fine structures (see step-like profiles in figures 2.4a, 2.4b, 2.4c) indicated formation of mixed layers: homogeneous layers of water separated by a thin interface with large gradients of temperature and salinity. Therefore, the fine thermohaline structures were investigated in many regions of the Ocean (Gregg, 1973 and 1976; Gregg and Briscoe, 1979; Gregg and Sanford, 1980; Marmorino, 1987; Stommel, 1993; Navrotsky 1999; Mordasova,

1999; Nakamura *et al.*, 2000), and some, were first observed recently in the White Sea (Latché *et al.*, 2002; Lukashin *et al.*, 2003).

The fine structures result mainly from the stirring and mixing processes that occur in the ocean and can be used as indicators of these processes. Turbulence is essentially a random process, which results in irregular fluctuations of temperature and salinity about their mean values. Much observed fine structure, however, is regular, and suggests that more specific processes are involved.

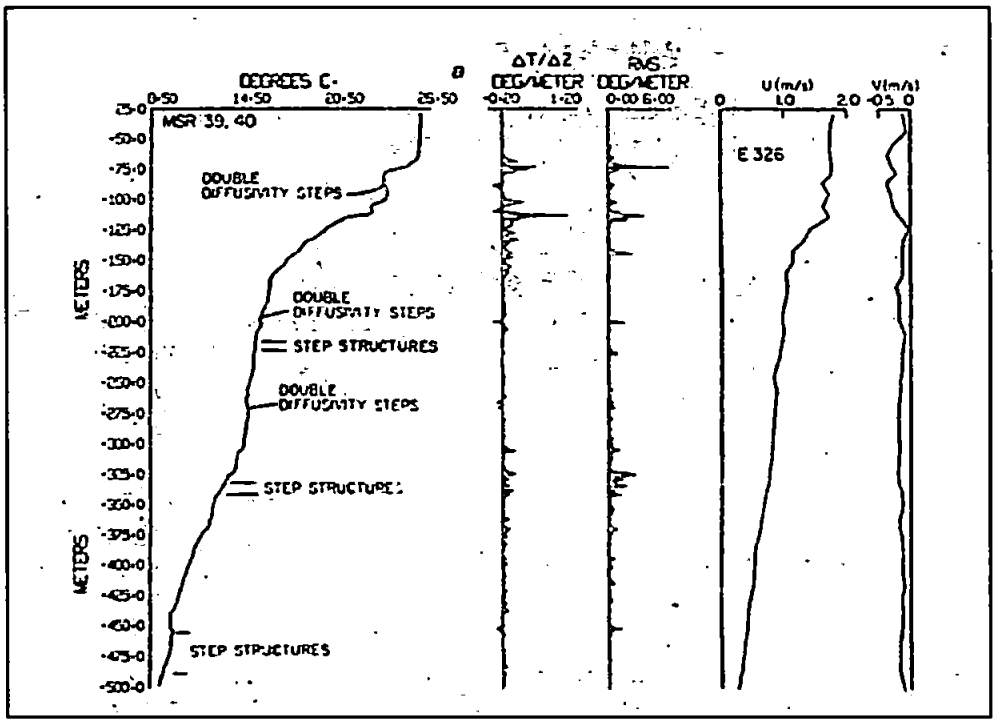


Figure 2.4a: Summary plots of two MSR (Micro-Structure Recorder) records taken in the middle of the Gulf Stream with the velocity profile. The double diffusivity steps are on the upper boundaries of salt-stabilized temperature inversions. Some of the step structures in monotonic regions may be due to salt fingering (Gregg and Sanford, 1980).

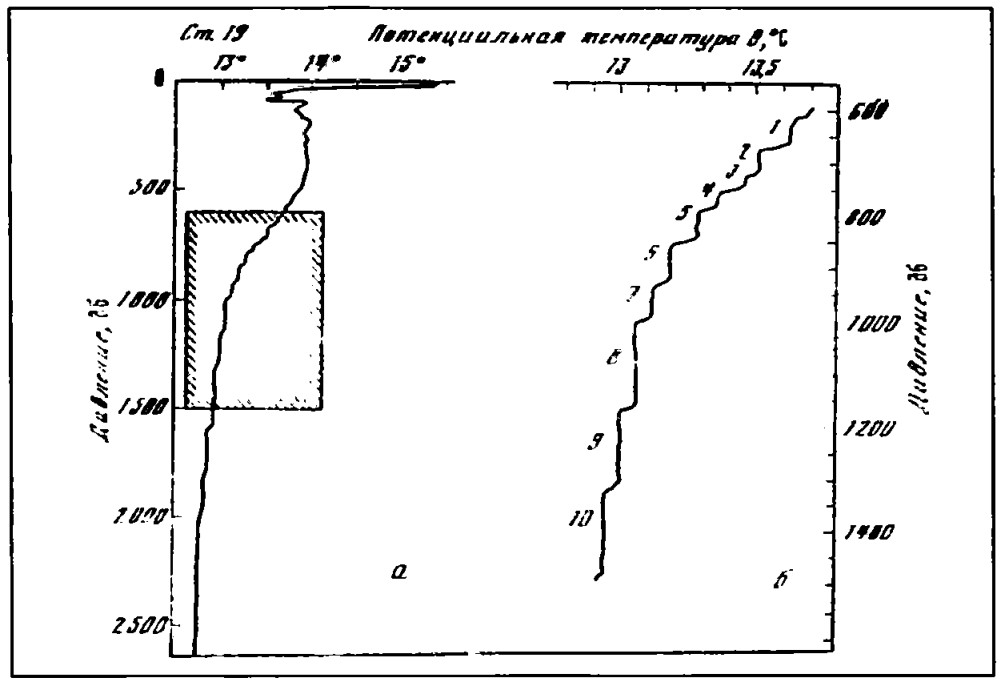


Figure 2.4b: Example of fine structures seen at station 19 in the vertical profile of potential temperature (a) from surface to bottom with a section (b) enlarged revealing 10 steps. Observations in the Tyrrhenian Sea (Molcard and Williams, 1975).

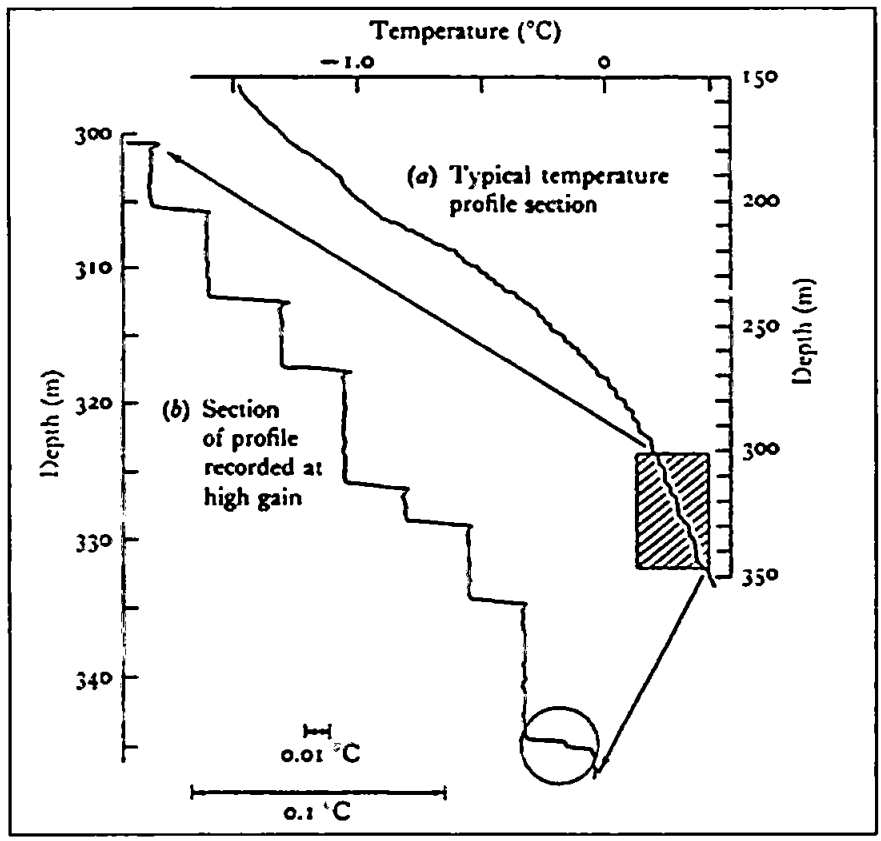


Figure 2.4c: Temperature profile under Arctic Ice Island T3, showing steps formed by the double-diffusive mechanism (Neal, Neshyba and Denner, 1969).

The scale of these fine-scale features varies considerably, some layers being 20-30m thick, whereas others, perhaps superimposed on them, are only less than a metre thick. There are very few observations of the lateral extent of these layers: it may be as much as tens of kilometres for the thicker layers, and perhaps hundreds of metres for the thinner layers. Temperatures may either decrease or increase with depth in these step-like profiles, but where the temperature increases with depth (temperature inversion), salinity also increases with depth so that the interfaces of the layers remain stable. When the temperature decreases with depth, salinity may either increase or decrease with depth. The molecular diffusion alone would eliminate the differences between adjacent layers of water, given sufficient time. The observed fine structure must therefore result from mixing activity or continual stirring, which produces the sharp contrasts between layers. Various hypotheses have been put forward to account for the microstructure. It is likely that a number of stirring processes are involved and that different processes dominate on different scales and in different parts of the ocean. The term of mixing activity according to Gregg (1976) is often referred to the rate at which temperature fluctuations are dissipated by diffusion, and also referred to the vertical heat fluxes resulting from small-scale turbulence. Schmitt (1994) reviewed double-diffusion in the ocean. When temperature and salinity both decrease with depth, a double diffusion process called salt-fingering occurs. In contrast, diffusive convection occurs when both temperature and salinity increase with depth. Figure 2.5 shows how the effect of the Salt-fingering process is to reduce the density of the lower layer and increase that of the upper layer, leading to instability in the system. Because the coefficient of molecular diffusion of heat is ~100 times greater than that of salt, the result is a convection pattern of sinking cells of salty water alternating with rising cells of less salty water. This process has been found and investigated within laboratory experiments (Stern, 1960; Turner and Stommel, 1964), and there is no conclusive evidence of its occurrence in the oceans on any major scale; and it is questionable whether this process could be significant on a large scale, for it is dependent on molecular processes.

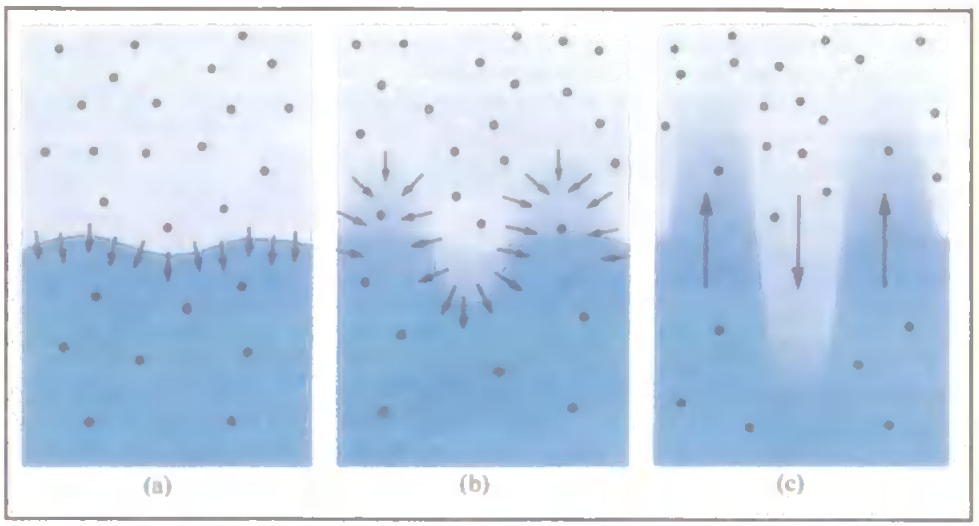


Figure 2.5: the change from a stable to an unstable density-depth profile when warm saline water (paler blue) overlies cooler and less saline water. (a) the more rapid diffusion of heat (arrows) than salt, leads to (b) and (c), the development of salt-fingers when the density profile becomes unstable (Gregg, 1973).

Turner (1973), however, showed that the relative strength of double-diffusion can be described by the gradient ratio of temperature and salinity, also called stability ratio or density ratio given in equation (2.1)

$$R_\rho = \frac{\alpha T_z}{\beta S_z} \qquad (2.1)$$

with $\alpha = -\rho^{-1}\frac{\partial \rho}{\partial T}$ (2.2) and $\beta = \rho^{-1}\frac{\partial \rho}{\partial S}$ (2.3)

where $\alpha$ in equation (2.2) is the thermal expansion coefficient, $\beta$ (2.3) is the haline contraction coefficient, $\rho$ is the density, and $T_Z$ and $S_Z$ are the vertical temperature and salinity gradients. Both forms of double-diffusion (diffusive convection and salt-fingering) are most intense when $R_\rho$ approaches 1. In the oceanic case where a horizontal front is cold and fresh on one side, $R_\rho$ is near 1 because T and S have an opposing effect on $\rho$ and compensate each other (Rudnick and Ferrari, 1999). Kelly (1984, 1990) derives expressions for the effective diapycnal heat and salt fluxes by double-diffusive processes as $R_\rho$ approaches 1.

The breaking of internal waves can also be another process to relate the presence of step-like structure. Wherever the water in the ocean is vertically stable, oscillations can

occur if the water is displaced vertically. Internal waves result, which can propagate energy through the ocean in rather the same way as surface waves do. Such waves forming at the interfaces of the layers of different density are associated with strong velocity shears, due to both the relative motion of the layers above and below and the orbital water motions associated with the waves. These shears can occasionally produce local instability in the form of billows or breakers, which lead to vigorous turbulent mixing of water immediately above and below the interface. The effect of this is to create an intermediate layer between the two original layers, and thus form two smaller steps in the vertical profile in place of one larger step. This can continue indefinitely with further steps in the vertical profile being formed on each occasion. The use of tracers has enabled divers to observe and film this process in the thermocline of Malta (Gregg, 1973).

Although some dynamics aspects in small-scale mixing have been considered to explain the presence of step-like profiles in terms of changes in conservative properties (temperature and salinity), the nature and the extent of such fine structures remain questionable in some part of the oceans.

# 2.5. Descriptive Oceanography of the White Sea

## 2.5.1. Introduction

The Norwegian explorer Ottar discovered the White Sea in 800 A.D. The White Sea is an arm of the Arctic Ocean reaching the north-western part of Russia, and named "Beloe More" in Russian. It is a semi-enclosed Arctic sea joined to the Barents Sea by the narrow and shallow Strait of 'Gorlo' ('neck' in Russian) situated between Cape Kanin and the Kola Peninsula (see figure 2.6). The Onega, Dvina, and Mezen Rivers, (which have given their names to the White Sea Bays) flow into the White Sea. Arkhangelsk is the biggest city of the study area situated at the estuary of Dvina Bay. The White Sea becomes icebound from the months September to June, hence shipping activity is heavy in summer. The Dvina, Volga, and Dnepr rivers connect the White Sea to the Caspian and the Black Seas. The White Sea can be regarded as an ecosystem which combines physical, chemical, biological and geological processes at different scales (Chugaynova *et al.*, 1993; Beloe more, 1994 and 1995; Berger *et al.*, 2001; Pertzova and Kosobokova, 2002b). An increased expedition activity in the White Sea was observed in the last decade (Dolotov and Lukashin, 2001). However, at the same time, problems have arisen related to the interpretation and the generalization of the observational results. Therefore this review consists of an up-to-date description of the hydrology of the White Sea, and underlines the main factors which form the regime and the hydrological signatures of the White Sea (Duvanin, 1983; Gidrometeorologiya, 1991). The factors that affect mostly the hydrology of the White Sea are:

- its geographical location with the half region of the White Sea located above the Arctic Polar Circle (66°33'N); severe climate conditions
- its small size sea compared with other Arctic seas
- its bottom topography and the shape of the coastlines
- the presence of estuaries and rivers of the White Sea Bays, providing important freshwater inputs
- the intensive exchange of water masses in the Gorlo Strait influenced by the tides.

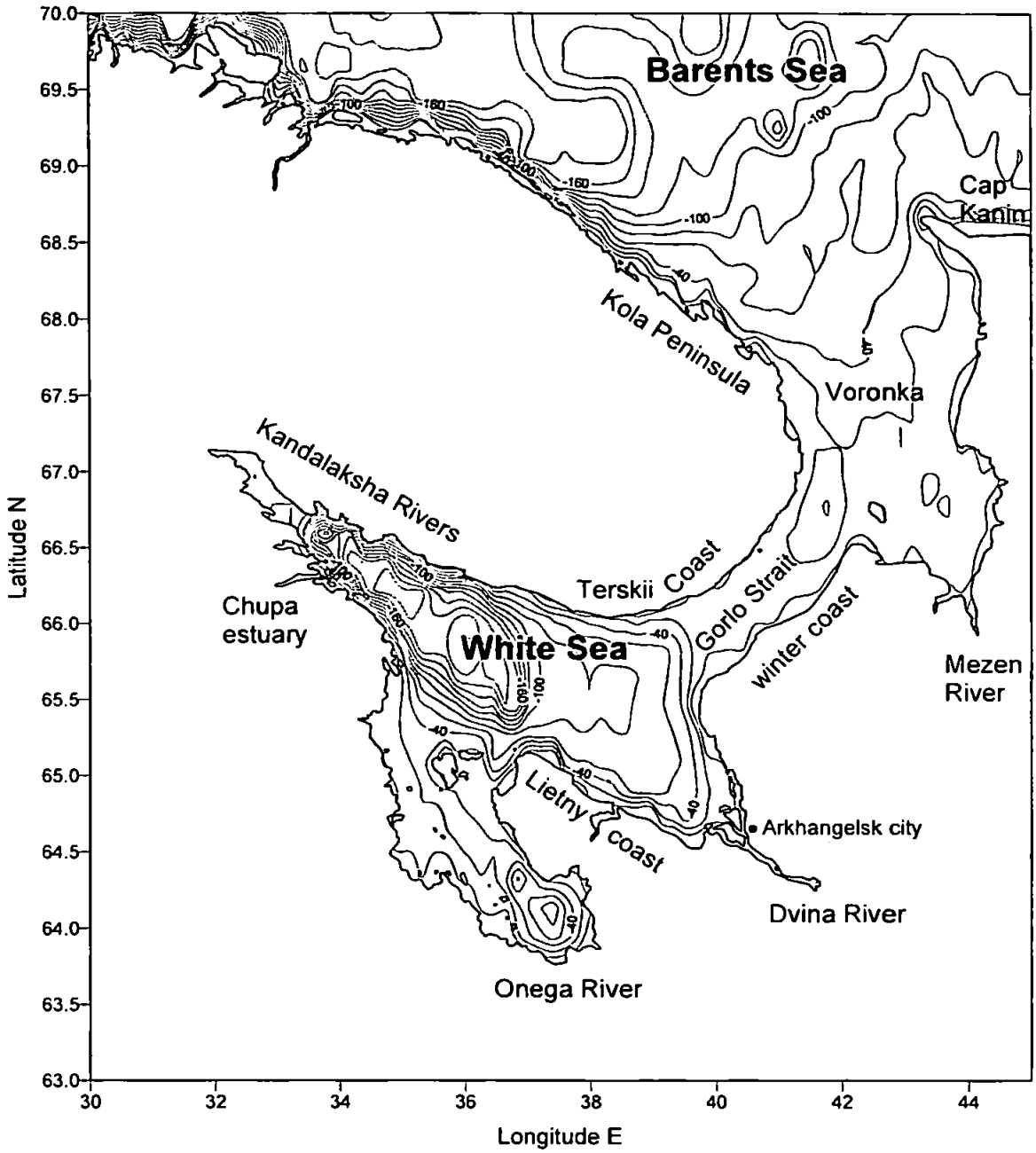


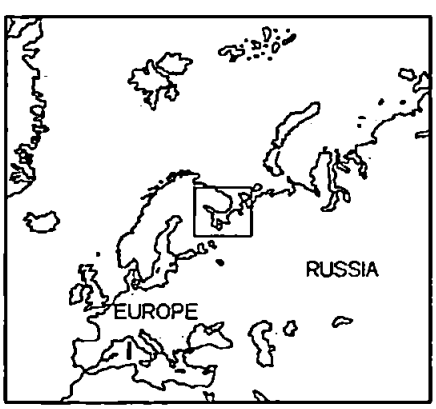


Figure 2.6: Location of the White Sea (beside) with (above) a detailed map (GEBCO, 5 miles resolution) showing its coastlines and isobaths (m); the main rivers of the White Sea Bays (Mezen, Dvina, Onega and Kandalaksha). In the northern part of the White Sea, the Basin (deepest part) connects to the Barents Sea (through Voronka) by the Gorlo Strait.

### 2.5.2. Topographic features and volume of waters

The area of the White Sea (figure 2.6) is relatively small and covers approximately a surface area of 90000 $km^2$, which is represented by a surface area of 34000 $km^2$ in its northern part; and 56000 $km^2$ in its southern part. Numerous islands cover in total an area of 800 $km^2$ (Klenova, 1966). The size of the White Sea extends 540 km along its latitudes and 550 km along its longitudes, considering the boundaries of the White Sea at the latitudes of Cape Kanin. The coastline of the White Sea has a perimeter of 5093 km. The White Sea has a maximum depth of 350 m located in the Basin adjacent to the Kandalaksha Bay, and an average depth of ~67 m.

The total volume of the White Sea waters is about 6000 $km^3$, which is represented by 2000 $km^3$ in the northern part including the Voronka, the Gorlo Strait and Mezen Bay, and 4000 $km^3$ in the southern part including the Basin of the White Sea, Dvina, Onega and Kandalaksha Bay. The average percentage of volume of water in the White Sea is given below in table 2.II. The Basin and the Kandalaksha Bay (with a maximum depth of ~300 m) are the deepest part of the White Sea, thus classified as a fjord-shape semi-enclosed sea. The presence of a shallow sill (with an average depth of 40-50 m) in the Gorlo Strait however restricts significantly the exchange of waters between the Barents Sea and the White Sea; the Gorlo Strait being 150 km long and 50 to 60 km wide.

| Vol. water % | Layers |
|---|---|
| 54 | 0-50 m |
| 23 | 50-100 m |
| 11 | 100-150 m |
| 7 | 150-200 m |
| 4 | 200-250 m |
| 1 | 250-300 m |

Table 2.II: Percentage of volume of waters in the White Sea per 50 m layer.

### 2.5.3. Water Masses

A simple view of the body of the White Sea waters is the inflow of saline waters from the Barents Sea and the outflow of less saline (fresh) surface waters from the White Sea Bays. However, the geomorphologic aspect of the White Sea subjected to Arctic atmospheric condition gives the picture of a complex flow system creating different modes of mixing in the formation of water masses. The combination of factors such as ice, the Arctic climate, the fresh water inputs, the different modes of mixing and turbulence (many islands) and topography (such as the sill of the Gorlo Strait) are strong potential forcings to generate the formation of water masses and fine thermohaline structure. The White Sea water types, which were first identified by Deryugin (1928) and later by Timonov (1947 and 1950), are recognised amongst Russian oceanographers (Gidrometeorologiya, 1991a). Their thermohaline characteristics and distribution are used for numerical models of the White Sea circulation run on a yearly basis. The water types are described below in the following sections. Figure 2.7 shows a schematic representation of the distribution of the water bodies of the White Sea during spring seasons (Gidrometeorologiya, 1991a).

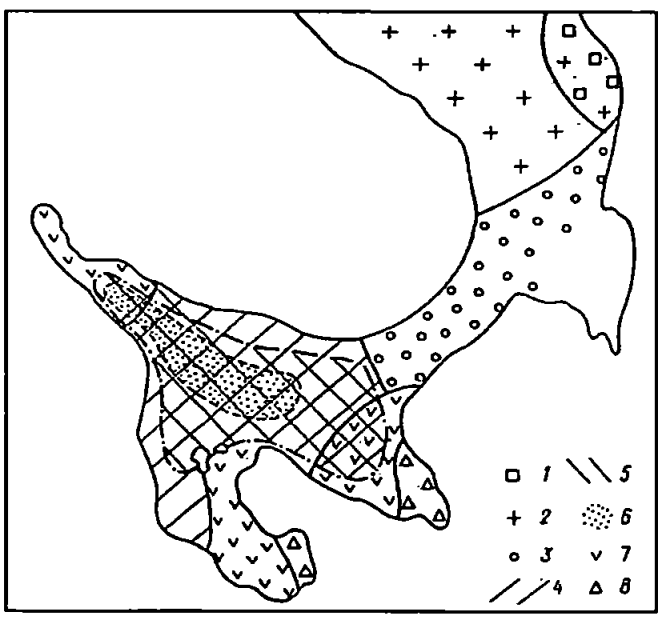


Figure 2.7: Distribution of the Water Types found in the White Sea regions during spring season. 1- Voronka Water, 2- Barents Sea Water; 3- Gorlo Strait Water (GSW); 4- White Sea Surface Water (WSSW); 5- White Sea Intermediate Water (WSIW); 6- Deep Water of the White Sea; 7- Fresh Waters of the White Sea Bays; 8- River Waters (Gidrometeorologiya, 1991a).

This distribution of the identified waters during spring do not vary at all in summer and in autumn hence remain the same, except for the river waters which are absent along the

coast of the White Sea Bays and for the fresh waters inside the White Sea Bays which have a maximum extent during spring (found around the mouth of the Bays), to a moderate spread in the Bays in summer and in autumn they occupies the same area as the river waters observed in spring.

**The Barents Sea and Voronka Waters**

The Barents Sea Water (BSW) is an Arctic water extending into the region of Voronka. The BSW is a homogeneous layer of water from surface to bottom as it propagates onto the shelf (Voronka). It has an approximate horizontal width of 15-20 miles from Kola Peninsula. The water has a salinity of 33 psu during summer and 34.5 psu during winter. Its temperature is 15°C in the warm season and reaches almost the freezing point in winter (being ice-free). The Voronka water however is confined to the east coast as a result of mixing with Barents Sea Water and fresh waters from Mezen Bay.

**The Gorlo Strait Water**

The Gorlo Strait Water (GSW) is strongly mixed by the tides propagating onto the shallow sill of Gorlo. The water is formed by intense mixing which involve the surface and fresh waters flowing out from the White Sea (24-25 psu) and the Barents Sea Water (30-33 psu) flowing in at the bottom layer of the Strait. As a result the GSW has salinity decreasing from 31 to 27-26.5 psu as it mixes from the north region (Voronka) to the south (entrance of the White Sea), and has salinity 30-29 psu in winter, due to none fresh surface outflow. The Gorlo water is thus typically and uniformly mixed by the tides. Its temperature is 5-6.3□C with a high level of oxygen during free-ice seasons.

**The Waters of the White Sea Bays**

The fresh waters found in the White Sea Bays (Onega, Dvina, and Kandalaksha Bay) have in summer the typical characteristics of temperature 16-17□C and salinity ≤ 20 psu and reach freezing point during winter. These estuarine waters present very low visibility (1-1.5 m), caused by the load of suspended particle matters, and a colour ratio index (as brown colour) of 17-21 (Gidrometeorologiya, 1991a). The circulation of these estuarine waters is confined to the upper layers of the White Sea Bays, and hence these fresh waters only mix horizontally with overlying waters. They contribute significantly

to the formation of the surface waters of the White Sea, which in summer are characterized by temperature 14-15°C and salinity 23-24 psu. In the north of Onega Bay, low temperatures are observed in the upper layer corresponding to the circulation of lenses.

**The White Sea Surface Water**

The surface and upper layer waters of the White Sea interacts horizontally with marginal waters from the White Sea Bays and vertically with underneath saline waters of the intermediate layers. The result is the formation of the WSSW characterized by salinity 25 psu during summer and low-salinity 20 psu during winter (due to ice formation). Their temperatures range from 15-to-20□C in summer and reach the freezing point in winter. The WSSW is defined by a surface layer of approximately 10-20 m thick, and in the water column below, the upper layers of the White Sea reach maximum 30-to-40 m depth, which represents 40% of the total volume of the White Sea.

**The White Sea Intermediate Water**

The White Sea Intermediate Water (WSIW) of the White Sea is characterized by salinity > 27.5 psu in summer and by > 28 psu in winter. The water is confined to the 50m isobaths of the White Sea reaching maximum ~120 m depth.

**The Deep Basin Water**

Underneath the intermediate layer at ~150 m and below, the deep water of the White Sea is hence confined to the Basin. The water is characterised by temperature -1.5□C and salinity 29.5-to-30 psu. This deep water of the White Sea does not vary seasonally or inter-annually in the Basin, and is therefore considered as stagnant water. However, due to the presence of oxygen showing yearly changes in the deep layer of the Basin, Timonov (1947) had suggested possible intrusion of water at certain deep levels with a source coming from Gorlo. The author stated that the month-period of January-March seems to be the most favourable seasonal period for the deep water of the Basin (with an increase temperature) to be removed by colder dense waters. Oscillating variation of oxygen was shown in the Basin with the decrease in summer and the increase in winter, suggesting deep water renewal phenomena.

### 2.5.4. Atmospheric conditions

The severe atmospheric conditions and ice in the White Sea have a direct and strong impact on the exchange of water masses between the Barents Sea and the White Sea (Deryugin, 1928; Timonov, 1947 and 1950), shown by its inter-annual oscillation after several different winter periods. Furthermore, the major part of the ice formed in the White Sea is likely to recirculate in the sea and not exchange much with the Barents Sea (Timonov, 1950). According to some calculations made using thermal balance equations derived from the atmospheric conditions, the results showed that the White Sea keeps the ice-sheet formed, hence melting near shore. This kind of process differs totally from those occurring in the Arctic coastal ocean; where freshwater influence the opening sea after formation of ice on the Arctic shelves. During winter the Barents Sea exports ice to the White Sea and gets some portion of drifted ice back from the White Sea during spring and early summer (Timonov, 1947). It hence provides a cross-shelf transport system for (aggregate) particulate matters to flow out of and into the White Sea.

During the long winter period (October-to-April), the White Sea Bays freeze over, hence estuarine water flowing into the White Sea are restricted. However, the period of May-early June is the ice-melting season, which brings a short period of extreme river flood. The monthly average air temperature during the warmest season is approximately 15°C near Arkhangelsk.

The air-sea interaction is therefore consequent in the White Sea notably with the area around Kandalaksha Bay located in the sub-arctic climatic zone, which has a predominant cyclonic weather (figure 2.8). The air temperature is below zero from mid-November to mid-May (e.g. -13°C in Arkhangelsk in January) and the estuaries are covered with 2m thick ice. The mean annual precipitation is ~400-500 mm, which is snow and rain falls in equal proportion. The climate can be summarised by two prevailing wind-directions (figure 2.8). The wind blows southerly and southwesterly during the winter period and changes to northerly and northeasterly during the summer-spring seasons. The characteristic wind speed is 5 to 10 m/s. Strong winds (> 15 m/s) most frequently blow in the autumn and winter and can last for 100-120 days in the northern part of the White Sea. Hence, in winter during strong winds, the ice can be pushed through the Gorlo Strait providing a mechanism for sea-ice water to flow out the White Sea and towards the Barents Sea. For example, a sea level rise of 1m in the north of the Gorlo region generated by strong southwesterly wind will cause an inflow of

Barents Sea Water into Gorlo according to mass conservation. However it is not systematic since the shallow sill of Gorlo restricts physically the intrusion of the BSW, enhanced with the shear stress acting at the bottom boundary, which however under certain conditions might entrain 'deep water particle' to flow in at the bottom of the Gorlo Strait.

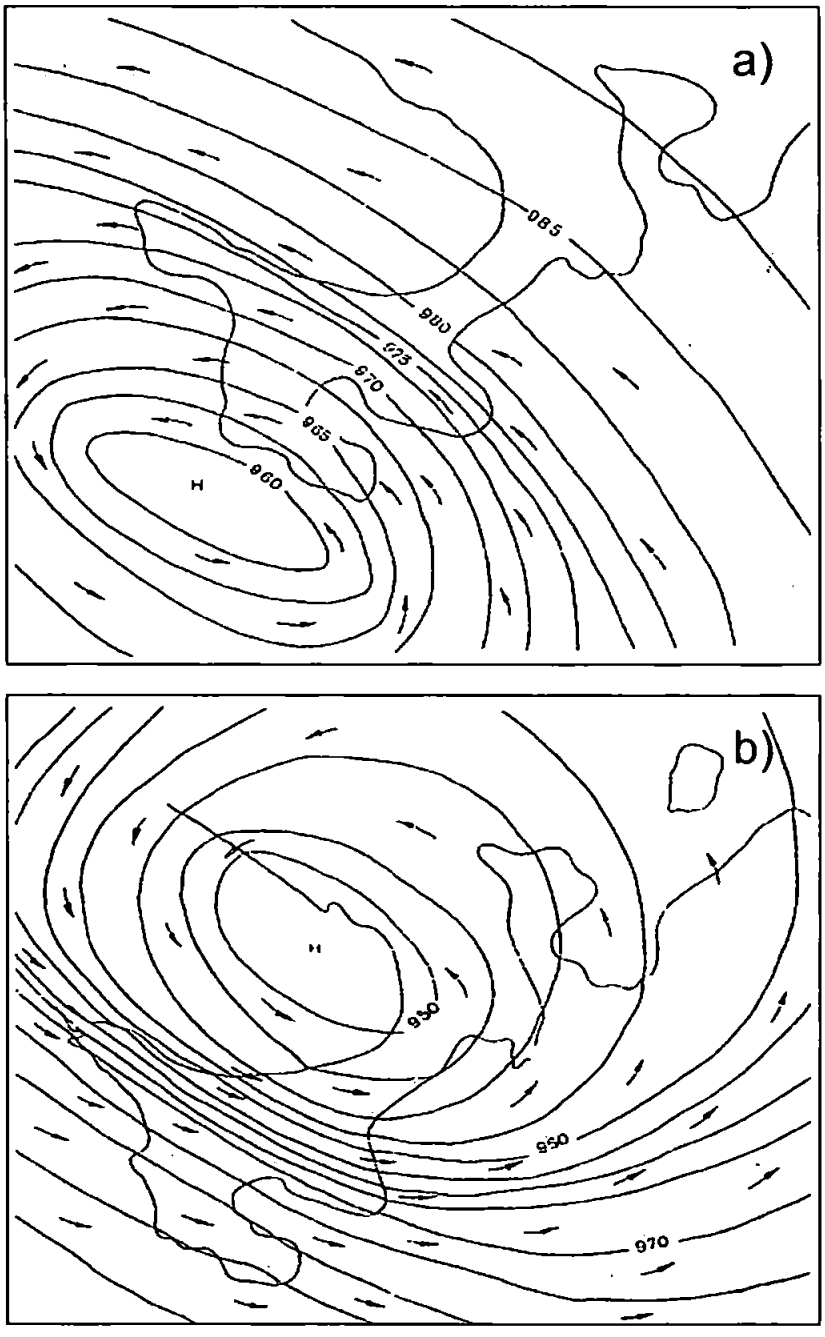


Figure 2.8: Predominance of a cyclonic weather above the White Sea showing the two prevailing wind-directions (a) southwesterly in winter and (b) northerly in summer and spring (Gidrometeorologiya, 1991a).

### 2.5.5. Tidal conditions

The tides in the White Sea are rather weak compared to other semi-enclosed seas (table 2.I). However the tides are not absent despite the strong tidal dissipation caused by the shallow sill of the Gorlo Strait, and are an important factor forming the hydrological regime of the White Sea. As reviewed by Deryugin (1928), the tidal energy is unequally distributed all over the White Sea area. For a total tidal energy (100%) transported from the Barents Sea into Voronka, 30% is dissipated in Voronka, 50% is scattered in the Mezen Bay, and only 20% of the tidal wave energy goes into the Gorlo Strait, but due to the reflection, only 6% propagates into the Basin and the Bays of the White Sea (Gidrometeorologiya, 1991a). The strong tidal dissipation within the Gorlo Strait is illustrated by the following average tidal velocities of only ~0.1 m/s in the Basin, by comparison with the tidal velocities of ~2 to 3 m/s in the Mezen Bay. An approximate tidal velocity in the Gorlo Strait estimated from Deryugin (1928) is 1-1.2 m/s with a tidal height of ~3 m. in the basin the tide height decrease to 1.5m and the velocities do not exceed 0.2 m/s. Approximately identical tides are observed in the Dvina Bay, but the velocity of the current at the apex are greater (up to 0.3 to 0.6 m/s). In Kandalaksha Bay, the topographic effect leads to an increase in tide height up to 2.5 m, but it manifests itself more notably in the tidal currents, which can reach 0.8 to 1.2 m/s. An approximate tidal circulation can be regarded with the phase and amplitude of the M2-tidal component (Nekrasov, 1975; Prandle, 1982) shown in figure 2.9. The propagation of the tidal wave into the Gorlo Strait and the Basin with the bays occurs with their partial reflection, diffraction and interference, resulting in a complex system of waves of different character: progressive, progressive-standing, and amphidromes. But according to Deryugin (1928), the tidal current does not contribute much to the water-mass exchange at the entrance of the White Sea, which is more influenced by the fresh surface outflow (Timonov, 1950). Deryugin (1928) showed that the tidal excursion does not exceed 16 km (tidal particle moving back and forth). However, residual-tidal currents were clearly reported in the Basin in a two tidal-cycle observation (Gidrometeorologiya, 1991a), which also agree with numerical results of a tidal circulation model in the White Sea using only a tidal forcing component.

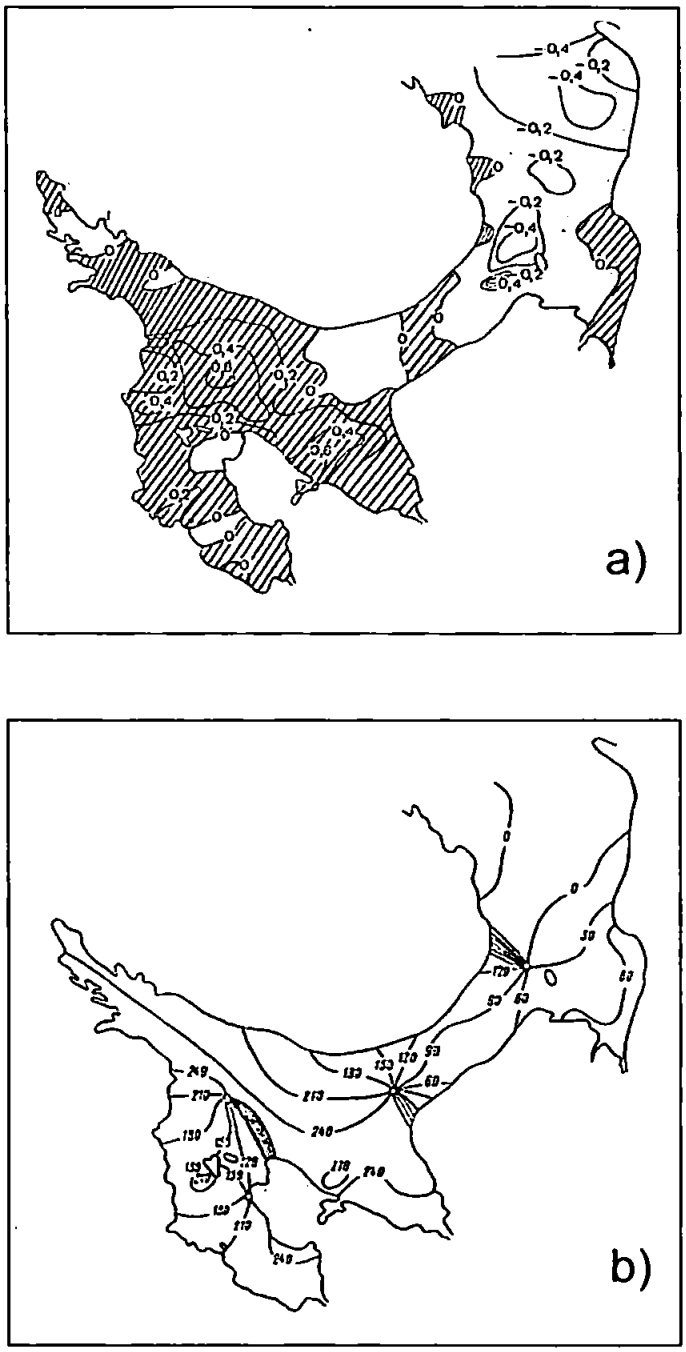


Figure 2.9: (a) Sea surface height in metre (shaded areas are positive values) derived from the M2-tidal constituent, and its corresponding phase (b) in the White Sea. (Gidrometeorologiya, 1991a).

### 2.5.6. Fresh water inflow

The fresh water inflow has a great influence on the salinity in the surface layer of the White Sea. The three largest rivers, Dvina, Mezen and Onega contribute a total river discharge of 2/3 of fresh water inputs in the White Sea (Duvanin, 1983). The Dvina

River alone contributes half of that ratio; the other half being equally distributed in the surface of the White Sea around the coasts south of Kandalaksha Bay and north of Onega Bay.

The annual sum of all the freshwater components of the White Sea budget is ~253 $km^3$ (Timonov, 1950; Duvanin, 1983), which is equivalent to a fresh surface layer of ~2.5 m thick spread all over the White Sea. The Basin and the Bays are the freshest part of the sea, and thus the layer of freshness, without considering the region of Gorlo, would be ~3.7 m thick, which is 4.7% of the total volume of the Basin plus the gulfs of the White Sea (Timonov, 1950). The consequences of fresh water inputs in the upper layers of the White Sea therefore facilitate the process of stratification particularly enhanced in the regions of Kandalaksha Bay and Dvina Bay. The winter-convection is hence bound to the pycnocline with a relatively fast formation of ice caused by these strong stratifications, which trigger rapid decrease of water temperature reaching fast the freezing point.

The balance of freshness of the White Sea is always positive due to the constant supply of river runoffs enhanced by the precipitations. A comparison with the Baltic Sea for example shows a freshness layer of only 1.1 m thick, which is ~4 m in the White Sea. The White Sea has the freshest index compared to other Russian seas. Approximately half of the total river inflows (Duvanin, 1983) contributing to the formation of the surface layer of the White Sea come with the spring flood season (high water discharges in May-June only). The lowest river flow is estimated as 25% of its average and constant supply during the high peak season (Elshin and Yu, 1979). The river flow (including the 3 Bays adjacent to the Basin) remarkably varies seasonally: relative low flows in summer and winter, slightly enhanced in autumn (just prior freezing) and very strong in spring at the ice-melting period. During this season of greatly enhanced flow (May and early June), the White Sea receives 60-70% of its annual-averaged river flow. In comparison, the rivers of the Kandalaksha Bay (Savenko, 2001) show seasonally invariant water discharge distribution. Lakes and swamps in these regions decrease the river inflow during spring season but increase the river flow in Kandalaksha Bay in summer and autumn. This phenomenon is usually more evident through the years with a very high-flood anomaly. Also it is worth noting that in the Basin of the White Sea, there are freshwater systems with a special regulation regime, which relate to the operating hydraulic engineering constructions.

### 2.5.7. Interactions and hydrological signatures

The annual estimation (with an approximate error of 20-30%) of the transport of surface outflow compensated by the near seabed inflow of saline water in the Gorlo Strait (Timonov, 1950) is ~2200 $km^3$ and 2010 $km^3$ respectively. The difference of water transport is mainly caused by the river runoffs (+190 $km^3$ per year). Significant results (Duvanin, 1983) emphasized the fact that the above water mass transport alter considerably the water circulation of the White Sea. The results from these studies have revealed some important hydrological signatures of the White Sea, which mainly arise from the interactions of rivers and fresh waters with saline waters. These are reported as 7 hydrological signatures which are enounced below with a schematic representation shown in figure 2.10.

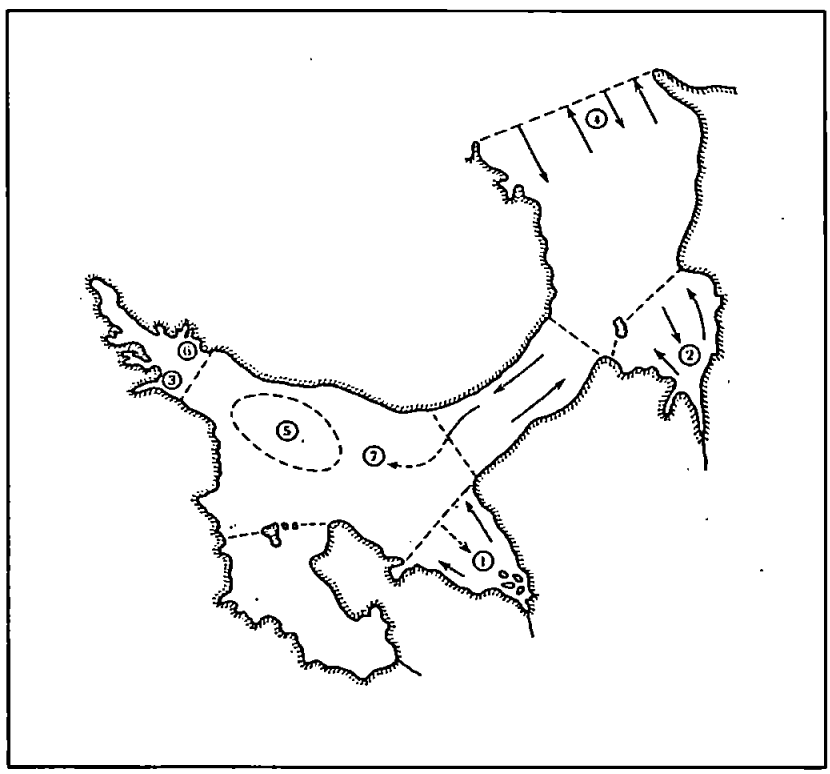

Figure 2.10: Schematic representation of the main hydrological signatures in the White Sea (Duvanin, 1983).

(1) The Dvina Bay is a perfect example of a big wide and moderate stratified estuary prevailed by horizontal circulation. Several oceanic features have shown the Dvina flow propagating along the Winter Coast. In some cases, a second flow of fresh water however less evident, was observed along the opposite coast (northeast) of the estuary.

Mass conservation and theoretical flow analysis suggest the existence of third flow of less fresh water in the centre of the Bay and propagating towards the estuary to compensate the two coastal currents. Observation of such circulation is well observed in summer and spring.

(2) The Mezen Bay represents a typical example a wide estuary entirely mixed vertically. The salinity field in the Bay is a good indication of the mixed water, and indicates a similar circulation as in Dvina, except that a saline current is well observed here in the centre of the Bay.

(3) Small region, such as Chupa located in the Kandalaksha Bay are associated to very narrow and partly mixed estuaries within a relative steady water circulation (Babkov, 1982). However these areas play an important role in the renewal mechanism of the intermediate water of the Basin. The flow circulation at the mouth of the estuary adjacent to the Basin involves some vertical mixing between the upper layers and the upper boundary layer of the intermediate water (50-to-100 m depth). An inferred contribution of the estuarine waters from the Kandalaksha Bay would represent 20-30% for the renewal of the intermediate layers of the Basin.

(4) A simple view of the water-exchange process occurring in the Gorlo Strait can be seen through the influence and the combined estuarine circulations. The zonal distribution of temperature and salinity in the White Sea as well as current measurements reveal the water-exchange driven by stream fluctuations.

(5) The variation of the freshness process, which can be interpreted as the variation of the thickness of the fresh water layer in the White Sea shows maximum values in the Basin region. However, considering the surface salinity distribution, the White Sea Bays appear with the lowest salinity. This contradiction is easily explained by the presence of river flow in the coastal areas. The Bays are therefore considered as transit areas. The Basin on the other hand represents the "stock area" where formation of fresh surface water (WSSW) takes place in thicker layers by comparison with the inner Bays.

(6) Observational data in the Umba river (see figure 3.2 in next chapter 3, for location) showed in winter a mixing zone between river and sea water, which scatters into a thin layer under the ice. This isolated layer considerably diminishes the winter vertical circulation. The winter convection depth in only 20 m in the late season, whereas it reaches a depth of 50-60 m elsewhere. As a result, the formation of a warm intermediate layer keeps developing during the winter season. Furthermore, this warm intermediate layer subsists during severe winter condition whereas for example in the Black Sea, a

cold intermediate layer develops in warmer overlying waters. It is an interesting hydrological phenomenon and a direct consequence of interlaying process between river and sea waters.

(7) These interlaying processes may define the water mass structure of the White Sea, although it has not been directly observed in the White Sea. However, the results showed that the formation of the surface, intermediate and deep waters of the White Sea are caused by mixing processes involving a complex combination of river, fresh waters and sea waters. The inferred process in the formation of water masses is that (i) the WSSW forms within the Basin area, (ii) that the WSIW goes into the deep part of the Basin as a source of saline (dense) water from the Gorlo Strait (GSW) in summer, and that (iii) the deep water of the White Sea is a result of intensive mixing with more saline water onto the Gorlo Strait in winter.

As a conclusion from these interactions, there is no sea water of salinity $\geq 31$ psu in the Basin and it cannot enter the White Sea either due to the water-exchange rate and the relatively strong tidal mixing in the Gorlo Strait.

The estimate of the deep water renewal of the White Sea based on the approximate calculations of Timonov (1950) is that within two years, the White Sea is renewed by 50% according to the water-exchange rate in the Gorlo Strait. Although it is fast for a water renewal process in semi-enclosed sea, complementary results from his study suggest that it happens since aeration of deep waters (deep oxygenated layers with oxygen content not lower than 70%) were observed in the White Sea. It has been also remarkable to observe that the origin of salt content in such layers differs notably from oceanic compounds. Hence, the balance and level of salt in the White Sea is controlled by the inflow of saline Barents Sea Water. The salinity rate in the White Sea is remarkably high-maintained in comparison with other semi-enclosed seas like the Baltic or the Black Seas. Timonov (1950) added that the exchange of water at the Strait with the Barents Sea control the salinity found in the deep layers.

### 2.5.8. Mixing processes

Several aspects of mixing are involved in the formation and distribution of water masses as reported by Timonov (1950) regarding the entire White Sea waters.

(i) The convective mixing is one of the first aspects. The winter convection takes place all around the White Sea except the west part of the Voronka region and Onega Bay.

Convective mixing does not play an important role in those areas because the water column there is entirely mixed all year round (no stratification occurs in summer and winter). On the other hand, in the Basin, Kandalaksha and Dvina Bays, and in particular marginal areas of the Basin, winter convection is important. Observations from Deryugin (1928) and later from Timonov (1950) confirmed the maximum winter-convection depth at ~50 m, which could be located deeper according to characteristic layers of turbulence.

(ii) The mixing induced by waves, during gales, drives vertical mixing reaching depth of maximum 15-20 m. It is well observed during the autumn period according to these strong gale-winds.

(iii) The mixing induced by tidal currents is clearly seen in the Gorlo Strait and in Voronka. In these areas, tidal currents produce intensive turbulent flows enhanced by the irregularities of the topography (narrow and shallow shelf, sill). In the western part of Voronka, the entire water column is vertically mixed throughout the year. The depth of mixing can be rather deep if strong-bottom currents circulate. In the Basin, the tidal currents are rather weak with episodic tidal mixing.

The role of wind-induced current for mixing in the Basin is also rather small due to strong stratifications set in the summer. The role of mixing from tidal condition however, can be seen in July-August by looking at the sea surface temperature gradient. Sharp sea fronts are observed between the area between the Basin and the Gorlo Strait. Bottom temperatures in the areas of intense mixing (such as in Gorlo) are anomalously high with an annual variability of ~10℃ observed in the bottom waters in comparison to those in the Basin. Two groups of regions in the White Sea can be distinguished by their hydrological structures: 1) Kandalaksha Bay, the Basin, Onega Bay and Voronka; 2) the Gorlo Strait and Dvina Bay. They are mostly dominated by stratification and mixing respectively. The mixing condition in Gorlo Strait is considerable as salinity drops by 4 psu at the bottom layers (salinity 25 at the surface and 29 in bottom waters). This variability has a direct impact on the marine biota, which subsist only in less saline water. Therefore rich oxygen and saline inflow from the Barents Sea represents the body to supply and maintain biological activity in the bottom waters of the White Sea. An intrusion of this saline body water has been referred by Deryugin (1928) while studying the distribution of phytoplankton. These biological tracers have indicated mixed-water inflows at deep and intermediate layers. During the period of October-November, Timonov (1950) reported in the centre part of the Basin, definite

observation of such intrusion in the 25-100 m layer was seen in a salt-finger shape. Possible intrusion of saline water in thicker layer was inferred by the author (Duvanin, 1983) shown in figure 2.10 (7). The author reported that this traced water mass and its thermohaline indexes should be similar to the Gorlo Water index.

### 2.5.9. Large-scale circulation and characteristics

The water circulation of the White Sea was first discussed by Deryugin (1928; see figure 2.11a) and later by Timonov (1947 and 1950; see figure 2.11b). The main factors governing the circulation are the fresh water inputs from rivers (as discussed earlier with surface residual outflow in the Gorlo Strait towards the Barents Sea). The latter contribute to the main observed cyclonic circulation in the Basin of the White Sea (Gidrometeorologiya, 1991a; see figure 2.11c). However, cyclonic and anticyclonic gyres exist in the Basin, generating local upwelling and downwelling of isothermals, referred to as the 'cold pole' and 'warm pole' by Deryugin, 1928 (figure 2.11a). Quasi-permanent flows were investigated using numerical models during the ice-free period (Gidrometeorologiya, 1991a). The results of the circulation scheme in the White Sea (figure 2.11b) are referred by Timonov (1950) in term of 4 flow-components that are:

(1)Thermohaline flows mainly formed by horizontal and vertical density distribution. It is assumed that these flows are mainly governed by large-scale atmospheric effects although it is known that tidal mixing dominates. (2)'Gradient currents' caused by sea level slope due to hydrological variation and water exchange with the Barents Sea. (3)Wind-driven and (4)tidal currents. Residual current as referred by Timonov (1950) are identified as excess of tidal streams.

According to the constant supply of fresh water inputs, the circulation of the upper layers, in the marginal areas of the Basin and near the White Sea Bays, is driven by a complex combination of baroclinic-barotropic currents, also involved within the atmospheric and horizontal gradient currents. Timonov (1950) also referred to the existence of vertical and horizontal surface circulation, based on observations. The dynamics of flow convergence and flow divergence exist which suggest downwelling motion near the coastal areas of Kandalaksha Bay and upwelling in the centre of the cyclonic gyre of the Basin. Ekman pumping was observed in the core of the cyclonic eddy of the Basin with intensive upwelling, enhanced by strong (quasi-permanent) wind.

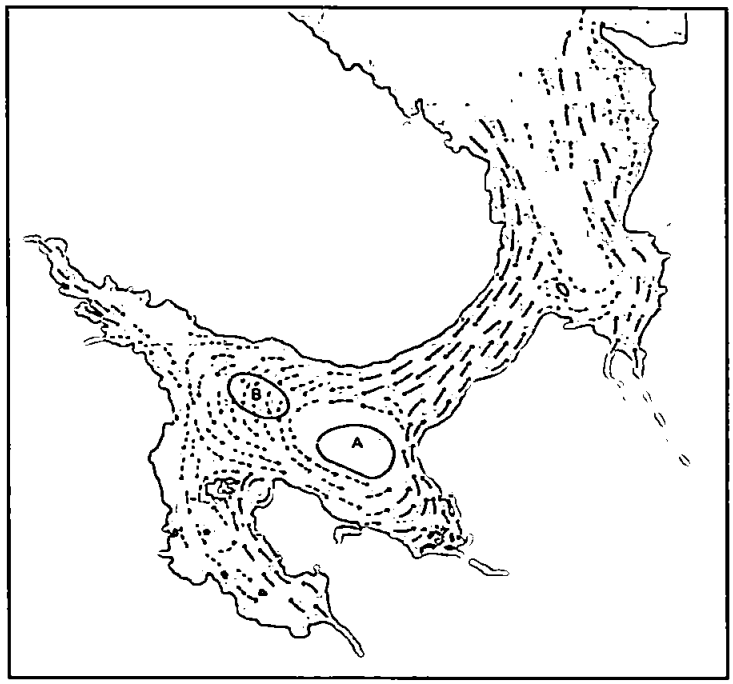


Figure 2.11a: Circulation scheme of the White Sea inferred (in dashed arrows) by Deryugin (1928). Dome-like elevation of isothermals was found in the hydrographic section in the outer region of Dvina Bay interpreted as a cyclonic vortex (A) and termed the 'cold pole'. Deryugin explained the deepening of the isothermals in the Basin (B), referred to as the 'warm pole' by the advection of warm waters from Gorlo to this region.

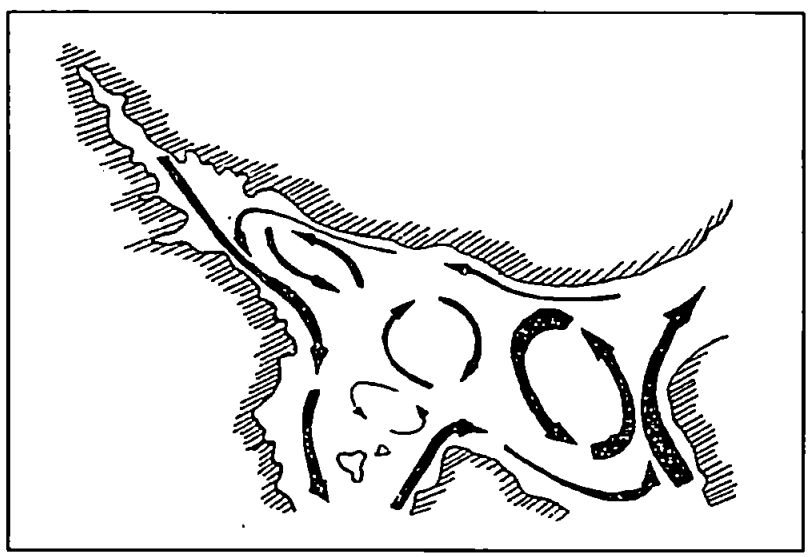

Figure 2.11b: Scheme of the surface circulation in the Basin of the White Sea (established by Timonov, 1947).

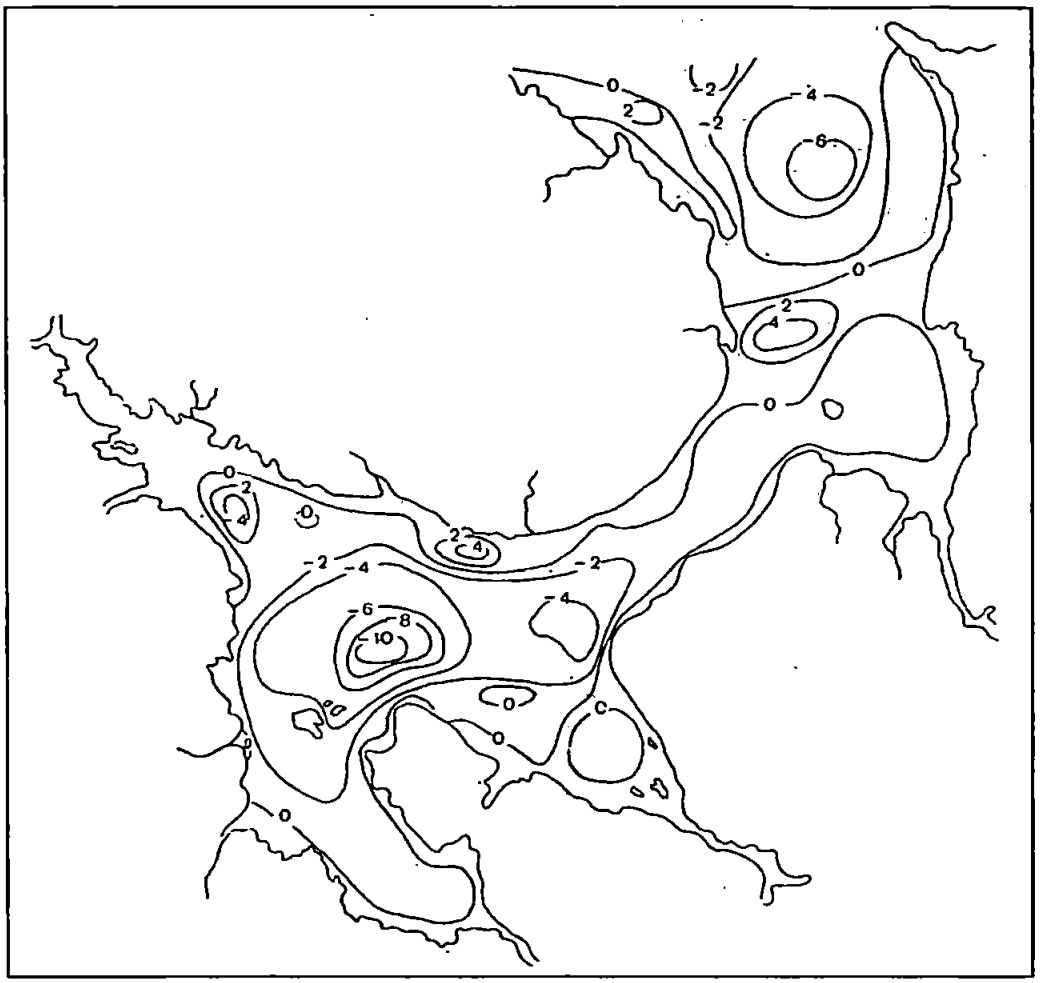


Figure 2.11c: Interannual average over 10 years of Sea Surface Height (cm) in the White Sea during ice-free period (Gidrometeorologiya, 1991a).

In conclusion, a simple view of the White Sea circulation is that the surface waters, considerably fresher than the intermediate layers, flush out of the White Sea into the Barents Sea due to constant and moderate river discharges in summer. The exchange of bottom waters with the Barents Sea, is however, much less frequent, depending again on the bottom turbulent flow in the shallow sill across the Gorlo Strait. Transport and advection of water masses, nearby estuaries, and from shelf to sea bottom, is poorly reviewed although previous works in the White Sea have shown that it is occurring in the northern part. Events of internal oscillations with tidal period are also of interest and might influence the formation and renewal of deep waters in the deepest part of the White Sea.

# Chapter 3: Observational programme and methodology

## 3.1. Introduction

The observational programme was designed to reveal a three-dimensional structure of the water masses in the northern part of the White Sea. The main emphasis was on small-scale thermohaline structure and on provision of a better understanding of the spatial extent of the identified water masses within their circulation during the ice-free period. The field phases were carried out from the 15$^{th}$ to the 23$^{rd}$ of June 2000, and from the 26$^{th}$ of May to the 3$^{rd}$ of June 2001. The following data were collected: temperature, salinity and density at more than 200 hydrographic stations. In addition, the satellite data of Sea Surface Temperature were obtained from Plymouth Marine Laboratory (PML, UK). The altimeter data were obtained from AVISO, which provides Sea Level Anomaly (SLA) products derived from the combined satellites TOPEX/POSEIDON and ERS1-2. The *in-situ* data were collected as part of the European projects (EU-INTAS-97-1881 and EU-INTAS-99-1600), which involved the Moscow State University and the P.P. Shirshov Institute of Oceanology. The oceanographic campaign of June 2000 was carried out on board *R/V Kartesh* (figure 3.1a,b); and the following year during May-June 2001, on board the research vessel Kuznetsov. The two oceanographic vessels were equipped with the same CTD SEACAT 19 profiler (shown in figure 3.1c) and GPS for the purposes of location.

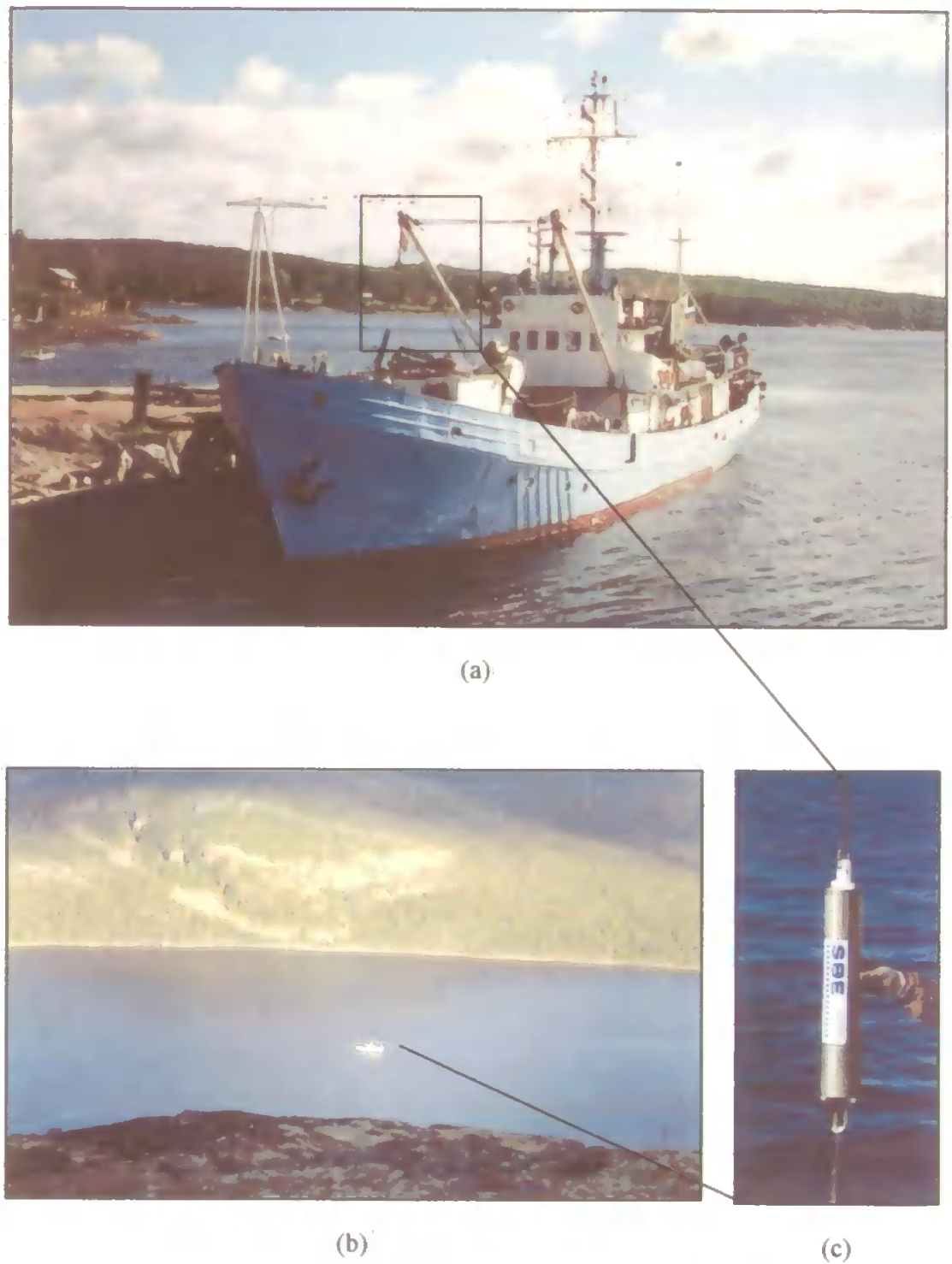


Figure 3.1: The *R/V Kartesh* (a) at the pier in the Chupa estuary (photo 14 June 2000), and (b) at a sampling station in Kandalaksha Bay (photo 20 June 2000) for CTD measurements (c) using a SBE SEACAT 19 profiler (photos courtesy: Prof. G. Shapiro).

## 3.2. Field sites and CTD measurements

### 3.2.1. Survey 2000

The aim of the hydrographic survey during summer 2000 was to study and identify the small-scale water structure and the inferred mixed layers (step-like structure) in the northern part of the White Sea, as well as to provide an insight of the spatial extent of these mixed layers. A particular interest focuses on the western region of the Gorlo Strait where formation of water masses occurs due to strong mixing. Therefore, a dense grid-coverage of stations was made in this area near Gorlo for investigating the small-scale mixing process (figure 3.2a), which has an important aspect in the relation to the formation of the complex structure of water masses in the White Sea. The physical measurements in that area near Gorlo and along the Terskii coast were done to investigate the presence of descending water (cascading events) as inferred by Timonov (1947 and 1950) and reported by Duvanin (1983). The water-exchange process occurring along the Gorlo Strait is a possibility for generating shelf-edge dense water, which may protrude down along the slope of the Basin of the White Sea. The grid-coverage near Gorlo is represented by 50 (n°17-66) hydrographic stations with a typical distance of about 5 km between the stations (see figure 3.2a). On the other side of the sea, the western study area was located in the shallow (40-60 m) Kandalaksha Bay and consisted of 40 (n°85-124) stations (see figure 3.2b). A sequence of cross transects in the Bay was placed to study a front generated from river waters and the offshore Basin waters, with few more stations along the estuaries and rivers. Between these areas (in the Basin), there were two extended sections along the Terskii Coast (Transects E2 and C, in figure 3.2b) and 8 shorter cross-shore sections (Transects G1-6 and C4-5, in figure 3.2b), providing another 62 stations (n°1-16/67-84/125-153). Hydrographic transects in the Basin were to investigate the water properties of other possible descent of waters or of advected waters along the Terskii shore (Transects F1-3; figure 3.2) coming from the Gorlo Strait. The oceanographic campaign was carried out between the 15th and the 23rd of June 2000 on board *R/V Kartesh* (see table information 'White Sea cruise 2000' in appendix A). This table shows the GPS coordinates of each station, with the time of the CTD deployments and records of water properties and maximum depth. During this cruise 2000, a total number of CTD stations represented 153 physical measurements recorded at a ~50 cm vertical resolution.

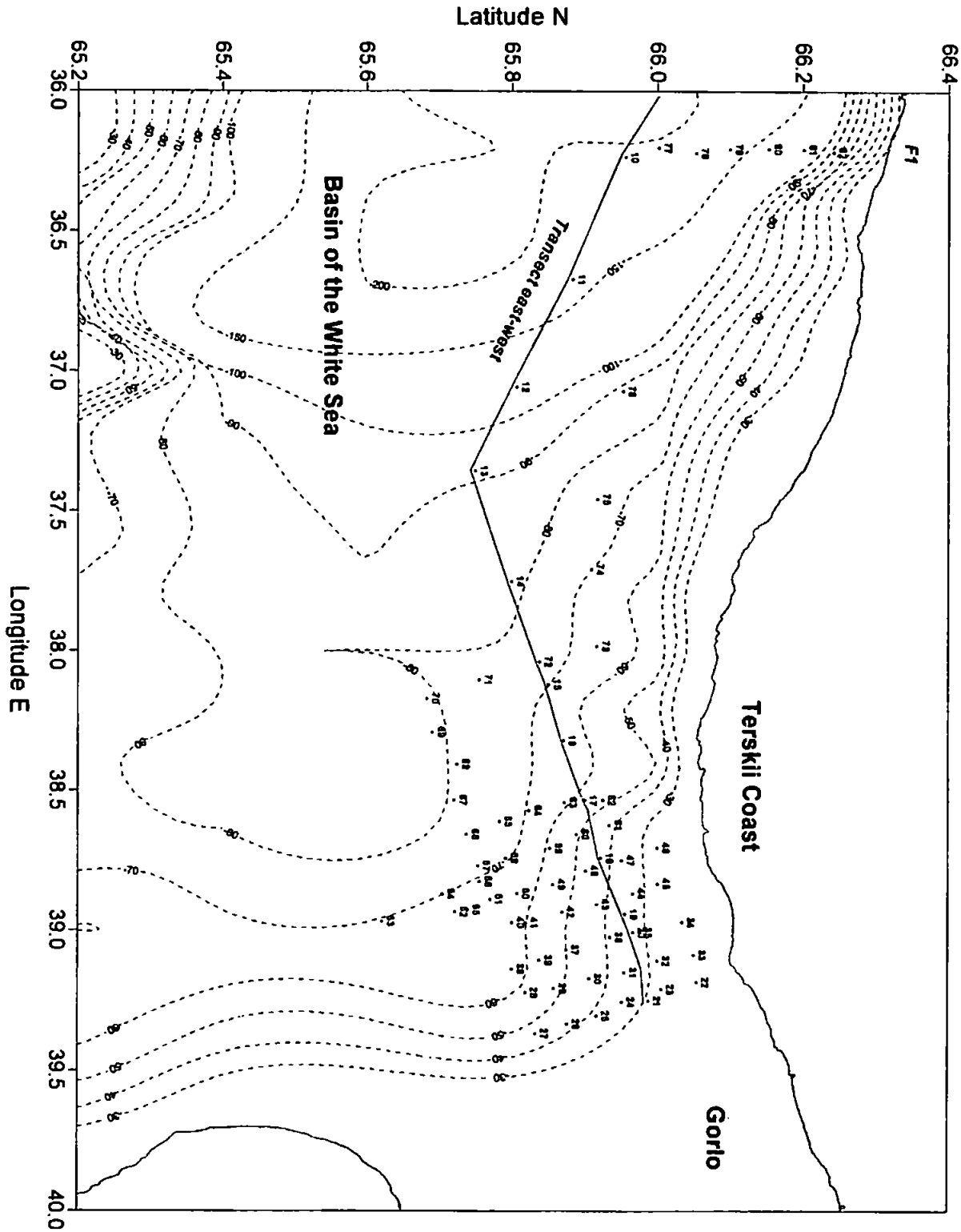


Figure 3.2a: Map survey 2000 in the northern part of the White Sea; west of Gorlo and adjacent to the Basin along the Terskii Coast. CTD stations are represented in blue (dots) with superimposed isobaths (m)

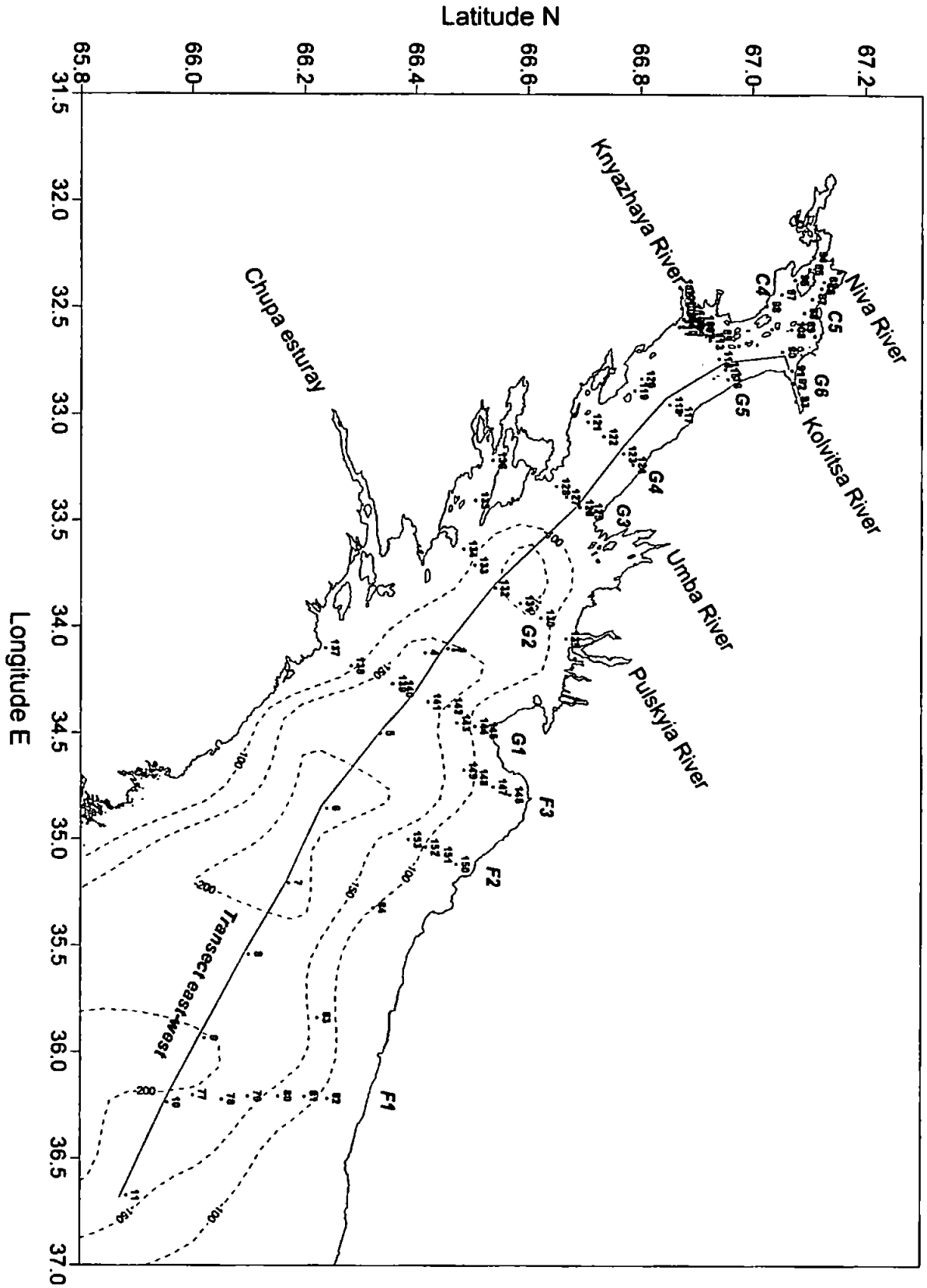


Figure 3.2b: Map survey 2000 of the northern part of the White Sea, in Kandalaksha Bay and adjacent to the Basin. CTD stations are represented in blue (dots) with superimposed isobaths (m).

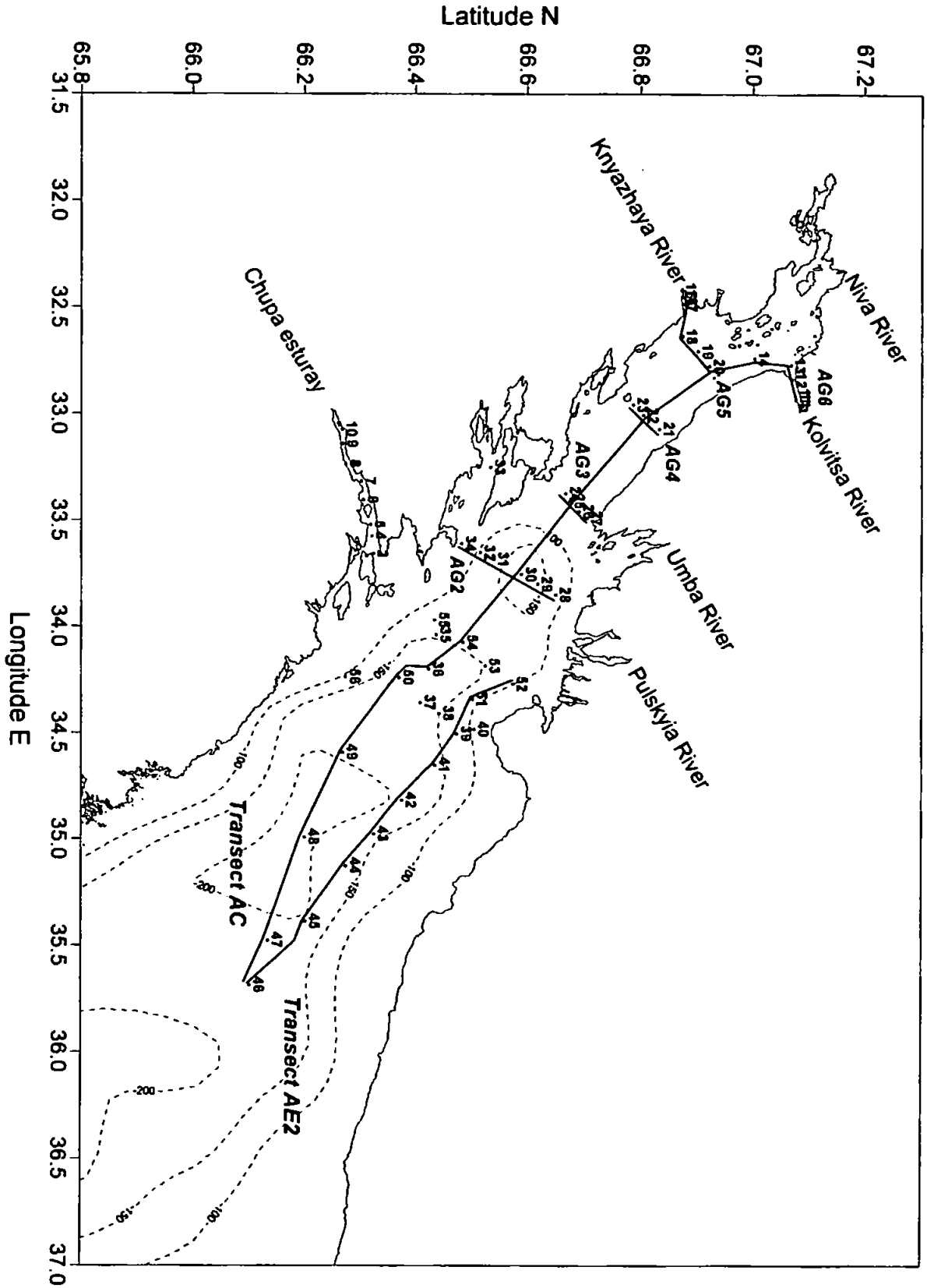


Figure 3.3: Location of CTD stations during survey 2001 in the Kandalaksha Bay and adjacent to the Basin of the White Sea, with superimposed isobaths (m). Transects AC and AE2 are sections used to compare hydrographical features with transects C and E2 from the survey 2000.

### 3.2.2. Survey 2001

Another oceanographic survey following the winter period 2000 was conducted in spring 2001 also on behalf of the INTAS-1881 project, on the research vessel Kuznetsov, equipped with the same CTD profiler as the previous summer cruise. The hydrographic measurements were made from the 26 of May 2001 to the 3rd of June 2001 (see table information 'White Sea cruise 2001' in appendix A). The cruise carried out 56 CTD measurements in Kandalaksha Bay and in the Basin. The CTD stations were intended to be at the same positions as those in summer 2000. The location of the CTD stations of cruise 'spring 2001' are shown in figure 3.3 with the corresponding hydrographic transects (Transect AG1-6; AC and AE2) to provide an inter-seasonal analysis of the water masses in Kandalaksha Bay and in the Basin of the White Sea.

## 3.3. CTD data processing

Preliminary CTD profiles on board the *Kartesh* showed the presence of step-like structures in the vertical distribution of temperature and salinity. In order to analyse mesoscale and specifically finer scale thermohaline structure, the CTD profiles must have a reasonable vertical resolution to carry on identifying such fine structure of thin mixed layers. Therefore, both the down-casts and up-casts of the CTD profiles, obtained during the both campaign (2000 and 2001) in the White Sea, were investigated to trace the vertical fine-scale structure of these mixed layers.

Normally a standard method for post-processing CTD data uses a bin-averaging scheme to reduce the instrumental noise; and this often results in the loss of very fine structure by over-smoothing the vertical step-like profiles. Furthermore, the use of a light-averaging scheme results in a large number of artificial steps not seen in the raw-data temperature. The source of artificial steps in the temperature profile is due to the fact that the vertical resolution of the pressure gauge is not equivalent to the high resolution of temperature sensors. In order to enhance the vertical resolution of the temperature and the salinity profiles without generating artificial steps, the pressure gauge must follow a correction procedure used by Frolov and Shapiro (1982). This approach in post-processing the CTD data is described in details in the following sections (see figure 3.4) within the standard procedure applied to the Sea-Bird-Electronic modules (SBE, 2000).

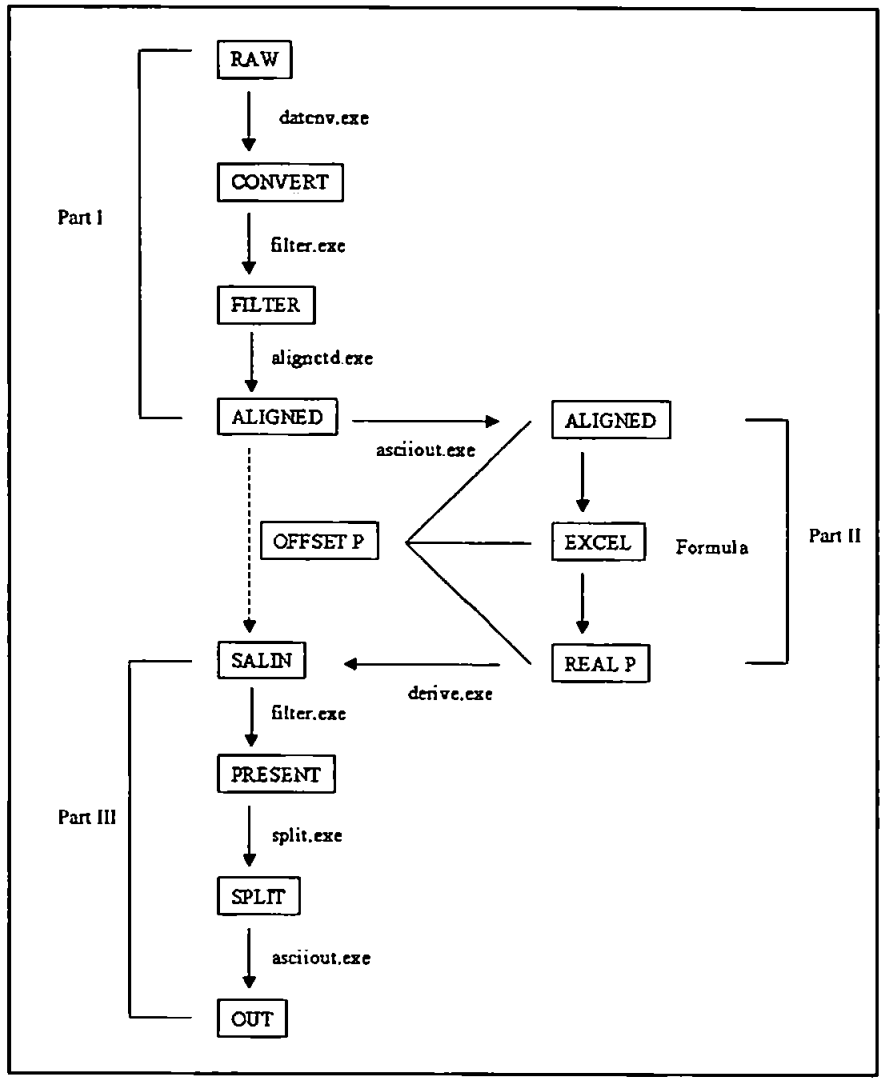


Figure 3.4: New approach scheme showing the three main parts for processing CTD data within the sequence of conventional applied SBE modules (.exe files; SBE, 2000). Part I: Corrections made to improve the resolution of vertical profiles (Frolov and Shapiro, 1982). Part II: Corrections applied to derive the 'real' pressure. Part III: Deriving and extracting high vertical-resolution CTD data.

The method of Frolov and Shapiro (1982) treats the pressure channel separately from conductivity and temperature channels. It is based on the fact that during the deployment of the CTD profiler by a motorised winch, the dependence of pressure upon time is much smoother than that of temperature and conductivity.

The speed for CTD sampling (down and up casts) was about 0.4 m/s (~5 samplings per metre) in deep stations (> 90 m) and slower with 0.2 m/s (~10 samplings per metre) in shallow stations (< 50 m) in order to get detailed structure of the upper active layers of the northern White Sea.

### 3.3.1. Sea-Bird Electronic module software

A number of conversion programs from SBE modules used the instrument configuration and calibration coefficients to create a converted engineering unit data file (.cnv). A configuration file called sea.con also stored in RAW, was generated using the module seacon.exe loading the instrument configuration. The pressure sensor was a strain gauge with the number of Ext volt sampled set to standard value (0). The number of 0.5 sec. intervals between samples is set to 1, given frequency 0 for temperature, frequency 1 for conductivity and pressure voltage. The SBE modules were operating on data files (.cnv) adding information to the header of the converted files. The header file records what module was applied on the data columns. The final converted data files included scan-numbers, temperature, conductivity, 'real' pressure, salinity and density, stored in the final directory called OUT, at the end of the technical procedure (figure 3.4). To get a high-quality CTD data, three major steps are considered for data processing.

**Part I: data filtering and aligning**

Firstly, it is important to take into account upcast and downcast measurements in order to establish the credibility of the observed fine structures in the vertical profiles along with readjusting the pressure component (figure 3.5a). Therefore, this part consists of re-adjusting the three oceanographic parameters (temperature, conductivity and pressure) before deriving the others (salinity, density, etc...). The SBE module datcnv.exe converts the raw-data in ASCII format (using the configuration file sea.con) providing columns of oceanographic parameters that are scan-numbers, temperature, conductivity and pressure; stored in folder CONVERT. Then, the module filter.exe applies a low pass filter to the data-columns, which forces the conductivity to have the same response as the temperature. In order to produce a zero phase (no time shift) the filter is first run forwards then backwards (all through the data-column including upcast and downcast measurements). Therefore a low pass filter of 1 sec. and 4 sec. is applied on conductivity and on pressure respectively (figures 3.5bcd). Then the module alignctd.exe aligns temperature, conductivity and pressure from the .cnv files and stored in the directory ALIGNED. Temperature and conductivity are aligned in time relative to pressure. This ensures that the calculations of salinity and density (as other oceanographic parameters) are made using measurements from the same parcel of water. In this case, an advance temperature relative to pressure is set to 0.5 sec.

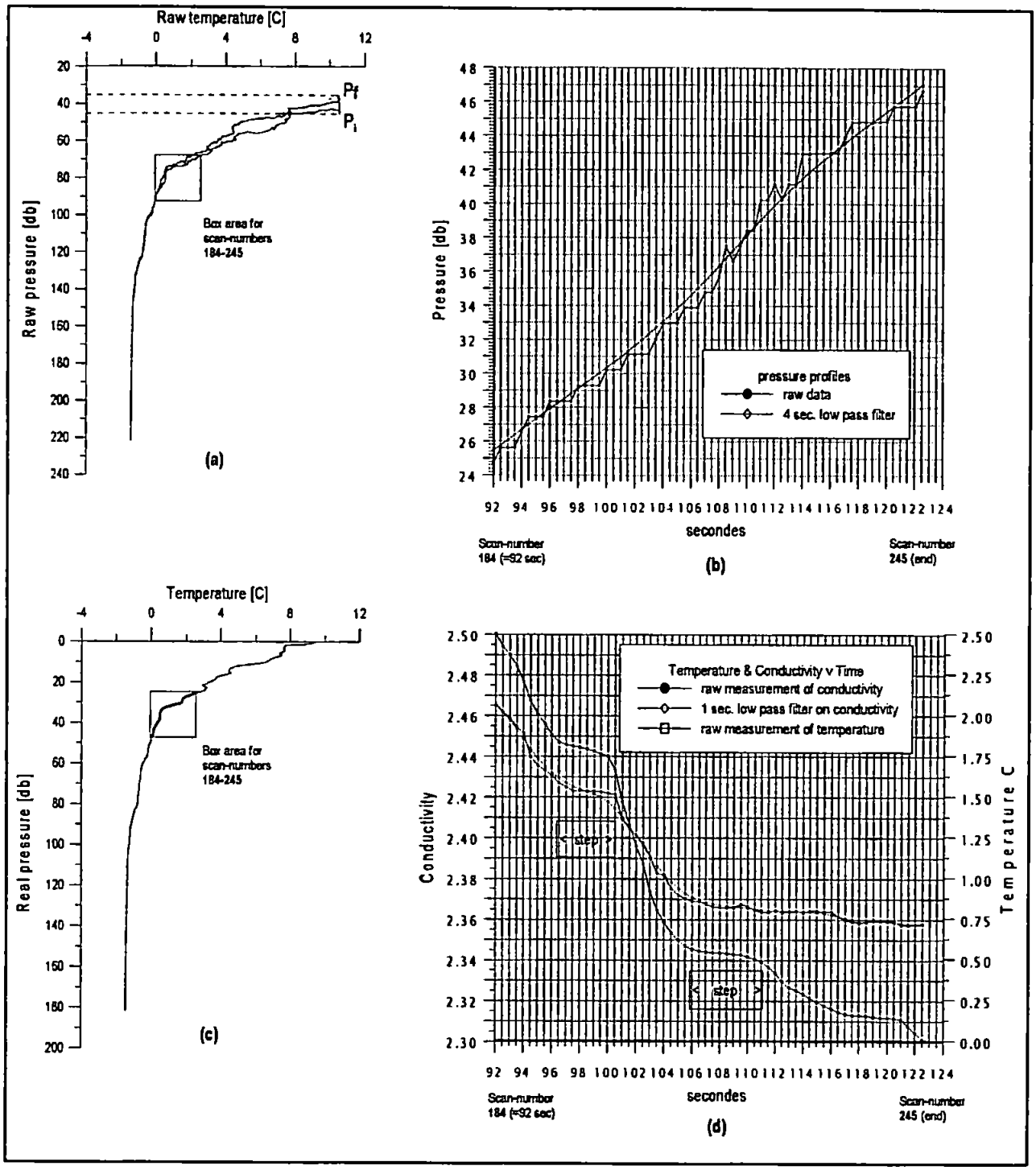


Figure 3.5: (a) Raw temperature against raw pressure measured at station 131 in Kandalaksha Bay, which shows the initial and final measured pressures ($P_i$ and $P_f > 0$). (b) The top enlarged picture shows the corresponding data of pressure from the box-section of (a) versus time-recordings. This shows the need to filter the pressure to remove artificial steps. (c) Same temperature profile as (a) with filtered and corrected pressure ('real pressure'). (d) The bottom enlarged picture of box-section (c), indicates two steps revealed in the raw temperature data, and in the corresponding conductivity data, which is also filtered to avoid artificial steps.

The reason for misalignments can be for inherent time delays (time constant) of sensor responses. It is known that measurements through depth with conductivity cells are recorded faster than temperature sensors made out of thick wires resulting in a time delay for the wire to warm up or to cool down.

**Part II: re-adjusting pressure**

The second part consists of re-calculating the pressure recorded during the downcast and upcast caused by the varying offset pressure. This is very important for the quality of the oceanographic data derived from the actual measured pressure. The pressure data show two positive different offset values at the sea surface level (figure 3.5a) before downcast and after upcast. This is due to the strain gauge device being stressed by the ambient forcing pressure, which has greater influence near the sea-bottom, showing in pressure profiles an increased pressure-bias from seabed up to surface. Therefore, it is thought appropriate to correct the measured pressure $P_m$ by deriving a 'real pressure' $P_r$ using the formula given below in equation (3.1), which minimises the pressure-bias variable $P_{offset}$, see equation (3.2), and set the initial and final offset pressure, respectively $P_i$ and $P_f$, to zero (the sea surface level).

$$P_r = P_m - P_{offset} \qquad (3.1)$$

$$P_{offset} = P_i + \frac{(P_f - P_i)}{n} \times n_i \qquad (3.2)$$

The variable n is the total number of scans (or records), and $n_i$ represents the $i^{th}$ scan-number. Once the data being processed and the headers of the data-files removed (using asciiout.exe), the real-pressure is calculated using EXCEL and stored in the directory REALP. However, the profile analysis of the 'new' pressure, for various few neighbouring stations, were made for the reliability of the data within the sight of any pressure differences observed between upcast and downcast. This indicates the quality of measurements done at stations where reasonable matches in pressure were observed, although measurements were done sometimes when the boat was drifting.

**Part III: data smoothing and extracting**

Finally, the third step in the data processing is that of smoothing the data before accessing them in the ASCII format. The module derive.exe (figure 3.4) reads the .cnv files and calculate the derived variables (following the international standard procedures for seawater: UNESCO, 1981), which are salinity (in practical scale unit: psu) and density $\sigma_t$ (kg/m$^3$) stored in the directory SALIN. A low pass filter is run on the salinity data using filter.exe to remove the background noise with a time constant set to 1.5 sec. (stored in directory PRESENT). Now that the data have been correctly processed with a quality control, the module split.exe split the upcast and downcast separately (folder SPLIT). Finally asciiout.exe allows once more accessing the files in a data format by removing the bad-flag numbers and the headers of the files.

In conclusion, this new approach of processing and profiling the CTD data allows detection of step-like profiles with a confidence level of ~1 m in the vertical resolution. However, for the sake of reliability of the analysis, only fine structures with a thickness of $\geq$ 2 m are treated.

## 3.4. Calculation of the horizontal distribution of parameters

To generate contours of horizontal distribution of temperature, salinity and density, a MATLAB program (see depthsection.m in appendix A) was first created to gather hydrographic data at selected stations in the northern White Sea. The generated output files include station coordinates and oceanic parameters, which are bin-averaged at 1m depth following a second MATLAB program (see interpol.m in appendix A) which uses a cubic spline interpolation for bin-averaging. Therefore, a data set of horizontal distribution of parameters is derived to analyse the extent and structure of the water masses in the surface layers, in the intermediate layers, and in the deeper layers. For example, the contours of temperature near the surface at about 5 m depth are compared with the SST images which were taken during the hydrographic survey 2000, hence providing an estimate circulation of the White Surface waters, also complemented by the calculation of its dynamic height.

## 3.5. Dynamic height

The dynamic height refers to the pressure associated with a column of water and is a useful geo-potential quantity to compare and validate Sea Level Anomalies (SLA) derived from the observation of satellite altimeters. The dynamic height (due to horizontal variations in temperature and salinity) is generated in the northern part of the White Sea to investigate the dynamic topography and its corresponding geostrophic circulation. The dynamic height (measured in dynamic metres: dyn) is given below in equation (3.3):

$$D(p_1, p_2) = \int_{p_1}^{p_2} \delta(T, S, p) dp \qquad (3.3)$$

where $p_1$ and $p_2$ are the two reference-levels of pressure, $\delta$ the specific volume anomaly, $T$ the temperature, $S$ the salinity, and $p$ the pressure. A dynamic metre represents the work done when a unit mass is displaced vertically for a distance of 1 metre, and is defined as 105 dyn-cm/gm or 10 J/kg. The bin-averaged output data from the interpol.m program are re-used to derive the dynamic height, which is calculated by using a third MATLAB program dyntopo.m shown in appendix A. For this calculation, the upper reference-level of pressure is 5 m and the lower reference-level is 100 m, which is considered as an average-depth for the lower boundary of the most active dynamic layers of the White Sea, and which also include the maximum of hydrographic stations for the study area.

## 3.6. Collection and processing of remote sensed data

### 3.6.1. Sea Surface Temperature images

The satellite images of Sea Surface Temperature (SST) were derived from AVHRR sensors and have been acquired from the Plymouth Marine Laboratory (PML). The available SST images during summer 2000 to be used to an estimate circulation of the White Sea (Chapter 7) are shown below in table 3.I. The observed mesoscale oceanic features will be complemented by the Sea Level Anomaly maps derived from the satellite altimeters.

| PML Remote Sensing Group | Dates of available SST images | | | | | | | | | |
|---|---|---|---|---|---|---|---|---|---|---|
| June 2000 | | | | 21 | 23 | 25 | 26 | 28 | 29 | 30 |
| July 2000 | 3 | 4 | 7 | 14 | 15 | 16 | 17 | 19 | 20 | 28 |

Table 3.I: Dates of available SST images used to investigate an estimate mesoscale circulation of the White Sea during summer 2000.

### 3.6.2. SLA products

The altimeter signal is a good oceanographic tool to look at the mesoscale activities in the open ocean. Recent works have shown that the use of combining two satellite altimeters, particularly TOPEX/POSEIDON and ERS1 flying during the same mission, improved the resolution of the time/space windows (Le Traon and Ogor, 1998; Latché, 1999). It therefore provides a comprehensive analysis for the formation and the circulation of mesoscale eddies (e.g. the observation of eddy-filament system by Barton *et al.*, 2000). Different validation gridding techniques are used to generate maps of SLA, which consist of combining altimeter data from different satellite flying simultaneously. This approach enables to generate more precise maps of SLA in terms of spatial and temporal coverage (Latché, 1999). The CLS Space Oceanography Division and the AVISO/Altimetry operations centre have recently produced a dataset (on CD-ROMs), which contains already gridded altimeter data products derived from combining satellites. This programme was part of the European Union' Environment and Climate project AGORA (ENV4-CT95601 13) and DUACS (ENV4-CT96-0357) with financial support from the CEO programme (Centre for Earth Observation) and Midi-Pyrénées regional council (France).

The SLA Processing starts with quality control and validation of the altimetric data and geophysical corrections (Le Traon *et al*, 1995). The altimeter measurement has to be corrected for instrumental errors, environmental perturbations (wet tropospheric, dry tropospheric and ionospheric effects), ocean wave influence (sea state bias), influence (ocean tide, Earth tide and pole tide) and inverse barometer effect. The most recently updated version of the Geophysical Data Records (GDR) software, the improved orbits (Le Traon and Ogor, 1998), the latest state of the art models and the homogeneous corrections are used (CSR3.0 tidal model, dry tropospheric and inverse barometer corrections).

Maps of Sea Level Anomalies (MSLA) are obtained using an improved space/time objective analysis method (Le Traon *et al.*, 1998) which takes into account long wavelength errors (i.e. correlated noise). The variance of the altimetric signal (and thus signal/noise ratio), which states its reliability to the SLA signal, depends on its geographical position. For each grid point, the data inside a time window of +/- 10 days is used for the satellite TOPEX/POSEIDON and a time window of +/- 18 days is used for the satellite ERS.

The SLA products are thus available every 10 days with a 0.25° x 0.25° grid resolution. They contain both the Sea Level Anomaly signal (in millimetres) and its error (as a percentage of the variance of the altimetric signal). An example of the variance of the altimetric signal (in % error) in the White Sea region is shown in figure 3.6 below.

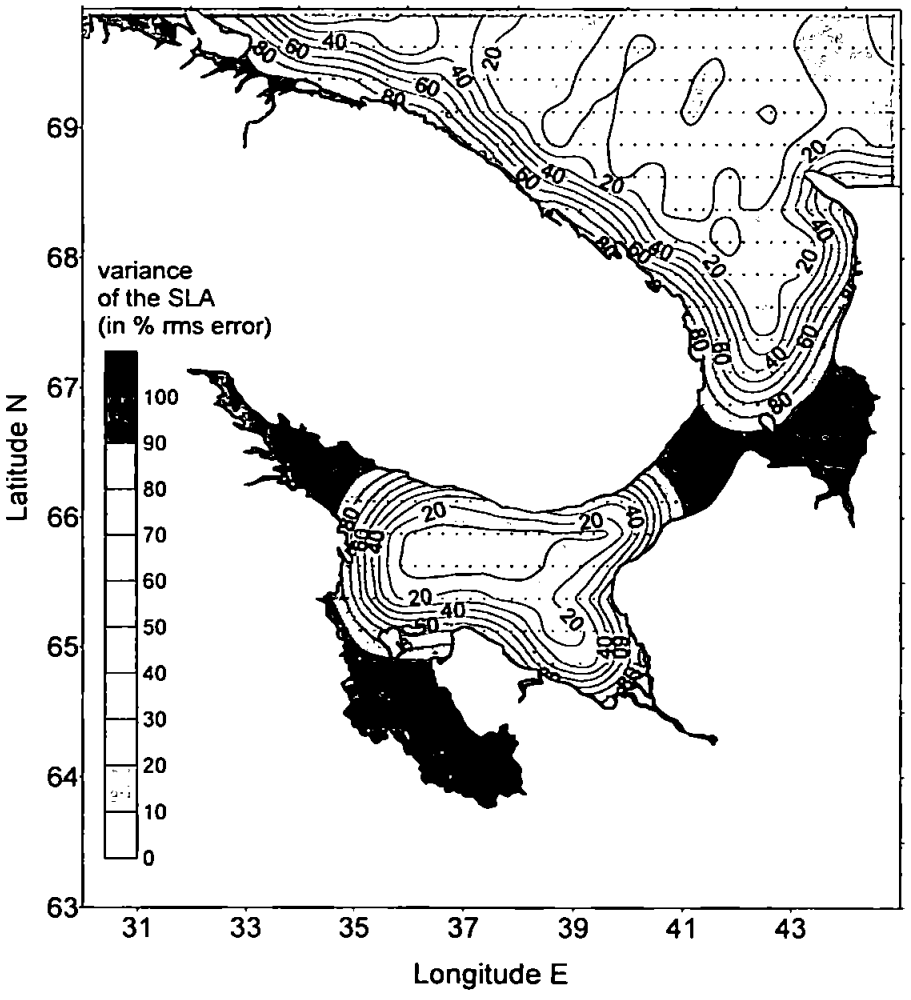


Figure 3.6: Contours of the variance of the altimetric signal (in % rms error) in the White Sea region superimposed with the grid coverage of the SLA data (0.25°x0.25°) derived for SLA data of June-July 2000.

### 3.6.3. Processing SLA data and calculating geostrophic surface velocity

The MSLA products (AVISO CDROMs) are organized under directories labelled TE_jjjjj.GZ, where jjjjj is the file date in days relative to 01 January 1950 (e.g. day 15635 = date October 22, 1992). One file represents one MSLA data (e.g.: the file named '15625' is the MSLA for 12 October 1992, which is followed by the file '15635': the MSLA data for 22 October 1992, etc ...). The data files are in ASCII format and gzip-compressed. The MSLA files are extracted for the White Sea region with a FORTRAN program readmsla.for (in appendix A). The data were flagged to 9999 and none reliable altimetric signal set to 100% variance error (e.g. lands, or near the coastlines and around islands).

Contours of SLA are made using the graphics software SURFER, which uses the Kriging method for contouring technique. The latter is a default method, which generates the best overall interpretation of most data-set, specifically with already gridded data.

A second program in FORTRAN (see Latché, 1999, appendix 3: eke.for) calculates the geostrophic velocity based on the extracted SLA data (MSLA). The coordinates of the geostrophic velocity are derived at the centre of each single square formed by the grid coverage of the individual squares formed by the SLA data. The magnitude and direction of the calculated velocity (symbolised by arrows) are superimposed on the SLA maps to provide a better scheme of the White Sea surface circulation. The SLA map is compared with the dynamic height (derived from the hydrographic survey 2000) to validate the observed mesoscale circulation.

## 3.7. Discussion

The CTD data processing technique introduced here focused on improving the vertical resolution of the profiles. This technique enables us the identification of vertical steps in the profiles with a confident level of about 1metre by looking at the down-cast and up-cast; although it is safer to analyse fine-mixed layers of $\geq 2$ metres thick. The accuracy within the vertical scale, in detecting the fine-mixed layers (vertical steps) in the CTD profiles, directly relies on the quality of re-adjusting the pressure obtained from the raw recorded measurements. The recorded measurements from the probe always indicated constant positive values of pressure at the beginning and end of each CTD cast, as indicated in figure 3.5a. Standard procedure recommends filtering the pressure, as it is

the case here (see figure 3.5b), to smooth and avoid artificial steps in the vertical profiles. Any slight error in the pressure, caused by the pressure-bias in the sensor might not be seen in the profile. Therefore this technique shows the importance of treating the raw pressure measured during down-cast followed by up-cast in order to subtract the so-called offset pressure, which includes the pressure-bias, illustrated in equations (3.1) and (3.2). Figure 3.5c shows the improvement in the pressure reading, therefore the depth of a water mass at a specific temperature or salinity can be read accurately, which is of importance for identifying the thermohaline properties of the fine-mixed layers and their vertical displacement in the water column.

The horizontal distribution of the mixed-layer was analysed by looking at the contours of horizontal temperature and salinity field at specific depths in the water column. The data at each CTD station were bin-averaged every metre using a cubic-spline interpolation. This interpolation technique is very convenient to derive the parameters such as temperature or salinity at every metre depth, but it may also derive values that are slightly different from what it should be at a metre depth in reality. However, this is unlikely to be the case here since the CTD measurements in this region of the White Sea are relatively dense within every metre. Most of the shallow CTD stations, presenting a maximum depth of < 60 m, show approximately 10 scans (recorded data) per metre, due to the unusual very low speed deployment of the probe. Therefore, errors within contours of temperature or salinity at a specific depth are relatively minor.

Contours of Sea Level Anomaly, however, need to be analysed with caution. The SLA data were already gridded when obtained from an improved space/time objective analysis method (LeTraon *et al.*, 1998), using altimetry data points averaged every 7 km along the ground-pass satellite. The errors within the gridded altimetry data product are revealed by the variance, as a percentage, of the altimetric signal. Therefore, when analysing the SLA map, it is important to remember the study regions that have errors in the variance of the altimetric signal of less than 20-30%. Contours of that percentage and less suggest reasonable data, which can be used for investigating an estimate circulation of the White Sea during summer (June-July) 2000 (see figure 3.6).

# Chapter 4: Fine thermohaline structures in the White Sea

## 4.1. Introduction

The characteristics of water masses in the White Sea are necessary to define the water mass transport, the hydrophysical processes or eco-biochemical cycles, which have been studied only recently (Yakushev and Mikhailovsky, 1993 and 1994; Korneeva and Luneva, 1999; Savinov *et al.*, 2000). The existence of a complex water mass structure in the White Sea has been long documented by Deryugin 1928; Timonov 1947 and 1950, Pantiulin 1974, Sukhovey 1986; Gidrometeorologiya, 1991; Howland *et al.* 1999). For instance, the most complex interaction of water masses occurs in the north-eastern part of the White Sea (Timonov, 1950; Gidrometeorologiya, 1991), specifically in the Gorlo Strait where strong tides contribute to the formation of mixed water masses. Despite such studies, it is clear that the details of the distribution and the circulation of complex water mass structure within the White Sea remain under researched (compared to many other semi-enclosed seas) mainly due to the lack of extensive high resolution measurements in the key areas of the semi-enclosed sea. Recent studies on the White Sea (on board *Kartesh* in June 2000*) show some preliminary evidence of fine step-like structures (Stommel and Fedorov, 1967; Cregg and Sanford, 1980) within water masses. But hitherto, no-one has been able to provide a detailed analysis of such structures during ice-free seasons. A detailed analysis which defines characteristics of water masses including step-like structures would be necessary to explain the physical processes which may affect the circulation or the eco-biochemical cycles within the White Sea. It is important to trace such fine step-like structures to see how they are distributed in the northern part of the White Sea and to relate them with the origin of their formation. It is likely that the Gorlo Strait represents the main mechanism to generate saline mixed waters which contributes strongly to the balance of the salinity ratio in the White Sea.

* The data shown in this study arise from the research cruise on board *R/V Kartesh*. I am grateful to Prof. G.I. Shapiro and Dr. A. Pantiulin who kindly collected the data.

An innovative presentation, in 3-D, of the water structure of the north-eastern part of the White Sea is given here in this chapter. This provides a conceptual model for the dynamics of the White Sea. It includes horizontal sections of temperature and salinity distribution (surface, intermediate and deep layers) and vertical profiles. The detailed temperature and salinity analysis provides characteristics of each water masse within step-like structures to reveal the key-elements of the dynamics of the White Sea in the regions: west of the Gorlo Strait, off the Terskii Coast, the Basin and in Kandalaksha Bay. The water masses in contact consist of 8 identified bodies known as (1) the Voronka Water, (2) the Barents Sea Water, (3) the Gorlo Strait Water, (4) the White Sea Surface Water of the Basin, (5) the White Sea Intermediate Water, (6) the White Sea Deep Water, (7) the White Sea Bays Fresh Waters, and finally (8) the River Waters. The Voronka Waters and the river Waters are well observed during spring seasons due to strong river discharges; however they are considered absent in summer and autumn due to mixing and less river runoff.

This chapter uses some material published in Lukashin *et al*, 2003, Oceanology, 43(2): 224-239. The candidate was the last author in this publication, which describes a large multidisciplinary study in the White Sea.

## 4.2. Structures of water masses

Vertical profiles at four selected stations in the eastern part (north coast and south of Gorlo) in the Basin and in Kandalaksha Bay are presented in figure 4.1. At station 21 (figure 4.1a), west of the Gorlo Strait, the water column is uniformly well mixed from 5-to-50 m, with the characteristic of 1.7°C and 27.1 psu. A very shallow and sharp thermocline occupies the surface separating warm (6°C) and fresh (25.4 psu) surface water from the mixed water. South of this station towards Dvina, the vertical profile of station 51 (figure 4.1b) presents a complex stepped structure with inversions. A very thin step near the surface (identified as step A, figure 4.1) is observed within the thermocline, and other step-like structures underneath are evident (step B and C). Above the thermocline, surface temperatures reach a maximum of 6.5°C and a corresponding surface salinity of 25.2 psu. Below the thermocline, between 20-65 m depth, the temperature is observed to be 0°C with a salinity range of 27 to 28 psu. In this profile, we note a similar thermohaline index from the thin quasi-homogeneous layer at 15 m (1.2°C; 27.2 psu) and the vertically mixed water from the north station 21 (1.7°C; 27.2 psu) although with a temperature variation of half a degree.

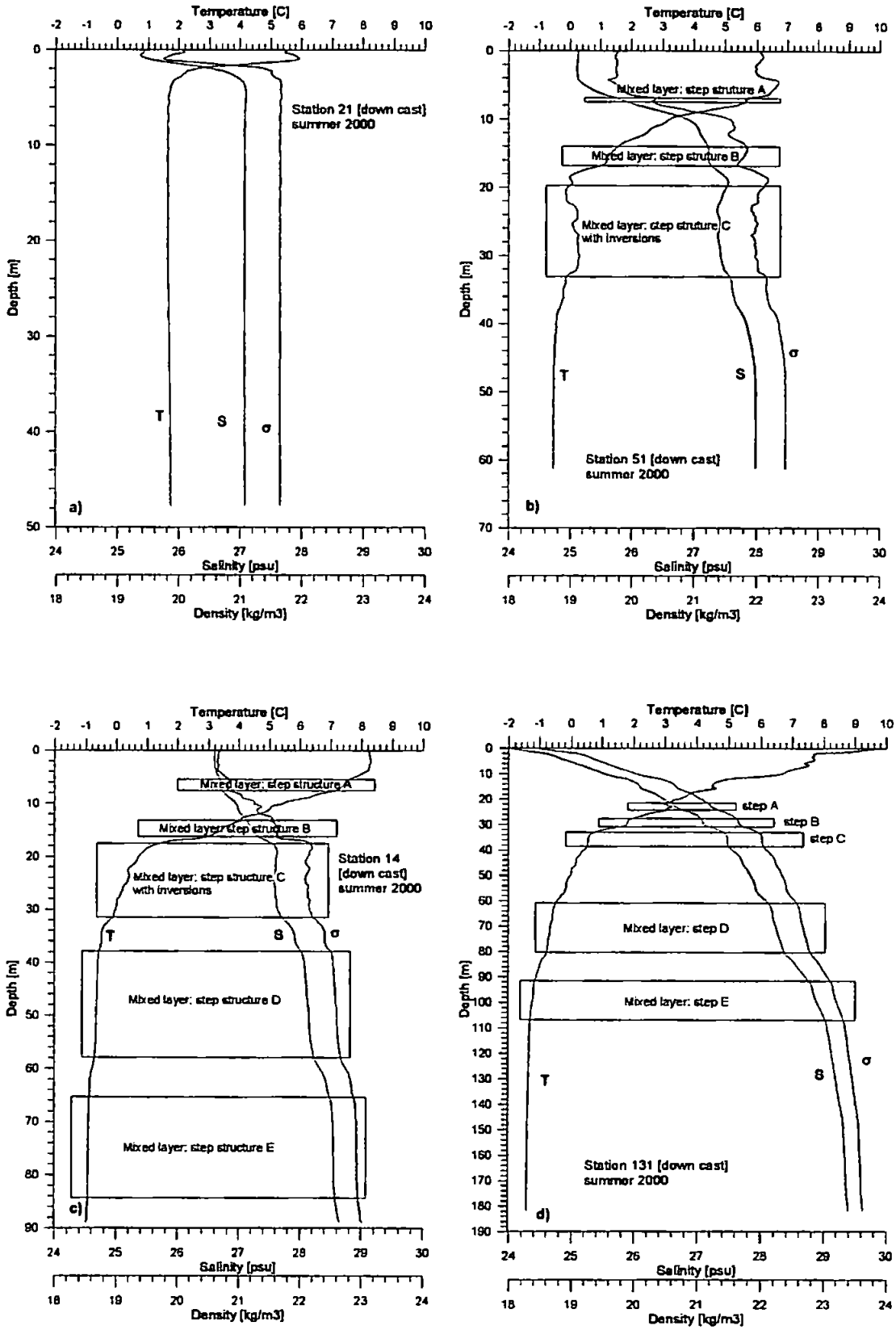


Figure 4.1: Vertical CTD profiles at stations (a) 21 in Gorlo, (b) 51 southwest of Gorlo, (c) 14 adjacent to the Basin offshore the Terskii Coast, (d) 131 in Kandalaksha Bay. Vertical step structure (A, B, C, D, E) indicate small scale quasi-homogeneous layers displayed with density inversion.

Further west of the area in the Basin, the profile at station 14 (figure 4.1c) shows bigger step-like structures, ranging between 10 to 20m layers thick. Three step-like structures are identified as "steps C, D, and E". Finer steps (~2 m thick) are also seen but it was difficult to label or trace them since they are part of the thermocline. Here step C represents some variation in the temperature (0.7 to 0°C) with constant salinity of 27.6 psu. Surface waters in the Basin have maximum temperature 8°C with salinity of about 26.6 psu. Then in deep waters, from 40 m to 90 m, the relative temperature variations are smaller compared to larger variations in salinity. Deeper, the profile shows the other 2 steps, named "step D and E", with respective characteristics of -0.6°C, 28.2 psu and -0.9°C, 28.5 psu. Further west in the deepest part of Kandalaksha Bay at station 131, the CTD profile shows a number of steps. The steps previously observed in the eastern station, in the Basin, and near Gorlo are interestingly present here displaying similar thermohaline properties as shown in figure 4.1d. Steps A, B are still located within the sharp thermocline, whereas steps C, D and E are located underneath in deeper water. Surface water is fresh (24 psu) and warm (near 9.5°C), and bottom water at 180 m depth is near -1.5°C and saline as 29.5 psu.

These selected CTD profiles were presented here to show the evidence of step-like structures in the water column in the northern White Sea. Although, the water is well stratified in Kandalaksha Bay, and well mixed in the western part of the Gorlo Strait, the steps are nevertheless present with different thicknesses and at varying depths. Each step was recorded at varying depths within temperature inversion in the vertical profiles. These relatively small-scale features are of complex structures since they show slight variation in either temperature or salinity or both according to all vertical profiles. These thermohaline variations observed in these quasi-homogeneous layers indicate gradual mixing with the surrounding resident waters.

The thermohaline observation of the entire set of CTD profiles for summer 2000 can be summarised as follows: (i) the surface temperature scale ranges from 3-to-10°C in both end areas (Kandalaksha Bay and Gorlo) whereas surface salinity varies from ~25.5 to 27 psu in the north Basin and from ~27 psu in Kandalaksha Bay to 19 psu in its estuaries. Some temperature inversions were seen in layers of 10-20 m. (ii) Mixed waters, in west of Gorlo, are seen at depth below 5 m to the shallow bottom (50 m) depicting a range of temperature and salinity values respectively of 0.5 to 3°C and 26.5 to 27.5 psu. (iii) Intermediate layers were defined as between 30 m and 100 m deep and revealed fine scale thermohaline structures such as steps with temperature inversion.

Distinct and bigger step-like structures were observed below 40-50m depth. Thermohaline values ranged from 27.5 to 28.5 psu and from 0.5 to -1°C. (iv) Deep layers were defined within very little variation in the thermohaline values from a depth of 120 m to 350 m, and mostly showed a stagnant water mass with a temperature of -1.5°C and a salinity of 29.5 psu, known as the bottom water of the White Sea.

Before analysis on small scale features is conducted there is a need to examine the mesoscale distribution of the water masses in the whole study area to identify their properties and variations through the water column. To do so, horizontal sections (including all CTD measurements from the cruise) at 5 m depth intervals (from surface to bottom) were generated to look at the temperature and salinity fields of the study area. As reviewed in the literature (Timonov, 1947 and 1950; Pantiulin 1974; Naletova and Sapozhnikov, 1993), the characteristic layers of surface waters, intermediate and deep waters are identified at respectively 0-30 m, 30-100 m and 100-300 m.

## 4.3. Distribution of Surface waters

The term "Surface layers" in the White Sea refers to a thin layer below the sea surface, bounded in general by a sharp thermocline during warm seasons, which reaches a maximum of 20 m depth. Figure 4.2 represents the horizontal distribution of temperature and salinity calculated near the surface at 5 m and at 20 m depth. The average surface temperature is about 7°C in the Basin of the White Sea and reaches 5°C towards Kandalaksha Bay (figure 4.2a) and inshore. In the north eastern sea, west of Gorlo, the water is colder 4°C and less near the Terskii Coast. The distribution of salinity at the surface, shown on figure 4.2b, is more uniform and spread in the Basin with a value of 26.6 psu, getting fresher with 23 psu in the estuaries of Kandalaksha Bay. In the west of Gorlo, fresher water is also observed, particularly in its south with a salinity of 25.4 psu, which shows the extent of the fresh Dvina water in the very surface layer. Below the surface at 20 m depth, temperature and salinity values change drastically, showing the presence of the sharp thermocline at shallow depth. The coldest temperatures (figure 4.2c) are located in the Basin with values reaching 1°C and less, then about 2°C near Gorlo and along the Terskii coast. Relative warmer water up to 5.5°C is nested inside Kandalaksha Bay, located above the deepest part. A salinity contour of 27.5 psu occupies the Basin (figure 4.2d) with more saline water in its core. Water with salinity of 27 psu is observed north of the eastern sea with less saline in the south with the present Dvina water.

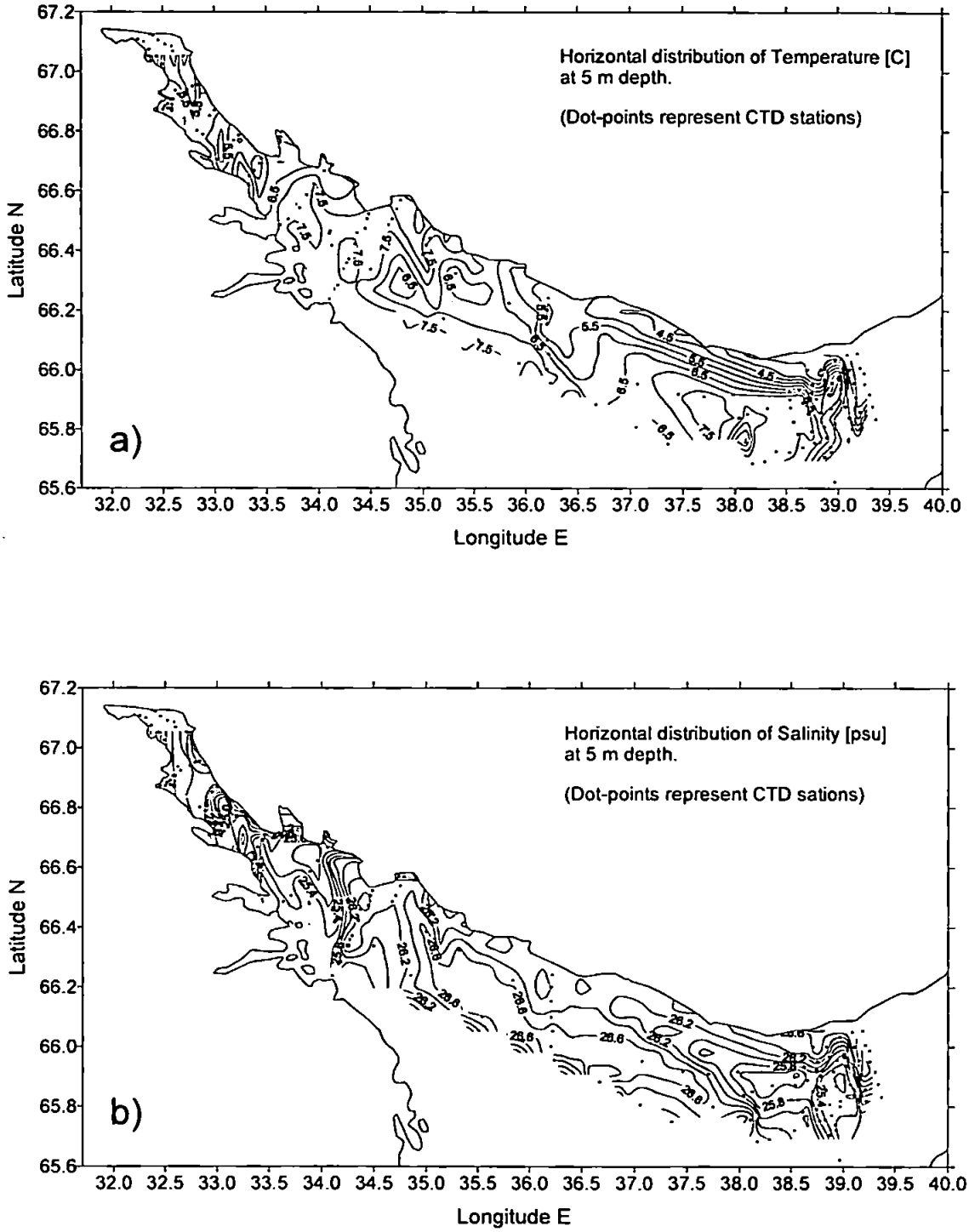


Figure 4.2: Horizontal distribution of (a) temperature and (b) salinity at 5m in the northern White Sea. The thermal front is evident is the Gorlo Strait as cold incoming GSW (<4°C) enters warmer surface waters (~7°C) of the White Sea. The second front located in Kandalaksha Bay is more obvious in the salinity field caused by runoffs of river waters (S varying from 15 psu at the head of Kandalaksha Bay to 25 psu at its mouth) interacting with White Sea surface waters (S~26 psu).

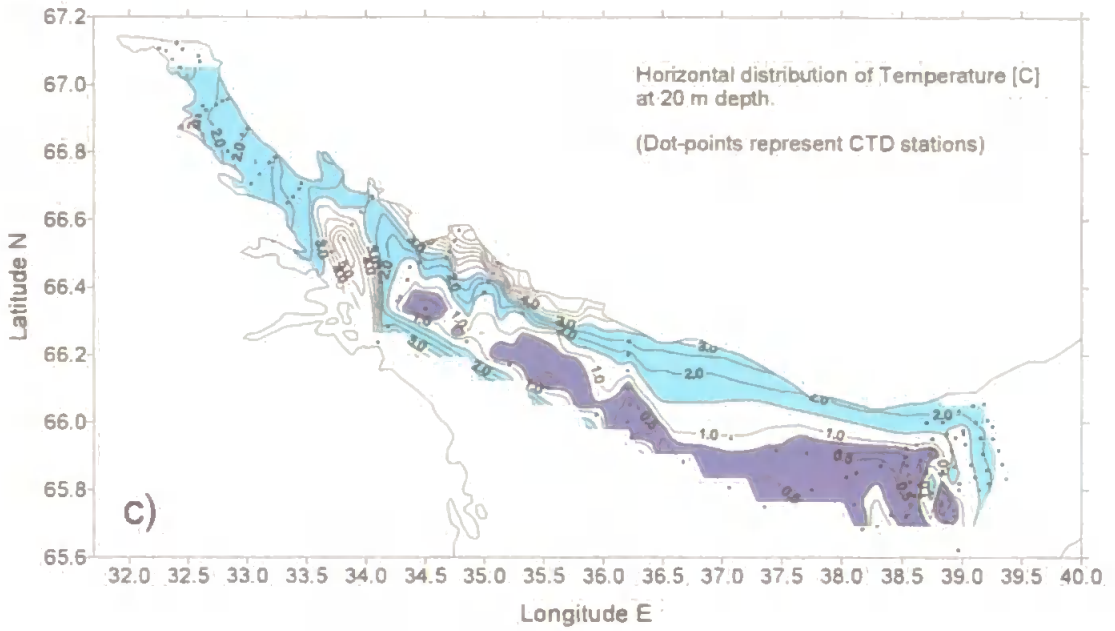


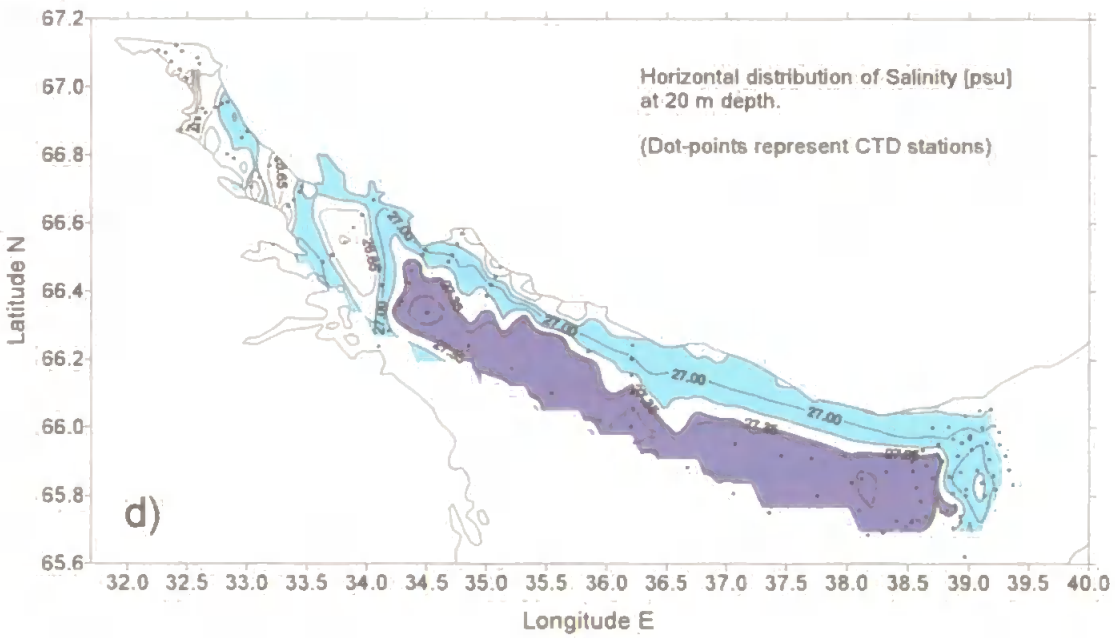


Figure 4.2: Horizontal distribution of (c) temperature and (d) salinity at 20m in the northern White Sea. Here we notice the incoming GSW, slightly modified by mixing with the White Sea waters (identified as the mixed layer step B) occupying the Terskii coast from Gorlo and all along the north coast of the Basin (shown by light blue colour). The distribution of the second mixed layers (step C) as shown by the deep-azure colour mainly occupies the Basin of the White Sea.

It is interesting to note a sharp front located west of Gorlo in the 5 m layer which suggests intrusion of cold and saline water coming from the Barents Sea through the Gorlo Strait. Some portion of the Gorlo Strait water is slightly advected along the Terskii Coast as shown by temperature and salinity contours of ~4°C and > 26.3 psu respectively. In the 20 m layer section, we can confirm that some of the mixed water from Gorlo is deflected along the Terskii Coast although interacting and mixing with the present White Sea Water. This is clearly shown by the temperature and salinity contours of 2°C and 27 psu. Furthermore, the extent of this advected water reaches the area of Kandalaksha Bay to finish in a rotating system adjacent to the front observed there with freshest water from rivers of Kandalaksha Bay in contact with White Sea Surface Water.

## 4.4. Distribution of Intermediate waters

At 30 m to lower depth (60 m), the feature observed in the distribution of the intermediate water is characterized by circular patch of both temperature and salinity gradients clearly matching the isobaths of the Basin. The temperature and salinity values vary from 0° to 1°C (figure 4.3a) and from 27.4 to 27.8 psu (figure 4.3b) respectively at 30 m; from 0.5° to -0.5°C (figure 4.3c) and from salinity 27.6 to 28 psu (figure 4.3d) at 45 m; from -0.35° to -0.8°C (figure 4.3e) and from salinity 28 to 28.4 psu (figure 4.3f) at 60 m. This present thermohaline gradient is likely to be associated with the cyclonic gyre of the Basin since the scale of this intermediate water occupies the whole Basin. At 30 m to 45 m depth, the thermohaline front near Gorlo located at longitude 39°E is well indicated in the temperature and salinity section (Figures 4.3a to 4.3d). It is interesting to note the elongated contours of salinity (27.2 to 27.4 psu) and temperature (0.5° to 1.2°C) along the Terskii coast emanating from the eastern front, west of Gorlo. This clearly suggests that the intrusion of the modified Gorlo water was mixed with the waters of the White Sea; however, some of the Gorlo waters were advected unchanged in the northward direction by the Terskii current.

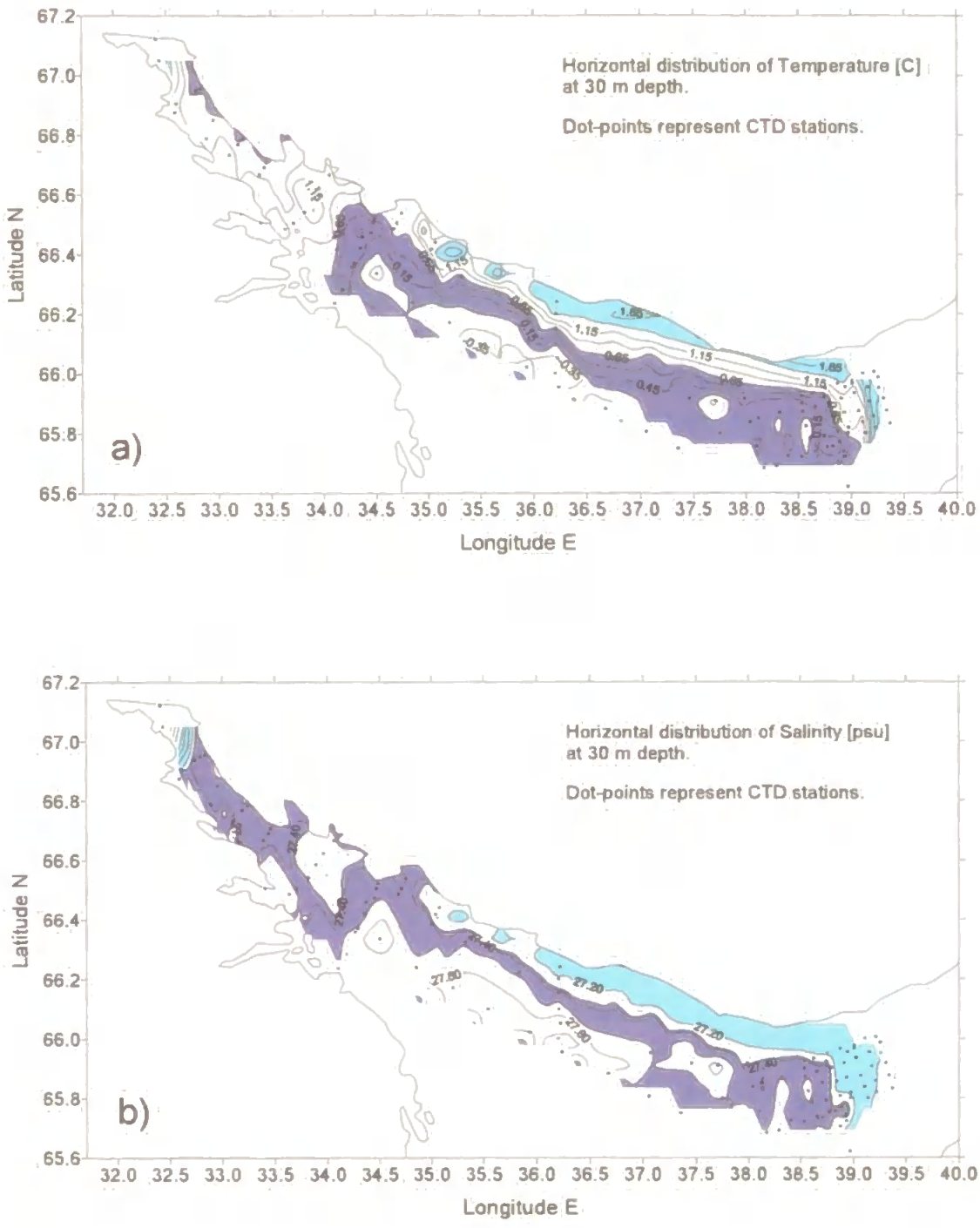


Figure 4.3: Horizontal distribution of (a) temperature and (b) salinity at 30m depth in the northern White Sea. Mixed bottom GSW (saline and cold, light blue) yet occupies the Terskii region, whereas offshore in the Basin, the mixed water (step C, deep-azure) has an elongated filament structure caused by the main cyclonic Basin circulation.

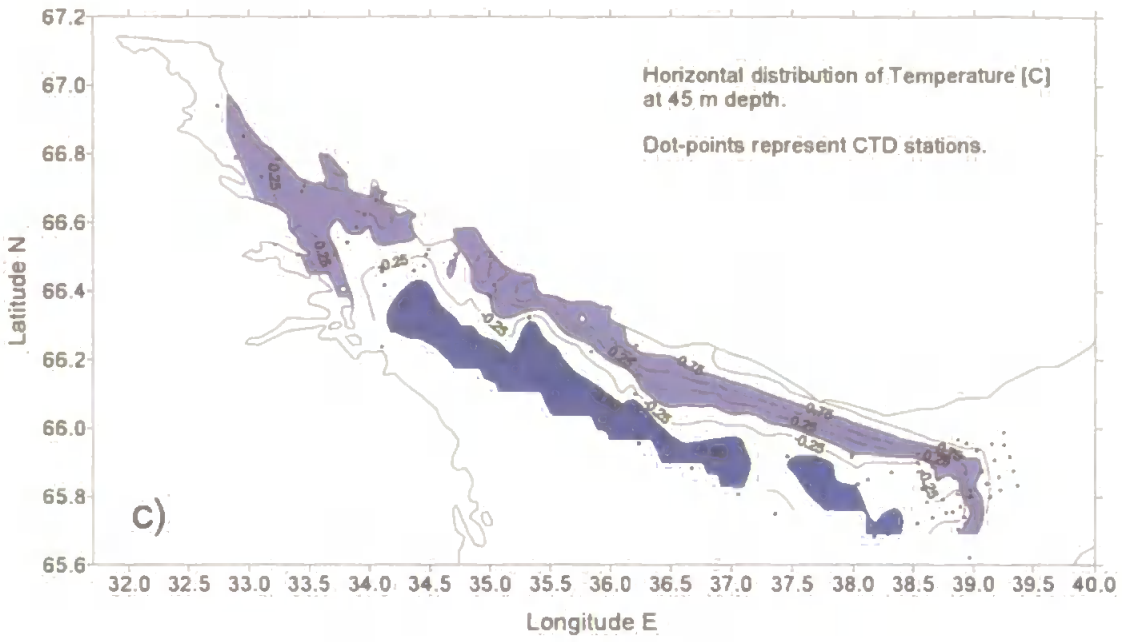


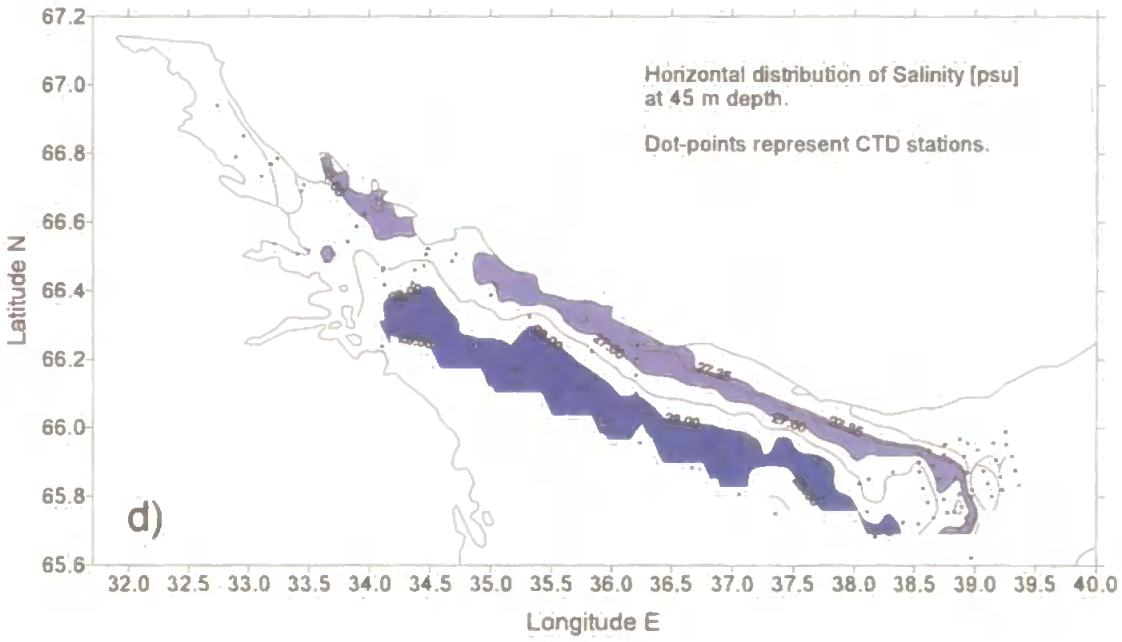


Figure 4.3: Horizontal distribution of (c) temperature and salinity (d) at 45m depth in the northern White Sea. Note the mixed layer (step C, deep-azure) spread at the bottom along the Terskii coast. The next identified mixed layer (step structure D, blue) now occupies the Basin of the White Sea.

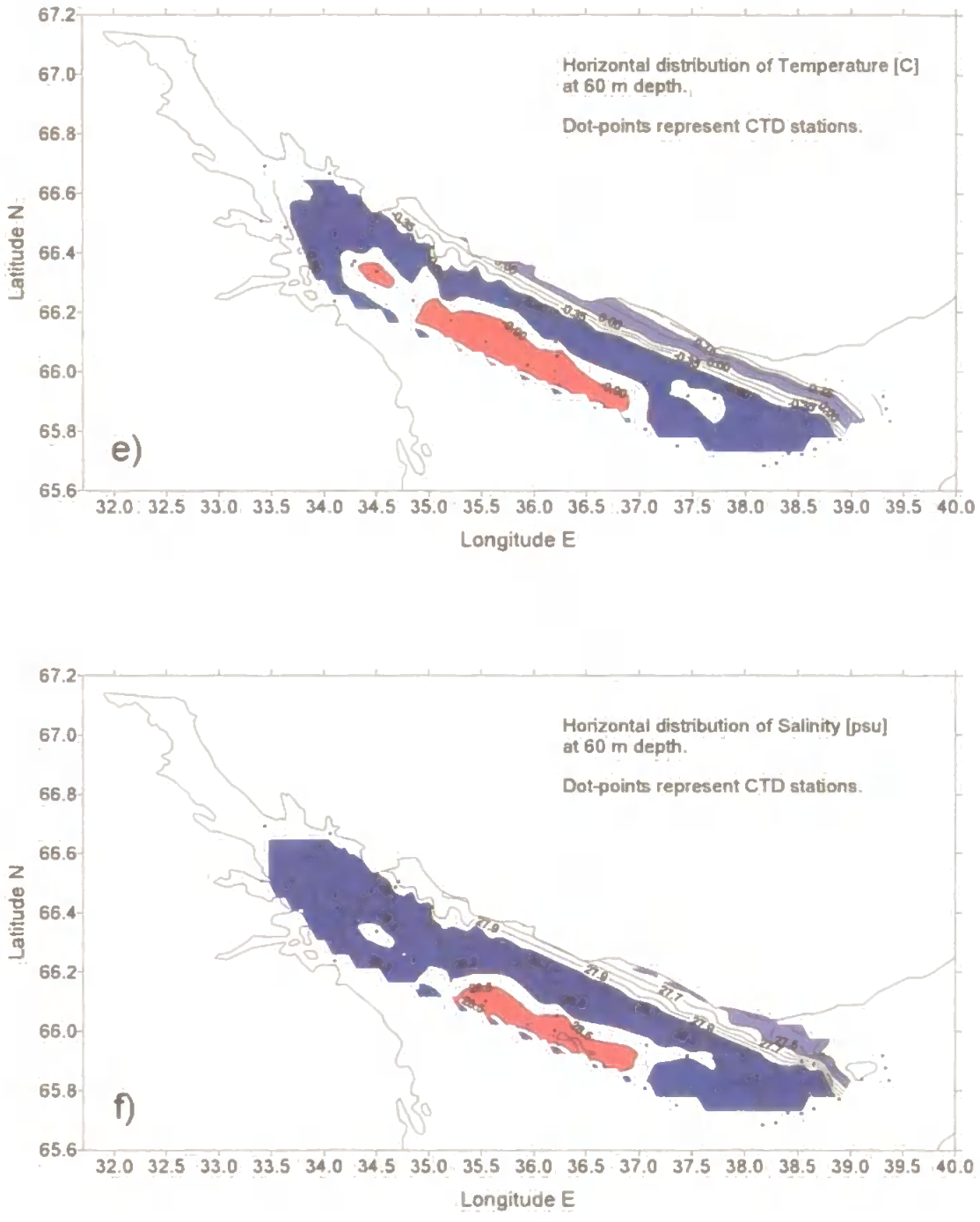


Figure 4.3: Horizontal distribution of (e) temperature and (f) salinity at 60m depth in the northern White Sea. The distribution of the mixed layers (step D in blue and step E in red) suggests the presence of the main cyclonic circulation nested in the Basin of the White Sea as shown by the sequence (see previous figures) of denser water dispatched in its centre.

## 4.5. Identification of mixed layers: Steps

A selection of CTD profiles (figures 4.1) have shown the evidence of step-like structures ranging from 1 to 58 m in thickness, suggesting the presence of several quasi-homogeneous mixed layers. However, their horizontal structures in particular need to be investigated. Therefore, a detailed analysis is run through the entire data set (see appendix B, tables 4.1 to 4.5), and resulted in the identification of five different mixed layers, labelled steps A, B, C, D and E (from surface to bottom: step A, the lightest mixed water, to step E, the denser mixed water). Table 4.1 below indicates the range of their thermohaline characteristics with assigned colours for layer identification in the hydrographic transects.

| | Salinity [psu ] | Temperature [°C] | Density $\sigma_t$ [kg.m$^{-3}$] | Colour |
|---|---|---|---|---|
| Step A | 25.5/26 | 3.5/7 | 20.2/20.8 | electric blue/orange |
| Step B | 26.65/27.2 | 1/3 | 21.2/21.75 | ice blue |
| Step C | 27.35/27.6 | 0/0.8 | 21.9/22.2 | deep azure/light blue |
| Step D | 28/28.4 | -0.8/-0.6 | 22.5/22.75 | blue |
| Step E | 28.5/28.7 | -1.15/-0.9 | 22.9/23.05 | red |

Table 4.1: thermohaline values characterizing the steps A, B, C, D, E indexed respectively with a colour for identification of the mixed layers in vertical and horizontal sections/transects.

The visual analytical approach also showed that the thermohaline index which identifies each step varies in depth according to their geographical location. These slight variations in either temperature or salinity or both are of interest because it may suggest the fact that meso or small scale mixing processes are occurring within the vicinity of these quasi-homogeneous layers, and/or suggest the fact that they differ from the source. The following sections describe in details the horizontal and vertical structure of the steps.

### 4.5.1. Distribution of step A

Step A is quite difficult to analyse since it is situated very close to the surface and also within the thermocline. In this study, step A was predominant in all stations except the

Basin of the White Sea in the very surface layer (figure 4.4a and table 4.1a and 4.1b in the appendix B), with a characteristic mean-depth of 10 m calculated at the middle of the mixed layer and an average thickness of 4 m. Figure 4.4a represents here the zonal distribution of step A in the northern White Sea. Values 1 show the presence of the step revealed in the CTD profiles whereas values 0 are non existent step.

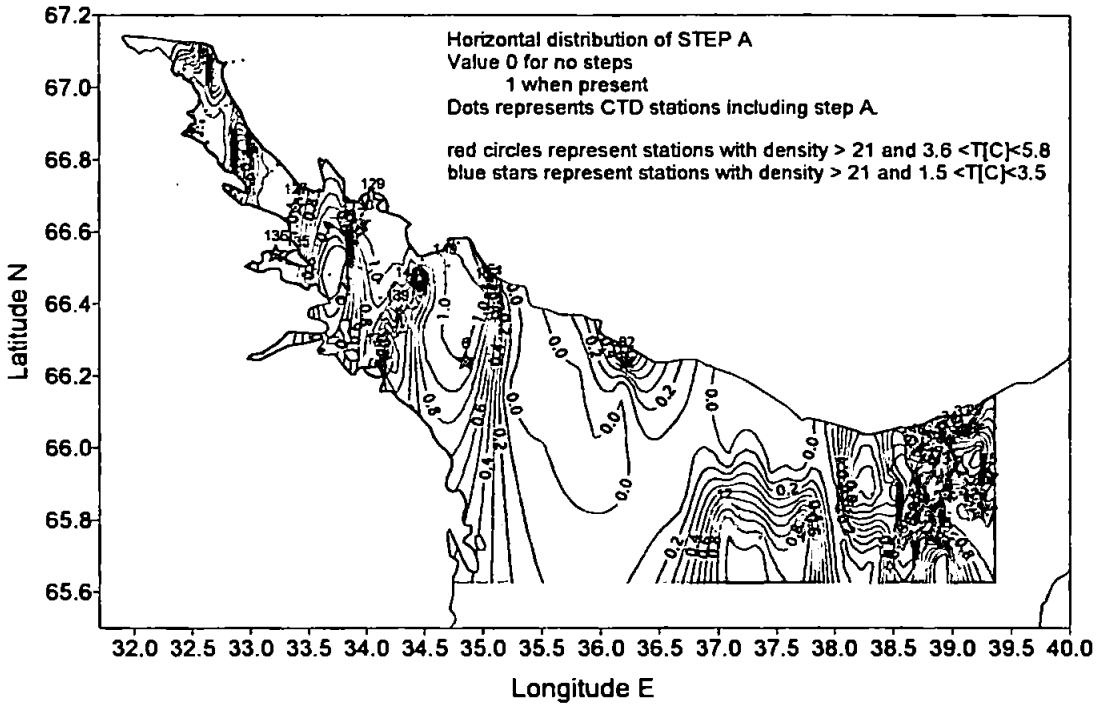


Figure 4.4a: Horizontal distribution of step A observed in the northern White Sea, cruise June 2000.

It shows Step A present in Kandalaksha Bay, west of Gorlo and in the area offshore Dvina adjacent to the Basin. It is very fresh and warm water, in principle originating from the rivers presenting a density of $\leq$ 21 kg.m$^{-3}$ (table 4.1a in appendix B). The absence of steps in the Basin of the white Sea is probably caused by summer stratification of surface layers with a sharp thermocline located relatively in shallow depth (5-20 m, see figure 4.1c). It is interesting to note a slight increase in density in step A (> 21 kg.m$^{-3}$) corresponding to cold values at some stations (table 4.1b in appendix B). Such densities associated with cold values of 1.5 to 3.5°C (see symbols blue-stars in figure 4.4a) suggest a contribution from the intrusion of the mixed Gorlo Strait Water. Such density in the indexes of step A are located near the Terskii Coast (with station 82) and a few in the north coast of Kandalaksha Bay. This shows and confirms that the Terskii current may play a role to displace and/or maintain fine mixed

water in the surface layer. Interestingly, stations with dense but less cold values of step A ranging from 3.6 to 5.8°C (see symbols red-circles in figure 4.4a) are located on the exact position of the two observed front zones, one located west of Gorlo and the second located seaward of Kandalaksha Bay. This again supports the fact that fresh surface water from Dvina may mix with surface water from the incoming mixed Gorlo Water, and that fresh surface water from Kandalaksha Bay also contribute to mixing with probably some surface water advected by the Terskii current. The latter is of interest since the dynamics of such fine mixed layers may relate to displaced waters from the recognised cyclonic circulation in the Basin (Timonov 1950; Gidrometeorologiya, 1991; Ivanov and Mikhailovsky, 1996; Semenov and Luneva, 1996 and 1999). Southwest of the Gorlo Strait, the mixed layer step A is generated by surface waters mixing with contribution from the Dvina waters, the strongest river discharge of the White Sea, which flows out through the Gorlo Strait.

### 4.5.2. Distribution of step B

Table 4.2 (see appendix B) shows the thermohaline values, depth and thickness of Step B from the visual analysis run through all CTD profiles 2000. The characteristics of this quasi-homogeneous layer indicate a mean depth of 20 m (calculated from the middle point of the layer) and an average thickness of about 11 m. The present layer is 10m below from the previous observed step A, and seen generally to be located right underneath the thermocline. Its water has a distinct index of more saline and colder values in comparison with the previous layer step A. The density has increased by 1.5, the salinity by 1 psu, and the temperature has cooled by 2.5°C. Evidence of step B is seen in the entire northern White Sea (figure 4.4b) apart from the area offshore Kandalaksha Bay and adjacent to the Basin. In table 4.2, it appears that a few stations present some distinct variations or fluctuations which are slightly out of the defined range of step B. At these stations, the layer presents slight denser and more saline water (blue stars in figure 4.4b representing stations 6, 13, 26, 126, 139, 141). This thermohaline index is seen in vertical profiles taken west of Gorlo, in the east part of the Basin, the Terskii shore, and in the whole region of Kandalaksha Bay including its estuaries and rivers. Indexes with warmer temperatures (red circles in figure 4.4b) are indicated by stations situated on the northern shore of Kandalaksha Bay, which suggest contribution of fresh and warm river waters to explain the presence of such step B in

these remote locations. Other locations are in the eastern part of the Basin which suggests some mixing occurring with yet the influence of the Dvina circulated water.

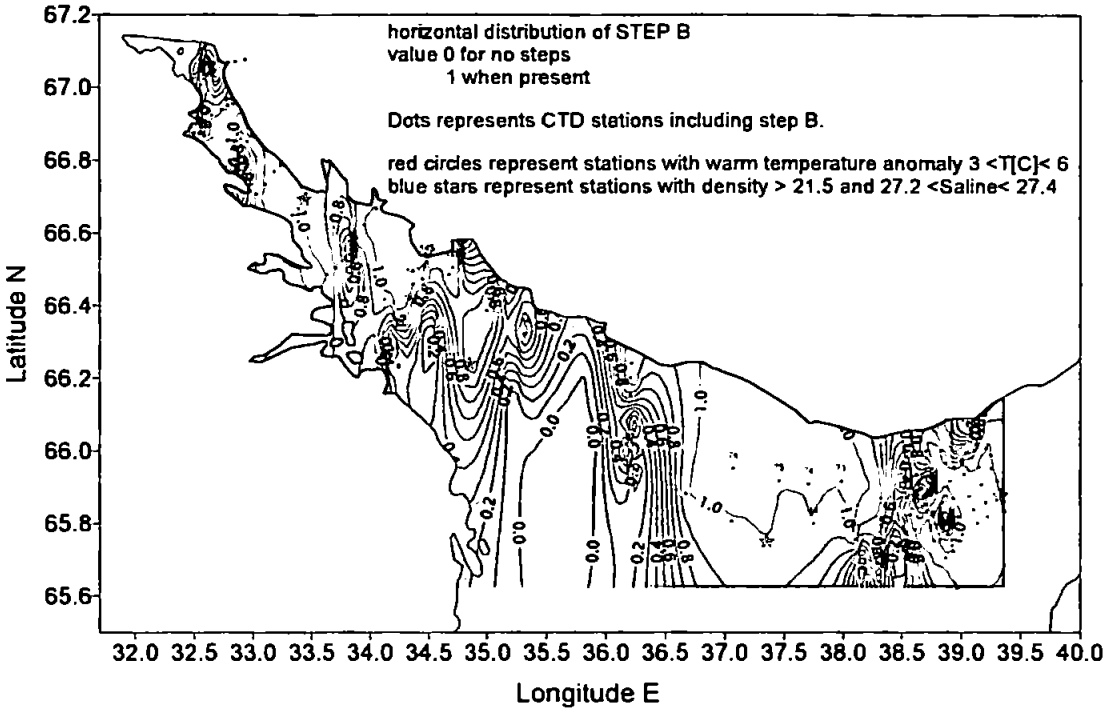


Figure 4.4b: Horizontal distribution of step B observed in the northern White Sea, cruise June 2000.

### 4.5.3. Distribution of step C

The step-like structure is very predominant in all stations of the survey. The mixed layer which has a temperature and a salinity of 0.5°C and 27.5 psu, is found at about 30m depth with an average thickness of 16m (see table 4.3 in appendix B). It is located 10m deeper than the former layer (step B). Step C is seen in the whole northern part of the White Sea (figure 4.4c); probably generated in the most western part of Gorlo since we observed gradual formation and presence of the step where the frontal zone is situated. Fluctuations in the quasi-homogeneous layer are mostly observed in the salinity field (see table 4.3), which reveal an increase in the density (reaching values of 22.2) when salinity has the highest values. On the other hand, the upper mixed layers which consist of step A and B show temperature fluctuations governing the density field. This is explained by the surface shield of the summer stratification in some places of the White Sea where topographic mixing is not present. In the case of the mixed layer step C, situated below 30 m, the salinity is likely to be a dominant factor in the density structure.

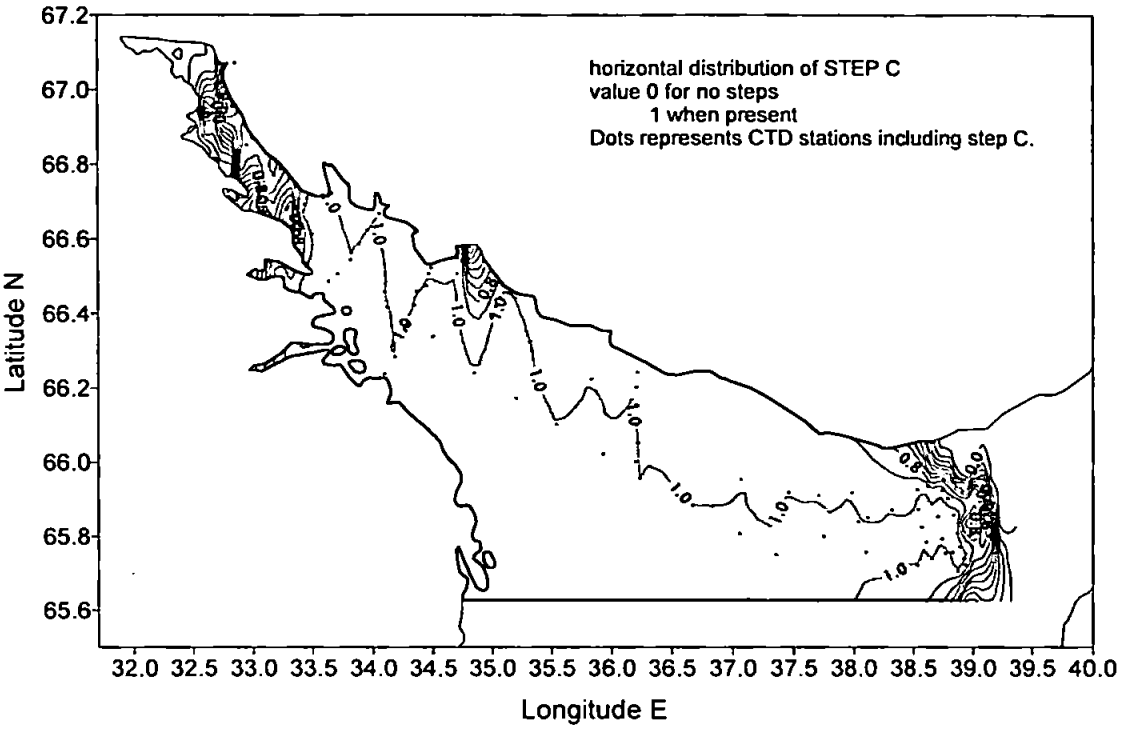


Figure 4.4c: Horizontal distribution of step C observed in the northern White Sea, cruise June 2000.

### 4.5.4. Distribution of step D

This mixed layer is located at an average depth of 56 m with an average thickness of 14m (table 4.4 in appendix B) and a range of temperature and salinity characterized by -0.8° to -0.6°C and 28 to 28.4 psu respectively (table 4.I). The layer 'step D' is clearly heavier than the previous observed layers located above in the water column, with temperatures below 0°C; and is likely to occupy the entire Basin (figure 4.4d).

### 4.5.5. Distribution of step E

This mixed layer is located at an average depth of 83 m, and its average thickness is about 16 m. The layer is located below the intermediate waters of the White Sea and its characteristics range from 28.5 to 28.7 psu and from -1.15° to -0.9°C (table 4.I and table 4.5 in appendix B). The two intermediate mixed layers step D and E have similarities in their spatial distribution (figures 4.4d and 4.4e). The deepest mixed layer is well characterized by negative temperatures occupying the Basin, therefore lying over the deep stagnant White Sea Water. Some distinct variation in temperature but less in salinity within the layer is evident in table 4.5.

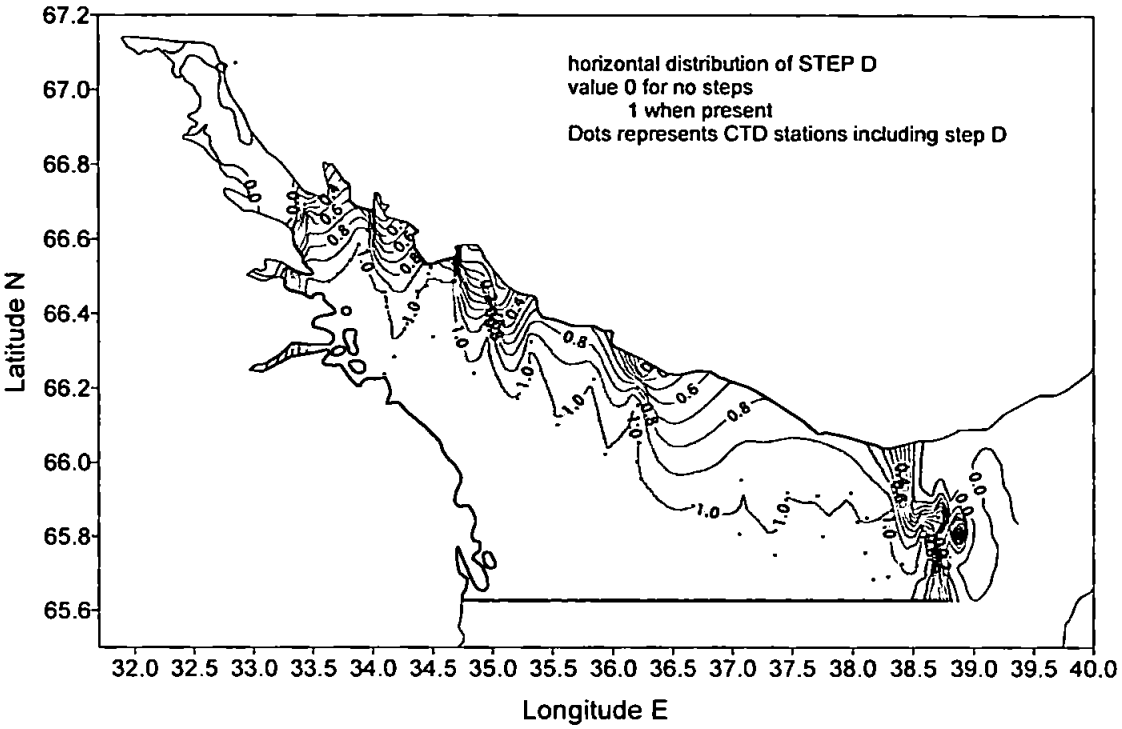


Figure 4.4d: Horizontal distribution of step D observed in the northern White Sea, cruise June 2000.

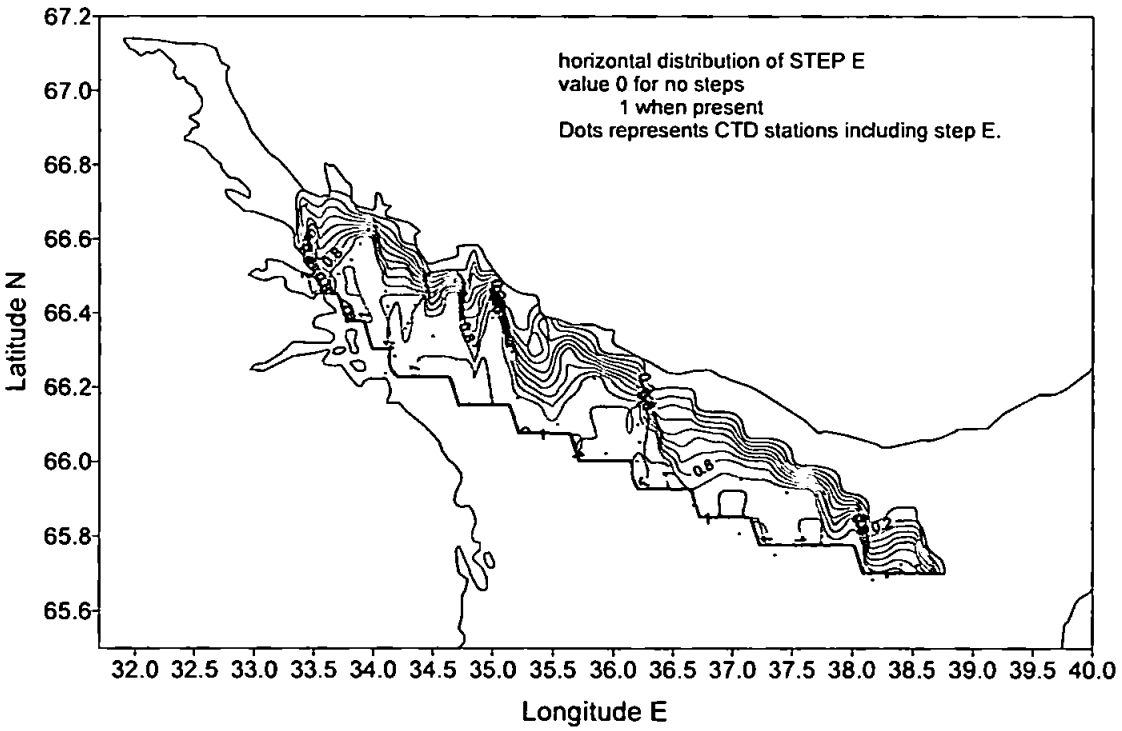


Figure 4.4e: Horizontal distribution of step E observed in the northern White Sea, cruise June 2000.

### 4.5.6. Vertical structure of the steps

The variation in depth and in thickness of the mixed layer A are represented by two selected transects (sections S1 and S2) across the northern White Sea (see figure 4.5). Along the sections S1 (offshore) and S2 (near shore), the step A is well present in Kandalaksha Bay, however it vanishes in the Basin and in the south-west region off the Gorlo Strait (shown in S1).

The data in section S1 confirm the absence of Step B in the area between Kandalaksha Bay and west of the Basin, (between stations 6 and 10) although step B is seen in section S2 near the Terskii shore. East of section S2, the thickness of the layer is nearly the depth of the water column (40-50 m). This mixed layer B can be regarded as the modified Gorlo Strait Water along the Terskii shore generated by tidal and topographic mixing. It is worth noting the oscillating behaviour within the thickness of the layer in both sections which might be related to tidal or residual tidal current (Semenov and Luneva, 1996 and 1999).

The vertical structure of the layer C as shown in figure 4.5 clearly indicates its formation and homogeneity in the whole water column (from 25 to 55 m) east of the two along shore sections S1 (station 39) and S2 (station 61). Moving west in the two sections, the vertical structure of the layer is nearly consistent in its thickness (however likely expanded offshore at some stations in section S1) and revealing internal oscillations. At the west end of the two sections, the mixed layer is likely to occupy the bottom of coastal water in Kandalaksha Bay. The mixed layer as seen in sections S1 and S2 has an extent of more than 300 km.

These two sections along the northern White Sea still reveal vertical oscillations of the mixed layer D at about 50 m depth and particularly emphasized in the offshore section S1 (although no clear evidence of step D near the Terskii shore in section S2). The oscillating shape is again well pronounced in the vertical structure of the mixed layer E (S1), and also in the shallow waters of the Terskii shore (S2).

In conclusion, the analysis of a 3-D structure of the five identified quasi homogeneous layers has revealed (i) the potential locations where they were generated and (ii) their shape and properties in the northern White Sea. The west part of the Gorlo Strait at the entrance of the White Sea seems to form such layers and it will be of interest to trace such features (by means of hydrographic transects) and use the above data to help define the physical processes described in the next section of this chapter.

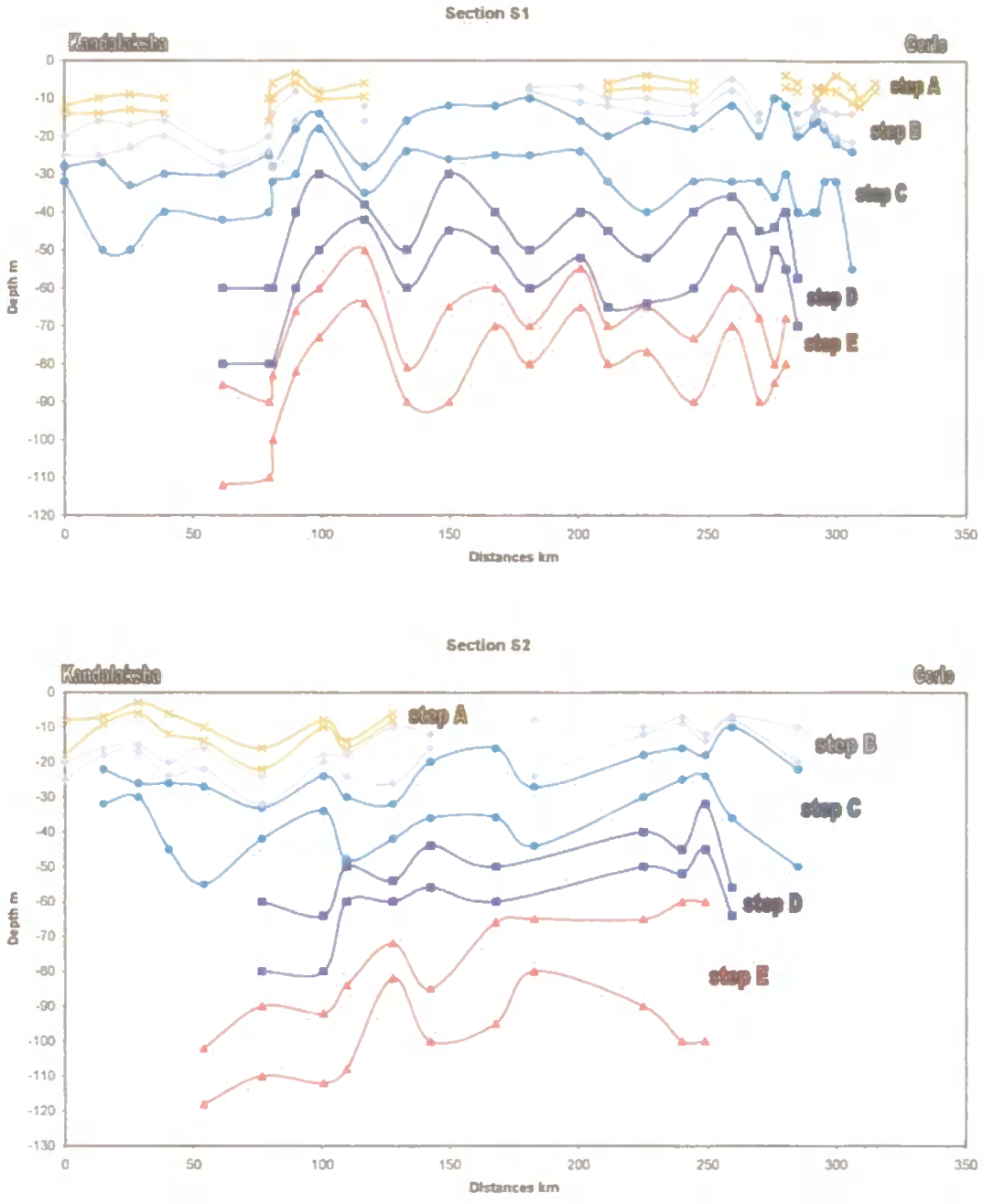


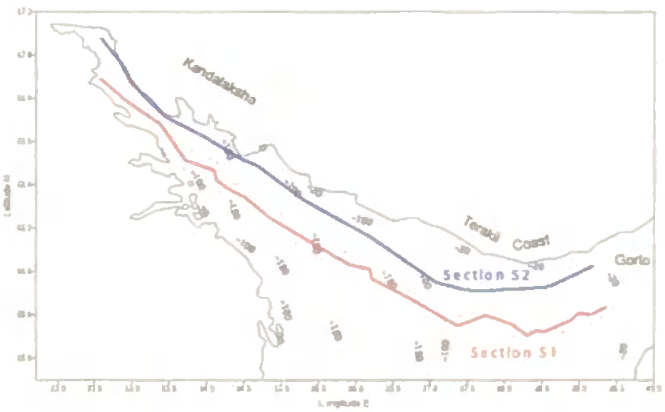


Figure 4.5: Sections along the northern White Sea (S1) close to the Terskii Coast and (S2) offshore across the Basin, as shown beside on the map with isobaths (broken lines). Vertical location and thickness (upper and lower boundaries) of the mixed layers (steps A, B, C, D and E) at stations along S1 and S2 reveal an oscillating pattern across the sea from Gorlo to Kandalaksha Bay, in June 2000.

## 4.6. A summer thermohaline intrusion

The longest transect across the White Sea (the east-west transect shown in figure 4.6 – insert- from survey 2000) illustrates the key physical processes in the northern White Sea. The vertical temperature distribution of that east-west section is shown on figure 4.6 (salinity and density distribution are shown in figures 4.6b and 4.6c in appendix B). The plot reveals the physical structure of water masses, some of which are related to the existence of the mixed layers displayed with filled coloured contours corresponding to the identified steps. The range to define the thermohaline values of each step has been narrowed in order to clarify the horizontal extent and the vertical structure of these mixed layers.

The vertically mixed water masses identified as step B (Gorlo Strait Water) and as step C show flow propagation in the Basin and Kandalaksha Bay in the form of layers constrained to the depths of 20 to 40 m with an extended length-scale of 400 km. Preliminary observations with transects (A, B and C) have dispatched a zonal extent of 30 km width for the intruded waters. These mixed layers (step A, B, C) represent the upper active layers. The mixed layers of Step A (that consist of fresh waters from Kandalaksha Bay, Dvina, and some surface water from Gorlo) are particularly confined to the very surface layers within strong stratification in the Basin which suppress the existence of such surface step-like structure (figure 4.6). The salinity and density distribution (figures 4.6b,c in appendix B) clearly separate surface fresh waters of Kandalaksha Bay from surface waters of the east part of the Basin and of the Gorlo Strait. West of transect (in figure 4.6), the salinity section shows the lowest salinity from estuary and river waters lying over the mixed layer A (located at ~10 m and sinking at 20 m depth towards the mouth of Kandalaksha Bay). This indicates less saline surface current influenced by the rivers of Kandalaksha Bay flowing into the White Sea influenced by some local circulation gyre. In turn, the less saline surface currents are compensated by slightly saltier water, such as the modified GSW, coming in the subsurface layers (step B). This is more evident with the presence of the mixed water (step B) lying in the bottom waters, far to the north-east on the shelf of Kandalaksha Bay, more specifically in the mouth of the Niva river. Colder temperatures (0.5°C) of step C at 40 m depth do not reach the bottom waters of the rivers and estuaries of Kandalaksha Bay, probably due to the presence of the shallow coastal topography and sill located north east of Kandalaksha Bay.

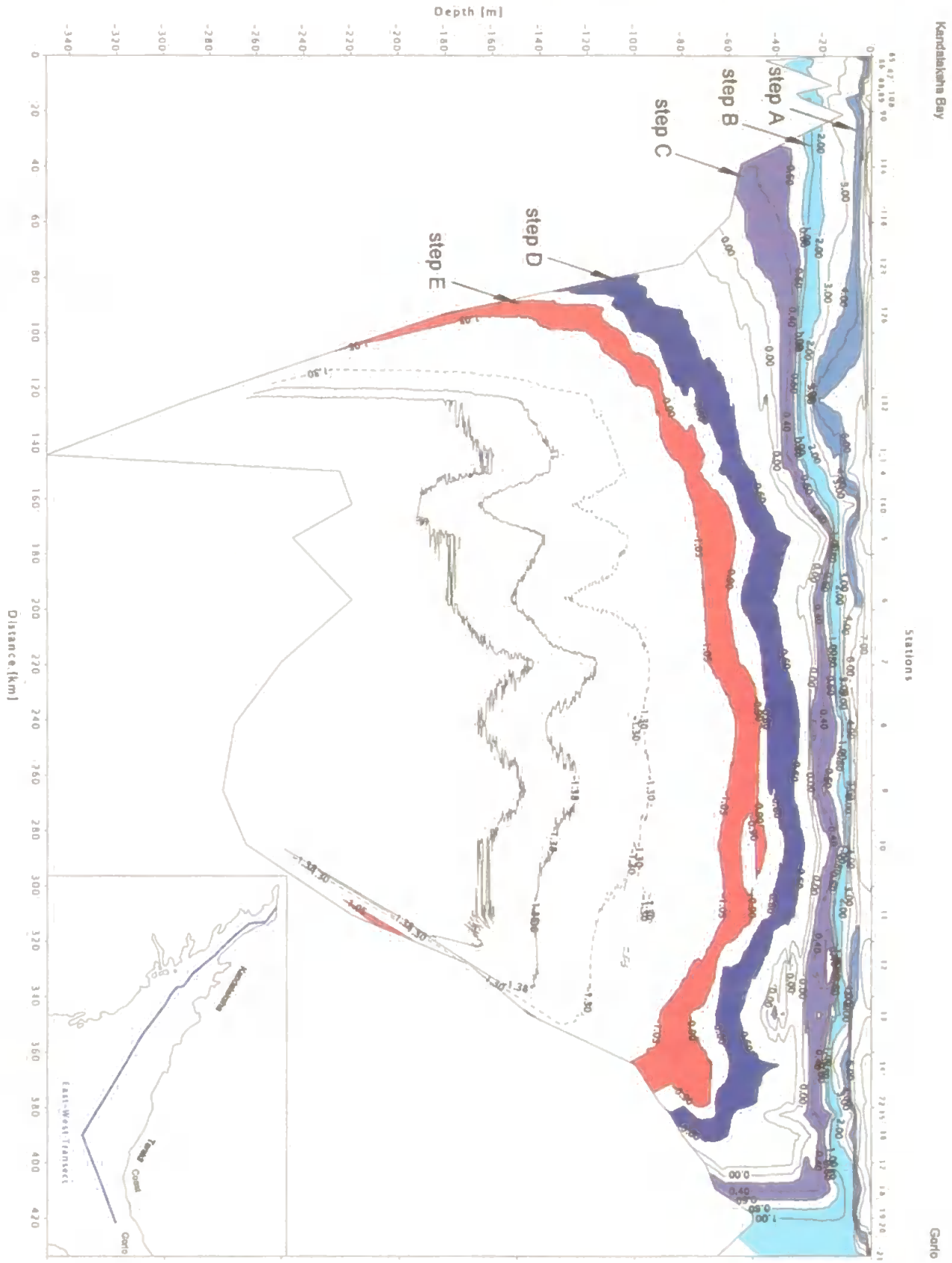


Figure 4.6: Vertical Temperature (°C) distribution along the East-west Transect, showing mixed layers A, B, C, D and E propagating across the White Sea, in June 2000. The active upper layer includes the mixed layers A, B, and C; the intermediate layer is well distinct by a dome structure (step D and E).

This can also be caused by the intensive stratification in summer in the estuaries of Kandalaksha Bay, which produces a sinking of the pycnocline, which reaches a depth of 50m, and so prevents saline water of the Basin from coming further on the shelf of Kandalaksha Bay. Below the mixed layer of step C (0.5°C; 27.5 psu), the intermediate water is found in the Basin (at about 50m and lower), and in Kandalaksha Bay (up to 120 m). These intermediate water masses form a dome-shape separating the upper layers from deep waters. A transect near the Terskii shore (transect F1 on figure 4.7) shows clearly the mixed layers occupying the Terskii coastal areas, namely the modified Gorlo Strait Water (step B) seen down to 30 m, the underneath layer of step C at 30 to 50 m and the two deepest mixed layers (step D and E) seen on the slope between 60 and 90 m depth.

## 4.7. A dome-shape structure

A distinct dome-like structure is revealed by the contours of the mixed layers of step D and E (seen in figure 4.6abc) which occupies the intermediate layer of the White Sea Basin (40-60 m). Beneath this dome-shaped structure, a pool of cold dense saline water is observed, confined to the fjord-type bathymetry of the Basin. The mixed layer of step E (-1°C; 28.5 psu) shows the boundary of the steady and stagnant deep water mass of the White Sea. The boundary layer is found to reach the coastal marine slope of the Terskii region as shown on transect F (figure 4.7). Pantiulin (1974 and 1990) has confirmed similar observations showing replenishment in this boundary layer which controls the mixing process. His results showed that the core of the boundary mixed layer restricts the penetration of water to the deep. The dome-like structure of these boundary layers may be caused by the main observed cyclonic gyre circulation (by referring to figure 2.11c) located in the Basin. Below these mixed layers, internal oscillations are seen in the core of the stagnant White Sea water by temperature contours of -1.3° to -1.4°C and salinity contours of 28.8 to 29.4 psu. It is worth noting west of transect (western part of the Basin, figure 4.6c) the shoreward deepening of isopycnals (drop of 60-80 m) of the boundary mixed layers starting from station 5 to station 123 (covering a distance of ~100 km). The resulting horizontal density gradient if it is a stationary case must be maintained by geostrophic currents. According to these parameters cited above, the resulting geostrophic velocity (by taking into account a density gradient of 0.5kg/m$^3$), gives a relative large velocity of ~0.4 m/s.

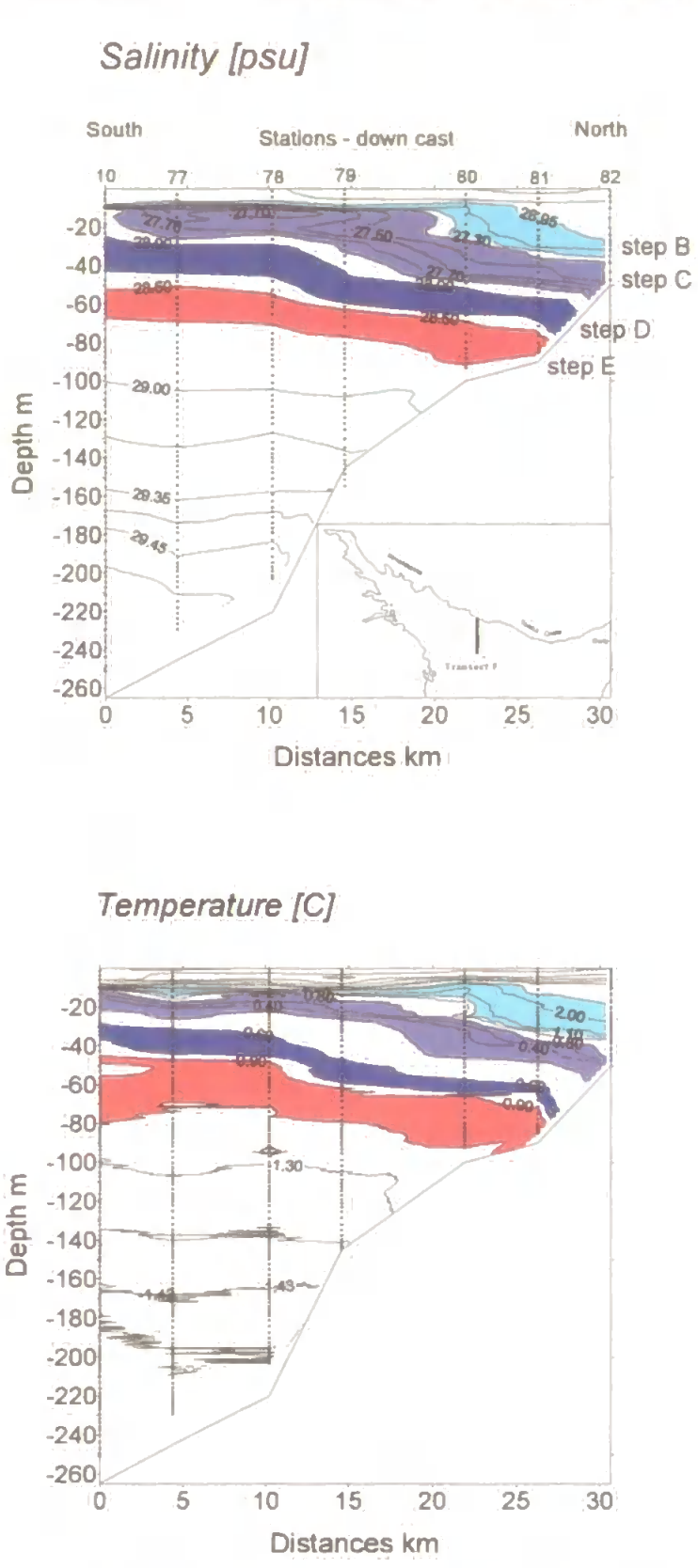


Figure 4.7: Vertical distribution of salinity and temperature at Transect F in north of Basin of the White Sea in June 2000. Note that the mixed layers B, C, D and E occupies the bottom slope of the Terskii region at their respective depth, with the distinct Terskii current entraining the mixed layer step B (stations 80 to 82; max depth ~30m and >10km broad from the Terskii coastline).

## 4.8. Conclusion

A conceptual model of the water structure has been produced using the results from the first high resolution hydrological survey of the northern part of the White Sea in June 2000. This has been summarized in a 3-D schematic of the water structure (figure 4.8), which reveals the important following key-points:

- A wide development of identified step-like (5 steps, 3-to-20 m thick) and inverse structures was revealed in the vertical profiles and distribution of temperature and salinity, revealing quasi-homogeneous layers with a horizontal extension up to 400 km.
- A complex distribution of structural combinations was observed in the studied area west of the Gorlo Strait which is found to be the principal area of their formation. In that area the following types of vertical distribution are recognised: (1) uniform down to the bottom deep-layer covered by warmer and desalinated surface waters, (2) distributions with monotonic changes in the characteristics, (3) two to three-step structures, and (4) temperature inversion structures.
- This hydrological diversity results mainly from the intensive tidal mixing and complicated interlaying between the incoming modified saline and cold waters of the Barents sea (penetrating north along the Terskii Coast) and the less dense advected desalinated warmer waters of the White Sea Bays (mainly from Dvina).
- The depths of upper and lower boundaries of the mixed layers (steps) are irregular. This is caused either by the variability of the process of formation of the steps and/or the variability of the advection mechanism.
- The two thickest dense mixed layers have dome-shape structure in the Basin which corresponds to the main cyclonic gyre of the Basin; and in the western part of the Basin they indicate the possibility of sinking (cascading) process over the slope from depths of ~80-100 m to ~180-200 m.

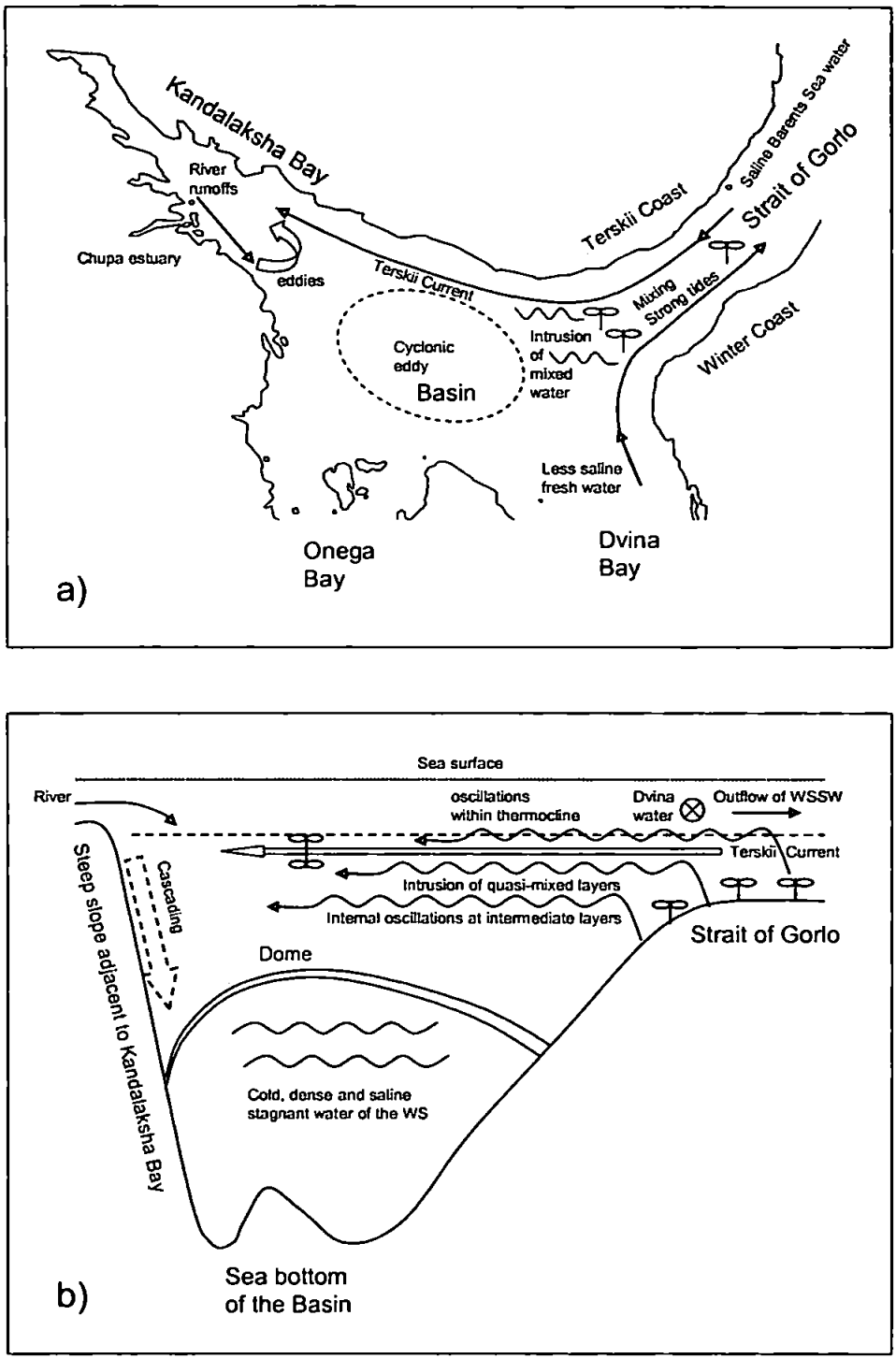


Figure 4.8: Schematic diagrams showing the key processes occurring in the northern White Sea based on the survey June 2000. The plan view (a) show the distribution of water masses mixing and contributing to the generation of eddies in the Basin and in Kandalaksha Bay with the formation of mixed layers originating at the shelf edge of the Gorlo Strait (by topographic stirring + strong tides). The vertical view (b) demonstrates the extent of the intrusion of the mixed layers in the water column propagating in the upper layers towards Kandalaksha Bay. Formation of a dome in the intermediate layers arises from the cyclonic gyre circulation of the Basin. Internal oscillations are within and under the domed boundary layer. Possible cascading event along the slopes in Kandalaksha Bay would renew the stagnant water of the Basin.

The analysis of the water mass structure in Kandalaksha Bay has shown at a series of CTD stations step-like structures, which relate to the intrusion of saline water. Formation of mixed layers is likely to be of local origin as they originate from tidal mixing over swells, banks, and steep slopes. The hydrological survey of summer 2000 has proven that mixed layers are formed at the edge of the shallow sill of the Gorlo Strait and propagate with slight modified properties in the region of Kandalaksha Bay. The survey also showed a high degree of desalination of the entire water Basin of the White Sea. The salinity of the subsurface layers showed gradual increase from 8 to 23 psu at its seaward boundary. The vertical temperature structure in the deep water part of the Basin has manifested no signs of a very cold intermediate layer, which suggests a mild preceding winter in the White Sea. Questions arise on the seasonal or interannual variability of the water structure, such as: (i) what would be the characteristics of inverse-layered structure seen in CTD profiles? (ii) Would the water structure change considerably seasonally? (iii) What is the extent of the saline mixed layer penetrating the Basin and Kandalaksha Bay following extreme winter condition? (iv) Would the excess of salinity driven by the intrusion of saline water form enough dense water on the shelf of Kandalaksha Bay and (v) trigger cascading event along the steepest slope of the White Sea (found in this area) therefore providing a replenishment of the deep water layers of the White Sea?

# Chapter 5: Interannual variability of the water mass structure

## 5.1. Introduction

The temporal variability of organic matter (Maksimova and Vladimirsky, 1990; Bek *et al.*, 1992; Agatova and Kirpichev, 2000), benthos (Bek, 1997; Azovsky *et al.*, 1998), of metals in sediment distribution (Millward *et al.*, 1999; Levchenko and Shcherbakov, 2000), zooplankton (Pertzova and Kosobokova 2002a) and of eco-biochemical cycles in the White Sea (Korneeva and Luneva, 1999; Savinov *et al.*, 2000) have been better documented than the studies based on the temporal variability of the hydrology and/or physics. However, the latter underlie various biogeochemical processes such as carbon-dioxide annual variability or chemico-biological cycles (Yakushev and Mikhailovsky, 1993 and 1994). The variability of chlorophyll and phytoplankton distribution has been also reported (Maksimova and Bondarenko, 1985; Smirnov *et al.*, 1989; Mordasova, 1999) although, the temporal scale of the dynamics of phytoplankton biomass has been poorly related to the hydrology and the physics. It was found (Ivanov and Mikhailovsky, 1996) that the long term variability of phytoplankton in the surface layers was more significant compared to the water layers at 10m and 25m, at which depth the variability was significant during only a very short time-period. Because the stratification of the water column determines the nature of the temporal scale, this anomaly in the distribution of phytoplankton may be related to the step-like structure in the water column, which was described in the previous chapter. The present chapter compares data sets collected during the survey 2000 and 2001* and data set of cruise 1991 (Gidrometeorologiya, 1991a) to estimate the variability of the water structure in Kandalaksha Bay and the adjacent waters of the White Sea proper. The study also focuses on the variability of the structure of the mixed layers which were identified for the first time in June 2000 (see chapter 4 and Lukashin *et al.*, 2003). Furthermore, the intrusion of the saline mixed layers has a considerable impact on the waters of Kandalaksha Bay and may contribute to the deep-water renewal mechanism of the White Sea.

* The data used in this study arise from a research cruise on board *Kuznetsov*. I am grateful to Dr. A. Pantiulin who kindly collected the data (May-June 2001).

Therefore, the distribution and characteristics of the dense waters in Kandalaksha Bay are compared using hydrographic transects from the three data sets. It is very likely that cascading events (Shapiro and Hill, 1997; Hill *et al.*, 1998; Shapiro and Hill, 2003) takes place along the steep slopes of Kandalaksha Bay, instead of occurring along the slopes from the shelf-edge of the Gorlo Strait at the entrance of the White Sea, as it was inferred previously (Timonov, 1950; Gidrometeorologiya, 1991a).

## 5.2. Hydrographical result 2001

### 5.2.1. CTD profiles

The details of the survey, in the north-eastern part of the White Sea, are given in section 3.2.2 with the location of the stations and the hydrographic transects shown in figure 3.3. The CTD profiles at stations 29 and 45 located in Kandalaksha Bay are shown on figure 5.1a and figure 5.1b. The profiles reveal a strong and sharp thermocline in the very surface layers, characterised by very strong temperature inversion, like the one observed at 30m depth. Step-like structures are still observed in the CTD profiles during this time of year 2001, with more pronounced inverse-layered structures than those observed in June 2000. The step-like profiles are present with a thickness varying from 10 m to > 20 m and positioned at different depths. All CTD profiles show that surface waters present a maximum temperature of 3°C whereas the bottom waters have constant temperature of −1.4°C. This cold water mass is seen at depth from 60 m (at the intermediate layers) and reaches the deepest part of Kandalaksha Bay/Basin area, observed at all CTD stations with a depth > 60m. In the Chupa estuary (see figure 3.3 at stations 1 to 10) the surface temperature varies along the estuary from 3 to 5°C maximum with the thermocline located near the sea surface (between 0 and 5 m). Below the thermocline the temperature reaches 1°C (figure 5.1c), with a temperature inversion seen in the layers between 30 and 40 m. The water at lower depth slowly decreases to 0.2°C from where it is mixed to the bottom. This bottom water presents similar characteristics compared to the mixed layer of Step C identified in June 2000. The present bottom mixed water is however slightly heavier here than in June 2000 below the 40 m layers. In the shallow coastal area at a location far north inside Kandalaksha Bay (stations 11 to 23), the characteristics of fresh surface waters range from 2 to 3°C and from 5 to 25.7 psu in temperature and salinity respectively. A detailed observation of CTD profiles in Kandalaksha Bay region shows that surface waters are relatively homogeneous within the first 15 m depth (figure 5.1d).

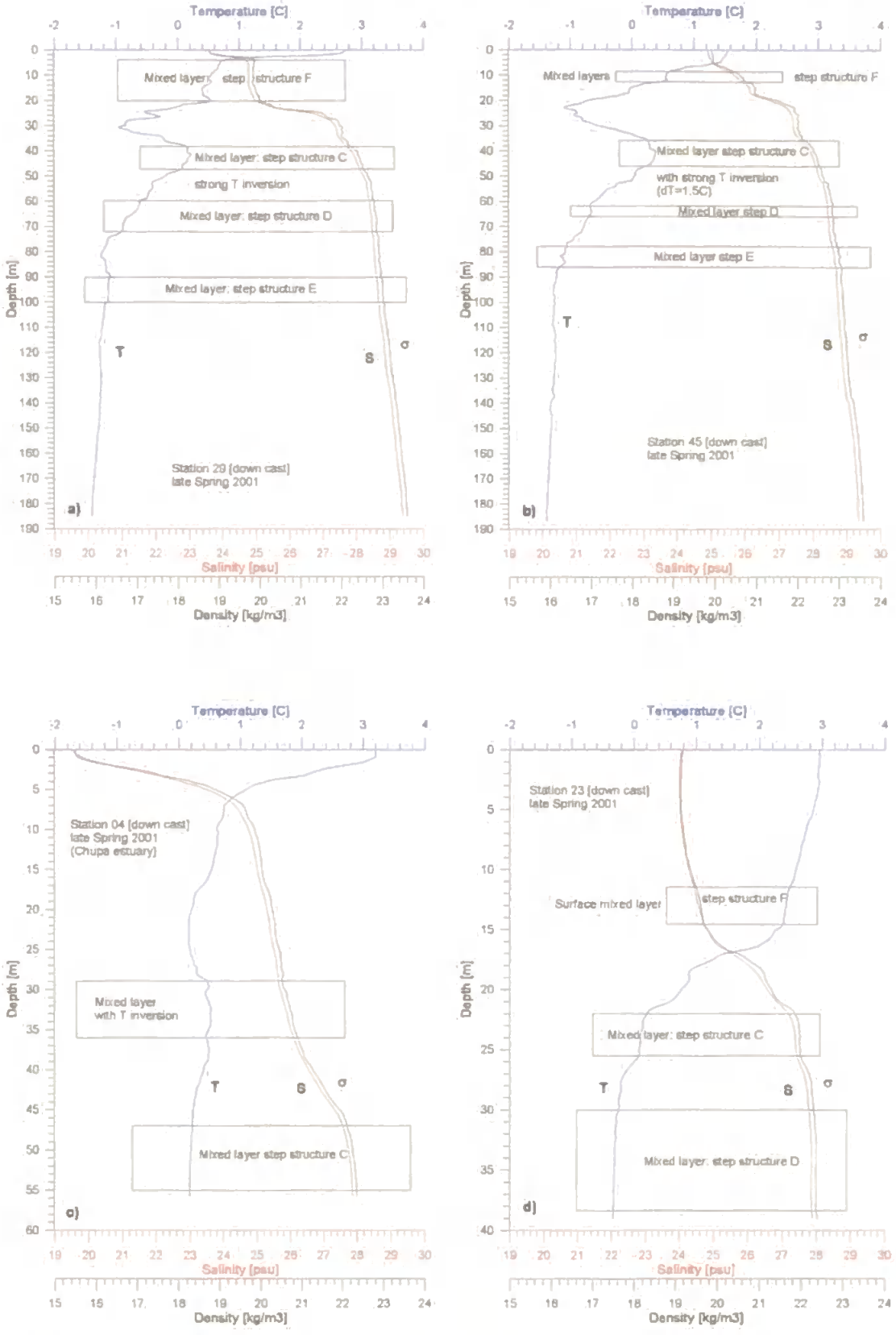


Figure 5.1: Vertical CTD profiles at stations (a) 29, (b) 45, (c) 04 and (d) 23 respectively during cruise 2001 in Kandalaksha Bay. Strong temperature inversions are seen within step structures indicating evidence of mixed layers and intrusion of water masses as previously observed in June 2000.

It is often observed that the bottom waters at these stations (with a maximum depth of 50 m) show similar characteristics to the step C identified in summer 2000. In the vertical profiles at the deepest stations (e.g. station 29) in Kandalaksha Bay, the thermocline is very pronounced: temperature decreases from 3° to -1°C in the first 30 m layers (figure 5.1a). The surface layers here are much colder in comparison with those in June 2000 (figure 4.1d) which show stronger temperature gradient of about 9°C observed in the first 30 m layers, due to a warmer surface occurring in summer. In the deepest part of the area, the profiles reveal numerous step-like structures in both upcast and downcast. Despite the fact that the surface layers show colder and denser values during the survey 2001 compared with the survey 2000, the step-like structures are nevertheless identified with similar characteristics as in the previous years (mainly referring to steps C, D, and E) although the mixed layers are slightly heavier waters at 30 m depth and deeper. However the mixed layer step C is an exception as it is well much denser in late spring 2001 than in June 2000, which shows the degree of contribution from the very coldest surface layers being free-iced generally in March. Furthermore, the process of ice melting in the surface layers emphasized the phenomenon of temperature inversion seen in the entire data set at depth between 40 and 50 m (figure 5.1b), which confirm the intrusion of relative warmer and saline water at such depth. The temperature inversion ranges from -1° to 0.4°C, and therefore is associated to the mixed layer identified as step C (June 2000), although more saline and denser. For example in Kandalaksha Bay (at station 38) a temperature inversion is observed within a step-like structure in the vertical profile between 44 and 50 m depths which correspond to the characteristic water mass of 0.4°C, 27.7 psu and 22.2 kg/m$^3$, in temperature, salinity and density respectively. The analysis of the characteristics of the step-like structures in the entire CTD profiles show a strong correlation with those identified from the previous survey in June 2000. In the following section, each step-like structure is analysed and compared with the previous survey 2000 to establish the variability of their structure through the water column and their distribution across the White Sea.

### 5.2.2. Identification of mixed layers: Steps

A visual analysis was made of the data set of the survey 2001 (56 CTD profiles) to investigate the shape of the mixed layers. The results clearly revealed 4 step-like structures in the vertical profiles recorded both from down and up cast measurements.

(1) The first mixed layer (called here step F) is observed in the surface layers (figure 5.1). The average depth location of the layer is at about 11 m with an average thickness of 5 m (table 5.1 in appendix C). The average thermohaline index characteristic of the surface mixed layer is 25 psu, 1.2°C and 20 kg/m$^3$ for salinity, temperature and density respectively. The mixed layer step F is fresh water with typical characteristics of river waters of Kandalaksha Bay and is present in all stations except those located in the south (such as in the Chupa estuary, which is too isolated from the adjacent Basin where surface mixing occurs resulting in the formation of the White Sea Surface Waters).

(2) The second observed quasi-homogeneous layer in the water column has similar characteristics to that of step C identified in survey 2000, which is named here step C 2001 (table 5.2 in appendix C). The step is found under the thermocline and predominant in the entire study area, even in the Chupa estuary. The average location and thickness of the mixed layer is about 36 m depth and about 7 m respectively. The mixed layer is identified by the characteristics of 27.6 psu, 0.1°C and 22.2 kg/m$^3$.

(3) The third homogeneous layer is observed beneath the former identified step C 2001 with remarkable similar characteristics to step D 2000, named here step D 2001. Its characteristics are shown in table 5.3 in appendix C. The vertical average position of the layer in the water column and its thickness are 55 m depth and about 9m respectively. The average characteristics of the mixed layer step D 2001 is 28.28 psu, -0.56°C and 22.7 kg/m$^3$. The step is also predominant at all stations deeper than 50 m.

(4) Finally the fourth and last evident step-like structure found underneath step D 2001, is named step E 2001. The mixed layer has the exact same average values in salinity (28.6 psu), temperature (-1°C) and density (23 kg/m$^3$) as in summer 2000 (table 5.4 in appendix C). The average vertical position of the layer is about 80 m depth with an average thickness of 13 m.

A number of horizontal distributions of water masses in Kandalaksha Bay/Basin area is drawn and analysed in the following section, to investigate oceanic features such as frontal zones and to study the variable extent of the mixed layers in Kandalaksha Bay, in particularly the intrusion of cold and saline water located in the active upper layers (0-60 m depth). Formation of dense water on the shelf in the bay is expected due to the presence of the mixed layer (step C 2001) slightly heavier than in June 2000 (table 5.I).

| Step A 2000 | Step F 2001 | Minimum values | | Maximum values | | Average values | |
|---|---|---|---|---|---|---|---|
| Salinity (psu) | | 25 | 23.5 | 27.2 | 26.1 | 26.06 | 25 |
| Temperature (°C) | | 1.5 | 0.1 | 7.8 | 2.7 | 4.16 | 1.22 |
| Density (kg/m$^3$) | | 19.6 | 19 | 21.6 | 20.9 | 20.64 | 20 |

| Step B 2000 | none | Minimum values | | Maximum values | | Average values | |
|---|---|---|---|---|---|---|---|
| Salinity (psu) | | 26.4 | | 27.3 | | 27 | |
| Temperature (°C) | | 1 | | 3 | | 2 | |
| Density (kg/m$^3$) | | 21 | | 21.75 | | 21.5 | |

| Step C 2000 | Step C 2001 | Minimum values | | Maximum values | | Average values | |
|---|---|---|---|---|---|---|---|
| Salinity (psu) | | 27.3 | 27.2 | 27.7 | 27.9 | 27.5 | 27.6 |
| Temperature (°C) | | 0 | -0.2 | 0.8 | 0.5 | 0.48 | 0.1 |
| Density (kg/m$^3$) | | 21.75 | 21.75 | 22.2 | 22.6 | 22 | 22.2 |

| Step D 2000 | Step D 2001 | Minimum values | | Maximum values | | Average values | |
|---|---|---|---|---|---|---|---|
| Salinity (psu) | | 27.8 | 27.85 | 28.4 | 28.5 | 28.2 | 28.28 |
| Temperature (°C) | | -0.8 | -0.8 | -0.4 | -0.2 | -0.6 | -0.56 |
| Density (kg/m$^3$) | | 22.3 | 22.3 | 22.8 | 22.93 | 22.6 | 22.7 |

| Step E 2000 | Step E 2001 | Minimum values | | Maximum values | | Average values | |
|---|---|---|---|---|---|---|---|
| Salinity (psu) | | 28.5 | 28.4 | 28.9 | 28.7 | 28.66 | 28.56 |
| Temperature (°C) | | -1.2 | -1.2 | -0.9 | -0.9 | -1 | -1.08 |
| Density (kg/m$^3$) | | 22.9 | 22.8 | 23.2 | 23 | 23 | 22.94 |

Table 5.I: thermohaline values recorded for the mixed layers observed during cruise 2000 and cruise 2001.

### 5.2.3. Distribution of water masses

In the surface layers at 5 m (figure 5.2a) slight saline (24.8 to 25.2 psu) and cold (1.2°C) water occupies the broader part of Kandalaksha Bay (above the trough), whereas the narrow parts of the Bay which consist of estuaries, rivers, and shallow coastal area are filled with relatively warm fresh water (< 24.2 psu and ~3°C). A clear front zone arises as a result of the two different water masses, located seaward and north of the Chupa estuary at 66.5°N latitude and 33.7°E longitude. The values of temperature and salinity gradient are ~2.5°C and 0.8 psu respectively. It is interesting to note just east of the front zone, a distinct patch of warm and fresh water probably coming from the river Pulskyia.

In the section below at 10 m depth (figure 5.2b), the above features are enhanced: coldest (about 0.2°C) and saline (25.4 to 25.8 psu) water fills the layer of the bay, whereas coastal areas (isobaths < 50 m depth) remain with the same index of fresh waters. On the north coast, near the river Pulskyia, the patch of warm and fresh water is still observed, as well as the front separating saline water from coastal water of Kandalaksha Bay. Saline and cold water is revealed down stream the Chupa estuary and extend inside the bay.

In the 20 m depth section (figure 5.2c), the distribution of temperature and salinity reveal dense waters on the coastal shelf in the northern part of Kandalaksha Bay with a salinity of 27.4 psu and a temperature of about 0°C (step C 2001). The distribution of such cold and saline water shows elongated structure across the steep slope at 3 different locations along the north coast. The salinity ranges from about 26.6 psu and temperature > 0°C in the centre of the Bay, changing to 27.7 psu and temperature < 0°C along the coastal area. On the other hand, less saline (25.8 to 26.6 psu) and still relative warm waters (from 0.2 to 1°C) compared to the surrounding waters, occupies the southern coast of Kandalaksha Bay. The separation of these water masses is evident with the thermal front still observed in the same shallow area.

Remarkably the next horizontal section at 30 m depth (figure 5.2d) shows dense water on the shallow shelf in the far north region of Kandalaksha Bay with highest salinity of 27.8 psu and a temperature of about -0.2°C (step C 2001). The dense water is surrounded by relative fresh coastal waters (salinity of less than 27.4 psu) with temperature > 0°C. The freshest water is observed in the Chupa estuary, therefore showing a saline front across the shelf at the mouth of the estuary.

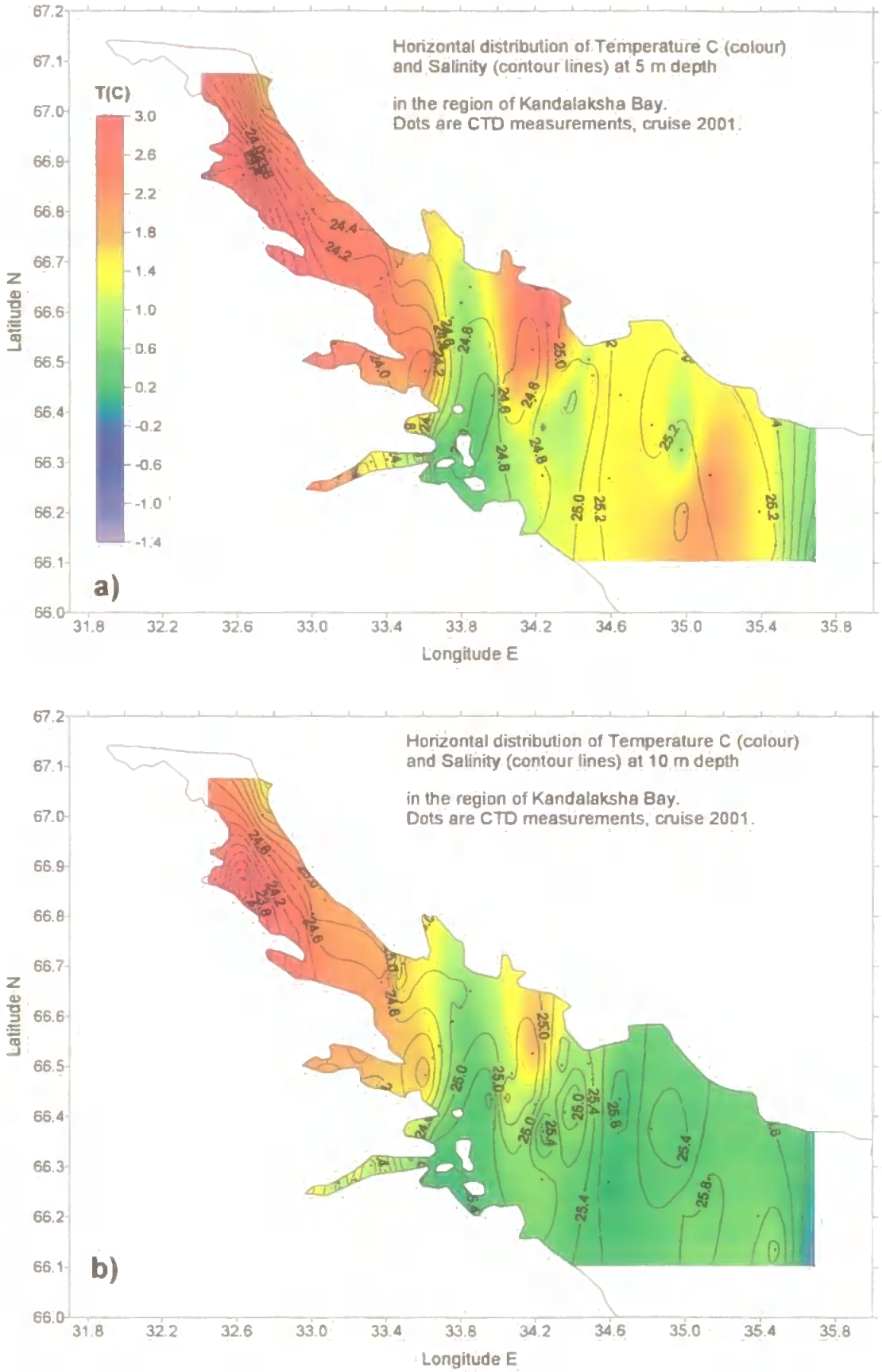


Figure 5.2: Horizontal distribution of temperature (image colour) and salinity (contour lines) at (a) 5m and (b) 10m depth in Kandalaksha Bay, cruise 2001.

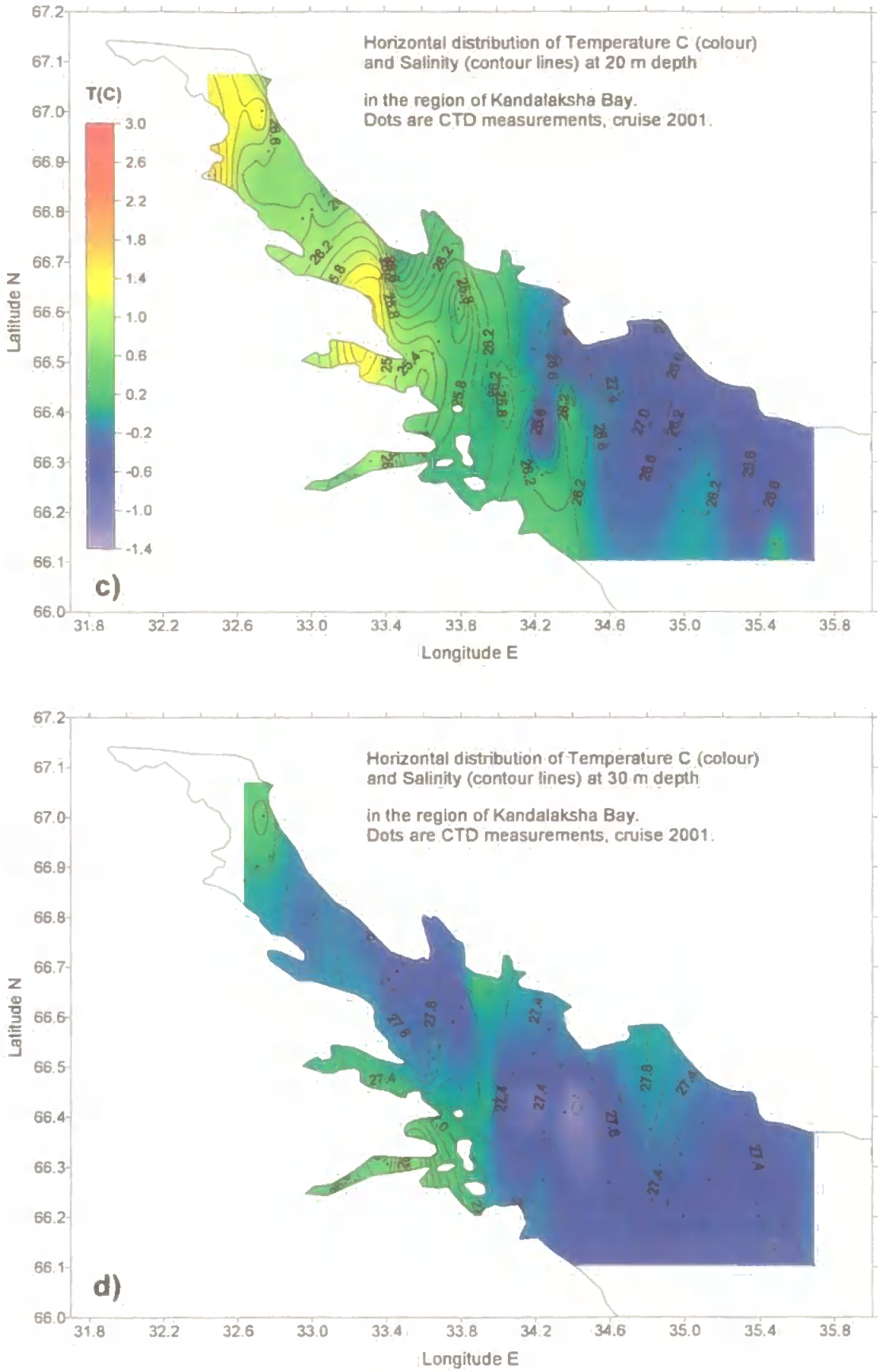


Figure 5.2: Horizontal distribution of temperature (image colour) and salinity (contours) at (c) 20m and (d) 30m depth in Kandalaksha Bay, cruise 2001.

The striking feature revealed in figure 5.2d is the bay filled with saline (27.4 psu) and cold (-0.4°C) water with some patches of relative saline but warmer water on the north coast. The contrast of water masses seen from the temperature distribution at 30 m (figure 5.2d) and the section at 45 m depth (figure 5.2e) is remarkable. The water in the bay is colder at 30 m than at 45 m and the structure of the density is stable because of very saline water at 45 m. The figures denote that a temperature inversion has occurred, regarded as an intrusion of relative warmer and saltier water at 45 m depth, as is shown on CTD profiles at stations 29 and 45 (figure 5.1a,b). The horizontal distribution of water mass at 45m depth shows distinct variations in salinity which has reached 28 psu and a temperature of ~0.3°C in the southwest area of the bay. The heavy water on the other hand is located in the northeast region characterized by salinity 28.3 psu and temperature -0.4°C. As it is noticed in the previous horizontal sections at 20 m and 30 m depth (figure 5.2c and 5.2d), relative dense water were observed in the same local areas. These coastal areas should be therefore regarded as potential regions (see arrows in figure 5.2e) where dense shelf water may be locally formed, and possible cascading events may occur, facilitated by the steep slope of Kandalaksha Bay.

Finally the 60m section (figure 5.2f) confirms that the heavy water is located all along the north coast of Kandalaksha Bay (identified by 28.5 psu and -0.5°C). The plot also shows a frontal zone located in the Chupa estuary displaying fresh water interacting with the intrusion of saline water now occupying the bottom layer at midway of the estuary. The results of the water mass distribution during the survey 2001 have clearly shown a penetration process of cold and saline water in the 30-50 m layers. Because the survey 2000 showed an oscillating "disturbance" in the structure of the saline mixed layer, the shape of the steps in 2001 are therefore investigated.

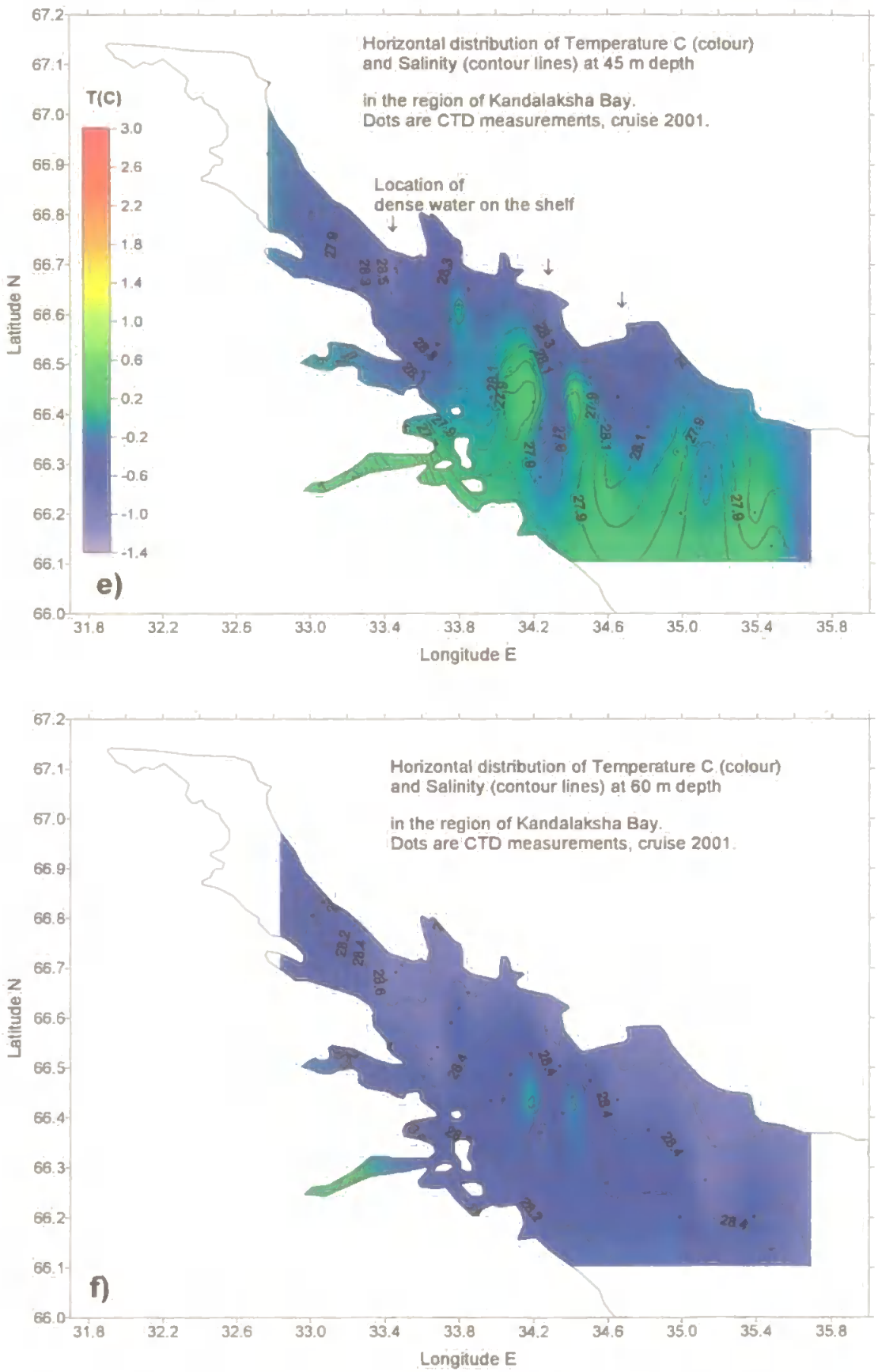


Figure 5.2: Horizontal distribution of temperature (image colour) and salinity (contours) at (e) 45m and (f) 60m depth in Kandalaksha Bay, cruise 2001.

### 5.2.4. The shape of the mixed layers

Two transects AC and AE2 (figure 5.3a and 5.3b) are used to investigate the vertical structure of the steps in 2001. Transect AC is located entirely across Kandalaksha Bay, whereas transect AE2 is located further onshore near the north coast of the Bay (see figure 3.3).

Oscillations in the depth of the mixed layers are clearly shown in figure 5.3a and 5.3b. The oscillations are evident for all the steps in the intermediate layers (~20 to 100 m) although the step F has very small amplitude. Near the coast (figure 5.3b), the oscillations have the form of sinusoidal curves (see steps C, D and E). On the same transect the mixed-layer step E exhibits a sinusoidal curve with a wavelength of ~32km and an amplitude of ~10 m. In the longest transect (figure 5.3a) the sinusoidal-shape of the mixed-layer (step E) has doubled in wavelength (about 69 km) but has the same amplitude. The physical origin for such observed distribution of mixed-layers in the water column may be related to either the presence of mesoscale eddies, inertial oscillations, or internal waves. The hypothesis of internal wave generation should be treated with caution because for example eddy effects were often misinterpreted as internal wave noise (LeBlond and Mysak, 1978; Pond and Pickard, 1983). However, internal waves may exist in the White Sea. A numerical study of the tidal circulation in the White Sea (Semenov and Luneva, 1999), although criticized due to a lack of high resolution observational data, showed that in the deep-water part of the White Sea (100 m depth and more), the interaction between tidal waves (important in the Voronka and the Gorlo Strait) and the relief at the entrance of the White Sea leads to the generation of intense internal waves in the semi-enclosed sea. If internal waves were present in the White Sea, they may be also responsible for mass transport (Inall *et al.*, 2001), lee-wave generation (Vlasenko *et al.*, 2002) or sediment transport and mixing (Shapiro *et al.*, 2000).

The hydrological results of the 2001 survey conducted in Kandalaksha Bay/Basin area has shown remarkable similarities with the former survey in 2000 in the identification of the steps (table 5.I), their structures and distribution. It suggests that the mixed layers might be inter-seasonal or permanent features in the White Sea (see table 5.I). It is of interest to compare the present case with previous oceanographic surveys (cruise 1991; Gidrometeorologiya, 1991) and clarify whether or not the mixed layers associated to the saline and cold intrusion are a persistent feature in the White Sea.

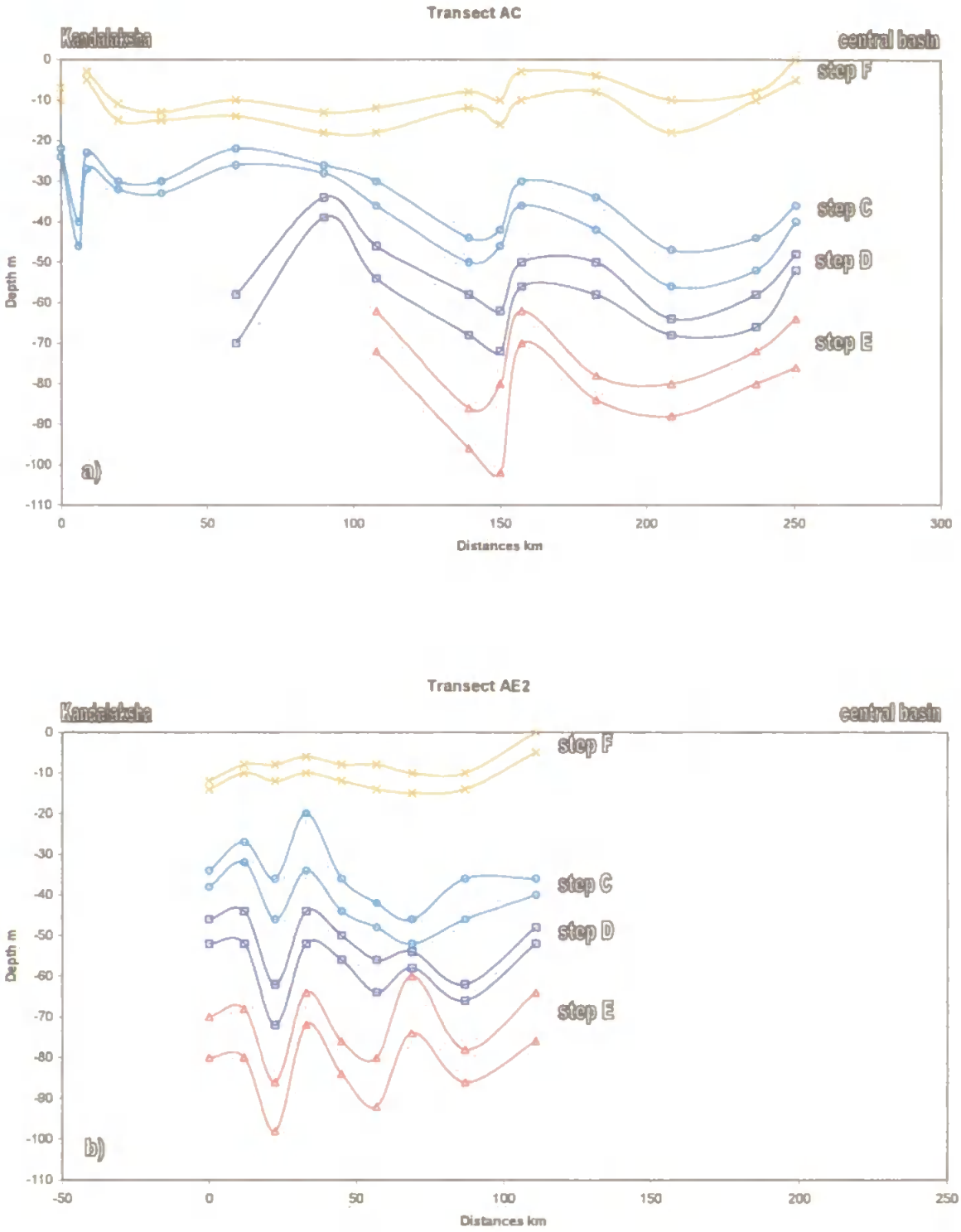


Figure 5.3: Vertical location and thickness of mixed layers observed in Kandalaksha Bay region and adjacent to the Basin at (a) transect AC (middle of Kandalaksha Bay) and (b) transect AE2 (north coast of the Bay). The charts show similar oscillating patterns from summer 2000 within the thickness of the steps F, C, D and E, cruise 2001.

## 5.3. Inter-seasonal comparison of water structure

The variability in the structures of water masses within step-like structures in the northern part of the White Sea is discussed here, including results from a previous data-set (survey 1991, Gidrometeorologiya, 1991). Although the CTD profiles obtained during the survey 1991 are of coarser vertical resolution (and furthermore bin-averaged each metre), the water masses are well identified enough for comparative analysis and the interlaying process can be observed via contours of transects. This section covers the following points: the thermohaline intrusion, the formation of dense water with possibility of cascading events, and finally the domed structure observed in the intermediate layers with isopycnal oscillations observed in the deep water of the White Sea.

### 5.3.1. A persistent thermohaline intrusion

The comparison of water masses and the core of mixed layers using T-S diagrams during the surveys 1991, 2000 and 2001 is addressed here by looking at four key-areas in the northern part of the White Sea: (a) southwest of the Gorlo Strait (figure 5.4a), (b) in the Basin offshore Terskii (figure 5.4b), (c) in the deepest part of Basin (figure 5.4c), and (d) in Kandalaksha Bay (figure 5.4d). On the T-S plots, the core of the mixed layers is revealed by the accumulation (or clusters) of marked symbols (identifying every measurements recorded in the water column), whereas sharp gradients are identified by distant (or sparse) symbols.

(a) In the southwest of Gorlo and off Dvina Bay (figure 5.4a), station 59 (summer 1991), although located further south in Dvina Bay, shows the DBW fresher and warmer (23 psu and 9°C), whereas station 53 (summer 2000) records salinity 25 psu and about 6°C in temperature. Beneath the surface layers, a thermal gradient (temperature decreasing from 5° to 1.5°C) is observed with constant salinity 26 psu. Vertical quasi-homogeneous water (Steps) were observed underneath the thermocline in summer 2000 (figure 4.6) suggesting fine mixed layers to form due to mixing with fresh surface waters. The TS curve at station 59 (figure 5.4a) here suggests such presence of mixing (at 11 m depth) with inferred water masses involved in the mixing (such as the Dvina Bay Waters and the White Sea Surface Waters), which result in a salinity and a temperature of about < 26 psu and 1.5°C respectively.

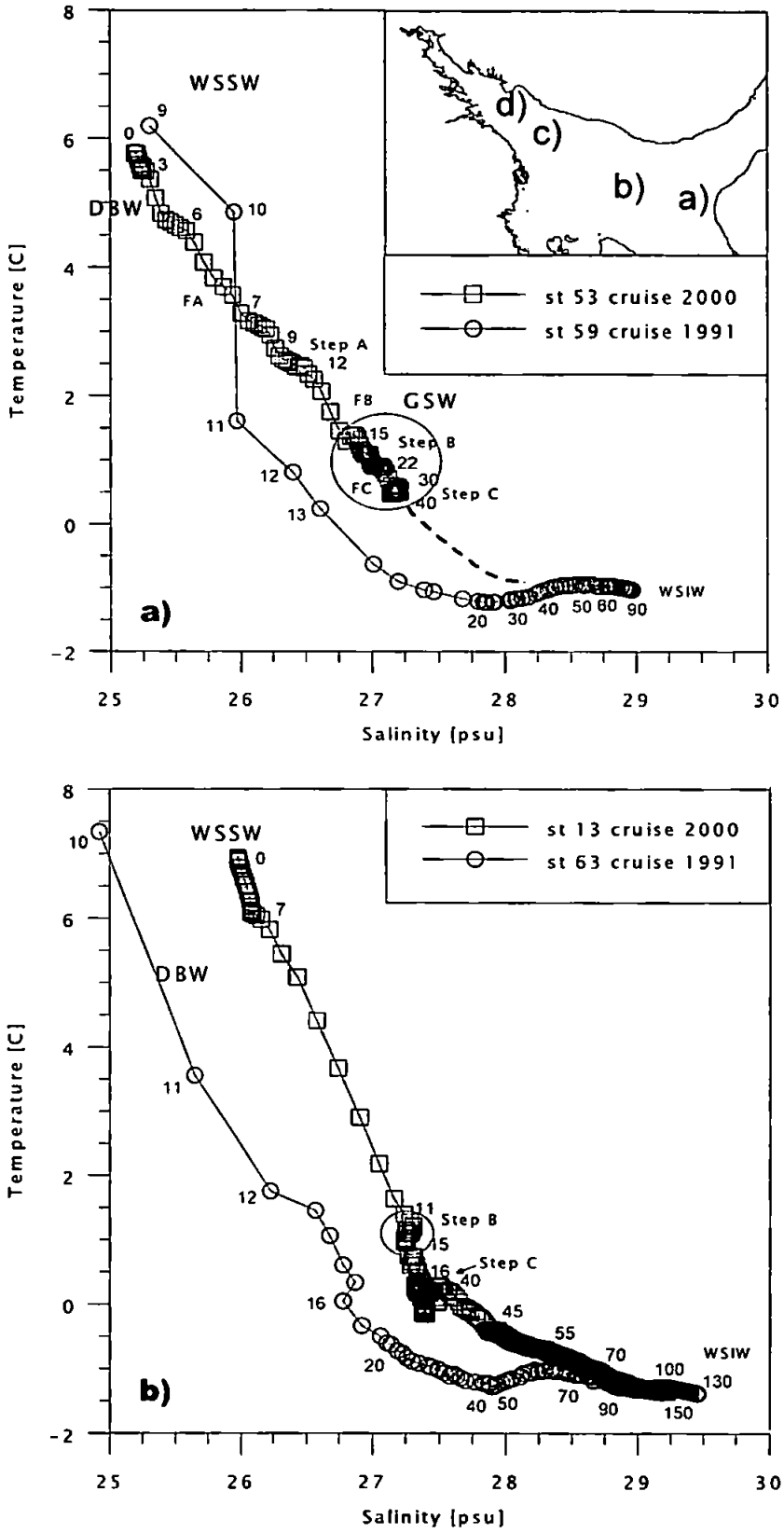


Figure 5.4: Comparison of water masses (a) during survey 1991, 2000 and 2001 at four selected location (a, b, c, d) in the White Sea using T-S diagram (a) south-west of Gorlo, and (b) in the Basin. Stations 53 (a) located on the shelf edge of Gorlo does not show the WSIW (broken lines) as shown at station 59, which is located on the shallow shelf slope. Clusters of symbols (dark points) represent quasi-homogeneous layers (steps) whereas sparse symbols show sharp thermohaline gradients. Numbers represent depth in metre.

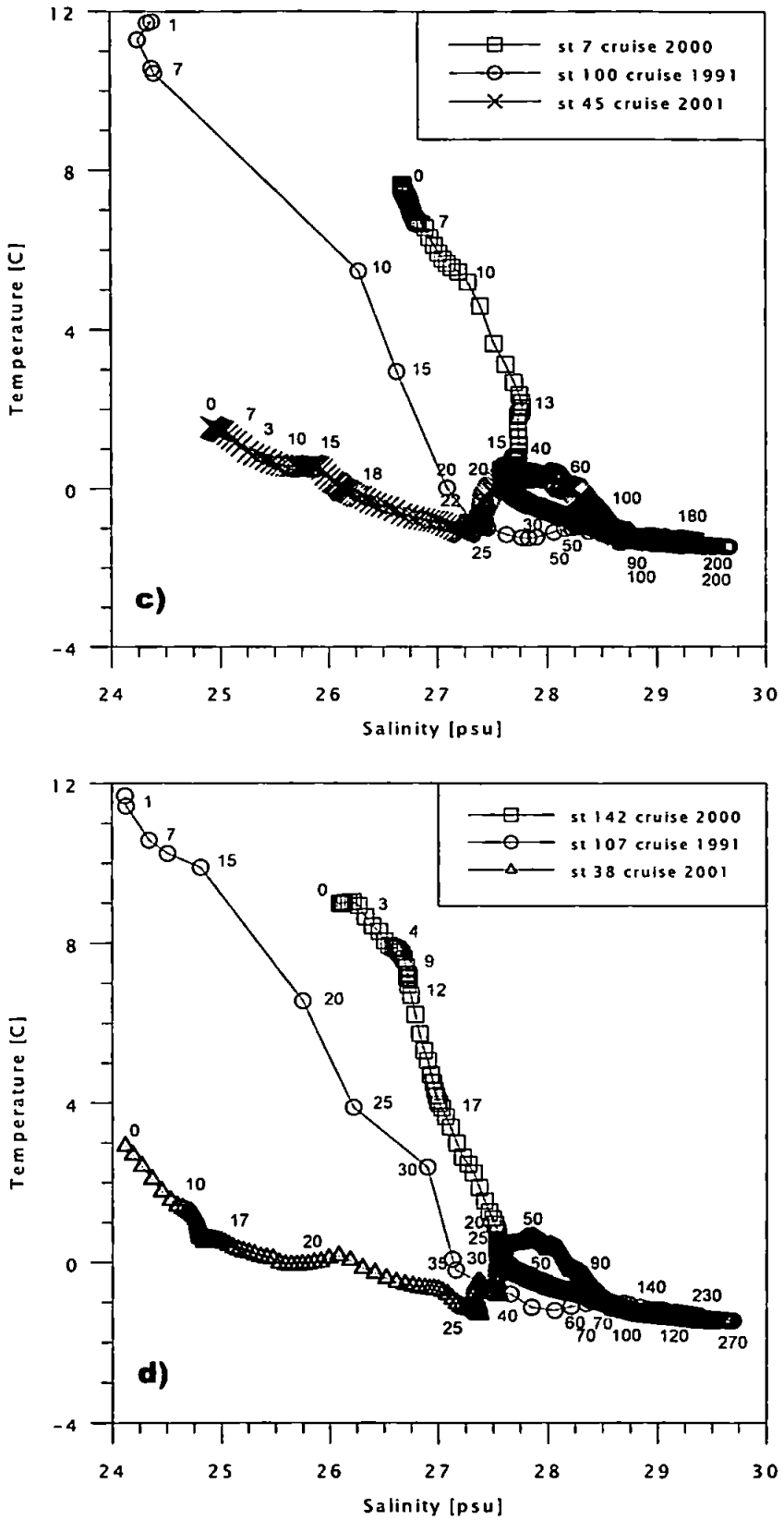


Figure 5.4: Comparison of water masses (a) during survey 1991, 2000 and 2001 at four selected location (a, b, c, d) in the White Sea using T-S diagram (c) in the Basin adjacent to Kandalaksha Bay and (d) in Kandalaksha Bay. Clusters of symbols represent quasi-homogeneous layers whereas sparse symbols show sharp thermohaline gradients. Numbers represent depth in metre.

The poor vertical resolution in the 1991 profiles does not allow the detection of the core of mixed layers, although in the T-S profile (figure 5.4a) the curve indicates a deflection towards a core water mass which has been identified as a step-like structure in the surface layer in summer 2000 (9-12 m in figure 5.4a) and also in 2001 (table 5.I), showing a salinity of ~26 psu and a temperature of ~1.5°C (at 11 m depth). This emphasises the fact that formation of fine structures has occurred in the surface layers. In the bottom layers, the index of the identified White Sea Intermediate Water mass (WSIW) is observed at station 59 (summer 1991) which is found slightly deeper compared with that of station 53 (summer 2000).

(**b**) In the Basin (figure 5.4b), the water column at station 63 in summer 1991 shows more freshness than in summer 2000. Both T-S curves display quasi-homogeneous water in the surface layers seen by the accumulation of symbols (0-7 m or 11-15 m depth at station 13, summer 2000). In summer 2000 the measurements show a mixed surface water of salinity 26 psu and 6-7°C (0-7 m depth), whereas in summer 1991, the index were 25 psu and about 8°C (at 10 m depth). Underneath the thermocline, the TS points at the two stations show a mixing zone (at 12-16 m depth in 1991 and at 11-15 m depth in 2000) which result in a core water mass of salinity ~26.8 psu and temperature 1°C. This mixed water mass is recognised as the step B identified in summer 2000. The next mixed layer (step C) which is present in the profile 2000 (at 16-40 m depth) is also observed here in profile 1991 with colder values (between 20-40 m depth). Both stations have also the exact bottom water mass of salinity 28.5 to 29.5 psu and temperature -1 to -1.5°C identified as the WSIW. This water mass can be associated as the core of the mixed layer (step E summer 2000 and 2001, see table 5.I) formed on the slope (between 60-150 m depth) just offshore the entrance of the White Sea.

(**c**) In the deepest part of Kandalaksha Bay, the three T-S curves (figure 5.4c) show a water mass involved in the mixing process occurring at 30 m depth. The three measurements show a fine homogeneous layer at the surface, which is the mixed layer associated with the WSSW. The surface mixed layer (0-7 m) has respectively salinity and temperature of 24.5 psu and 10-12°C in 1991, 26.7 psu and 7-8°C in 2000 and, 25 psu and 1-2°C in 2001. Other steps are obvious in the T-S plot at station 2001 with the clear intrusion of the water mass identified by salinity 27.7 psu and T ~1°C, notably the mixing zone which appears in the data 2000 and also in the data 1991, revealing a much colder water (about -1°C), recognised as step E, the WSIW.

(d) Finally, further north-east near the north coast of Kandalaksha Bay, at station 38 (in 2001) the T-S diagram clearly shows the water mass intrusion of salinity 27.5 psu and temperature ranging from 0.5 to 1°C. In 2000, the intrusion had a water slightly fresher and colder (27.5 psu and 0°C), whereas in 1991 the water mass had salinity 27 to 27.5 psu and temperature -0.5°C. Steps are also present at the surface depicted by the accumulation of T-S points (symbols) at 10-17 m depth (at station 38 in 2001).

Mixed layers are evident in summer 2000 and 2001 but less obvious in 1991 because of the poor vertical resolution of the CTD profiles, although core of mixed layers are well identified in figure 5.4b, which shows some mixing zone of the transformed GSW. Nevertheless the data-set has shown that there is evidence of such fine mixing processes occurring every year, observed in form of layers with relatively small variations in their characteristics, in particularly the formation and intrusion of the 20-40 m mixed layers. The physical process of mixing, generating that particular layer, originates from the interaction of the intrusion of the transformed GSW with overlying waters. The circulation of this intrusion is, however, not clear although it originates in the southwest part of Gorlo Strait (figure 4.6). Other step-like structures are observed deeper (such as step D and E) and they may be related to the general circulation of the Basin which brings water mass in contact notably between the intermediate waters from the White Sea Bays and the vertically mixed water originating on the shallow slope of the Gorlo Strait. It is interesting to compare the hydrographic transects in 2001 (located in Kandalaksha Bay) with that of 1991 (in the Basin and in Kandalaksha Bay). This would complement the interannual identification of water mass signatures depicted on the east-west transect 2000 (figure 4.6). The transect 2001 (figure 5.5a) along the Kandalaksha Bay reveals an elongated water mass at 40m depth which corresponds to the intrusion of saline water which was characterized in transect 2000 by the contours of salinity 27.25 to 27.75 psu, and temperature 0.3 to -0.1°C. The water mass is present in the bottom layers of the coastal areas of Kandalaksha Bay between 40 to 60 m depth in 2001 in the same manner as it is in 2000. However, it is interesting to see that the intrusion (at stations 30 to 46 in transect 2001) is situated in deeper layers than in June 2000 (situated at only 20m depth). Formation of surface waters in the Bay (WSSW) can be traced by the mixed layer identified by Step F in summer 2001, which has contours of salinity 24.75 to 26 psu and temperature of 0.8 to 2°C (figure 5.5a).

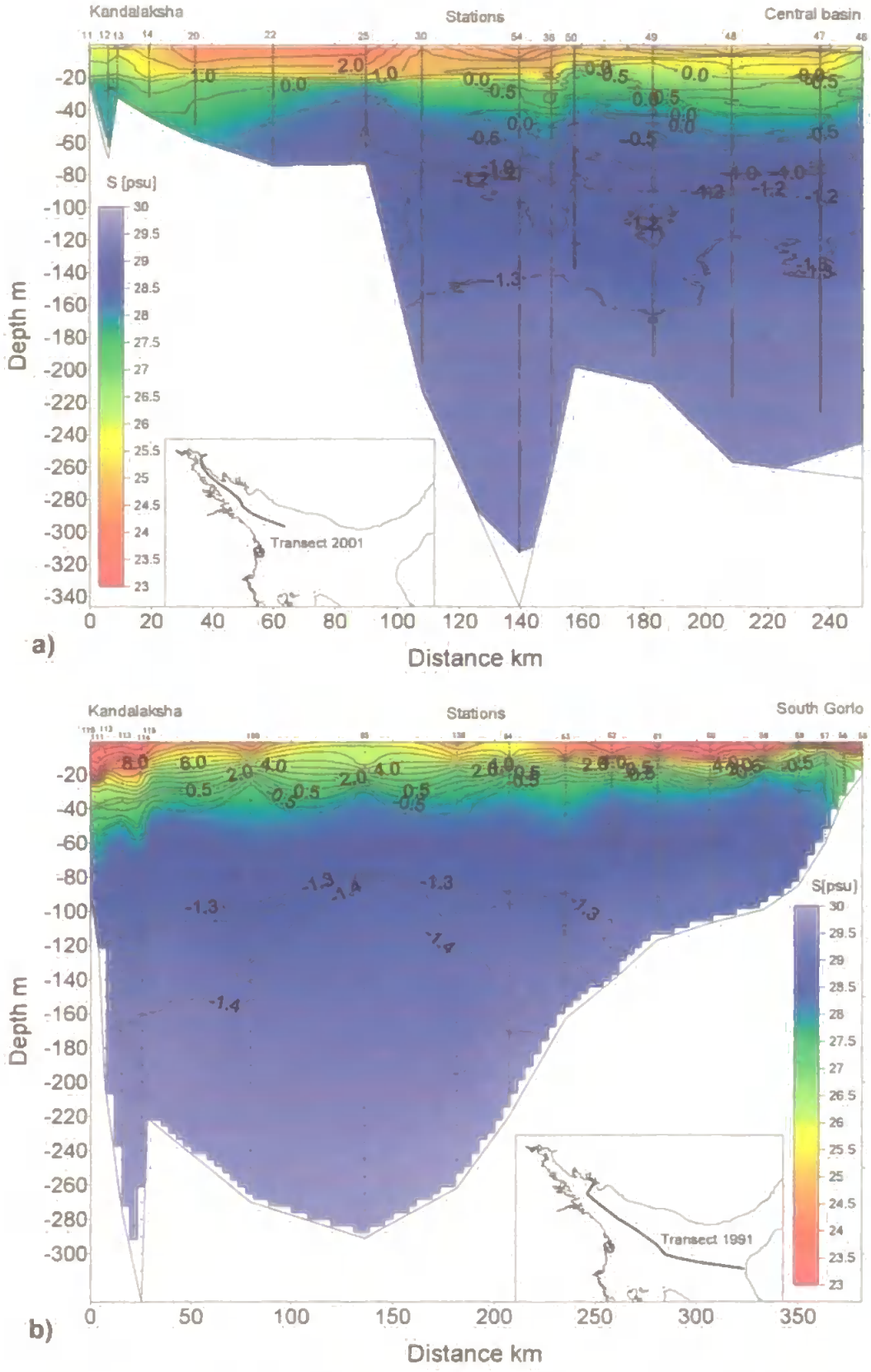


Figure 5.5: Vertical section of Temperature (contours) and salinity (colour) along the (a) east-west transect 2001 and the (b) east-west transect 1991. Note the dome shape of isotherm -1.3°C (b) in the Basin (st 95) and (a) oscillating near Kandalaksha Bay with the sinking isotherm -1.2°C along the steep shelf slope.

This water mass comes from rivers, particularly from the Kolvitsa River (stations 11, 12, 13; see figure 3.3), and extends from east to west into the centre of the Bay in the first 10 m layers.

In summer 1991, the same index of water mass for the identified mixed layer (step C) observed in 2000 is revealed by contours of salinity (27 to 27.5 psu) and temperature (0.5 to 2°C) in the east-west Transect 1991 (figure 5.5b). The signature of this water mass along that transect is remarkably similar to that of summer 2000. The water is vertically mixed south of the Gorlo Strait between 20 and 40 m depth on the slope and propagates in a thin layer. A rough estimation of its thickness is 10 m, but thinner in the Basin, located in the 30 m depth within an oscillating structure. The mixed surface water mass step A (figure 4.6) associated with the WSSW is also observed in the Basin in summer 1991, with contours of salinity 25-26 psu and temperatures 7-8°C (figure 5.5b). Off Dvina Bay and south of Gorlo, the layer is observed in the first 10 m layers (at stations 55 to 63), then the layer rises to the surface forming the WSSW in the Basin (at stations 64 to 100 along the transect 1991 in figure 5.5b). On the other end, east of the transect, the water mass is seen in the bottom coastal area of Kandalaksha Bay at about 20 m depth and the thermohaline contours rise to the surface from the Bay to Basin (at stations 114, 115, 100). The possibility of rising isopycnals may be due to the presence of an eddy located in the Basin.

| Comparison of the intrusion of the modified GSW. | 1991 | 2000 | 2001 |
|---|---|---|---|
| Step B | (b) at 12-16m depth<br>~1°C; 26.8 psu | (b) at 11-15m depth<br>~1°C; 27.2 psu | (c) at 10-15m depth<br>~1°C; 26 psu |
| Step C | (b) at 20-40m depth<br>~-1°C; 27.5 psu<br><br>(c) at 30-40m depth<br>~-1°C; 27.7 psu<br><br>(d) at ~50m depth<br>-1° to 1°C; 27.5 to 28 psu | (b) at 16-40m depth<br>0°C; 27.5 psu<br><br>(c) at 15-25m depth<br>0.5°C; 27.5 psu<br><br>(d) at ~50m depth<br>-1° to 1°C; 27.5 to 28 psu | (c) at 35-45m depth<br>0.4°C; 27.8 psu<br><br>(d) at ~50m depth<br>-1° to 1°C; 27.5 to 28 psu |

Table 5.II: Comparison of the characteristics of mixed water mass (steps B, C) in the water column seen as an intrusion of the modified GSW in the northern part of the White Sea. Bold characters (b,c,d) indicate the location of the measurements in the White Sea (see figure 5.4a, insert) for the three data-set (1991, 2000, 2001).

The three surveys have shown the evident and persistent intrusion of the vertically mixed water formed in the southwest part of the Gorlo Strait, caused by topographic stirring and strong tides (see table 5.II). The mixed water circulates in thin layers in the northern White Sea between 30 and 40 m depth and down to 50 m in the region of Kandalaksha Bay. The formation of the WSSW was also seen and evident in the Basin caused by advection of fresh waters from the White Sea Bays, in particular from Dvina and Kandalaksha Bay. The formation of such saline mixed layers and their elongation in the northern White Sea has an important impact for the water renewal of the semi-enclosed sea. Formation of dense water on the shelf of Kandalaksha Bay may result from the advection of such mixed saline layers, and may cascade into the deepest part of the White Sea.

### 5.3.2. Dense water formed on the coastal slopes of Kandalaksha Bay

According to Timonov, the intrusion of saline water from the Barents Sea flowing through the Gorlo Strait should protrude down slope into the deep part of the White Sea (figure 2.2). However it is not the case here in the west part of the Gorlo Strait since the data from survey 2000 has not shown any evidence of such cascading event inferred by oceanographers. No dense water was actually observed on the shelf and the slopes south-west of the Gorlo Strait despite the dense coverage of stations in that region during the survey 2000 (figure 4.6). This was not even observed in the hydrographic transect in 1991 (figure 5.5b). Instead of water cascading into the Basin, the results show a persistent intermediate boundary layer in the form of a domed structure occupying the entire Basin of the White Sea. The boundary layer is recognised as one of the observed mixed layers (shown from surveys 1991, 2000 and 2001). The intermediate boundary layer is seen at depth varying from 80-90 m to 120-140 m which separates the upper active layers (from 0 to 60 m) penetrating further down the water column from the stagnant water of the White Sea lying at the bottom of the Basin.

The physical process to explain the water renewal in the White Sea, according to the results of the study here from the three different surveys (figure 4.6 and figures 5.5a,b), is the persistent intrusion of saline water onto the shallow coastal slopes of Kandalaksha Bay, which is the coldest area of the White Sea therefore facilitating the formation of the excess of dense water (see Shapiro *et al.*, 2004). Dense water on the shelf is formed there since the winter convection in that area reaches quickly the 40-50 m bottom depth (Timonov, 1950; Pantiulin, 1974). The mixed layers such as Step D and E in June 2000

(figure 4.6) were found along the steep slope of Kandalaksha Bay slipping down, originally formed on the shallow slopes by vertical mixing south-west of the Gorlo Strait. This observation strongly suggested a possible deep water renewal mechanism (figure 4.8) in the White Sea as the identified intrusion of the modified GSW in thin elongated layer reveals deposition of saline water on the shelf of Kandalaksha Bay. Cascading events are therefore likely to occur with the formation of dense water on the north-eastern shelf of the White Sea rather than on its western part.

For example, in the Chupa estuary, in summer 1991 (figure 5.6a) formation of relatively dense water is observed on the slope at the head of the estuary (at stations 120 and 121) between 40 and 60 m depth, denoted by contours of salinity 26 psu and temperature 0.5°C. Formation of dense water along-slope has been documented by Shapiro and Hill (1997) with similar water structures protruding down-slope. In the transect 1991 (figure 5.6a) similar thermohaline characteristics and structure of the mixed layers (very thin layer in the first 20 m depth) known as step A (in summer 2000) or step F (in summer 2001) are observed. Contours suggest that the water has intruded into the head of the estuary and occupies the bottom layers with salinity 25.5-26 psu. Colder temperature such as 0.5°C may facilitate dense water with salinity 26 psu and more on the slope of the Chupa estuary. Formation of such dense water on the same slope at 30 m to 40 m (at station 6 and 7) in transect 2001 (figure 5.6b) are observed with contours of salinity 26.75-27 psu and temperatures of 0.5°C and less. The results indicate that cascading events are likely to occur at the mouth of the Chupa estuary with the salt water deposit seen at the bottom layers. Mixed layers are intruding the mouth of the estuary providing the salt deposit, whereas colder temperature at these depths triggers the formation of dense water along the slope.

On the shelf edge in Kandalaksha Bay, south of transect G3 in summer 2000 (figure 5.6c), the water mass has a salinity of 27.5 to 27.8 psu and temperatures of 1.2 to 0.4°C on the slope between 35 m and 55 m depth. No descent water is observed here. However, south of the same transect in late spring 2001 (figure 5.6d), the water mass on the slope (between 65m and 75m depth at station 24 and 25) has a salinity of 28.5 to 28.65 psu and a temperature of -0.5 to -1°C. Contours of salinity 28.65 psu and more show water descending alongslope close to 90m depth with contours of 28.7 psu and -1.05°C in salinity and temperature respectively.

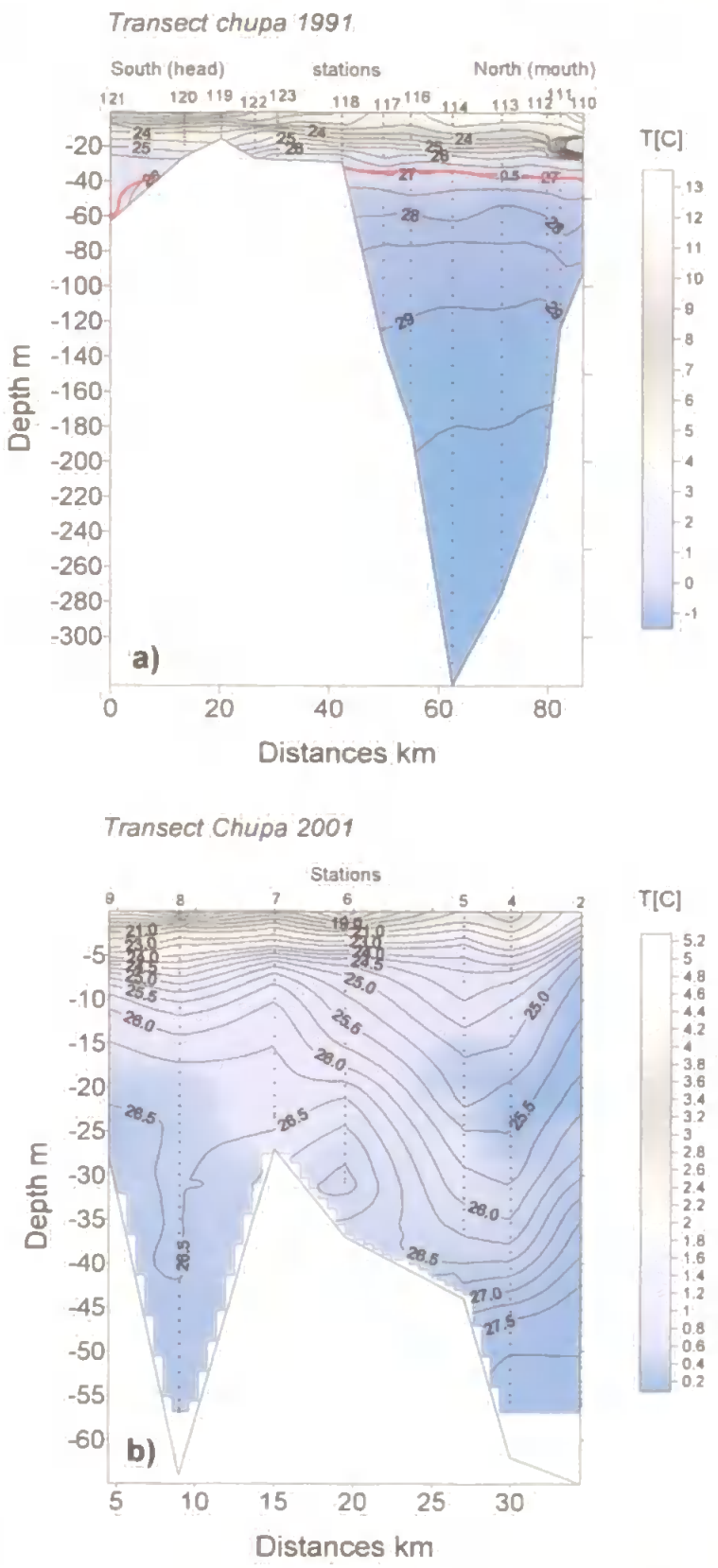


Figure 5.6: Contours of Salinity superposed with temperature image map along transect Chupa estuary (a) during cruise 1991 and (b) during cruise 2001. Note the water mass (isotherm 0.5°C, S=27) propagating at 20m (a) and at 30m (b) with formation of lens head of the estuary.

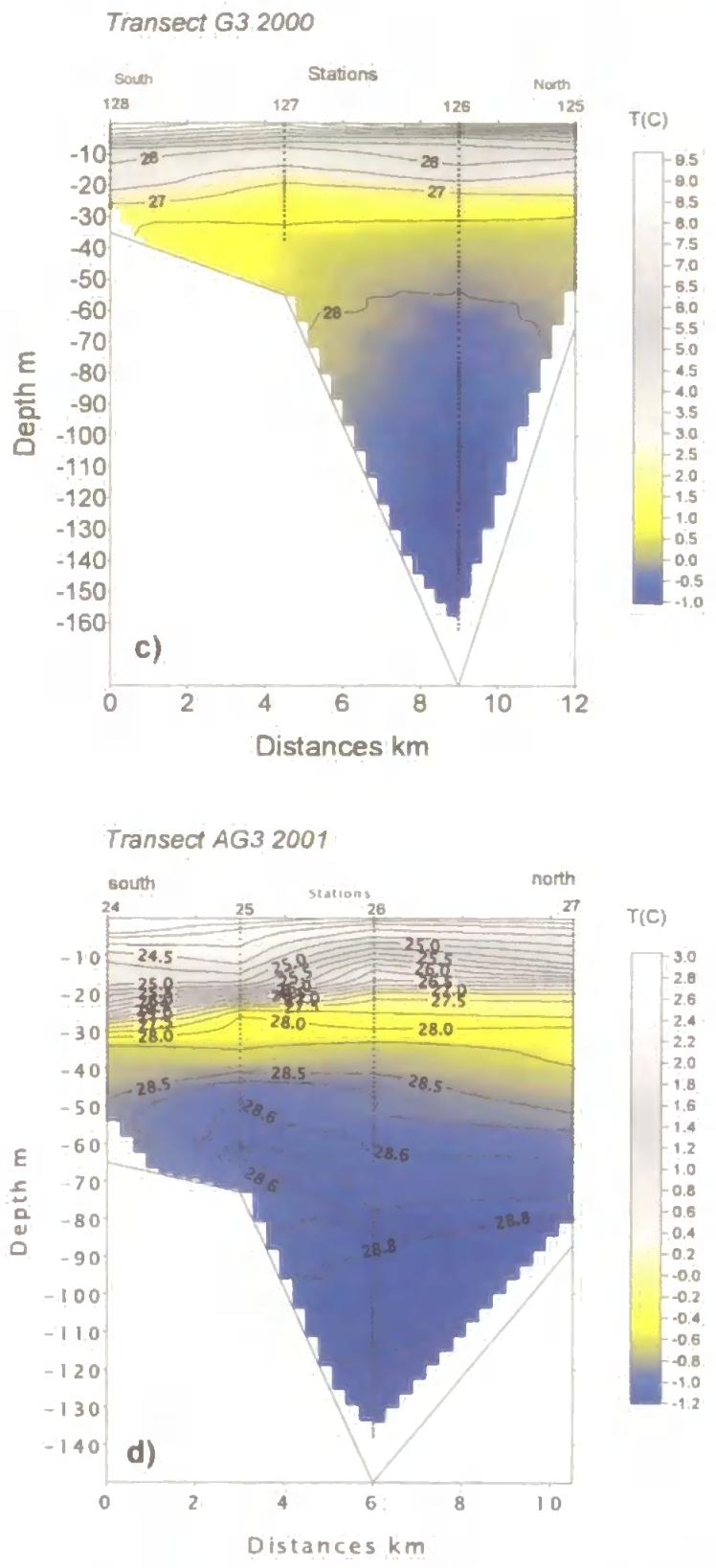


Figure 5.6: Contours of Salinity superposed with temperature image map (c) along transect G3 during cruise 2000 and (d) along transect AG3 during cruise 2001

The feature from the comparison of the hydrology in the study area for the two surveys 2000 and 2001 is the saline intrusion with salinity contours of 28-28.5 psu and temperatures of 0 to -0.8°C, at 30-40 m depth during survey 2001. The intrusion is found much deeper during June 2000 (at station 126) at depth between 70 m and 110 m.

Further on the shelf, south of transect G4 (figure 5.6e), the intrusion in the 20-40 m layers (stations 121 and 122) have a saline water of 26.5-27.25 psu whereas in late spring 2001 (figure 5.6f) the mixed layer has increased in salinity to 27.2-28 psu. Below that depth, clear observation of dense water is formed alongslope between 50 and 80 m in late spring 2001. It shows coldest temperature of -0.5°C matching salinity contour 28 psu, with the highest salinity 28.2 psu (and coldest temperature of -0.65°C) located on the slope in the core of the dense water. The shape of the along-slope dense water has the characteristics of '*head-up*' lenses as documented in Shapiro and Hill (2003).

Moving further into Kandalaksha Bay with transect G5 (figure 5.6g), the intrusion of the identified water (step C: 27.5 psu, 0.5°C) in summer 2000 occupies the bottom layer (35 to 50 m). South of this transect (at station 101 and 102) the strong saline front caused by river runoffs in the summer is vertically apparent at 5 to 20 m depth, which stop the saline intrusion to go further north onto the shelves of Kandalaksha Bay. No relatively dense water is observed on the slope. However, in late spring 2001 (figure 5.6h) the saline front (present in 2000) is not evident here, and contours of salinity show a weak horizontal front with presence of saline water (contours 27 psu) in the 20-25 m layers. Dense water is shown on that same transect along-slope (at 25 to 40 m depth) during this time of year. The temperature has reached nearly 0°C with salinity 27.7 psu in the core of the along-slope dense water.

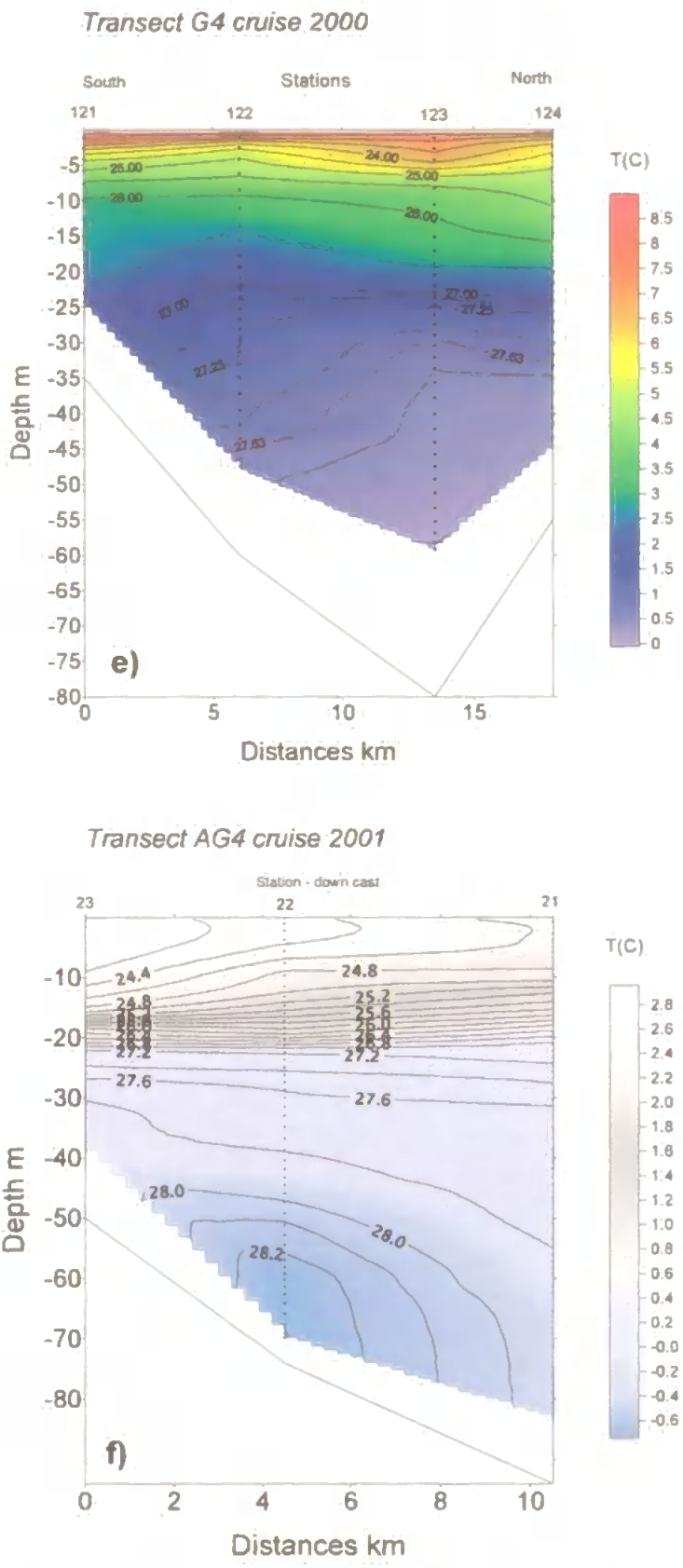


Figure 5.6: Contours of Salinity superposed with temperature image map (e) along transect G4 during cruise 2000 and (f) along transect AG4 during cruise 2001. Note the formation of lens of dense water on the coastal slope of Kandalaksha Bay (S=28, T=-0.5°C) along transect AG4.

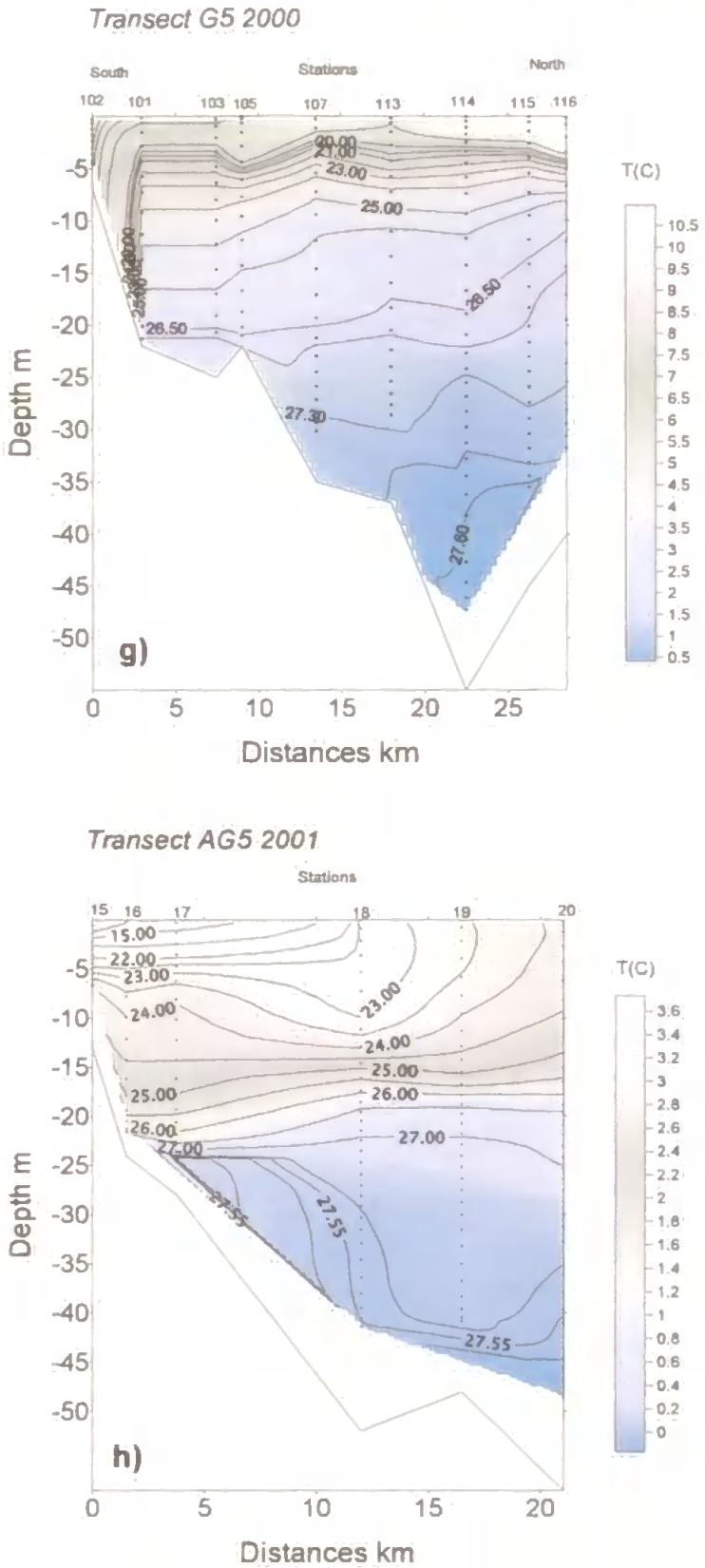


Figure 5.6: Contours of Salinity superposed with temperature image map (g) along transect G5 during cruise 2000 and (h) along transect AG5 during cruise 2001. Same feature with formation of lens of dense water with the saline water mass (S=27, T~0.5°C) propagating at 20m.

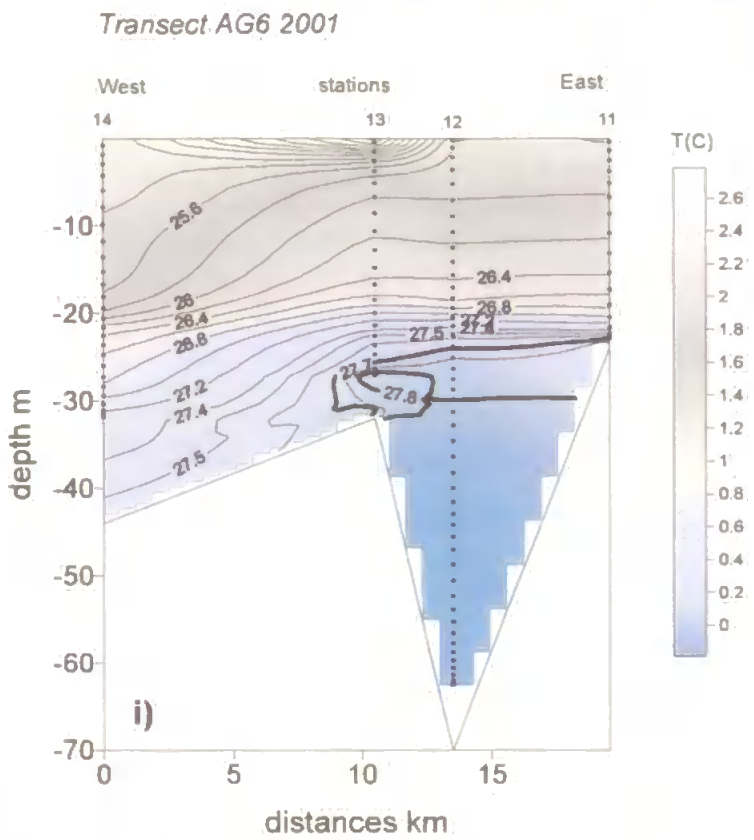


Figure 5.6: Contours of Salinity superposed with temperature image map along transect (i) AG6 during cruise 2001. Note the dense water mass (isohaline 27.8) in the trough and spilling over the shelf slope in the north coast of Kandalaksha Bay.

In the remote and shallow places in the north of Kandalaksha Bay, near Kolvitsa River (see figure 3.3), formation of dense water spilling down slope is observed in transect AG6 (figure 5.6i) during survey 2001. The contours of salinity 27.7 and 27.8 psu show markedly the core of the dense water on the shelf edge with temperature contour reaching 0°C. Such a phenomenon occurred the year before (in 2000) as shown in transect C5 (figure 5.6j). The densest water (27 psu; 1.5°C, known as the modified GSW) occupies the deep (at stations 89 and 108) and covered by a water of salinity 25.25-25.5 psu. The temperature field in that transect shows cold water of 2 to 3°C (salinity 25.25 to 25.75 psu) on the sill edge, which probably results in the formation of dense water, which protrudes further down the slope. Observations in June 2000 in the estuary of the Kolvitsa River revealed a 3-layered circulation (Lukashin *et al.*, 2003).

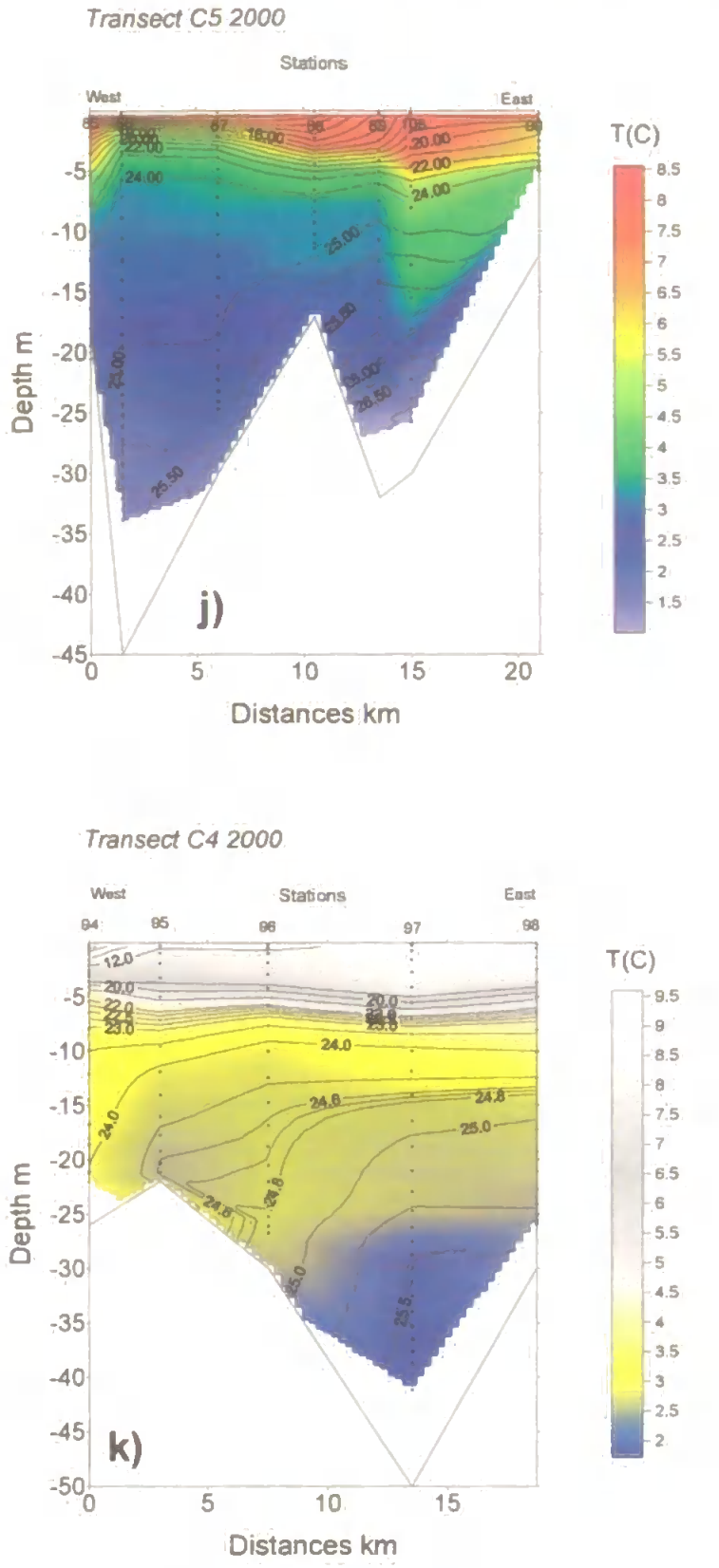


Figure 5.6: Contours of Salinity superposed with temperature image map along transect (j) transect C5 and (k) C4 during cruise 2000.

The warm and desalinated surface layer of 2 m thick was underlain by a layer with temperature and salinity distribution similar to those in the swell region; this represents the zone of the influence of the compensational current of saline water (the GSW). This is also occurring in the neighbouring coastal area as shown in transect C4 (figure 5.6k) with formation of relative dense water on the shallow sill edge (at 25 m depth, at station 95) depicted by contours of salinity 24.6 to 24.75 psu. The coldest temperature recorded at these shallow depths ranges from 2.6 to 2.65°C. The formation of dense water with such temperatures seems however more complicated than simple winter vertical convection with probably some salinisation caused by ice generation.

In conclusion, the formation of dense water yielding to cascading events is mainly observed along the coastal slopes of Kandalaksha Bay and at the mouth of the Chupa estuary in late spring 2001. Some were observed in summer 2000 in the far remote and shallow places in the north of Kandalaksha Bay but the characteristic of the waters was far less dense compared to the observed waters in 2001 (which are furthermore located deeper). Such dense waters have the salinity of 28 to 28.7 psu and the temperatures of -0.4 to -1°C and are mainly found on the shelf edge or along-slope on the coastal areas at depth between 50 and 80 m. This water mass is the east-formed mixed layer seen at the intermediate layers. It is presented as a dome shape structure seen across the entire Basin of the White Sea and its asymmetry (mixed layers deepening in Kandalaksha Bay) suggests the topography in Kandalaksha Bay to be of favourable site for cascading events.

### 5.3.3. Dome-shape structure and internal oscillation in deep layers

Oscillations of deep layers of homogeneous layers (from 90 to 200 m depth) are clearly observed in the east-west transect in summer 2000 (figure 4.6). The oscillations are seen in the Basin (at stations 1 to 10) by contours of temperature -1.3°, -1.38° and -1.42°C and contours of salinity 29, 29.30 and 29.40 psu. Such oscillations are also observed in late spring 2001 (figure 5.5a) in Kandalaksha Bay and the Basin (at stations 54 to 46), although the amplitude and the phase of the oscillations are less pronounced than in the former summer of 2000. The domed structure however is not clearly present in this transect between Kandalaksha Bay and the Basin as it is depicted in summer 2000 by the mixed layers step D and E. In summer 1991 (figure 5.5b) contours of temperatures -1.25°, -1.30° and -1.40°C well depict the domed structure located between 120 and 140

m depth. The dome may be associated with the cyclonic circulation in the surface layers of the Basin (at stations 64, 136, 95, 100), which is investigated in more detail in the next Chapter 7. In summer 2000 and late spring 2001, the oscillations present similarities in amplitude and phase as shown at stations 5, 6, 7 in June 2000 (figure 4.6) and at stations 50, 49, 48 in 2001 (figure 5.5a). By comparison, the contours of salinity 29 psu (in late spring 2001) show the oscillating water from 160 m depth (at station 49) to 120 m depth (at the neighbouring station 48) which in summer 2000 oscillates only from 120 m (at station 6) to 100 m (at neighbouring station 7). Therefore the amplitude of the oscillations is about 10m in summer 2000 and twice as big in late spring 2001. The presence of internal oscillations in deep layers might be related to or caused by water cascading on the steep slopes of Kandalaksha Bay disturbing the deep and stagnant water of White Sea, although the presence of internal waves in the White Sea may also contribute to the generation of such internal oscillations. In the transect 2000 (figure 4.6) the identified mixed layers are penetrating along-slope at 100 to 220 m depth (stations 123, 126), therefore disturbing and compressing the deep water which respond to it by oscillating motions. In transect 2001 (figure 5.5a), the same scenario occurs: contours of temperature -1.20°C and salinity 28.66 show water protruding down the steep slope (stations 25, 30) in the same location as in summer 2000, causing the disturbed deep water to oscillate (see contours -1.25° to -1.35°C). Consequently, such observation of internal oscillations in deep layers (water of -1.3°C) may be the result of cascading events occurring on the steepest slope of Kandalaksha Bay adjacent to the Basin. However, further investigation and more detailed observations on the process of cascading should be necessary in future work.

## 5.4. Discussion

The presence of fine step-like structures within the sharp thermocline in the 10-20m layers in Kandalaksha Bay and in the Basin were regarded as a result of complex mixing between the southwest Gorlo surface water (advected by the Terskii Current), the water mass coming from Dvina and the north-eastward surface waters (from Kandalaksha Bay), which therefore form the White Sea surface waters in the northern Basin. They were identified by the thermohaline index in relation to these mixed layers, defined as Step A (figure 4.1) during summer 2000 and as step F (figure 5.1) during late spring 2001. East-west transects have shown the depth of their formation by vertical

mixing on the shallow sill (shelf edge) of the Gorlo Strait caused by strong tides. The formation of these surface mixed layers (step A or F) therefore depends on the less saline waters brought from the Dvina Bay, which mainly flow out of the White Sea through the Gorlo Strait along the Winter coast (see figure 4.8a). Deeper in the water column, the mixed-layers (such as Step C) are also formed southwest of the Gorlo Strait and vertically mixed from 20 m to bottom down the slope with considerably less freshwater contribution. This is well noted in late spring 2001 with the mixed layer of step C showing more saline and slightly colder water, also because of smaller river discharges occurring during this time of year.

The dynamics of the intrusion of the fine mixed layer (step C), revealed by its thickness and lateral extent (during the three surveys), are still open to discussion. The layer generated on the shallow sill of Gorlo by strong tides was seen to propagate in the first 20-40 m layers providing salt water in the far remote places in the north of Kandalaksha Bay. The average thermohaline index recorded for this mixed layer step C (table 5.I) during summer 2000 and late spring 2001 showed a temperature varying from 0° to 0.5°C, a salinity of 27.5 psu, and a density of 22. The presence of such a layer was also observed in summer 1991 (figure 5.5b) with the same thermohaline values, which reveal the elongated thin layer in the 20-40 m layers from the Gorlo Strait to Kandalaksha Bay. The present results suggest the intrusion to be a permanent feature spread in the northern part of White Sea. Its dynamical process may be related to tidal residual currents (Gidrometeorologiya, 1991a) confined to the first 50m depth layer, due to the presence of a domed structure maintained by strong salinity and density gradients which prevent water mass from penetrating deeper into the Basin. A schematic diagram was presented in figure 4.8 to show the mechanism associated with the formation of such mixed layers. Despite the weak level of tidal energy in the White Sea, tides and their spring-neap cycle variability have been reported by Howland *et al.* (1999) to influence the circulation in the Chupa estuary and contribute to the dynamics of the estuary by generating a water mass in the upper layers. They observed that during their seasonal cruises, the water of the estuary had a salinity ranging from 20 to 27 psu in summer (in July) 1994; from 24 to 27 psu in autumn (in September) 1995; and from 20 to 28 psu in spring (in May) 1997. These waters consist partially of seawater in the immediate coastal zone and correspond to our identified water masses of step A (the fresher), step B (modified GSW) and step C present in the Chupa estuary in summer 2000 and late spring 2001. Howland *et al.* (1999) found that the observed salinity distributions in the Chupa estuary are generated by the interaction of mixing and

advective processes in the whole estuary. They reported that during spring tides, an intrusion of intermediate layers is advected up-estuary, which is the case during the spring survey of 2001. It is also inferred that freshwater inflow in summer plays an important part in the dynamics of the White Sea, generating cyclonic circulation in the Basin which would explain the predominant domed structure seen in the intermediate layers of the White Sea in summer 2000 and 1991. The dome was identified in summer 2000 by step D and E with water temperature of -0.5° to -1°C and in 1991 by water of temperature -1° to -1.3°C. The existence of this intermediate water was described by Timonov (1947, 1950) as an entire source which acts as a boundary layer; he reported a penetration depth of 50 m during winter convection process. The hypothesis here is that the formation of the mixed water at the intermediate layers is formed due to friction with a tidal residual current acting in the upper active layers and shaped as a dome caused by the predominant cyclonic gyre of the Basin. Based on hydrological stations located south of Gorlo and near Onega Bay, Pantiulin (1974) has reported evidence of the likelihood thermohaline index of the deep water of Onega and of Gorlo with that of the intermediate water in the Basin and Kandalaksha Bay. The source of this water was explained by oxygen maxima found in its core showing good aeration due to winter convection and also explained by the circulation of tidal mixing in the southwest of the Gorlo Strait.

Oscillations of the depths of the mixed layers were evident during the surveys 2000 and 2001 and also below the domed structure in the deep layers (> 120 m). These oscillations were associated with the intrusion of the modified GSW. The intrusion of saline water has been observed at the mouth of the Chupa estuary (Howland *et al.*, 1999) with also vertical oscillations (reported at diurnal/semi-diurnal: 12.25h frequencies) in the temperature and salinity field. However, below the domed structure of temperature isolines, the oscillations may also result from the disturbance of the stagnant water caused by intrusion of water cascading along the steep slope of Kandalaksha Bay. The results from the surveys revealed that the formation of dense water in this area was originally caused by the constant intrusion of the saline mixed layers. The latter explain one of the hydrological signatures of the White Sea described by Timonov (1950) concerning the deep water replenishment mechanism.

## 5.5. Conclusion

The results in this chapter have shown a detailed analysis of the mesoscale and small-scale structure of the water masses in the northern part of the White Sea (west of Gorlo, in the Basin, and in Kandalaksha Bay). Three data-sets (1991, 2000 and 2001) have been used to compare the hydrological features summarized below:

- The interannual comparison of fine structures revealed that step-like structures and inversions were observed in the data sets from the two surveys (2000 and 2001). In both cases, four steps were identified with same characteristics and thicknesses in a range of 3 to 20 m (see table 5.1). The coarse vertical resolution of the data set 1991, however, did not permit a comparison of the fine structures.
- The interannual comparison of the distribution of water masses in the Kandalaksha Bay revealed the presence of a distinct saline front in 2000 and 2001. The front exists in the same location (33.8-34°E, 66.5°N) resulting from the interaction of the Kandalaksha waters (25.4 psu; 7°C in 2000 / 24.2 psu; 3°C in 2001) and the surface Basin waters (26.6 psu; 7°C in summer 2000 / 25.2 psu; 1.2°C in late spring 2001).
- West of the front, and at depth ≥ 20 m, dense water (27.4 to 27.8 psu; 0 to -0.2°C) was observed alongside the north coast of Kandalaksha Bay (see figures 5.2c, d, e) in late spring 2001 and none observed in summer 2000, which was mainly located offshore in the centre of the bay. A relatively warm and saline intermediate layer (28 to 28.3 psu; 0.3 to 0.5°C) was observed in the 40-60 m layer in late spring 2001, whereas it was less obvious in summer 2000. However, this indicated that in both cases an intrusion of the mixed layers.
- The comparison of hydrographic transects, during surveys 1991 and 2000 across the northern part of the sea, showed that the intrusion of the mixed layers is located in the vicinity of a turbulent boundary layer (~50 m depth). The latter separates the active upper layers from stagnant waters of the Basin. This boundary layer was inter-annually found within a domed structure in the Basin. The asymmetry of the domed-layer, seen in the western part of the Basin during survey 2000, indicated the possibility of descending water along the steep slope of Kandalaksha Bay.
- The comparison of a number of hydrographic transects in the north of Kandalaksha Bay revealed pool of dense water more pronounced on the shelf

edge in late spring 2001 than in summer 2000. In the adjacent waters of the Basin, the dense water (28.6 psu; -1°C) was found along the steep slope of Kandalaksha Bay, between 80 and 140 m depth in late spring 2001; and found at deeper location, between 120 to 200 m depth in summer 2000. Other patches of relatively less dense water (28.3 psu; -0.5°C) in the form of lenses were observed onto the shelf-edge of Kandalaksha Bay during survey 2000 and 2001. Another patch of slightly less dense water (26 psu; 0.5°C) was identified in the bottom layers of the Chupa estuary during survey 1991 and 2001. The interannual structure of the water masses in the north of Kandalaksha Bay supports the hypothesis that the formation of dense water and descending water occurs on the shelf-edge and along the slope of Kandalaksha Bay.

# Chapter 6: Mixing processes west of the Gorlo Strait

## 6.1. Introduction

The hydrographic survey in the test area in the Gorlo region in summer 2000 revealed a very complicated structural combination of water mass distribution, such as the formation of intermittent mixed layers (Chapter 4 and 5). These features are generated southwest of the Gorlo Strait with strong interaction between the transformed saline and cold Barents Sea waters penetrating from the north, and the less dense warmer waters of the White Sea supplied from the south. The Gorlo Strait, which connects the White Sea to the Barents Sea (via the so called Voronka region) is only 50-60 km wide, 150 km long and typically 40 m deep. The Voronka region is known to have very strong tides, which come from the Barents Sea and are enhanced by the funnel-like shape of the Voronka and Mezen Bay. However most of the tidal energy is reflected back at the entrance toward the Gorlo Strait. As reviewed in the literature (Gidrometeorologiya, 1991a), only 20% of incoming tidal energy enters the Gorlo Strait and only 6% enters the White Sea Basin. Tidal currents in Gorlo are strong and the maximum velocity is about 1 to 1.2 m/s, which is mainly observed along the Terskii coast. In the summer there are five identified water masses in the region adjacent to the White Sea and to the Gorlo Strait, which are involved in the mixing process (see chapter 2, figure 2.2; Gidrometeorologiya, 1991a). These are the well mixed Gorlo Strait Water (GSW), a thin layer (about 10 to 20 m) of the White Sea Surface Water (WSSW), fresher Bay Waters, colder White Sea Intermediate Water (WSIW), which generally has the temperature -0.2 to -0.9°C, and the White Sea Deep Water (WSDW) below 100 m.

Although mixing processes have been studied previously in the White Sea, they are still not well understood due to their complex nature. Standard hydrographic sections have been carried out across the Voronka and the Gorlo Strait (Gidrometeorologiya, 1991), mainly by using Nansen bottles during the last intensive survey 1991. The analysis of these data revealed the following features of the mixing processes. Traditionally, it has been thought (Gidrometeorologiya, 1991a) that the waters in Voronka and the Gorlo

Strait are well mixed from the bottom to the surface, excluding the period after spring river flood when low salinity waters enter the Gorlo from the Dvina Bay. However, the analysis of recent data obtained during the survey 2000 has shown below that this concept is not relevant to the south-western part of the Gorlo Strait for the period of June 2000. A "belt" of maximum salinity gradients (salinity front) was found to be located in the southern part of Voronka (Pantiulin, 1990), where salinity changes from 34 to 30 psu. Waters with salinity about 30 psu and temperature of −1.5°C penetrates into the southern part of Gorlo only during the second half of the winter to renew the bottom waters in the deep Basin of the White Sea. The Gorlo Strait is the only route for water exchange between the Barents Sea and the White Sea, and so an analysis of mixing processes in the Gorlo Strait based on recent observations from a dense network of CTD measurements using modern oceanographic technology is addressed here.

This chapter is based on the paper by Shapiro *et al*, 2003, Oceanology, 43 (Suppl. 1): S26-S31. The candidate was the second author in this publication, which describes the mixing processes of the Gorlo Strait of the White Sea.

## 6.2. Materials and observations

A CTD survey was carried out from the 17 to 21 of June 2000 over a rectangular area located in the Gorlo Strait adjacent to the shallow regions of the White Sea Basin and Dvina Bay (figure 6.1a), to study the distribution of water masses and mixing. The measurements were taken in that region where water masses come into contact from the Basin, Dvina Bay and the Gorlo Strait. The mixing process is intensified by strong tides, shallow and ragged bottom topography. The survey consisted of 50 stations and was part of the multidisciplinary EU-INTAS project: Mesoscale Physical and Biogeochemical Processes in Coastal Waters of the Russian Arctic (Lukashin *et al.*, 2003). The measurements were taken using the research vessel *Kartesh*, with typical distances between stations being 3-6 km. Vertical profiles of temperature and salinity were obtained with a CTD probe SBE-19 from Sea Bird Electronics with a vertical resolution of about 0.2 m (in shallow regions) to 0.4 m (see chapter 3 for the methodology).

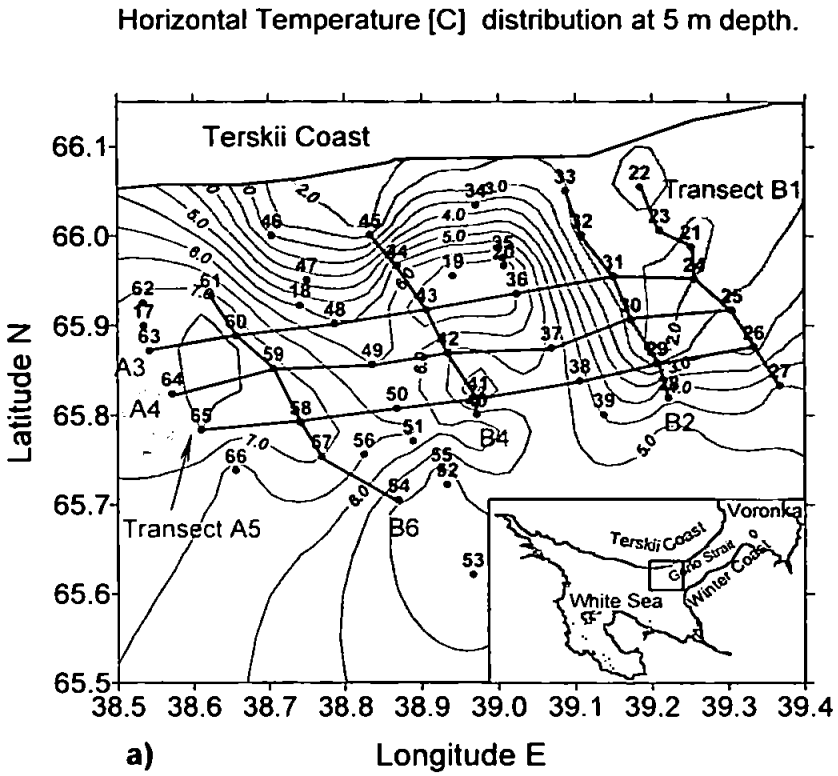


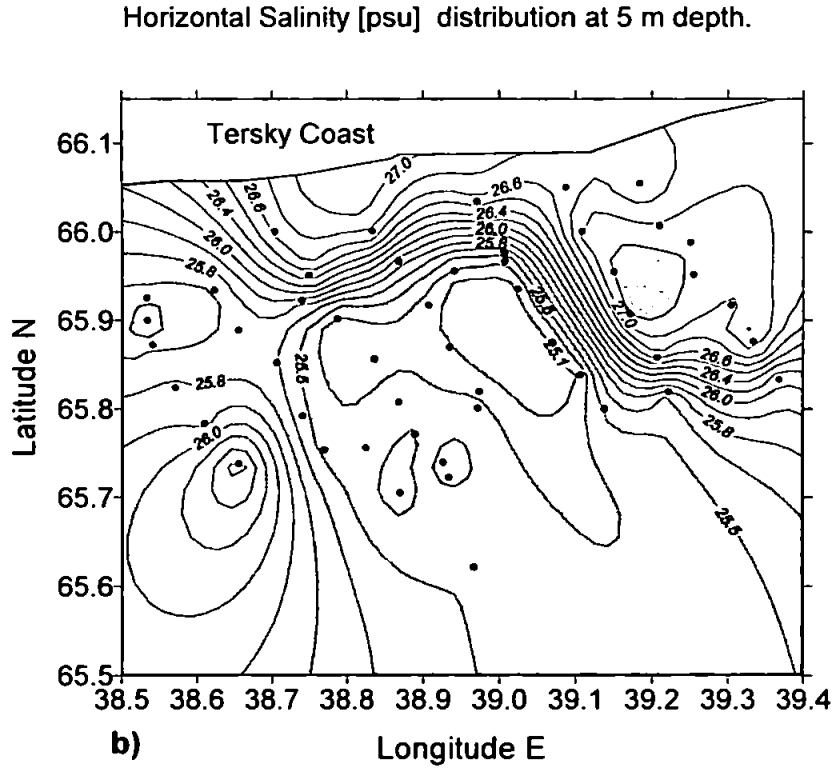


Figure 6.1: Distribution of (a) temperature and (b) salinity at depth 5m in the mixing area at the south-western end of the Gorlo Strait, June 2000. Note the meandering surface front and formation of lenses on its left.

Both downcast and upcast were recorded to monitor any changes of water properties due to the ship drift caused by tidal currents during the period of measurements at a station (about 10 minutes). Throughout the survey the weather was calm with wind speeds never exceeding force 2 on the Beaufort scale.

The study includes comprehensive analysis of 3D water mass structure, and it is based on horizontal charts of temperature and salinity distribution at various depths, vertical cross sections along and across the Gorlo Strait, temperature-salinity diagrams, vertical profiles at individual station and analysis of temperature and salinity fluctuations in the areas of strong mixing. The results of the analysis are presented in the following section and supported by a selection of plots, which reveal the mesoscale horizontal structure and the small-scale vertical structure of water masses.

## 6.3. Water Masses in contact

Generally, the large-scale distribution of hydrographic parameters in the White Sea was typical for early summer conditions (Gidrometeorologiya, 1991a). However, the dense grid of stations and high vertical resolution of newly obtained data allowed us to study the water mass distribution and mixing in greater detail.

The chart of temperature and salinity distribution (figures 6.1a,b) at the depth of 5m clearly shows the spatial structure of water masses in the near-surface layer. Their horizontal structures may change with depth therefore deeper sections are of interest namely at 20 m (figures 6.1c,d), and at 40 m (figures 6.1e,f). These horizontal sections are chosen to represent these water masses in contact respectively at the "intermediate" and at the bottom boundary layers. As we can see on these charts, the northern and north-eastern parts of the study area are occupied by the modified Gorlo Strait Water (GSW) with a core identified as T=2°C, S=27.2 psu all through the water column (see stations 21 to 24). The 'source current' (Gidrometeorologiya, 1991a) brings into the Gorlo Strait waters from Voronka, where it is well mixed due to intensive tidal mixing.

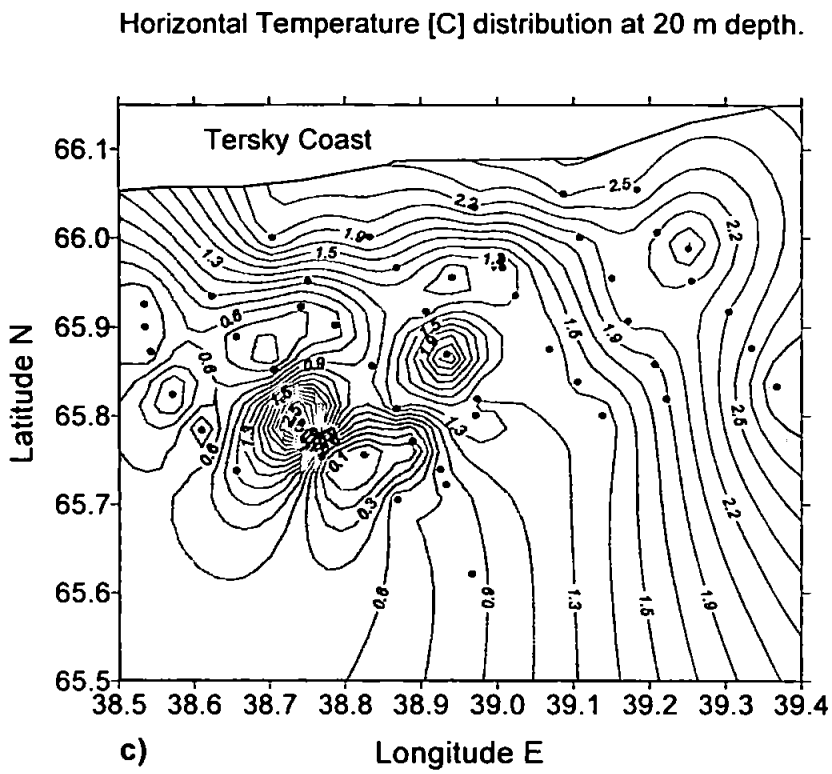


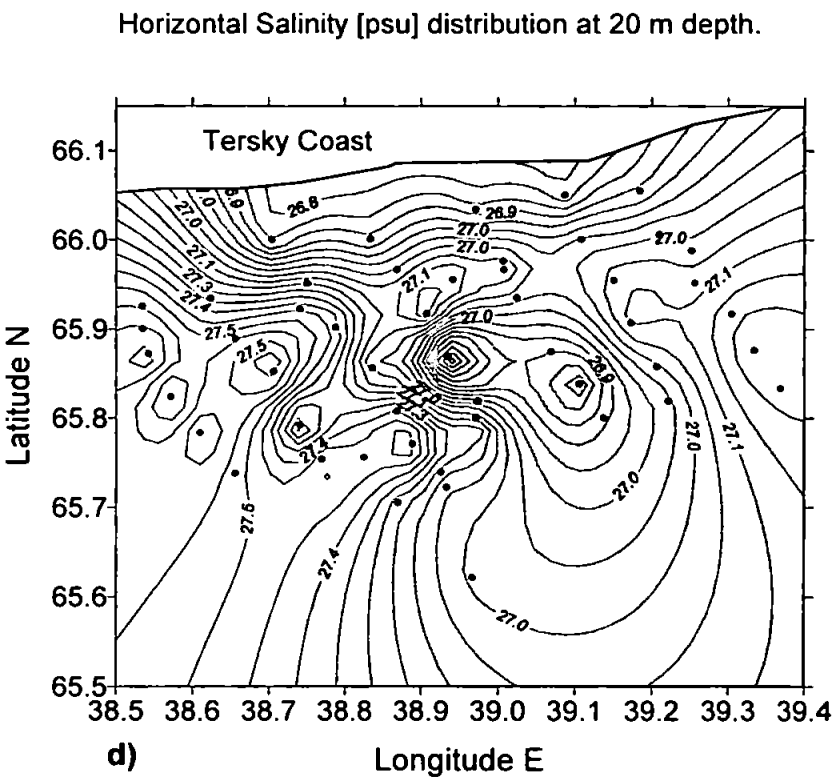


Figure 6.1: Distribution of (c) temperature and (d) salinity at depth 20m in the mixing area at the south-western end of the Gorlo Strait, June 2000. The front is still evident in the temperature field and less obvious in salinity. Local circulation (Terskii current, Dvina gyre) shows mesoscale eddy activities and formation of lenses. Interaction or partial coalescence of lenses is observed here exchanging water and energy with the White Sea waters.

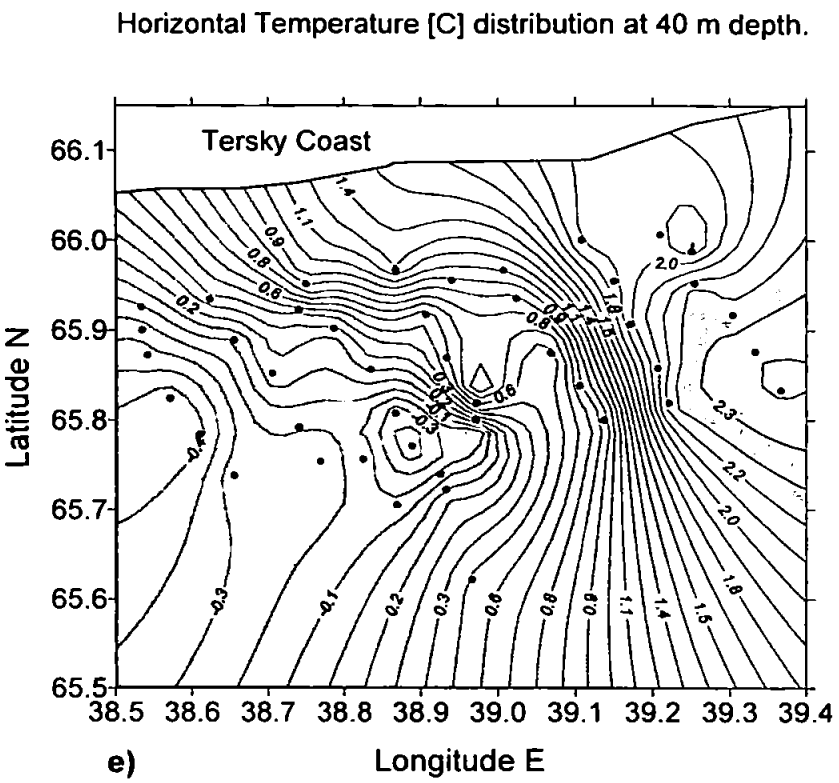


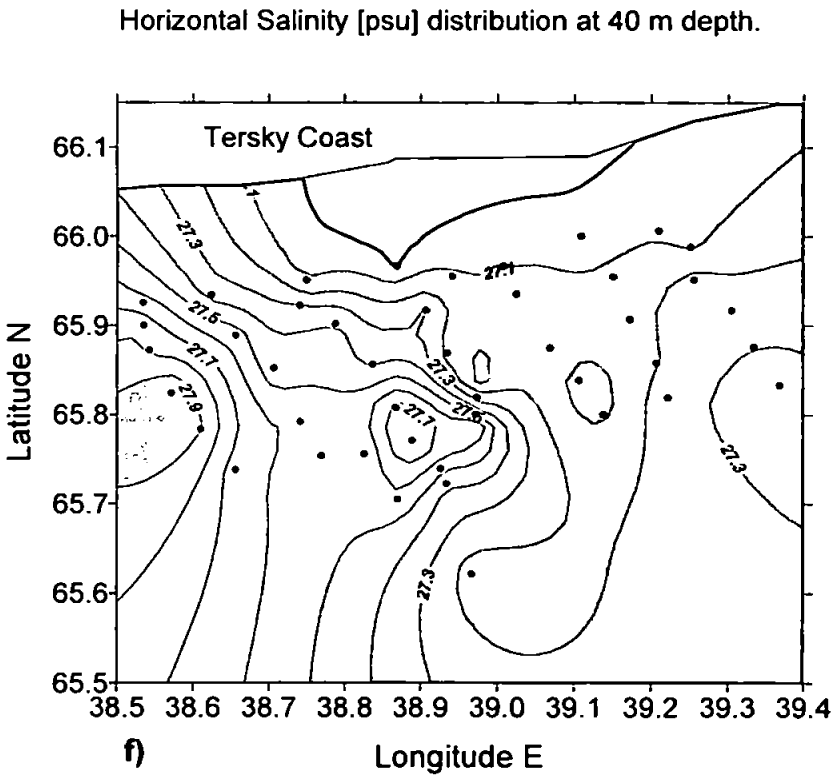


Figure 6.1: Distribution of (e) temperature and (f) salinity at depth 40m in the mixing area at the south-western end of the Gorlo Strait, June 2000. Note the presence of the (eddy) ring detached to the left of the front which separate bottom GSW from waters in the White Sea.

In the surface layers (figure 6.1ab), the warmest was the White Sea Surface Water (WSSW; T=7°C; S=25.5 psu), shown at stations 62 to 65. This water mass occupied the western side, whilst fresher and slightly colder Dvina Bay Water (DBW, T=5°C; S=24.8 psu) was advected from the south, probably by the cyclonic Dvina Bay gyre (Timonov, 1950). The influence of this gyre and the adjacent Terskii Coastal Current (Gidrometeorologiya, 1991a) is evident from the intrusion of colder GSW into the western end of the Gorlo Strait along the Terskii Coast in the north.

The next sections at 20 m depth (figure 6.1cd) for temperature and salinity distribution show a complex scenario of water masses in contact. Small and mesoscale eddy activities are taking place at a depth slightly underneath the thermocline. Relative warm temperatures (> 2°C) of the mixed GSW still occupy the north and north-eastern part of the area, although less saline water is observed along the Terskii Coast. Comparatively, cold temperatures and fresher water from the south of Dvina (T=1.9 to 0.8 °C, S=26.6 to 27 psu) bars the intrusion of the GSW, eroding its core. The fresh water from the Dvina river flowing in a cyclonic gyre enters the western area, which interacts with the colder and more saline water from the White Sea. These contacting water masses are likely to generate eddy-like structures.

Near the bottom layers at 40m depth (figure 6.1ef), it is worth noting that the modified GSW (looking at contours of T=2.3°C and S=27.3 psu) stretches to the southern area from the Terskii Coast where the DBW occupied the surface layers in the first place. More saline and colder temperatures are clearly present in the western area from the White Sea waters (shown by contours of T=-0.4°C and S=27.9 psu). Note that contours of temperature and salinity show an eddy-like structure, observed in the centre of the area with coldest temperature and saline water in its core (T=-0.3°C, S=27.7 psu). This can be explained by the presence of the two water masses in contact that is the deep DBW with the White Sea waters, thereby generating mesoscale eddies.

## 6.4. Mesoscale eddy formation

In the central part of the area the measurements reveal a mesoscale patch (lens) of WSSW in the surface layers (figure 6.1ab), which is surrounded by colder GSW from the north and a mixture of GSW/DBW in the south. Despite having a diameter of only 7-8 km and a thickness of 8-10 m (figure 6.1g, stations 43), the core of the lens is well defined and occupied by four adjacent CTD stations (the duration of these

measurements lasted 20 hours). The lens is separated by a sharp thermocline (a drop in temperature by 6°C in 5m depth) from the underlying water. This thermohaline feature is indicative of the initial stages of a mesoscale eddy formation, a process well observed in various parts of the World Ocean (Filyushkin and Plakhin, 1995; Shapiro and Meschanov, 1996) but which has not been reported in the White Sea before. The formation of the lens might be forced by the baroclinic instability of the thermohaline front and associated current or alternatively by intensification of the Dvina Bay gyre due to increase of fresh water discharge. South of this lens, there is a small patch of surface Dvina Bay Water, however it was evident only at station 41 and it is not possible to resolve its horizontal structure.

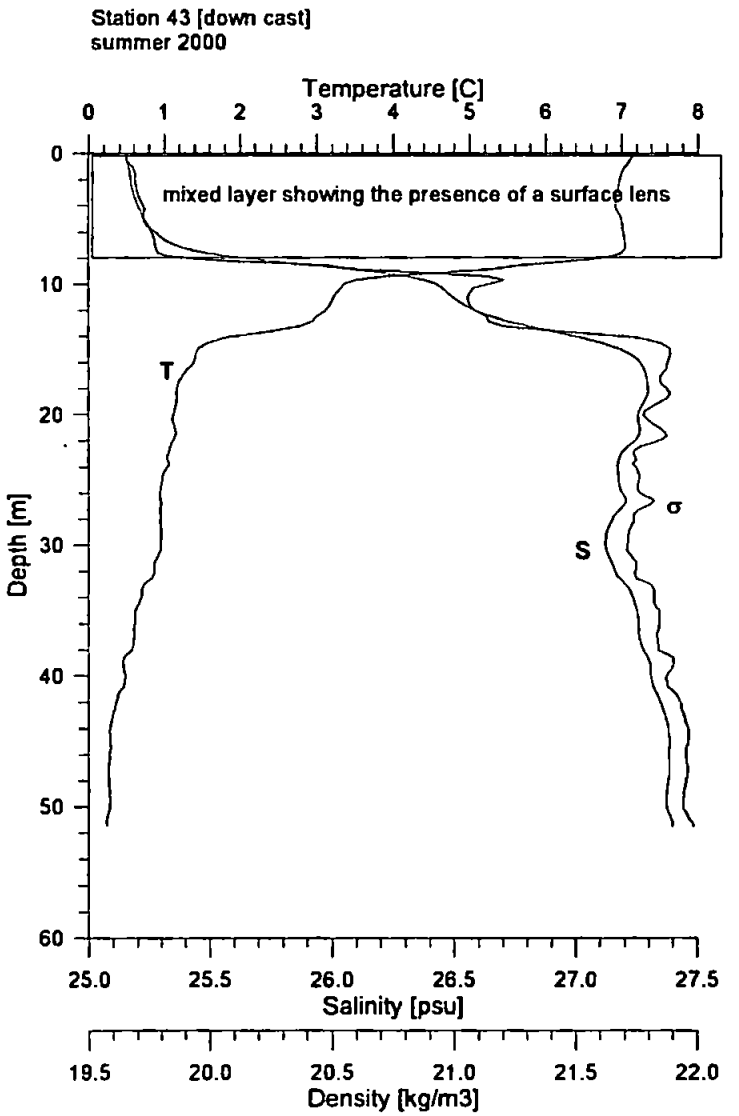


Figure 6.1g: CTD profile at station 43 measured in the south-west of the Gorlo Strait, June 2000. Note the structure of a lens at the surface with a thickness of 8-10m.

Underneath the thermocline, at 20 m depth (figure 6.1cd), the observed "anticyclonic" lens of the WSSW is still present with its core centred on stations 19 and 43. South of the area, an inferred "cyclonic" lens is formed (core located at station 42), with a diameter of 7-8 km and a thickness of 4-6 m (see transect B4 in figure 6.2d at station 42). It is located underneath the observed small patches of the surface Dvina Bay Water, well separated by the sharp thermocline. It is worth noting the similar characteristic of the 3 eddy-like structures (showing a core of 2°C). One is centred on station 21 (the core of the GSW), the second one on station 42 in the centre area and another one on station 58 located in the White Sea waters. A possible mechanism for the GSW to enter the central area is through formation of lenses. It is not clear from the salinity distribution whether one can infer such formation of lenses, and whether they propagate into the White Sea area, but the salinity and the temperature at the core of these lenses are likely to be similar to that of the GSW on the Terskii shore. Chlorophyll, PH, oxygen or other tracers, although absent from the data set would help to identify whether these lenses are of same water properties and confirm their origin. The "formed" lens (generated from the GSW) in the south-western area is however associated with the eddy-like structure observed in the vertical profiles at station 51. As discussed in the previous paragraph (water masses in contact), the WSSW interacting with the gyre of the DBW, are likely to form a small-scale eddy-like structure seen at the most southern area. The structure of the eddy has intensified as shown by the increase of temperature gradient (steeper surface topography), associated with the presence of the White Sea Intermediate Water (WSIW). The section of temperature distribution at 20 m depth denotes a vortex-like structure of that "anticyclonic" eddy with the associated lens centred on station 58. The temperature at the core-eddy is about 0.1°C and reaches -0.4°C near the bottom layers at 40m depth, whereas the salinity increases to > 27.7 psu, provided typical values of the WSIW.

In conclusion, the results showed that the water exchange in the Gorlo Strait leads to the formation of mesoscale eddies and lenses propagating at different layers caused by the variety of structural combinations of water masses present in that region (Lukashin *et al*, 2003; Shapiro *et al.*, 2003). The intrusion of the GSW, strongly dependent on the tides and mixing with fresh water surface current, therefore shows its importance in the dynamics and structure of the water at the entrance of the White Sea. A more detailed analysis of its vertical distribution is given in the following section.

## 6.5. Intrusion of the GSW

Contours of salinity and temperature in Transect B1 (figure 6.2a) clearly show the incoming Gorlo Strait Water. This water mass is present in Transect B1 through the entire water column and at the bottom, with the exception of fresh surface water probably already mixed (from 10m depth to the surface). The contours of salinity 27.05 psu and temperature 2.4°C show the limit of the Gorlo Strait Water in summer 2000, which are separated from fresher and warmer water in the surface layers. A "core" of the GSW can be identified with values of temperature colder than 2.0°C. The salinity distribution clearly indicates this core with contours of 27.05 psu on figure 6.1b.

In the shallow White Sea Basin area adjacent to the Gorlo Strait (figure 6.2b), the "core" of the Gorlo Strait Water is considerably reduced across the strait due to mixing caused by surrounding water masses, such as the presence of the Dvina surface water, which is well noted with a maximum salinity of 25.3 psu and minimum temperature of 4.8°C (figure 6.2b) at stations 28 and 29 (south of the transect B2). In the thin surface layer (5-15 m depth), sharp gradients of temperature and salinity at stations 29-30 show a region of mixing between the Dvina surface water and the Gorlo Sea Water. In the shallow areas close to the Terskii shore (stations 32-33) the water is well mixed with fresher water compared with that of the Gorlo Strait Water. This probably implies topographic stirring near the bottom (at 25-30 m depth) and mixing with fresher and warmer WSSW coming from the Basin with local circulation gyres. The GSW enters into the northern White Sea along the Terskii Coast and flows within the Terskii current with slight changes in its water properties as a result of these mixing processes. At the frontal zone the GSW also mixes with the WSSW just below the thermocline (stations 30, 31), at depths of 10-35 m (figure 6.2b). At these depths the temperature of the GSW and WSSW differs by only 0.5°C compared to the 4.6°C temperature difference in the surface layers (< 10 m depth). The lenses of water observed at 10-35 m depth are regarded as the modified water that is produced by the mixing of the GSW and the WSSW at the frontal zone. Different types of mixing occur here producing a complex picture for the structure of the generated mixed waters. The intensity in mixing and the location of the front are an important aspect regarding the formation of these mixed waters, some of which take their properties from the "source" water. Such mixed waters enter the northern part and the Basin of the White Sea. The frontal zones and the mixing areas are therefore analysed in more detail in the following section to explain the range of various horizontal structures found in the west part of the Gorlo Strait.

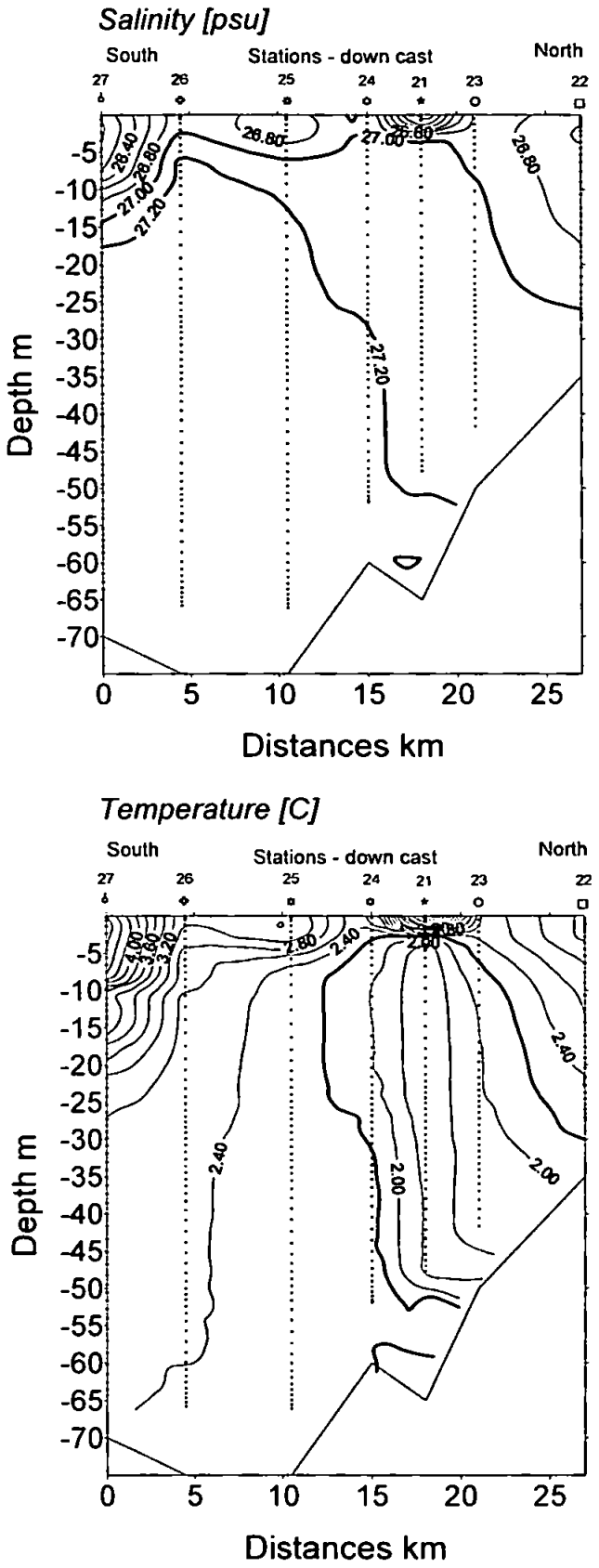


Figure 6.2a: Transect B1, Cross Section of vertical salinity and temperature distribution southwest of Gorlo in June 2000. Note the presence of the incoming GSW identified by its core with isotherms 2.2°C and isohaline 27.2 psu flowing along the Terskii coast.

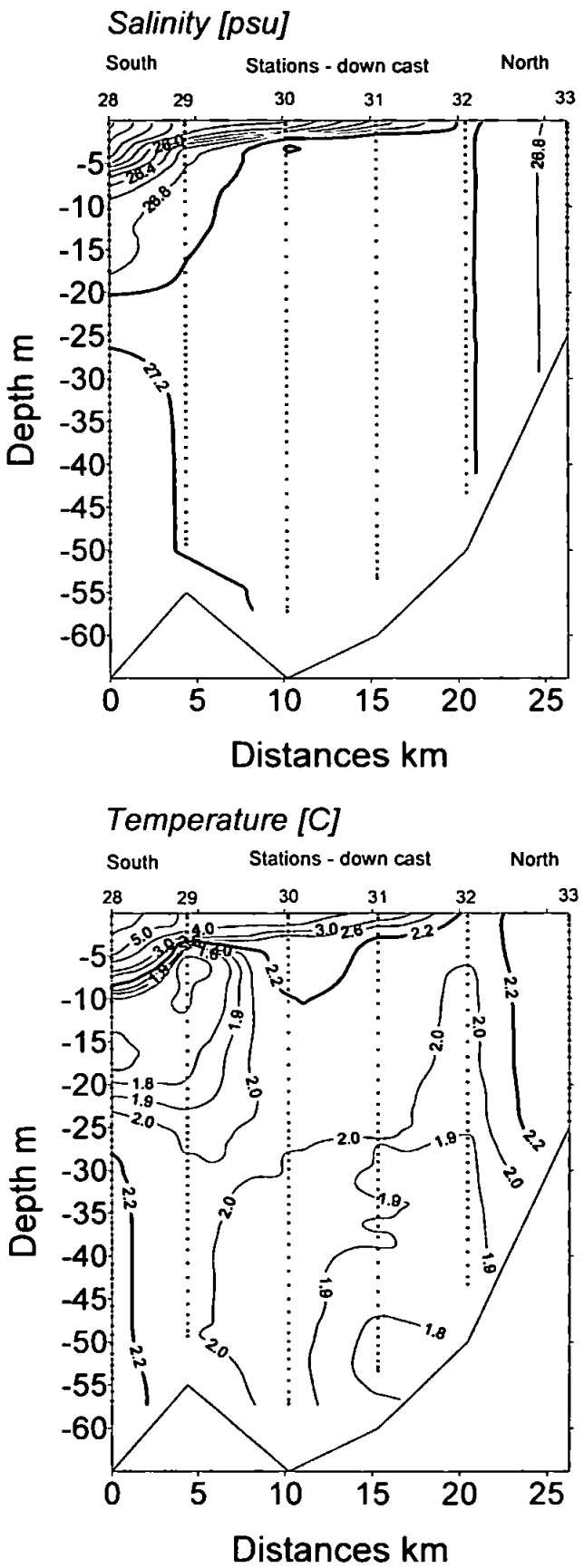


Figure 6.2b: Transect B2, cross section of vertical salinity and temperature distribution southwest of the Gorlo Strait in June 2000. Here, we note the core of the GSW (at the bottom) across the Strait start in contact with cold and fresh water (10-25m) south of transect as we move toward the White Sea entrance.

## 6.6. Frontal zones and mixing areas

Alongshore cross sections (transect A3, A4 and A5, figure 6.1) across the thermal front are analysed here to identify the area where bottom mixing occurs more intensively (figure 6.2cde). It is expected that areas of strong mixing should be separated from the source water masses by a sharp front. The transect A3, close to the Terskii Coast (figure 6.2c), denotes cold and saline White Sea Intermediate Water (WSIW, T=-1°C, S=28.5 psu which was identified as the mixed layers step E in summer 2000; table 5.I). This water mass is located at > 25 m and is believed to be formed by previous winter cooling and salinisation due to the incoming current from the Gorlo Strait along the Terskii Coast. The current brings more saline Barents Sea water, modified through stirring and mixing in the Voronka Bay and in the Gorlo Strait. Three distinct water masses are observed here: the WSSW, the GSW and the WSIW. The warm mesoscale "patch" (discussed in the section above as the inferred anticyclonic eddy, 7-8 km in diameter) lies in the surface waters to a maximum 5-8 m depth, depicted at stations 43 and 36. Clearly here in the northern area, the WSSW flows above the sharp thermocline (salinity gradient 2 and temperature gradient above 4°C in less than 10 m) which is at a depth about 10 m, and is literally stopped by a strong thermal front. The frontal zone well depicted at between stations 36 and 31, reveals the presence of the GSW entering the White Sea along the Terskii Coast. The thermal front here is strikingly well observed through the entire water column, to the bottom depth (60 m).

At station 48, colder water than that of the WSSW is observed. This may be coastal water advected offshore. This implies some local circulation gyre, caused perhaps by the influence of the Dvina Bay circulation and/or by Terskii current meandering in the surface, initiated by baroclinic instabilities. This assumes that surface mixing occurs mainly between waters from the Terskii shore and the incoming WSSW in this northern area. Below the thermocline at 20 to 60 m, at the location of the shallow shelf edge, and left (south-west) of the front, mixing areas take place. Topographic stirring is likely to mix waters originating from a source such as bottom GSW and bottom-slope waters occupied by the WSIW. Underneath the thermocline, about 30 m depth, mixing also occurs, seen by the trends of salinity and temperature contours.

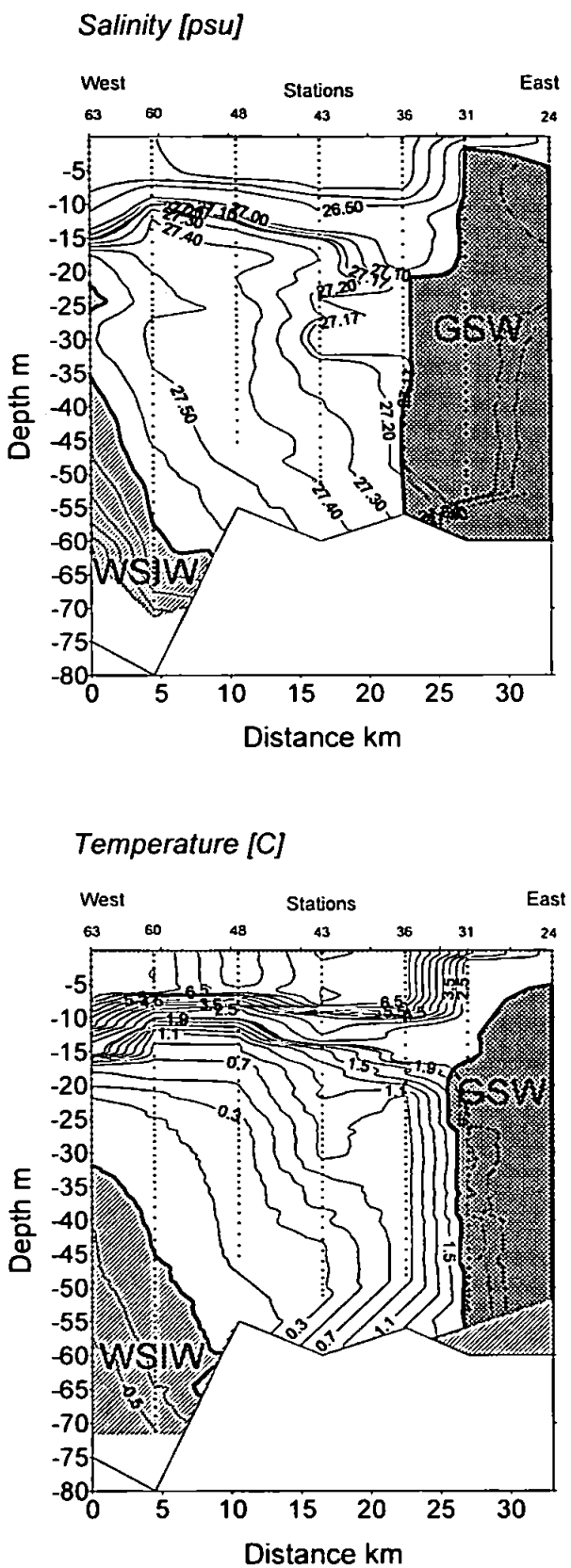


Figure 6.2c: Transect A3, section along coastline northeast of the White Sea, June 2000. Note the two contact water masses (GSW, WSIW) separated by strong front and located under sharp thermocline at 10-15m depth.

The transect A4 avoids the warm mesoscale patch or "anticyclonic lens" but clearly shows four water masses (presence of DBW) and their complex interaction in the south-western end of the Gorlo Strait (figure 6.2d). The location of the meandering front as shown by the three sections of horizontal distribution of temperature and salinity, gives a clear picture to the horizontal extent of the DBW flowing northward to meet the GSW and the WSSW. The river discharges (important in summer) from Dvina play an important contribution in the formation of the mixed waters in the surface layers in the northern part of the area. The DBW contributes to fresh the already mixed waters in the north from WSSW and GSW, probably strengthening the formation of the lens observed at stations 42 at 20 m depth (figures 6.1cd). The Gorlo Strait Water on the eastern side of the transect A4 is well mixed below 5-7 m and is covered by a duvet of warmer surface water, which could be attributed to the summer heating (figure 6.2d). Surface waters from the Basin (west of transect) and Dvina Bay (centre) occupy a thin layer not penetrating deeper than 8-10 m. The mixing area between WSSW and DBW is concentrated in a narrow band not exceeding 5 km. The temperature front between warmer GSW and colder WSIW occupies the water column from 15-25 m down to the seabed. Frontal mixing takes place in a strip between 20 and 25 km width and coincides with the shallowest area on the transect. The resultant water mass leaks into the White Sea as a thin intrusion at a depth of 15-25 m. Along its way the water mixes with the overlying DBW and WSSW, producing well-developed temperature and salinity inversions as well as quasi-homogeneous layers. These thin layers are regarded as the origin of formation of mixed layers identified by the step-like structures seen in the vertical profiles.

Further south of Transect A5, the mixing is well pronounced between a surface patch of DBW centred on station 38 and the GSW in a thickness layer of about 15 m below 5-10 m depth. This resultant mixed water has a temperature of 1.5°C and more, and a salinity of 26.7 psu and more. Below 25 m to the seabed, the thermal front is well present and wide as 15 km as we see the WSIW occupying some part of the shallow shelf from water depth 40 m to bottom (65 m). Topographic stirring is likely to contribute to form a shelf water mass (0.5° to 0.9°C and 27.1 to 27.5 psu), however mixing underneath the thermocline, west of the Transect in layers of 20 to 40 m, is also shown (as in Transect A4; figure 6.2d), provided similar thermohaline properties of that of the formed shelf water.

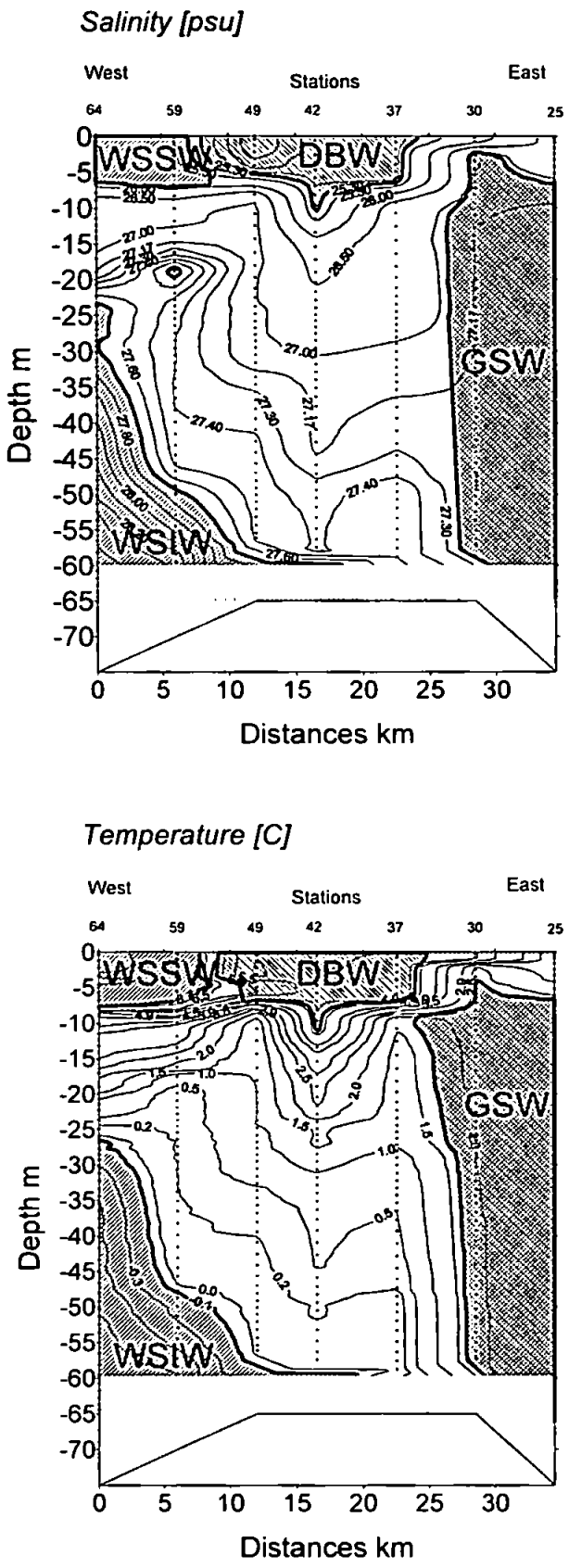


Figure 6.2d: Transect A4, cross section along the Terskii shore, near the Gorlo Strait, White Sea June 2000. The four water masses are in contact showing complex frontal and mixing zones.

The characteristics of such 'shelf water' are revealed by the contours in figure 6.2e and demonstrate that this mixed water mass propagates in a thin layer above the WSIW and right underneath the thermocline. The mixed layer deepens and gets thicker from east to west of the Transect. Its thickness is now about 10 m associated with a temperature drop of 5 to 6°C. The surface waters formed by the WSSW and DBW (west of the Transect A5) therefore do not mix with the underlying already mixed layer and the WSIW. Near the central area, at station 50 and 41, a thermal front appears in the 5-8 m surface with a 2°C temperature gradient. This local front arises from the presence of the westerly WSSW and the DBW localised in the central-east area that has probably originated or detached from the inferred cyclonic Dvina Bay gyre. The intrusion of the DBW is responsible for adding complex local circulation such as lenses or eddy features in the south-western area of the Gorlo Strait, and for mixing with the GSW in the surface layers.

South to centre of the Transect B4 (figure 6.2f) in the 10 m surface, Dvina water of 5°C mixes with WSSW, with a cold core observed at station 41. The location of mixing and frontal zones are well observed in the temperature field rather than the corresponding salinity with clear temperature gradient (> 2°C) between the WSSW and the DBW. However, lenses are likely to be formed because of this temperature gradient. Further west and south of transect B6 (figure 6.2g), a small thermal front of the same temperature gradient is localised at stations 54 and 57. A long tongue of the WSSW occupying the surface areas is observed here from the centre part of the transect to its north part. The front separating the incoming "source" water of Gorlo from White Sea waters is seen throughout the entire water column in the north at station 44 and 45. However, it is less obvious further west near the Terskii Coast with Transect B6. As shown on previous transects, topographic stirring mixes water near the Terskii Coast at 30m depth. At the bottom at 55m, lies a core of different mixed water (salinity 27.3 psu; T ~0.5°C), which is formed at that depth by WSIW mixing with GSW. The associated front is observed from depth 20 m to bottom shown by the measurements done at stations 40 and 41, localised in the central zone of the whole studied area. Beneath the thermocline at ~20 m, the complex and interesting mixing takes place at station 42, as was shown in the transect A4. Additional observations on the nature of the "lens" observed at 20 m depth in figure 6.1c is given here in the cross transect B4. These two perpendicular transects plus the horizontal distribution clearly show the three dimensional structure of this lens. It has a diameter of ~8-10km and a thickness of about 20 m. The properties of the lens are a salinity of 27.1 to < 26.3 psu and a temperature

ranging from 1.9 to 3°C. The formation of this lens in the 10-30m layer is certainly due to the intrusion of the DBW diffusing its water properties and mixing with the overlying waters such as the modified GSW from the Terskii Coast, the shallow-shelf mixed water (near bottom core: S ~27.5 psu, T ~0.5°C), and probably the WSIW in the vicinity of the 30m depth. On cross section B6 (figure 6.2g), the WSIW is clearly present with temperature 0.1°C reaching 30 m depth. A similar lens structure is observed at 20 m depth centred on station 58. Its diameter is of same order (~10 km) as its eastern counterpart but less thick as ~5 m. The vertical thermohaline distribution confirms the same water characteristics in a narrow layer at 20 m. The bottom mixed water generated on the shallow shelf has now been advected above the WSIW as shown by the selected contours of S=27.5 psu and T=0.5°C in transect B6. This mixed layer is confined to 20 and 40 m depth. The lens is also present at station 58; however less thick within the mixed layer increasing the production of turbulence at its low boundaries, which likely provides a mechanism to sustain mixing with the WSIW. The production of turbulence can be regarded through the temperature or salinity fluctuations (or both), reflecting the intensity of mixing, which is addressed in the following section.

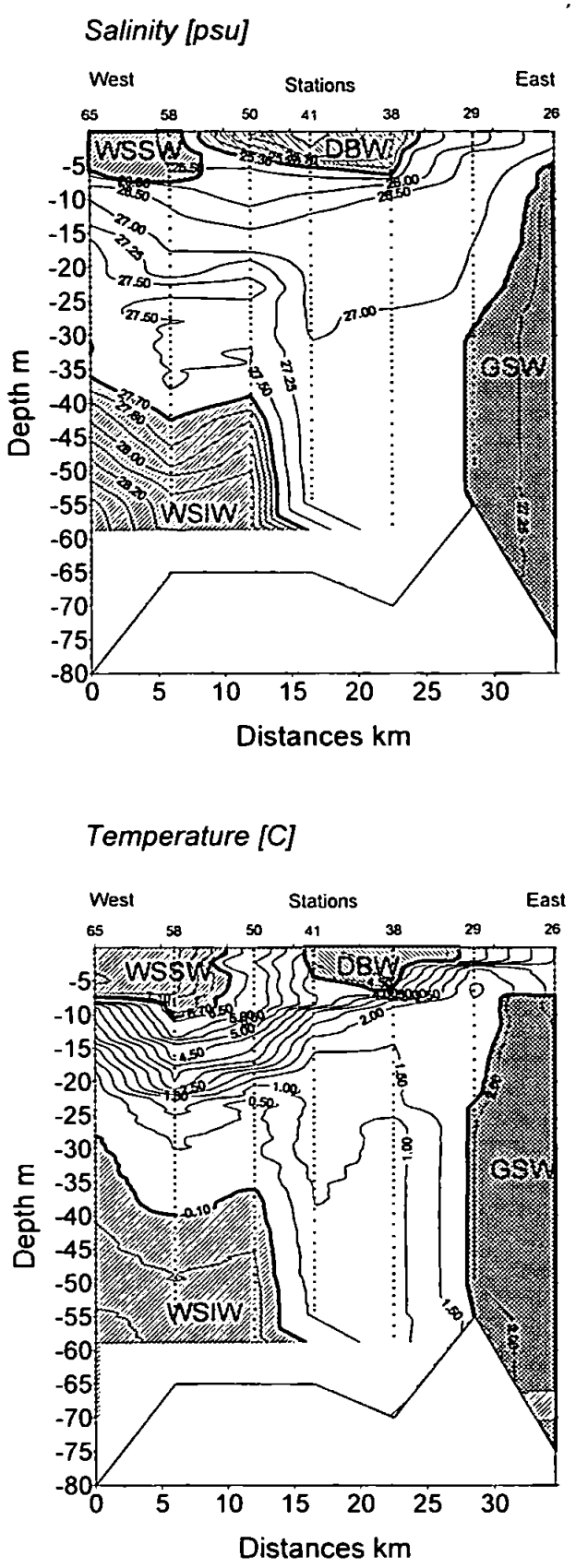


Figure 6.2e: Transect A5, section along coastline northeast of the White Sea, June 2000. Note the strong topographic mixing in the bottom layer with a frontal zone (GSW/WSIW) and lateral mixing under the thermocline where transformed GSW (15-25m) leaks into the White Sea in form of layers.

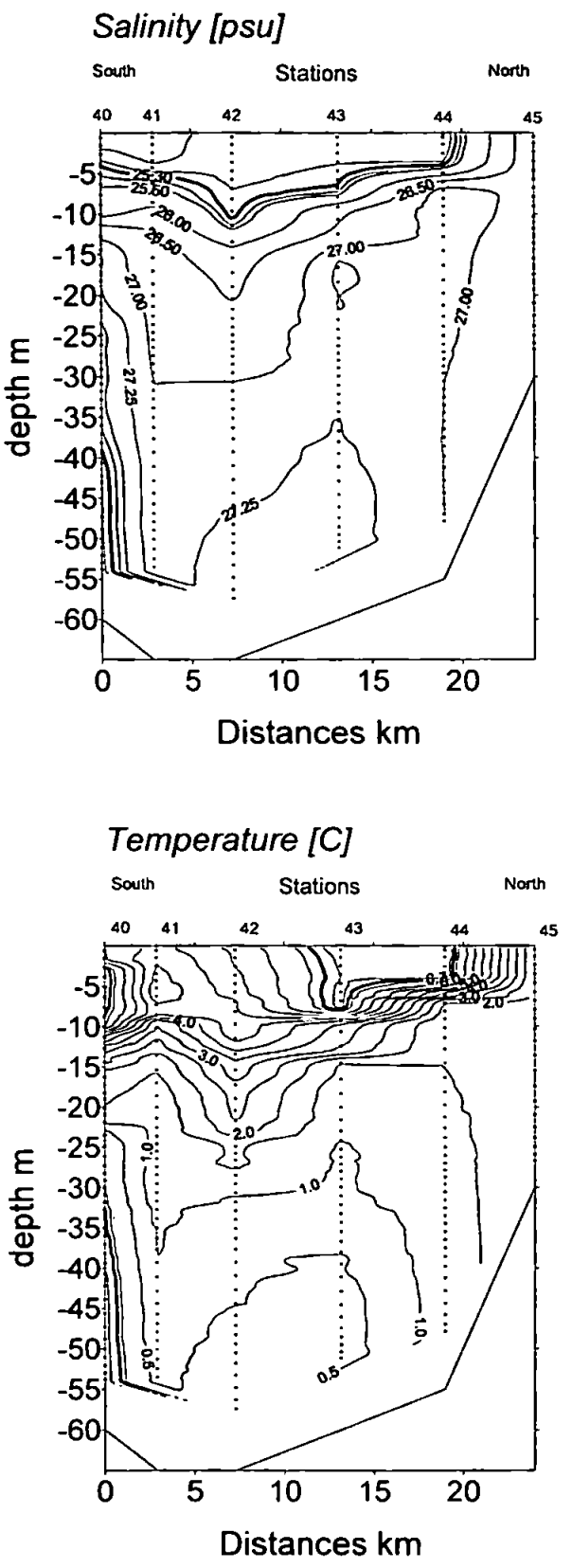


Figure 6.2f: Transect B4, section cross shore northeast of the White Sea, June 2000.

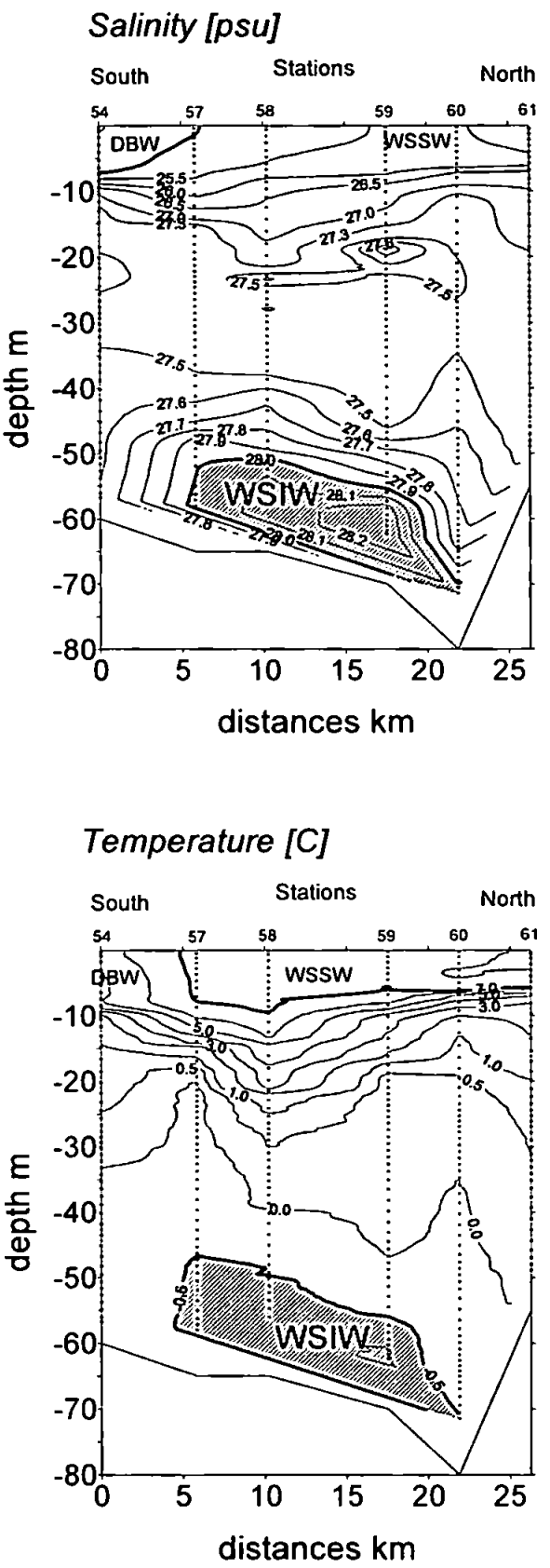


Figure 6.2g: Transect B6, section cross shore northeast of the White Sea, June 2000.

## 6.7. Intensity of mixing processes

Within the stratified layers, the intensity of mixing is controlled by the balance of production of turbulent energy by baroclinic shear currents, which facilitates mixing, and the hydrostatic stability of the water column, which suppresses mixing. The intensity of mixing can be regarded as the degree of reduction of the core of identified water masses. Therefore, T-S diagrams are useful tools to determine clearly the "core" of water masses, sometimes to localise fronts and mixing areas, and to identify mixed waters.

Core water masses and their mixtures are seen on the T-S diagrams (figure 6.3). In order to keep the figure clear, only three stations from the transect A4 are plotted (figure 6.3a), at station 25, 42 and 64 representing the eastern end, centre and the west of transect, respectively. The same approach is repeated with the northern thermal front localised at stations 17, 20 and 32 (figure 6.3b). South-western stations (58, 51, 54 and 53) are also selected to get additional information on the degree of mixing between local and possibly advected water masses (figure 6.3c).

Quasi-homogeneous layers previously formed may also mix with identified water masses due to local circulation. The diagrams (figures 6.3abc) show individual vertical measurements by unconnected symbols, so the core of a water mass or quasi-homogeneous layer (step-like structure) is located at a region where the density of these points is greatest in the T-S profile. On the other hand, stratified waters are represented by sparse points. Station 25 reveals the most uniform water, although two clusters, i.e. colder GSW and warmer and slightly fresher surface water are easily identified. Measurements at station 64 reveals three main water masses, cold and saline WSIW, warm and less saline WSSW, and a small amount of GSW penetrating into the Basin at 15-20 m depth in the form of a quasi-homogeneous layer. Measurements at station 32 clearly illustrate the source of the GSW on the Terskii Coast, revealed here as a single point. Located west of the thermal front, station 20 denotes two clusters of water: the WSSW and a saline water on the shallow-shelf (10 m to bottom 45 m), which presents a similar water characteristic to the GSW but 1 °C colder. Station 17 reveals the three water masses: the WSSW, the WSIW and the GSW. It is well stratified between the WSSW and the GSW, which progressively mixes with an underlying quasi-homogeneous layer (identified as step C in summer 2000) at 20 m depth.

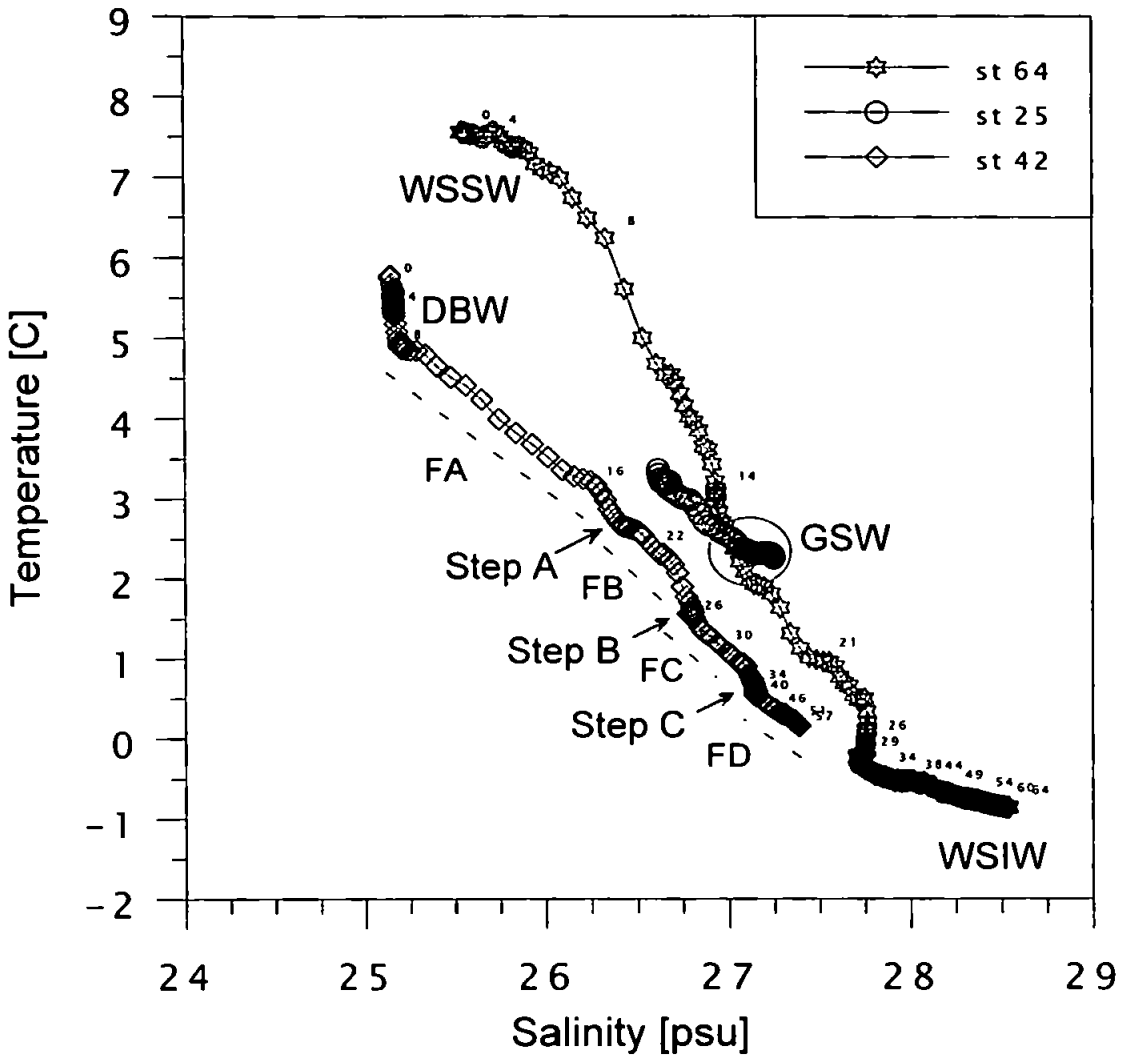


Figure 6.3a: T-S diagram of selected stations from Transect A4 showing the contacting water masses and different aspects of mixing in the south-west part of the Gorlo Strait. Depth of measurements (every 20 data points) is marked on the right hand side of the symbols. Sparse symbols show strong gradients and high density of symbols represents a core of water.

This mixed layer (step C) has originated from topographic stirring on the shallow-shelf, and is seen as a mixed layer propagating above the WSIW at ~30m depth.

At the south-west station 58 (figure 6.3c) the measurements shows the WSSW, a quasi-homogeneous layer (Step C) and the WSIW in the T-S profile. At the south-most station 53, however, the data show only the DBW and the mixed layer (Step C) at the bottom (22 to 45 m). At the station 51 the data indicates that DBW overlies surface water mixing with WSSW. Below, strong stratification appears and some mixing occurred within the vicinity of the thin layer which consists of the GSW. Dark symbols show the presence of a colder and more saline mixed layer (T=0°C and S=27.5 psu), which can

be interpreted as the previously formed Step C rather mixing strongly with WSIW clearly present at the sea bottom. Less presence of WSIW on the shelf, in the south area at station 54, rather suggests that temperature fluctuations are occurring in the upper layer, caused by the GSW that lies in a thin layer (10-12 m), creating turbulence or thermohaline fluctuation within the mixed layer (Step C). These fluctuations decrease along with the depth due to the presence of deep cold and saline near-uniformed mixed layers.

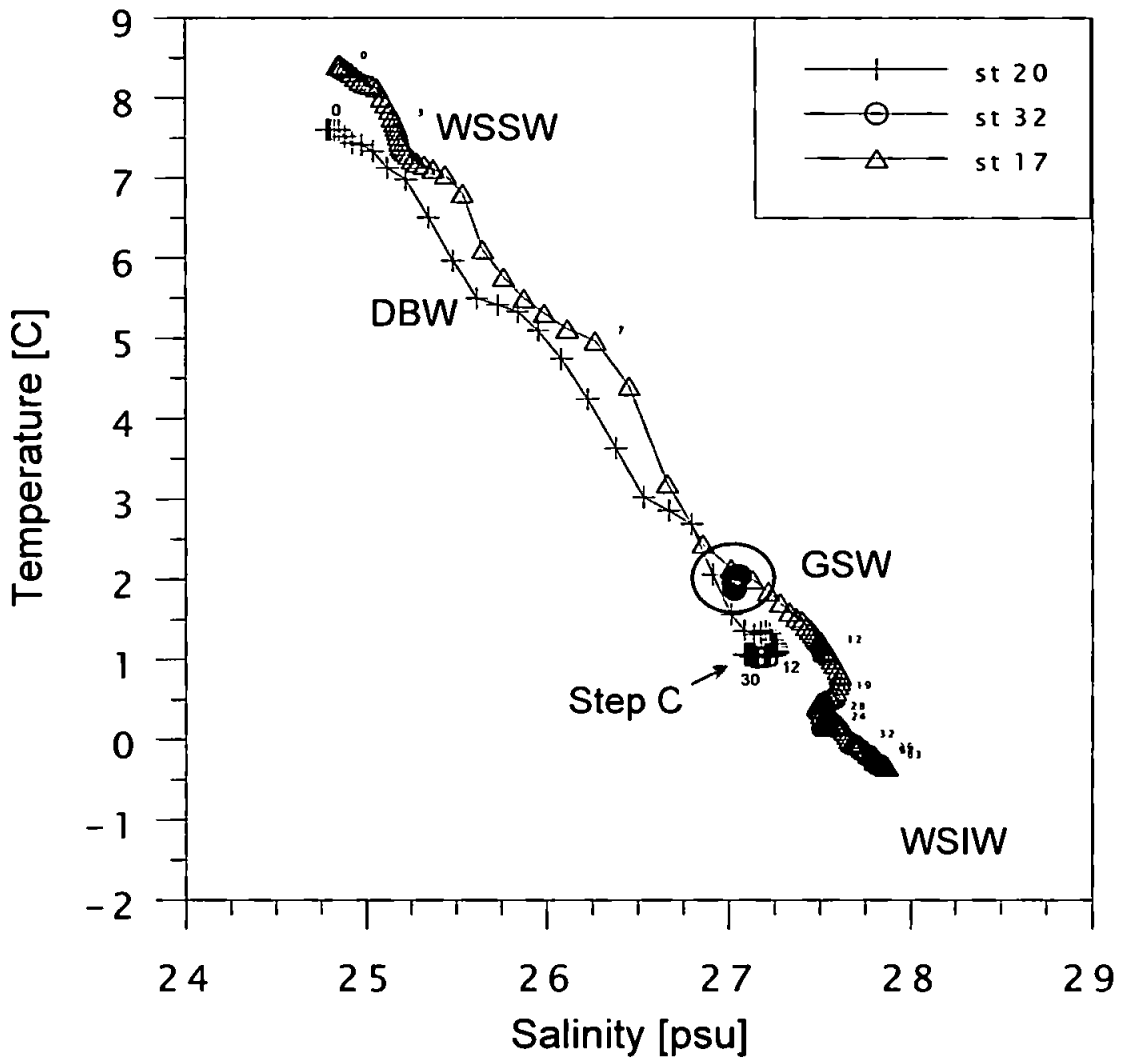


Figure 6.3b: T-S diagram of selected northern stations along the Terskii Coast showing the contacting water masses and different aspects of mixing in the south-west part of the Gorlo Strait.

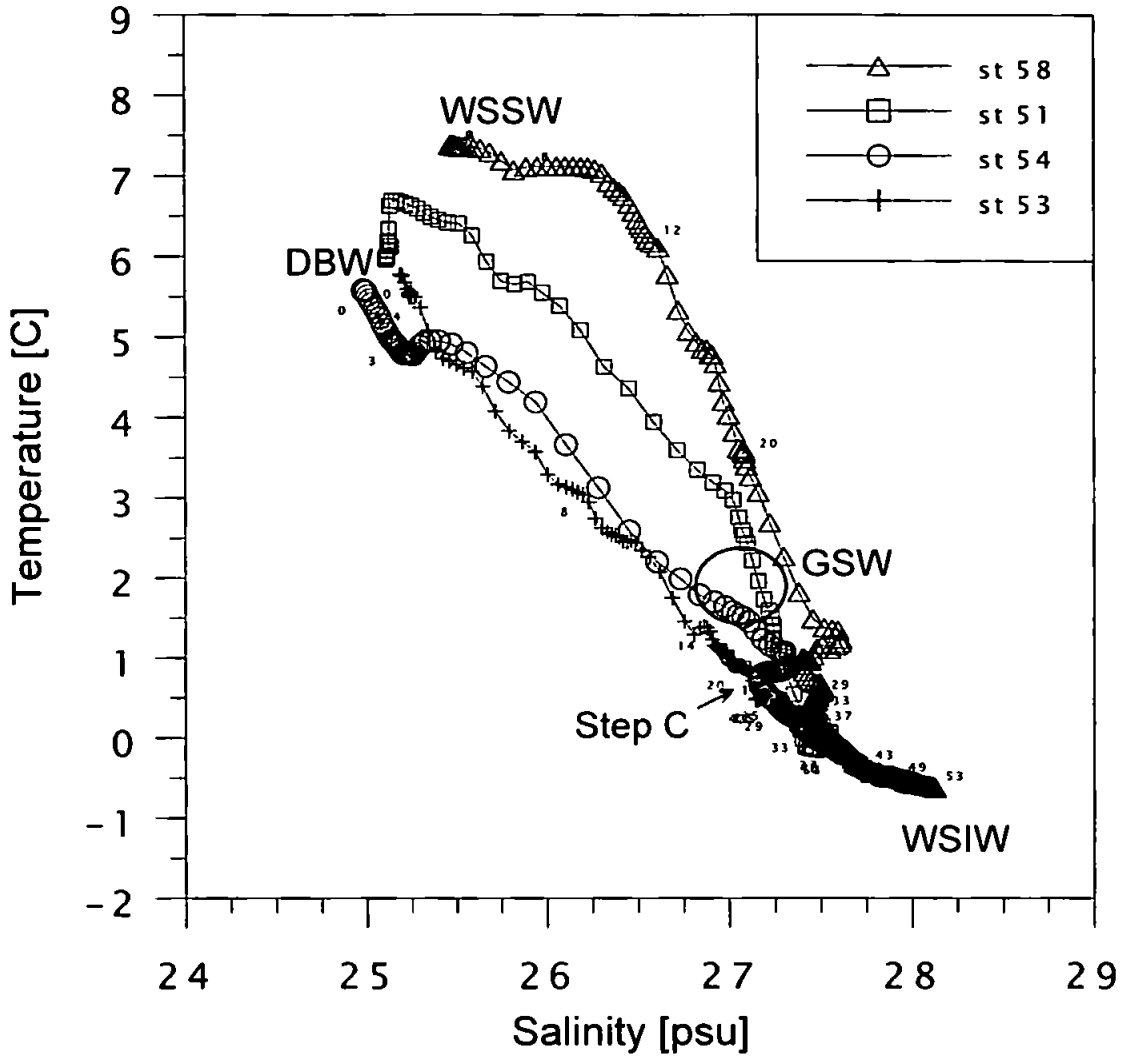


Figure 6.3c: T-S diagram of selected southern stations showing the contacting water masses and different aspects of mixing in the south-west part of the Gorlo Strait.

The most interesting and complex picture of the mixing process was observed at station 42. The temperature profile (figure 6.4) revealed a vertical distribution of core water masses and quasi-homogeneous layers seen as steps. Formation of such steps is likely to show stages of mixing at various depths, with presence of interlayer fluctuations.

These fluctuations were obtained by subtracting the averaged profile from the original high-resolution profile. Smoothing was performed by a running mean method with an averaging window of 15 data points. The top of the water column there, referred to figure 6.4 and figure 6.5, is occupied by modified DBW from the sea surface down to 6 m, marked DBW.

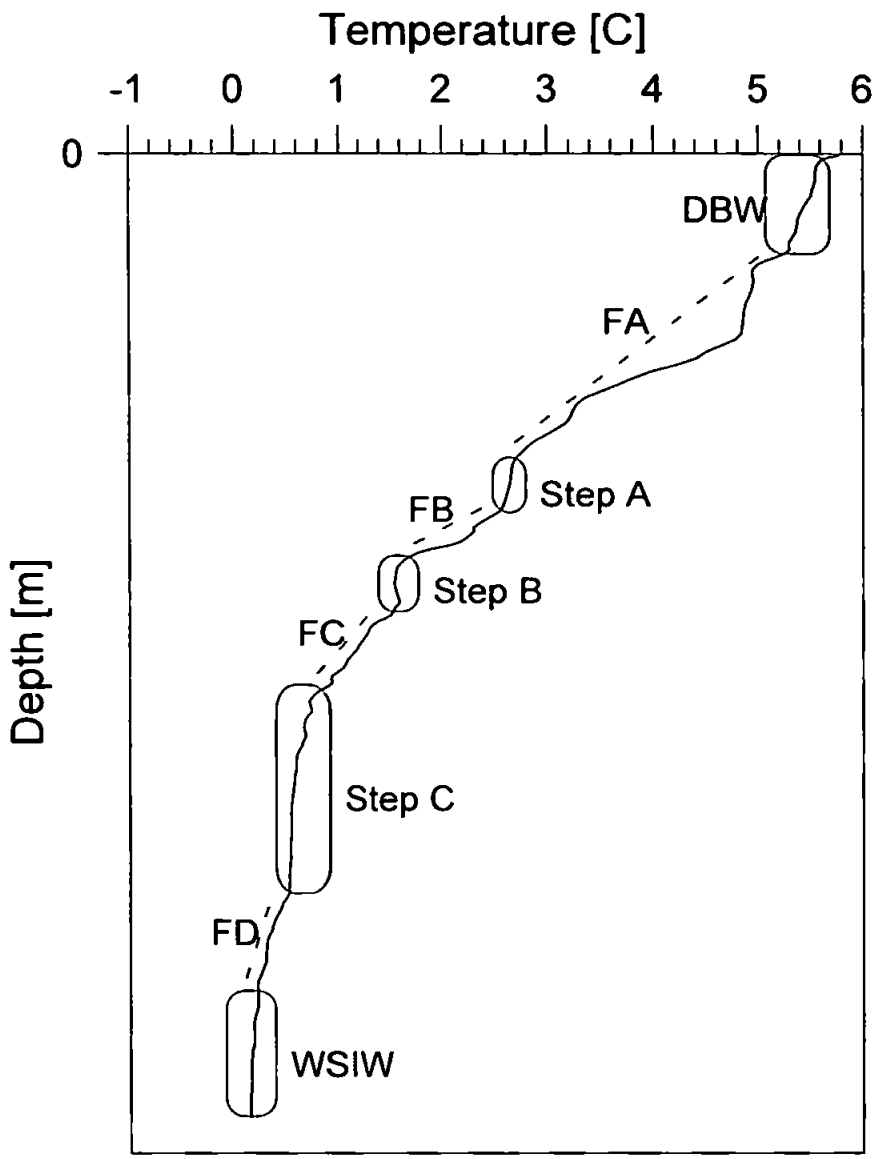


Figure 6.4: Temperature profile at station 42 showing the mixing region marked as anomaly fluctuations (FA, FB, FC, FD) and identified water masses with already mixed water from observed quasi-homogeneous layers (steps A, B, C).

At lower depths, a sharp stratified pycnocline (marked as FA) is observed and ends at 17m depth. Further down a 4 m thick homogeneous layer is found (Step A), which contains the mixture of DBW, GSW and small percentage of WSIW. Beneath the mixed layer, stratified layers FB and FC connect the temperature inversion (Step B, at 24-28 m) and the deep homogeneous layer (Step C, at 36-44 m). Mixed water with strong contribution of WSIW occupies the near bottom layer. Temperature fluctuations at station 42 are shown in figure 6.5.

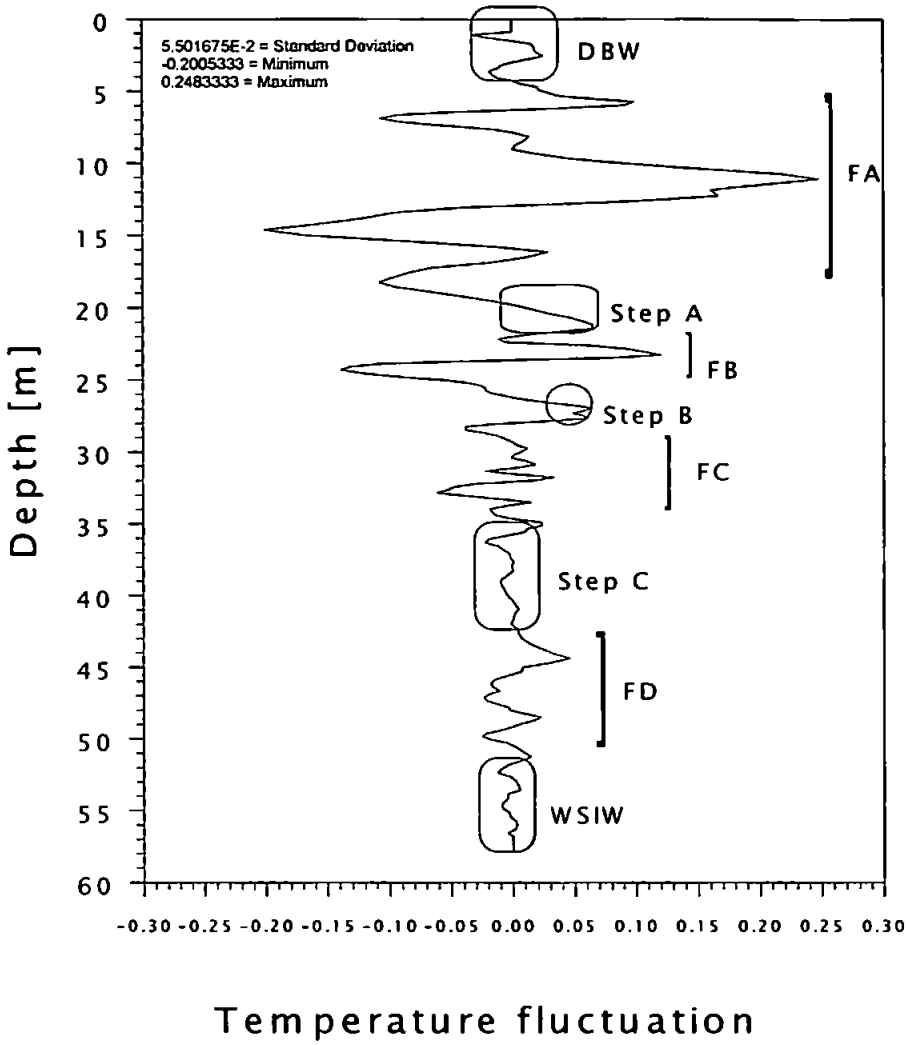


Figure 6.5: Temperature fluctuation at station 42 with marked water masses and mixed layers

The most intensive oscillations here, with maximum T'=0.25°C, are related to the thermocline (marked as FA), which separates surface DBW from modified waters of step A. Strong fluctuations are evident near the bottom despite the layer being already nearly homogeneous. Temperature and salinity fluctuations at stations of transect A4 are shown in figure 6.6 in appendix D. The biggest oscillations along the transect A4, T'=0.5°C and S'=0.1, are related to the lower boundaries of the sharp thermocline. These were identified as FA. West of transect, at stations 49 and 59, no fluctuations at 15-20 m depth reveal within vertical profiles the layer of modified GSW. Smaller fluctuations at 45 m (T'=0.05°C, S'=0.02) relate the strong contribution of the WSIW with the uniformly mixed layer identified as Step C. Strong evidence of fluctuations is seen in figure 6.7 in appendix D at station 58 at 20-25 m depth, which explains the

presence of the modified GSW in formation of a lens at ~20 m depth, therefore creating turbulence within the underlying mixed layer (step C).

## 6.8. Conclusion

The high-resolution CTD survey in summer 2000 has revealed the mechanism of mixing of different water masses in the south-western part of the Gorlo Strait of the White Sea. Four water masses have come into contact, identified as the GSW (T=2°C, S=27.2 psu), the WSSW (T=7°C; S=25.5 psu), the DBW (T=5°C; S=24.8 psu) and the WSIW (T=-1°C, S=28.5 psu).

The measurements were carried out soon after the maximal intrusion of the Dvina Bay Waters into the Gorlo area, and at the time of measurements the incoming waters from Voronka were warmer and saltier than the home waters of the White Sea. However, results show that the interaction of surface fresh waters (DBW/WSSW) with the GSW generate mesoscale eddies and formation of lenses (7-8 km and 8-10 m thick). Lenses are likely to propagate into the White Sea as they detach from the local circulation (Terskii current, Dvina gyre) although they may collide again with the system. Formation of mesoscale eddies and/or lenses, apparently due to baroclinic instability, extend the length of the boundary that separates differing water masses and hence facilitates horizontal mixing This kind of system was reported in the Gulf Stream with interaction or partial coalescence of rings along the stream (Richardson, 1980; Gregg and Sanford, 1980).

The intrusion of the GSW was clearly evident in the White Sea waters, separated either by a sharp thermocline or by fronts. The core of the GSW was considerably reduced across the Strait towards the entrance of the White Sea, although its water properties were slightly reduced along the Terskii coast as entrained by the Terskii current, provided resultant mixed water to be advected into the White Sea Basin along the Terskii Coast.

Mixing processes included vertical stirring (highly enhanced by strong tides in the Gorlo Strait) and horizontal exchanges through interleaving at the thermal and salinity fronts. At the surface, meandering fronts are initiated by baroclinic instabilities caused by local gyre mainly influenced by the Dvina Bay circulation and/or the Terskii current (see Dvina Bay cyclonic gyre in figure 2.11b; Timonov, 1947). Near the bottom mixed

waters are formed by topographic stirring and separated by a front originating from a source such as the bottom GSW and the bottom-slope WSIW.

The intensity of mixing is well indicated by analysis of temperature and salinity fluctuations. The greatest fluctuation occurred under the thermocline connected to the intrusion of the GSW and the supply of fresh water coming from the south of the White Sea (formation of lens). Observations of interlayer fluctuations also prove stages of mixing at various depths between mixed layers and the core of water masses (DBW at the surface, WSIW near the bottom).

# Chapter 7: Estimates of mesoscale circulation

## 7.1. Introduction

The first scheme of a general circulation of the White Sea was proposed by Deryugin in 1928. His work was based on the postulate that all semi-enclosed seas in the northern hemisphere have an anticlockwise circulation. Such circulation was explained either by the predominance of cyclonic wind over the seas or by the combination of river inflow and the Coriolis force. The constant fresh inputs from the White Sea Bays, starting to act when the surface ice sheet melts in March, generate an outflow surface current of fresh water through the Gorlo Strait. Deryugin (1928) concluded that the nature of such surface currents were responsible for the observation of the main cyclonic circulation (see figure 2.11c) in the White Sea (Gidrometeorologiya, 1991). However, Deryugin's circulation scheme stood on indirect methods to derive current velocities, there by leaving the general circulation with inferred currents (figure 2.11a). The circulation scheme of the White Sea has been slightly improved by Timonov (1947 and 1950) using measurements and a dynamical approach to calculate currents near Kandalaksha and Onega Bay (see figure 2.11b). Numerical models have attempted to resolve the tidal circulation of the White Sea (Semenov and Luneva, 1996 and 1999), and hydrological conditions in the White Sea Bays were investigated during the summer 1991 and 1997 (Agatova and Kirpichev, 2000), but none of the previous studies have directly shown the importance of the outflow current of fresh surface water contributing to, for example, the formation of mixed layers (see Chapter 4 and 5) observed in the White Sea. The mixing of complex structure of water masses (notably the intrusion of saline water with the fresh surface waters of the White Sea Bays) southwest of the Gorlo Strait (Chapter 6) results in the formation of mixed layer with slight changes in their characteristic properties (for example the GSW is modified along the Terskii coast, partially caused by lateral and/or vertical mixing) as they propagate in the semi-enclosed sea. It is important to study the surface circulation of the White Sea to reveal the existing relation between fresh water inputs from the White Sea Bays, which can be

traced by AVHRR satellite sensors, and the surface dynamics, which can be derived from satellite altimeters.

The present chapter here introduces recent observations of mesoscale features in the circulation of the White Sea using in situ measurements (horizontal distribution of temperature and surface dynamic height) to validate satellite images, such as maps of Sea Surface Temperature and Sea Level Anomaly. The chapter focuses on the important contribution of the fresh water inputs from the White Sea Bays and its variability which is relevant to the dynamics of the White Sea (figure 4.8) in the upper layers (0-50 m). It also focuses on the variability of the cyclonic gyre in the Basin, which is likely to facilitate the intrusion of the Gorlo Strait Water (GSW) associated with the Terskii Current. The maxima of river discharge during summer season are traced to observe any changes in the surface circulation of the White Sea disregarding the wind factor. The results lead to some hypothesis about the mesoscale eddy activity in the White Sea, notably the main cyclonic circulation of the Basin and mesoscale eddies in the Voronka region. A number of consecutive Sea Surface Temperature (SST) and corresponding Sea Level Anomaly (SLA) images show the important contribution of the freshwater runoffs in the dynamics of the surface circulation of the White Sea.

## 7.2. The use of satellite images

The circulation of the White Sea during the period of summer 2000 is assessed using satellite images such as Sea Surface Temperature (SST) images and Sea Level Anomaly (SLA) maps. Figures 7.1 and 7.2 shows respectively the SST and SLA images processed at a time that corresponds best with the duration of the White Sea campaign 2000. The SLA maps allow to identify the mesoscale eddy circulation, and the SST images allow to identify small-scale oceanic features. Selected maps of SLA and SST are compared with horizontal distribution of water masses and dynamical height (see chapter 3 for its calculation) derived from the hydrographical survey 2000 to validate the mesoscale structure and circulation of the surface waters of the White Sea.

The available SST images of the White Sea have been processed at the Plymouth Marine Laboratory (PML) for the two month period of June and July 2000 (see table 3.I in chapter 3 for the dates; and see appendix E figures 7.10 to 7.25 for the corresponding SST images).

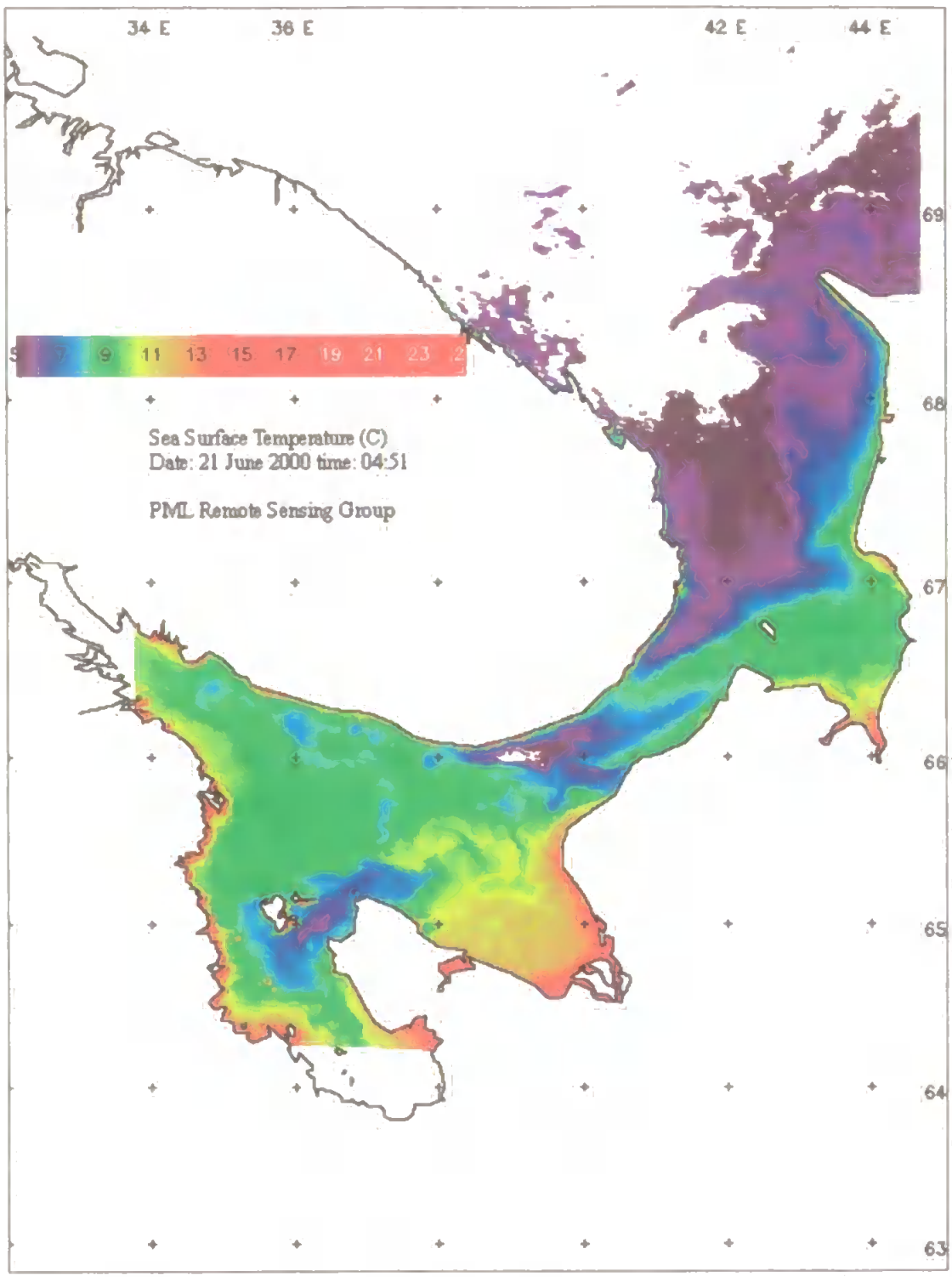


Figure 7.1: Sea Surface Temperature image taken the 21 June 2000 in the White Sea.

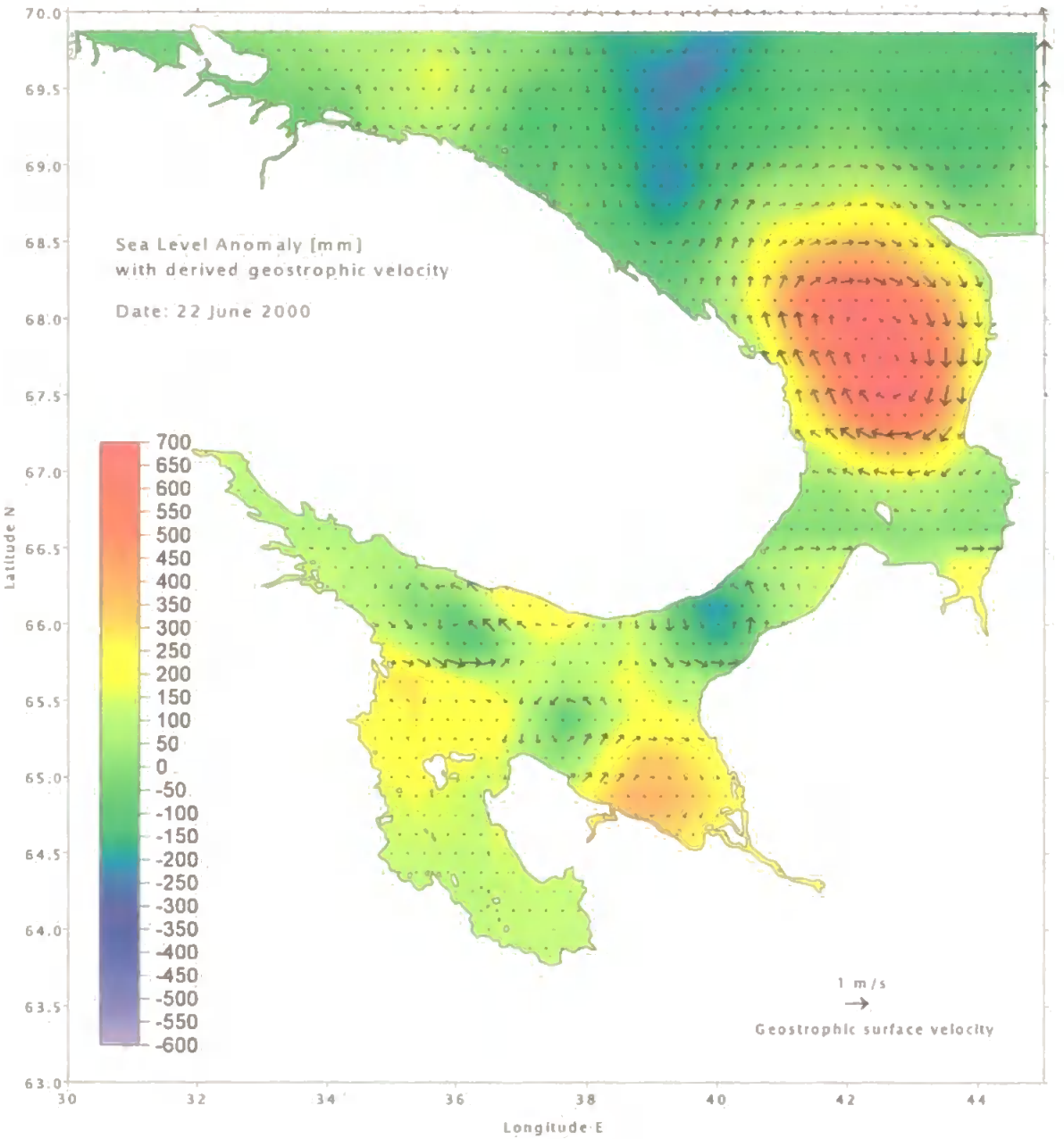


Figure 7.2: Sea Level Anomaly image map of the White Sea with geostrophic surface velocity derived from SLA data for the 22 June 2000.

Maps of Sea Level Anomalies (MSLA) derived from the altimeter data products, were generated by the CLS Space Oceanography Division.

The spatial resolution of the SLA data is a quarter of a degree in latitude and longitude and the sequence of SLA maps are every 10 days. The SLA altimeter products have been extracted from a database provided by the AVISO project (Le Traon *et al.*, 1995; Le Traon and Ogor, 1998; Le Traon *et al.*, 1998). Contour maps of errors, as a

percentage of the altimetric signal variance, were drawn (see figure 3.6 in chapter 3) to indicate the location of reliable altimetric signals in the White Sea with a signal errors of < 20%. Reasonable altimetric signals were obtained in areas such as the Basin, offshore from the White Sea Bays (~25 km away from the coast), the western part of the Gorlo Strait, the Voronka region and the Barents Sea. Geostrophic currents have been derived from the SLA product for every 10 days (Latché, 1999) and superposed on the MSLA to get a better picture of the general circulation of the White Sea.

### 7.2.1. SST and *in-situ* temperature distribution

According to the CTD measurements, which were taken between the 16-to-19 June 2000 (station 10 to 82) around Terskii-Gorlo and from 20-to-23 June around the area of Kandalaksha Bay and the Basin, it is therefore better to compare contours of surface temperature (figure 7.3a) for the area of Gorlo with the SST 21 June (figure 7.1), and the area around Kandalaksha Bay / Basin with the SST 23 June (figure 7.3b). The horizontal temperature distribution at 5 m depth in the northern part of the White Sea (figure 7.3a) show reasonable agreements with the temperature gradient shown by the SST images taken on the 21$^{st}$ and the 23$^{rd}$ of June 2000 (figures 7.1 and 7.3b).

The observed surface features are: (i) the Terskii current associated with cold water, (ii) small eddies confined to Kandalaksha Bay and the Basin and (iii) frontal zones which separate estuarine warm and fresh surface waters from cold saline waters.

(i) The Terskii current (constrained to maximum 30 m depth, Deryugin, 1928; Timonov 1947 and 1950) is revealed here by the cold surface temperature (< 7°C). The distribution of such cold water in the SST image indicate clearly that the Terskii Current is a source of entrainment for the intrusion of the modified GSW to reach the waters of Kandalaksha Bay (figure 7.3b and figure 7.10 in appendix E). The water strongly mixes with the tides in Gorlo (Chapter 6) forming the GSW: T=2°C; S=27.2 psu (in summer 2000). The GSW penetrates into the White Sea in fine oscillating mixed layers (Chapter 4 and 5) and mixes again with the White Sea waters with some GSW left to flow along with the Terskii current (figure 7.3) to gradually mix with near-surface estuarine and river waters along the north coast of Kandalaksha Bay.

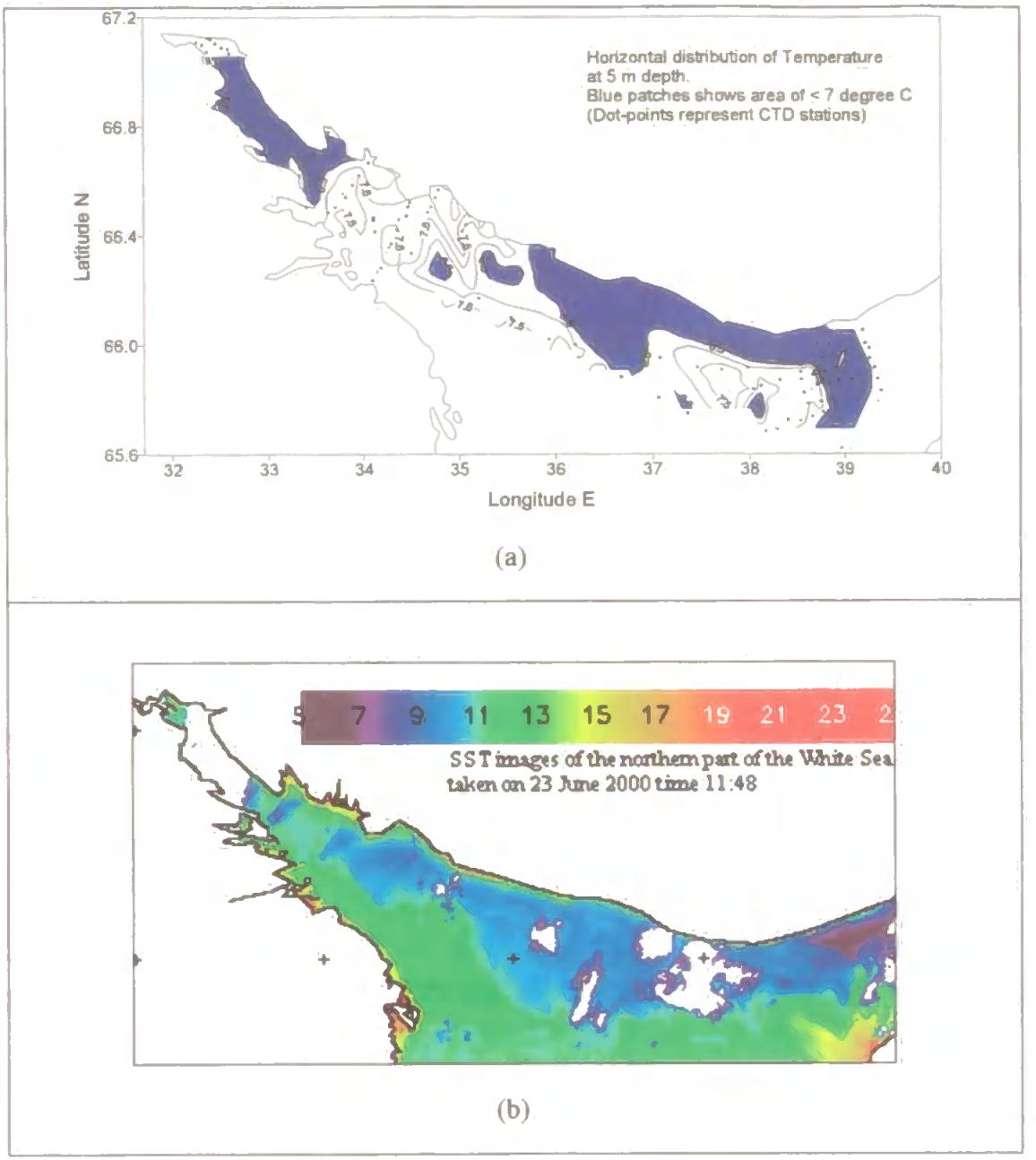


Figure 7.3: (a) Contours of temperature at 5m depth derived from CTD measurements (17-23 June) compared with (b) the SST image taken on the 23 June 2000, in the northern part of the White Sea. The cold water is located along the Terskii coast (associated with the Terskii Current) and mesoscale eddies are observed in the Basin/Kandalaksha Bay.

(ii) The surface fronts are well observed in figure 7.1 and 7.3a, one located at the entrance of the White Sea and the second in Kandalaksha Bay and off the Chupa estuary. This shows the extent of the Basin water mixing with the Gorlo Water on one end, and on the other end, mixing with the Terskii coastal waters and fresh and warm

Kandalaksha waters. In Kandalaksha Bay, the temperature gradient at the front is about 4°C in the surface layer (10-20 m), and decreases to < 1°C at > 30 m depth (see figures 4.3a and 4.3c).

(iii) Mesoscale eddies are generated due to the different water masses into contact (see figure 6.1a). Previous studies (Gidrometeorologiya, 1991) have confirmed the predominant cyclonic circulation (see figure 2.11c) in the Basin which is partially associated with the Terskii current. The SST (figure 7.1) shows here a numbers a small gyre along the Terskii coast (blue patches) which are likely to be small and local cyclonic features, resulting from interacting water masses (Basin Waters and coastal waters). At 30m deep (see figure4.3a in chapter 4) the contour line of temperature 1°C depicts the main cyclonic system of the Basin here in June 2000, confined to the Terskii shore with local meanders associated with small scale eddies (at 35-36°E and ~66.4°N). In Kandalaksha Bay, and off the Chupa estuary, anticyclonic and cyclonic eddies are observed in the SST (figure 7.3b). The cyclonic eddy (66.3°N, 34.5°E) has a core temperature identified as < 6.5°C at 5m (figure 7.3a) and < 1°C at 20m (see figure 4.2a). The anticyclonic eddy (66.5°N, 34°E) has a core temperature of > 7.5°C at 5m depth and ~5°C at 20 m depth. The analysis of the SLA maps will confirm the mesoscale circulation of the White Sea, in the Basin in particular; however it will not resolve the circulation inside the Kandalaksha Bay. Therefore the SLA map (22 June 2000) is complemented with the dynamic height in the region of the northern White Sea to support the observations.

### 7.2.2. SLA and dynamic height

The SLA data with the corresponding dynamic height in the northern White Sea derived from the survey 2000 are analysed and compared here to support the observation of the mesoscale features shown by the SST image and the *in-situ* temperature field (figure 7.3). The dynamic height for Kandalaksha Bay-Basin was calculated using a surface reference level of 5 m depth and a bottom reference level of 100m depth (figure 7.4). The results derived from the two data-sets effectively corroborate and show the presence of the cyclonic eddy. The structure of the eddy observed through the SLA map follows strikingly the 100 m isobaths of the Basin adjacent to Kandalaksha Bay, showing both negative values of SLA (-0.25 m) and of dynamic height (-0.25 dyn).

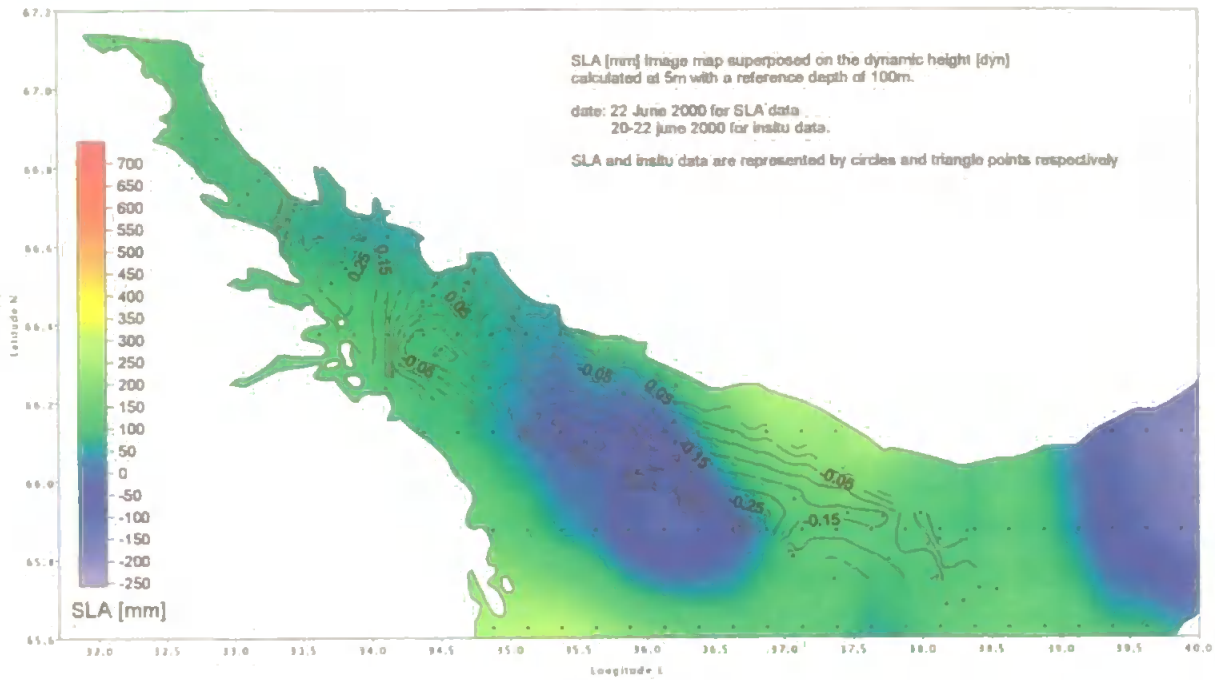


Figure 7.4: Contours of dynamic height (dyn) calculated at 5m depth with a reference level of 100m, superposed on image map SLA (in millimetres), in the northern part of the White Sea.

Surface currents are derived from the SLA data, based on geostrophic assumption. Their calculations permit to give a rough estimation of the amplitude and direction of the surface currents in the White Sea (figure 7.2). These currents superimposed on the SLA maps give a better picture to further analyses on the summer circulation of the White Sea. The results from the satellite images are validated by the corresponding *in-situ* measurements which have clearly identified the main cyclonic circulation in the Basin. The front zone located off the Chupa estuary is also well depicted in the dynamic height with the contours of 0.1 to 0.2 dyn. The local circulation associated to the front zone suggests an anticyclonic eddy nested inside Kandalaksha Bay (figure 7.4) with contours of 0.25 dyn. The constant inputs of river runoff deflecting to the right (figure 7.1) from the Chupa and Onega estuaries in summer plus the intrusion of the modified Gorlo water along the Terskii Coast maintain the main cyclonic gyre of the Basin as well as preserving the salinity ratio of the WSSW (Timonov, 1950). The cyclonic eddy (figure 7.2) observed through the SLA map on the 22$^{nd}$ of June justify the dome-like structure

(figure 4.6) of the intermediate mixed layers (at 60 to 120 m depth) confined to the Basin.

The horizontal distribution of salinity and temperature at 60 m depth (figure 4.3f), reinforce the fact that the circulation at the intermediate layer is well dissociated from the active upper layers which confirm the status of intermediate layer (identified here as step D and E; see Chapter 4 and 5) as a boundary layer. Near Kandalaksha Bay, the SLA geostrophic velocity is < 0.5 m/s, which agrees with the results found in Howland *et al.* (1999).

The downwelling isotherms depicted in the east west transect (figure 4.6), with its centre located at station 132 (near the deepest part of Kandalaksha Bay) also reinforce, despite the lack of reliable SLA data near the coast of Kandalaksha Bay, the presence of a small anticyclonic eddy (also revealed by the dynamic height contours of 0.25 dyn in figure 7.4). Its existence can be explained by the possible entrainment of potential vorticity caused by its larger neighbouring cyclonic eddy in Basin but also caused by the front zone which the circulation of river waters flowing out of Kandalaksha Bay with the intrusion of saline water (Terskii Current). Furthermore, both eddies are nested respectively in the two deepest topographic troughs (or depression) of the White Sea.

### 7.2.3. Mesoscale eddy activities from SLA and SST

The SST (figure 7.1) and the SLA (figure 7.2) images clearly show the presence of the main cyclonic gyre nested in the Basin in June 2000. Off the Lietny coast, a hammer-like shape feature is observed in the SST on the 21 June and shown in the SLA maps as a vortex system. It is present 10 days earlier in June 12 (figure 7.6 in appendix E) with an estimated geostrophic velocity of 0.5 m/s. This coastal jet system arises from the presence of a cyclonic eddy off Dvina near cape Lietny, associated with the observed anticyclone gyre of the bay. The SST image on the 21 June did not indicate fresher (and warmer) surface water in the Dvina Bay nor in June 8 (figure 7.12 in appendix E) indicating a very low river discharge. However, the cyclonic eddy situated off the cape Lietny at the mouth of Dvina Bay in figure 7.5 and 7.6 in appendix E show some agreements with the results of Timonov (1947, see figure 2.11b), which support the reliability of the SLA data.

### 7.2.4. Summary of validating satellite images

Satellite images such as SST and SLA can be used to assess the circulation of the White Sea during summer 2000. The comparisons between *in-situ* and satellite images have shown good agreements and also with previous studies in the general circulation scheme of the White Sea. Before analysing further satellite images of the White Sea, the main and interesting key-points outlined from that preliminary comparative analysis are given as follows:

- The water from the Barents Sea entering Gorlo and the northern part of the White Sea is markedly revealed by sharp contrast of colour in the SST image of 21$^{st}$ and 23$^{rd}$ of June, indicating presence of interfering water masses.
- Horizontal sections of temperature distribution (at 5 m and 20-30m depth) illustrate the elongated water mass of Gorlo carried northward by the Terskii Current (known to follow the 30 m isobaths).
- The frontal zones at the entrance near Gorlo and in Kandalaksha Bay.
- The main and predominant cyclonic gyre in the Basin, which refers to figures 2.11a and 2.11c, explains the domed structure of the intermediate mixed layers in the White Sea.

## 7.3. The White Sea circulation in June-July 2000

The results from the satellite images obtained for the period of June-July 2000 show that Deryugin's assumptions (1928) concerning some of the inferred local circulation of the White Sea were correct (figure 2.11a), although it is likely to be more complex. The sequence of satellite images reveal that cyclonic gyres are likely to dissipate relatively fast to be replaced by anticyclones being formed, probably in respond to the variability of freshwater inputs in the White Sea Bays. The evident oceanic feature observed here in the sequence of SST images (figure 7.10 to 7.25 in appendix E) is the variation of maximum river runoff well indicated during all summer by yellow patches revealing warm and fresh surface water in the White Sea Bays. The stronger the contrast of colour the maximum of freshwater inputs is indicated. The analysis of the sequence of SST images during summer 2000 enables us to classify here by order of importance the contribution of river discharges for the White Sea circulation which are: 1) river Dvina,

2) river Onega, 3) rivers of Kandalaksha, and finally 4) river Mezen. Coastal along-slope currents were identified from SST images as filaments (elongated colour patches) revealing fresh water masses flanking the coastlines.

### 7.3.1. Entrance of the White Sea: the Gorlo Strait

The outflow-inflow system contributing to the water mass exchange in the Gorlo Strait is well denoted by a sharp contrast of colour indicating a frontal temperature gradient, seen in the SST images on the 21 June (figure 7.1) and on the 17 July (figure 7.22 in appendix E). Previous studies have indirectly traced the intrusion of the Barents Sea water in the Gorlo Strait by looking at the distribution of phytoplankton (Deryugin, 1928), but none have directly documented the intrusion of the modified GSW into the White Sea using SST images (see feature in figures 7.10 to 7.25 in appendix E). On the other hand, the SLA data are not reliable in the Gorlo Strait since the channel is too narrow (~50 km across) for the altimeters to resolve the SLA signal.

### 7.3.2. White Sea Bays and the Basin

Cyclonic eddies in the White Sea Bays are well depicted in the SLA maps such as in Dvina, Onega and Mezen. The calculation of salinity anomaly by Pantiulin (1974) has shown a warm pole around Kandalaksha and a cold pole in the Basin. These poles are eddies as discussed in the sections above, and are well detected in the SLA image (figure 7.2). Furthermore it is supported by the SST images which indicate quite clearly the importance of the river discharges flowing into the White Sea in a clockwise circulation. The sequence of SST images also indicates clearly the fluctuation of the river discharge. The structure of the main cyclonic gyre in the Basin varies considerably (figure 7.5 to 7.6 in appendix E) probably due to low contribution of river discharges. The SLA-derived geostrophic velocity is estimated at 0.5 m/s which correlates with the surface currents calculated from the numerical model (Gidrometeorologiya, 1991) using only permanent thermohaline forcing scheme. An anticyclonic eddy (SLA maps 2, 12 July: figures 7.7 and 7.8 in appendix E) is formed offshore Onega Bay and south of Kandalaksha, probably resulting from the presence of cyclonic activity inside Onega Bay. In a week's time, this anticyclone has moved northward (SLA map 22 July: figure 7.9) and set in the Basin, reversing the whole circulation of the White Sea Basin. It is very much difficult to relate the reversed circulation of the Basin to any changes in the

freshwater inputs from the White Sea Bays since the entire White Sea is covered by yellow patches which only indicate very warm surface layers (SST 17, 19, 20 July: figures 7.22 7.24 in appendix E). However, Lednev (1934) observed such an anticyclonic gyre in the Basin during summer. He reported that this 'anticyclonic dome' is of interest since downwelling (descent of waters) have been observed and constrained within it, according to flow convergence.

## 7.4. Discussion

Fresh water currents were clearly indicated on the sequence of SST images as filaments deflected in an anticlockwise direction, preserving the constant freshness of the upper layers in the White Sea Bays with some contribution to the general circulation of the White Sea, but notable in Dvina and Kandalaksha Bays. The fluctuation of river runoff during summer was seen through the SST images, altering local circulation and small-scale structures of eddies inside the White Sea Bays. Previous studies on the dynamics of the White Sea circulation (Gidrometeorologiya, 1991), excluding the atmospheric forcing component, have shown that it is driven mainly by residual tidal currents associated with baroclinic currents. Tidal currents have an important contribution in the general outflow current and circulation in some part of the White Sea. To rate the contribution of tidal and non-periodic (baroclinic) flow among the general flow circulation of the semi-enclosed sea, a ratio was introduced to differentiate them. Positive ratios, indicating that tidal streams exceed currents, were found mainly in the Basin and Gorlo, whereas negative ratios were found near Kandalaksha and Dvina Bays, showing the tidal regime as relatively non-existent. The comparison of observational data using SLA map (figure 7.2) and results from numerical models (Gidrometeorologiya, 1991a) showed good agreements in the regions where the tides prevail in the White Sea circulation with a consequent tidal flow: in the Mezen Bay (with 1.8m/s predicted), in the Voronka and in the Gorlo Strait (1.2m/s predicted). With reliable SLA signals (see SLA signal error in figure 3.6) in the Basin of the White Sea, the SLA data have generated a reasonable surface topographic map to analyse the White Sea circulation. The variation of the surface elevation seen through the SLA maps may reflect either the tidal residual circulation (mainly observed in Voronka and Mezen Bay, e.g. the resulting strong anticyclone nested in the Voronka region, in figure 7.2), or the thermohaline circulation (which mainly results from the strong river discharges in the White Sea bays). However, it is not very clear whether or not the SLA data can show

the main contribution from the tidal residual and/or thermohaline flow in the observed circulation, as observations (Gidrometeorologiya, 1991a) show these currents of the same orders of magnitude in the Basin (e.g. baroclinic flows were observed up to 0.3m/s in the surface layer (0-10 m) but only < 0.05m/s below (> 15 m depth); and predicted tidal flow was given 0.3 m/s, in the Basin). Therefore, the mesoscale circulation was estimated knowing the potential areas in the White Sea where tidal residual circulation and thermohaline circulation prevail.

In the north of Voronka, the cold and saline Barents Sea Water enters Voronka (known to be entirely vertically mixed due to strong tides); as it approaches Kola Peninsula, it flows in the shallow Gorlo Strait forming the modified Gorlo Strait Water. The tidal residual flow in the Voronka reinforced by river runoffs from Mezen (SST 21 June 2000, figure 7.1) was the mechanism entraining the strong observed anticyclonic eddy nested in Voronka (figure 7.2). The corresponding SLA-geostrophic velocity at the edge of the anticyclone was about 0.80 m/s, which corroborates the results of the numerical model (Gidrometeorologiya, 1991) based only on the "permanent thermohaline flow" forcing. This suggested a relatively low contribution from the tidal residual component in the circulation in Voronka around the 22 June 2000, but an important contribution from the baroclinic flow (originating from the constant positive White Sea outflow in the surface layer of the Gorlo Strait). Following the summer observations, two hypotheses arise:

(i) Mesoscale activities in Voronka showed a large anticyclonic gyre. The eddy had a weak structure in the first weeks of June (SLA maps 2, 12 June: figure 7.5 and 7.6), which may be caused by less freshwater inputs from Dvina and Mezen rivers. However, at the end of June and beginning of July, the structure of the anticyclone had strengthened and extended to the Barents Sea (SLA map 02, 12 July: figures 7.7 and 7.8 in appendix E) associated with strong river discharges (SST 25, 26, 28, 29, 30 June, 15 to 20 July: figures 7.11 to 7.15 and 7.20 to 7.24 in appendix E).

(ii) The mesoscale circulation in Voronka reversed to cyclonic gyres (SLA map 02 June, 22 July: figures 7.5, 7.9 in appendix E) when the Mezen river shows reasonable runoffs (SST 19-20 July: figure 7.23-7.24 in appendix E). A cyclonic eddy was formed in the Mezen Bay entrained by the well defined filament of fresh water which also contributed to a strong outflow jet observed offshore (formation of the west cyclone and the east anticyclone, nested at the entrance of Voronka, see SLA map 22 July, figure 7.9 in

appendix E) also possibly sustained by the constant outflow of surface White Sea waters originated mainly from Dvina Bay which is the case here in 20 July.

The small scale 'anticyclonic dome' (B) referred by Deryugin (1928) (figure 2.11a) adjacent to the Basin area was associated with descending waters constrained within the eddy. The anticyclone has been depicted here by the satellite images and needs to be investigated in the next cruise conducted in the White Sea, since it may facilitate shelf-edge dense water from Kandalaksha Bay to protrude down slope into the deep layers of the Basin.

The hypothesis for the formation of the mesoscale anticyclonic gyre of the Basin might correlate with the 2 large cyclonic eddies, one located in Dvina Bay, the second off Onega Bay adjacent to the Basin. The second may be formed by responding to a large extent of fresh surface water flowing along the western flank of Onega Bay (SST 15 to 20 July, figures 7.20 to 7.24). The freshwater discharges in Kandalaksha also may be an important factor to weaken or change flow direction in the surface layers in the north of Kandalaksha Bay close to the Terskii shore (SST 20 July: figure 7.24). However it is possible that during spring tides, tidal residual current in the White Sea may contribute as much as baroclinic current in the surface layers to sufficiently change and reverse the Basin cyclonic gyre to an anticyclonic circulation.

## 7.5. Conclusion

The satellite images used to investigate the mesoscale oceanic features in the White Sea were validated with good agreement between the satellite data and the observations based on surface dynamic height and horizontal surface temperature field. The use of SST images allows the tracing features of freshwater circulation in the White Sea Bays. Fresh surface currents generated from river discharges were observed as elongated filaments of water flanking the coasts and extending in an anticlockwise direction. Some of the SST images showed the intrusion of the Barents Sea water entering the Gorlo Strait as a filament of water propagating northward along the Terskii coast and in Kandalaksha Bay. The SLA maps were used to investigate the shape and the circulation of the mesoscale eddies with an accurate SLA signal near Kandalaksha Bay, in the Basin, and in the Voronka, however not precisely accurate along the coastline and

therefore discredited near the estuaries. The complex circulation of the White Sea was nevertheless observed inside and outside the White Sea Bays by means of SST images. The analysis of the sequence of satellite images has proved that, in the surface layers, the circulation of the White Sea is very much dependent on the White Bay currents with a probably small contribution from tidal residual currents (of same magnitude of order in the surface layers in the Basin). The sequence of satellite images has revealed fluctuations in the river discharges (coming from Kandalaksha, Onega and Dvina Bays), which have a direct impact on the general flow circulation of the White Sea, since baroclinic flow dominate the local circulation of the White Sea Bays. It has an important impact on the formation of the mixed layers found in the south-west region of the Gorlo Strait. It is an open challenge for numerical modellers to distinguish the real contribution of the tidal residual currents in the Basin, which are often of the same magnitude of order as the baroclinic currents (strongly variable with the river discharges) in the surface layers of the White Sea.

# Chapter 8: Isopycnal and Diapycnal analysis on the Gorlo Strait Water displacement

## 8.1. Introduction

The small scale mixing processes play an important role in the thermohaline structure transformation of the Gorlo Strait Water (GSW). This water originated from the Barents Sea, enters the White Sea through the Gorlo Strait and is vertically mixed due to strong tides. It then flows along the northern part of the White Sea Basin as a filament (Terskii current) at 20 to 40 m depth. The interaction of more saline and colder GSW with surface Basin waters and north-western resident waters of Kandalaksha Bay occurs at different spatial and temporal scales. As a result, its thermohaline characteristics are transformed.

One of the possible processes of mixing at the mesoscale, reported in Chapter 6, is the interaction between the Surface White Sea Water and the GSW in the western part of the Gorlo Strait. Other interactions between saline waters and fresh resident waters of Kandalaksha Bay were reported in Chapter 4 and 5, and advection of saline water into the Chupa estuary (in the 5-20 m layers) were confirmed by Howland *et al.* (1999). Such advection of saline water at the mesoscale may be driven by a residual tidal current or might be induced by tidally generated internal lee waves as is the case for the semi-enclosed Basin of Trondheim in Norway (Vlasenko *et al.*, 2002). The circulation of the White Sea in summer 2000 (Chapter 7) has shown the main cyclonic gyre in the Basin to be a potential mechanism to transform some of the modified GSW intruding into the White Sea along the Terskii Shore. The saline and modified GSW, observed through the formation of numerous mixed layers spread in the northern White Sea, may have some portions entrained by the gyre system of the Basin in the upper layers (0-50 m) resulting in a water mass transport toward the interior of the Basin (Timonov, 1950; Inall *et al*,. 2001). At a smaller scale the inhomogeneities in the fine structure or step-like structures (Chapter 4 and 5), recorded in the vertical profiles of temperature and

salinity, are explained by the occurrence of complex small-scale mixing processes (Pingree, 1972; Yemel'yanov and Federov, 1985; Shapiro and Emel'yanov, 1989; Shapiro and Emelianov, 1994). From the energetic point of view it means that the spreading of kinetic energy from the mesoscale to smaller scales is reflected in the different shapes of fine structural inhomogeneities (Fedorov, 1978).

The shape of fine structural inhomogeneities has a relationship with the small-scale mixing process modes (Zhurbas and Lips, 1987). The diapycnal mode leads, as a rule, to the creation of step-like structures or shapes in the vertical thermohaline profiles (Fedorov, 1978; Zurbas and Ozmidov, 1987), whereas the isopycnal mode leads to the formation of inversion-like shapes (Ruddick and Turner, 1979; Woods, 1980). The statistical analysis of fine structural inhomogeneities shapes (Zhurbas and Lips, 1987) allows the evaluation of the diapycnal or isopycnal nature, and the quantification of the intensities of the diapycnal or isopycnal modes of small scale mixing.

The present study* in this chapter therefore investigates the diapycnal or isopycnal modes of small scale mixing intensity responsible for the occurrence of such mixed layers in the northern White Sea. The study takes on board the data-set from the survey 2000 and 2001, based on the diapycnal/isopycnal mode analysis. The aim of the chapter focuses on the mesoscale interaction between eddies (the main cyclonic circulation of the Basin) and the intrusion of the GSW, which is reflected in the small-scale mixing processes.

## 8.2. Material and methods

### 8.2.1. The GSW displacement

A mesoscale structure, formed by an eddy associated with the Terskii current in the northern White Sea Basin, was detected on the SST image of 21$^{st}$ June 2000, complemented with the SLA map of the 22$^{nd}$ June 2000, as shown in figures 7.1 and 7.2. The eddy centred at 66°N and 36°E had a diameter of ~120 km. The intrusion of a mixed layer known as the modified GSW into the White Sea was observed for 400km long and ~20 m in thickness along the Terskii shore. The advected mixed water is entrained by the cyclonic eddy/Terskii current system from the Gorlo Strait to Kandalaksha Bay. The Terskii current had the same spatial scale as the Basin cyclonic gyre.

*I am grateful to Dr. M. Emelianov for providing the code of the software and to S. Villeneuve who partly contributed in the data processing, as part of his training research period within the Shelf Sea Oceanography and Meteorology research group.

To obtain the thermohaline structure of the Terskii/Basin circulation and to analyse its influence on the mesoscale water displacement, 17 CTD stations from cruise 2000 were selected in the eastern area near the Gorlo Strait and 5 sections of CTD stations including data from cruise 2000 and data from cruise 2001, were made in the western area near Kandalaksha Bay (figure 8.1). Stations near the Gorlo Strait include either up or down cast measurements (Chapter 3) depending on the least inversion density observed in the vertical profiles. The results show that not all the measurements can be represented (figures 8.2 and 8.3); therefore a few stations, providing a good geographical representation of the area, are selected from downcast measurements at stations: 21, 22, 28, 30, 32, 44, 45, 59, 61, 63; and from upcast measurements at stations 33, 36, 40, 41, 42, 49, 51, 66. The data selected in Kandalaksha Bay for summer 2000 and late spring 2001 present no density inversions in the vertical profiles. These selected stations are represented by triangular symbols west of the Gorlo Strait and in Kandalaksha Bay (figure 8.1). In Kandalaksha Bay, sections of CTD stations are investigated to study a comparative analysis of the mode of mixing on the transformed GSW. The sections are: the cross section S1 (stations d138 to d145 from survey 2000; and stations d37 to d40, d50 and d56 from during survey 2001); the cross section S2 (stations d130-d133 from survey 2000; and stations d28-d32 from survey 2001); the along section S4 (stations d84, d153, d149 from survey 2000; and stations d39-d45, d28 from survey 2001); and finally the along section S5 (stations d5-d8 from survey 2000; and stations d32, d35, d46-d50 from survey 2001).

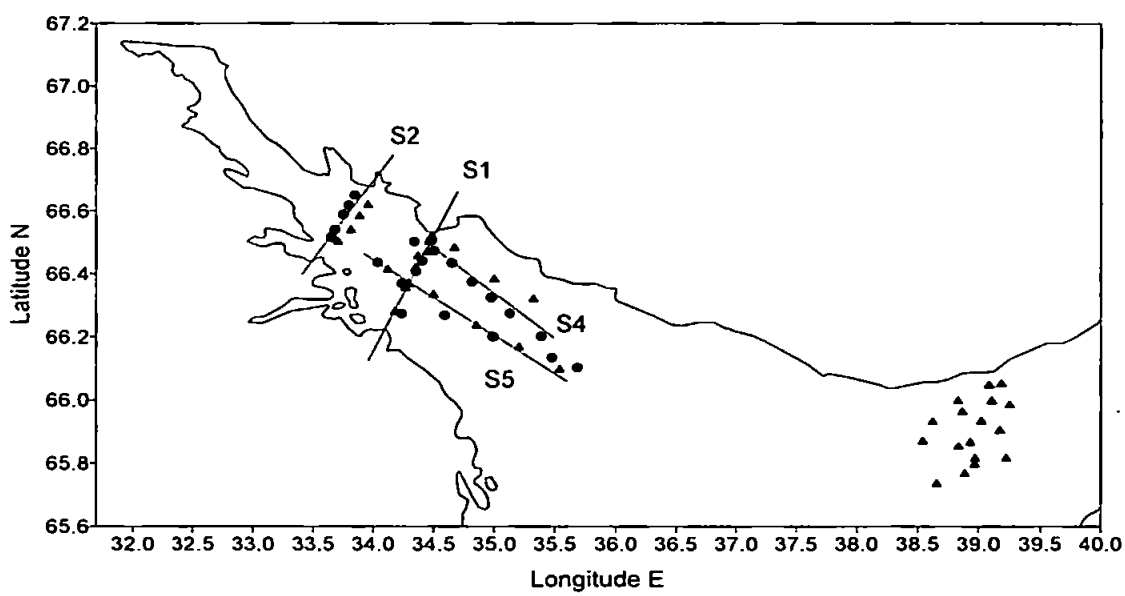


Figure 8.1: Sections (S1, S2, S3, S5) of CTD stations during cruise 2000 (triangular symbols) and 2001 (dots) to investigate the mesoscale displacement of the GSW, west of Gorlo Strait and in Kandalaksha.

### 8.2.2. Statistical method of fine structure inhomogeneity analysis

The software for investigating the diapycnal or isopycnal mode of mixing in the White Sea was used by Shapiro and Emelianov (1994) for their investigation in the relationship between characteristics of the mesoscale and fine structure in the Antarctic polar front zone. This software was made available for the present study thanks to Dr. Emelianov. The software is a program written in Quick Basic slightly modified to input CTD data taken from the White Sea. The program calculates temperature and salinity fluctuations, then derives the parameters $\alpha$ and $\beta$ (the thermal expansion and haline compression coefficients) to finally calculates the Pingree angle (Pingree, 1972) and the density ratio $R_\rho$ (see section 2.4 in chapter 2), which is a coefficient corresponding to diapycnal mixing (see section 8.3.2).

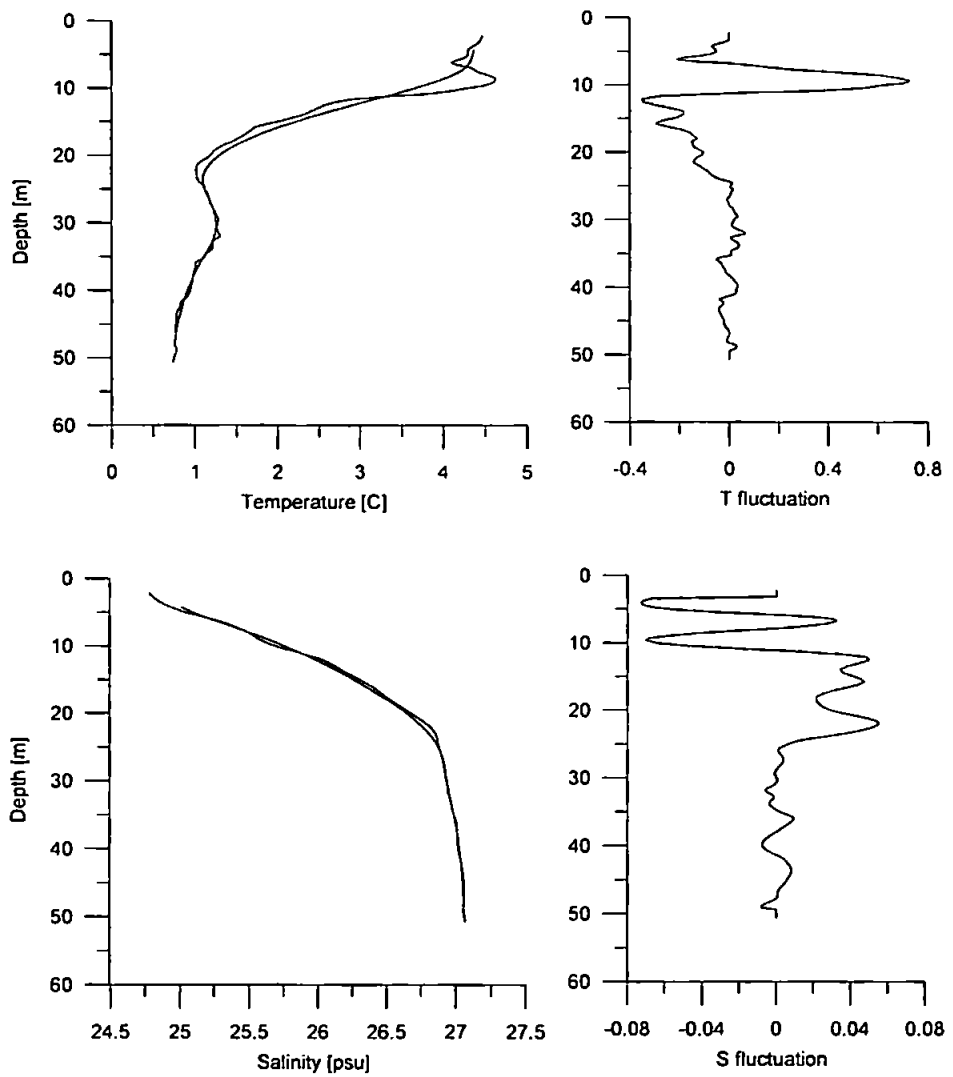


Figure 8.2: Smoothed profiles and fluctuations of temperature and salinity derived from original CTD downcast measurements at station 41

### Data filtering and pulsating components

To highlight the inhomogeneities in the fine structure, the temperature and salinity fluctuations (or pulsating components) are derived from the vertical profiles (see figure 8.2). To do this, the cosine filter was used and the mean profiles were subtracted from the original profiles (Fedorov, 1978). The temperature fluctuation ($T'$) and the salinity fluctuation ($S'$) are subtracted from the original CTD profile smoothed using the window width of $\lambda$=40 in the cosine filter. The filter represents 40 data points that is approximately 14 m in depth taken for all selected CTD stations, which separates the average profile from high frequency fluctuations. These temperature and salinity fluctuations according to Pingree (1972) determine the mode of small scale mixing process which causes inhomogeneities in the fine structure in the vertical profiles.

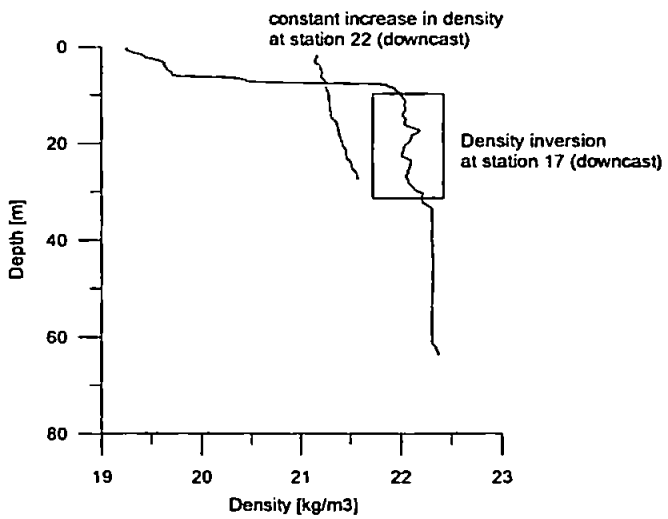


Figure 8.3: Density profiles showing density inversion at downcast station 17 and none at downcast station 22, cruise 2000.

### Density inversion problem

Within the 50 stations taken during the cruise summer 2000 in the west part of the Gorlo Strait, some measurements revealed many density inversions in the vertical profiles. An example of such density inversions is shown in figure 8.3 taken from the downcast measurements at station 17. For it, the calculation of the thermal expansion and haline compression coefficients, and so the Pingree angle and $R_\rho$ would be inconsistent because of the instability of the density of the water. Therefore stations in the west region of the Gorlo Strait were selected according to the density of water with

depth showing fewer or no density inversions by looking at downcast and up cast measurements for each station. Reasonable density structure such as shown in figure 8.3 at station 22 is taken into account for deriving the parameters described above.

## 8.3. Analysis of small scale structures

### 8.3.1. The ($\beta S'$, $\alpha T'$) plane

The nature of the inhomogeneities derived from the vertical profiles are analysed in the ($\beta S'$, $\alpha T'$) plane, where $T'$ and $S'$ are the temperature and salinity inhomogeneities (or fluctuations) normalised by the thermal expansion ($\alpha$) and the haline contraction ($\beta$) coefficients. The calculation of $\alpha$ and $\beta$ involved all the measurements in the water column (except from a surface and a bottom layer cut-off: the first and last 20 measurements). The results of the inhomogeneities in the fine structure analysis, at for example station 66 and 30, are plotted in the ($\beta S'$, $\alpha T'$) plane (figure 8.4). Each individual thermohaline fluctuation is represented as a point in the ($\beta S'$, $\alpha T'$) plane and the ensemble of fluctuations seen the CTD profile form a cloud of points (Zhurbas and Lips, 1987). The fit line for this cloud of points is called the Pingree Line and defines an inclination angle $\varphi_p$ called the "Pingree angle", with respect to the horizontal $\beta S'$ axis. This angle depends on the mode of mixing, which causes the inhomogeneities of temperature and salinity (Shapiro and Emelianov, 1994).

### 8.3.2. Isopycnal and Diapycnal mode of mixing

Situations occur, particularly in the vicinity of thermohaline fronts, when fine structure inhomogeneities of temperature and salinity are largely compensated in the density field, and the $T_Z$ or $S_Z$ profile or both have inversion layers in which the gradients change sign to the opposite of the corresponding mean gradients. The former case (as reviewed in section 2.2) is referred to fine 'step-like' structure and the latter as 'intrusive' fine structure. The stepped fine structure is generally attributed to local vertical mixing of various types and to the kinematics effect of internal waves (Zhurbas and Ozmidov, 1987; Fedorov, 1978). Intrusive fine structure results from interleaving of waters with different T and S characteristics, and the quasi-horizontal movements of water layers may have various origins (Ruddick and Turner, 1979; Woods, 1980).

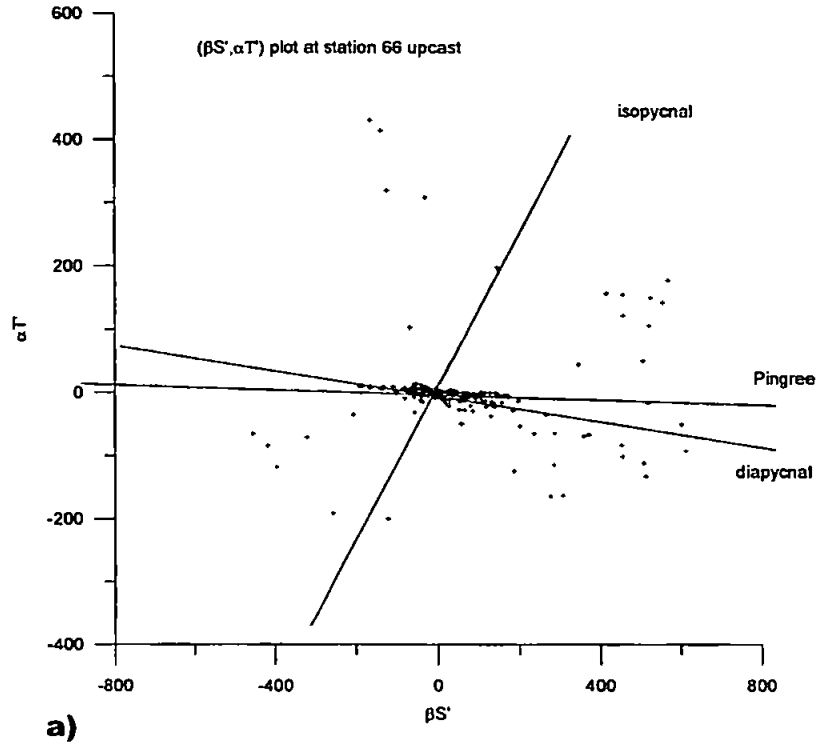


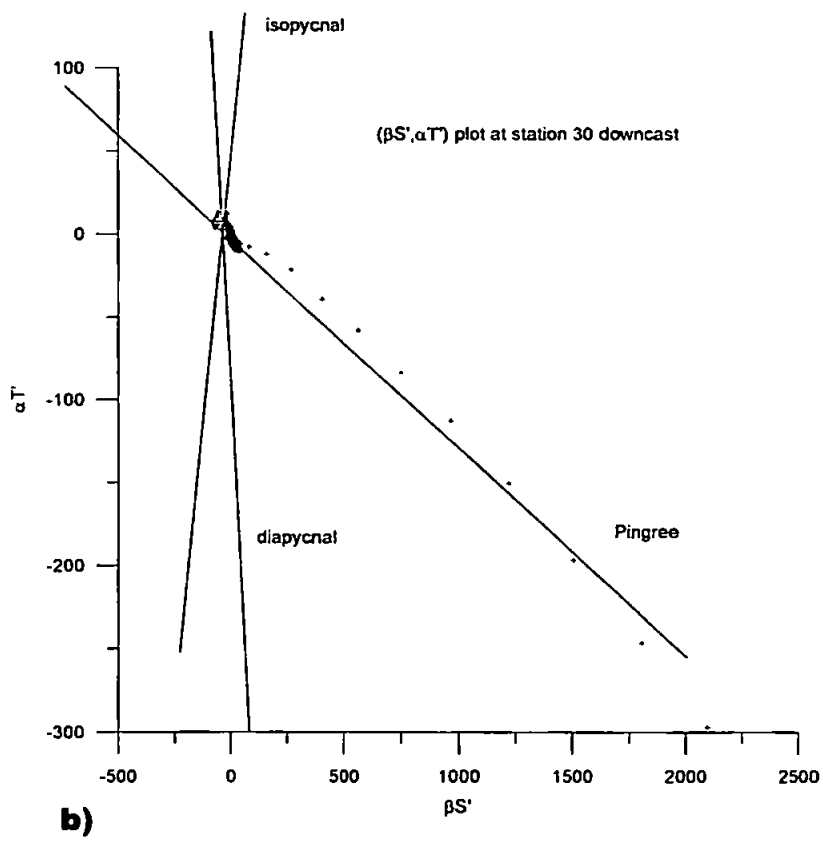


Figure 8.4: ($\beta S'$, $\alpha T'$) plots calculated at (a) upcast station 66 and (b) downcast station 30.

Note that processes generating stepped and intrusive fine structure are correlated and in particular that it is possible for the evolution of a stepped thermohaline structure to result from the transformation of an intrusive fine structure by convective double-diffusion mechanisms (Zhurbas and Ozmidov, 1983).

Considering the fine structure fluctuations of temperature T' and salinity S' (e.g. by using a cosine filter on the initial T and S profile), then, according to Pingree (1972), condition (8.1) below will be satisfied for isopycnal advection processes ('isopycnic intrusion'):

$$\alpha T' = \beta S' \text{ (Isopycnal mode)} \qquad (8.1)$$

and the followed condition (8.2) for fine step-like structures formed by vertical mixing processes:

$$\frac{T'}{S'} = \frac{\overline{T}_z}{\overline{S}_z} \text{ (Diapycnal mode)} \qquad (8.2)$$

where $\overline{T}_z$ and $\overline{S}_z$ are the mean vertical temperature and salinity gradients in the depths range under consideration. Equations (8.1) and (8.2) are used to determine the type of fine structure when analyzing the field observation. So multiplying the left and right parts of the equation (8.2) by $\alpha/\beta$ the relationship (8.2) can be rewritten as follows:

$$\frac{\alpha T'}{\beta S'} = \frac{\alpha \overline{T}_z}{\beta \overline{S}_z} = R_\rho \qquad (8.3)$$

where $R_\rho$ is known as the density ratio reported by Turner (1973) and Ruddick (1983). Therefore the program uses the equation (8.3) to calculate the parameter $R_\rho$ and the Pingree angle ($\varphi_i$), which are both reported in the ($\beta S'$, $\alpha T'$) plane. To calculate the two parameters, a few modifications were made to the program. The increment of the data which normally operates for downcast measurements was simply reversed in the case of upcast measurements. The pressure unit is changed to Bars for density calculations. Modifications were also made in the code of the program to allow reading unfixed length of data column varying according to CTD stations.

Based on the relationships introduced by Pingree (1974), two characteristic lines as shown in figure 8.4 were introduced on the ($\beta S'$, $\alpha T'$) plane: the Isopycnal Line, defined by the following equation (8.4) which characterizes pure isopycnal mode of mixing:

$$tg\varphi_i = 1 \qquad (8.4)$$

and the Diapycnal Line, defined by the following equation (8.5) which characterizes a pure diapycnal mode of mixing.

$$tg\varphi_i = R_\rho \qquad (8.5)$$

The analysis of inhomogeneities in the fine structure, at station 66 (figure 8.4a), shows the mode of mixing to be diapycnal since the Diapycnal Line is in the proximity of the Pingree Line. However, in some cases it is difficult to judge the proximity of the Pingree Line either to the Isopycnal Line or the Diapycnal Line. An example is showed in figure 8.4b at station 30. Therefore to identify the nature of the inhomogeneities in the fine structure, the parameter γ (in equation 8.6) was introduced by Emelianov (1993) when it is difficult to differentiate the proximity of the Pingree Line to the Isopycnal Line or to the Diapycnal Line.

$$\gamma = \frac{(tg\varphi_P - tg\varphi_i)}{(tg\varphi_d - tg\varphi_i)} \qquad (8.6)$$

When $\gamma < 0.5$, the fine structure temperature and salinity fluctuations were mainly formed by isopycnal mode of mixing, and by diapycnal mode of mixing when $\gamma > 0.5$. However the equation for $\gamma$ (8.6) has been rewritten for more convenience by introducing the new parameter called $\delta$ (Shapiro and Emelianov, 1994) shown below in the equation (8.7). This parameter $\delta$ is used here in this study and integrated into the program to better differentiate the two mode of mixing.

$$\delta = \frac{\phi - 1}{|R_\rho| - 1} \qquad (8.7)$$

The Pingree angle here is symbolised by $\phi$. By comparison with the parameter $\gamma$, if $\delta >$ 0.5, the mode of mixing is more diapycnal; if $\delta < 0.5$ the mode of mixing is then more isopycnal.

### 8.3.3. The mode of small-scale mixing west of Gorlo Strait

The program has run successfully for the selected quality CTD measurements in the study area of the Gorlo Strait. The program has performed the calculation for the Pingree angle, the parameters $R_\rho$ and $\delta$ for each station of the study area. The results are shown in the table 8.I which also show the maximum depth used for the analysis of the fine structure inhomogeneities.

| Stations | Pingree angle ($tg\varphi_p$) | Max depth [m] | δ | Mode of mixing |
|---|---|---|---|---|
| u49 | -0.43 | 55 | 0.508928571 | diapycnal |
| u51 | -0.31 | 55 | 0.616071429 | diapycnal |
| u42 | -0.19 | 50 | 0.704347826 | diapycnal |
| u40 | -0.33 | 50 | 0.572649573 | diapycnal |
| u33 | -0.035 | 20 | 0.790983607 | diapycnal |
| u66 | -0.006 | 65 | 0.871929825 | diapycnal |
| u41 | -0.36 | 50 | 0.571428571 | diapycnal |
| u36 | -0.38 | 45 | 0.52991453 | diapycnal |
| d61 | -0.44 | 45 | 0.4375 | isopycnal |
| d45 | -0.2 | 25 | 0.941176471 | diapycnal |
| d28 | -0.25 | 55 | 0.700934579 | diapycnal |
| d32 | -0.38 | 40 | 0.056363636 | isopycnal |
| d21 | -0.18 | 45 | 0.76635514 | diapycnal |
| d22 | -0.2 | 25 | 0.701754386 | diapycnal |
| d30 | -0.13 | 55 | 0.2175 | isopycnal |
| d63 | -0.35 | 60 | 0.546218487 | diapycnal |
| d44 | -0.27 | 45 | 0.553030303 | diapycnal |

Table 8.I: Mode of small-scale mixing west region of the Gorlo Strait for selected stations during cruise 2000.

The overall result shows a diapycnal mode of mixing, which is expected in the shallow region of the Gorlo Strait where tides are strongly present and the water mass well vertically mixed on the sill. However, the parameter $\delta$ also indicates that the diapycnal regime changes consequently to the isopycnal regime as it is observed at stations 61, 30 and 32. To quantify the intensity of the two modes of mixing west of the Gorlo Strait, a 3-D plot of the parameter δ is shown in figure 8.5.

The horizontal plane represents the geographical location of the stations in the western part of the Gorlo Strait and the vertical axis represents the variation of $\delta$, indicating high intensity of isopycnal mixing at the lowest values of $\delta$, and diapycnal mixing for high values of $\delta$. A distinct local zone is revealed in figure 8.5 showing high intensity of isopycnal mixing located at longitudes 39.1°E to 39.2°E and latitude 65.9°N. This observation confirms horizontal process discussed in Chapter 6 concerning the formation of eddies or lenses west of the Gorlo Strait as a result of the water mass mixing between the intrusion of saline GSW and advected water from the extent Dvina Bay gyre (Shapiro *et al.*, 2003). Predominant thermohaline fine structures (mixed layers) and fluctuations occurring in the west region of the Gorlo Strait are associated

with various water mass of different origins, therefore influencing and modifying the saline GSW. By using the method described above, the inhomogeneities in the fine structure in the dynamically active layer (0-50 m depth) is analysed in the following section to study the spatial distribution of the intensities of diapycnal and isopycnal modes of small scale mixing, which transform in a complex manner the intrusion of the GSW in the northern part of the White Sea.

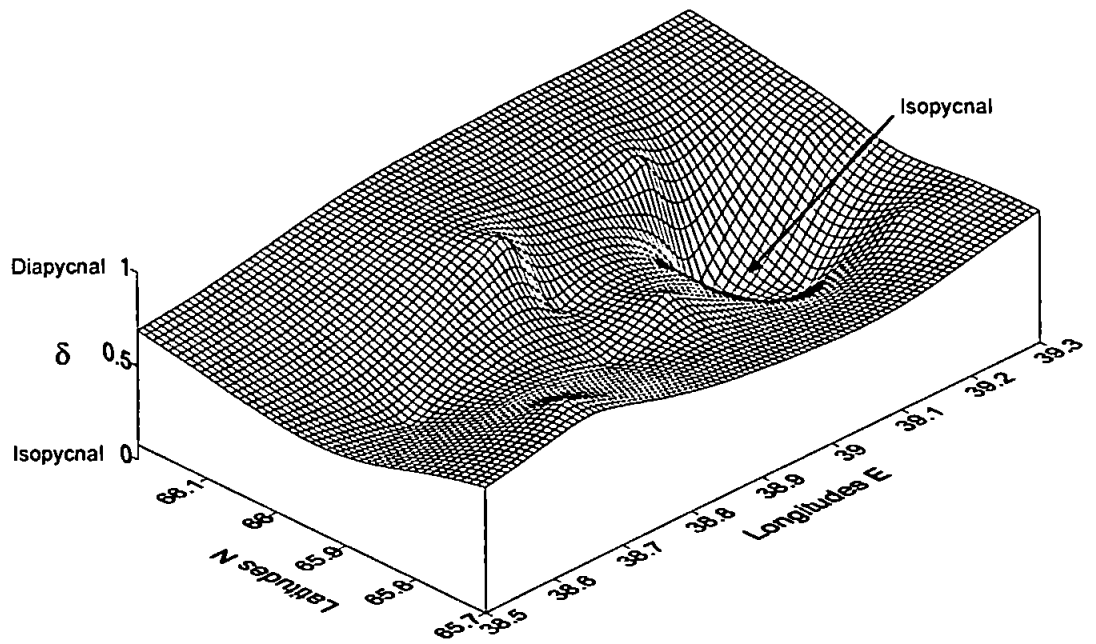


Figure 8.5: 3-D plot of the distribution of the isopycnal and diapycnal modes of mixing in the investigated area west of the Gorlo Strait, cruise 2000.

### 8.3.4. Spatial distribution of the transformed GSW: intensities of diapycnal and isopycnal mode

Following the results obtained in Chapter 4 (figure 4.1), in Chapter 6 and shown in the T-S diagram (figure 8.6) in the region west of the Gorlo Strait, three step-like structures are observed in summer 2000: steps A, B and C (Lukashin *et. al.*, 2003). The formation of mixed layer A is caused by fresh surface water mixing between Dvina Bay water and the already mixed WSSW plus some from the GSW. However the formation of steps B and C occurring underneath the sharp summer thermocline in the active layer (10-40 m) are regarded as two slight different types of transformed GSW. These mixed water masses (steps B and C) are tidally generated on the sill and projected in thin layers into the Basin probably caused and maintained by a residual tidal current or by the

generation of lee-waves. The latter have been recently studied and reported by Vlasenko *et al.* (2002) in a similar type of semi-enclosed sea which presents also a shallow sill at its entrance.

The T-S diagram (figure 8.6) shows the core of the GSW (T=~2.5°C; S=~27.25 psu) and the 2 signatures of the transformed GSW: (i) step B with 1°<T<2°C and 26.4<S<27.2 psu; (ii) step C with 0°<T<0.8°C and 27.3<S<27.5 psu. The spatial distribution of the two transformed water masses in the Gorlo Strait (figure 8.7) at 25 m depth shows the eroded intrusion of GSW as a front zone formed in the northeast region of study area. Step B is therefore located in the front zone at the edge of the main Basin cyclonic gyre along the Terskii slope. Step C is however located in the south-west part of the area, within the Basin influenced by the main cyclonic circulation. The T-S curves (figure 8.6) have a lot of irregularities in the 10-40m layers which suggest small-scale mixing processes.

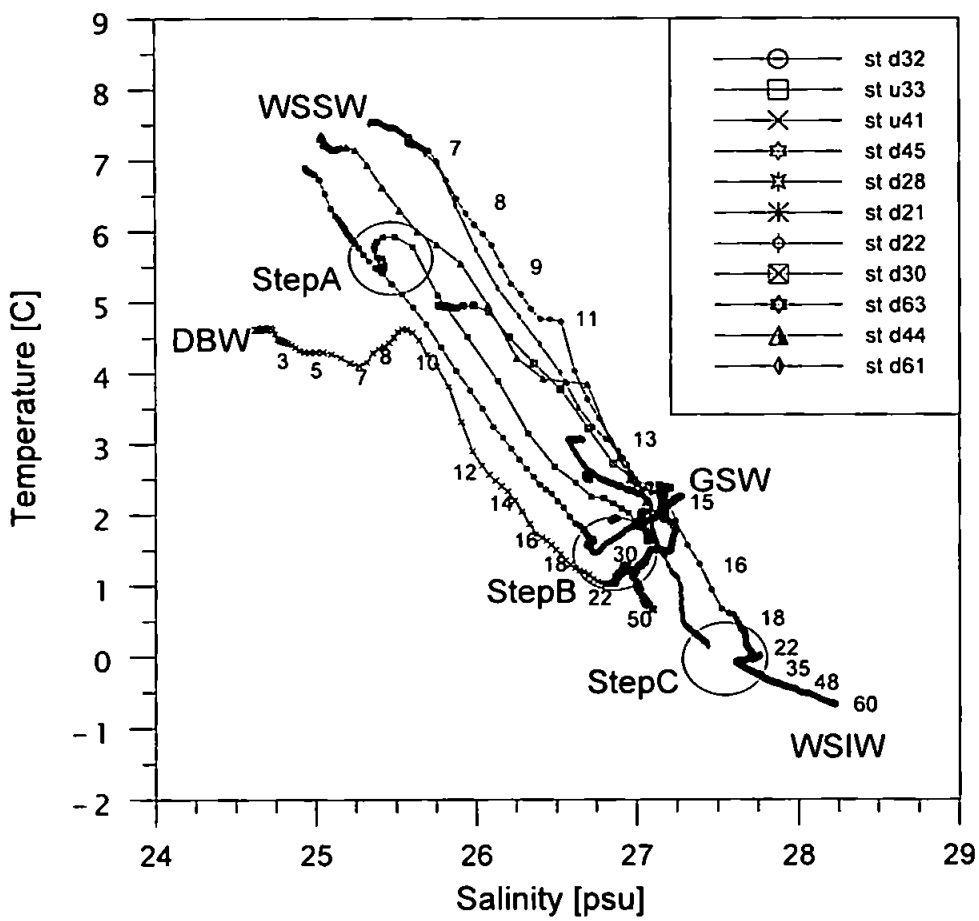


Figure 8.6: T-S diagram showing the variation of transformed GSW related to the formation of mixed layers at selected stations west of the Gorlo Strait. Depths of measurements are marked at stations 41 and 63.

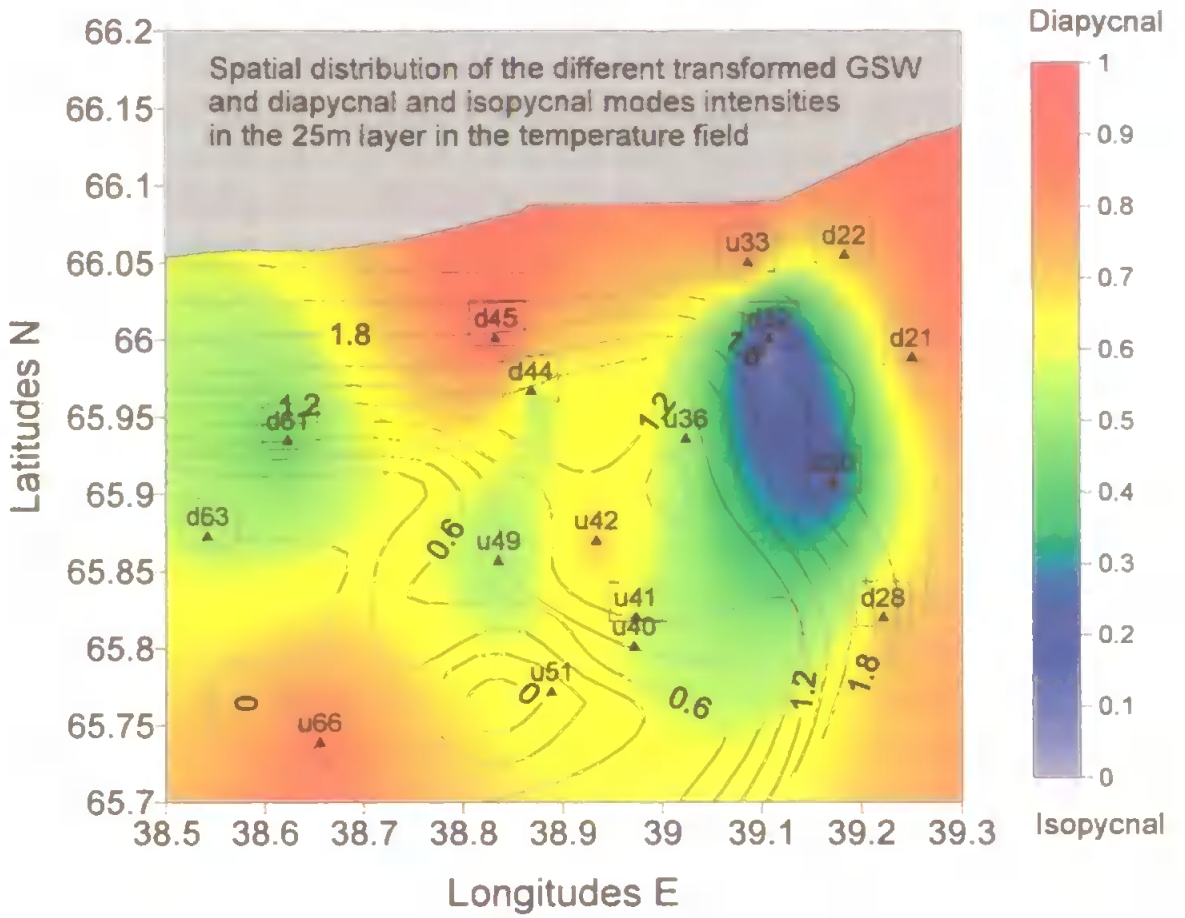


Figure 8.7: Spatial distribution of the different transformed GSW and diapycnal and isopycnal modes intensities in the 25m layer of the temperature field.

The spatial distribution of intensities of diapycnal and isopycnal modes superimposed on an *in-situ* temperature field at the 25 m depth (figure 8.7) is discussed below according to the intensity of each mode of mixing in the study area.

(i) The transformed GSW step B is vertically mixed by topographic stirring and tides (at stations 22, 33, 45) which is shown by predominant diapycnal mode of mixing.

(ii) Along the Terskii coast and slightly offshore (at stations 44, 61, 63) the diapycnal mode of mixing changes to the isopycnal regime, which indicates that transformed GSW step B is remixed with the waters circulating within the main rotating cyclonic gyre of the Basin, which are also influenced by freshness coming from the extent of the Dvina gyre. However, the two modes co-exist in this part of the study area with slight isopycnal predominance near the coast which emphasizes the fact that the Terskii

current entrains the modified GSW (step B), as was well depicted from the SST image (figure 8.1).

(iii) In the east part of the chart, the front divides the incoming new GSW (at stations 21, 22) from the old transformed GSW; forming the mixed layer step C (stations 30, 32, 36). The isopycnal mode of mixing strongly predominates here (see blue patches in figure 8.7).

(iv) In the west part of the chart, adjacent to the Basin is found the transformed GSW (step C) in the diapycnal mode (stations 51, 66).

(v) The presence of small scale eddies and lenses discussed in chapter 6 (Shapiro *et al.*, 2003) transforming some part of the incoming GSW (old) to new GSW into the White Sea is a reasonable explanation which is justified here by the slight intensity of isopycnal modes seen from stations 36, 40, 41, 44, 49 and 51.

### 8.3.5. Modes of mixing of the GSW in Kandalaksha Bay

The method to analyse the inhomogeneities of the fine structure has been repeated for the data set of summer 2000 and late spring 2001 in Kandalaksha Bay. The region of interest is the western edge of the main cyclonic eddy in the Basin carrying modified GSW along the Terskii coast. The results from Chapter 4 and 5 have shown the predominant structure of mixed layers at such depth (step B, C) during summer 2000 and late spring 2001, which are now known to be associated with the intrusion of saline water seen here by the two transformed GSWs. The analysis provides more details about the modes of small-scale mixing concerning the transformation of the GSW in the 10-60 m layer, while propagating further north in Kandalaksha Bay.

The results shown below in the T-S diagram (figure 8.8) at selected stations 2001 indicates clearly the mixing zone ($-0.5°<T<0.5°C$; $27.5<S<28$ psu) caused by the intrusion of the transformed GSWs.

The results of the inhomogeneity analysis in Kandalaksha Bay are shown in the ($\beta S'$, $\alpha T'$) planes (see appendix F) and summarized in table 8.II. The Pingree angle was approximately zero in the entire data set, therefore the determination of the Isopycnal Line and Diapycnal Line are referred to the horizontal axis of each ($\beta S'$, $\alpha T'$) planes.

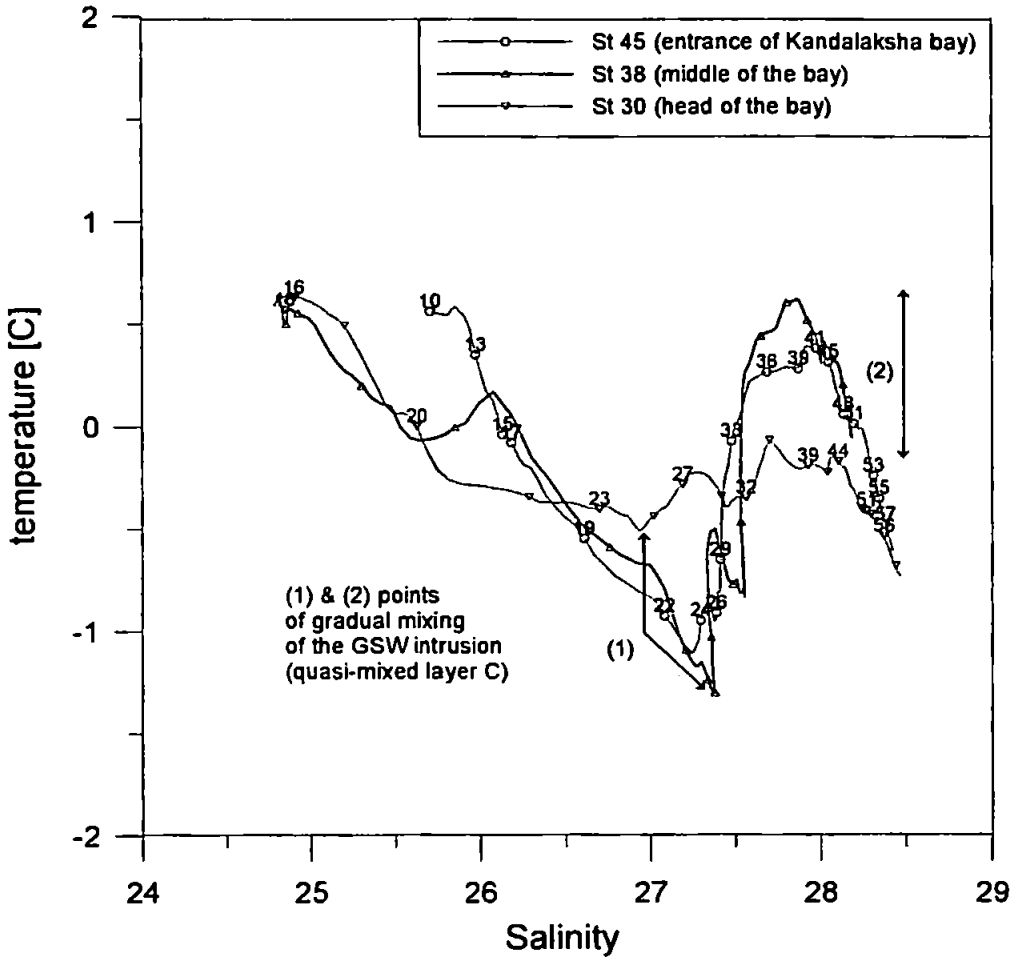


Figure 8.8: T-S curves obtained in 3 different parts of Kandalaksha Bay (station 2001) showing the signatures of the transformed GSW propagating into the Bay in the 10-60m layer. Depths are allocated beside the T-S curves to show the gradual mixing of the warm and saline (transformed GSW) mixed layer with Kandalaksha waters.

In the first 60 m layer, all the ($\beta S'$, $\alpha T'$) plots (see appendix F) revealed a succession of isopycnal (iso) and diapycnal (dia) modes of mixing, in the water column identified respectively from surface to bottom as iso1, dia1, iso2, and dia2. The relationship between the observed fine structure of the transformed GSWs (steps B, C) and the mode of small-scale mixing is revealed by relating the average-depth of the mixed layers (B, C) with that of the modes of mixing. This is observed by means of vertical sections S1, S2, S4 and S5 in figure 8.9, which clearly position the 2 modes of mixing and the mixed layers in the water column (both represented by lines + symbols for identification). For example in section S1 during summer 2000 (figure 8.9cd), the upper boundary of iso1 ("iso1-max") shows the beginning of the isopycnal mode which occupies the surface layer (10-30 m) observed at station d138. Below 30 m depth, the regime slightly

changes to diapycnal mode (dia1) characterized by the upper boundary layer "dia1-max" (at 32 m). The next upper boundary layer at lower depth terminates the diapycnal regime as the isopycnal mode start to prevail (iso2), and so on. The results in figure 8.9 are examined according to the following key-dynamical areas (figure 8.1) such as (i) the filaments of GSW along the Terskii coast (S4) meandering into Kandalaksha Bay (S1), (ii) the anticlockwise circulation nested inside the bay (S2), and finally (iii) some portion of modified GSWs deflected in the mouth of the Bay (S5) by the Basin cyclonic gyre.

| Stations 2001 | Pingree angle: $tg(\varphi_i)$ | Max depth [m] | | Stations 2000 | Pingree angle: $tg(\varphi_i)$ | Max depth [m] |
|---|---|---|---|---|---|---|
| d28 | -0.030 | 135 | | d130 | -0.19 | 220 |
| d29 | -0.013 | 180 | | d131 | -0.22 | 180 |
| d30 | -0.020 | 195 | | d132 | -0.49 | 265 |
| d31 | -0.020 | 245 | | d133 | -0.17 | 175 |
| d32 | -0.010 | 190 | | d84 | -0.42 | 80 |
| d39 | -0.050 | 245 | | d153 | -0.06 | 135 |
| d40 | -0.030 | 230 | | d149 | -0.3 | 165 |
| d41 | -0.015 | 200 | | d138 | -0.18 | 160 |
| d42 | -0.040 | 190 | | d139 | -0.12 | 180 |
| d43 | 0.010 | 200 | | d140 | -0.23 | 200 |
| d44 | -0.030 | 195 | | d141 | -0.14 | 240 |
| d45 | -0.020 | 185 | | d142 | -0.18 | 270 |
| d46 | 0.010 | 245 | | d143 | -0.3 | 245 |
| d47 | 0.010 | 225 | | d144 | -0.26 | 185 |
| d48 | -0.010 | 215 | | d145 | -0.12 | 100 |
| d49 | -0.070 | 190 | | d6 | -0.17 | 200 |
| d50 | -0.020 | 135 | | d5 | -0.22 | 225 |
| d35 | -0.020 | 205 | | d7 | -0.23 | 210 |
| | | | | d8 | -0.22 | 250 |

Table 8.II: Results of the Pingree angle for the stations 2000 and 2001 in the investigated area of Kandalaksha Bay.

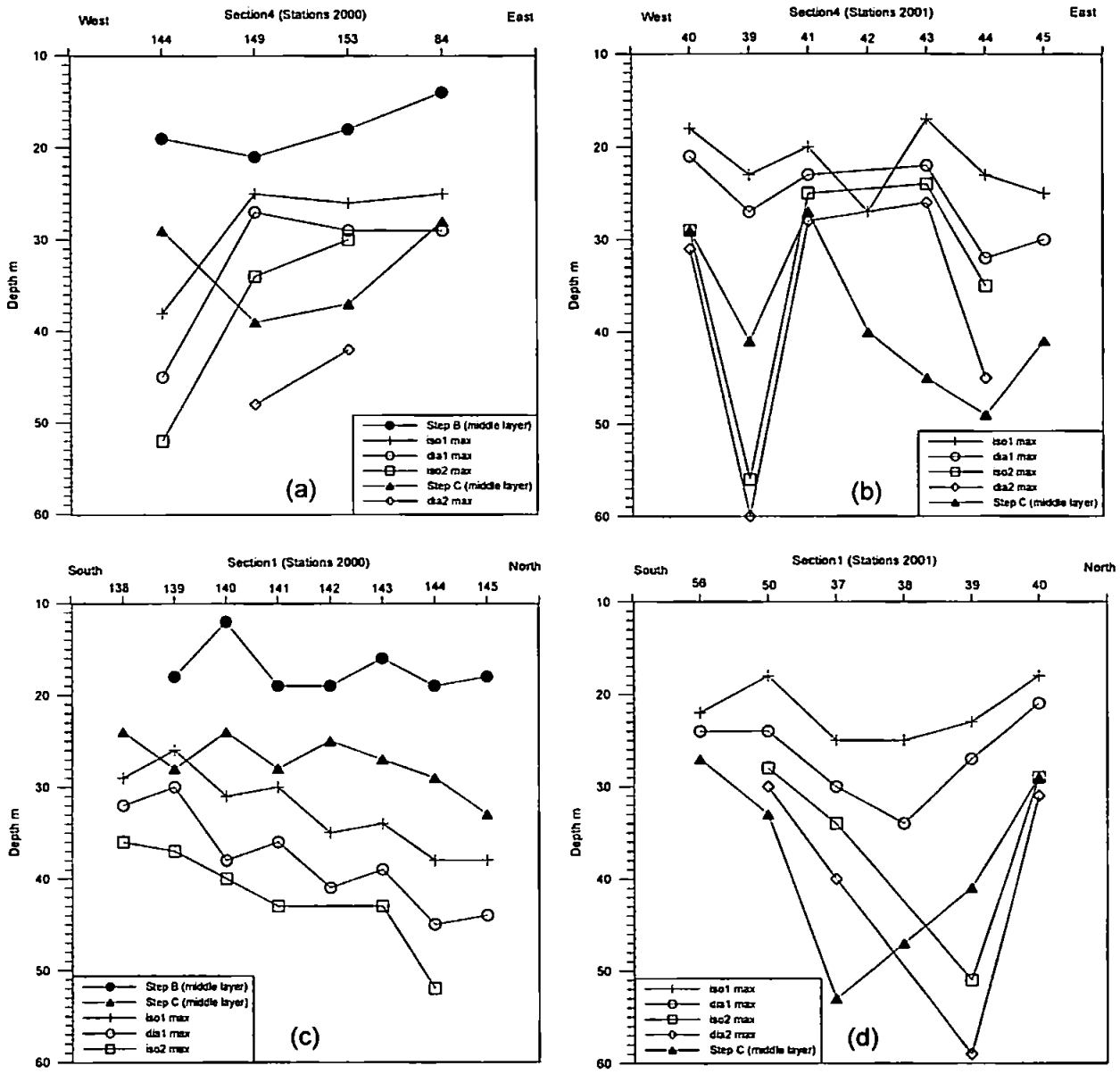


Figure 8.9: Vertical position in the water column of the diapycnal and isopycnal mode of mixing associated to the formation of the mixed layers of the transformed GSWs along the section S4 (a) in 2000, (b) and 2001, and S1 (c) in 2000, (d) and 2001.

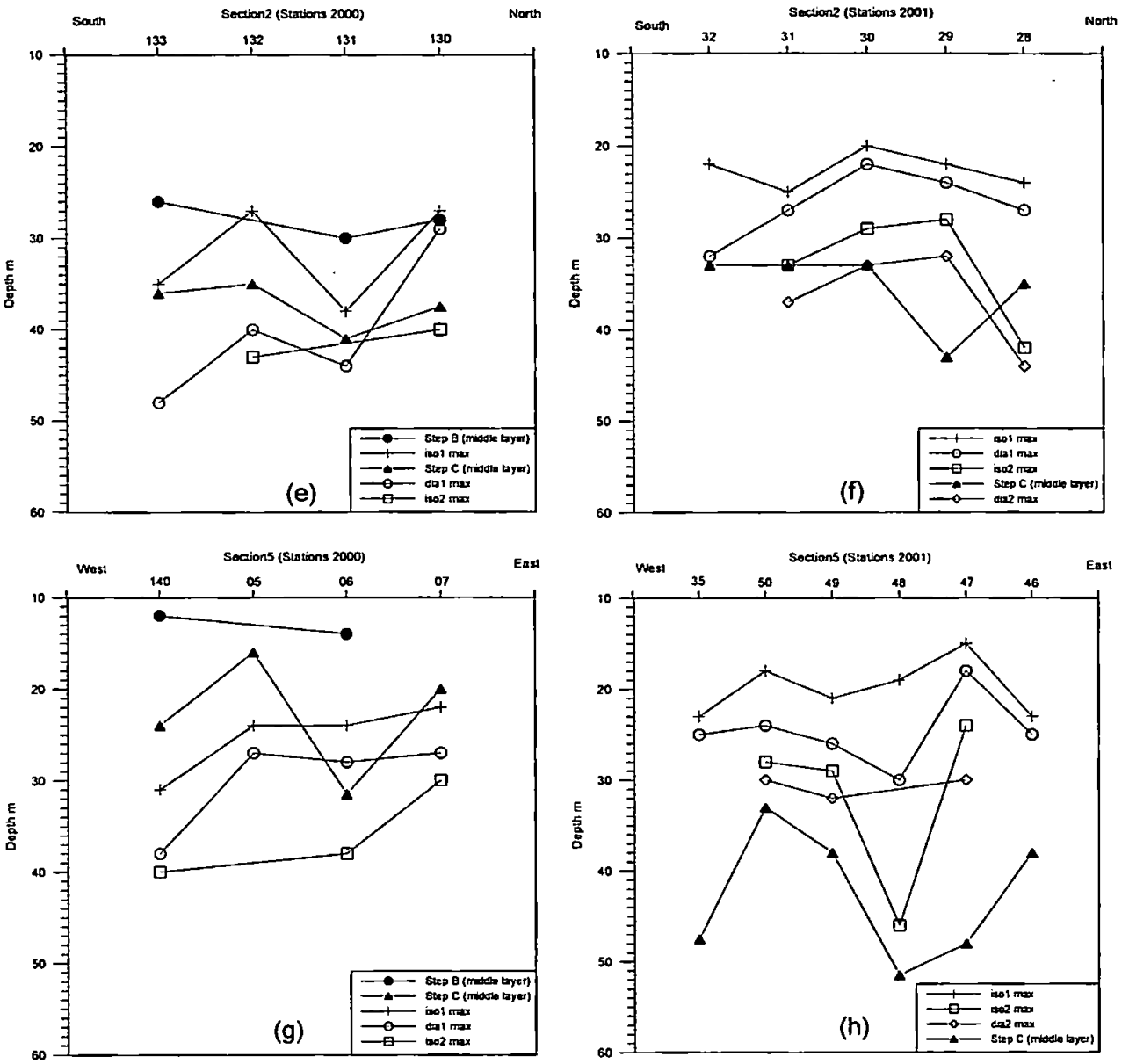


Figure 8.9: Vertical position in the water column of the diapycnal and isopycnal mode of mixing associated to the formation of the mixed layers of the transformed GSWs along the section S2 (e) in 2000, (f) and 2001, and S5 (g) in 2000, (h) and 2001.

The results also provide some discussion on the variability of the two modes of mixing concerning the modified GSWs during summer 2000 and late spring 2001:

(i) Along the Terskii coast (S4), the mode of mixing is isopycnal for Step B in summer 2000 (figure 8.9a), although below 30m, step C has a diapycnal mode of mixing. In 2001, the layer step C is also in diapycnal mode (figure 8.9b) west of the section (offshore in the Bay), and slightly change to isopycnal as it approaches the coastal Terskii current which terminates into the residual cyclonic circulation of the bay (stations 39, 40, in 2001). At the front zone section (S1) across the bay, the mode of mixing for the two transformed GSWs is mainly isopycnal observed in summer 2000 (figure 8.9c) and in late spring 2001 (figure 8.9d).

(ii) Along the section (S2)which crosses the core of the local anticyclonic gyre, the mode of mixing is mainly isopycnal for the mixed layer B observed at 30m depth in summer 2000 (figure 8.9e). However, below that depth, the mode of mixing changes to diapycnal mode associated to the mixed layer C, which nevertheless present isopycnal mixing at the northern coast of the Bay. This remark confirms the advection process of the modified GSWs along the northern coast of Kandalaksha Bay. The data in 2001 confirm the diapycnal mode of the mixed layer C at the centre of the eddy (figure 8.9f). However, the mixed layer C has an isopycnal mode of mixing observed at the margins of the eddy along the southern and northern coast of the Bay.

(iii) Along the section S5, the mode of mixing here is mainly isopycnal in summer 2000 found for the modified GSWs (figure 8.9g). However, the layers have a regime mainly diapycnal in late spring 2001 (figure 8.9h). The change of mode of mixing may be related to the change of local flow circulation at the mouth of the bay, which cannot be justified here due to the lack of SST images during that period of time. However, it is probable that the diapycnal mode of mixing prevails within the core of the eddy, suggesting a displacement of the predominant cyclonic circulation extended to the shallow area of Kandalaksha Bay also probably combined with a weak saline front across the bay caused by very weak river discharges, which in probable in late spring after severe winter conditions.

## 8.4. Conclusion

The analysis of the data, in the west part of the Gorlo Strait, has demonstrated that the main cyclonic circulation with the well known Terskii current deflects a portion of the intrusion of the GSW. The spatial distribution of small-scale process intensities at the 25m layer shows that the area of the entrainment is connected with the north-eastern part of the cyclonic eddy associated with the extended Dvina Bay gyre, characterized by the highest intensity of isopycnal mode of mixing. Along the Terskii slope, the two modes of mixing co-exist for the formation of the transformed GSW (identified as step B in Chapter 4) which is entrained by the Terskii current at shallow depth (30 m). The spatial distribution of diapycnal mode intensity however marks the area occupied by the other transformed GSW (identified as step C in Chapter 4 and 5) located further offshore. In summer 2000 in Kandalaksha Bay, the transformed GSWs are deflected from the north coast to the south by the cyclonic circulation, which is marked mainly by the isopycnal mode in the first 30m layers. In late spring 2001, the intrusion of mixed saline water from the Basin towards Kandalaksha Bay is also mainly isopycnal at depth between 30m and 50m and also across the Bay (from north to south). The diapycnal mode of mixing associated to the step C in summer 2000 was marked in the core of an anticyclone nested further north inside Kandalaksha Bay.

The results obtained in this study showed that the mesoscale Basin eddies play an important role in the redistribution of the intrusion of the GSW throughout the White Sea Basin. Parts of the GSW are captured, mixed and re-circulate within the main cyclonic eddy of the Basin. Small-scale mixing is one of the important mechanisms that participate in the GSW thermohaline structure transformation. The spatial distribution of the intensities of the diapycnal and isopycnal modes of small-scale mixing has been used as tracers of differently transformed GSW mesoscale displacement in the active 10-60 m depth layers of the White Sea.

# Chapter 9: Conclusion

In this last chapter of this thesis, the principal results are presented here from the previous chapters, and are discussed according to the research objectives as stated in the Introduction (Chapter 1). Finally, some recommendations for future research are given.

## 9.1. Summary of the results

Previous works carried in the White Sea have been reviewed in Chapter 2 and a few dynamical questions such as deep-water renewal and fine-scale (stepped) structure of the water masses in the White Sea were addressed. The EU-INTAS and Russian national projects have responded to the importance of understanding the dynamics of the White Sea by providing valuable data-sets, which were collected particularly in the northern regions of the White Sea. The northern part of the White Sea is considered as the most dynamical area, with the presence of strong tides in its north-east part (Gorlo and Voronka); and conversely with the presence of strong summer stratifications and freshwater runoff on the other side of the sea, in its north-west part (Kandalaksha Bay). The combination of these processes and local gyre circulation resulted in the formation of fine structures in the vertical profiles, at which the vertical resolution was improved (as discussed in Chapter 3) to determine and analyse the nature, the extent and the processes of such fine- structure within the mesoscale circulation of the White Sea.

The main results from the chapters of this thesis are summarized below:

1. The complex water mass occurring west of the Gorlo Strait has denoted fine scale thermohaline features and water mass formation, which were thoroughly studied in Chapters 4 and 5 during the two surveys 2000 and 2001. The data analysis for temperature, salinity and density has revealed the distinct signatures of step-like structures in the profiles which clearly indicated striking similarities in the characteristic of the water masses. The high-resolution CTD survey has revealed the mechanism of mixing of four different water masses west of the Gorlo Strait: the GSW, the DBW, the WSSW and the WSIW, each separated either by a sharp thermocline or by hydrographic fronts.
2. Five quasi-homogeneous layers and temperature inversions were identified during survey 2000 and confirmed with four of approximately same

characteristics during the survey 2001. Contour plots across the northern White Sea from Gorlo to Kandalaksha Bay were used to show the prominent thermohaline features on a horizontal scale of 400 km (entire distance across the White Sea from the Gorlo Strait to the north of Kandalaksha Bay). The intrusion of the east-generated water mass from Gorlo was evident in the whole sections of the northern White Sea during the three surveys 1991, 2000 and 2001. Pool and lenses of denser waters were reported in the far remote places of north Kandalaksha Bay, evident in late spring 2001 rather than in summer 2000, suggesting possible cascading events. Contour plots along the whole section across the northern part of the White Sea suggest descent of the densest mixed layers along the steep slope of Kandalaksha Bay adjacent to the Basin. The mixed layer of dense waters in Kandalaksha is reported deeper in late spring 2001 than in summer 2000, at depth varying from 80-120 m to 140-200 m. Other descents of dense water, identified in the coastal area of Kandalaksha Bay were related to the characteristic water mass of the mixed layer propagating from the west region of the Gorlo Strait to the Kandalaksha Bay in the 20-50 m layer. The results have shown that temperature cooling, in the area of Kandalaksha Bay, is likely to be the mechanism to form dense water with salt content deposit brought with the intrusion of the transformed GSW.

3. The intrusion of the GSW is found in the entire section of the White Sea in the vicinity of the active upper boundary layer (maximum depth ~50 m), which separates surface and intermediate waters from stagnant deep-water masses. The boundary layer in the Basin has a domed structure as a result of upwelling circulation caused by the presence of the nested cyclonic gyre in the centre of the Basin, observed through satellite images during summer 2000. The detailed analysis of the mixed layers, showing variation in thickness and depth, strongly suggest that they are formed by turbulent boundary mixing. These mixing processes are likely lead by lateral salt fluxes in the overlaying pycnocline (due to the freshness of river runoff) and associated to the mesoscale cyclonic eddy of the Basin and are sustained by tidal variability in the underlying pycnocline. Internal oscillations have been observed below intermediate depth within the deep water masses during surveys 2000 and 2001. This is likely to be caused by downslope penetration of shelf water that can be accounted for excess density of shelf-edges waters in the coastal area of Kandalaksha Bay. The results in chapter 6 were located in the west region of the Gorlo Strait, where water exchange

takes place between the Barents Sea and the White Sea. The advection of the Dvina Bay Waters west of the Gorlo Strait played an important role for the water mass exchange at the entrance of the semi-enclosed sea. Mixing processes, west of Gorlo, included vertical stirring and horizontal exchanged through interleaving at the thermal and salinity fronts. Formation of mesoscale eddies and lenses, apparently due to baroclinic instability, extended the length of the boundary that separates differing water masses and hence facilitates horizontal mixing. Vertical mixing in the whole water column near the Terskii coast (30 m isobaths) was highly enhanced by strong tides in the Gorlo Strait. The resultant mixed water was advected into the White Sea Basin along the Terskii Coast.

4. The mesoscale circulation in the Basin therefore has an important role in water exchange and certainly in the water renewal of the White Sea since it deflects portions of the GSW being identified at various stations across the northern White Sea, and localised within few metres underneath the thermocline. The results in chapter 7 showed good agreements between near-surface *in-situ* and satellite observations. Calculation of the dynamic height has identified mesoscale eddies in Kandalaksha Bay and the Basin. The sequence of SLA complemented by the SST images has suggested the important contribution of thermohaline circulation to the overall dynamical circulation of the White Sea in summer 2000. The main feature detected was the filament of modified GSW along the Terskii coast associated with the cyclonic gyre of the Basin.

5. Chapter 8 investigated the nature of the different modified GSW seen as the intrusion of saline water observed during the survey 2000 and 2001. A statistical method of fine structure inhomogeneity analysis was used to relate the formation of the mixed layer with the modes of small-scale mixing processes. High intensity of isopycnal mode of mixing showed the contribution of the extended Dvina Bay gyre into transforming some of the incoming GSW which has resulted in the formation of lenses. Along the Terskii slope, the two modes of mixing co-exists with more transformation of parts of the GSW carried away by the Terskii current (constricted to the 30 m isobaths). The spatial distribution of diapycnal mode intensity however marked the formation of the east-generated mixed layers (0.5°C; 27 psu) in the area adjacent to the Basin. In the region of the Kandalaksha Bay, a portion of the transformed GSW was entrained from the north coast to the south by the cyclonic gyre of the Basin marked by isopycnal

mode of mixing in the 10-30 m layer during the survey 2000 and in the 30-50 m layer during survey 2001. The diapycnal mode of mixing in Kandalaksha Bay however is marked by the core of the local anticyclonic gyre nested further north inside Kandalaksha Bay. The present results have shown that the mesoscale Basin circulation plays an important role in the redistribution of the incoming GSW throughout the White Sea Basin capturing part of the recently incoming GSW, and to put it in contact with more transformed GSW inside its own cyclonic circulation. Small-scale mixing is one of the important mechanisms that participate in the GSW thermohaline structure transformation. The intensity of diapycnal and isopycnal was used as tracers to monitor the different transformed GSW mesoscale displacement in the active 10-60 m depth layers.

## 9.2. Recommendations for future work

The findings of this study based on the observational results have provided a better understanding of the mesoscale physical processes of the White Sea, notably the formation of the fine mixed layers and the mechanism of the deep water renewal of the White Sea. However, a change in the characteristics of the thermohaline structure of the White Sea may alter or prevent such processes. Therefore numerical models along with high-resolution *in-situ* measurements at specific locations of the White Sea are needed to determine the main parameters and factors responsible for influencing such processes. A tidal numerical model of the White Sea should be run to investigate the tidal residual component in the mesoscale circulation of the White Sea. Further *in-situ* measurements on cascading should be carried out in the northeast region of the sea and in Kandalaksha Bay, where it occurs (personal communication). A numerical model based on investigating stratified and sheared turbulent boundary layers should be developed for the case of the White Sea. This should be able to reproduce the fine-scale quasi-homogeneous layers in order to investigate the small-scale parameterizations of the fine structure observed in the White Sea. A coupled model such as POLCOM-ERSEM model can be used to approach the complex spatio-temporal marine ecosystem processes of the region of Kandalaksha Bay/Basin of the White Sea (e.g. to study the response of zooplankton populations to physical forcing). And finally a coupled hydrodynamic – sea ice model can be develop to carry out simulations to investigate the physical processes in dense and deep water formation on ice-covered seas in the White Sea, complemented by winter *in-situ* observations.

# Appendix A: Log book station and computing programs

## A.1. Table info cruise 2000

| CTD SEACAT 19 profiler | | | | | | |
|---|---|---|---|---|---|---|
| Table White Sea cruise: summer 2000; vessel: *Kartesh* | | | | | | |
| No. STATIONS | LAT in dec. | LON in dec. | DEPTH (m) | DATE (June 2000) | TIME | COMMENTS |
| 1.1 | 66.4671 | 34.1095 | 350 | 15 | 14,00 | |
| 1.2 | 66.4580 | 34.1032 | 300 | 15 | 17,00 | |
| 4 | 66.4172 | 34.1227 | 225 | 15 | 23,51 | |
| 5 | 66.3373 | 34.5012 | 245 | 16 | 01,20 | |
| 6 | 66.2398 | 34.8545 | 220 | 16 | 02,50 | |
| 7 | 66.1718 | 35.2059 | 250 | 16 | 04,18 | |
| 8 | 66.1010 | 35.5413 | 270 | 16 | 05,50 | |
| 9 | 66.0221 | 35.9348 | 275 | 16 | 07,37 | |
| 10 | 65.9559 | 36.2365 | 265 | 16 | 09,15 | |
| 11 | 65.8834 | 36.6722 | 220 | 16 | 11,13 | |
| 12 | 65.8069 | 37.0565 | 170 | 16 | 13,05 | T-INVERSION |
| 13 | 65.7502 | 37.3559 | 145 | 16 | 14,40 | INTRUS.;BOTTOM MIXED L. |
| 14 | 65.8000 | 37.7516 | 100 | 16 | 16,17 | 2 MIXED LAYERS |
| 15.1 | 65.8504 | 38.1204 | 85 | 16 | 17,45 | 2 MIXED LAYERS |
| 15.2 | 65.8504 | 38.1204 | 85 | 16 | 17,58 | 2 MIXED LAYERS |
| 16 | 65.8711 | 38.3201 | 80 | 16 | 18,45 | 2 MIXED LAYERS |
| 17 | 65.9003 | 38.5347 | 70 | 16 | 19,50 | BOTT.MIXED LAYER |
| 18 | 65.9229 | 38.7409 | 66 | 16 | 20,45 | BOTT. MIXED LAYER |
| 19 | 65.9558 | 38.9411 | 50 | 16 | 21,30 | BOTT.MIXED LAYER |
| 20 | 65.9669 | 39.0072 | 50 | 16 | 22,00 | ZOO, PHYTO,CHEM |
| 21 | 65.9882 | 39.2510 | 65 | 17 | 00,47 | MIXED |
| 22 | 66.0548 | 39.1839 | 35 | 17 | 02,25 | "CASCADING" AREA STARTS |
| 23 | 66.0065 | 39.2097 | 50 | 17 | 02,55 | |
| 24 | 65.9518 | 39.2551 | 60 | 17 | 03,40 | WIND NW 7M/S |
| 25 | 65.9173 | 39.3043 | 75 | 17 | 04,10 | |
| 26 | 65.8765 | 39.3335 | 75 | 17 | 04,40 | |
| 27 | 65.8334 | 39.3678 | 70 | 17 | 05,17 | |
| 28 | 65.8194 | 39.2215 | 65 | 17 | 05,56 | |
| 29 | 65.8582 | 39.2066 | 55 | 17 | 06,30 | |
| 30 | 65.9070 | 39.1718 | 65 | 17 | 07,12 | |
| 31 | 65.9550 | 39.1500 | 60 | 17 | 07,46 | |
| 32 | 66.0008 | 39.1082 | 50 | 17 | 08,18 | |
| 33 | 66.0504 | 39.0870 | 25 | 17 | 08,59 | |
| 34 | 66.0347 | 38.9706 | 25 | 17 | 09,43 | |
| 35 | 65.9766 | 39.0064 | 50 | 17 | 10,17 | |
| 36 | 65.9357 | 39.0241 | 56 | 17 | 10,98 | |
| 37 | 65.8752 | 39.0687 | 65 | 17 | 11,28 | |
| 38 | 65.8386 | 39.1057 | 70 | 17 | 12,00 | |
| 39.1 | 65.8005 | 39.1374 | 65 | 17 | 12,33 | |
| 39.2 | 65.8005 | 39.1374 | 65 | 17 | 12,40 | |
| 40 | 65.8008 | 38.9716 | 60 | 17 | 13,19 | |
| 41 | 65.8197 | 38.9734 | 65 | 17 | 15,41 | BATTERY SWAP |
| 42 | 65.8696 | 38.9343 | 65 | 17 | 16,24 | |
| 43 | 65.9176 | 38.9071 | 60 | 17 | 16,58 | |
| 44 | 65.9668 | 38.8685 | 55 | 17 | 17,38 | |
| 45 | 66.0012 | 38.8334 | 30 | 17 | 18,05 | |

| | | | | | | |
|---|---|---|---|---|---|---|
| 46 | 66.0006 | 38.7040 | 30 | 17 | 18,35 | |
| 47 | 65.9514 | 38.7501 | 55 | 17 | 19,44 | |
| 48 | 65.9021 | 38.7871 | 55 | 17 | 20,15 | |
| 49 | 65.8566 | 38.8360 | 65 | 17 | 20,50 | Two mixed layers. Batometr. |
| 50 | 65.8079 | 38.8682 | 65 | 17 | 23,25 | |
| 51 | 65.7714 | 38.8891 | 65 | 17 | 23.5 | Inversion. |
| 52 | 65.7227 | 38.9334 | 55 | 18 | 00,40 | 3 layers |
| 53 | 65.6219 | 38.9667 | 50 | 18 | 01,24 | |
| 54 | 65.7055 | 38.8700 | 60 | 18 | 02,10 | |
| 55 | 65.7398 | 38.9258 | 55 | 18 | 04,10 | |
| 56 | 65.7563 | 38.8251 | 65 | 18 | 04,40 | |
| 57 | 65.7541 | 38.7691 | 65 | 18 | 05,00 | |
| 58 | 65.7924 | 38.7415 | 65 | 18 | 05,30 | |
| 59 | 65.8525 | 38.7062 | 70 | 18 | 06,10 | |
| 60 | 65.8892 | 38.6560 | 80 | 18 | 07,00 | |
| 61 | 65.9346 | 38.6236 | 55 | 18 | 07,30 | |
| 62 | 65.9258 | 38.5339 | 55 | 18 | 08,17 | |
| 63 | 65.8724 | 38.5421 | 75 | 18 | 08,52 | |
| 64 | 65.8242 | 38.5713 | 75 | 18 | 09,27 | |
| 65 | 65.7839 | 38.6099 | 80 | 18 | 10,02 | |
| 66 | 65.7384 | 38.6558 | 80 | 18 | 10,35 | |
| 67 | 65.7216 | 38.5335 | 90 | 18 | 11,20 | |
| 68 | 65.7252 | 38.4053 | 100 | 18 | 12,57 | |
| 69 | 65.6916 | 38.2910 | 120 | 18 | 13,30 | |
| 70 | 65.6837 | 38.1706 | 120 | 18 | 14,07 | |
| 71 | 65.7560 | 38.1038 | 90 | 18 | 15,08 | |
| 72 | 65.8385 | 38.0390 | 90 | 18 | 16,00 | |
| 73 | 65.9171 | 37.9835 | 95 | 18 | 16,50 | |
| 74 | 65.9097 | 37.7083 | 120 | 18 | 18,00 | |
| 75 | 65.9182 | 37.4573 | 100 | 18 | 19,00 | |
| 76 | 65.9527 | 37.0716 | 110 | 18 | 20,30 | |
| 77 | 66.0019 | 36.2025 | 245 | 18 | 23,20 | |
| 78 | 66.0528 | 36.2217 | 220 | 19 | 00,05 | |
| 79 | 66.1000 | 36.2073 | 145 | 19 | 00,45 | |
| 80 | 66.1536 | 36.2059 | 100 | 19 | 01,30 | |
| 81 | 66.2012 | 36.2083 | 90 | 19 | 02,00 | |
| 82 | 66.2417 | 36.2179 | 50 | 19 | 02,40 | |
| 83 | 66.2236 | 35.8387 | 110 | 19 | 03,35 | |
| 84 | 66.3238 | 35.3228 | 95 | 19 | 05,40 | |
| 85 | 67.1259 | 32.3762 | 18 | 19 | 16,20 | |
| 86 | 67.1212 | 32.4076 | 45 | 20 | 00,00 | |
| 87 | 67.1051 | 32.4564 | 30 | 20 | 02,10 | |
| 88 | 67.0907 | 32.5230 | 17 | 20 | 02,55 | |
| 89 | 67.0854 | 32.5867 | 32 | 20 | 03,25 | |
| 90 | 67.0524 | 32.7052 | 12 | 20 | 04,10 | |
| 91.1 | 67.0691 | 32.7931 | 36 | 20 | 04,40 | Kolvitsa, current start |
| 91.2 | 67.0691 | 32.7931 | 36 | 20 | 09,15 | |
| 91.3 | 67.0691 | 32.7931 | 36 | 20 | 13,00 | |
| 91.4 | 67.0691 | 32.7931 | 36 | 20 | 18,00 | Kolvitsa, current finish |
| 92 | 67.0710 | 32.8546 | 65 | 20 | 19,25 | |
| 93 | 67.0760 | 32.9374 | 25 | 20 | 22,40 | (current at 23,00) |
| 94 | 67.1076 | 32.2589 | 26 | 21 | 04,10 | |
| 95 | 67.1000 | 32.3175 | 22 | 21 | 04,30 | |
| 96 | 67.0743 | 32.3680 | 30 | 21 | 05,00 | |
| 97 | 67.0510 | 32.4363 | 50 | 21 | 06,40 | |
| 98 | 67.0249 | 32.4909 | 30 | 21 | 07,00 | |
| 99 | 66.9369 | 32.6247 | 35 | 21 | 07,50 | |
| 100 | 66.8730 | 32.5014 | 25 | 21 | 09,00 | Knazhaja |
| 101 | 66.8731 | 32.4505 | 22 | 21 | 13,00 | |
| 102 | 66.8693 | 32.4035 | 7 | 21 | 14,16 | |
| 103 | 66.8839 | 32.5189 | 25 | 21 | 17,10 | |

| | | | | | | |
|---|---|---|---|---|---|---|
| 104 | 66.8763 | 32.5534 | 30 | 21 | 17,25 | |
| 105 | 66.8907 | 32.5509 | 22 | 21 | 17,35 | |
| 106 | 66.9063 | 32.5728 | 25 | 21 | 17,45 | |
| 107 | 66.9069 | 32.6021 | 35 | 21 | 17,55 | |
| 108 | 67.0683 | 32.6003 | 30 | 21 | 18,10 | |
| 109 | 66.8886 | 32.5909 | 30 | 21 | 18,20 | |
| 110 | 66.8758 | 32.5875 | 40 | 21 | 18,35 | |
| 111 | 66.8684 | 32.5898 | 35 | 21 | 18,50 | |
| 112 | 66.9060 | 32.6015 | 37 | 21 | 20,50 | |
| 113 | 66.9237 | 32.6530 | 37 | 21 | 22,30 | |
| 114 | 66.9397 | 32.7390 | 55 | 21 | 22,55 | |
| 115 | 66.9506 | 32.7892 | 45 | 21 | 23,30 | |
| 116 | 66.9555 | 32.8345 | 40 | 21 | 23,50 | |
| 117 | 66.8694 | 33.0017 | 40 | 22 | 00,45 | |
| 118 | 66.8513 | 32.9555 | 60 | 22 | 01,05 | |
| 119 | 66.7895 | 32.8892 | 60 | 22 | 01,25 | |
| 120 | 66.8019 | 32.8333 | 35 | 22 | 01,50 | |
| 121 | 66.7061 | 33.0369 | 35 | 22 | 03,00 | |
| 122 | 66.7341 | 33.1040 | 60 | 22 | 03,20 | |
| 123 | 66.7690 | 33.1854 | 80 | 22 | 03,50 | |
| 124 | 66.7863 | 33.2367 | 55 | 22 | 04,10 | |
| 125 | 66.7087 | 33.4564 | 65 | 22 | 05,15 | |
| 126 | 66.6922 | 33.4378 | 180 | 22 | 05,35 | |
| 127 | 66.6681 | 33.3883 | 55 | 22 | 06,10 | |
| 128 | 66.6502 | 33.3379 | 35 | 22 | 06,35 | |
| 129 | 66.6675 | 34.0563 | 75 | 22 | 09,15 | |
| 130 | 66.6231 | 33.9580 | 245 | 22 | 09,50 | |
| 131 | 66.5866 | 33.8895 | 200 | 22 | 10,25 | |
| 132 | 66.5429 | 33.8177 | 290 | 22 | 11,05 | |
| 133 | 66.5058 | 33.7098 | 200 | 22 | 14,30 | |
| 134 | 66.4862 | 33.6338 | 140 | 22 | 15,10 | 2 stup., rezk. promezh. termoklin |
| 135 | 66.5073 | 33.4048 | 115 | 22 | 16,45 | |
| 136 | 66.5381 | 33.2175 | 60 | 22 | 17,35 | |
| 137 | 66.2375 | 34.1001 | 115 | 22 | 23,20 | |
| 138 | 66.2837 | 34.1842 | 160 | 23 | 00,10 | |
| 139 | 66.3585 | 34.2679 | 200 | 23 | 01,30 | |
| 140 | 66.3718 | 34.2927 | 220 | 23 | 02,05 | |
| 141 | 66.4226 | 34.3532 | 260 | 23 | 02,45 | |
| 142 | 66.4598 | 34.3726 | 290 | 23 | 06,00 | |
| 143 | 66.4739 | 34.4518 | 265 | 23 | 06,30 | |
| 144 | 66.5064 | 34.4685 | 210 | 23 | 07,15 | |
| 145 | 66.5228 | 34.4865 | 125 | 23 | 08,05 | |
| 146 | 66.5689 | 34.7900 | 30 | 23 | 09,40 | |
| 147 | 66.5392 | 34.7537 | 70 | 23 | 10,05 | |
| 148 | 66.5060 | 34.7079 | 105 | 23 | 10,30 | |
| 149 | 66.4865 | 34.6747 | 190 | 23 | 10,55 | |
| 150 | 66.4727 | 35.1173 | 35 | 23 | 12,35 | |
| 151 | 66.4421 | 35.0735 | 60 | 23 | 13,00 | |
| 152 | 66.4185 | 35.0366 | 120 | 23 | 13,25 | |
| 153 | 66.3867 | 35.0011 | 180 | 23 | 13,55 | |

# A.2. Table info cruise 2001

| CTD SEACAT 19 profiler | | | | | | | |
|---|---|---|---|---|---|---|---|
| Table White Sea cruise: spring 2001, vessel: *Kuznetsov* | | | | system uploaded | COMMENTS | | |
| data filename [.hex] | station | latitude | longitude | date | time | depth seabed[m] | |
| new3600 | 1 | 66 16.7 | 33 14.3 | 26.may.01 | 08:10 | 72 | |
| new3700 | 2 | 66 19.7 | 33 39.7 | 26 may.01 | 09:30:00 | 65 | |
| new3900 | 3 | 66 16.7 | 33 14.3 | 27 may.01 | 11:00:00 | 65 | |
| new4000 | 4 | 66 19.4 | 33 34.7 | 27-May-01 | 15:46:19 | 62 | |
| new4100 | 5 | 66 19.2 | 33 31.2 | 27-May-01 | 16:08:25 | 44 | |
| new4200 | 6 | 66 18.6 | 33 24.3 | 27-May-01 | 16:44:12 | 37 | |
| new4300 | 7 | 66 18.2 | 33 19.0 | 27-May-01 | 18:12:29 | 27 | |
| new4400 | 8 | 66 16.7 | 33 14.0 | 27-May-01 | 19:02:52 | 64 | |
| new4500 | 9 | 66 16.2 | 33 08.8 | 27-May-01 | 21:29:33 | 28 | |
| new4600 | 10 | 66 16.1 | 33 04.5 | 27-May-01 | 21:55:23 | 32 | |
| new4700 | 11 | 67 04.9 | 32 56.1 | 28-May-01 | 08:26:20 | 24 | |
| new4801 | 11a | 67 04.9 | 32 56.1 | 28-May-01 | 08:46:04 | 24 | |
| new4900 | 12 | 67 04.2 | 32 50.6 | 28-May-01 | 12:18:07 | 70 | |
| new5000 | 13 | 67 04.0 | 32 46.4 | 28-May-01 | 15:11:29 | 32 | |
| new5100 | 14 | 67 00.3 | 32 44.6 | 28-May-01 | 16:22:46 | 44 | |
| new5200 | 15 | 66 52.5 | 32 25.3 | 28-May-01 | 18:04:57 | 13 | |
| new5300 | 16 | 66 52.6 | 32 27.1 | 28-May-01 | 19:12:20 | 24 | |
| new5400 | 17 | 66 52.7 | 32 29.1 | 28-May-01 | 20:07:36 | 28 | |
| new5500 | 18 | 66 52.7 | 32 38.2 | 29-May-01 | 05:44:18 | 52 | |
| new5600 | 19 | 66 54.2 | 32 42.5 | 29-May-01 | 06:12:00 | 48 | |
| new5700 | 20 | 66 55.5 | 32 46.8 | 29-May-01 | 06:39:49 | 58 | |
| new5800 | 21 | 66 50.0 | 33 04.5 | 29-May-01 | 09:28:05 | 94 | |
| new5900 | 22 | 66 48.5 | 33 00.6 | 29-May-01 | 09:57:09 | 74 | |
| new6000 | 23 | 66 47.4 | 32 57.7 | 29-May-01 | 12:21:54 | 50 | |
| new6100 | 24 | 66 40.1 | 33 22.7 | 29-May-01 | 13:51:55 | 65 | |
| new6200 | 25 | 66 40.9 | 33 24.9 | 29-May-01 | 14:17:20 | 73 | |
| new6300 | 26 | 66 41.9 | 33 27.8 | 29-May-01 | 16:24:52 | 150 | |
| new6400 | 27 | 66 42.6 | 33 29.6 | 29-May-01 | 16:48:00 | 87 | |
| new6500 | 28 | 66 39.1 | 33 51.0 | 29-May-01 | 18:00:22 | 155 | |
| new6600 | 29 | 66 37.2 | 33 48.0 | 29-May-01 | 18:43:00 | 155 | |
| new6700 | 30 | 66 35.7 | 33 45.4 | 29-May-01 | 19:18:07 | 213 | |
| new6800 | 31 | 66 32.8 | 33 41.0 | 30-May-01 | 01:38:11 | 260 | |
| new6900 | 32 | 66 31.0 | 33 39.1 | 30-May-01 | 02:10:35 | 216 | |
| new7000 | 33 | 66 32.2 | 33 15.0 | 30-May-01 | 09:59:04 | 96 | |
| new7100 | 34 | 66 29.0 | 33 36.9 | 30-May-01 | 11:12:13 | 135 | |
| new7300 | 35 | 66 26.4 | 34 02.5 | 30-May-01 | 12:42:53 | 223 | |
| new7400 | 36 | 66 25.7 | 34 12.0 | 30-May-01 | 13:30:13 | 265 | |
| new7500 | 37 | 66 24.9 | 34 21.7 | 30-May-01 | 14:58:14 | 278 | |
| new7600 | 38 | 66 26.9 | 34 24.8 | 31-May-01 | 00:39:59 | 287 | |
| new7700 | 39 | 66 28.7 | 34 30.4 | 31-May-01 | 03:02:49 | 264 | |
| new7800 | 40 | 66 30.6 | 34 29.0 | 31-May-01 | 07:17:48 | 256 | |
| new7900 | 41 | 66 26.2 | 34 39.2 | 31-May-01 | 08:06:36 | 230 | |
| new8000 | 42 | 66 22.8 | 34 49.0 | 31-May-01 | 08:55:19 | 217 | |
| new8100 | 43 | 66 19.8 | 34 58.9 | 31-May-01 | 09:45:19 | 232 | |
| new8200 | 44 | 66 16.8 | 35 07.9 | 31-May-01 | 10:34:18 | 213 | |
| new8300 | 45 | 66 12.2 | 35 23.4 | 31-May-01 | 11:39:15 | 213 | |
| new8400 | 46 | 66 06.3 | 35 41.3 | 31-May-01 | 13:37:38 | 267 | |
| new8500 | 47 | 66 08.2 | 35 28.9 | 31-May-01 | 19:13:50 | 264 | |
| new8600 | 48 | 66 12.1 | 34 59.8 | 31-May-01 | 20:58:03 | 257 | |

| | | | | | | | |
|---|---|---|---|---|---|---|---|
| new8700 | 49 | 66 16.2 | 34 35.9 | 01-Jun-01 | 02:13:01 | 209 | |
| new8800 | 50 | 66 22.3 | 34 14.7 | 02-Jun-01 | 10:02:13 | 198 | |
| new8901 | 51 | 66 30.3 | 34 20.9 | 02-Jun-01 | 19:39:48 | 276 | 260 zonding |
| new9000 | 52 | 66 34.8 | 34 16.3 | 02-Jun-01 | 20:21:10 | 201 | |
| new9100 | 53 | 66 31.9 | 34 11.2 | 02-Jun-01 | 21:09:19 | 275 | |
| new9200 | 54 | 66 29.3 | 34 04.8 | 02-Jun-01 | 21:58:47 | 346 | max depth |
| new9300 | 55 | 66 26.1 | 33 58.2 | 02-Jun-01 | 22:43:00 | 187 | |
| new9400 | 56 | 66 16.7 | 34 14.3 | 03-Jun-01 | 00:57:07 | 68 | |

# A.3. MATLAB programs: depthsection.m

```
%       Matlab Program "depthsection.m"
%       that select depth for various station files
%       spaced on regular and identical step and record its
%       Temperature, salinity & density sigma-t.
%       This program is aimed at horizontal depth-section contours.
%       Ask files that have been interpolated using cubic spline method.

clear all;

%       load station info: num, lat, Lon
coord=load('e:\Phd_project\region_section\castlocation.txt');

%       change to current directory for interpolated datafiles
cd e:\Phd_project\region_section\all_station\v_interpol_data\  %dir in my office computer

%       name the outfile as a string to formulate several output files
filename='depthm.dat';

%       enter the depth(s) and number of station files
d=input('Enter the depth of section(s) -as INTEGER- e.g. [5:5:250]\n');
d=d'
numstat=input ('Enter the total number of station file for section\n');

%       initialise multidimentional matrix 500x5 repeated the number of stations, set to 0
z=zeros(500,5,numstat);

%       do a loop for opening Id station file, later stored in the multi-D matrix z
for n=1:numstat                         %39 station in Kandalaksha
stat=input('Enter the station as a number (eg: 1.1 for d01_1)\n');
[fid,pathname]=uigetfile('*.dat','open the station file you just typed',50,50);

        %       return if none (if cancel the open box, no error shows on the prompt command)
        if fid == 0
                return;
        end

%       put coordinate position in matrix stat
        for c=1:length(coord);
                if stat==coord(c,1);stat=[coord(c,1) coord(c,3) coord(c,2)];
                end
        end

        %       load file
        x=load(fid);
        %       resize matrix x (filled by 0) to that of z and stored in matrix z(page number n)
        [l g]=size(x);
        xx=zeros(500-l,5);
```

```
        x=[x' xx'];
        x=x';
        z(:,:,n)=x;

        %       seek the selected depth in data column of matrix z
        %       store "[Station num., Lon, Lat], depth, Temp., Salin., Dens., Cond."
        %       in the multi-D Matrix data
        for j=1:length(d);
                for i=1:length(z);
                        if z(i,1,n)==d(j);
                        data(n,:,j)=[stat z(i,:,n)];
                        end
                end
        end
end
%       write in output file
for j=1:length(d);
        deep=num2str(d(j));
        out=strrep(filename,'m',deep);
        DLMWRITE(out,data(:,:,j),'\t');
end
fclose('all')
```

# A.4. MATLAB programs: interpol.m

```
%       Matlab Program "interpol.m"
%       that applies a regular interval through data columns
%       using cubic spline interpolation for
%       Depth, Temperature, salinity & density sigma-t.
%       This program is aimed at horizontal depth-section contours.

clear all;

%       change to directory whilst opening data
cd e:\Phd_project\ctd2000\ctd_profiles\      %dir in my office computer

%       open infile and load it
[fid,pathname]=uigetfile('*.dat','open CTD data file ',50,50);

%       return if none (if cancel the open box, no error shows on the prompt command)
if fid == 0
        return;
end

x=load(fid);

%       interpolate data column on regular interval using cubic spline
%       starting from surface 1m to deep cast.
%       AND STORE IN THE MATRIX DATA
depth=1:1:round(max(x(:,4)));
temp=spline(x(:,4),x(:,2),depth);
salin=spline(x(:,4),x(:,5),depth);
dens=spline(x(:,4),x(:,6),depth);
cond=spline(x(:,4),x(:,3),depth);
data=[depth',temp',salin',dens',cond'];

%       write on output file, saveas eg: id01_1.dat
```

```
        out=['i' fid];
        DLMWRITE(out,data,'\t');

fclose('all')
```

# A.5. MATLAB programs: dyntopo.m

```
% Matlab program "dyntopo.m" to calculate the dynamic height
% input data must have a (positive) depth bin-average of 1
% unit of dynamic height is x10^5 dyn-cm/gm.

% initialise parameters and matrix of density sigma_t
g=9.81;  %m/s^2
rho0=1000;
dsurf=input('Enter surface reference depth (positive integer) \n');
dbottom=input('Enter the bottom reference depth (positive integer) \n');
stns=input('Enter the number of stations \n');

data_size=dbottom-dsurf+1;
sig=zeros(data_size,stns);
%sig=zeros(dbottom,stns);
m=0;

% at that point, the station files should be renamed to follow an increased number
% e.g.: d01.asc, d04.asc, d153.asc... should then be: d01.asc, d02.asc, d03.asc...
for i=1:stns
  clear dens de n
  m=m+1;
  if i<10
    filename=(['d0',int2str(i),'.asc']);
  else
    filename=(['d',int2str(i),'.asc']);
  end

  dens=dlmread(filename,' ');  % need ' '='space' to read data as in a matrix
  length=size(dens,1);
  de=dens(dsurf:length,6);
    n=size(de,1);
    for j=1:n
    sig(j,m)=de(j);
    end
end


for i=1:data_size
  suma=0;
  points=stns;
  for j=1:stns
    if sig(i,j)==0
      points=points-1;
    else
      suma=suma+((sig(i,j)*10^-3)+1);
    end
  end

  meandens(i)=suma/points;
end

for i=1:data_size
```

```
  for j=1:stns
    if sig(i,j)==0
      deltarho(i,j)=0;
    else
      deltarho(i,j)=((sig(i,j)*10^-3)+1)-meandens(i);
    end
  end
end


for j=1:stns
  H(j)=(-g/rho0)*sum(deltarho(:,j));% In dynamic meters.
  % problem by dividing by rho0(=1000)..because output data are 1000 times smaller.??
  % need to ask cecilia or vladimir for the equation...
end

dyn=[1:1:stns; H]';
save dyn.dat dyn -ascii;
```

# A.6. FORTRAN program: readsla.for

```
      PROGRAM READ_MSLA


!     modified by Lolo the 02 March 2002.

!     this program reads a SLA (Sea Level Anomaly) map file
!     the map is obtained by objective analysis of SLA data
!     This example shows how to read the first file in your list
!     corresponding to the date 17325 (June 8, 1997)

!     TE = sea level anomaly in  millimeters (Topex Ers merged)
!     ER = quadratic mapping error in %
!     over continents or near the coast or in the absence of data
!     TE = 9999 and ER = 100

      implicit none

      integer*2 alatmi,alonmi,mii,mjj,ic,jc
      real*4 itlat,itlon
      REAL ALONP,ALATP
      integer*4 te,er
      character*80 nomfic

!     open input and output files
      open(unit=20,file='TPERS-SLA.dat',status='unknown')
      open(10,file='MSLA_HH_TPERS_17325.ASC',status='old',form='formatted')

!     start to read geographical coordinates and parameters for grid points
      read(10,'(A80)') nomfic

      read(10,120)alatmi,alonmi,itlat,itlon,mii,mjj

120   format(2i6,2f8.2,2i6)

!     mii= number of grid point in latitude
!     mjj= number of grid point in longitude
!     itlat, itlon = grid size in degrees
```

```
!       start to do loop to calculate grid point coordinates and read respective SLA
        DO 1 JC=1,MJJ
        DO 2 IC=1,MII

!       latitude and longitude of grid point can be obtained as follows :

                ALONP=ALONMI+ITLON/2.+ITLON*(JC-1)
                ALATP=ALATMI+ITLAT/2.+ITLAT*(IC-1)

        read(10,100)TE,ER
100     format(i6,i4)

!       record and print SLA grid point for the White Sea box coordinates
        if ((alatp.le.70).and.(alatp.ge.63)) then
                if ((alonp.le.45).and.(alonp.ge.30)) then
                        if ((TE.ne.9999)) then

                        WRITE(6,*) ALATP,ALONP,TE,ER
11                      format(i4,i4,f5.2,f5.2)
                        WRITE(20,*) ALATP,ALONP,TE,ER
                        endif
                endif
        endif

2       continue
1       continue

!       end program
        CLOSE(10)
        close(20)

        END
```

# Appendix B: Mixed layer identification

## B.1 Salinity and density distribution at the east-west transect

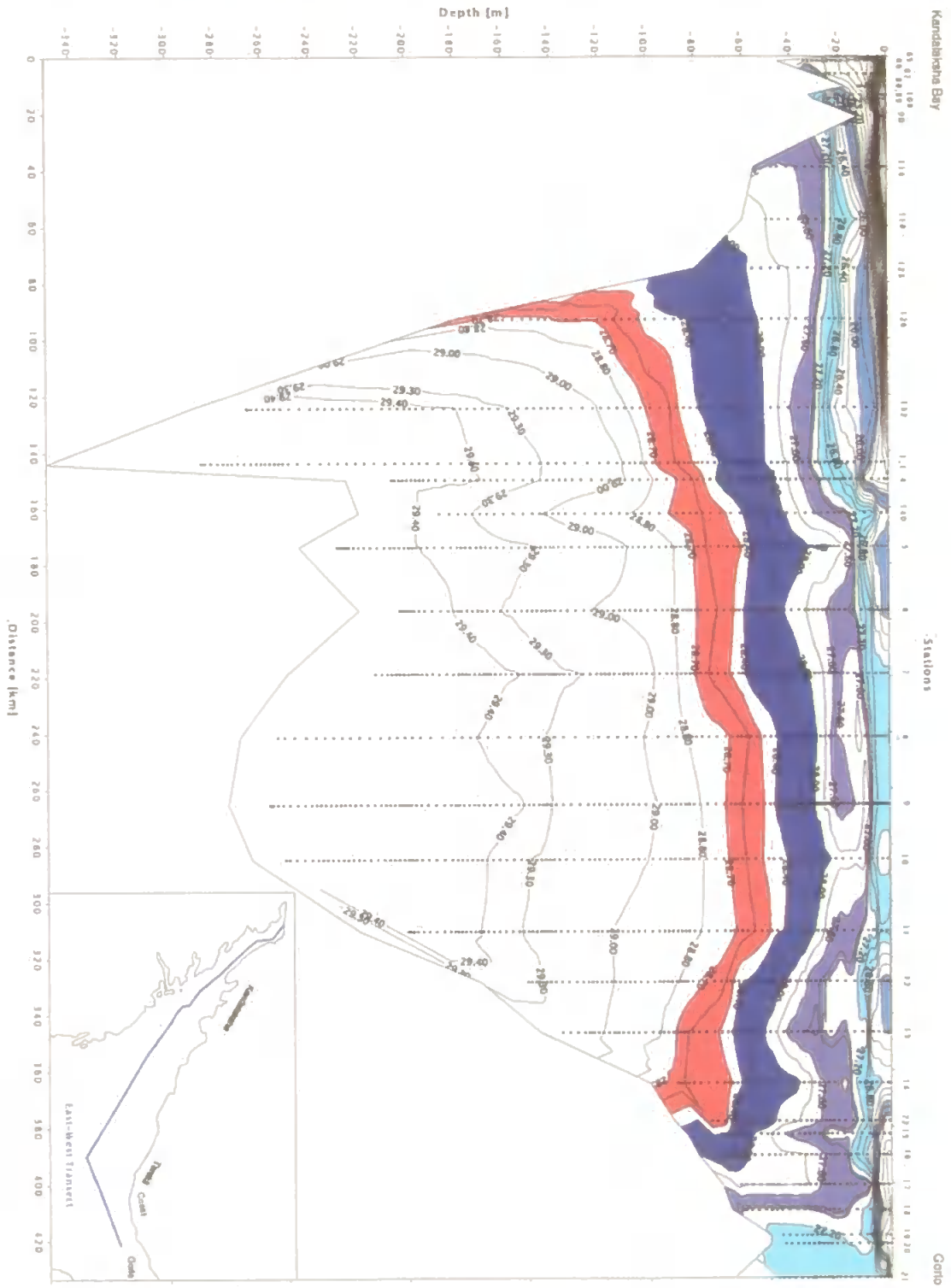


Figure 4.6b: Vertical salinity [psu] distribution along the East-west Transect, showing mixed layers A, B, C, D and E propagating across the White Sea, in June 2000. The active upper layer includes the mixed layers A, B, and C; the intermediate layer is well distinct by a dome structure (step D and E).

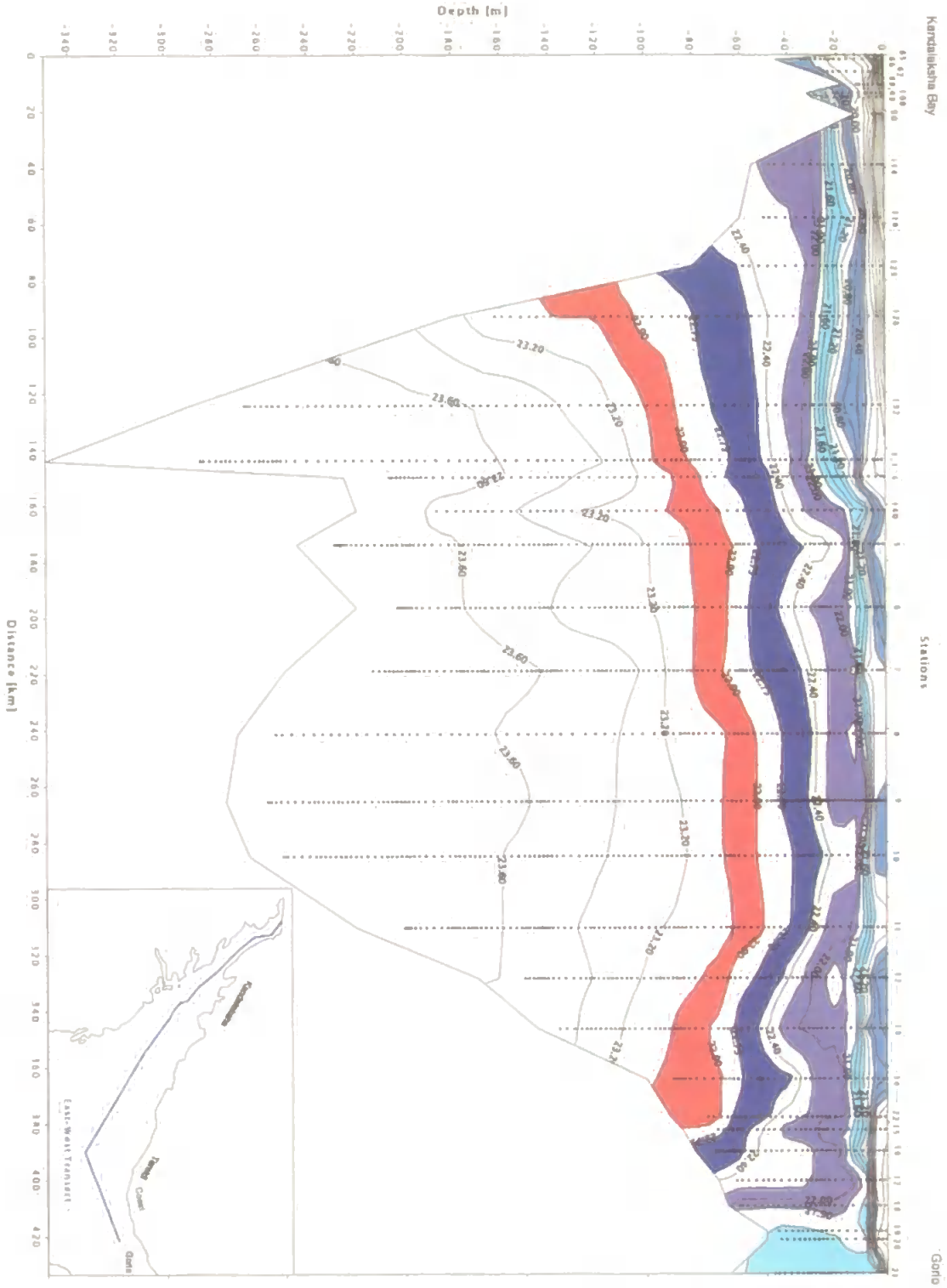


Figure 4.6c: Vertical density [kg/m3] distribution along the East-west Transect, showing mixed layers A, B, C, D and E propagating across the White Sea, in June 2000. The active upper layer includes the mixed layers A, B, and C; the intermediate layer is well distinct by a dome structure (step D and E)

# B.2 Tables of the thermohaline index of the mixed layers A, B, C, D, E – survey 2000.

Table 4.1a: Mixed layer A (density ≤ 21), White Sea cruise 2000

| ST_NUMBER | upper_layer[m] | lower_layer[m] | middle_layer | thickness | salinity | Temperature | density |
|---|---|---|---|---|---|---|---|
| 1.1 | 10 | 16 | 13 | 6 | 26 | 6 | 20.4 |
| 4 | 6 | 10 | 8 | 4 | 25.2 | 7.3 | 19.6 |
| 5 | 8 | 10 | 9 | 2 | 26.4 | 5.8 | 20.7 |
| 13 | 4 | 8 | 6 | 4 | 26.1 | 6.1 | 20.5 |
| 14 | 6 | 8 | 7 | 2 | 26.7 | 7.3 | 20.7 |
| 15.1 | 6 | 8 | 7 | 2 | 25.5 | 6.6 | 20 |
| 16 | 6 | 8 | 7 | 2 | 25.9 | 6 | 20.3 |
| 17 | 6 | 7 | 6.5 | 1 | 26.2 | 5.2 | 20.4 |
| 18 | 4 | 8 | 6 | 4 | 25.9 | 5.4 | 20.2 |
| 19 | 6 | 7 | 6.5 | 1 | 25.7 | 5.5 | 20.2 |
| 20 | 5 | 6 | 5.5 | 1 | 25.6 | 5.3 | 20.3 |
| 27 | 6 | 8 | 7 | 2 | 26.2 | 4.4 | 20.7 |
| 37 | 7 | 9 | 8 | 2 | 26.3 | 2.8 | 20.9 |
| 38 | 4 | 6 | 5 | 2 | 25.2 | 4.3 | 20 |
| 39 | 7 | 11 | 9 | 4 | 25.6 | 4.1 | 20.2 |
| 40 | 4 | 10 | 7 | 6 | 25.5 | 6.8 | 20 |
| 41 | 9 | 10 | 9.5 | 1 | 26.2 | 3 | 20.95 |
| 42 | 14 | 22 | 18 | 8 | 26.4 | 2.6 | 21 |
| 48 | 6 | 8 | 7 | 2 | 26.25 | 3.6 | 21 |
| 49 | 6 | 8 | 7 | 2 | 25.5 | 4.5 | 20.4 |
| 51 | 7 | 8 | 7.5 | 1 | 25.9 | 5.6 | 20.3 |
| 63 | 9 | 11 | 10 | 2 | 26.9 | 4.8 | 20.9 |
| 66 | 6 | 8 | 7 | 2 | 26.8 | 5.8 | 21 |
| 67 | 4 | 7 | 5.5 | 3 | 26.2 | 6.6 | 20.8 |
| 89 | 8 | 12 | 10 | 4 | 25.6 | 3 | 20 |
| 91.3 | 10 | 14 | 12 | 4 | 26 | 3 | 20.2 |
| 92 | 14 | 17 | 15.5 | 3 | 25.2 | 3.4 | 20 |
| 93 | 8 | 11 | 9.5 | 3 | 25 | 4.2 | 20.1 |
| 97 | 25 | 40 | 32.5 | 15 | 25.6 | 2 | 20.1 |
| 98 | 15 | 25 | 20 | 10 | 25 | 2.5 | 20 |
| 99 | 10 | 17 | 13.5 | 7 | 25.8 | 3 | 20.5 |
| 100 | 10.5 | 14 | 12.25 | 3.5 | 25.5 | 3.8 | 20 |
| 101 | 13 | 16 | 14.5 | 3 | 25.5 | 3 | 20.4 |
| 103 | 12 | 18 | 15 | 6 | 25.2 | 3.6 | 20.2 |
| 104 | 12 | 18 | 15 | 6 | 25.4 | 3.2 | 20.2 |
| 105 | 9.5 | 14 | 11.75 | 4.5 | 25.2 | 3.5 | 20 |
| 106 | 10 | 16 | 13 | 6 | 25 | 3.5 | 20 |
| 107 | 8 | 18 | 13 | 10 | 25.5 | 3.5 | 20.2 |
| 108 | 8 | 18 | 13 | 10 | 25.5 | 3.5 | 20.2 |
| 109 | 17 | 20 | 18.5 | 3 | 26 | 2.5 | 20.5 |
| 110 | 12 | 14 | 13 | 2 | 25.2 | 3.5 | 20.2 |
| 111 | 9 | 10 | 9.5 | 1 | 25 | 4 | 20.2 |
| 112 | 9 | 17 | 13 | 8 | 25.5 | 3.5 | 20.5 |
| 113 | 8 | 10 | 9 | 2 | 25 | 3.8 | 20 |
| 114 | 8 | 10 | 9 | 2 | 25.2 | 3.2 | 20.2 |
| 115 | 6 | 10 | 8 | 4 | 25 | 3.2 | 20.2 |
| 116 | 7 | 9 | 8 | 2 | 25.6 | 3 | 20.5 |
| 117 | 3 | 6 | 4.5 | 3 | 25 | 5 | 20 |
| 120 | 10 | 14 | 12 | 4 | 25.8 | 3.3 | 20.25 |
| 121 | 5 | 7 | 6 | 2 | 25 | 4.2 | 19.8 |
| 122 | 9 | 13 | 11 | 4 | 26.2 | 3 | 20.8 |
| 123 | 8 | 16 | 12 | 8 | 26 | 3.8 | 20.6 |
| 124 | 6 | 12 | 9 | 6 | 25.4 | 4.4 | 20.2 |

| | | | | | | | |
|---|---|---|---|---|---|---|---|
| 125 | 10 | 14 | 12 | 4 | 26 | 3.8 | 20.6 |
| 126 | 14 | 18 | 16 | 4 | 26.2 | 3.5 | 20.6 |
| 127 | 10 | 14 | 12 | 4 | 26.4 | 3.2 | 21 |
| 128 | 7 | 19 | 13 | 12 | 26 | 3.8 | 20.6 |
| 130 | 16 | 22 | 19 | 6 | 26.4 | 3.2 | 21 |
| 142 | 10 | 12 | 11 | 2 | 26.7 | 7.2 | 20.9 |
| 144 | 8 | 10 | 9 | 2 | 26.6 | 7.8 | 20.7 |
| 145 | 9 | 12 | 10.5 | 3 | 26.6 | 5.6 | 20.9 |
| 146 | 9 | 16 | 12.5 | 7 | 26.48 | 6.7 | 20.74 |
| 147 | 9 | 18 | 13.5 | 9 | 26.48 | 6.8 | 20.55 |
| 148 | 13 | 15 | 14 | 2 | 26.5 | 7.6 | 20.7 |
| 153 | 6 | 8 | 7 | 2 | 26.9 | 6.8 | 20.9 |
| | | | | | | | |
| mean | 8.72 | 12.86 | 10.79 | 4.14 | 25.82 | 4.47 | 20.41 |

Table 4.1b: Mixed layer A (density ≥ 21), White Sea cruise 2000

| ST_NUMBER | upper_layer[m] | lower_layer[m] | middle_layer | thickness | salinity | Temperature | density |
|---|---|---|---|---|---|---|---|
| 6 | 6 | 12 | 9 | 6 | 26.8 | 3.5 | 21.4 |
| 12 | 6 | 8 | 7 | 2 | 26.4 | 5.5 | 21.1 |
| 22 | 2 | 4 | 3 | 2 | 26.55 | 3 | 21.15 |
| 25 | 2 | 4 | 3 | 2 | 26.75 | 3 | 21.25 |
| 28 | 10 | 18 | 14 | 8 | 26.7 | 1.5 | 21.35 |
| 29 | 3 | 5 | 4 | 2 | 26.7 | 1.7 | 21.3 |
| 33 | 2 | 10 | 6 | 8 | 26.7 | 2.1 | 21.295 |
| 34 | 4 | 8 | 6 | 4 | 26.6 | 3 | 21.2 |
| 42 | 14 | 22 | 18 | 8 | 26.4 | 2.6 | 21 |
| 43 | 10 | 14 | 12 | 4 | 26.6 | 3 | 21.1 |
| 44 | 6 | 8 | 7 | 2 | 26.3 | 4 | 21.1 |
| 46 | 3 | 4 | 3.5 | 1 | 26.65 | 2.9 | 21.25 |
| 48 | 6 | 8 | 7 | 2 | 26.25 | 3.6 | 21 |
| 55 | 8 | 14 | 11 | 6 | 26.5 | 2.5 | 21.2 |
| 56 | 9 | 12 | 10.5 | 3 | 26.8 | 2.4 | 21.2 |
| 58 | 15 | 17 | 16 | 2 | 26.85 | 4.7 | 21.2 |
| 66 | 6 | 8 | 7 | 2 | 26.8 | 5.8 | 21 |
| 82 | 8 | 28 | 18 | 20 | 26.6 | 2.5 | 21.3 |
| 127 | 10 | 14 | 12 | 4 | 26.4 | 3.2 | 21 |
| 129 | 8 | 14 | 11 | 6 | 26.5 | 3.8 | 21.2 |
| 130 | 16 | 22 | 19 | 6 | 26.4 | 3.2 | 21 |
| 131 | 20 | 26 | 23 | 6 | 26.5 | 3.2 | 21.2 |
| 135 | 10 | 14 | 12 | 4 | 26.7 | 4 | 21.2 |
| 136 | 14 | 16 | 15 | 2 | 26.7 | 3 | 21.2 |
| 137 | 20 | 22 | 21 | 2 | 26.9 | 4.5 | 21.3 |
| 139 | 8 | 12 | 10 | 4 | 27 | 4.4 | 21.4 |
| 141 | 10 | 12 | 11 | 2 | 26.9 | 4.4 | 21.4 |
| 149 | 14 | 16 | 15 | 2 | 26.9 | 4.7 | 21.3 |
| 151 | 20 | 22 | 21 | 2 | 26.8 | 3.1 | 21.36 |
| 152 | 7 | 10 | 8.5 | 3 | 27.2 | 3.6 | 21.6 |
| | | | | | | | |
| mean | 9.23 | 13.47 | 11.35 | 4.23 | 26.66 | 3.41 | 21.22 |

Table 4.2: Mixed layer B, White Sea cruise 2000

| ST_NUMBER | upper_layer[m] | lower_layer[m] | middle_layer | thickness | salinity | Temperature | density |
|---|---|---|---|---|---|---|---|
| 1 | 20 | 24 | 22 | 4 | 26.85 | 2 | 21.5 |
| 4 | 14 | 28 | 21 | 14 | 27 | 2.5 | 21.6 |
| 6 | 12 | 16 | 14 | 4 | 27.3 | 1.5 | 21.9 |
| 11 | 7 | 11 | 9 | 4 | 27.3 | 2.9 | 21.7 |
| 12 | 10 | 12 | 11 | 2 | 26.9 | 2.4 | 21.5 |
| 13 | 10 | 14 | 12 | 4 | 27.25 | 1.1 | 21.85 |
| 14 | 12 | 14 | 13 | 2 | 27.2 | 3.5 | 21.6 |
| 15 | 10 | 15 | 12.5 | 5 | 27.1 | 1.8 | 21.6 |
| 16 | 11 | 17 | 14 | 6 | 26.9 | 2.2 | 21.5 |
| 19 | 8 | 45 | 26.5 | 37 | 27.1 | 1 | 21.7 |
| 20 | 8 | 45 | 26.5 | 37 | 27.1 | 1 | 21.7 |
| 21 | 4 | 40 | 22 | 36 | 27 | 1.6 | 21.6 |
| 22 | 10 | 15 | 12.5 | 5 | 26.7 | 2.6 | 21.8 |
| 23 | 10 | 25 | 17.5 | 15 | 27.05 | 2 | 21.6 |
| 24 | 0 | 55 | 27.5 | 55 | 27.15 | 2.2 | 21.655 |
| 25 | 8 | 65 | 36.5 | 57 | 27.25 | 2.3 | 21.75 |
| 26 | 10 | 65 | 37.5 | 55 | 27.3 | 2.5 | 21.775 |
| 27 | 30 | 65 | 47.5 | 35 | 27.3 | 2.5 | 21.8 |
| 28 | 20 | 60 | 40 | 40 | 27.3 | 2.2 | 21.75 |
| 29 | 28 | 50 | 39 | 22 | 27.2 | 2 | 21.7 |
| 30 | 2 | 60 | 31 | 58 | 27.2 | 2 | 21.7 |
| 31 | 2 | 55 | 28.5 | 53 | 27.13 | 2 | 21.7 |
| 32 | 2 | 45 | 23.5 | 43 | 27.03 | 2 | 21.6 |
| 35 | 6 | 40 | 23 | 34 | 27 | 1.2 | 21.65 |
| 36 | 12 | 20 | 16 | 8 | 26.8 | 2 | 21.5 |
| 37 | 10 | 25 | 17.5 | 15 | 26.75 | 1.3 | 21.5 |
| 38 | 10 | 22 | 16 | 12 | 26.7 | 1.5 | 21.3 |
| 39 | 14 | 24 | 19 | 10 | 26.8 | 1.25 | 21.5 |
| 40 | 14 | 22 | 18 | 8 | 27.2 | 1.5 | 21.7 |
| 41 | 20 | 55 | 37.5 | 35 | 27 | 1.2 | 21.6 |
| 42 | 24 | 28 | 26 | 4 | 26.8 | 1.5 | 21.4 |
| 43 | 14 | 32 | 23 | 18 | 27.25 | 1.2 | 21.75 |
| 44 | 10 | 50 | 30 | 40 | 27 | 1.5 | 21.6 |
| 45 | 5 | 25 | 15 | 20 | 26.85 | 1.95 | 21.45 |
| 46 | 10 | 25 | 17.5 | 15 | 26.75 | 2.2 | 21.375 |
| 47 | 18 | 50 | 34 | 32 | 27.1 | 1 | 21.6 |
| 48 | 8 | 10 | 9 | 2 | 27 | 2.2 | 21.5 |
| 49 | 10 | 30 | 20 | 20 | 27.1 | 1 | 21.75 |
| 51 | 13 | 18 | 15.5 | 5 | 27.1 | 1.2 | 21.7 |
| 52 | 14 | 23 | 18.5 | 9 | 27.05 | 0.8 | 21.8 |
| 53 | 13 | 22 | 17.5 | 9 | 26.9 | 1 | 21.5 |
| 54 | 12 | 24 | 18 | 12 | 27.2 | 0.8 | 21.8 |
| 55 | 16 | 20 | 18 | 4 | 27.1 | 1 | 21.8 |
| 56 | 12 | 14 | 13 | 2 | 27 | 1.3 | 21.6 |
| 57 | 12 | 15 | 13.5 | 3 | 26.8 | 3.5 | 21.2 |
| 58 | 18 | 22 | 20 | 4 | 27 | 3.5 | 21.5 |
| 59 | 10 | 16 | 13 | 6 | 27.1 | 2.5 | 21.4 |
| 61 | 10 | 20 | 15 | 10 | 27.1 | 1.5 | 21.6 |
| 63 | 13 | 16 | 14.5 | 3 | 27 | 2.3 | 21.6 |
| 64 | 10 | 20 | 15 | 10 | 27 | 2.5 | 21.4 |
| 65 | 12 | 14 | 13 | 2 | 27.2 | 2.4 | 21.6 |
| 66 | 14 | 18 | 16 | 4 | 27.3 | 2.2 | 21.8 |
| 69 | 14 | 16 | 15 | 2 | 27.1 | 3.8 | 21.55 |
| 71 | 5 | 8 | 6.5 | 3 | 27 | 5 | 21.2 |
| 72 | 10 | 12 | 11 | 2 | 27.2 | 2.5 | 21.7 |
| 73 | 7 | 8 | 7.5 | 1 | 26.8 | 3 | 21.4 |
| 74 | 12 | 14 | 13 | 2 | 27.15 | 3.4 | 21.5 |

| | | | | | | | |
|---|---|---|---|---|---|---|---|
| 75 | 7 | 9 | 8 | 2 | 27.3 | 3.2 | 21.8 |
| 76 | 10 | 12 | 11 | 2 | 27.3 | 3.6 | 21.8 |
| 77 | 7 | 8 | 7.5 | 1 | 27.3 | 3.8 | 21.8 |
| 80 | 8 | 24 | 16 | 16 | 27.25 | 1.1 | 21.8 |
| 81 | 8 | 30 | 19 | 22 | 27.1 | 2 | 21.7 |
| 82 | 32 | 35 | 33.5 | 3 | 27.2 | 1.3 | 21.75 |
| 84 | 12 | 16 | 14 | 4 | 26.9 | 4.5 | 21.3 |
| 91 | 18 | 21 | 19.5 | 3 | 26.4 | 2 | 21 |
| 92 | 20 | 24 | 22 | 4 | 26.4 | 2 | 21 |
| 93 | 16 | 22 | 19 | 6 | 27 | 2 | 21 |
| 99 | 21 | 24 | 22.5 | 3 | 26.75 | 1.8 | 21.25 |
| 100 | 20 | 24 | 22 | 4 | 27 | 1.8 | 21.5 |
| 104 | 23 | 24 | 23.5 | 1 | 26.4 | 1.6 | 21.2 |
| 106 | 18 | 22 | 20 | 4 | 26.4 | 2 | 21.5 |
| 107 | 20 | 30 | 25 | 10 | 27 | 1 | 21.8 |
| 108 | 20 | 25 | 22.5 | 5 | 26.8 | 1.5 | 21.8 |
| 110 | 20 | 25 | 22.5 | 5 | 26.4 | 1.8 | 21 |
| 111 | 24 | 27 | 25.5 | 3 | 27 | 1.6 | 21.5 |
| 112 | 18 | 22 | 20 | 4 | 26.5 | 2 | 21.25 |
| 113 | 12 | 18 | 15 | 6 | 26.2 | 2.5 | 21 |
| 114 | 14 | 22 | 18 | 8 | 26.4 | 2.5 | 21 |
| 115 | 14 | 20 | 17 | 6 | 27 | 1.6 | 21.25 |
| 116 | 16 | 18 | 17 | 2 | 27.2 | 1.5 | 21.6 |
| 117 | 15 | 17 | 16 | 2 | 26.8 | 2.2 | 21.5 |
| 118 | 12 | 22 | 17 | 10 | 26.8 | 2.2 | 21.25 |
| 120 | 16 | 25 | 20.5 | 9 | 27 | 2 | 21.5 |
| 121 | 10 | 20 | 15 | 10 | 26.25 | 2.7 | 21 |
| 122 | 17 | 23 | 20 | 6 | 27 | 1.8 | 21.4 |
| 123 | 18 | 22 | 20 | 4 | 26.6 | 2.5 | 21.2 |
| 124 | 20 | 24 | 22 | 4 | 26.8 | 2 | 21.4 |
| 125 | 16 | 22 | 19 | 6 | 26.8 | 2.2 | 21.4 |
| 126 | 22 | 30 | 26 | 8 | 27.2 | 1.5 | 21.9 |
| 127 | 16 | 20 | 18 | 4 | 26.85 | 2 | 21.5 |
| 128 | 20 | 24 | 22 | 4 | 26.6 | 2.8 | 21.3 |
| 129 | 15 | 22 | 18.5 | 7 | 27 | 2.8 | 21.7 |
| 130 | 24 | 32 | 28 | 8 | 27.2 | 1.2 | 21.6 |
| 131 | 28 | 32 | 30 | 4 | 27.1 | 1.8 | 21.6 |
| 133 | 24 | 28 | 26 | 4 | 27.2 | 1.6 | 21.7 |
| 134 | 14 | 26 | 20 | 12 | 27 | 2 | 21.45 |
| 135 | 20 | 28 | 24 | 8 | 27.1 | 1.6 | 21.7 |
| 136 | 22 | 26 | 24 | 4 | 27.2 | 1.2 | 21.7 |
| 137 | 23 | 26 | 24.5 | 3 | 27.2 | 2 | 21.7 |
| 139 | 16 | 20 | 18 | 4 | 27.4 | 1.5 | 21.85 |
| 140 | 8 | 16 | 12 | 8 | 27.1 | 2.7 | 21.6 |
| 141 | 16 | 22 | 19 | 6 | 27.3 | 1.4 | 21.85 |
| 142 | 18 | 20 | 19 | 2 | 27 | 4.2 | 21.4 |
| 143 | 14 | 18 | 16 | 4 | 26.9 | 6 | 21.1 |
| 144 | 18 | 20 | 19 | 2 | 27.1 | 3.6 | 21.5 |
| 145 | 14 | 22 | 18 | 8 | 26.9 | 3.4 | 21.4 |
| 147 | 22 | 24 | 23 | 2 | 27.32 | 2.4 | 21.8 |
| 148 | 18 | 20 | 19 | 2 | 27.1 | 4.3 | 21.45 |
| 149 | 18 | 24 | 21 | 6 | 27.15 | 1.8 | 21.7 |
| 151 | 23 | 30 | 26.5 | 7 | 26.92 | 2.2 | 21.54 |
| 152 | 15 | 38 | 26.5 | 23 | 27.3 | 1.6 | 21.7 |
| 153 | 10 | 26 | 18 | 16 | 27.3 | 1.6 | 21.8 |
| | | | | | | | |
| mean | 14.32 | 25.45 | 20.04 | 11.52 | 26.99 | 2.12 | 21.54 |

Table 4.3: Mixed layer C, White Sea cruise 2000

| ST_NUMBER | upper_layer[m] | lower_layer[m] | middle_layer | thickness | salinity | Temperature | density |
|---|---|---|---|---|---|---|---|
| 1.1 | 25 | 40 | 32.5 | 15 | 27.4 | 0.5 | 22 |
| 4 | 28 | 32 | 30 | 4 | 27.4 | 0.6 | 22 |
| 5 | 14 | 18 | 16 | 4 | 27.6 | 0.5 | 22.2 |
| 6 | 28 | 35 | 31.5 | 7 | 27.6 | -0.1 | 22.1 |
| 7 | 16 | 24 | 20 | 8 | 27.7 | 0.5 | 22.05 |
| 8 | 12 | 26 | 19 | 14 | 27.7 | 0.6 | 22.2 |
| 9 | 12 | 25 | 18.5 | 13 | 27.6 | 0.5 | 22 |
| 10 | 10 | 25 | 17.5 | 15 | 27.8 | 0.2 | 22.2 |
| 11 | 16 | 24 | 20 | 8 | 27.5 | 0.5 | 22.1 |
| 12 | 20 | 32 | 26 | 12 | 27.3 | 0.4 | 21.9 |
| 13 | 16 | 40 | 28 | 24 | 27.5 | 0.3 | 22 |
| 14 | 18 | 32 | 25 | 14 | 27.55 | 0.5 | 22.05 |
| 15.1 | 16 | 45 | 30.5 | 29 | 27.4 | 0.2 | 21.9 |
| 16 | 18 | 28 | 23 | 10 | 27.5 | 0.5 | 22 |
| 17 | 16 | 30 | 23 | 14 | 27.5 | 0.5 | 22 |
| 18 | 8 | 60 | 34 | 52 | 27.3 | 0.5 | 21.9 |
| 36 | 20 | 50 | 35 | 30 | 27.3 | 0.8 | 21.75 |
| 37 | 32 | 60 | 46 | 28 | 27.3 | 0.5 | 21.9 |
| 38 | 24 | 65 | 44.5 | 41 | 27.1 | 0.8 | 21.65 |
| 39 | 24 | 55 | 39.5 | 31 | 27.1 | 0.8 | 21.7 |
| 40 | 22 | 32 | 27 | 10 | 27.6 | 0 | 22 |
| 42 | 32 | 45 | 38.5 | 13 | 27.2 | 0.5 | 21.75 |
| 43 | 34 | 50 | 42 | 16 | 27.3 | 0.5 | 21.8 |
| 47 | 6 | 16 | 11 | 10 | 27.4 | 1 | 22 |
| 48 | 14 | 45 | 29.5 | 31 | 27.4 | 0.7 | 22 |
| 49 | 32 | 55 | 43.5 | 23 | 27.5 | 0.3 | 22 |
| 50 | 20 | 36 | 28 | 16 | 27.5 | 0.5 | 22 |
| 51 | 18 | 32 | 25 | 14 | 27.5 | 0 | 22 |
| 52 | 24 | 50 | 37 | 26 | 27.3 | 0.4 | 21.9 |
| 54 | 24 | 60 | 42 | 36 | 27.4 | 0.2 | 22 |
| 55 | 22 | 50 | 36 | 28 | 27.5 | 0 | 22 |
| 56 | 16 | 40 | 28 | 24 | 27.35 | 0 | 22 |
| 57 | 15 | 40 | 27.5 | 25 | 27.5 | 0 | 22 |
| 58 | 24 | 40 | 32 | 16 | 27.5 | 0.5 | 22 |
| 59 | 18 | 48 | 33 | 30 | 27.45 | 0.2 | 22 |
| 60 | 12 | 32 | 22 | 20 | 27.4 | 0.4 | 22 |
| 61 | 20 | 50 | 35 | 30 | 27.35 | 0.5 | 21.9 |
| 62 | 10 | 50 | 30 | 40 | 27.5 | 0.5 | 22 |
| 63 | 18 | 32 | 25 | 14 | 27.6 | 0 | 22.2 |
| 64 | 22 | 28 | 25 | 6 | 27.7 | 0.5 | 22.2 |
| 65 | 16 | 40 | 28 | 24 | 27.7 | 0.2 | 22.2 |
| 66 | 20 | 40 | 30 | 20 | 27.5 | 0.2 | 22 |
| 67 | 12 | 30 | 21 | 18 | 27.4 | 0.3 | 22 |
| 68 | 10 | 36 | 23 | 26 | 27.4 | 0.5 | 22 |
| 69 | 20 | 32 | 26 | 12 | 27.6 | 0.3 | 22.1 |
| 70 | 14 | 32 | 23 | 18 | 27.55 | 0.5 | 22 |
| 71 | 12 | 32 | 22 | 20 | 27.5 | 0.5 | 22 |
| 72 | 18 | 25 | 21.5 | 7 | 27.5 | 0.5 | 22 |
| 73 | 10 | 36 | 23 | 26 | 27.4 | 0.4 | 22 |
| 74 | 18 | 24 | 21 | 6 | 27.6 | 0.3 | 22.1 |
| 75 | 16 | 25 | 20.5 | 9 | 27.55 | 0.5 | 22 |
| 76 | 18 | 30 | 24 | 12 | 27.7 | 0.5 | 22.2 |
| 77 | 11 | 25 | 18 | 14 | 27.5 | 0.5 | 22.1 |
| 78 | 16 | 22 | 19 | 6 | 27.7 | 0.6 | 22.1 |
| 79 | 16 | 24 | 20 | 8 | 27.6 | 0.6 | 22.1 |
| 80 | 24 | 44 | 34 | 20 | 27.5 | 0.4 | 22 |
| 81 | 30 | 48 | 39 | 18 | 27.5 | 0.5 | 22 |
| 82 | 38 | 45 | 41.5 | 7 | 27.4 | 0.8 | 21.8 |
| 83 | 16 | 40 | 28 | 24 | 27.5 | 0.5 | 22.1 |

| | | | | | | | |
|---|---|---|---|---|---|---|---|
| 84 | 20 | 36 | 28 | 16 | 27.5 | 0.5 | 22 |
| 91.3 | 23 | 30 | 26.5 | 7 | 27.6 | 0.3 | 22 |
| 92 | 24 | 28 | 26 | 4 | 27.6 | 0.5 | 22 |
| 99 | 27 | 30 | 28.5 | 3 | 27.5 | 0.9 | 22 |
| 110 | 28 | 32 | 30 | 4 | 27.4 | 0.8 | 21.9 |
| 112 | 14 | 30 | 22 | 16 | 27.3 | 1 | 21.9 |
| 114 | 24 | 50 | 37 | 26 | 27.6 | 0.5 | 22 |
| 115 | 22 | 36 | 29 | 14 | 27.5 | 0.5 | 22 |
| 116 | 22 | 32 | 27 | 10 | 27.6 | 0.8 | 22 |
| 117 | 26 | 30 | 28 | 4 | 27.4 | 1.25 | 21.9 |
| 118 | 24 | 50 | 37 | 26 | 27.6 | 0.5 | 22 |
| 119 | 27 | 50 | 38.5 | 23 | 27.6 | 0.5 | 22 |
| 122 | 33 | 50 | 41.5 | 17 | 27.4 | 0.6 | 22 |
| 123 | 25 | 60 | 42.5 | 35 | 27.75 | 0.5 | 22.1 |
| 124 | 26 | 45 | 35.5 | 19 | 27.6 | 0.5 | 22.1 |
| 125 | 27 | 55 | 41 | 28 | 27.7 | 0.3 | 22.1 |
| 126 | 32 | 44 | 38 | 12 | 27.7 | 0.2 | 22.1 |
| 127 | 30 | 40 | 35 | 10 | 27.5 | 0.6 | 22 |
| 129 | 26 | 48 | 37 | 22 | 27.6 | 0.8 | 21.9 |
| 130 | 33 | 42 | 37.5 | 9 | 27.4 | 0.6 | 21.95 |
| 131 | 34 | 48 | 41 | 14 | 27.6 | 0.5 | 22.1 |
| 132 | 30 | 40 | 35 | 10 | 27.4 | 0.5 | 22 |
| 133 | 30 | 42 | 36 | 12 | 27.55 | 0.5 | 21.9 |
| 134 | 28 | 40 | 34 | 12 | 27.4 | 1 | 21.9 |
| 135 | 32 | 56 | 44 | 24 | 27.5 | 0.5 | 22 |
| 136 | 33 | 40 | 36.5 | 7 | 27.5 | 0.7 | 22 |
| 137 | 26 | 36 | 31 | 10 | 27.5 | 0.4 | 22.1 |
| 138 | 20 | 28 | 24 | 8 | 27.5 | 0.5 | 22.1 |
| 139 | 24 | 32 | 28 | 8 | 27.6 | 0.5 | 22 |
| 140 | 18 | 30 | 24 | 12 | 27.55 | 0.5 | 22 |
| 141 | 24 | 32 | 28 | 8 | 27.5 | 0.6 | 22 |
| 142 | 20 | 30 | 25 | 10 | 27.55 | 0.3 | 22 |
| 143 | 22 | 32 | 27 | 10 | 27.5 | 0.5 | 22 |
| 144 | 24 | 34 | 29 | 10 | 27.5 | 0.5 | 22 |
| 145 | 26 | 40 | 33 | 14 | 27.5 | 0.5 | 22 |
| 147 | 25 | 40 | 32.5 | 15 | 27.44 | 0.5 | 22 |
| 148 | 28 | 48 | 38 | 20 | 27.5 | 0.5 | 22 |
| 149 | 30 | 48 | 39 | 18 | 27.4 | 0.4 | 22 |
| 151 | 42 | 45 | 43.5 | 3 | 27.5 | 0.5 | 22 |
| 152 | 42 | 50 | 46 | 8 | 27.4 | 0.5 | 22 |
| 153 | 32 | 42 | 37 | 10 | 27.5 | 0.5 | 22 |
| | | | | | | | |
| mean | 22.14 | 38.58 | 30.36 | 16.44 | 27.4944 | 0.4795 | 22.002 |

Table 4.4: Mixed layer D, White Sea cruise 2000

| ST_NUMBER | upper_layer[m] | lower_layer[m] | middle_layer | thickness | salinity | Temperature | density |
|---|---|---|---|---|---|---|---|
| 1.1 | 60 | 80 | 70 | 20 | 28.4 | -0.8 | 22.8 |
| 4 | 60 | 80 | 70 | 20 | 28.3 | -0.8 | 22.8 |
| 5 | 30 | 50 | 40 | 20 | 28 | -0.6 | 22.5 |
| 6 | 38 | 42 | 40 | 4 | 27.9 | -0.5 | 22.4 |
| 7 | 50 | 60 | 55 | 10 | 28.3 | -0.8 | 22.7 |
| 8 | 30 | 45 | 37.5 | 15 | 28.2 | -0.7 | 22.7 |
| 9 | 40 | 50 | 45 | 10 | 28.3 | -0.8 | 22.8 |
| 10 | 50 | 60 | 55 | 10 | 28.4 | -0.8 | 22.8 |
| 11 | 40 | 52 | 46 | 12 | 28.4 | -0.8 | 22.8 |
| 12 | 45 | 65 | 55 | 20 | 28.3 | -0.7 | 22.7 |
| 13 | 52 | 64 | 58 | 12 | 28.2 | -0.6 | 22.6 |
| 14 | 40 | 60 | 50 | 20 | 28.1 | -0.6 | 22.5 |
| 15.1 | 70 | 80 | 75 | 10 | 28.4 | -0.8 | 22.8 |
| 16 | 60 | 75 | 67.5 | 15 | 28.1 | -0.5 | 22.6 |
| 50 | 50 | 60 | 55 | 10 | 28.1 | -0.5 | 22.5 |
| 59 | 60 | 64 | 62 | 4 | 28.3 | -0.6 | 22.7 |
| 64 | 40 | 52 | 46 | 12 | 28.1 | -0.6 | 22.5 |
| 65 | 55 | 70 | 62.5 | 15 | 28.5 | -0.6 | 22.85 |
| 66 | 60 | 70 | 65 | 10 | 28.5 | -0.6 | 22.8 |
| 67 | 40 | 55 | 47.5 | 15 | 27.9 | -0.5 | 22.4 |
| 68 | 44 | 50 | 47 | 6 | 27.8 | -0.4 | 22.4 |
| 69 | 45 | 60 | 52.5 | 15 | 28.3 | -0.6 | 22.7 |
| 70 | 48 | 60 | 54 | 12 | 28.3 | -0.7 | 22.7 |
| 71 | 36 | 45 | 40.5 | 9 | 27.9 | -0.5 | 22.4 |
| 72 | 50 | 65 | 57.5 | 15 | 28.2 | -0.6 | 22.8 |
| 73 | 56 | 64 | 60 | 8 | 28.3 | -0.6 | 22.7 |
| 74 | 32 | 45 | 38.5 | 13 | 28.2 | -0.5 | 22.75 |
| 75 | 45 | 52 | 48.5 | 7 | 28.1 | -0.5 | 22.6 |
| 76 | 40 | 50 | 45 | 10 | 28.2 | -0.6 | 22.6 |
| 77 | 32 | 42 | 37 | 10 | 28.3 | -0.7 | 22.7 |
| 78 | 30 | 40 | 35 | 10 | 28.3 | -0.5 | 22.6 |
| 79 | 36 | 45 | 40.5 | 9 | 28 | -0.5 | 22.4 |
| 80 | 48 | 56 | 52 | 8 | 28 | -0.5 | 22.4 |
| 81 | 48 | 70 | 59 | 22 | 28.4 | -0.8 | 22.8 |
| 83 | 50 | 60 | 55 | 10 | 28.2 | -0.6 | 22.6 |
| 84 | 44 | 56 | 50 | 12 | 28 | -0.5 | 22.5 |
| 92 | 30 | 60 | 45 | 30 | 28.2 | -0.6 | 22.5 |
| 126 | 62 | 80 | 71 | 18 | 28.2 | -0.5 | 22.6 |
| 130 | 60 | 80 | 70 | 20 | 28.2 | -0.6 | 22.6 |
| 131 | 60 | 80 | 70 | 20 | 28.2 | -0.6 | 22.4 |
| 132 | 60 | 75 | 67.5 | 15 | 28.2 | -0.6 | 22.6 |
| 133 | 60 | 80 | 70 | 20 | 28.2 | -0.6 | 22.65 |
| 134 | 60 | 80 | 70 | 20 | 28.2 | -0.6 | 22.6 |
| 135 | 66 | 80 | 73 | 14 | 28.2 | -0.6 | 22.8 |
| 137 | 48 | 70 | 59 | 22 | 28.15 | -0.6 | 22.8 |
| 138 | 48 | 60 | 54 | 12 | 28.2 | -0.7 | 22.8 |
| 139 | 60 | 75 | 67.5 | 15 | 28.4 | -0.8 | 22.8 |
| 140 | 40 | 60 | 50 | 20 | 28.1 | -0.6 | 22.5 |
| 141 | 60 | 74 | 67 | 14 | 28.4 | -0.8 | 22.8 |
| 142 | 62 | 75 | 68.5 | 13 | 28.35 | -0.8 | 22.7 |
| 143 | 56 | 76 | 66 | 20 | 28.2 | -0.6 | 22.6 |
| 144 | 64 | 80 | 72 | 16 | 28.2 | -0.6 | 22.6 |
| 145 | 48 | 74 | 61 | 26 | 28.2 | -0.7 | 22.7 |
| 148 | 56 | 62 | 59 | 6 | 27.9 | -0.5 | 22.3 |
| 149 | 50 | 60 | 55 | 10 | 27.8 | -0.4 | 22.3 |
| 153 | 54 | 60 | 57 | 6 | 28.2 | -0.8 | 22.7 |
| | | | | | | | |
| mean | 49.25 | 63.13 | 56.19 | 13.88 | 28.19 | -0.62 | 22.63 |

Table 4.5: Mixed layer E, White Sea cruise 2000

| ST_NUMBER | upper_layer[m] | lower_layer[m] | middle_layer | thickness | salinity | Temperature | density |
|---|---|---|---|---|---|---|---|
| 1.1 | 90 | 110 | 100 | 20 | 28.6 | -1 | 23 |
| 4 | 80 | 100 | 90 | 20 | 28.7 | -1.15 | 23 |
| 5 | 60 | 80 | 70 | 20 | 28.5 | -1.15 | 22.9 |
| 6 | 50 | 64 | 57 | 14 | 28.4 | -0.9 | 22.7 |
| 7 | 85 | 90 | 87.5 | 5 | 28.7 | -1.15 | 23.05 |
| 8 | 65 | 90 | 77.5 | 25 | 28.7 | -1.15 | 23.05 |
| 9 | 60 | 70 | 65 | 10 | 28.7 | -1.15 | 23.05 |
| 10 | 70 | 80 | 75 | 10 | 28.7 | -1.15 | 23.05 |
| 11 | 50 | 65 | 57.5 | 15 | 28.7 | -1.15 | 23.05 |
| 12 | 70 | 80 | 75 | 10 | 28.7 | -1 | 23 |
| 13 | 65 | 92 | 78.5 | 27 | 28.6 | -1 | 22.9 |
| 14 | 70 | 90 | 80 | 20 | 28.55 | -0.9 | 22.9 |
| 67 | 68 | 80 | 74 | 12 | 28.6 | -0.8 | 22.95 |
| 68 | 80 | 85 | 82.5 | 5 | 28.7 | -0.9 | 23 |
| 69 | 68 | 90 | 79 | 22 | 28.7 | -1 | 23 |
| 70 | 65 | 85 | 75 | 20 | 28.6 | -1 | 23 |
| 71 | 60 | 70 | 65 | 10 | 28.5 | -0.8 | 22.9 |
| 72 | 68 | 75 | 71.5 | 7 | 28.6 | -0.9 | 23 |
| 74 | 60 | 100 | 80 | 40 | 28.6 | -1 | 23 |
| 75 | 65 | 90 | 77.5 | 25 | 28.6 | -1 | 22.9 |
| 76 | 65 | 80 | 72.5 | 15 | 28.6 | -1 | 23 |
| 77 | 60 | 70 | 65 | 10 | 28.6 | -1 | 23 |
| 78 | 60 | 80 | 70 | 20 | 28.7 | -1 | 23 |
| 79 | 65 | 80 | 72.5 | 15 | 28.6 | -1 | 23 |
| 80 | 66 | 95 | 80.5 | 29 | 28.6 | -1 | 23 |
| 81 | 80 | 88 | 84 | 8 | 28.7 | -1 | 23 |
| 83 | 85 | 100 | 92.5 | 15 | 28.8 | -1 | 23.1 |
| 126 | 102 | 118 | 110 | 16 | 28.6 | -0.9 | 23 |
| 130 | 90 | 110 | 100 | 20 | 28.8 | -1.15 | 23.05 |
| 131 | 94 | 110 | 102 | 16 | 28.9 | -1.15 | 23.05 |
| 132 | 90 | 100 | 95 | 10 | 28.8 | -1 | 23 |
| 133 | 82 | 112 | 97 | 30 | 28.6 | -1 | 23 |
| 134 | 100 | 106 | 103 | 6 | 28.8 | -1.15 | 23 |
| 137 | 80 | 100 | 90 | 20 | 28.5 | -1 | 22.95 |
| 138 | 80 | 92 | 86 | 12 | 28.8 | -1.15 | 23 |
| 139 | 90 | 106 | 98 | 16 | 28.8 | -1.15 | 23.05 |
| 140 | 66 | 82 | 74 | 16 | 28.7 | -1 | 22.95 |
| 141 | 84 | 108 | 96 | 24 | 28.7 | -1.15 | 23.05 |
| 142 | 95 | 110 | 102.5 | 15 | 28.7 | -1.15 | 23.05 |
| 143 | 80 | 90 | 85 | 10 | 28.5 | -1 | 22.9 |
| 144 | 92 | 112 | 102 | 20 | 28.85 | -1.2 | 23.2 |
| 149 | 84 | 108 | 96 | 24 | 28.8 | -1.15 | 23.1 |
| 152 | 66 | 76 | 71 | 10 | 28.6 | -1 | 23 |
| 153 | 72 | 82 | 77 | 10 | 28.7 | -1.15 | 23 |
| | | | | | | | |
| mean | 74.48 | 90.93 | 82.70 | 16.45 | 28.66 | -1.04 | 23.00 |

# Appendix C: Mixed layer identification

## C.1 Tables of thermohaline index of the mixed layers F, C, D, E – survey 2001.

Table 5.1: Mixed layer F, White Sea cruise 2001

| stations | upper_layer[m] | lower_layer[m] | middle_layer | thickness | salinity | Temperature | density |
|---|---|---|---|---|---|---|---|
| | | | | | | | |
| 2 | 6 | 20 | 13 | 14 | 25.5 | 0.1 | 20.5 |
| 3 | 8 | 14 | 11 | 6 | 24.8 | 0.6 | 19.9 |
| 11 | 7 | 10 | 8.5 | 3 | 26.1 | 1.6 | 20.8 |
| 11a | 9 | 12 | 10.5 | 3 | 26 | 1.6 | 20.7 |
| 13 | 3 | 5 | 4 | 2 | 25.3 | 1.7 | 20.6 |
| 14 | 11 | 15 | 13 | 4 | 25.5 | 1.8 | 20.4 |
| 15 | 6 | 7 | 6.5 | 1 | 23.5 | 2.7 | 19 |
| 16 | 18 | 20 | 19 | 2 | 25 | 1.9 | 19.8 |
| 17 | 10 | 14 | 12 | 4 | 24.2 | 2.6 | 19.5 |
| 19 | 16 | 17 | 16.5 | 1 | 25.2 | 2 | 20.1 |
| 20 | 13 | 15 | 14 | 2 | 25 | 2.2 | 19.9 |
| 21 | 6 | 10 | 8 | 4 | 24.8 | 2 | 19.8 |
| 22 | 10 | 14 | 12 | 4 | 24.9 | 2.1 | 19.9 |
| 23 | 11 | 15 | 13 | 4 | 24.6 | 2.4 | 19.6 |
| 24 | 11 | 18 | 14.5 | 7 | 24.9 | 1.9 | 19.9 |
| 25 | 13 | 18 | 15.5 | 5 | 24.8 | 1.7 | 19.8 |
| 26 | 7 | 10 | 8.5 | 3 | 25.3 | 1.4 | 20.2 |
| 27 | 8 | 12 | 10 | 4 | 25 | 1.7 | 20 |
| 28 | 6 | 14 | 10 | 8 | 24.8 | 0.7 | 19.8 |
| 29 | 4 | 20 | 12 | 16 | 24.8 | 0.5 | 19.8 |
| 30 | 12 | 18 | 15 | 6 | 24.8 | 0.6 | 19.84 |
| 31 | 12 | 18 | 15 | 6 | 24.8 | 0.7 | 19.9 |
| 32 | 10 | 14 | 12 | 4 | 24.5 | 1.4 | 19.6 |
| 33 | 8 | 20 | 14 | 12 | 24.4 | 1.8 | 19.4 |
| 34 | 16 | 20 | 18 | 4 | 24.8 | 0.7 | 19.8 |
| 35 | 8 | 16 | 12 | 8 | 24.5 | 1.2 | 19.6 |
| 36 | 10 | 16 | 13 | 6 | 24.8 | 0.6 | 19.9 |
| 37 | 6 | 10 | 8 | 4 | 24.8 | 0.9 | 19.8 |
| 38 | 10 | 18 | 14 | 8 | 24.8 | 0.6 | 19.8 |
| 39 | 8 | 12 | 10 | 4 | 25.3 | 1 | 20.2 |
| 40 | 6 | 12 | 9 | 6 | 25.2 | 0.7 | 20.2 |
| 41 | 6 | 10 | 8 | 4 | 25.8 | 0.6 | 20.6 |
| 42 | 8 | 12 | 10 | 4 | 25.3 | 0.5 | 20.2 |
| 43 | 8 | 14 | 11 | 6 | 25.3 | 0.3 | 20.2 |
| 44 | 10 | 15 | 12.5 | 5 | 25.9 | 0.2 | 20.8 |
| 45 | 10 | 14 | 12 | 4 | 25.8 | 0.6 | 20.6 |
| 46 | 0 | 5 | 2.5 | 5 | 26 | 1.6 | 20.9 |
| 47 | 8 | 10 | 9 | 2 | 25.2 | 0.9 | 20.1 |
| 48 | 10 | 18 | 14 | 8 | 25.8 | 0.5 | 20.65 |
| 49 | 4 | 8 | 6 | 4 | 25.3 | 1.5 | 20.2 |
| 50 | 3 | 10 | 6.5 | 7 | 25.1 | 0.9 | 20.05 |
| 51 | 8 | 10 | 9 | 2 | 25.3 | 0.9 | 20.2 |
| 52 | 12 | 14 | 13 | 2 | 25.2 | 1.1 | 20.1 |
| 53 | 13 | 16 | 14.5 | 3 | 25.1 | 1 | 20.1 |
| 54 | 8 | 12 | 10 | 4 | 24.8 | 1 | 20 |
| 55 | 10 | 18 | 14 | 8 | 25.6 | 0.2 | 20.5 |
| 56 | 3 | 7 | 5 | 4 | 24.7 | 1.3 | 19.8 |
| | | | | | | | |
| mean | 8.84 | 13.74 | 11.29 | 4.91 | 25.03 | 1.22 | 20.03 |

Table 5.2: Mixed layer C, White Sea cruise 2001

| stations | upper_layer[m] | lower_layer[m] | middle_layer | thickness | salinity | Temperature | density |
|---|---|---|---|---|---|---|---|
| | | | | | | | |
| 2 | 44 | 56 | 50 | 12 | 27.6 | 0.2 | 22.2 |
| 3 | 46 | 56 | 51 | 10 | 27.6 | 0.2 | 22.2 |
| 4 | 46 | 56 | 51 | 10 | 27.8 | 0.2 | 22.2 |
| 11 | 22 | 24 | 23 | 2 | 27.5 | 0.4 | 22.05 |
| 11a | 22 | 24 | 23 | 2 | 27.4 | 0.3 | 22.05 |
| 12 | 40 | 46 | 43 | 6 | 27.85 | -0.2 | 22.45 |
| 13 | 23 | 27 | 25 | 4 | 27.65 | 0.05 | 22.1 |
| 14 | 30 | 32 | 31 | 2 | 27.2 | 0.3 | 21.75 |
| 17 | 23 | 25 | 24 | 2 | 27.5 | 0.15 | 22 |
| 18 | 23 | 45 | 34 | 22 | 27.45 | 0.1 | 22 |
| 19 | 29 | 43 | 36 | 14 | 27.4 | 0.1 | 22 |
| 20 | 30 | 33 | 31.5 | 3 | 27.4 | 0.05 | 22 |
| 21 | 26 | 30 | 28 | 4 | 27.4 | 0 | 22 |
| 22 | 22 | 26 | 24 | 4 | 27.3 | 0 | 21.9 |
| 23 | 22 | 26 | 24 | 4 | 27.3 | 0.15 | 21.85 |
| 24 | 27 | 29 | 28 | 2 | 27.2 | 0 | 21.8 |
| 27 | 22 | 26 | 24 | 4 | 27.5 | -0.05 | 22 |
| 28 | 32 | 38 | 35 | 6 | 27.8 | 0.3 | 22.3 |
| 29 | 38 | 48 | 43 | 10 | 27.8 | 0.2 | 22.4 |
| 30 | 30 | 36 | 33 | 6 | 27.5 | -0.2 | 22.1 |
| 31 | 28 | 38 | 33 | 10 | 27.7 | -0.05 | 22.3 |
| 32 | 28 | 38 | 33 | 10 | 27.7 | -0.05 | 22.3 |
| 34 | 24 | 27 | 25.5 | 3 | 27.5 | 0 | 22.2 |
| 35 | 44 | 51 | 47.5 | 7 | 27.8 | 0.1 | 22.3 |
| 36 | 42 | 46 | 44 | 4 | 27.6 | 0.4 | 22.25 |
| 37 | 50 | 56 | 53 | 6 | 27.6 | 0.4 | 22.4 |
| 38 | 44 | 50 | 47 | 6 | 27.7 | 0.4 | 22.2 |
| 39 | 36 | 46 | 41 | 10 | 27.6 | -0.1 | 22.1 |
| 40 | 26 | 32 | 29 | 6 | 27.6 | -0.1 | 22.2 |
| 41 | 20 | 34 | 27 | 14 | 27.9 | -0.1 | 22.3 |
| 42 | 36 | 44 | 40 | 8 | 27.9 | 0.3 | 22.3 |
| 43 | 42 | 48 | 45 | 6 | 27.9 | 0.2 | 22.4 |
| 44 | 46 | 52 | 49 | 6 | 27.8 | 0 | 22.3 |
| 45 | 36 | 46 | 41 | 10 | 27.8 | 0.4 | 22.4 |
| 46 | 36 | 40 | 38 | 4 | 27.8 | -0.1 | 22.3 |
| 47 | 44 | 52 | 48 | 8 | 27.8 | 0.1 | 22.4 |
| 48 | 47 | 56 | 51.5 | 9 | 27.8 | 0.2 | 22.35 |
| 49 | 34 | 42 | 38 | 8 | 27.75 | 0.5 | 22.3 |
| 50 | 30 | 36 | 33 | 6 | 27.7 | 0 | 22.3 |
| 51 | 27 | 32 | 29.5 | 5 | 27.6 | -0.2 | 22.1 |
| 52 | 34 | 38 | 36 | 4 | 27.8 | 0 | 22.6 |
| 53 | 40 | 50 | 45 | 10 | 27.8 | 0.1 | 22.3 |
| 54 | 44 | 50 | 47 | 6 | 27.8 | 0.3 | 22.35 |
| 55 | 32 | 40 | 36 | 8 | 27.8 | 0.2 | 22.3 |
| 56 | 26 | 28 | 27 | 2 | 27.5 | 0 | 22.2 |
| | | | | | | | |
| mean | 32.64 | 39.38 | 36.01 | 6.74 | 27.63 | 0.10 | 22.20 |

Table 5.3: Mixed layer D, White Sea cruise 2001

| stations | upper_layer[m] | lower_layer[m] | middle_layer | thickness | salinity | Temperature | density |
|---|---|---|---|---|---|---|---|
| | | | | | | | |
| 21 | 62 | 86 | 74 | 24 | 27.9 | -0.45 | 22.4 |
| 22 | 58 | 70 | 64 | 12 | 28.3 | -0.8 | 22.75 |
| 23 | 30 | 40 | 35 | 10 | 27.85 | -0.3 | 22.3 |
| 24 | 35 | 43 | 39 | 8 | 28.4 | -0.8 | 22.8 |
| 25 | 34 | 39 | 36.5 | 5 | 28.2 | -0.6 | 22.6 |
| 26 | 34 | 42 | 38 | 8 | 28.4 | -0.8 | 22.8 |
| 27 | 30 | 40 | 35 | 10 | 28.1 | -0.5 | 22.6 |
| 28 | 52 | 60 | 56 | 8 | 28.5 | -0.8 | 22.8 |
| 29 | 60 | 72 | 66 | 12 | 28.4 | -0.8 | 22.93 |
| 30 | 46 | 54 | 50 | 8 | 28.2 | -0.4 | 22.64 |
| 31 | 40 | 44 | 42 | 4 | 28.3 | -0.3 | 22.6 |
| 32 | 50 | 54 | 52 | 4 | 28.4 | -0.6 | 22.8 |
| 33 | 62 | 90 | 76 | 28 | 28.5 | -0.65 | 22.9 |
| 34 | 48 | 56 | 52 | 8 | 28.3 | -0.5 | 22.7 |
| 35 | 58 | 74 | 66 | 16 | 28.3 | -0.5 | 22.7 |
| 36 | 62 | 72 | 67 | 10 | 28.2 | -0.3 | 22.7 |
| 37 | 60 | 66 | 63 | 6 | 28.2 | -0.3 | 22.6 |
| 38 | 60 | 72 | 66 | 12 | 28.2 | -0.2 | 22.6 |
| 39 | 62 | 72 | 67 | 10 | 28.4 | -0.7 | 22.8 |
| 40 | 48 | 62 | 55 | 14 | 28.3 | -0.7 | 22.8 |
| 41 | 44 | 52 | 48 | 8 | 28.3 | -0.7 | 22.7 |
| 42 | 50 | 56 | 53 | 6 | 28.2 | -0.2 | 22.6 |
| 43 | 56 | 64 | 60 | 8 | 28.3 | -0.7 | 22.8 |
| 44 | 54 | 58 | 56 | 4 | 28.3 | -0.7 | 22.7 |
| 45 | 62 | 66 | 64 | 4 | 28.4 | -0.7 | 22.8 |
| 46 | 48 | 52 | 50 | 4 | 28.1 | -0.7 | 22.6 |
| 47 | 58 | 66 | 62 | 8 | 28.2 | -0.7 | 22.7 |
| 48 | 64 | 68 | 66 | 4 | 28.4 | -0.5 | 22.8 |
| 49 | 50 | 58 | 54 | 8 | 28.2 | -0.5 | 22.7 |
| 50 | 50 | 56 | 53 | 6 | 28.4 | -0.8 | 22.8 |
| 51 | 44 | 52 | 48 | 8 | 28.3 | -0.5 | 22.7 |
| 52 | 46 | 52 | 49 | 6 | 28.4 | -0.8 | 22.8 |
| 53 | 56 | 68 | 62 | 12 | 28.3 | -0.4 | 22.6 |
| 54 | 58 | 68 | 63 | 10 | 28.3 | -0.5 | 22.6 |
| 55 | 52 | 62 | 57 | 10 | 28.3 | -0.45 | 22.7 |
| | | | | | | | |
| mean | 50.94 | 60.17 | 55.56 | 9.23 | 28.28 | -0.57 | 22.70 |

Table 5.4: Mixed layer E, White Sea cruise 2001

| stations | upper_layer[m] | lower_layer[m] | middle_layer | thickness | salinity | Temperature | density |
|---|---|---|---|---|---|---|---|
| | | | | | | | |
| 26 | 56 | 80 | 68 | 24 | 28.6 | -1 | 23 |
| 27 | 58 | 82 | 70 | 24 | 28.7 | -1 | 23 |
| 28 | 80 | 96 | 88 | 16 | 28.6 | -1.2 | 23 |
| 29 | 90 | 100 | 95 | 10 | 28.64 | -1.18 | 23 |
| 30 | 62 | 72 | 67 | 10 | 28.5 | -0.9 | 22.9 |
| 31 | 54 | 70 | 62 | 16 | 28.6 | -1.1 | 23 |
| 32 | 60 | 68 | 64 | 8 | 28.5 | -1 | 22.9 |
| 34 | 80 | 88 | 84 | 8 | 28.7 | -1 | 23 |
| 35 | 82 | 90 | 86 | 8 | 28.6 | -1.05 | 23 |
| 36 | 80 | 102 | 91 | 22 | 28.5 | -1.1 | 22.9 |
| 37 | 82 | 92 | 87 | 10 | 28.6 | -1.1 | 22.9 |
| 38 | 80 | 92 | 86 | 12 | 28.5 | -1 | 22.9 |
| 39 | 86 | 98 | 92 | 12 | 28.6 | -1.15 | 23 |
| 40 | 66 | 90 | 78 | 24 | 28.6 | -1 | 22.9 |
| 41 | 64 | 72 | 68 | 8 | 28.5 | -1.1 | 22.9 |
| 42 | 76 | 84 | 80 | 8 | 28.5 | -1.1 | 22.9 |
| 43 | 80 | 92 | 86 | 12 | 28.6 | -1.2 | 23 |
| 44 | 60 | 74 | 67 | 14 | 28.4 | -1.2 | 22.9 |
| 45 | 78 | 86 | 82 | 8 | 28.6 | -1.1 | 23 |
| 46 | 64 | 76 | 70 | 12 | 28.5 | -1 | 22.8 |
| 47 | 72 | 80 | 76 | 8 | 28.4 | -1 | 22.85 |
| 48 | 80 | 88 | 84 | 8 | 28.6 | -1.1 | 23 |
| 49 | 78 | 84 | 81 | 6 | 28.4 | -1 | 22.9 |
| 50 | 62 | 70 | 66 | 8 | 28.5 | -1 | 22.9 |
| 51 | 68 | 80 | 74 | 12 | 28.6 | -1.1 | 22.9 |
| 52 | 70 | 80 | 75 | 10 | 28.6 | -1 | 23 |
| 53 | 80 | 100 | 90 | 20 | 28.6 | -1.2 | 23 |
| 54 | 86 | 96 | 91 | 10 | 28.6 | -1.15 | 22.95 |
| 55 | 83 | 104 | 93.5 | 21 | 28.6 | -1.2 | 22.9 |
| | | | | | | | |
| mean | 73.00 | 85.72 | 79.36 | 12.72 | 28.56 | -1.08 | 22.94 |

# Appendix D: Profiles of temperature and salinity fluctuations west of the Gorlo Strait - survey 2000

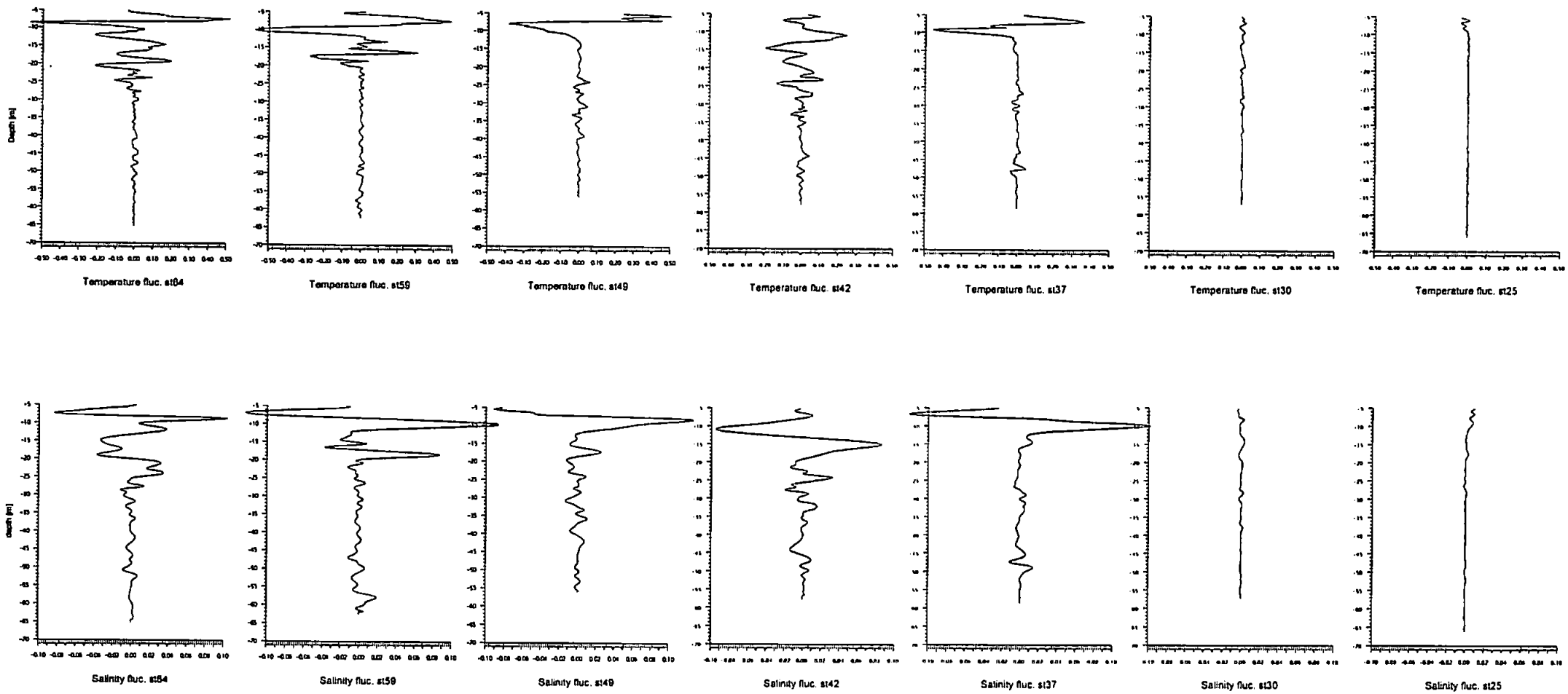


Figure 6.6: Temperature and salinity fluctuations derived at stations of transect A4

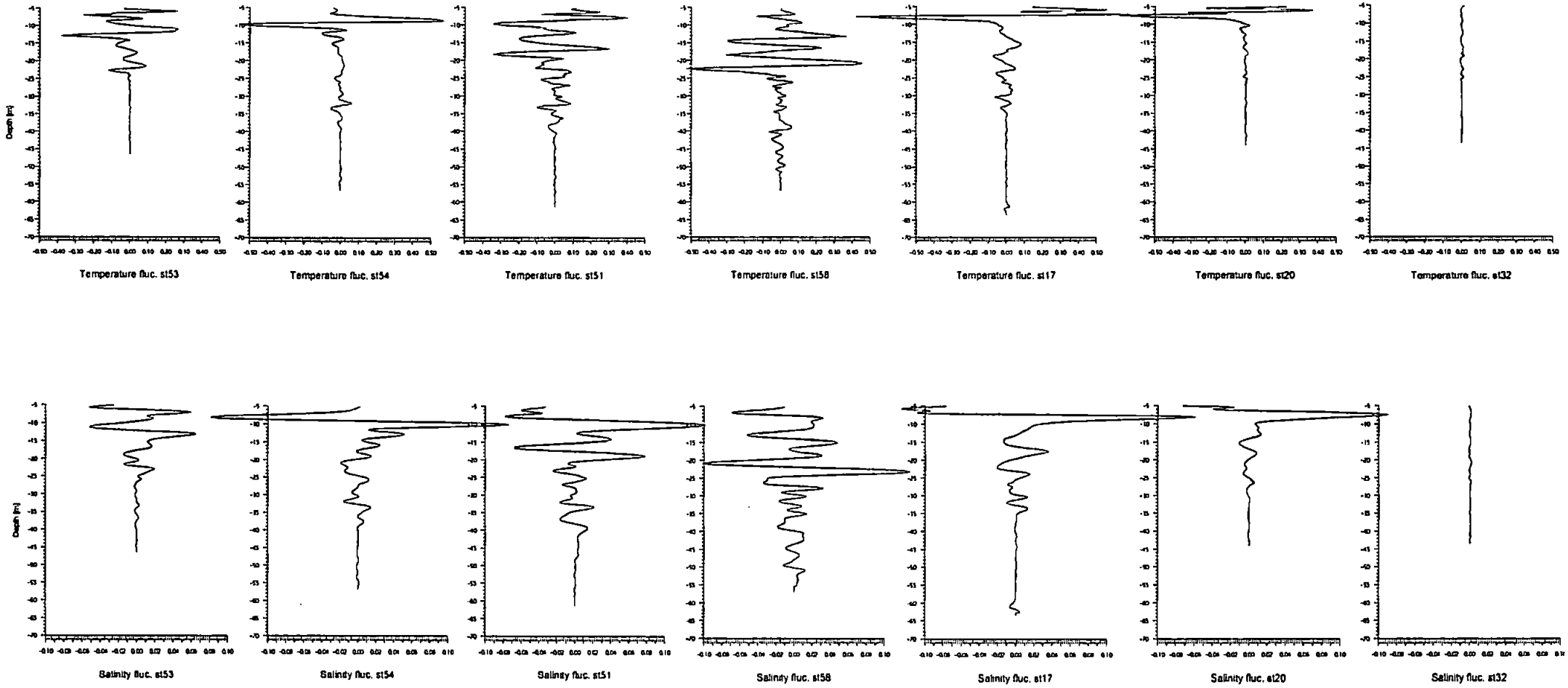


Figure 6.7: Temperature and salinity fluctuations at selected south-western and northern stations

# Appendix E: Panel of SST and SLA maps

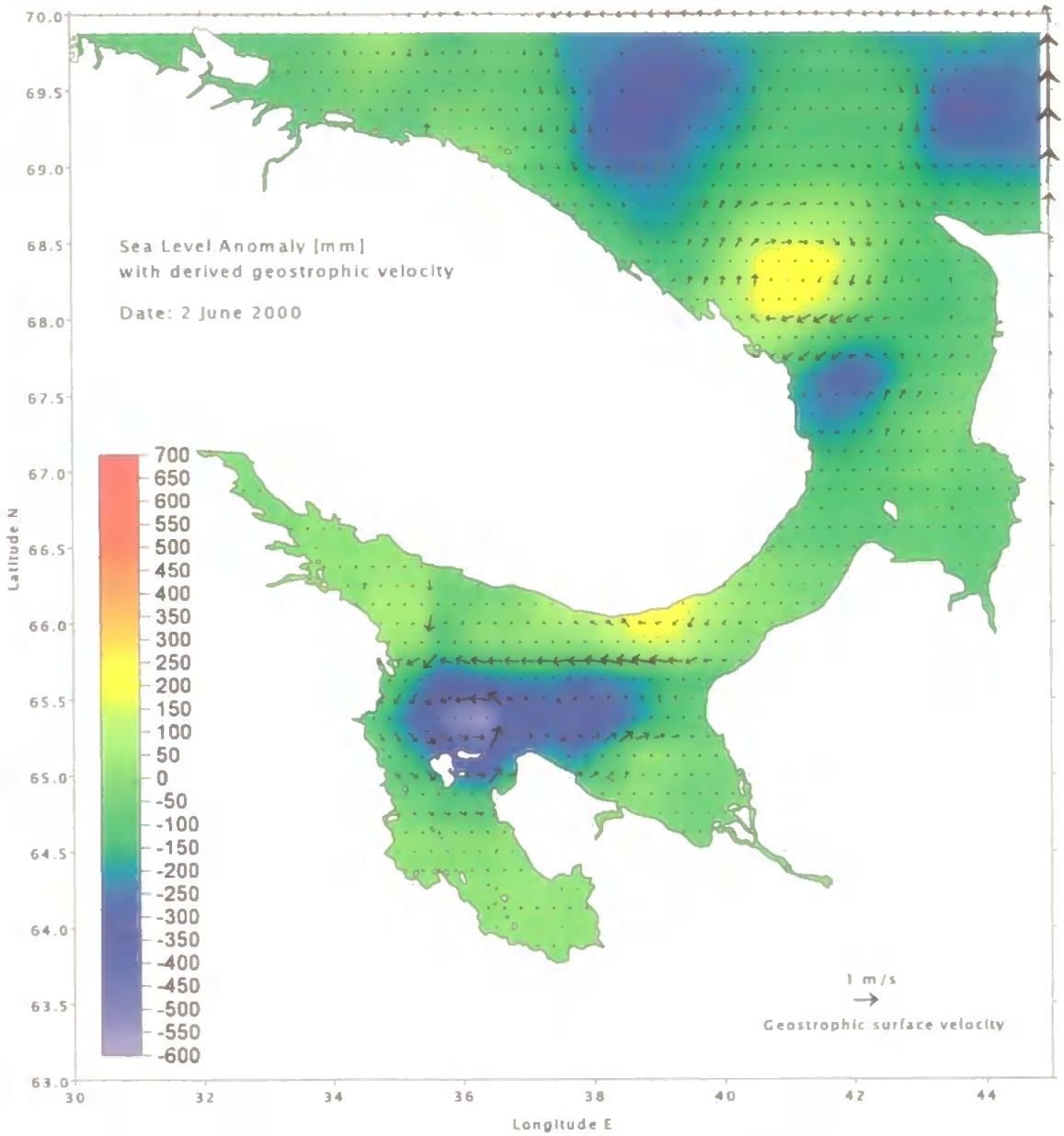


Figure 7.5: SLA map with derived geostrophic surface velocity for 2 June 2000.

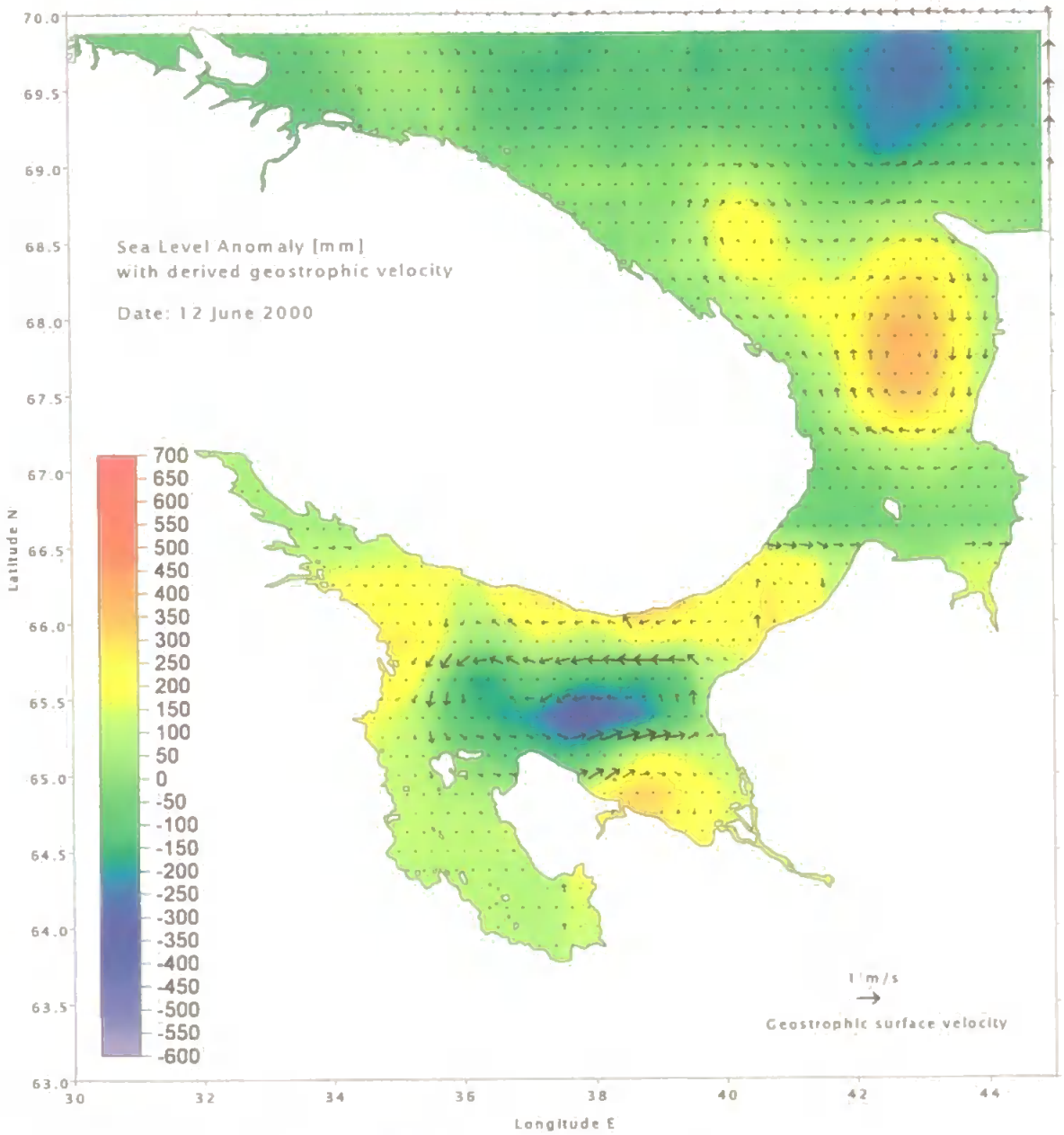


Figure 7.6: SLA map with derived geostrophic surface velocity for 12 June 2000.

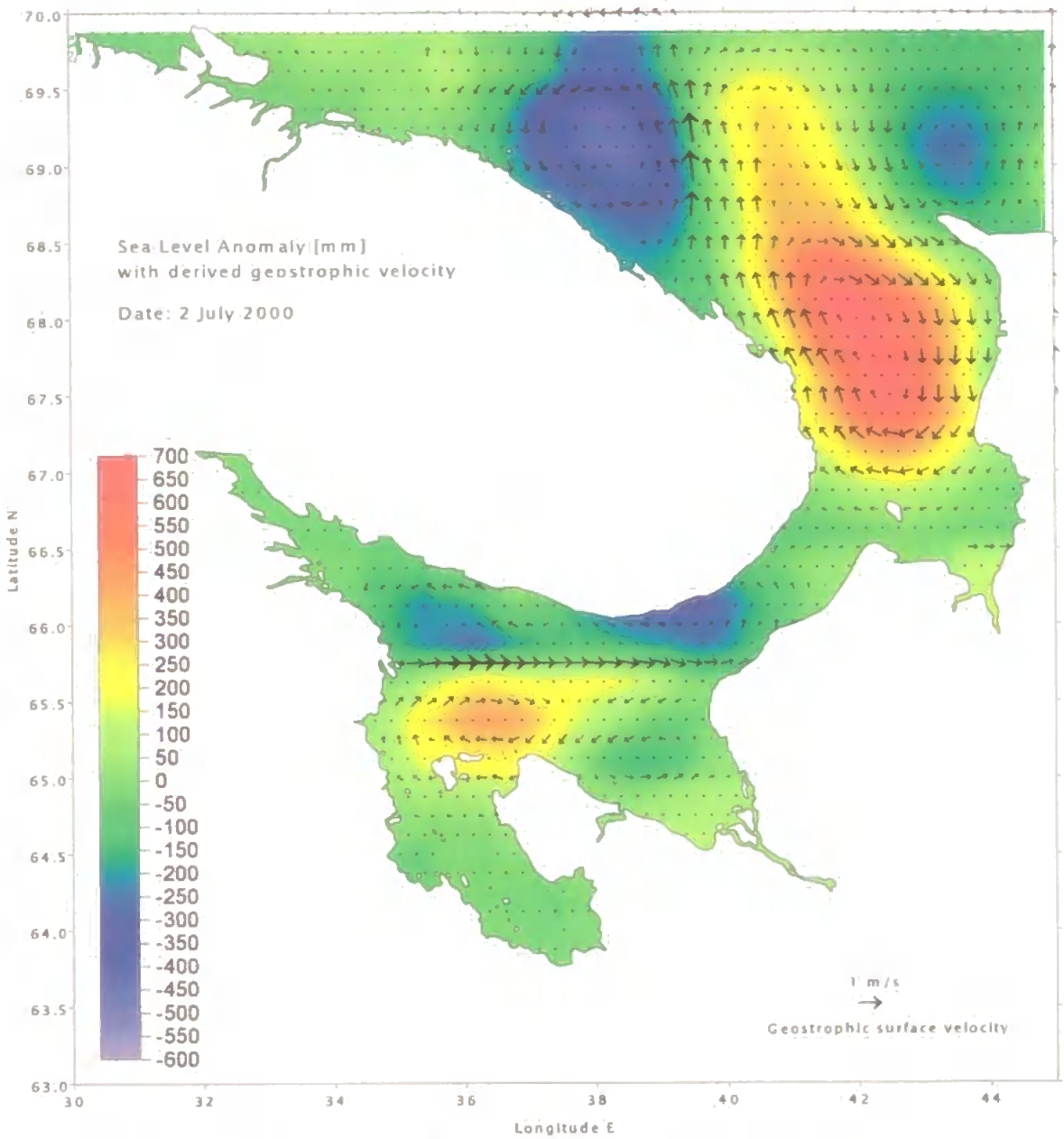


Figure 7.7: SLA map with derived geostrophic surface velocity for 2 July 2000.

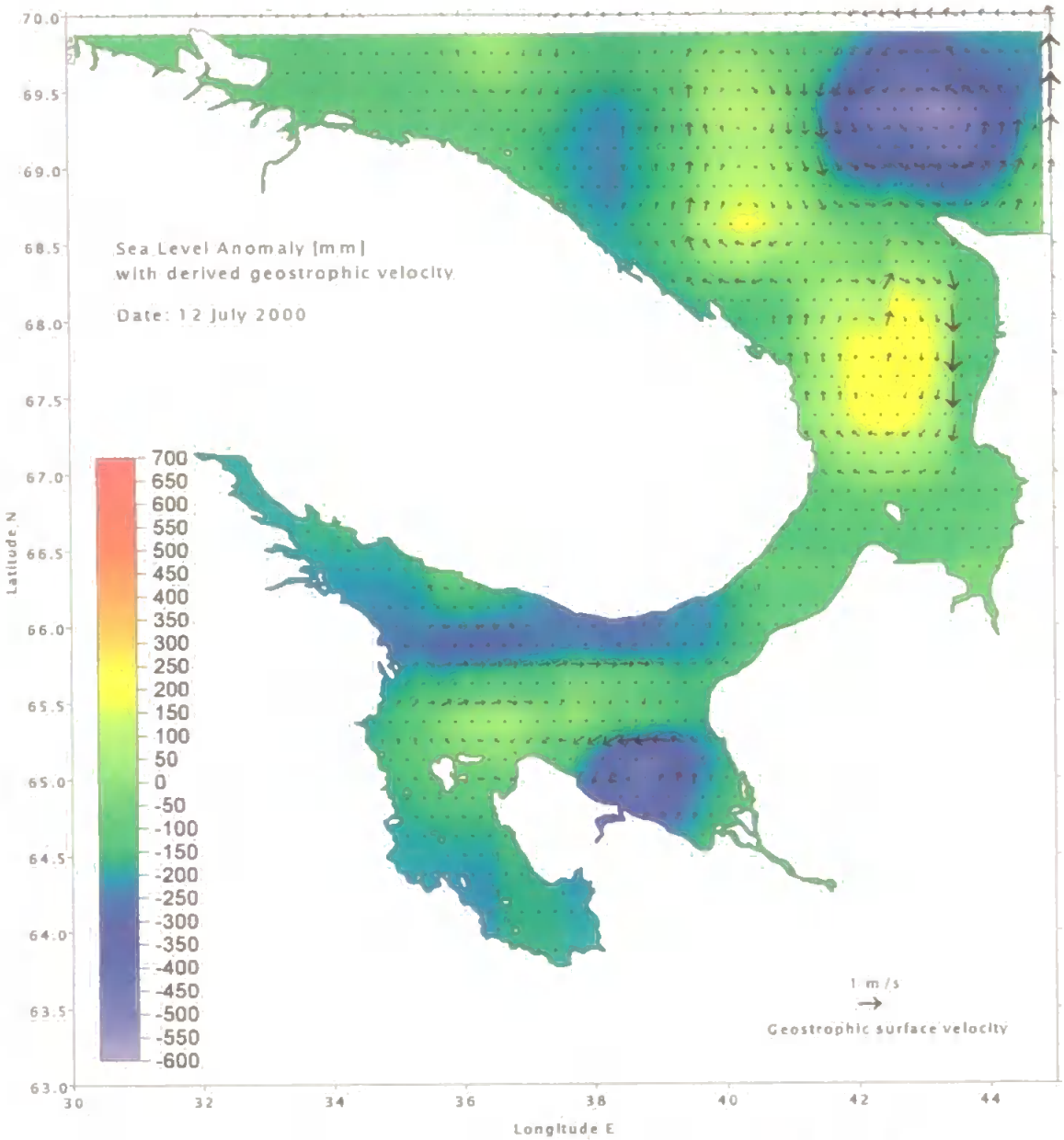


Figure 7.8: SLA map with derived geostrophic surface velocity for 12 July 2000.

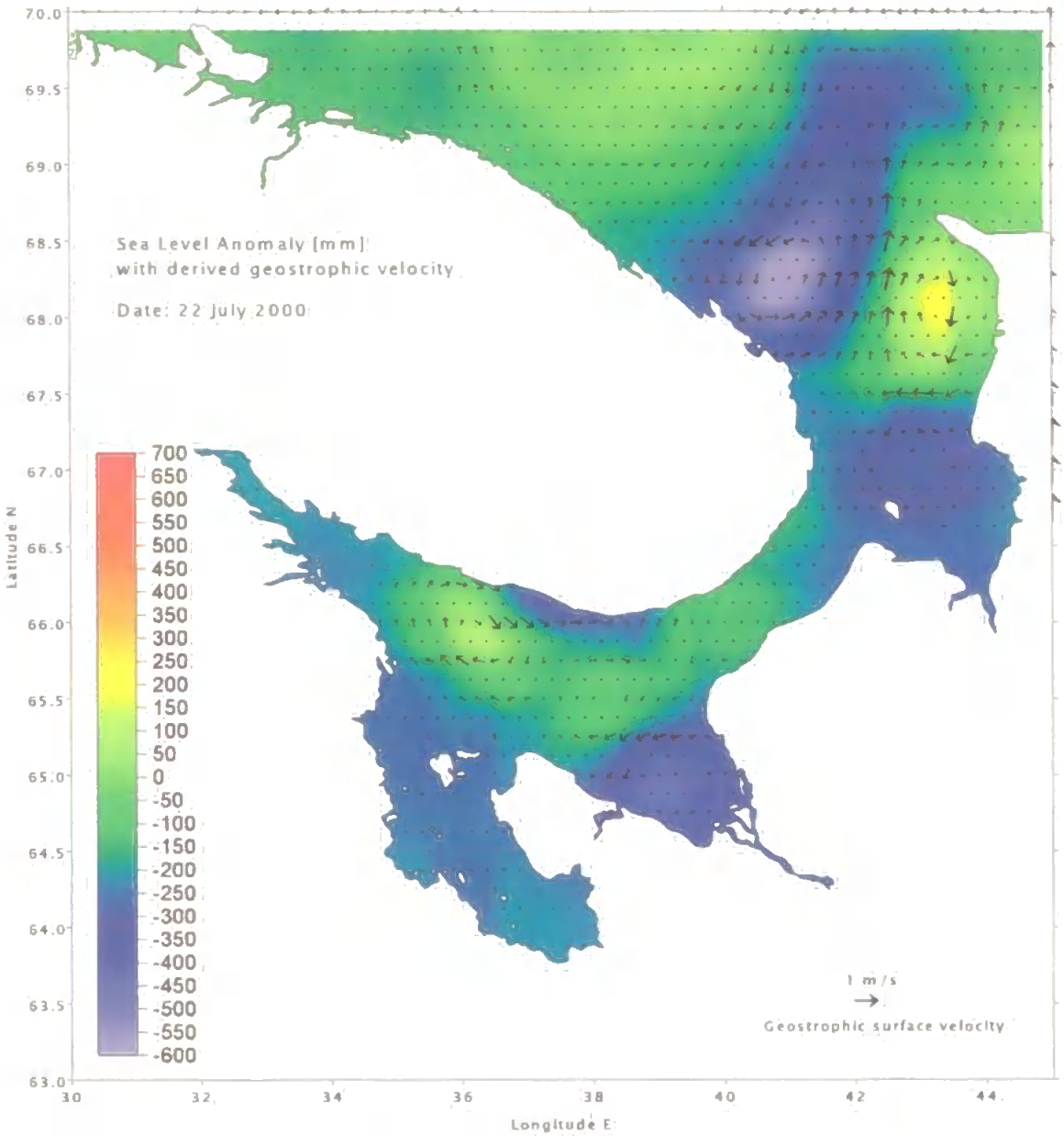


Figure 7.9: SLA map with derived geostrophic surface velocity for 22 July 2000.

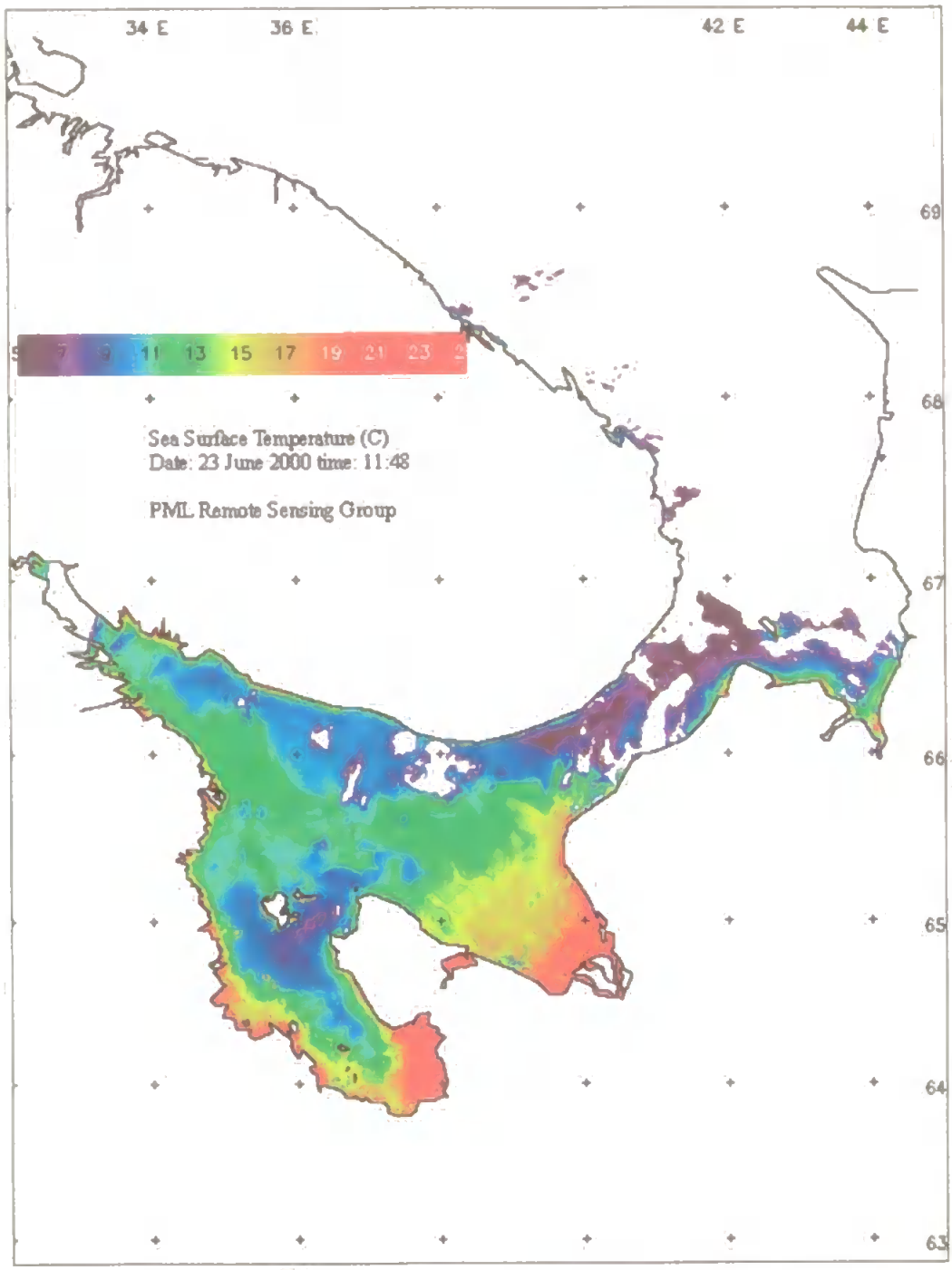


Figure 7.10: SST image taken the 23 June 2000.

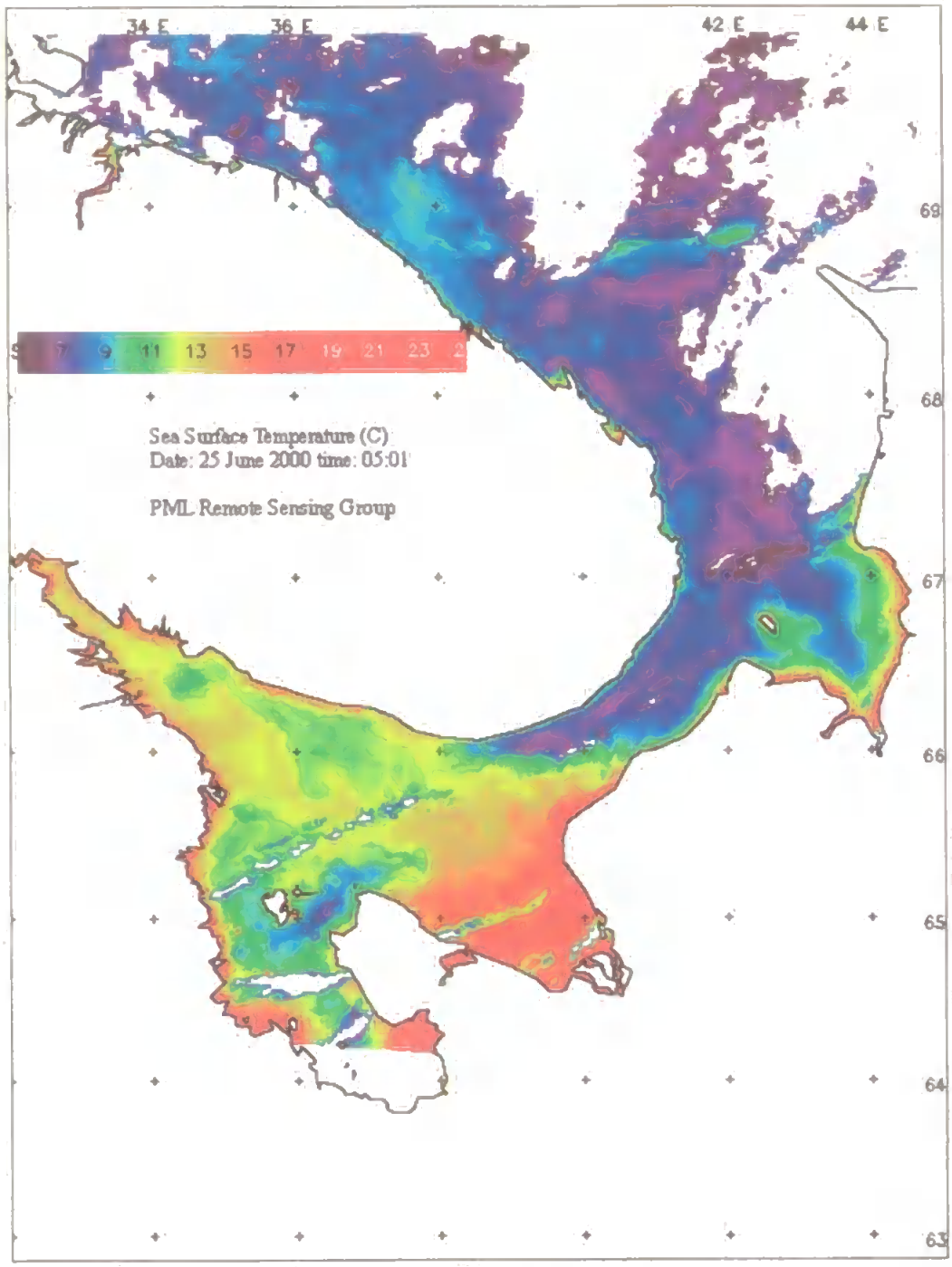


Figure 7.11: SST image taken the 25 June 2000.

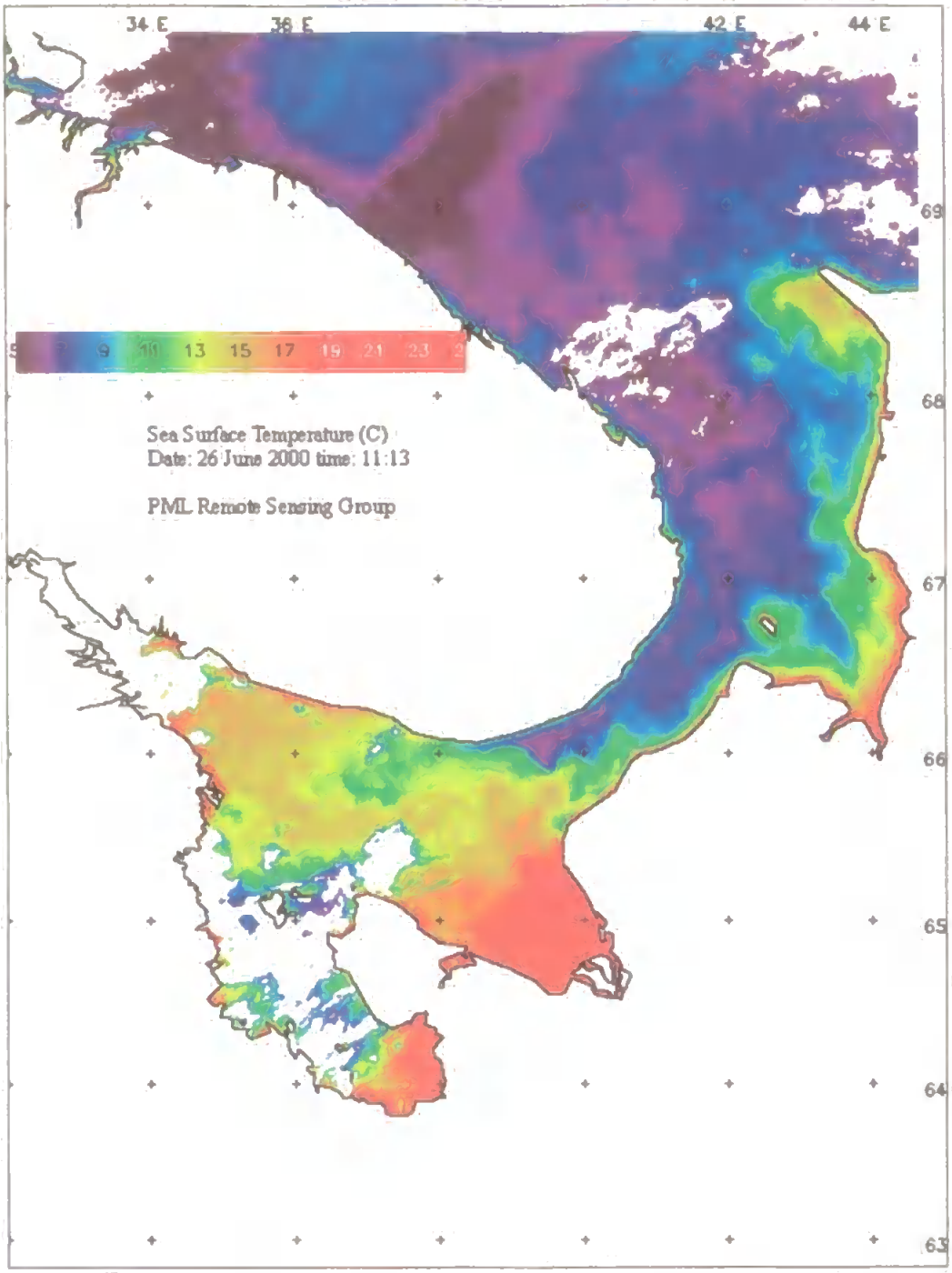


Figure 7.12: SST image taken the 26 June 2000.

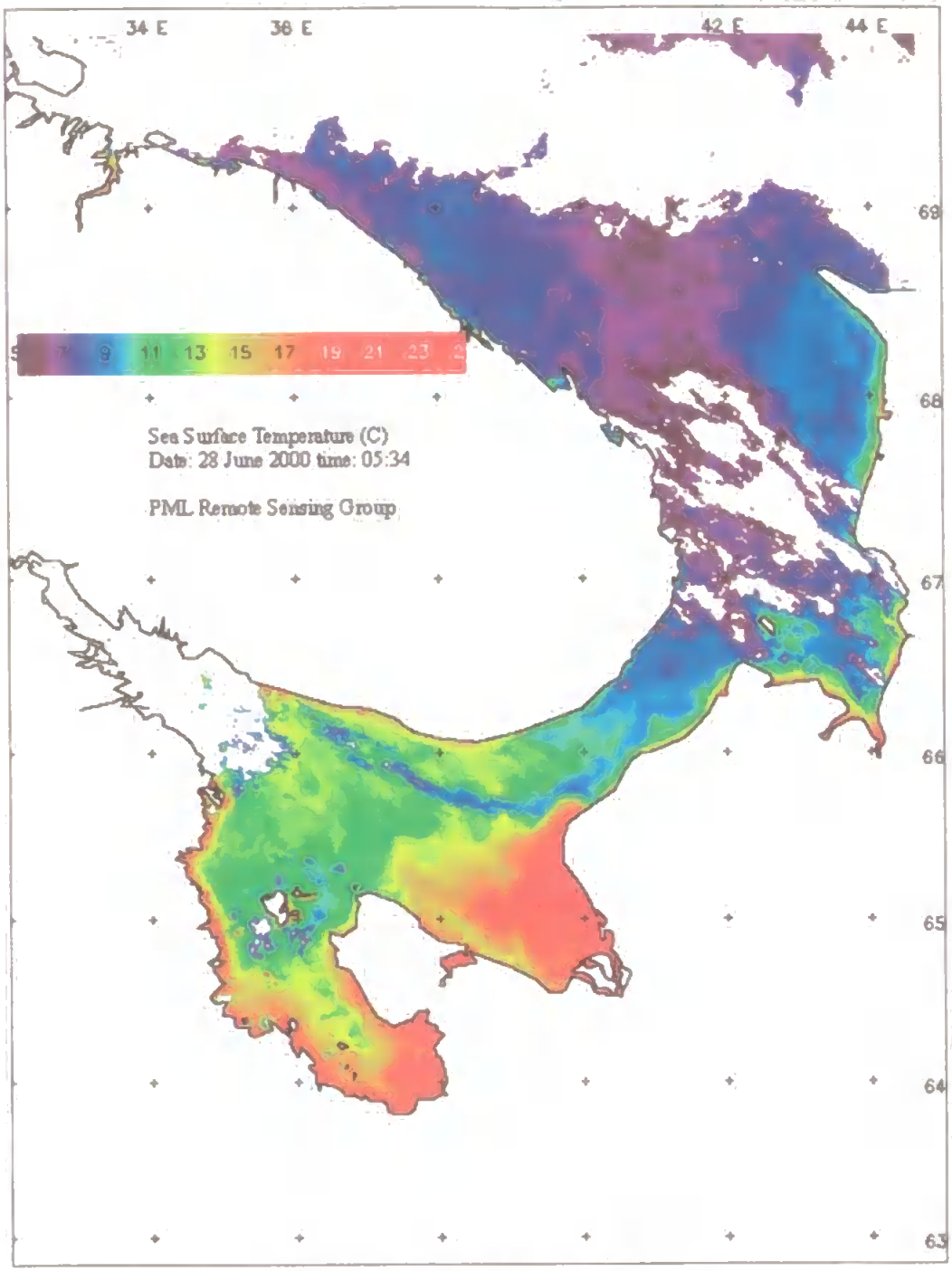


Figure 7.13: SST image taken the 28 June 2000.

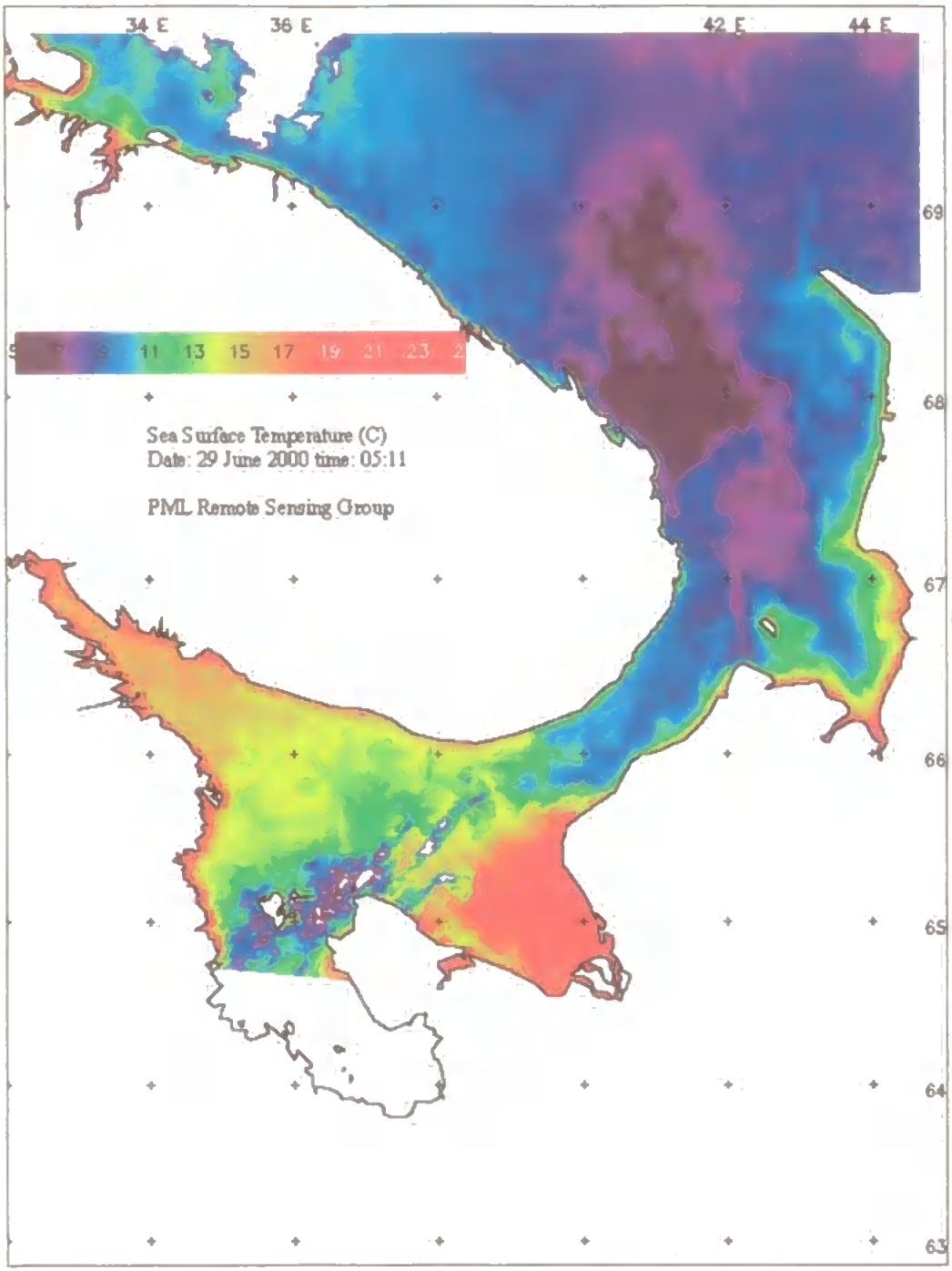


Figure 7.14: SST image taken the 29 June 2000.

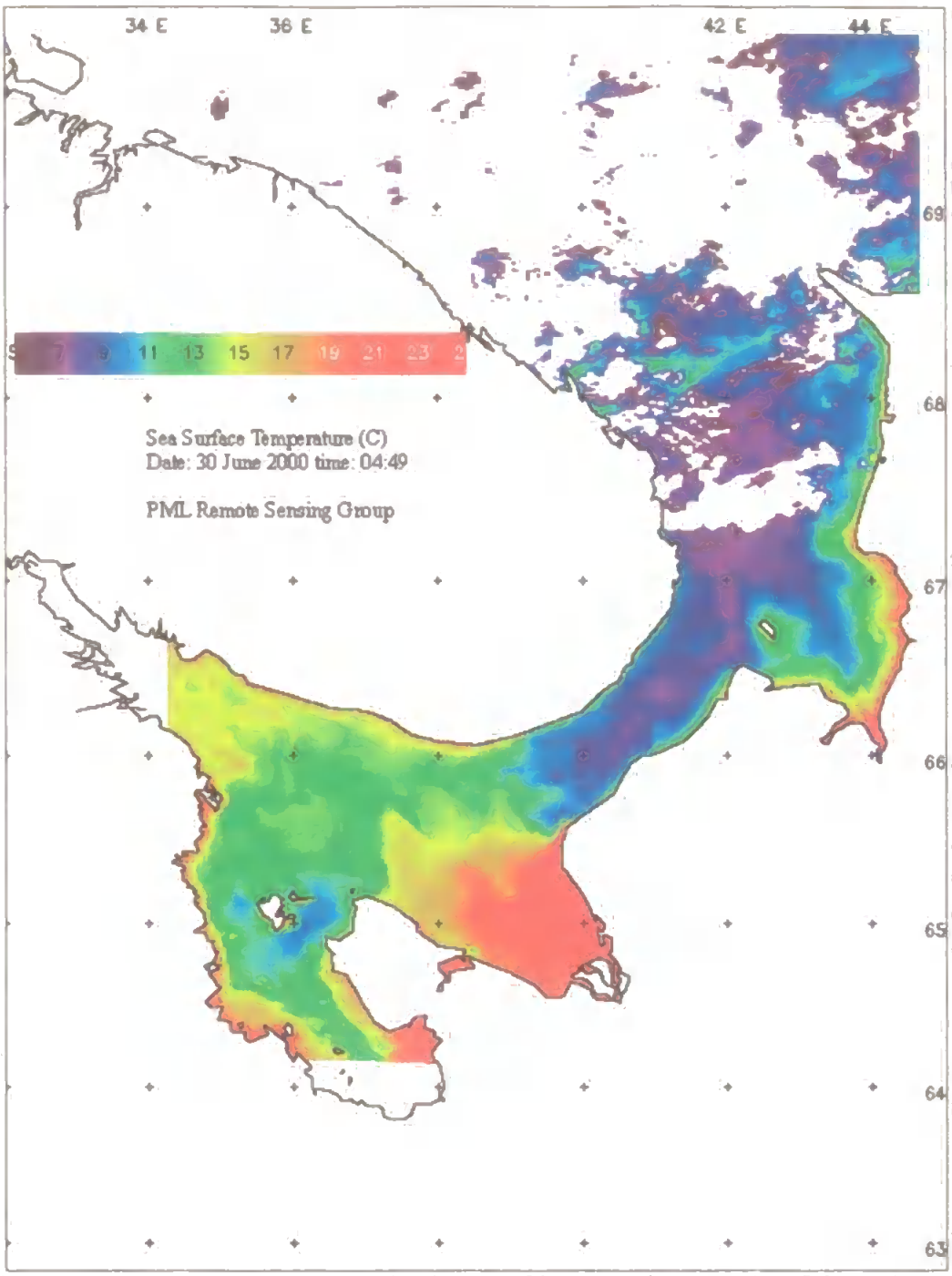


Figure 7.15: SST image taken the 30 June 2000.

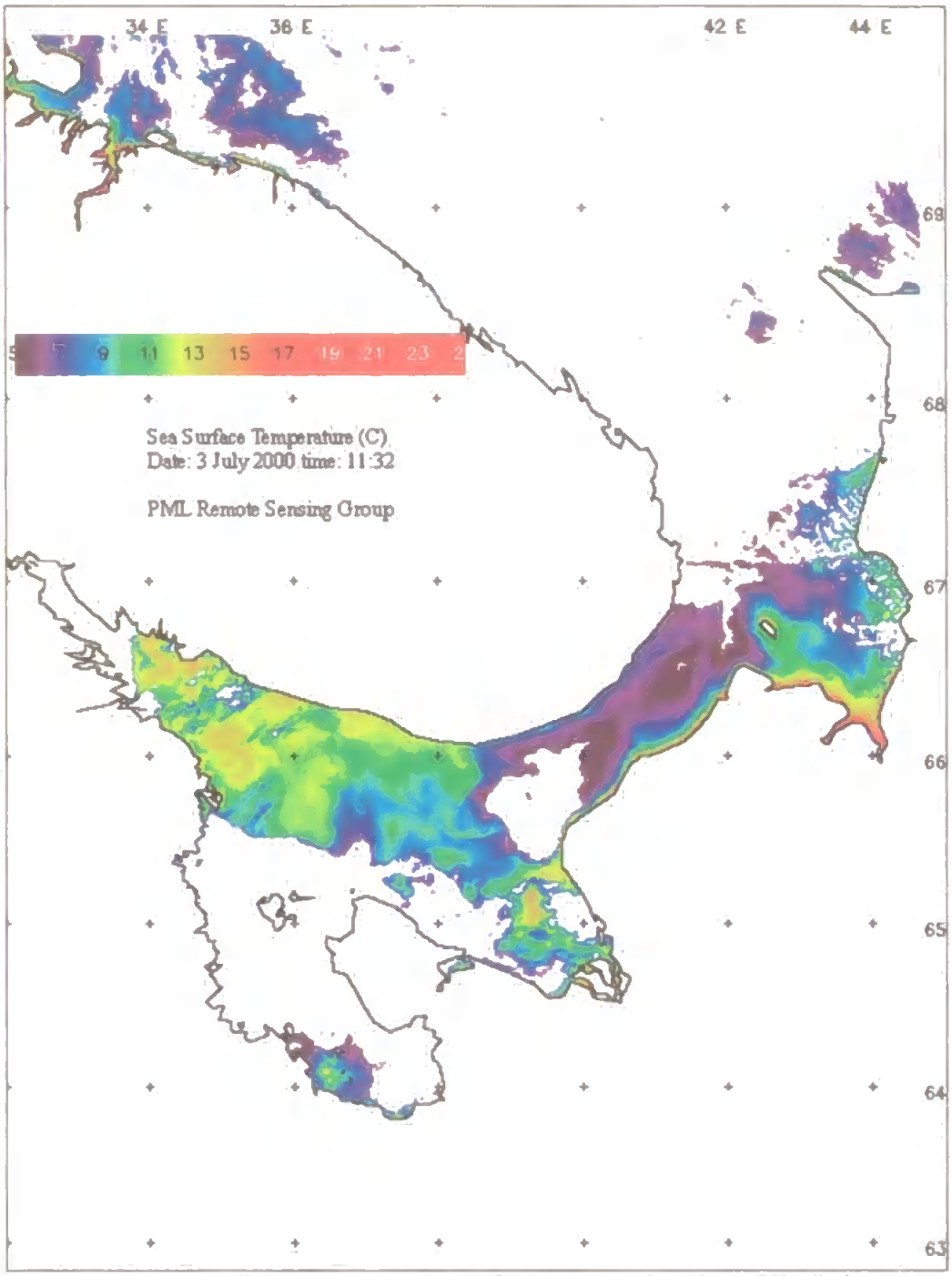


Figure 7.16: SST image taken the 3 July 2000

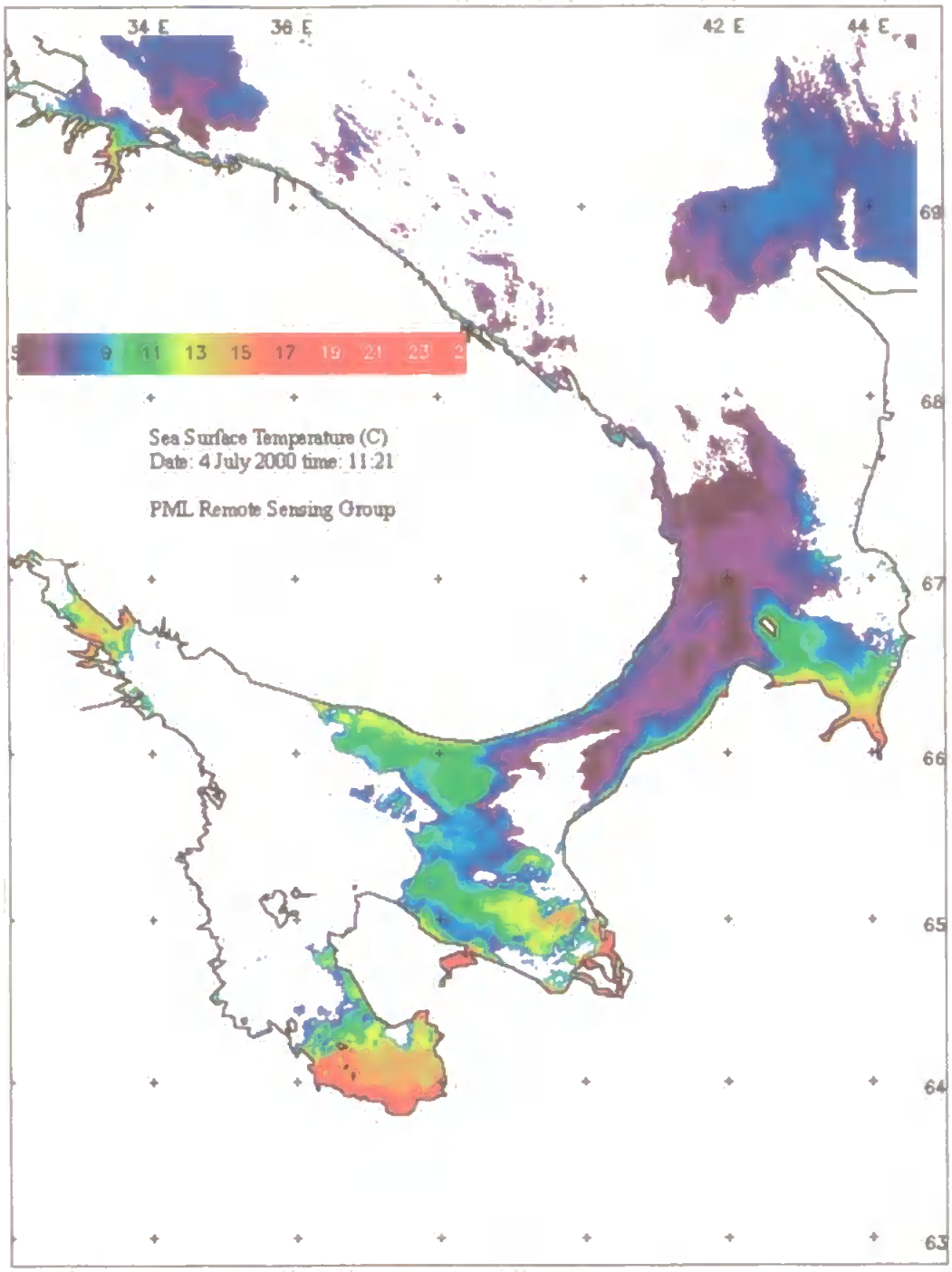


Figure 7.17: SST image taken the 4 July 2000

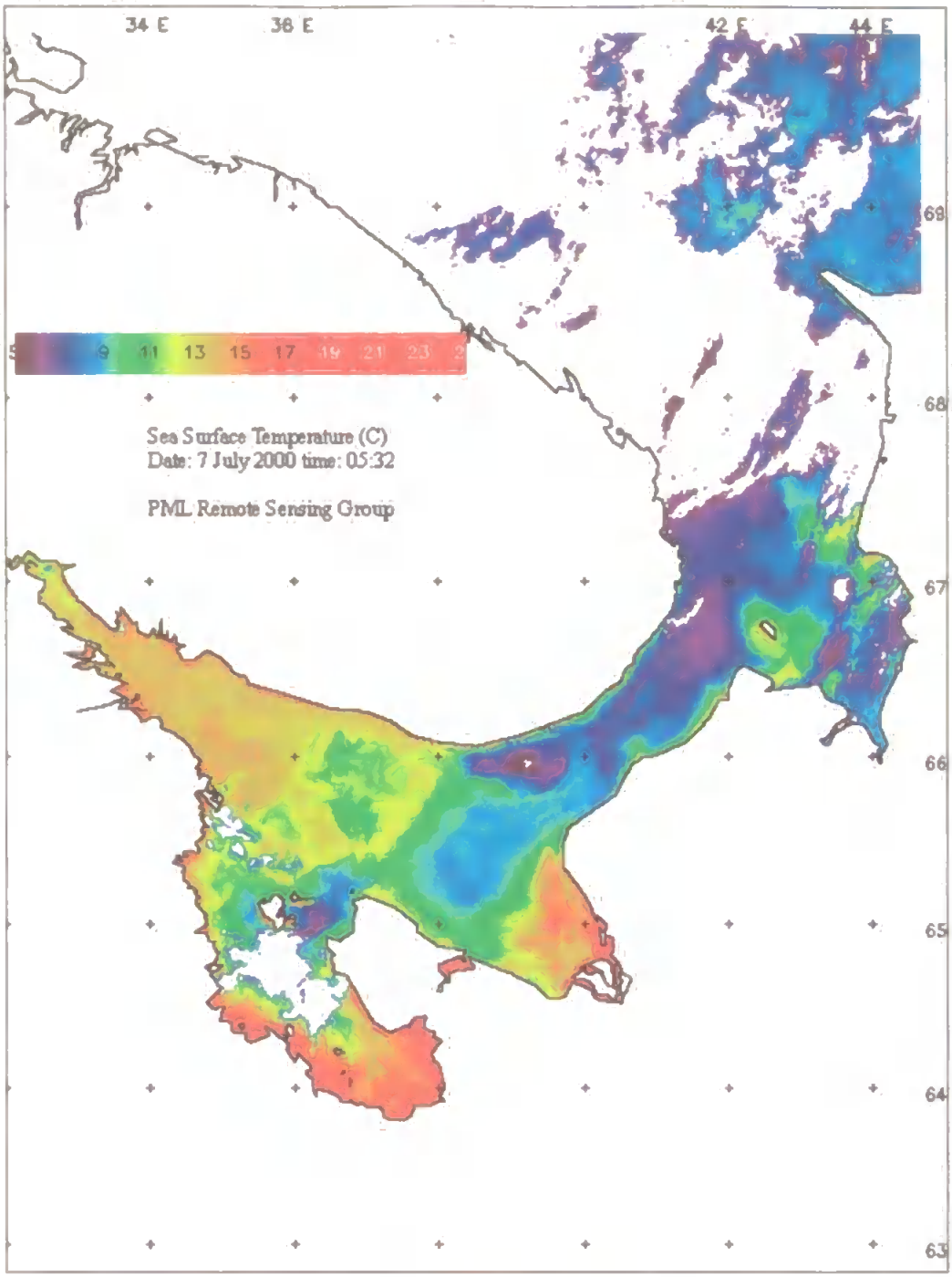


Figure 7.18: SST image taken the 7 July 2000.

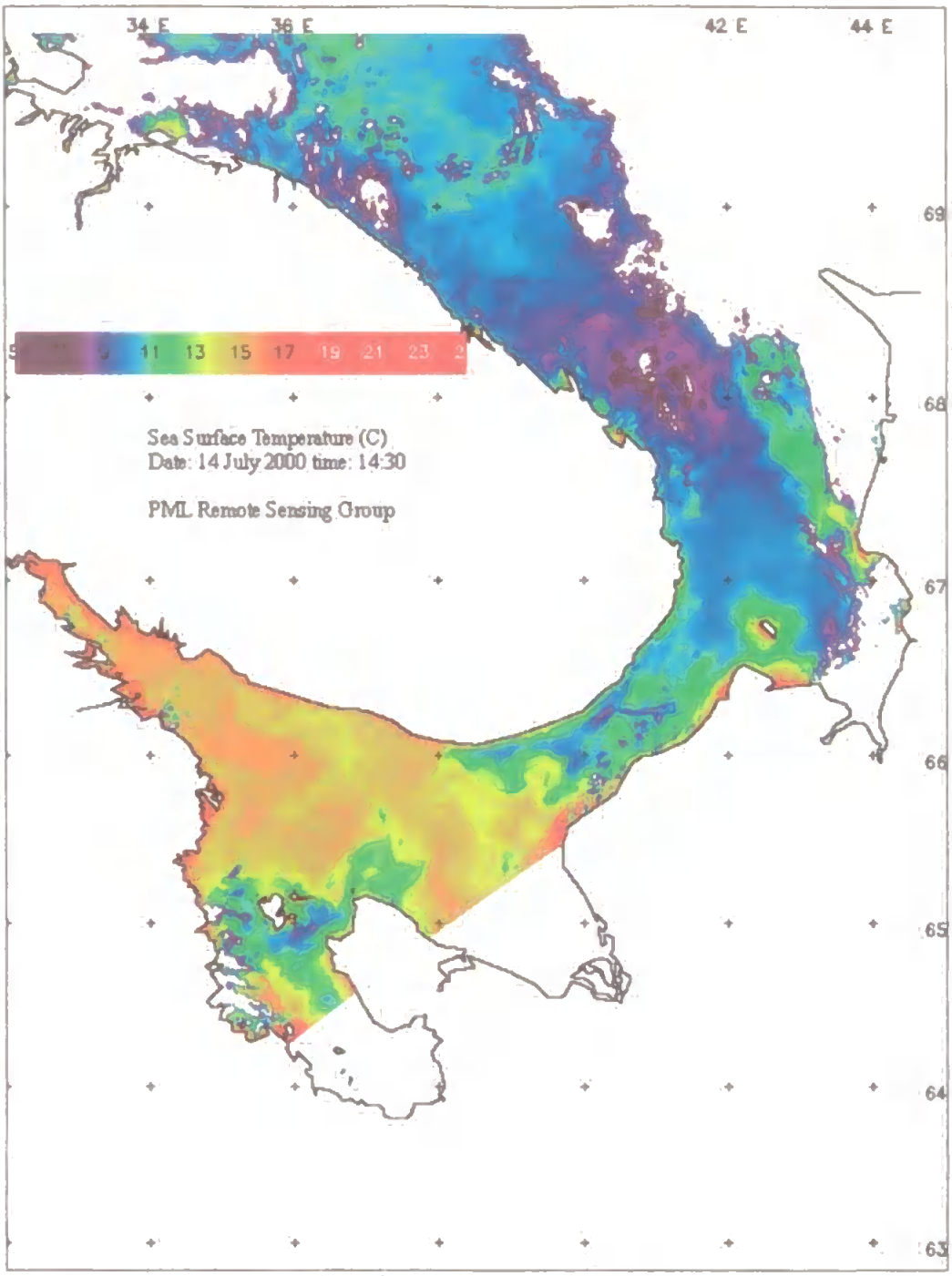


Figure 7.19: SST image taken the 14 July 2000.

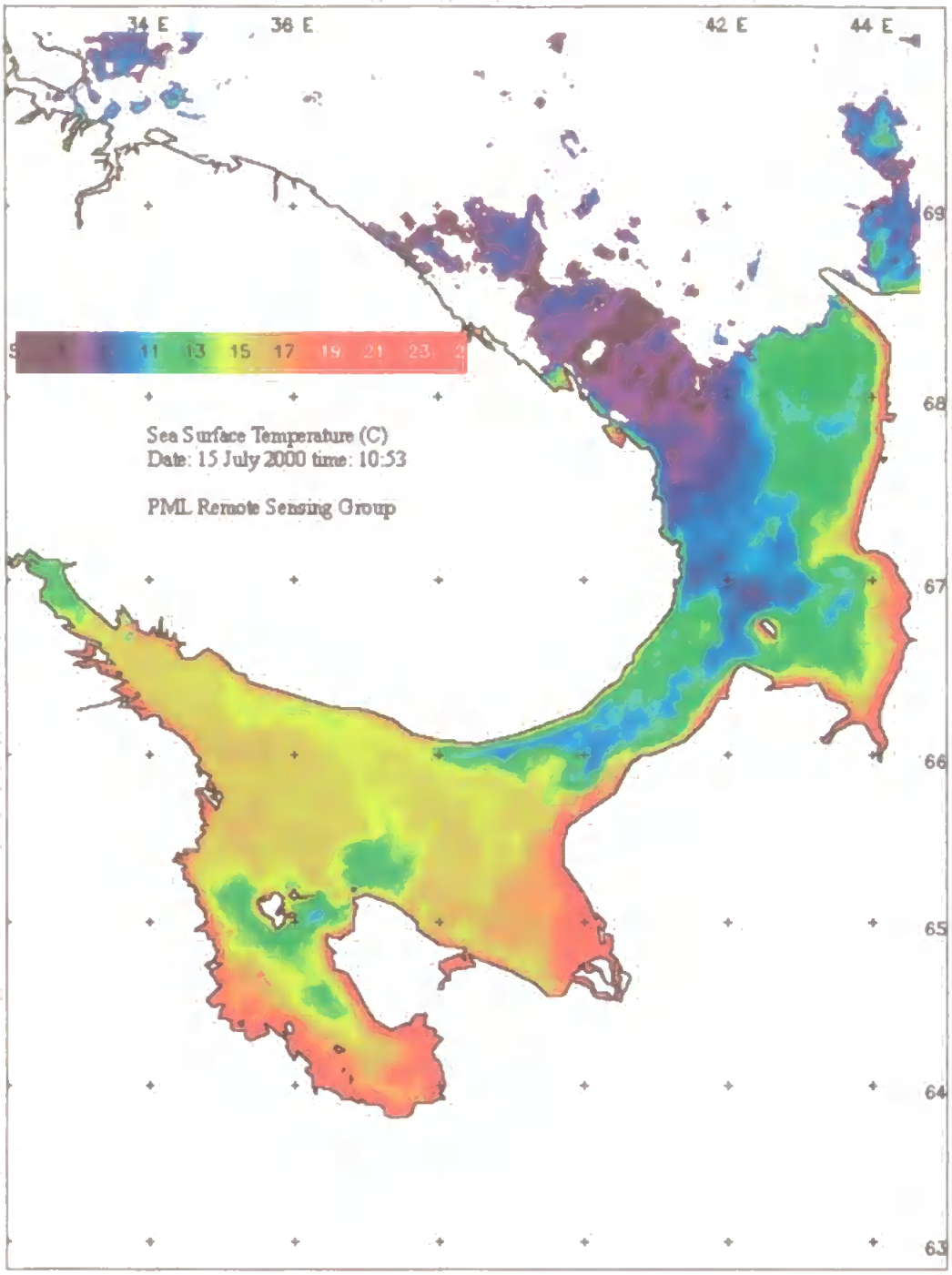


Figure 7.20: SST image taken the 15 July 2000.

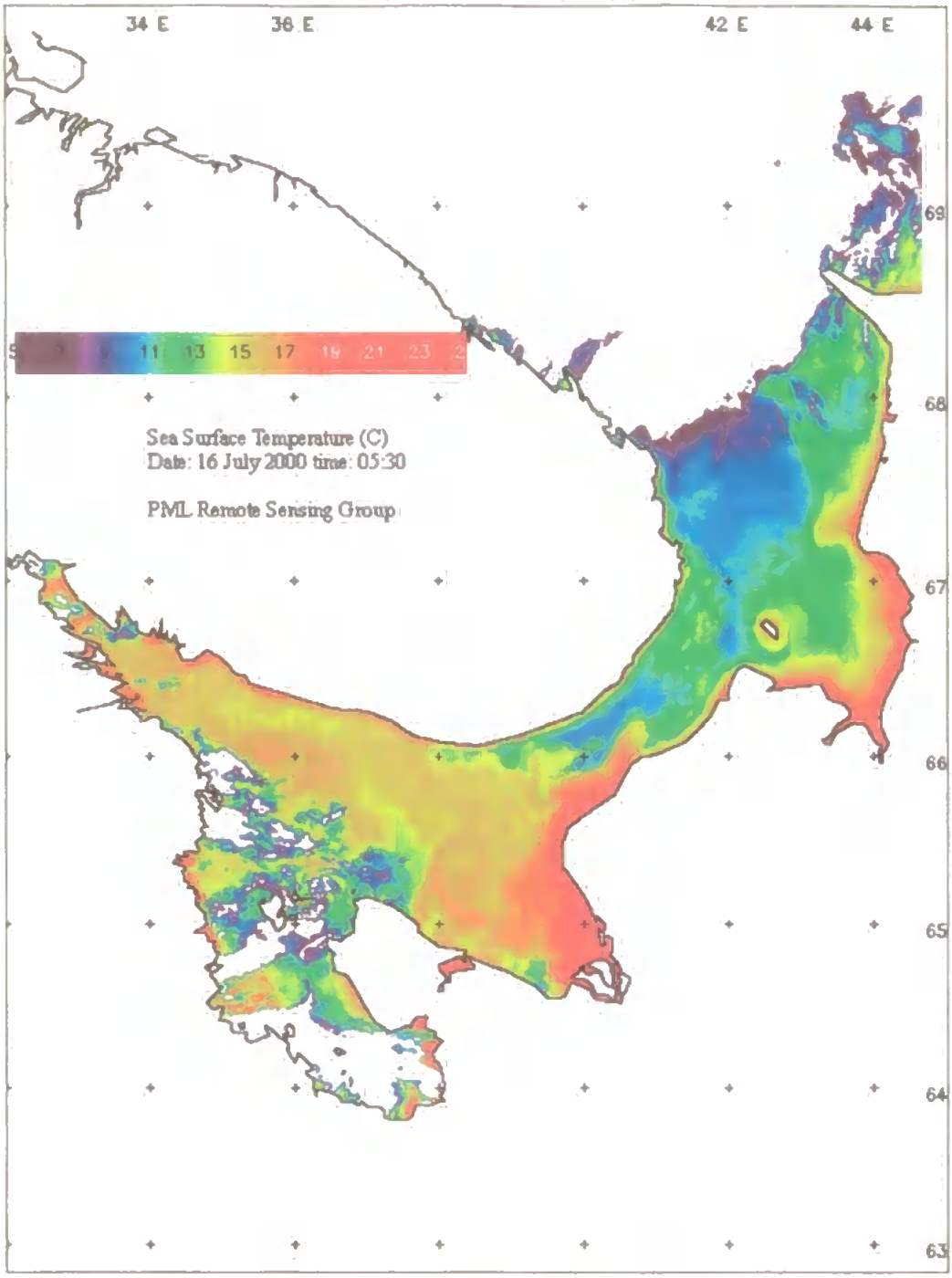


Figure 7.21: SST image taken the 16 July 2000

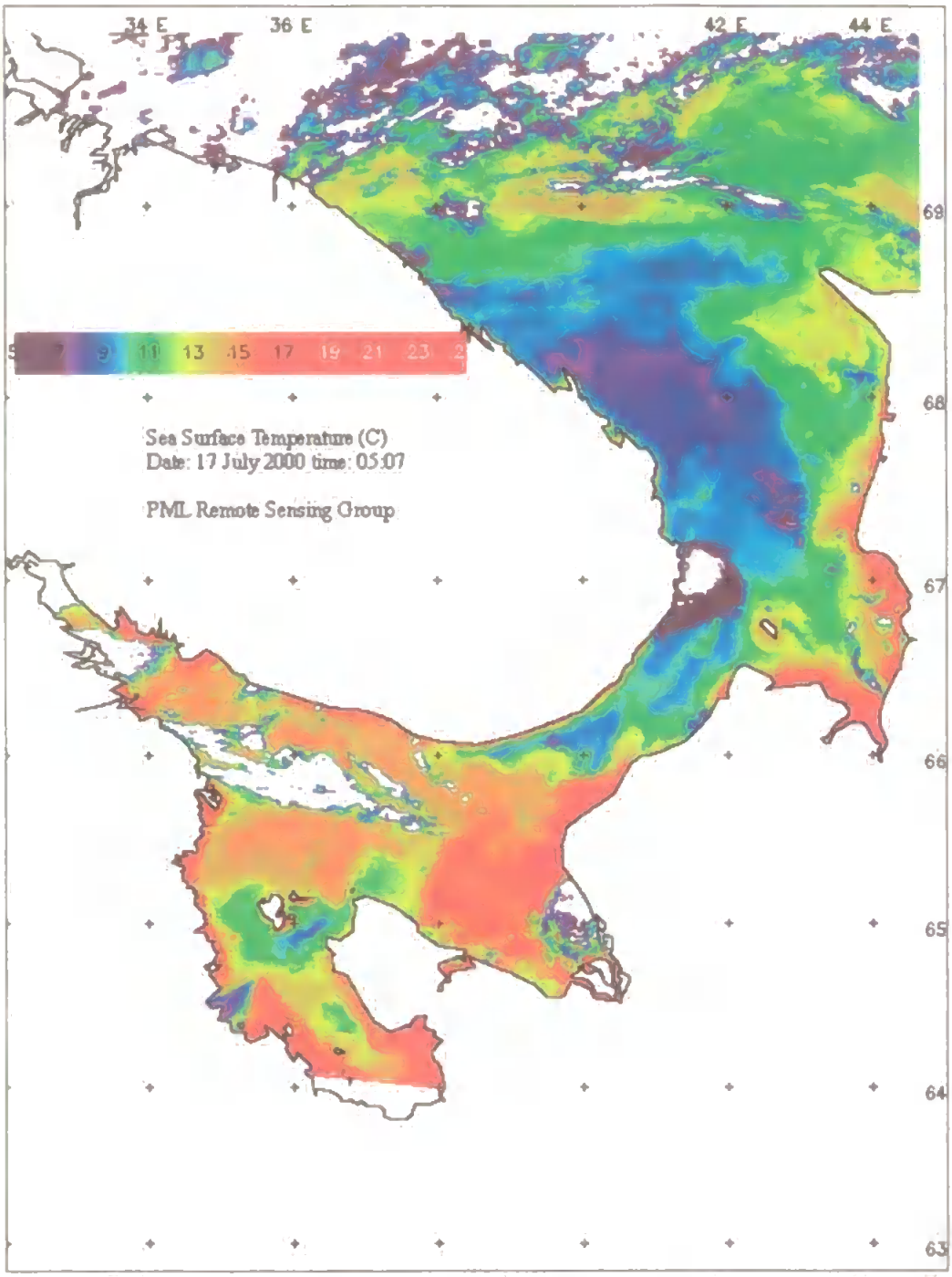


Figure 7.22: SST image taken the 17 July 2000.

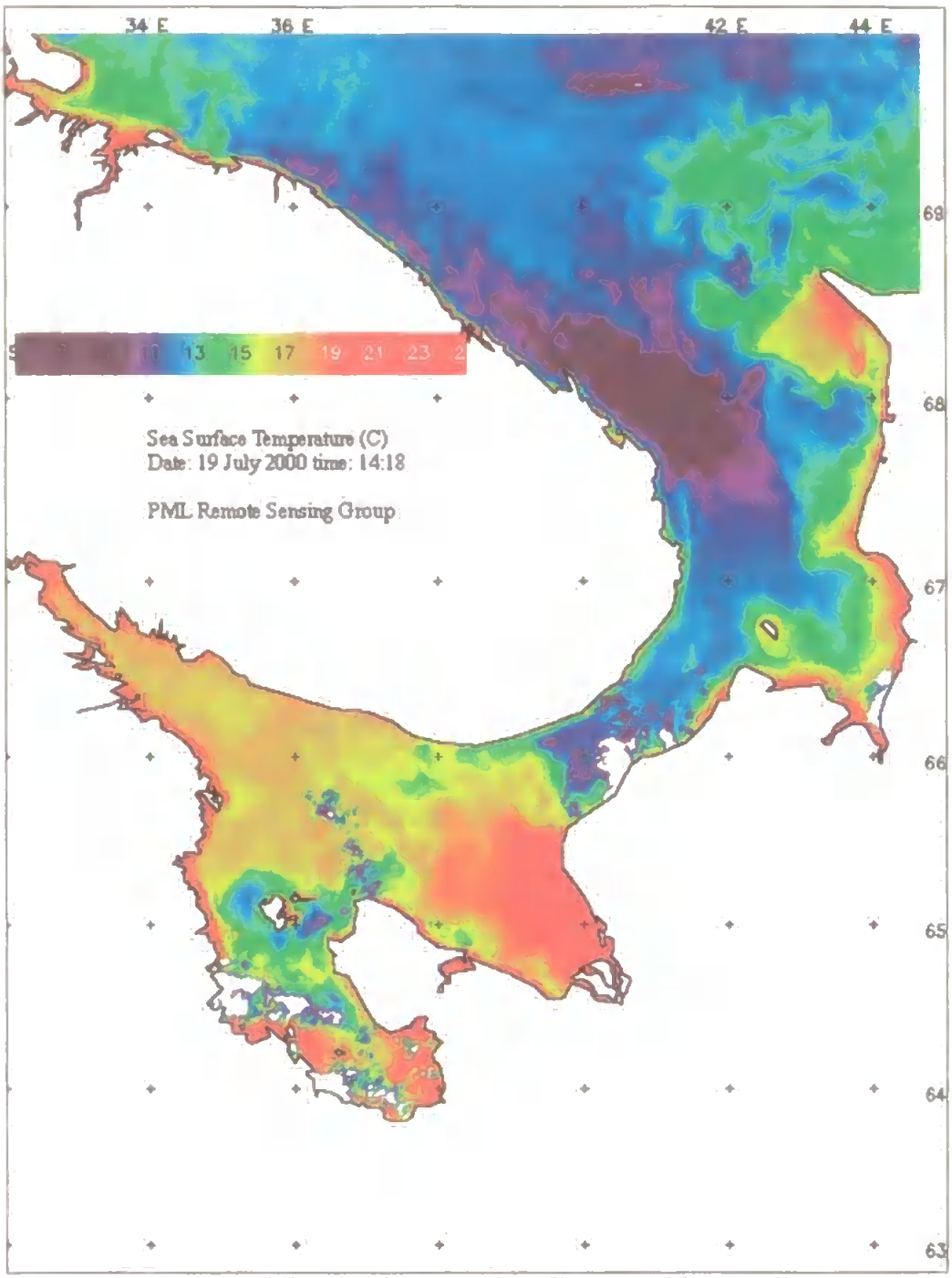


Figure 7.23: SST image taken the 19 July 2000.

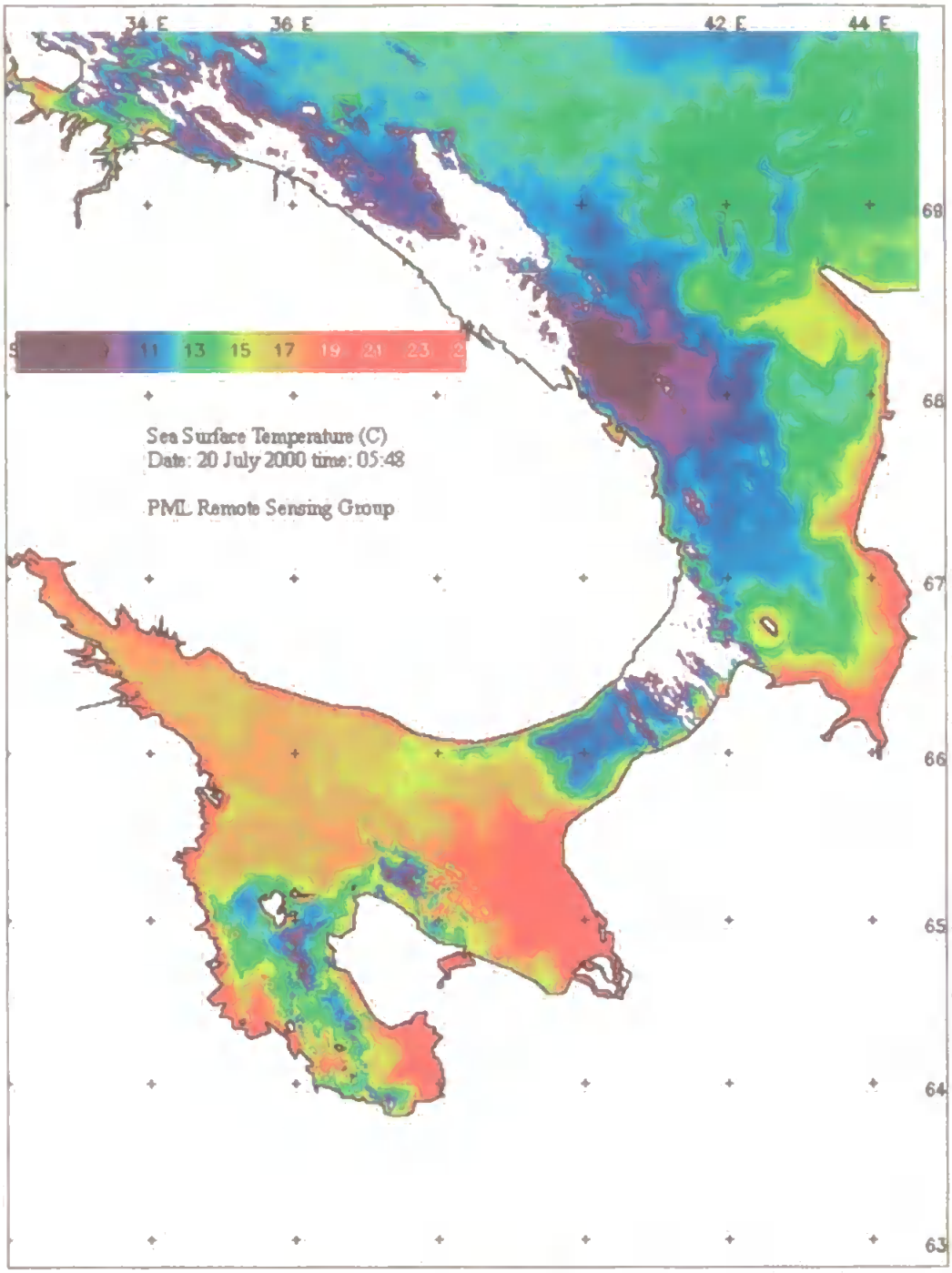


Figure 7.24: SST image taken the 20 July 2000.

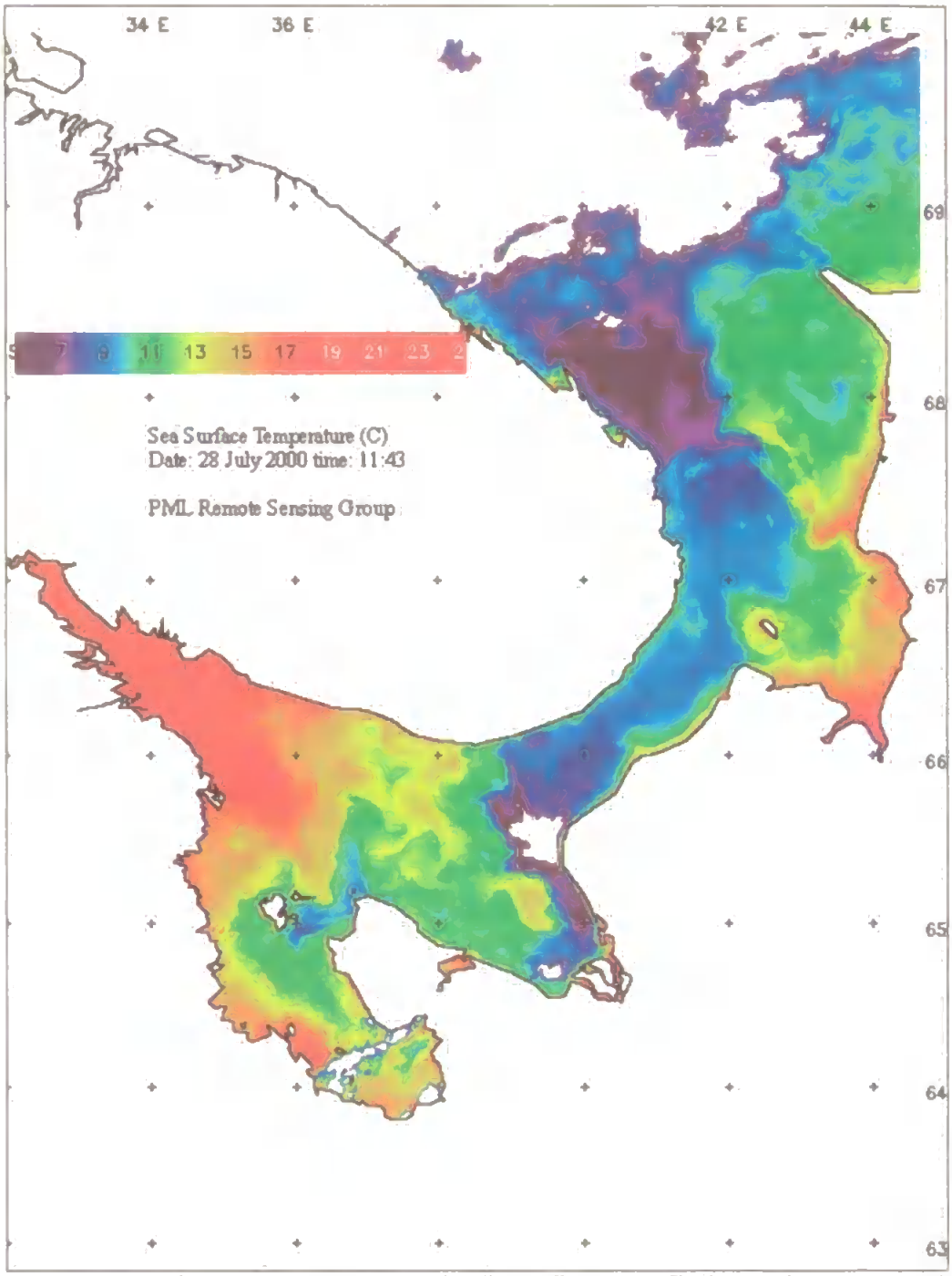


Figure 7.25: SST image taken the 28 July 2000

# Appendix F: Fine structure inhomogeneities analysis

## A.7. F.1 Plates (βS', αT') at stations during survey 2000.

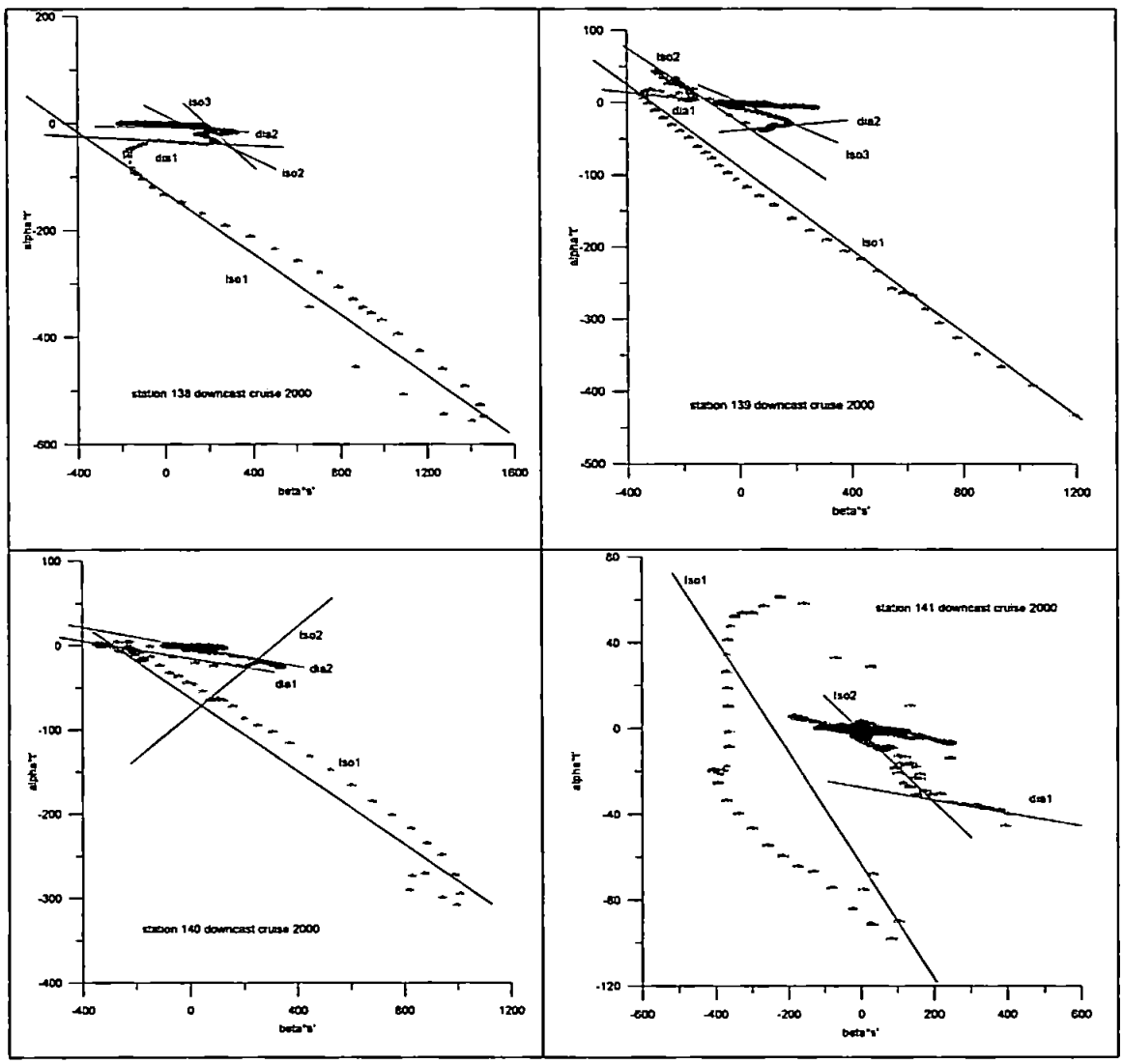

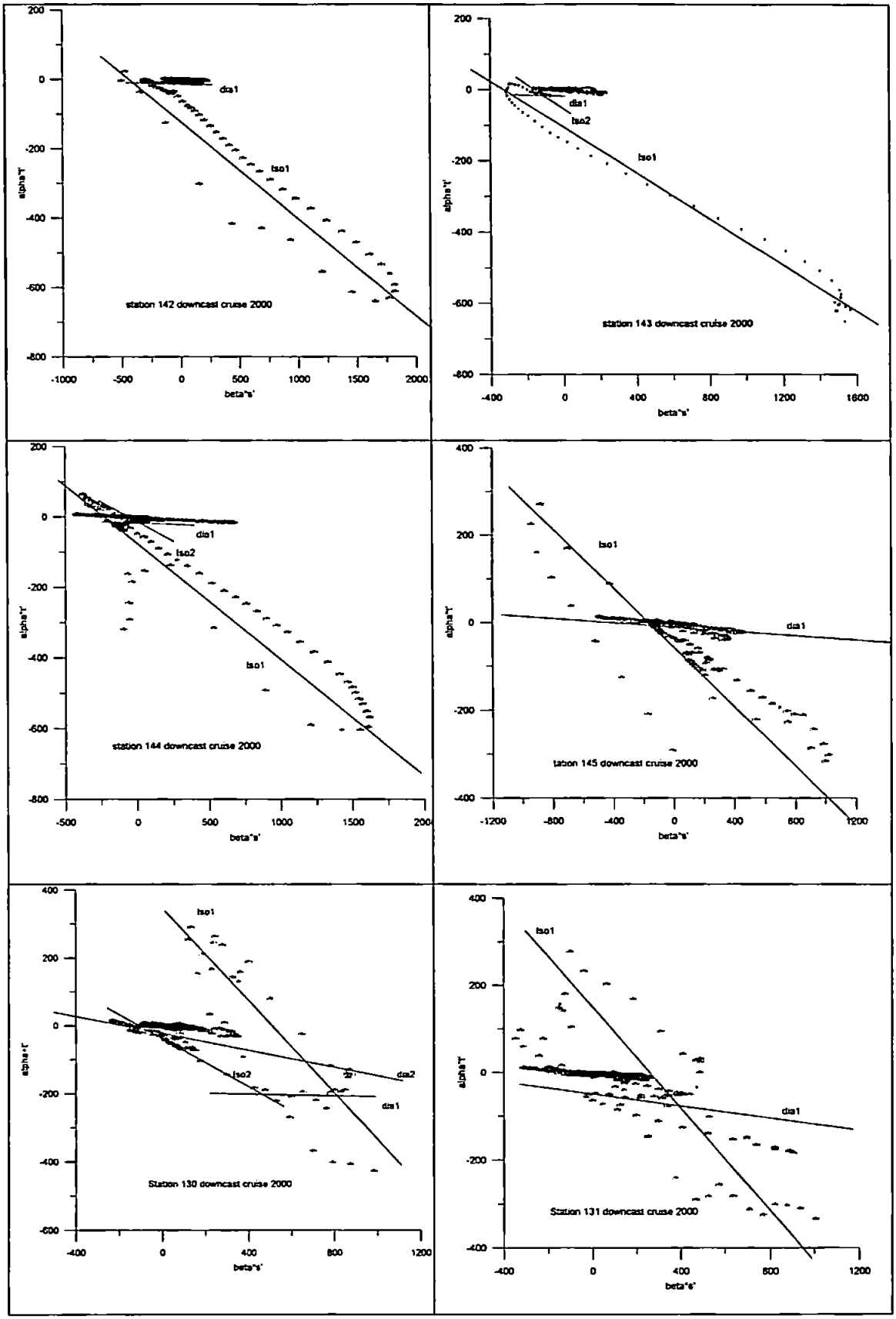
dia1
iso1
station 142 downcast cruise 2000
alpha'r'
beta's'
dia1
iso2
iso1
station 143 downcast cruise 2000
alpha'r'
beta's'
dia1
iso2
iso1
station 144 downcast cruise 2000
alpha'r'
beta's'
iso1
dia1
tation 145 downcast cruise 2000
alpha'r'
beta's'
iso1
iso2
dia2
dia1
Station 130 downcast cruise 2000
alpha'r'
beta's'
iso1
dia1
Station 131 downcast cruise 2000
alpha'r'
beta's'

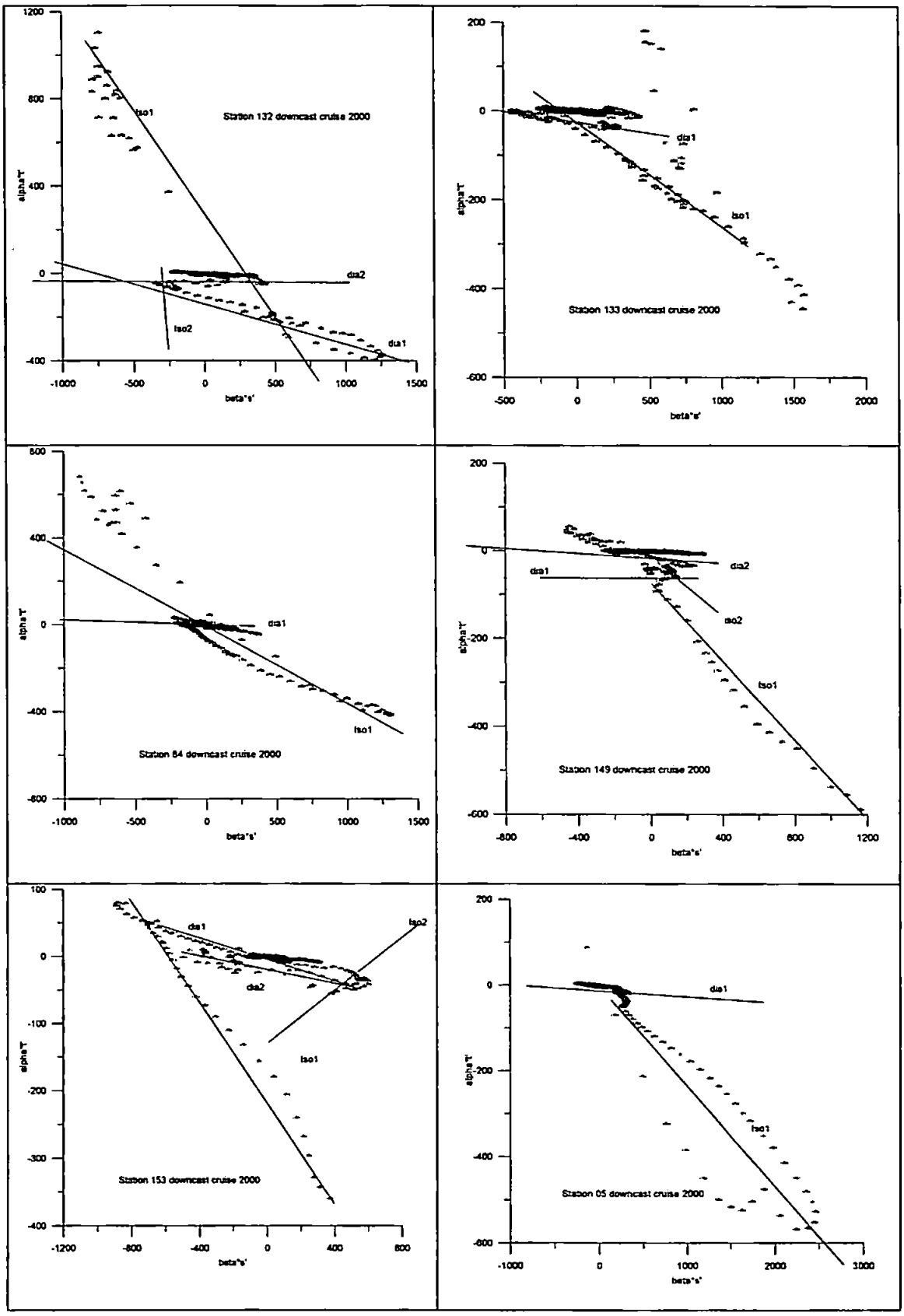
Station 132 downcast cruise 2000
iso1
dia2
iso2
dia1
alpha'T'
beta's'
Station 133 downcast cruise 2000
dia1
iso1
Station 84 downcast cruise 2000
dia1
iso1
Station 149 downcast cruise 2000
dia1
dia2
iso2
iso1
Station 153 downcast cruise 2000
dia1
iso2
dia2
iso1
Station 05 downcast cruise 2000
dia1
iso1

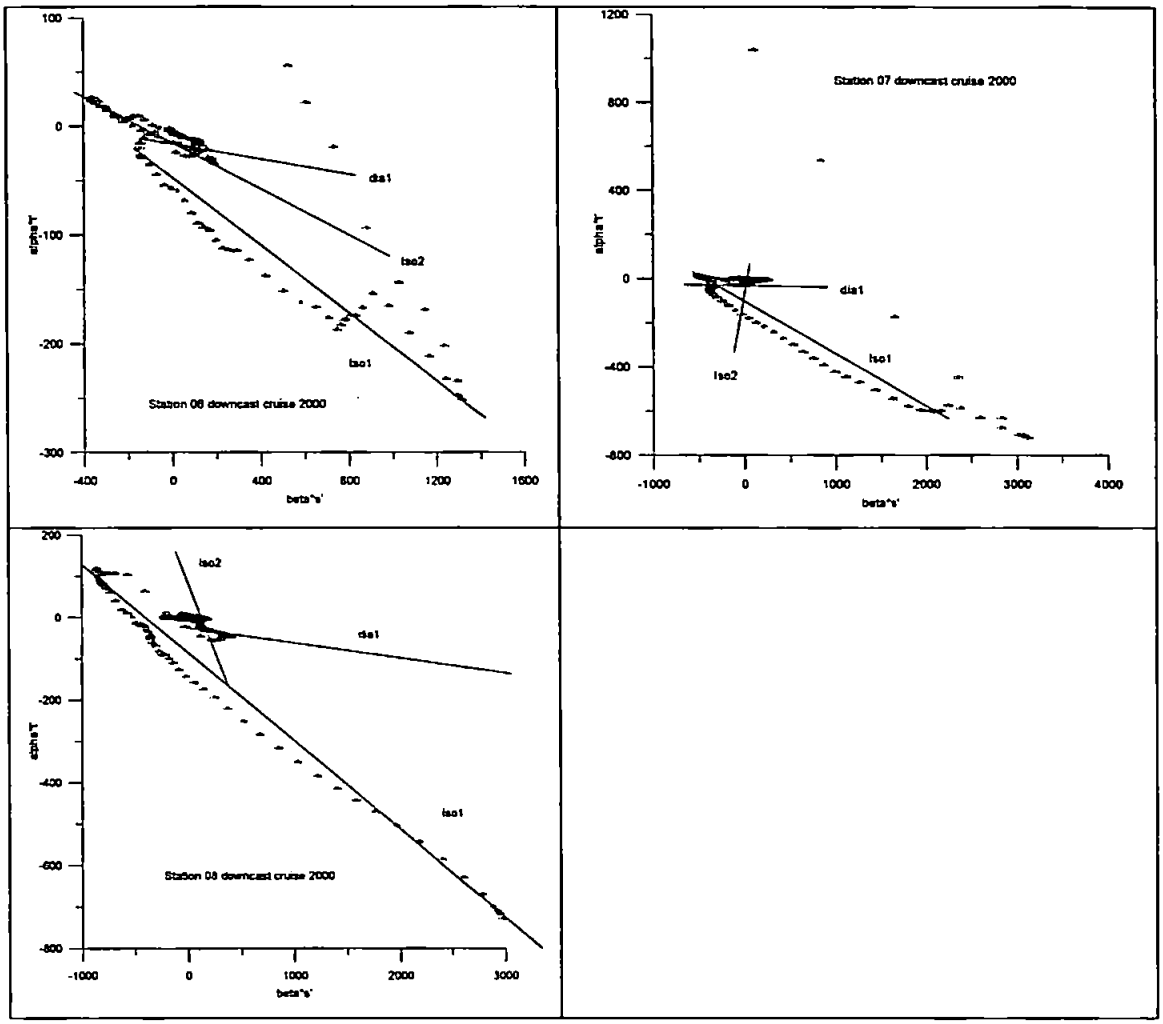
Station 06 downcast cruise 2000
dia1
iso2
iso1
alpha*T
beta*s'
Station 07 downcast cruise 2000
dia1
iso1
iso2
alpha*T
beta*s'
iso2
dia1
iso1
Station 08 downcast cruise 2000
alpha*T
beta*s'

# F.2 Plates (βS', αT') at stations during survey 2001

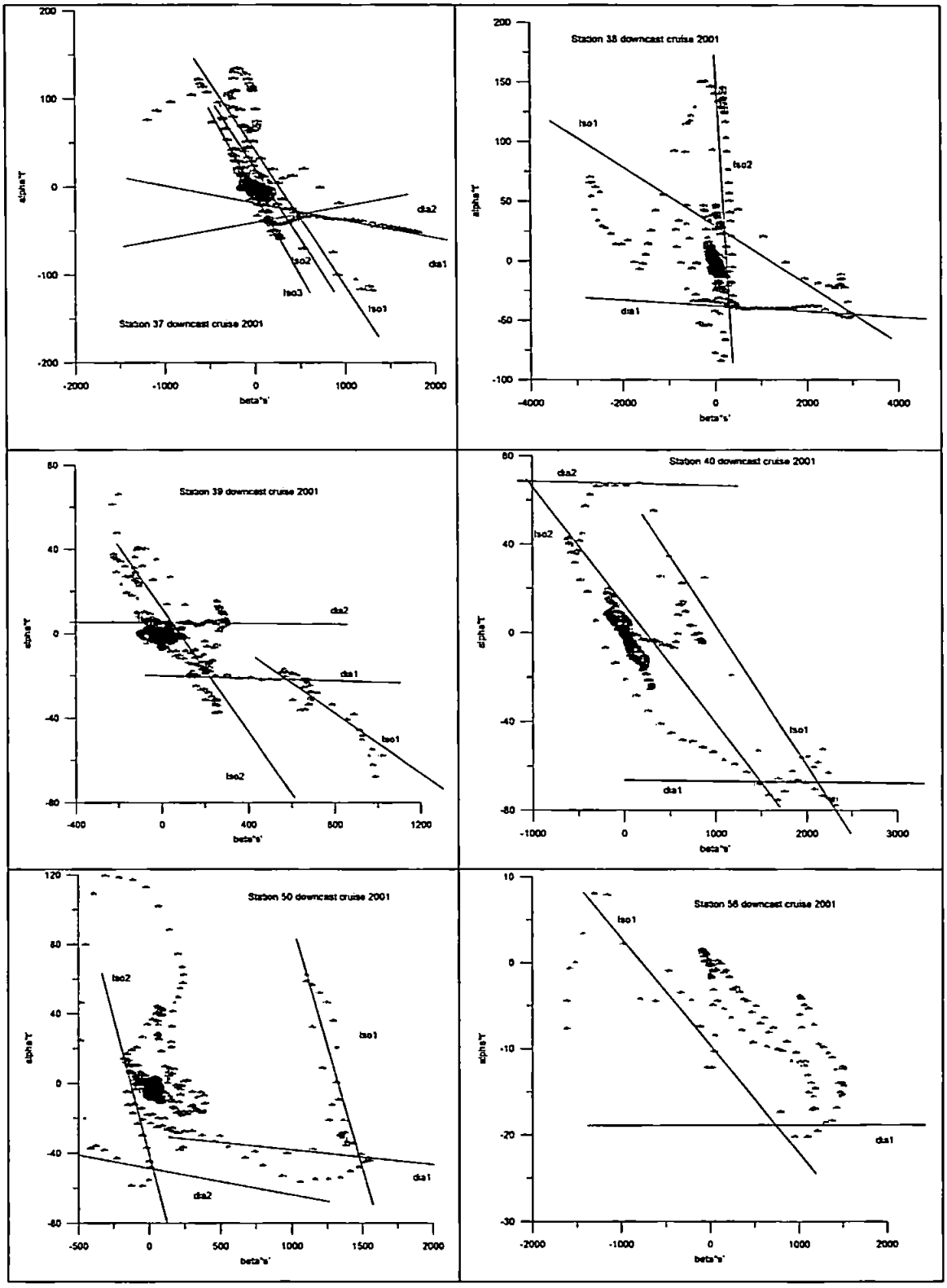

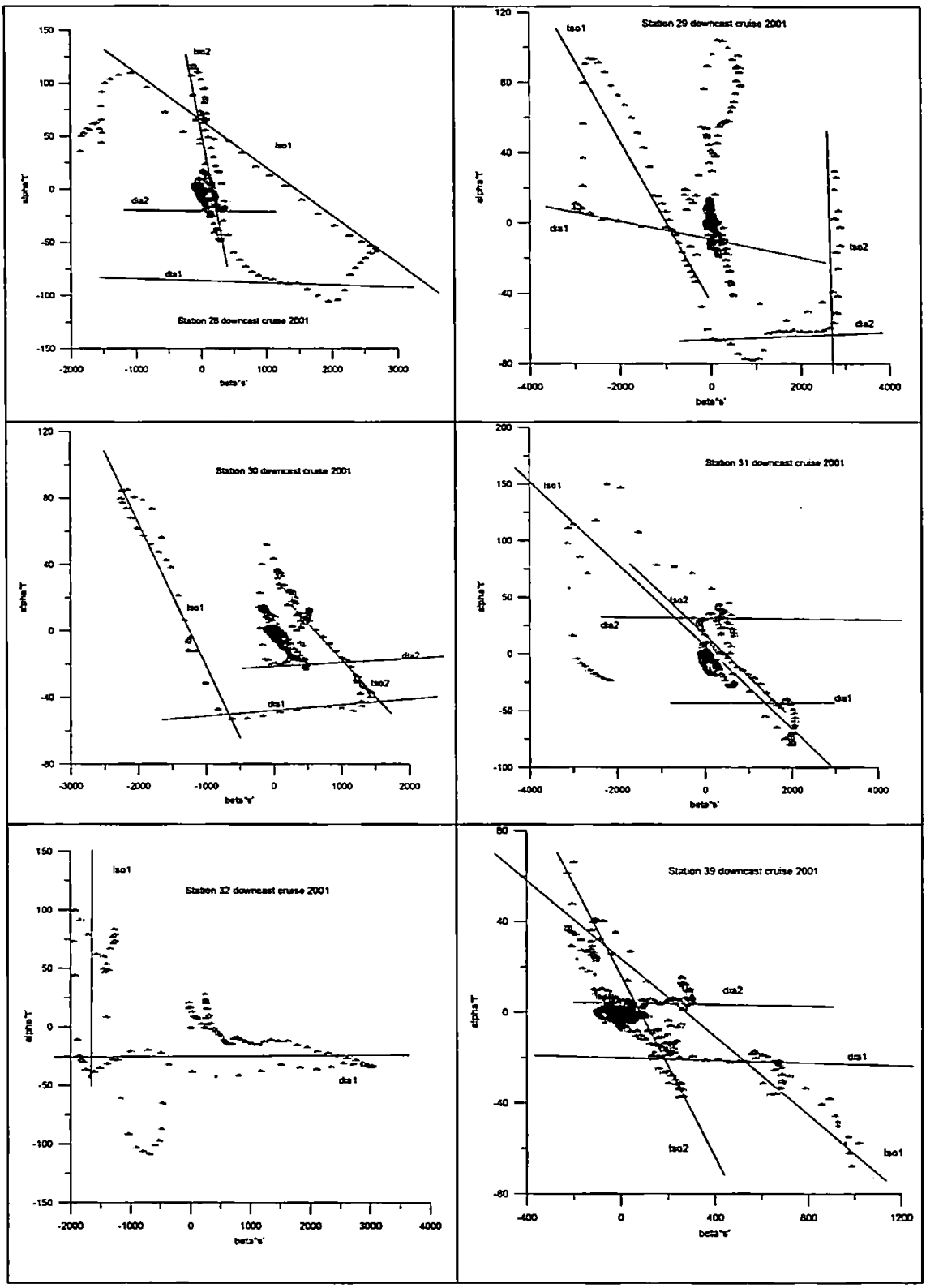
Station 28 downcast cruise 2001
Station 29 downcast cruise 2001
Station 30 downcast cruise 2001
Station 31 downcast cruise 2001
Station 32 downcast cruise 2001
Station 39 downcast cruise 2001
alpha'T
beta's'
lso1
lso2
dsa1
dsa2

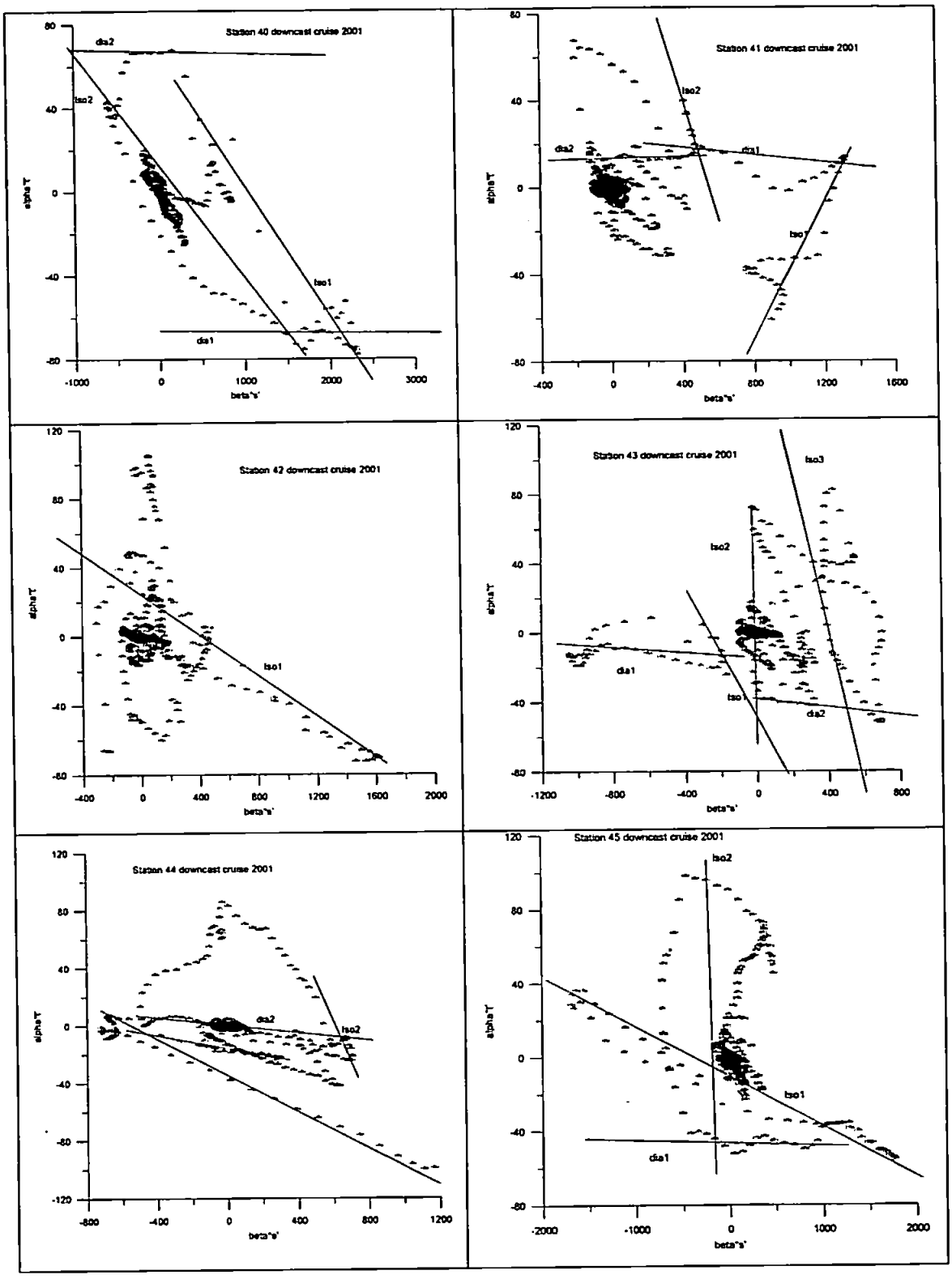
Station 40 downcast cruise 2001
Station 41 downcast cruise 2001
Station 42 downcast cruise 2001
Station 43 downcast cruise 2001
Station 44 downcast cruise 2001
Station 45 downcast cruise 2001
alpha'T
beta's'
da1
da2
iso1
iso2
iso3

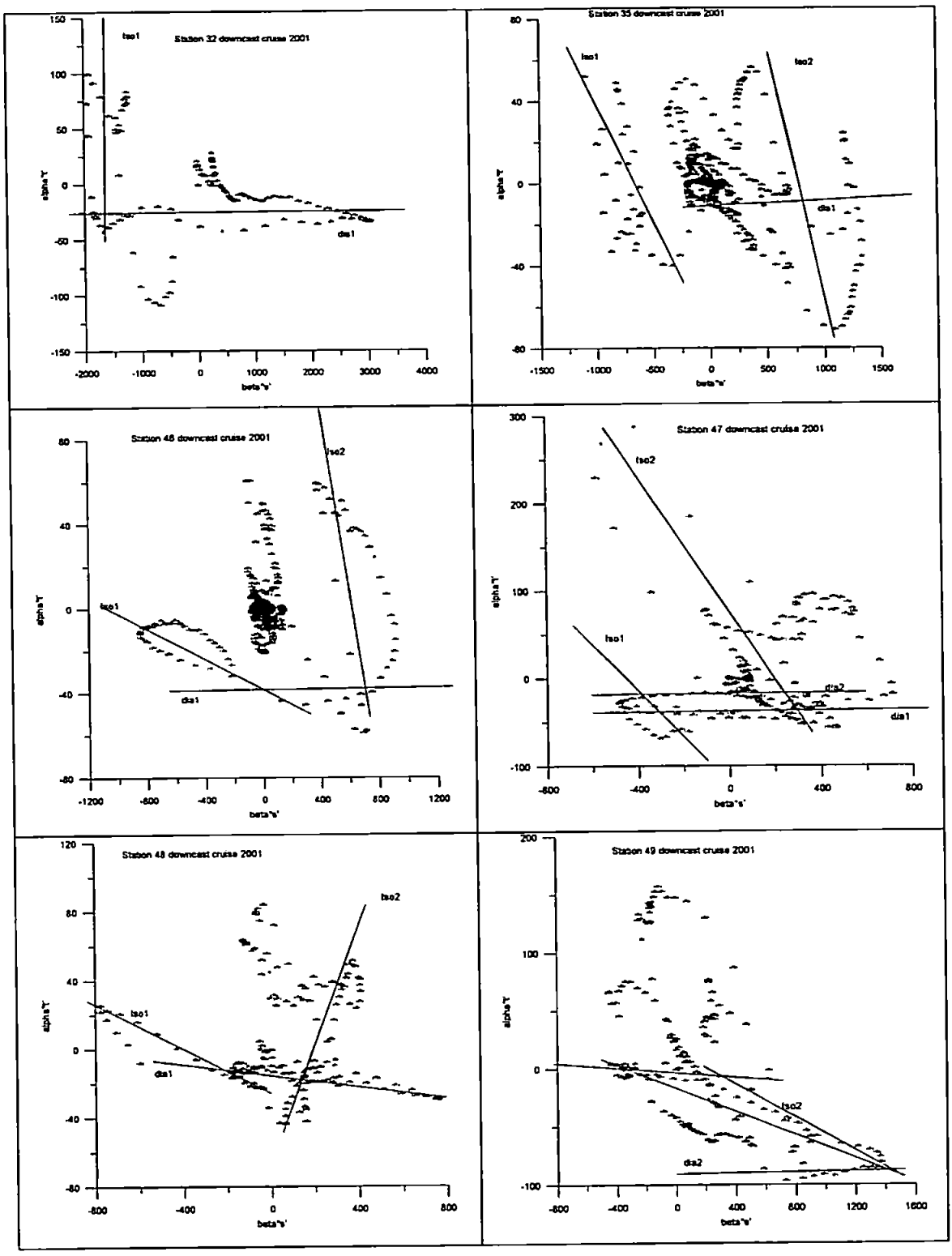
Station 32 downcast cruise 2001
Station 35 downcast cruise 2001
Station 46 downcast cruise 2001
Station 47 downcast cruise 2001
Station 48 downcast cruise 2001
Station 49 downcast cruise 2001
alpha'T'
beta's'
lso1
lso2
dla1
dla2

## REFERENCES


Aagaard K. and Carmack E.C., 1989. The role of sea ice and other freshwater in the Arctic Ocean. J. Geophys. Res., 94, 14485-14498.

Agatova A.I. and Kirpichev K.B., 2000. Organic matter in the White Sea: Interannual variability of organic matter distribution. Oceanology, 40, 791-795.

Altshuller (Альтшулер) V.M., Sustavov Yu.M. 1970. The exchange of energy between the White and the Barents Seas. Trudi PINRO. 27. (Russian journal)

AVISO: Archiving, Validation and Interpretation of Satellite Oceanographic data. (http://www.aviso.oceanobs.com/)

Azovsky A.I., Obridko S.V., Burkovsky I.V., and Stoljarov A.P., 1998. Community structure of transitive zones under the condition of complex environmental gradients (an example of macrobenthos of the Chernaya estuary, the Kandalaksha Bay, the White Sea). Okeanologiya, 38, 412-420.

Babkov A.J., 1982. Brief Hydrological characteristics of the Chupa Inlet of the White Sea. Exploration of the Fauna of the Sea, 27, 3-12 (Russian journal).

Barton E.D., Basterretxea G., Flament P., Mitchelson-Jacob E.G., Jones B., Arístegui J., and Herrera F., 2000. Lee region of Gran Canaria. Journal of Geophysical Research, 105, C7, 17173-17193.

Bek T.A., Sharnaud N.M., Shcherbakov F.A., and Potapova L.I., 1992. Genesis of the sediments organic-matter of the White Sea. Okeanologiya, 32 (6), 1131-1138.

Bek T.A., 1997. A biotic basis for the distribution of coastal macrobenthos in the White Sea. Okeanologiya, 37, 881-886.

Beloe more, 1994. Kompleksnye issledovaniya ekosistemy Belogo morya: Sbornik trudov (Multidisciplinary Studies of the White Sea Ecosystem. Collection of Papers), Sapozhnikov, V.V., Ed., Moscow: Vses. Nauch.-Issl. Inst. Rybn. Khoz. Okeanogr.

Beloe more, 1995. Biologicheskie resursy i problemy ikh ratsional'nogo ispol'zovaniya. Chast' 1-2 (The White Sea: Biological Resources and Problems of Their Rational Use, Parts 1-2), St. Petersburg: ZIN RAN, Issledovaniyafauny morei, vol. 42(50).

Bergamasco A. and Gačić M., 1996. Baroclinic response of the Adriatic Sea to an episode of bora wind. J. Physic. Oceangr. 26(7), 1354-1369.

Berger V., Dahle S., Galaktionov K., *et al*, 2001. White Sea. Ecology and Environment, St. Petersburg-Tromso: Derzavets.

Bergström S. and Carlsson B., 1994. Rive, runoff to the Baltic Sea, 1950-1990. Amhio, 23(4-5), 280-287.

Bethoux J. P. and Gentili B., 1994. The Mediterranean Sea, a test area for marine and climatic interactions. In Ocean Processes in Climate Dynamics. Global and Mediterranean Examples, P. Malanotte-Rizzoli and A. R. Robinson, (eds). Kluwer Academic Publishers, NATO/ASI Series, Vol. 419. Kluwer Academic Publishers. Dordrecht, The Netherlands, pp. 239 254.

Bignami F., Salusti E., and Schiarini S. 1990. Observation on a bottom vein of dense water in the southern Adriatic and Ionian Seas. Journal of Geophysical Research, 95, 7249-7259.

Brown J., Hill A.E., Fernand L., and Horsburgh K.J., 1999. Observations of a seasonal jet-like circulation at the central North Sea cold pool margin. Estuarine Coastal and Shelf Sciences, 48, 343-355.

Bryden H. and Kinder H.T, 1992. Flow through the Strait of Gibraltar. In Rapp. Comm. Int. Mer. Medit., 33, 211.

Bryden H.L., Candela J. and Kinder T.H., 1994. Exchange through the Strait of Gibraltar. Prog. Oceanogr., 33, 201-248.

Candela J., 1991. The Gibraltar Strait and its role in the dynamics of the Mediterranean Sea. Dynam. Atmos. Oceans, 15, 267 299.

Chugaynova V.A., Nesvetova G.I., Konnov V.A., and Maximova M.P., 1993. Organic Nitrogen and Phosphorus in the bays of the White Sea. Okeanologiya, 33 (2), 201-209.

Church J.A., Bethoux J.P. and Theocharis A., 1998. Semi-enclosed seas, Islands and Australia. The Sea, 11, edited by Allan R. Robinson and Kenneth H. Brink.

Cooper L.H.N. and Vaux D., 1949. Cascading over the continental slope of water from the Celtic Sea. Journal of Marine Biological Association, 28, 719-750.

Cregg M.C., and Sanford T.B., 1980. Signatures of Mixing from the Bermuda Slope, the Sargasso Sea and the Gulf Stream. J. of Phys. Oceanogr., 10, 105-127.

Damm P., Hinzpeter H., Luthardt H. and Terzenbach U., 1994. Seasonal and interannual variability in the atmosphere and in the sea. In Circulation and Contaminants Fluxes in the North Sea. J. Sündermann, ed. Springer-Verlag, Berlin, 654 pp.

Deryugin (Дерюгин) K.M., 1928. Fauna of the White Sea and Conditions of Its Dwelling, Issledovaniya morei SSSR, no. 7-8, Leningrad. (Фауна Белого моря и условия ее существования, Исследования морей СССР, вып. 7-8, Л., 1928, 511с.)

Dolotov Yu.S., and Lukashin, V.N., 2001. Expeditions to the White Sea on R/Vs *Ekolog* and *Kartesh* in 2000, Okeanologiya, vol. 41, no. 5, pp. 790-795.

Duvanin A.I., 1983. Interaction of the ocean and the environment. Moscow State University, (Взаимодействие океана с окружающей средой, М., МГУ, 1983).

Edwards F.J., 1987. Climate and oceanography. In Red Sea, A. J. Edwards and S. M. Head, eds. Pergamon Press, Oxford, pp. 45-69.

Elshin (Елшин Ю.А.) Yu.A., 1979. Inflow of river water into the Barents and White Seas and its oscillations in intra- and inter-annual transect. Vodnie Resursi, 2, 65-69. (Russian journal)

Emelianov M.V., 1993. Mesoscale and fine structure of the frontal zones in the Atlantic sector of the Southern Ocean. PhD Thesis, P.P. Shirshov Institute of Oceanology, Moscow: 194pp (Russian text).

Eshel G., Cane M.A. and M. Benno Blumenthal, 1994. Modes of subsurface, intermediate, and deep water renewal in the Red Sea. J. Geophys. Res., 99(C8), 15941-15952.

Fedorov K.N., 1978. Fine structure of hydrophysical fields in the ocean. In: Okeanologiya. T.1 (Oceanology. Vol.1). Moscow, Nauka Press, pp. 113-147.

Filyushkin, B.N. and Plakhin, E.A., 1995. Experimental Study of the First Stage of Mediterranean Water Lens Fonnation, Okeanologiya, , vol. 35, pp. 875-882.

Foster T.D. and Carmack E.C., 1976. Frontal zone mixing and Antarctic bottom water formation in the south Weddell Sea. Deep-Sea Research, 20, 301-317.

Frolov and Shapiro, 1982. 41 cruise of R/V Akademik Kurchatov.

Furnes G.K., 1980. Wind effects in the North Sea. J. Phys. Oceanogr., 10, 978-984.

Garrett C., 1994. The Mediterranean Sea as a climate test Basin. In Ocean Processes in Climate Dynamics: Global and Mediterranean Examples, P. Malanotte-Rizzoli and A. R. Robinson, eds. NATO/ASI Ser. Vol. 419. Kluwer Academic Publishers, Dordrecht, The Netherlands, pp. 227 237.

Georgopoulos D., Theocharis A. and Zodiatis G., 1989. Intermediate water formation in the Cretan Sea (S. Aegean Sea). Oceanol. Acta, 12(4), 353-359.

Gidrometeorologiya, 1991a. Gidrometeorologiya i gidrokhimiya morei SSSR. T II, Beloe more. (Hydrometeorology and Hydrochemistry of the Seas of the USSR. Vol.2, The White Sea), Glukhovskoi, B.Kh. Ed., St. Petersburg: Gidrometeoizdat, no.1. (Гидрометеорология и гидрохимия морей СССР, т.II, Белое море, Вып. 1, Гидрометеорологические условия, Гидрометеоиздат, 1991).

Gidrometeorologiya, 1991b. Gidrometeorologiya i gidrokhimiya morei SSSR. (Hydrometeorology and Hydrochemistry of the Seas of the USSR), Simonov, A.I. and Al'tman, E.N., Eds., Leningrad: Gidrometeoizdat, no.2.

Gill A.E., 1973. Circulation and bottom layer production in the Weddell Sea. Deep-Sea Research, 20, 111-140.

Gladyshev S., Martin S., Riser S., and Figurkin A., 2000. Dense water production on the northern Okhotsk shelves: Comparison of ship-based spring-summer observations for 1996 and 1997 with satellite observations. Journal of Geophysical Research, 105, 26281-26299.

Gordeev, V.V., 1983. Rechnoi stok v okean i cherty ego geokhimii (Riverine Runoff into the Ocean and Features of Its Geochemistry), Moscow: Nauka (Russian journal).

Gow A.J. and Tucker W.B., 1990. Sea ice in polar regions. In Polar Oceanography, Part A, Physical Science, W.O. Smith, ed. Academic Press, San Diego. Calif., 406 pp.

Gregg M.C., 1973. The microstructure of the ocean. Sci.Am., 228, 65-77.

Gregg M.C., 1976. Temperature and Salinity Microstructure in the Pacific Equatorial Undercurrent. Journal of Geophysical Research, 81, No.6, 1180-1196.

Gregg M.C. and Briscoe M.G., 1979. Internal waves, fine structure, microstructure and mixing in the ocean. Reviews of Geophysics and Space Physics, 17, 1524-1547.

Gregg M. C. and Sanford T. B., 1980. Signatures of Mixing from the Bermuda Slope, the Sargasso Sea and the Gulf Stream. Journal of Physical Oceanography, 10, 105-127.

Gustafsson B. and Stigebrandt A., 1996. Dynamics of the freshwater-influenced surface layers in the Skagerrak. J. Sea Res. 35(1-3), 39 53.

Hill, A.E., James I.D., Linden P.F., Matthews J.P., Prandle D., Simpson J.H., Gimtrowicz E.M., Smeed D.A., Lwiza K.M.M., Durazo R., Fox A.D., and Bowers D.G., 1993. Dynamics of tidal mixing fronts in the North Sea. Philos. Trans. R. Soc. London Ser. A, 343, 431-446.

Hill A.E., Horsburgh K.J., Garvine R.W., Gillibrand P.A., Slesser G., Turrell W.R., and Adams R.D., 1997. Observations of a density-driven recirculation of the Scottish Coastal Current in the Minch. Estuarine Coastal and Shelf Sciences, 45, 473-484.

Hill A.E., Souza A.J., Jones K., Simpson J.H, Shapiro G.I., McCandliss R., Wilson H. and Leftley J., 1998. The Malin Cascade in winter 1996. Journal of Marine Research, 56, 87-106.

Horsburgh K.J., Hill A.E., Brown J., 1998. A Summer Jet in the St George's Channel of the Irish Sea. Estuarine, Coastal and Shelf Science, 47, 285-294.

Horsburgh K.J., Hill A.E., Brown J., Fernand L., Garvine R.W., Angelico M.M.P., 2000. Seasonal evolution of the cold pool gyre in the western Irisha Sea. Progress in Oceanography, 46(1), 1-58.

Howland R.J.M, Pantiulin A.N., Millward G.E. and Prego R., 1999. The hydrography of the Chupa Estuary, White Sea, Russia. Estuarine, Coastal and Shelf Science, 48, 1-12.

Hunter J.R., 1986. The physical oceanography of the Arabian Gulf: a review and theoretical interpretation of previous observations. Proc. First Gulf Conference on Environment and Pollution, Kuwait, February 7-9, 1982, R. Halwagy, D. Clayton and M. Behbehani, eds. pp. 1-23.

Huntley D.A., 1980. Tides on the North-West European Continental Shelf. In The North-West European Shelf Seas: The Seabed and the Sea in Motion. II. Physical and Chemical Oceanography and Physical Resources, F. T. Banner, M. B. Collins and K. S. Maisse, eds. Elsevier, Amsterdam, pp. 301-351.

Huthnance J.M., 1995. Circulation, exchange and water masses at the ocean margin: the role of physical processes at the shelf edge. Progress in Oceanography, 35, 353-431.

Inall M.E., Shapiro G.I., and Sherwin T.J., 2001. Mass transport by non-linear internal waves on the Malin Shelf. Continental Shelf Research, 21 (13-14), 1449-1472.

Ivanov S.S. and Mikhailovsky G.E., 1996. Multifractal features of the White Sea phytoplankton annual variability. Okeanologiya, 36, 875-882.

Ivanov V.V., Shapiro G.I., Huthnance J.M., Aleynik D.L., Golovin P.N., 2003. Cascades of Dense Water Around the World Ocean. Progress in Oceanography (published).

Kelly D.E., 1984. Effective diffusivities within oceanic thermohaline staircases. Journal of Geophysical Research, 89, 10484-10488.

Kelly D.E., 1990. Fluxes through diffusive staircases: a new formulation. Journal of Geophysical Research, 95, 3365-3371.

Kinder, T.H. and Parilla G., 1987. Yes, some of the Mediterranean outflow does come from great depth. J. Geophys. Res., 92(C3), 2901-2906.

Kitani K., 1973a. An oceanographic study of the Okhotsk Sea: particularly in regard to cold waters. Bull. Far. Seas Fish. Res. Lab., 9, 45-76.

Kitani k., 1973b. On the transition layer in the Okhotsk Sea. Bull. Jpn. Soc. Fish. Oceanogr., 22, 1-9.

Klenova M.V., 1966. Barents Sea and White Sea. The Encyclopedia of Earth Sciences Series. (Fairbridge, R. W., ed.). Vol. 1. Reinhold Publishing Corporation, pp. 95-101.

Korneeva G.A. and Luneva M.V., 1999. Ecobiochemical investigation of the White Sea water. Izvestiya Akademii Nauk Seriya Biologicheskaya, 5, 592-601.

Kõuts T. and Omstedt A., 1993. Deep water exchange in the Baltic Proper. Tellus, 45A, 311-324.

Krauss W. and Brügge B., 1991. Wind-produced water exchange between the deep Basins of the Baltic Sea. J. Phys. Oceanogr., 21, 373-384.

Lacombe H. and Richez C., 1982. The regime of the Strait of Gibraltar. In Hydrodynamics of Semienclosed Seas, J. C. J. Nihoul, ed., Vol. 34. Elsevier, Amsterdam, pp. 13-71.

Latché L., 1999. Canary Eddy-Filament revealed by altimetry. MSc Thesis. School of Ocean Sciences, University of Wales, Bangor, Menai Bridge, Wales, pp.70.

Latché L., Shapiro G.I., and Pantiulin A.N., 2002. Thermohaline Intrusion in the White Sea in June 2000, 27th General Assembly of the European Geophysical Society, Nice, France (21-26 April 2002). (http://www.cosis.net/abstracts/EGS02/03437/EGS02-A-03437.pdf)

Lavin M.F., Gaxiola-Castro G., Robles J.M., and Richter K., 1995. Winter water masses and nutrients in the Gulf of California. Journal of Geophysical Research, 100, 8587-8605.

Le Traon P.Y., Gaspar P., Bouyssel F., and Makhmara H., 1995. Using TOPEX/POSEIDON data to enhance ERS-1 data. J. Atm. Ocean. Techn., 12, 161-170.

Le Traon P.Y. and Ogor F., 1998. ERS-1/2 orbit improvement using TOPEX/POSEIDON: the 2 cm challenge. J. Geoph. Res., 103, C4, 8045-8057.

Le Traon P.Y., Nadal F., and Ducet N., 1998. An improved mapping method of multi-satellite altimeter data. J. Atm. Ocean. Techn., 25, 522-534.

LeBlond P.H. and Mysak L.A., 1978. Waves in the Ocean. Elsevier, Amsterdam, 602pp.

Lednev V.A. (Леднев В.А.), 1934. Maps of the steady currents of the White Sea. (К карте постоянных течений Белого моря. Зап. по гидрографии, №2).

Lennon G.W., Bowers D.G., Nunes R.A., Scott B.D., Ali M., Boyle J., Wenju C., Herzfeld M., Johansson G., Nield S., Petrusevics P., Stephenson P., Suskin A.A., and Wijffels S.E.A., 1987. Gravity currents and the release of salt water from an inverse estuary. Nature, 327, 696-697.

Levchenko O.V. and Shcherbakov F.A., 2000. Some features of the bottom structure in the eastern part of the White Sea. Oceanology, 40 (6), 882-890.

Li L., Wimbush M., Watts D.R., and Lee T.N., 1986. Variability of thermal structure off Georgia, winter 1978. Continental Shelf Research, 6, 561-584.

Luick J.L. and Tomczak M., 1994. On the formation and spreading of the Bass Strait cascade. Continental Shelf Research, 14, 385-399.

Lukashin V.N. , Kosobokova K.N., Shevchenko V.P., Shapiro G.I., Pantulin A.N., Pertzova N.M., Savenko A.V., Deev M.G.,, Kljuvitkin A.A., Novigatsky A.N.,

Prego R., Latché L., 2003. Results of multi-disciplinary oceanographic observations in the White Sea, June 2000. Oceanology, 43(2), 237-253.

Maksimova M.P. and Bondarenko A.I., 1985. Chlorophyll in the White Sea water. Okeanologiya, 25 (5), 813-818.

Maksimova M.P., and Vladimirsky S.S., 1990. Organic-carbon and formation of Organic-matter in the gulfs of the White Sea. Okeanologiya, 30, 64-69.

Malanotte-Rizzoli P., 1991. The northern Adriatic as a prototype of convection and water mass formation on the continental shelf. In Deep Convection and Deep Water Formation in the Oceans, P. C. Chu and J. C. Gascard, eds. Elsevier, New York, pp. 229-239.

Marmorino G.O. 1987. Observations of small-scale mixing processes in the seasonal thermocline .1. salt fingering. Journal of physical oceanography. 17, p 1339-1347.

MEDOC Group, 1970. Observation of formation of deep water in the Mediterranean Sea, 1969. Nature, 227, 1037-1040.

Melling H. and Lewis E.L., 1982. Shelf drainage flows in the Beaufort Sea and the effect on the Arctic Ocean pycnocline. Deep-Sea Research, 29, 967-985.

Millward G.E., Rowley C., Sands T.K., Howland R.J.M., and Pantiulin A., 1999. Metals in the sediments and mussels of the Chupa estuary (White Sea) Russia. Estuarine Coastal and Shelf Science, 48 (1), 13-25.

Molcard R. and Williams A.J., 1975. Deep stepped structure in the Tyrrhenian sea. Mem. Soc. Roy. Sci., Liège, ser. 6, VII, 191-210.

Morcos, S.E., 1970. Physical and chemical oceanography of the Red Sea. Oceanogr. Mar. Biol. Annu. Ret, 8, 73-202.

Mordasova N.V., 1999. Chlorophyll in the White Sea. Ices Journal of Marine Science, 56, 215-218.

Nakamura T., Awaji T., Hatayama T., Akimoto K., Koho T., Kawasaki Y. and Fukasava M., 2000. The generation of large-amplitude unsteady lee waves by subinertial tidal flow: a possible vertical mixing mechanism in the Kuril Straits. J. of Phys. Oceanogr., 30, 1601-1621.

Naletova I.A. and Sapozhnikov V.V., 1993. Nutrients and production-destruction processes in the White Sea. Okeanologiya, 33 (2), 195-200.

Nansen F., 1912. Das Bodenwasser und die Abkuhlung des Meeres. Int.Rev.ges.Hydrobiol.Hydrog., Bd v, 1-42.

Nansen F., 1913. The waters of the north-eastern North Atlantic. Internationale Revue der Gesamten Hydrobiologie und Hydrographi, 4, 139.

Navrotsky V.V., 1999. Mixing caused by internal waves and turbulence: a comparative analysis. Journal of Marine Systems, 21(1-4), 131-145.

Neal V.T., Neshyba S. and Denner W., 1969. Thermal stratification in the Arctic Ocean. Science, 166, 373-4. (p. 270).

Nekrasov A.V. (Некрсов А. В), 1975. Tidal wave in Shelf seas. Gidrometeoizdat, Leningrad, 245p. (Приливные волны в окраинных морях. –Л.: Гидрометеоиздат, 1975. -245с.)

Oguz T. and Rozman L., 1991. Characteristics of the Mediterranean underflow in the southwestern Black Sea continental shelf/slope region. Oceanologica Acta, 14, 433-444.

Ohtani K. and Azumaya T., 1995. Interannual change of the sea conditions on the continental shelf and its itilluence on abundance of walleye Pollock in the eastern Bering Sea. Can. J. Fish. Aquat. Scii., spec. publ.

Otto L., Zimmerman J.T.F., Furnes G.K., Mork M., Saetre R. and Becker G., 1990. Review of the physical oceanography of the North Sea. Neth. J. Sea Res.. 26(2), 161-238.

Ovchinnikov I.M., 1984. The formation of intermediate water in the Mediterranean sea. Oceanology, 24, 168-173.

Özsoy E., Ünlüata Ü., and Top Z., 1993. The evolution of the Mediterranean water in the Black Sea: interior mixing and material transport by double diffusive intrusions. Progress in Oceanography, 31, 275-320.

Pantiulin A.N., 1974. Some features of the water structure in the White Sea. Tr.Belomorskoi biologicheskoi stantsii MGU (Moscow: Mosk. Gos. Univ.), no.4, 7-13. (Некоторые особенности структуры вод белого моря. Биология Белого моря, Труды Беломорской биологической станции МГУ, Т.4, М., МГУ, 7-13).

Pantiulin A.N., 1990. On the Formation and Variability of the Water Structure in the White Sea. Biological Resources of the White Sea, (Biologicheskie resursy Belogo moray) Matekin, P.V., Ed., Moscow: Moscow State University, pp.9-16. (О формировании и изменчивости структуры вод Белого моря. Биологические ресурсы Белого моря:, М. 1990, с.9-16).

Pertzova N.M. and Kosobokova K.N., 2002a. Interannual Changes in the Biomass and Distribution of Zooplankton in Kandalaksha Bay of the White Sea, Okeanologiya, 42 (2), 1-9.

Pertzova N.M. and Kosobokova K.N., 2002b. Zooplankton of the White Sea. History of Investigations and the Present State of Knowledge-A Review, Berichte zur Polarforschung, 359, 30-41.

Pfirman S.L, Eicken H., Bauch D. and Weeks W.F. 1995. The potential transport of pollutants by Arctic seas. Science of the Total Environment, 159, 129-146.

Pices Working Group 1, 1995. The Okhotsk Sea and Oyashio Region. In PICES Sci. Rep. 2, L.D. Talley and Y. Nagata, eds. Sidney Columbia, Canada, 227 pp.

Pingree R.D., 1972. Mixing in the deep stratified ocean. Deep-Sea Res., 19 (8), 549-561.

Pond S. and Pickard G.L., 1983. Introductory Dynamical Oceanography. 2nd Edition, Butterworth Heinemann, Oxford, 329pp.

Prandle D., 1982. The vertical structure of tidal currents. Geophys. Astr. Fluid Dyn., 22, 29-49.

Prell W.L., 1984. Variation of monsoonal upwelling: a response to changing solar radiation: climate processes and climate sensitivity. Geophys. Monogr., 29, 48-57.

Prell W.L. and Van Campo E., 1986. Coherent response of Arabian Sea upwelling and pollen transport to late Quaternary monsoonal winds. Nature, 323, 526 528.

Prell W.L. and Kutzbach J.E., 1987. Monsoon variability over the past 150,000 years. J. Geophys. Res., 92, 8411-8425.

Quadfasel D., Rudels B., and Hirz K., 1988. Outflow of dense water from a Svalbord fjord into Fram Strait. Deep-Sea Research, 35, 1143-1150.

Richardson P.L., 1980. Gulf Stream Ring Trajectories. Journal of Physical Oceanography, 10, 90-104.

Royer T.C., 1981. Baroclinic transport on the Gulf of Alaska. II. Fresh water driven coastal current. Journal of Marine Research, 39, 251-266.

Royer T. C., 1982. Observations of the Alaska Coastal Current. In Coastal Oceanography, H- G- Gade, A. Edwards and H. Svendsen, eds. Plenum Press, New York- pp. 9-30.

Ruddick B.R. and Turner J.S., 1979. The vertical length scale of double-diffusive intrusions. Deep Sea research, 26 (8A), 903-914.

Ruddick B., 1983. A practical indicator of the stability of the water column to double-diffusive acting. Deep Sea Research, 30 (10A), 1105-1107.

Rudnick D.L. and Ferrari R., 1999. Compensation of horizontal temperature and salinity gradients in the ocean mixed layers. Science, 283, 526-529.

Savenko A.V., 2001. Hydrochemical Structure of the Mouth Areas of Minor Rivers Flowing into Kandalaksha Bay of the White Sea. Okeanologiya, 41 (6), 835-843.

Savinov V.M., Savinova T.N., Carroll J., Matishov G.G., Dahle S., and Naes K., 2000. Polycyclic aromatic hydrocarbons (PAHs) in sediments of the White Sea, Russia. Marine Pollution Bulletin, 40, 807-818.

SBE, 2000. Sea-Bird Electronic software and manual (March 2000) for SEACAT SBE 19 CTD profilers. (http://www.seabird.com)

Schmitt R.W., 1994. Double diffusion in oceanography. Annual Review of Fluid Mechanics, 26, 255-285.

Semenov E. V. and Luneva M. V. 1996. Numerical Simulation of Tidal and Thermohaline Circulation of the Waters of the White Sea., Izvestiya Akademii Nauk Fizika Atmosfery I Okeana (News of Russian Academic of Sciences – Physics of Atmosphere and Ocean), 32 (5), 704-713.

Semenov E. V. and Luneva M. V. 1999. Combined Effect of Tide, Stratification, and Vertical Turbulent Mixing on the formation of Hydrophysical Fields in the White Sea. Izvestiya Akademii Nauk Fizika Atmosfery I Okeana (News of Russian Academic of Sciences – Physics of Atmosphere and Ocean), 35 (5), 660-678.

Shapiro G.I. and Emel'yanov M.V, 1989. Mesoscale Structure of the Hydrophysical Fields in the Region of Intensive Crill Fishery and Its Relation to the Hydrochemical and Hydrobiological Characteristics of the Waters, Antarktika, Moscow: Nauka, 28, 121-136.

Shapiro G.I. and Meschanov S.L., 1991. Distribution and spreading of Red Sea Water and salt lens formation in the northwest Indian Ocean. Deep-Sea Res., 38(l), 21-34.

Shapiro G.I and Emelianov M.V., 1994. The mesoscale and fine structure water characteristics relationship in the Antarctic polar front zone. Okeanologica, 34(2), 206-211.

Shapiro G.I and Meschanov S.L., 1996. Spreading pattern and mesoscale structure of Mediterranean outflow in the Iberian Basin estimated from historical data. J. Mar. Sys., 7, 337-348.

Shapiro G.I, Meschanov S.L. and Emelianov M.V., 1996. Mediterranean lens "Irving" after its collision with seamounts. Oceanol. Acta, 18(3), 309-318.

Shapiro G.I and Hill A.E., 1997. Dynamics of dense water cascades at the shelf edge. Journal of Physical Oceanography, 27, 2381-2394.

Shapiro G.I., Shevchenko V.P., Lisitsyn A.P., Serebryany A.N., Politova N.V., and Akivis T.M., 2000. Influence of internal waves on the suspended sediment distribution in the Pechora Sea. Doklady Earth Sciences, 373, 899-901.

Shapiro G.I. and Hill A.E., 2003. The alternative density structures of cold/salt water pools on a sloping bottom: the role of friction. J. Phys. Oceanogr., 33 (2), 390-406.

Shapiro G.I., Latché L., Pantiulin A.N., 2003. Mixing processes in the Gorlo Strait of the White Sea. Oceanology, 43(1), 26-31. In Geophysical Research Abstracts, Vol. 5, 14781, EGS-AGU-EUG Joint Assembly, Nice, France, 06-11 April 2003. (http://www.cosis.net/abstracts/EAE03/14781/EAE03-J-14781.pdf).

Shapiro G.I., Huthnance J.M., and Ivanov V.V., 2004. Dense water cascading off the continental shelf. J. Geophysical Research, 108, C12, Art. No.3390.

Simpson J.H., and Bowers D., 1981. Models of the stratification and frontal movements in shelfs seas. Deep See Res., 28A(7), 727-738.

Simpson J.H., 1997. Tidal processes in shelf seas. In The Sea, 10, the Global Coastal Ocean: Processes and Methods, K.H. Brink and A.R. Robinson, eds. Wiley, New York, Chap. 5.

Smirnov N.A., Fedorov V.V., and Fedorov V.D., 1989. Functional ecological description of seasonal development of the White Sea phytoplankton. Zhurnal Obshchei Biologii, 50 (3), 353-365.

SMIS-IKI-RAN : Space Monitoring Information Support laboratory (SMIS) of the Space Research Institute (IKI RAN) (http://smis.iki.rssi.ru).

Stern M.E., 1960. The 'salt-fountain' and thermohaline convection. Tellus, 12, 172-175.

Stommel H., and Fedorov K.N., 1967. Small-scale structure in Temperature and Salinity near Timor and Mindanao. Tellus, 19, N2, 306-325.

Stommel H.M., 1993. A conjectural regulating mechanism for determining the thermohaline structure of the oceanic mixed layer. Journal of Physical Oceanography, 23(1), 142-148.

Sukhovey V.F. (Суховей В.Ф.), 1986. Seas of the World Ocean, Leningrad, Hydrometeoizdat. (Моря Мирового Океана. Ленинград Гидрометеоиздат).

Timonov V.V., 1947. Schematic of the General Water Circulation in the Basins of the White and the Barents Seas and Origin of Its Abyssal Waters, Trudy GOIN, no. 1 (13), pp. 118-131. (Схема общей циркуляцин Бассейна Белого моря и происхождение его глубинных вод. «Тр. ГОИН», вып. 1(13)).

Timonov V.V, 1950. Principal Features of the Hydrological Regime of the White Sea. Pamyati Yu. M Shokal,'Fkogo, (Yu.M. Shokal'skii in Memoriam), Moscow, pp.206-235. (Главные Особенности Гидрологического режима Белого моря. В сб.: «Памяти Ю. М. Шокальского», ч. 2. М. (Moscow)).

Tomczak M., 1985. The Bass Strait water cascade during winter 1981. Continental Shelf Research, 4, 225-278.

Tomczak M., 1987. The Bass Strait water cascade during summer 1981-1982. Continental Shelf Research, 7, 561-572.

Turner J.S. and Stommel H., 1964. A new case of convection in the presence of combined vertical salinity and temperature gradients. Proceeding of National Academy of Science, 52, 49-53.

Turner J.S., 1973. Buoyancy Effects in Fluids. Cambridge University Press, Cambridge, 367pp.

UNESCO, Tenth Report of the Joint Panel on Oceanography Tables and Standards (1981). UNESCO Technical Papers in Marine Science, No.36, p.24. (Contains the definitions of the PSS 78 and IES 80).

Vlasenko V., Stashchuk N., and Hutter K., 2002. Water exchange in fjords induced by tidally generated internal lee waves. Dynamics of Atmospheres and Oceans, 35, 63-89.

Watanabe K., 1963. On the reinforcement drift of the East Sakhalin current preceding the ice season off the coast of Hokkaido: study in sea ice in the Okhotsk Sea (IV). Oceanogr. Mag., 14, 117-130.

Watanabe T. and Wakatsuchi M., 1998. Formation of 26.8-26.9 water in the Kuril Basin of the Sea of Okhotsk, as a possible origin of the North Pacific Intermediate Water. J. Geophys. Res., 103, C2, 2848-2865.

Whitehead J.A., 1987. Dense water off continents. Nature, 327, 656.

Woods J.D., 1980. The generation of thermohaline fine structure at fronts in the ocean. Ocean Modeling, 32, 1-4.

Yakushev E.V. and Mikhailovsky G.E., 1993. Modelling of the chemico-biological cycles in the White Sea – Calculations of Nitrogen, Phosphorus and Oxygen annual variability. Okeanologiya, 33 (5), 695-702.

Yakushev E.V. and Mikhailovsky G.E., 1994. Modelling of the chemico-biological cycles in the White Sea – The Carbon-dioxide annual variability calculations. Okeanologiya, 34 (2), 240-247.

Yasuoka T., 1967. Hydrography in the Okhotsk Sea. Oceanogr. Mag., 19, 61-72.

Yasuoka T., 1968. Hydrography in the Okhotsk Sea. Oceanogr. Mag., 20, 55-63.

Yemel'yanov M.V. and Fedorov K.N., 1985. Structure and transformation of intermediate waters of the Mediterranean Sea and Atlantic Ocean. Oceanology, Engl. transl., 25, v.2, 155-161.

Zhurbas V.M. and Ozmidov R.V., 1983. Production of stepped fine structure of the ocean by thermohaline intrusions. Izv. AN SSSR. Fiz. Atmosf. i okeana, 19, No.12, 1295-1302.

Zhurbas V.M. and Ozmidov R.V., 1987. Forms of stepped structures in the ocean thermocline and mechanisms of their generation. Okeanologiya, 24(2), 197-203.

Zhurbas V.M. and Lips U.K., 1987. Discrimination of main Types of Thermohaline Fine Structure in the Ocean, Oceanography, 27(4), 416-420.

Zoccolotti L. and Salusti E., 1987. Observations of a vein of very dense marine water in the southern Adriatic Sea. Continental Shelf Research, 7, 535-551.

Zore-Armanda M., 1969. Water exchange between the Adriatic and the eastern Mediterranean. Deep Sea Res., 16, 171-178.

## RELEVANT PUBLICATIONS

Lukashin V.N. , Kosobokova K.N., Shevchenko V.P., Shapiro G.I., Pantulin A.N., Pertzova N.M., Savenko A.V., Deev M.G.,, Kljuvitkin A.A., Novigatsky A.N., Prego R., Latché L., 2003. Results of multi-disciplinary oceanographic observations in the White Sea, June 2000. Oceanology, 43(2), 237-253.

Shapiro G.I., Latché L., Pantiulin A.N., 2003. Mixing processes in the Gorlo Strait of the White Sea. Oceanology, 43(1), 26-31.

Oceanology, Vol. 43, No. 2, 2003, pp. 224–239. Translated from Okeanologiya, Vol. 43, No. 2, 2003, pp. 237–253.


MARINE GEOLOGY

# Results of Multidisciplinary Oceanographic Studies in the White Sea in June 2000

V. N. Lukashin[1], K. N. Kosobokova[1], V. P. Shevchenko[1], G. I. Shapiro[1,4], A. N. Pantyulin[2], N. M. Pertzova[2], M. G. Deev[2], A. A. Klyuvitkin[1], A. N. Novigatskii[1], K. A. Solov'ev[2], R. Prego[3], L. Latche[4]

[1] *Shirshov Institute of Oceanology, Russian Academy of Sciences, Moscow, Russia*
[2] *Moscow State University, Moscow, Russia*
[3] *Institute for Marine Research, Vigo, Spain*
[4] *Institute for Marine Research, Plymouth University, UK*

Received April 12, 2002

**Abstract**—Multidisciplinary oceanographic studies of the White Sea were carried out in the regions of the Gorlo, of the Basin, and of Kandalaksha Bay including the estuaries of the Niva, Kolvitsa, and Knyazhaya rivers. The hydrographic survey revealed long-living stepwise structures and inversions in the vertical profiles of temperature and salinity formed due to the tidal mixing of saline and cold Barents Sea waters and warmer White Sea waters in the Gorlo area. The biological studies revealed the principal features of the distribution, abundance, and species composition of phyto- and zooplankton in all the areas studied. They showed the tolerance of the principal zooplankton species to desalination in the estuaries. The studies of the suspended matter in the estuaries clearly demonstrated physical and chemical transformations of the matter supplied by the rivers. The data on the vertical particle flux in the deep-water part of Kandalaksha Bay showed the difference between the subsurface layer and the near-bottom layer, which could result from the sinking of the products of the spring phytoplankton bloom and from the supply of the suspended terrigenous matter from the nepheloid layer formed by the tidal currents.

## INTRODUCTION

Multidisciplinary oceanographic studies of the White Sea represent an important task at the present-day stage of the development of marine sciences. This inland sea of Russia is the most reachable for the studies; nevertheless, it is almost unknown from the systematic point of view. Due to the multiyear efforts of the scientists of Moscow State University (MSU) and the Zoological Institute, Russian Academy of Sciences, implementing both in marine expeditions and at the *Pertzov* and *Kartesh* White Sea biological stations [1, 13–25, 31, 33–35], as well as to the research performed by the All-Union and Polar institutes for marine fishery and oceanography [7, 28], the information on the hydrological parameters and the biological structure of the sea is the most abundant. Also available are the results of the geological studies performed by the scientists from All-Union Geological Institute and from the Laboratory for Shelf Studies of the Shirshov Institute of Oceanology, Russian Academy of Sciences (IORAS), aimed at the examination of the geological structure of the seafloor and its sedimentary cover [11, 12]. Along with this, one can state a significant deficit in the knowledge on the interrelations between the hydrophysical, biological, and geochemical processes in the White Sea and their role in the formation of the sediment fluxes toward the floor; on the riverine discharge of the sedimentary matter, its substantial and chemical composition, and the transformation of the matter supplied by the rivers; and on the hydrophysical, biological, and geochemical processes in the zone of mixing between the riverine and marine waters.

At the end of the 1990s, the Russian scientific community developed a series of national and international projects concerning system studies of the White Sea (INTAS 94-391, INTAS 96-1359, INTAS 97-1881, ICA2-CT-2000–10053, White Sea System-2000, and others). This paper presents the results of the studies implemented within the framework of the INTAS 97-1881 project from June 15 to 24, 2000, in the White Sea from aboard the R/V *Kartesh* by the IORAS together with the Geographical and Biological Faculties of MSU and Plymouth University (UK).

The objective of the project was a multidisciplinary study of the mesoscale hydrophysical, biogeochemical, and biological processes in the region of the Gorlo, in the deep-water part of the White Sea and in the zone of the marginal filter, and in the estuaries of the minor rivers flowing into Kandalaksha Bay. On the basis of the hydrophysical, biological, and sedimentation properties, we studied the mesoscale and fine structure of the water masses, the interaction between the deep-water and shallow-water areas, the vertical matter fluxes in these regions, the substantial and chemical composition

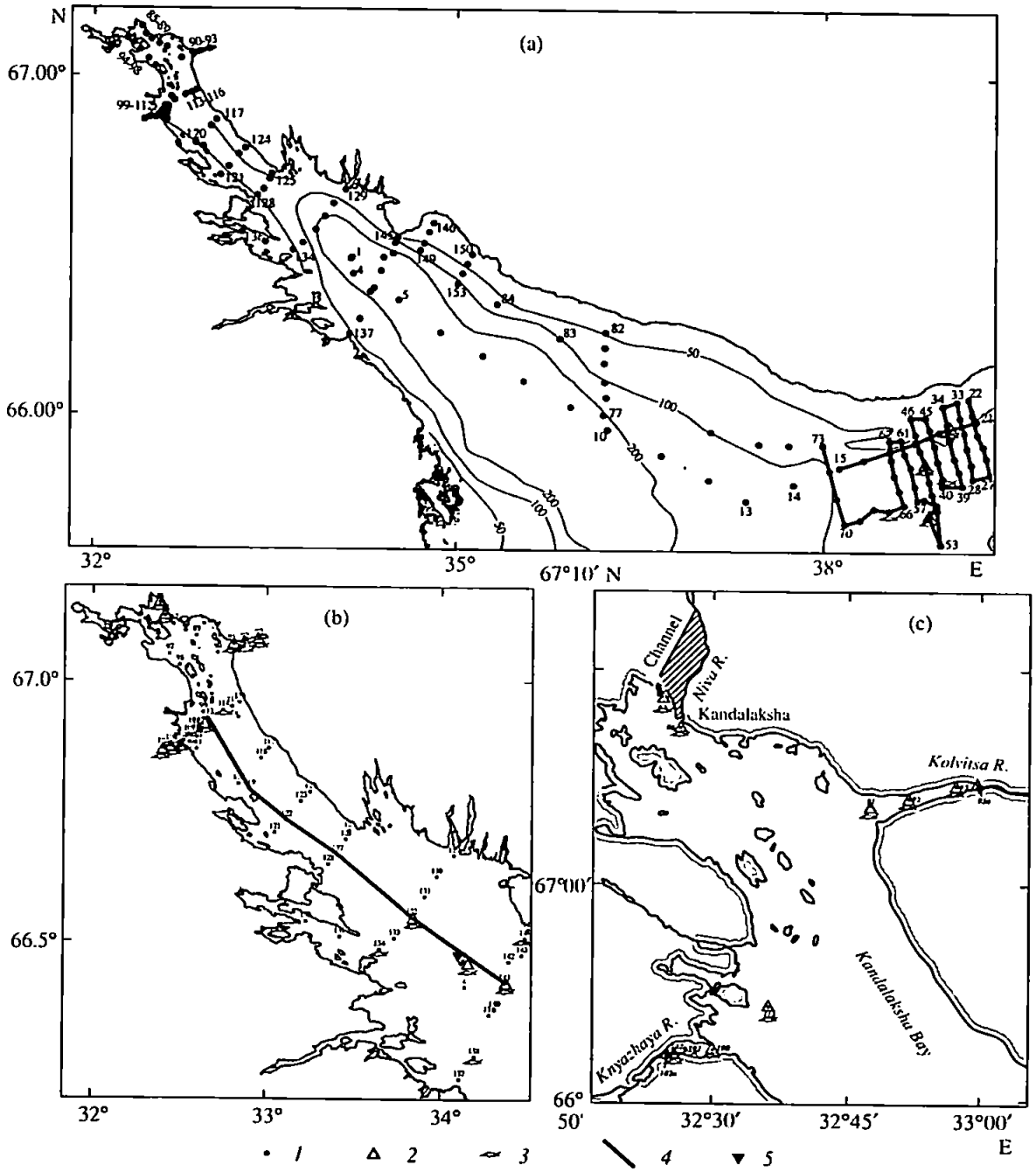


Fig. 1. Schematic of the station location. (a) Northwestern part of the White Sea; (b) location of the cross section along Kandalaksha Bay; and (c) near-mouth regions. (*1*) CTD probings; (*2*) water suspension sampling; (*3*) plankton net hauls; (*4*) cross section location; and (*5*) location of the station with sediment traps.

of the matter, and the processes of interaction between the riverine and marine waters in the estuaries of the minor rivers flowing into Kandalaksha Bay. The studies were implemented through the measurements of temperature, salinity, current velocity and direction, hydrochemical parameters, composition and distribution of phyto- and zooplankton, and the degree of transformation of the sedimentary matter delivered by the rivers. We examined the factors determining the features of the distribution and mutual interaction between different components of phyto- and zooplankton and estimated the contribution of biota to the production of biomass

and to the sedimentation process. The studies were also aimed at assessment of the upper layer of the bottom sediments.

## MATERIALS AND METHODS

The studies were performed in the northern part of the White Sea within three principal regions: (1) west of the Gorlo of the White Sea, (2) in the deep-water part of Kandalaksha Bay and in the basin off the Terskii Coast, and (3) in the estuaries of three minor rivers (the Niva, Kolvitsa, and Knyazhaya rivers) flowing into Kandalaksha Bay (Fig.1). On the whole, 154 stations were observed including 153 stations with CTD probing with a SBE 19 probe (Sea-Bird Electronics). At 25 stations, in parallel with the hydrological observations, we determined dissolved oxygen concentrations and pH values in situ with the help of a HI.9142 portable oximeter (Hanna) and Ekotest-110 ionometer. In total, 150 determinations were implemented at characteristic levels with regard to the vertical distribution of the hydrological parameters. At 18 stations located in the estuaries of the minor rivers of Kandalaksha Bay, in addition to the standard hydrochemical determinations ($O_2$ and pH), we collected water samples with a 30-l plastic bottle sampler with their subsequent preservation in order to study the features of migration of chemical elements (Si, P, Sr, Ca, F, and B) in the zones of mixing between the reservoir and marine waters [27].

Temperature and salinity measurements were performed from a drifting vessel; in order to check the identification of the fine structure of the water masses, profiles were recorded at both the probe sinking and surfacing. Signal processing was implemented following the technique suggested by M.F. Frolov and G.I. Shapiro with corrections in the readings of the pressure gauge; this allowed us to improve the vertical resolution of the temperature and salinity profiles from 1 to 0.4 m.

At anchor stations, we measured the current velocities and directions with a VALEPORT impeller with remote recording of the readings. In Kolvitsa Inlet, a half-day-long station with current measurements at 8 levels was observed.

The suspended matter samples were collected from the plastic water bottle samplers from various levels. About 150 samples were obtained by filtering through nuclear screens 47 mm in diameter with a pore size of 0.45 μm; about 75 samples were obtained by filtering through GF/F glass fiber screens 47 mm in diameter. In addition, 50 samples of filtrate were taken for determination of heavy metal concentrations.

Phytoplankton samples were collected from the bottle samplers from the levels where suspended matter samples were also taken. The samples were preserved in a 0.1% formalin solution. On the whole, 59 samples at 13 stations were collected. The processing of non-concentrated samples (50 ml in volume) and the counting of mass forms of phytoplankton <20 μm in size were performed in a Fuchs–Rosenthal chamber over two weeks after their acquisition. Then, the samples were fixed in a 1% formalin solution for subsequent concentrating and counting of large (>20 μm) and low-abundant forms.

The zooplankton samples were collected with a Juday net with an opening of 37 cm and a gauze filtering cone with a mesh size of 180 μm by layer-by-layer vertical hauls in the water column from the surface to the bottom. The sampling levels were chosen with regard to the data on the vertical water structure acquired in the course of the hydrophysical probing. The samples were preserved in a 4% formalin solution. In total, 74 zooplankton samples at 22 stations were collected.

In order to study the vertical fluxes of the sedimentary matter in the deep-water part of Kandalaksha Bay at a point with a sea depth of 320 m, we installed a mooring station supplied with minor sediment traps. The exposure equaled to 7.83 days. The samples were fixed in a 2% formalin solution.

The samples of the bottom sediments (upper layer of the sediments 0–1 cm) were collected with a grab sampler in the river estuaries and in the central part of Kandalaksha Bay. The sediments were described, then dried at a temperature of 60°C and packed for the subsequent processing at the land laboratory.

## RESULTS

### *Hydrophysical Studies*

The hydrophysical studies off the Terskii Coast, in the deep-water part of the Basin, and in Kandalaksha Bay of the White Sea showed a wide development of stepwise and inverse structures in the vertical distributions of temperature and salinity. At a significant part of the stations, different numbers of steps (from one to five) 3–20 m thick were observed in the profiles of a single or both characteristics mentioned (Figs. 2a–2d). Another feature consists of the breaks in the vertical distribution plots recorded at a series of stations. The most complicated distribution of structural combinations was observed in a test area in the Gorlo region, which represents the principal area of their formation. Here, we recognized the following types of vertical distribution: (1) uniform down to the bottom deep-water layer covered by warmer and desalinated surface waters, (2) distributions with monotonic changes in the characteristics, (3) two- and three-step structures, and (4) structures with a temperature inversion. This kind of diversity is formed as a result of intensive tidal mixing and complicated interlayering between the transformed saline and cold waters of the Barents Sea penetrating from the north and the less dense desalinated warmer waters of the White Sea supplied from the south.

In the open part of the sea, in the intermediate layer 20–90 m, thick stepwise structures are observed (from one to three structures at each of the stations) with a

horizontal extension up to 400 km (Fig. 3d). They are separated by water layers with enhanced vertical gradients of both temperature and salinity. The two thickest layers (hatched in Fig. 3d) have dome-shaped outlines corresponding to the principal cyclonic gyre in the basin. The temperature distribution observed in the western part of the basin indicates the possibility of sinking (cascading) of the mixed waters over the slope from depths of 80–100 to 180–200 m. Although additional studies are required to recover the true mechanism of the cascading, one can expect that it has an advective–gravitational origin, similar to that of the process of the slipping down of the dense waters over the northwestern shelf of Europe [32]. In the 0- to 20-m subsurface layer, we often observed less stable interlayers of mixed waters 3–5 m thick, which are best manifested in salinity profiles (Fig. 2d). The depths of the upper and lower boundaries of the mixed layers are irregular. This is caused, first, by the variability of the process of the formation of stepwise structures and, second, by the variability of the advection mechanism; probably, the presence of inertial oscillations also plays its part. As one can see from Fig. 3d, the stepwise structures are mainly formed in the shallow-water part of the Gorlo where homogeneous layers attain the shape of vertical columns forming sharp surface temperature fronts. This kind of fronts is not manifested in satellite images due to the screening effect of the warm surface waters. A similar phenomenon was observed in the Scotia Sea in the Antarctic [29]

We managed to resolve the mesoscale water structure due to the dense network of stations in a minor test area in the northern part of the Gorlo, where the intensity of the subsurface fronts reached 0.6°C per 10 km. From the fact that, in the direction from the basin toward the Gorlo region, the interlayers of the mixed intermediate waters continuously transfer to quasi-homogeneous volumes of the near-bottom waters, one can suggest that the protection mechanism of their formation is related to the turbulent mixing induced by strong tidal currents and bottom friction. This process, as well as the water advection from the Gorlo region to the deep-water part of the sea, proceeds most intensively during the spring tide periods, when the velocities of the tidal currents are two- to threefold greater than those during the neap tides; the horizontal displacements of the water masses over a tidal cycle are correspondingly greater. Therefore, the tidal "plunger" operates more efficiently providing the basin with recurrent portions of water.

The hydrological survey of Kandalaksha Bay showed a high degree of desalination of the entire water basin. The salinity of the subsurface layer gradually increased from 8‰ in the top part of the bay up to 23‰ at its seaward boundary. The vertical temperature structure in the deep-water part of the basin manifests no signs of a cold intermediate layer; this suggests a mild preceding winter in the White Sea (Figs. 3a, 3b). At a series of stations stepwise structures were observed,

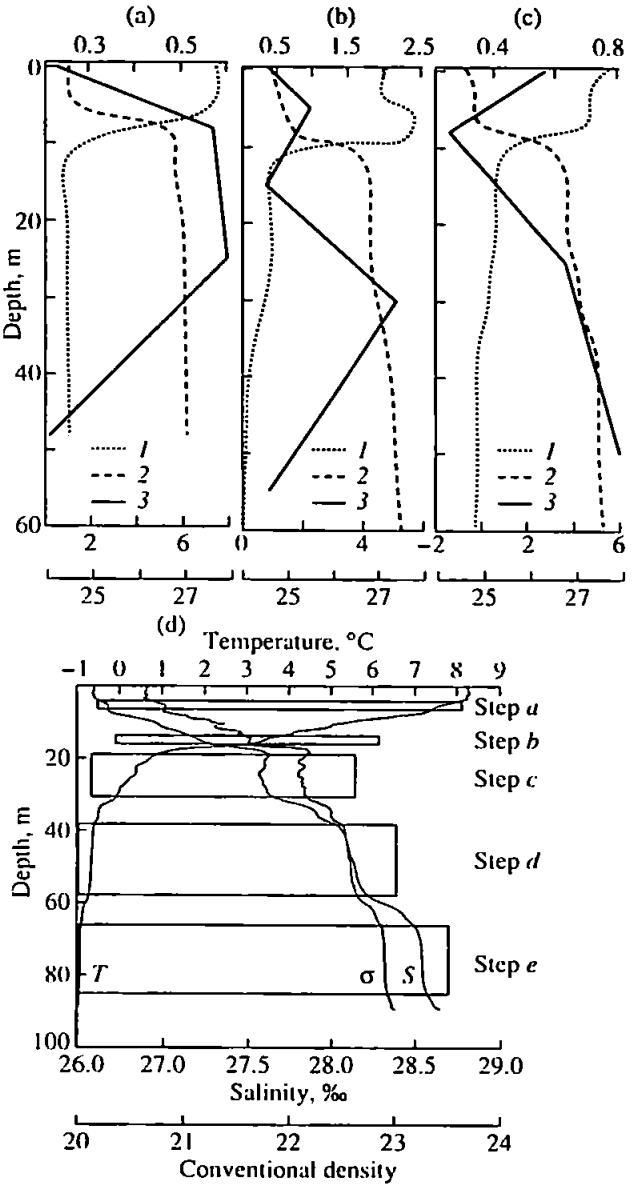


Fig. 2. Distributions of temperature ($T$, °C), salinity ($S$, ‰) and suspended matter concentrations (mg/l) at stations (a) 20, (b) 49, (c) 54 in the Gorlo region, and (d) fine structure profiles at station 14 in the deep-water part of the basin. (*1*) Temperature, (*2*) salinity, and (*3*) suspended matter concentration.

including those located in the near-bottom layer. This allows one to suppose that the stepwise features could be of a local origin; they might be generated by the tidal mixing over swells, banks, and steep slopes.

The observations in the estuaries of the Kolvitsa and Knyazhaya rivers showed strong two-layered circulations accompanied by the entrainment effects at the boundary between the currents. The velocities of the sink surface current in the top part of the estuary of the

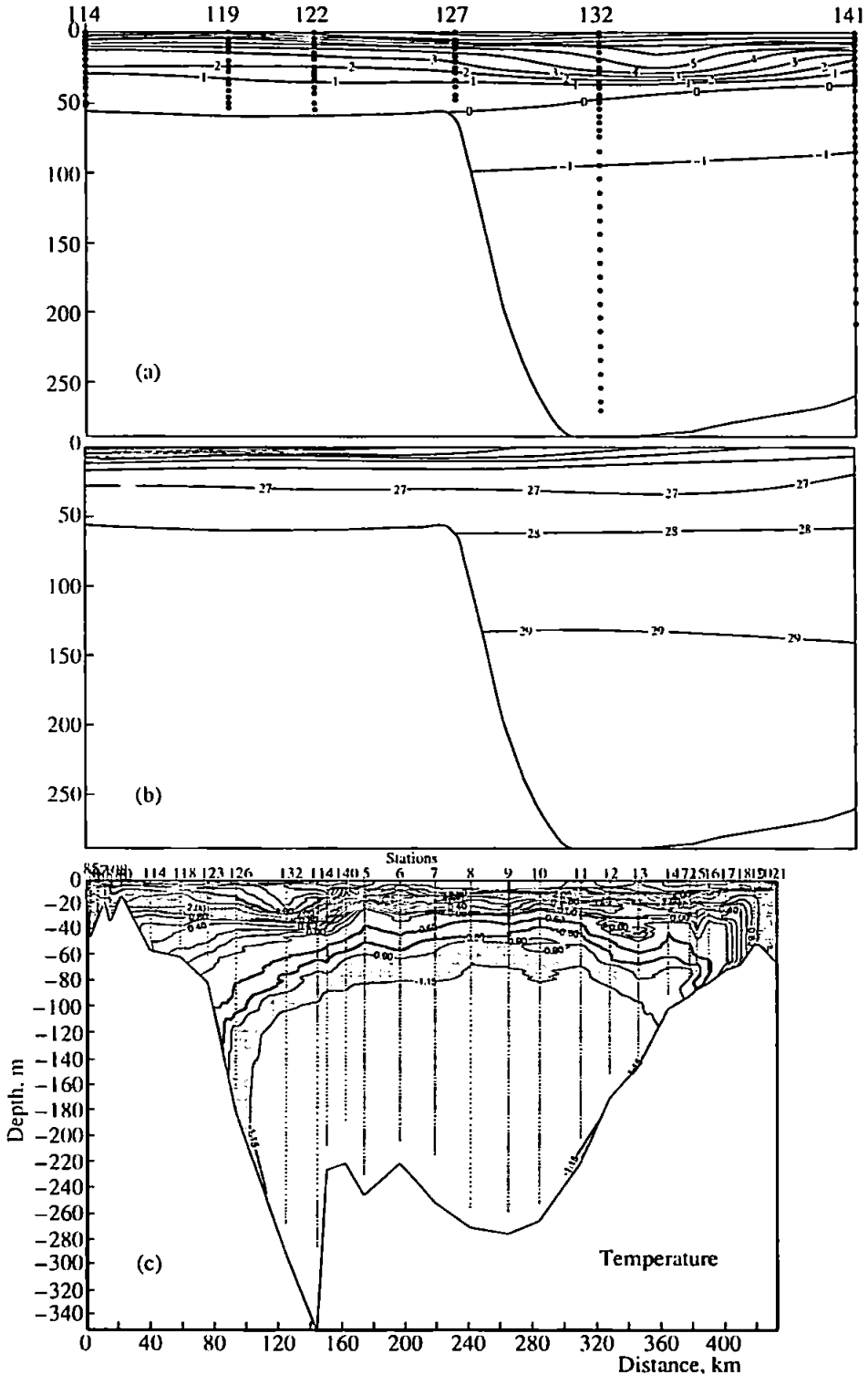


Fig. 3. Distributions of (a) temperature, *T*, °C, (b) salinity, *S*, ‰, in the axial section along Kandalaksha Bay, and (c) temperature distribution over the longitudinal profile Kandalaksha–Gorlo. Two of the three quasihomogeneous interlayers observed at the intermediate level and one of two in the subsurface layer are hatched.

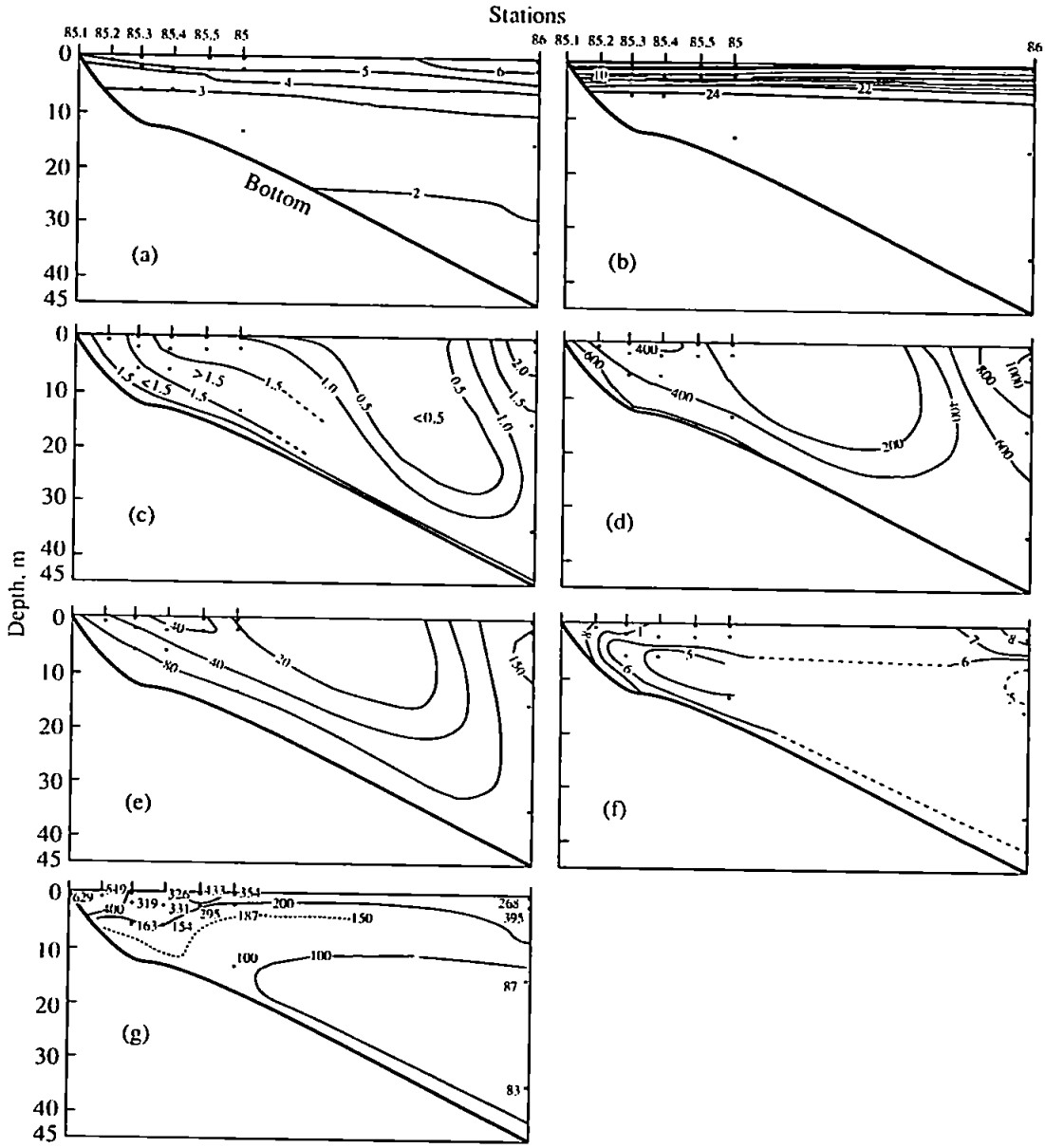


Fig. 4. Distributions of (a) temperature ($T$, °C), (b) salinity ($S$, ‰), concentrations of (c) suspended matter (mg/l), (d) Si (μg/l), and (e) Al (μg/l), (f) Si : Al ratio, and (g) $C_{org}$ concentrations (μg/l) in the Niva River estuary.

Knyazhaya River reached 90 cm/s; at a depth of 4 m, the current was replaced by an oppositely directed one with a maximum velocity of 20 cm/s. At the exit from the estuary, a small-scale surface was performed; it showed that the desalinated waters spread in the form of a train rather than as a compact jet.

In the estuary of the Kolvitsa River, the thickness of the desalinated surface layer was 1.2 m and the velocity of the sink current at the surface reached 16 cm/s. Its replacement by a backward current occurred at a depth of 2.5 m. The hydrological structure in the Kolvitsa River estuary was three-layered. The warm and desalinated surface layer 2 m thick was underlain by a layer with temperature and salinity distributions similar to those in the swell region representing the zone of the influence of the compensational current arriving from the sea. At depths of 20–25 m, the pycnocline is located; deeper begins the water layer of the estuary basin with $T = -0.8$°C and $S = 28.2$‰. The above difference of the deep water temperature in situ from the freezing point suggests a more complicated process of its formation rather than a high degree of its transfor-

mation. This process seems to be more complicated than simple winter vertical convection with salination from ice generation.

### *Hydrochemical Studies*

The studies performed in the estuaries of the minor rivers of the Kandalaksha Bay catchment (the Niva, Kolvitsa, and Knyazhaya rivers) allowed A.V. Savenko to recognize the nonconservative behavior of phosphates and silicon [27]. Both in the riverine waters and at the seaward boundary of the mixing zone, phosphate concentrations are low and comprise 0.006–0.010 and 0.003 mg P/l, respectively. Therefore, the removal of the main amounts of $PO_4^{3-}$ occurs as early as in the zone of the riverine water domination. The maximum phosphate removal determined from the maximum deviations of the observed data from the conservative behavior trend is noted at a chloride concentration of 3.5 g/l. In contrast to phosphates, dissolved silicon is most intensively absorbed in the zone of the predominance of marine waters. The maximum removal of dissolved silicon observed at chloride concentrations of about 9 g/l depends directly on the silicon concentrations in the mouths of the Niva, Kolvitsa, and Knyazhaya rivers—1.0, 2.2, and 1.7 mg/l, respectively.

On the contrary, the behavior of strontium, potassium, fluorine, and boron in the estuaries of the rivers studied follows conservative mixing laws. Under a chloride concentration change from 0.02–0.06 to 15 g/l, a linear increase in the strontium and potassium concentrations takes place. At the transition from the riverine to marine waters, the value of the Sr : Ca weight ratio remains approximately the same, equal to 0.02–0.03, which suggests a similar ability of strontium and potassium to accumulate in the waters with an elevated mineralization.

With the growth of the chloride content, the fluorine and boron concentrations in the estuaries of the Niva, Kolvitsa, and Knyazhaya rivers also linearly increase. At the transition from the riverine to marine waters, the F : Cl and B : Cl ratios monotonically decrease; their changes are most significant at the initial stage of the mixing between the riverine and marine waters, and the ratios reach constant values at chloride concentrations greater than 3 g/l [27].

### *Biological Studies*

The composition of both phyto- and zooplankton in the three regions studied—west of the Gorlo, in the central deep-water part of the sea, and in the estuary zone—was noticeably different. According to the data by T.N. Rat'kova, in terms of both biomass and abundance, phytoplankton was dominated by small flagellates; however, active bloom was noted only in the Gorlo region. The diatoms of this region were dominated by *Sceletonema costatum*, a mass form of the summer period typical of eutrophicated waters. Zooplankton was poor in terms of abundance (mean abundance value over the water column of 2000 ind./m$^3$). Juveniles of the mass Arctic copepod *Calanus glacialis* (nauplii and copepodites I–III) dominated its composition together with the Arctic–boreal species *Pseudocalanus minutus*.

In the central deep-water region we noted bloom of the flagellate alga *Phaeocystis* sp. Zooplankton was dominated by the species of the Arctic assemblage—copepods *C. glacialis* (represented by two generations), *Metridia longa, P. minutus*, and chaetognath *Sagitta elegans*. The vertical distribution of the zooplankton abundance was typical of the spring period with a clearly expressed maximum near the surface (>25000 ind./m$^3$ in the layer 0–10 m) and a sharp drop in the deeper layers (down to 40 ind./m$^3$ in the layer 200–300 m). A rather high biomass value and a distinct separation of different generations of *C. glacialis* over the water column were noted. In the surface layer 0–10 m, juveniles (nauplii and copepodites I–III) were abundant, while the individuals of the overwintered generation (copepodites V–VI) had already descended down to depths greater than 50 m.

In all of the three estuaries studied, we noted the bloom of the flagellate algae *Phaeocystis* sp., while diatoms were dominated by pennate forms. The composi-

**Table 1.** Percentage of freshwater, euryhaline, and marine species in the total abundance of zooplankton (ind./m$^3$) in the estuary of the Knyazhaya River, Kandalaksha Bay of the White Sea

| Station no. | Station 102 | Station 101 | | Station 100 | | |
|---|---|---|---|---|---|---|
| Date | June 21, 2000 | June 21, 2000 | | June 21, 2000 | | |
| Sea depth, m | 7 | 22 | | 25 | | |
| Layer, m | 0–6 | 0–6 | 6–20 | 0–3 | 3–10 | 10–22 |
| Salinity | 5.68–7.55 | 7.74–22.9 | 23.0–26.9 | 4.86 | 22.8 | 27.6 |
| Total abundance, ind./m$^3$ | 26880 | 47460 | 18464 | 3992 | 13740 | 9363 |
| Freshwater (%) | 17.7 | 0.7 | 0.7 | 27.8 | 0 | 0 |
| Euryhaline (%) | 7.0 | 4.2 | 3.7 | 29.2 | 1.5 | 0.03 |
| Marine (%) | 75.3 | 95.0 | 95.0 | 43.0 | 98.5 | 99.97 |

**Table 2.** Percentage of freshwater, euryhaline, and marine species in the total abundance of zooplankton (ind./m$^3$) in the estuary of the Niva River, Kandalaksha Bay of the White Sea

| Station no. | Station 85 | | | Station 86 | | |
|---|---|---|---|---|---|---|
| Date | June 19, 2000 | | | June 20, 2000 | | |
| Sea depth, m | 18 | | | 45 | | |
| Layer, m | 0–3 | 3–8 | 8–14 | 0–3 | 3–25 | 25–40 |
| Salinity | 6.65–21.0 | >21.0 | 26.8 | >1.23 | 2.0–27.0 | 27.0–27.2 |
| Total abundance, ind./m$^3$ | 1893 | 28716 | 28438 | 11128 | 5508 | 4333 |
| Freshwater (%) | 18.1 | 0.007 | 0 | 8.3 | 2.1 | 0.03 |
| Euryhaline (%) | 4.6 | 1.04 | 0.03 | 16.9 | 4.1 | 2.7 |
| Marine (%) | 77.3 | 98.9 | 99.97 | 74.8 | 93.8 | 97.27 |

tion and distribution of zooplankton occurred to be rather diverse. At a series of stations in the estuaries of the Niva and Knyazhaya rivers (stations 85, 100; Tables 1, 2), in the desalinated surface layer 0–3 or 0–6 m at a salinity of 1.2–6.5‰, we observed both freshwater (*Bosmina coregoni, Sida crystallina, Linocalanus glimaldii*, Cyclopoida, Rotatoria) and euryhaline species resistant to strong desalination (*Podon leukarti, Evadne nordmanii, Acartia longiremis, A. bifilosa, Centropages hamatus*, and *Derjuginia tolli*). However, both in this layer and beneath it, common marine neritic species *Pseudocalanus minutus, Oithona similis, Metridia longa, Calanus glacialis, Sagitta elegans, Microsetella norvegica*, and others dominated in terms of both species number and abundance of planktonic organisms. Among the latter, *P. minutus* dominated (up to 63% of the total zooplankton abundance). The presence of freshwater species in the upper desalinated layer at these stations undoubtedly implied a significant influence of the freshwater runoff; meanwhile, the total zooplankton abundance in this layer was usually extremely low. In deeper layers, due to the sharp salinity increase up to 21–27‰, freshwater species were almost completely absent and only marine species were encountered. The abundance of zooplankton in these layers increased by a factor of 40–150 due to the occurrence of marine forms, which suggests an intensive inflow of marine waters in the lower layers reaching even the innermost parts of the estuaries (see Tables 1, 2). The general character of the distribution and composition of zooplankton was quite similar to that described by M.E. Vinogradov *et al.* [2] in the waters of the Yenisei River estuary, where they observed a distinct separation of the upper desalinated riverine layer from the lower marine layer with a relatively high salinity. The plankton of the brackish-water assemblage inhabiting the desalinated surface waters of the Yenisei estuary was also poor in abundance; in the deeper more saline waters, the plankton biomass was significantly higher due to the presence of marine species.

In addition, in the estuaries of the Niva and Knyazhaya rivers, we discovered one more type of zooplankton distribution. Thus, at stations 86, 101, and 102, in spite of the strong desalination of the surface layer, the maximum zooplankton abundance was observed precisely near the surface. In so doing, freshwater and euryhaline species in the surface layer were not abundant, while the abundance of marine species reached high values (see Tables 1, 2). The features of the vertical distribution of abundance were similar to those in the open part of Kandalaksha Bay with a maximum at the surface and subsequent decrease with depth. Most probably, in this kind of small estuary, the zooplankton distribution and its species composition are determined not only by the degree of the surface water desalination and the salinity gradient value in the upper layer but also by the direction and intensity of the dominating currents. Probably, a certain role belongs to the tidal currents as well. In the region of stations 86, 101, and 102, the influence of the marine water inflow during our studies seemed to be stronger than that of the freshwater runoff. The great number of marine forms at all of the stations and their high abundance even in the desalinated surface layer shows that the impact of marine waters on the biota of the estuaries of the minor rivers of Kandalaksha Bay is generally very significant. This also implies that a number of marine species are resistant to strong desalination and easily withstand a salinity drop down to 6–8‰.

The estuary of the Kolvitsa River, representing a bucket-shaped inlet with a maximum depth of 75 m and a swell at a depth of 20 m at its boundary with Kandalaksha Bay, is somewhat different from the two above-described estuaries in the zooplankton composition. Despite the significant desalination of the surface 8- to 10-m layer, at three stations performed in this estuary, no freshwater species were observed; brackish-water species composed from 11 to 81.3%, while the rest of the plankton was represented by marine forms (Table 3). At all of these three stations, the absolute abundance values of euryhaline species were very close ranging from 3125 to 4550 ind./m$^3$; however, due to the

**Table 3.** Percentage of freshwater, euryhaline, and marine species in the total abundance of zooplankton (ind./m$^3$) in the estuary of the Kolvitsa River, Kandalaksha Bay of the White Sea

| Station no. | Station 93 | | Station 92 | | | Station 91 | | |
|---|---|---|---|---|---|---|---|---|
| Date | June 21, 2000 | | June 20, 2000 | | | June 20, 2000 | | |
| Sea depth, m | 25 | | 65 | | | 36 | | |
| Layer, m | 0–8 | 8–22 | 0–10 | 10–28 | 26–55 | 0–10 | 10–25 | 25–34 |
| Salinity | 0.5–17.5 | 17.9–28.2 | 4.9–16.8 | 23.0–28.6 | >28.6 | 15.9–19.9 | 20.0–27.8 | >27.8 |
| Total abundance, ind./m$^3$ | 28396 | 8864 | 10188 | 5526 | 1272 | 5349 | 4455 | 3842 |
| Freshwater (%) | 0 | 0 | 0 | 0 | 0 | 0 | 0 | 0 |
| Euryhaline (%) | 11.0 | 0.02 | 44.7 | 4.5 | 0.05 | 81.3 | 3.0 | 3.5 |
| Marine (%) | 89.0 | 99.98 | 55.3 | 95.5 | 99.95 | 18.7 | 97.0 | 96.5 |

changes in the percentage of marine species, their proportion in the plankton of the surface 0- to 10-m layer increased from the inner part of the estuary toward its periphery. With regard to the composition of marine species, age composition of their populations, and character of their vertical distribution, the Kolvitsa estuary was quite similar to Kandalaksha basin. At all of the stations in the estuary, the maximum zooplankton abundance was observed in the surface layer, gradually decreasing with depth.

On the whole, in all three estuaries, a very high zooplankton abundance was observed. In the estuaries of the Kolvitsa, Niva, and Knyazhaya rivers its value averaged over the entire water column ranged from 4180 to 16000, from 5490 to 22420, and from 11650 to 26 950 ind./m$^3$, respectively. The maximum abundance was confined to the stations closest to the river mouths, while toward the outer parts of the estuaries it gradually decreased. From the three estuaries studied, the richest in terms of abundance was the Knyazhaya Inlet.

### *Geological Studies*

The geological research included the studies of the suspended matter in the mixing zones of the minor rivers flowing into Kandalaksha Bay (the Niva, Kolvitsa, and Knyazhaya rivers) and over a longitudinal profile in the central part of the bay and of the studies of the sedimentary matter fluxes and bottom sediments in its deep-water part. In this part of the White Sea, especially in the estuaries of the minor rivers, neither suspended matter and its composition nor vertical particle fluxes has been studied to date; therefore, the data presented here are pioneering.

Figures 4–6 show the cross sections of distribution of temperature, salinity, and concentrations of suspended matter and selected chemical elements (Si, Al, and $C_{org}$) over profiles running from the mouth areas of the rivers of Kandalaksha Bay. The coldest water was observed in the estuary of the Niva River; here, the surface water temperature was 4.5–6°C. In the estuaries of the Kolvitsa and Knyazhaya rivers, the water is warmer; its temperature reaches 7–8°C. The gradients of the temperature changes with depth are not great, and the position of the jump layer is defined by the distribution of salinity. The salinity data allow one to realize the water structure in the estuaries and the character of the zone of mixing between the riverine and marine waters. For example, in the Niva estuary, the salinity change from <2 up to 24‰ occurs within a layer less than 5 m thick; the respective values for the Kolvitsa and Knyazhaya rivers are 10 and 12 m. These data suggest a high intensity of the fresh water supply. It is known that the strongest transformation of the riverine matter supplied the seas is confined to the salinity range from 2 to 10‰, which is favorable for the flocculation of the matter delivered by the rivers and for colloid coagulation [4, 8, 9, 31, 38]. This salinity range is observed in the upper part of the jump layer at small (less than 1.5 km) distances from the mouths.

The estuaries under consideration are characterized by extremely small concentrations of suspended matter (less than 1.5 mg/l) in the river parts of the mixing zones (see Figs. 4–6). The principal reason for this lies in the low suspended matter concentrations in the rivers flowing into the White Sea from Karelia and Kola Peninsula. Their runoffs are controlled by the Niva hydroelectric power station, Lake Kolvitsa, and the reservoir of Knyazhaya Inlet. These rivers, as well as all the others, are characterized by a reduction in the surface suspended matter concentration with distance from the mouth down to <0.5 mg/l. In the cross section off the Niva River, this regularity is broken by a fourfold concentration increase at the terminal station of the section (station 86). This seems to be caused by the riverine water runoff of the second channel of the Niva River (see Fig. 4b), which has a great length and catchment area and therefore supplies greater amounts of suspended matter. In the water column of all the rivers, an

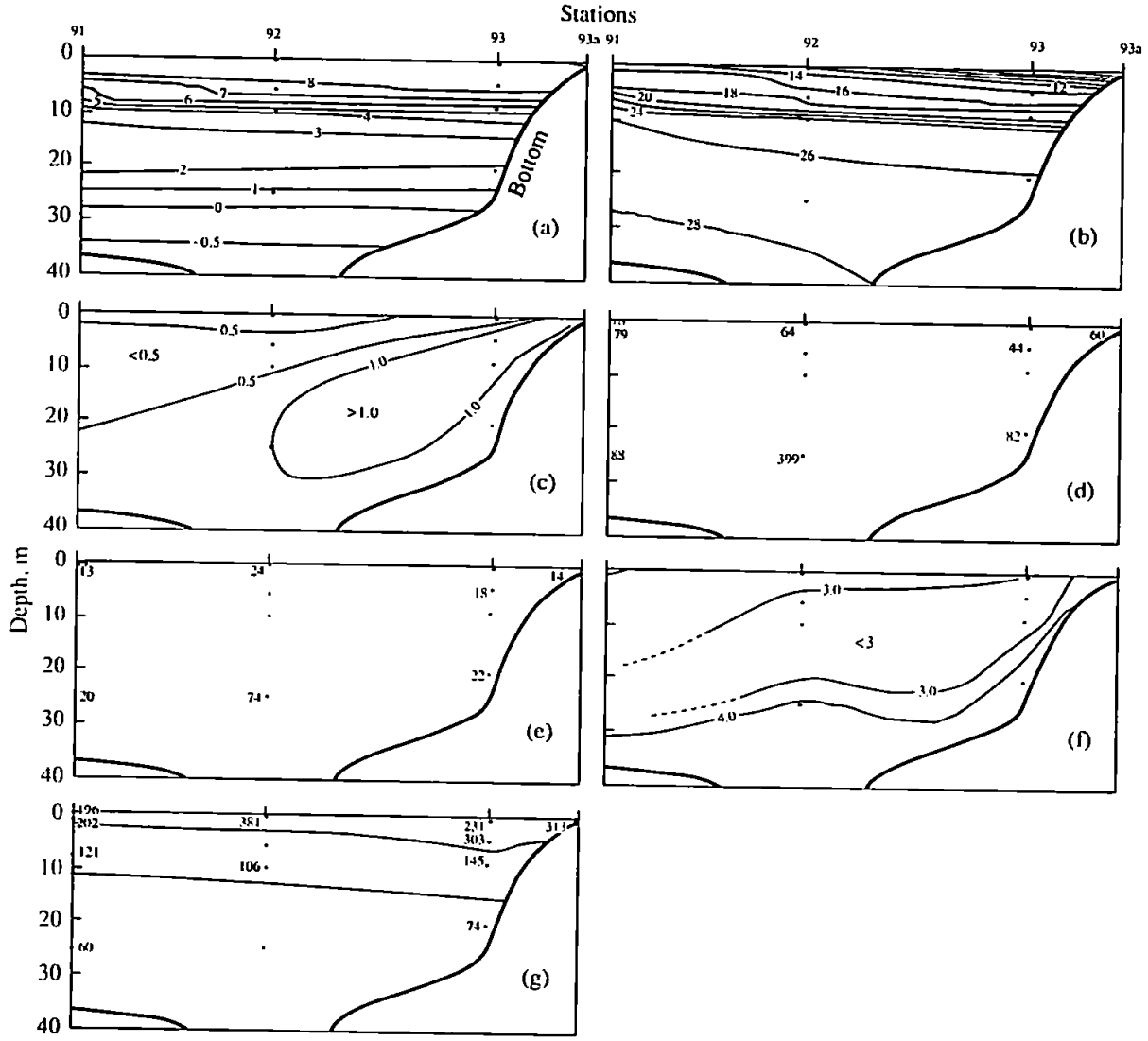


Fig. 5. Distributions of (a) temperature ($T$, °C), (b) salinity ($S$, ‰), concentrations of (c) suspended matter (mg/l), (d) Si (μg/l), and (e) Al (μg/l), (f) Si : Al ratio, and (g) $C_{org}$ concentrations (μg/l) in the Kolvitza River estuary.

inclined layer with enhanced concentrations is observed extending seaward from the mouth areas. In this layer, suspended matter concentrations are higher than in the overlying and underlying waters; they are also greater than those in the freshwater parts of the estuaries. The concentration increase starts in the region of the salinity growth from 2‰; this is especially well manifested in the cross section from the mouth of the Knyazhaya River (Fig. 6c). Undoubtedly, the formation of this layer is related to the processes of transformation of the riverine matter at the river–sea barrier.

The data on the distribution of the chemical elements composing the bulk of the suspended matter (Si, Al, and $C_{org}$) also point to the transformation of the matter. The most representative data were acquired in the Niva estuary (Figs. 4d–4g). In Fig. 4d, the silicon distribution features high concentrations in the upper layers adjacent to the near-mouth parts of the estuaries of both river channels; this peak is caused by the presence of great amounts of diatoms (see above). The concentrations fall with distance from the mouths and with depth. The concentrations of aluminum, which serves as a marker of terrigenous and autigenous matter in estuaries [38], grow with depth (Fig. 4e). The values of the Si : Al ratio decrease with depth; its minimum values are confined to the layer of enhanced suspended matter concentrations (Fig. 4f). Beneath this layer, the values of Si : Al increase slightly; this is likely to be related to the resuspension of the bottom sediments resulting in the growth of the concentrations of both Si

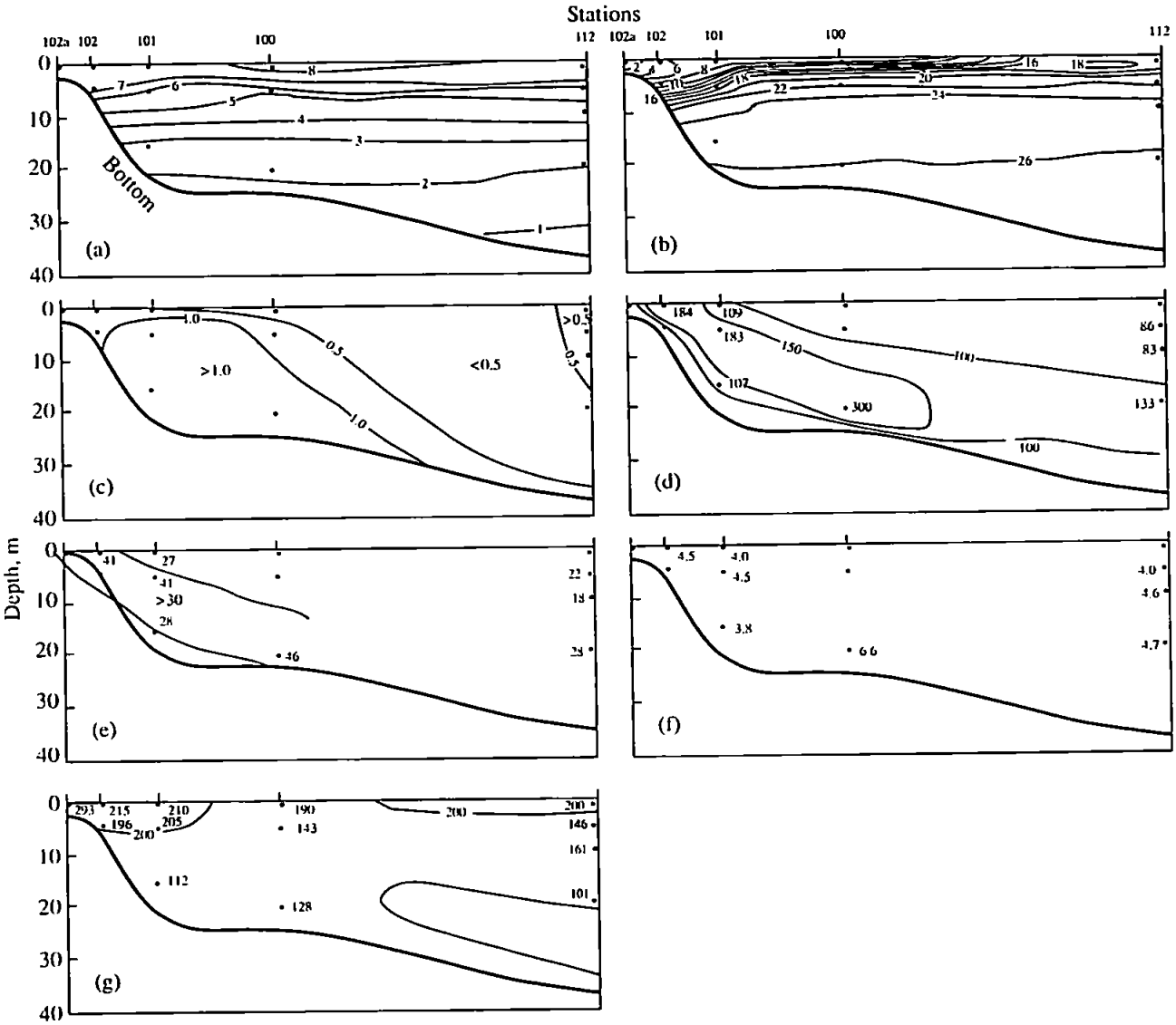


Fig. 6. Distributions of (a) temperature (*T*, °C), (b) salinity (*S*, ‰), concentrations of (c) suspended matter (mg/l), (d) Si (μg/l), (e) Al (μg/l), (f) Si : Al ratio, and (g) $C_{org}$ concentrations (μg/l) in the Knyazhaya River estuary.

and Al. For the Kolvitsa estuary, the information on Si and Al is nominal (Figs. 5d–5f); nevertheless, judging from the values shown in the sections, one can also expect a slight growth in their concentrations. The regularities in the distribution of the chemical element concentrations are similar for all of the rivers. The values of the Si : Al ratio decrease in the layer of the enhanced suspended matter concentrations and increase in the near-bottom layer due to the turbidization of the bottom sediments.

In the surface layer (down to 5 m) of the near-mouth parts of all of the rivers, the concentrations of organic carbon are also high (Figs. 4g–6g); they fall with the distance from the mouth and with depth. Here, the high concentrations of $C_{org}$ are caused by the development of diatoms and flagellates; in so doing, about one-third of $C_{org}$ is provided by diatoms. The organic carbon concentrations in the near-mouth areas of other rivers are lower, though the features of its distribution are the same. Here, flagellates are mostly encountered.

Thus, the materials obtained show that, in the estuarine parts of the minor rivers of Kandalaksha Bay under consideration, one can clearly recognize the results of the physicochemical processes of transformation of the matter supplied by the rivers; this is manifested in the increase of the suspended matter concentrations with salinity changes due to coagulation of the colloids of the clay minerals delivered by the rivers and, partly, of

**Table 4.** Concentrations of suspended matter and suspended chemical elements at stations in the Gorlo region

| Station no. | Coordinates | | Sea depth, m | Level, m | Suspended matter concentration, mg/l | Chemical elements, μg/l | | | | | | | |
|---|---|---|---|---|---|---|---|---|---|---|---|---|---|
| | latitude, N | longitude, E | | | | $C_{org}$ | N | C : N | P | Si | Al | $Si_{am}$ | Terrigenous matter |
| 20 | 66°57.63′ | 39°02.78′ | 55 | 0 | 1.05 ± 0.45 | 164 | 25.4 | 7.5 | 1.9 | 54 | 9.2 | 25.4 | 107 |
| | | | | 8 | 0.93 ± 0.27 | 216 | 32.0 | 7.9 | 4.7 | 223 | 25.8 | 144.0 | 300 |
| | | | | 25 | 1.3 ± 0.30 | 102 | 13.4 | 8.9 | 2.9 | 293 | 63.4 | 99.4 | 739 |
| | | | | 50 | 1.0 ± 0.20 | 96 | 12.0 | 9.3 | 2.5 | 253 | 56.6 | 80.7 | 660 |
| 49 | 65°52.50′ | 38°52.00′ | 65 | 0 | 1.23 ± 0.23 | 447 | 73.9 | 7.1 | 5.0 | 279 | 32.6 | 179.9 | 380 |
| | | | | 5 | 2.11 ± 1.72 | 498 | 75.4 | 7.7 | 1.4 | 84 | 8.8 | 57.7 | 102 |
| | | | | 15 | 0.68 ± 0.18 | 125 | 18.5 | 7.8 | nd | 136 | 34.1 | 31.7 | 397 |
| | | | | 30 | 0.80 ± 0.10 | 76 | 10.6 | 8.3 | 2.2 | 212 | 49.9 | 59.4 | 582 |
| | | | | 55 | 0.56 ± 0.15 | 77 | 8.8 | 10.2 | 1.2 | 123 | 22.5 | 54.3 | 263 |
| 54 | 65°42.43′ | 38°52.26′ | 60 | 0 | 1.3 ± 0.40 | 537 | 80.1 | 7.8 | 3.4 | 339 | 77.4 | 102.5 | 902 |
| | | | | 8 | 2.0 ± 0.70 | 476 | 72.4 | 7.7 | nd | nd | nd | nd | nd |
| | | | | 15 | 1.03 ± 0.30 | 195 | 28.2 | 8.1 | nd | nd | nd | nd | nd |
| | | | | 25 | 1.35 ± 0.53 | 105 | 14.3 | 8.6 | nd | nd | nd | nd | nd |
| | | | | 50 | 1.48 ± 0.44 | 169 | 19.4 | 10.1 | nd | nd | nd | nd | nd |

**Table 5.** Concentrations of the principal chemical elements in the materials of sediment traps and the vertical fluxes of the sediment-forming components

| Chemical element | Concentrations, % | | Sediment-forming components | Fluxes, mg $m^{-2}$ $day^{-1}$ | |
|---|---|---|---|---|---|
| | 55 m | 270 m | | 55 m | 270 m |
| $C_{org}$ | 6.85 | 6.4 | Organic matter | 85.2 | 136.1 |
| $C_{carb}$ | 1.14 | 0.68 | $CaCO_3$ | 59.1 | 60.6 |
| Si | 30.06 | 29.1 | $SO_{2am}$ | 337.7 | 469.1 |
| Al | 1.54 | 2.78 | Terrigenous matter | 111.6 | 344.3 |
| Si : Al | 19.5 | 10.5 | Total | 593.6 | 1010.1 |
| $C_{org}$/P (at.) | 111 | 83 | Bulk flux | 622 | 1063 |

the organic matter. This process is favored by the small concentrations of the terrigenous suspended matter driven by the rivers due to the controlled runoff of them.

The data on the distribution of temperature, salinity, and concentration of suspended matter and chemical elements in its composition over a cross section along Kandalaksha Bay are presented in Table 4 and in Fig. 7. They show that, in the seaward direction, the temperature in the surface layer decreases, while its salinity increases. A certain distortion of the relatively even distribution of these characteristics was observed at station 3, which was performed a week before the other stations of the section. At this station, we noted a growth in the concentrations of suspended matter, silicon, aluminum, and organic carbon, which can be related to the diatom bloom at the time of the observations. The suspended matter distribution is characterized by a growth of concentrations with depth, which may be caused by the sinking of the suspended matter formed during the spring phytoplankton bloom to the deeper layers and by the delivery of the suspended matter formed by the resuspension of the bottom sediments by tidal currents to the deep-water part of the bay. This is confirmed by the data on the sediment fluxes in the deep-water part of the bay obtained at station 2, located in the vicinity of station 3 (Table 5).

In the southern part of the Gorlo of the White Sea, suspended matter was collected at three stations. The sedimentary matter concentration at station 20 closest to the shore is characterized by a relatively even distri-

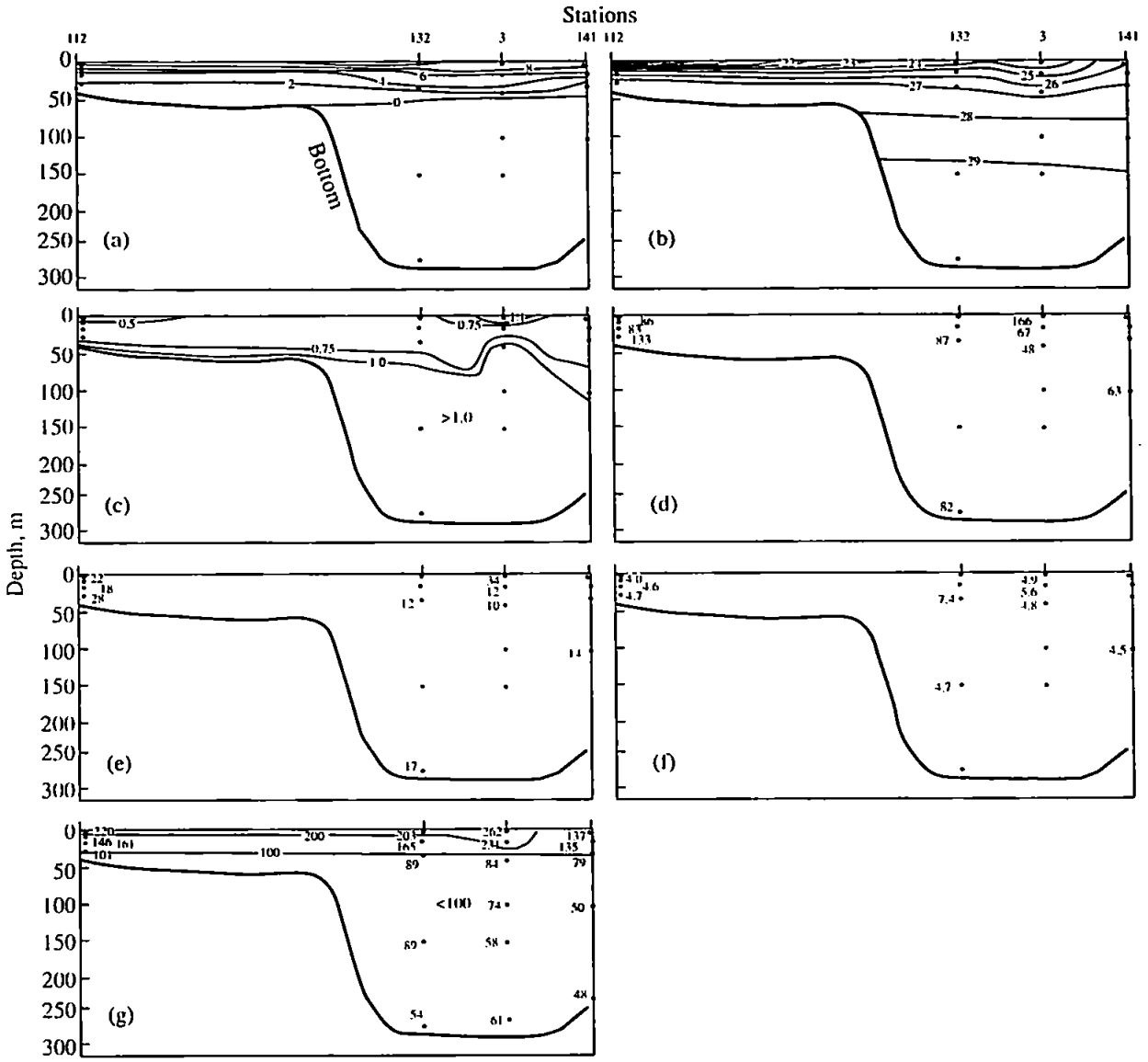


Fig. 7. Distributions of (a) temperature (*T*, °C), (b) salinity (*S*, ‰), concentrations of (c) suspended matter (mg/l), (d) Si (μg/l), (e) Al (μg/l), (f) Si : Al ratio, and (g) $C_{org}$ concentrations (μg/l) in the axial cross section along Kandalaksha Bay.

bution curve (see Fig. 2a) free from significant deviations. At station 49 located in the central part of the Gorlo, we observed elevated concentrations in the upper mixed layer with a maximum in the jump layer; deeper, the concentrations decrease and reach their minimum near the bottom (see Fig. 2b). At station 54 (in the central part of the Gorlo) the suspended matter concentrations are maximum in the density jump layer, then they decrease, and grow again in the near-bottom layer (Fig. 2c). The distribution of chemical elements shows (Table 4) an enrichment of the upper mixed layer in organic carbon and silicon; judging from the values of the silicon-to-aluminum ratio, a significant part of the silicon is related to the diatom plankton. Beneath the jump layer, both the $C_{org}$ concentrations and atomic C : N ratio increases at all of the stations; this implies a partial destruction of organic matter. Beneath the jump layer, the concentrations of Si at station 20 increase, while at station 49 they decrease; however, at both of the stations, the values of the Si : Al ratio fall with depth. This suggests that the principal silicon carriers are terrigenous alumosilicates. The increase with depth in the suspended matter concentration, especially in its terrigenous component, at stations 20 and 54 seems to point to a supply of the suspended matter entrained

from the bottom and delivered by the Barents Sea water over the Gorlo swell.

An examination of the particle fluxes showed that the overall flux values are surprisingly high as compared to the data obtained in the Barents and Kara seas [37]. In Table 5 we present the concentrations of chemical elements and the fluxes of the sediment-forming components of the matter precipitating within the water column. Among the chemical elements, the highest concentrations belong to silicon; those of organic carbon, calcium carbonate, and aluminum are significantly lower; while the phosphorus concentrations are two orders of magnitude smaller. The Si : Al ratios show that the precipitating matter is dominated by the biogenic silica derived from the diatom plankton rather than by the silicate silica. In the lower layer (270 m), the concentrations of all the elements except for Al are lower than in the upper layer. The atomic C : P ratio at a depth of 55 m is close to the value characteristic of plankton [36], while in the deeper layers it decreases. Commonly, the values of this ratio increase with depth since phosphorus refers to the most labile components of organic matter. The increase of this ratio in the deep layer probably suggests an additional delivery of inorganic phosphorus to the suspended matter due to its sorption over the clayey matter and Fe hydroxides, as was reported for the sedimentary fluxes in the Norwegian Sea [9].

The fluxes of the sediment-forming components are calculated from the concentrations of chemical elements, which provide the values of concentrations of the sediment-forming components, and from the values of the total fluxes. The content of organic matter was determined by multiplying the $C_{org}$ concentration by a factor of 2 [38]. The content of the diatom opal was estimated by the terrigenous matrix technique from the Si : Al value characteristic of the terrigenous matter. The suspended terrigenous matter consists mostly of clayey matter, and the ratio between the elements cited in the continental clays equals 3.05 [26]. Thus, the content of the terrigenous Si in the matter should be equal to the content of Al multiplied by 3.05, while the content of the siliceous (diatom) Si may be evaluated as total Si minus terrigenous Si. The content of the terrigenous matter is determined as the Al concentration multiplied by a factor of 11.65, which is obtained from the aluminum content in platform clays [26].

The data on the calculated fluxes of sediment-forming components show that the values for the 270-m level are higher than those for the 55-m level for almost all of the components. The carbonate flux values were close to each other and occurred to be the least; presumably, this was caused by the low amount of carbonate-concentrating organisms in the White Sea [1]. The fluxes of organic matter and amorphous silica equally increase (approximately 1.5-fold) which seems to imply one and the same group of planktonic carriers of these components. The elevated fluxes at the lowermost level are caused by the diatom bloom at the beginning of the exposure (see above). The increase in the terrigenous flux is especially great at the lower level (more than threefold), which results, similarly to the case of suspended matter, from the supply of the entrained matter of the bottom sediments to the basin.

In Table 6 we present the structure of the matter fluxes and the estimates of the percentages of their biogenic (organic matter, silica of the diatoms, and calcium carbonate) and terrigenous components. From the table, one can see that the compositions of the matter in the fluxes at both of the levels are close to one another. A twofold increase is noted only for the terrigenous matter at the lower level.

The upper layer of the bottom sediments (0–1 cm) collected in the estuarine zones of the Niva and Kolvitsa rivers is represented by oxidized silty–clayey ooze with a minor admixture of fine-grained sand. In the estuary of the Knyazhaya River, beneath the mainstream of the flow, fine-grained sand is encountered, while in the seaward part of the estuary, silty–clayey ooze is sampled. In the central part of Kandalaksha Bay, the sediments are clayey with an admixture of fine-grained sand covered with a fine oxidized layer less than 0.3 cm thick.

## CONCLUSIONS

The presence of long-living stepwise and inversive structures in the vertical distributions of temperature and salinity were for the first time established in the deep-water part of the White Sea and in Kandalaksha Bay. These structures seem to be formed in the region of the Gorlo due to intensive tidal mixing and complicated interlayering between transformed cold saline waters of the Barents Sea penetrating from the north and desalinated warmer White Sea waters supplied from the south. Subsequently, these structures propagate into the White Sea over a distance of about 400 km. The intermittency of the layers with respect to

**Table 6.** Structure of the matter fluxes in the deep-water part of Kandalaksha Bay

| Station no., depth | Level, m | OM, % | $SiO_{2am}$, % | $CaCO_3$, % | Terrigenous matter, % |
|---|---|---|---|---|---|
| 3 | 55 | 13.7 | 53.3 | 9.5 | 22.2 |
| 320 m | 270 | 12.8 | 40.9 | 5.7 | 39.8 |

the vertical is probably caused by the enhanced degree of turbulent mixing in shallow-water areas in the spring tide periods. In the estuaries of the minor rivers of Kandalaksha Bay, strong two-layered circulations were recognized: sink surface currents of desalinated waters with great velocities (up to 90 cm/s) overlay weaker countercurrents of the White Sea waters.

The hydrochemical studies in the estuaries of the minor rivers of Kandalaksha Bay showed that the changes in the concentrations of phosphates and silicon upon mixing between the riverine and marine waters proceeds in a nonconservative way, while the behavior of strontium, potassium, fluorine, and boron follows the laws of conservative mixing.

The biological studies showed that phytoplankton is everywhere dominated by flagellates both in terms of biomass and abundance (their bloom was noted everywhere). The diatom abundance was smaller, and in the near-mouth regions they were represented by pennate forms. In the Gorlo region, zooplankton, represented mostly by the juveniles of the Arctic copepod *Calanus glacialis*, was poor both in species and quantitative respects. In the central deep-water region, the zooplankton was dominated by the same species; however, its biomass was relatively high. In all of the estuaries, an extremely high zooplankton abundance was observed. The maximum abundance was observed at the stations closest to the river mouths; toward the outer parts of the estuaries it decreased. The composition and distribution of zooplankton in the near-mouth regions were rather diverse. The presence of freshwater species in the desalinated surface layer suggested a strong influence of the freshwater runoff. In the deeper layers, freshwater species completely disappeared due to the sharp salinity growth. The great amount of marine forms at all of the stations and their high abundance in the desalinated layer shows that the influence of marine waters on the biota is rather strong; meanwhile, many marine species demonstrate high resistance to significant desalination and easily withstand a salinity drop down to 6–8‰.

The study of the distribution and composition of suspended matter in the estuaries of the minor rivers of Kandalaksha Bay showed a clear manifestation of the physicochemical processes of transformation of the matter supplied by the rivers. They result in an increase in the concentrations of suspended matter and its components—organic and terrigenous matter ($C_{org}$, Al, and Si)—under salinity growth from 2 to 10‰. The suspended matter distribution over the median cross section of Kandalaksha Bay is characterized by an even distribution over the density jump layer and an increase in the concentrations with depth, which is likely to be related to the sinking of the suspended matter formed during the period of the spring phytoplankton bloom to deeper layers and to the delivery of the terrigenous suspended matter resuspended from the bottom sediments by the tidal currents to the deep-water part of the bay. The same reasons are responsible for the differences in the vertical matter fluxes at different levels and in the composition of the precipitating matter.

## ACKNOWLEDGMENTS

The expedition was successful due to the assistance of the crew of R/V *Kartesh* and her Captain Ya.E. Stel'makh; the authors are grateful to all of them. The authors are also grateful to T.N. Rat'kova for the studies of the phytoplankton composition. This study was supported by the INTAS Foundation, project no. INTAS-97-1881.

## REFERENCES

1. *Beloe more. Biologicheskie resursy i problemy ikh ratsional'nogo ispol'zovaniya. Chast' 1–2* (The White Sea: Biological Resources and Problems of Their Rational Use, Parts 1–2), St. Petersburg: ZIN RAN, *Issledovaniya fauny morei*, vol. 42(50), 1995.
2. Vinogradov, M.E., Shushkina, E.A., Lebedeva, L.P., and Gagarin, V.I., Mesoplankton of the Eastern Part of the Kara Sea and the Estuaries of the Ob and Yenisei Rivers, *Okeanologiya*, 1994, vol. 35, no. 4, pp. 716–723.
3. *Gidrometeorologiya i gidrokhimiya morei SSSR* (Hydrometeorology and Hydrochemistry of the Seas of the USSR), Simonov, A.I. and Al'tman, E.N., Eds., Leningrad: Gidrometeoizdat, 1991, no. 2.
4. Gordeev, V.V., *Rechnoi stok v okean i cherty ego geokhimii* (Riverine Runoff into the Ocean and Features of Its Geochemistry), Moscow: Nauka, 1983.
5. Dolotov, Yu.S., Kovalenko, V.N., Lifshits, V.Kh., *et al.*, On the Dynamics of Water and Suspended Matter in the Estuary of the Keret' River (Karelian Coast of the White Sea), *Okeanologiya*, 2002, vol. 42, no. 5, pp. 765–774.
6. Dolotov, Yu.S. and Lukashin, V.N., Expeditions to the White Sea on R/Vs *Ekolog* and *Kartesh* in 2000, *Okeanologiya*, 2001, vol. 41, no. 5, pp. 790–795.
7. *Kompleksnye issledovaniya ekosistemy Belogo morya: Sbornik trudov* (Multidisciplinary Studies of the White Sea Ecosystem. Collection of Papers), Sapozhnikov, V.V., Ed., Moscow: Vses. Nauch.-Issl. Inst. Rybn. Khoz. Okeanogr., 1994.
8. Lisitsyn, A.P., Marginal Filter of the Ocean, *Okeanologiya*, 1994, vol. 34, no. 5, pp. 735–747.
9. Lukashin, V.N., Bogdanov, Yu.A., Shevchenko, V.P., *et al.*, Studies of the Vertical Fluxes of Sedimentary Matter and Its Composition in the Norwegian Sea in the Summer Months of 1991–1995, *Geokhimiya*, 2000, no. 2, pp. 197–212.
10. Lukashin, V.N., Lyutsarev, S.V., Krasnyuk, A.D., *et al.*, Suspended Matter in the Estuaries of the Ob and Yenisei Rivers (By the Materials of Cruise 28 of R/V *Akademik Boris Petrov*, *Geokhimiya*, 2000, no. 12, pp. 1329–1345.
11. Medvedev, V.S. and Krivonosova, N.M., Studies of the Quantitative Distribution of Suspended Matter in the Near-Shore Waters of the White Sea, *Okeanologiya*, 1968, vol. 8, no. 6, pp. 1001–1016.
12. Nevesskii, E.N., Medvedev, V.S., and Kalinenko, V.V., *Beloe more: Sedimentogenez i istoriya razvitiya v golo-*

*tsene* (The White Sea: Sedimentogenesis and Evolution History in the Holocene), Moscow: Nauka, 1977.

13. Pantyulin, A.N., Some Features of the Water Structure in The White Sea, *Tr. Belomorskoi biologicheskoi stantsii MGU* (Moscow: Mosk. Gos. Univ.), 1974, no. 4, pp. 7–13.
14. Pantyulin, A.N., Povalishnikova, E.S., Zakharova, E.A., and Khoulend, R., Hydrological and Hydrochemical Features of the Minor Estuaries in Kandalaksha Bay of the White Sea, *Vestn. Mosk. Univ., Ser. 5: Geogr.*, 1994, no. 5, pp. 86–96.
15. Pertzova, N.M., Zooplankton of Kandalaksha Bay of the White Sea, *Tr. Belomorskoi biologicheskoi stantsii MGU* (Moscow: Mosk. Gos. Univ.), 1970, vol. 3, pp. 34–45.
16. Pertzova, N.M., On the Quantitative Vertical Distribution of Zooplankton in Kandalaksha Bay of the White Sea, *Kompleksnye issledovaniya prirody okeana* (Multidisciplinary Studies of the Nature of the Oceans), Moscow: Mosk. Gos. Univ., 1971, no. 2, pp. 153–162.
17. Pertzova, N.M., Zooplankton Distribution in the Basin and Kandalaksha Bay of the White Sea, *Tr. Belomorskoi biologicheskoi stantsii MGU*, Moscow: Mosk. Gos. Univ., 1980, vol. 5, pp. 49–68.
18. Pertzova, N.M., Zooplankton of the White Sea Gorlo and Mezen' Bay, *Ekologiya i fiziologiya zhivotnykh i rastenii Belogo morya* (Ecology and Physiology of Animals and Plants of the White Sea), Moscow: Mosk. Gos. Univ., 1983, vol. 6, pp. 17–25.
19. Pertzova, N.M., On the Ecology of the Boreal Copepods *Centropages hamatus* and *Temora longicornis* in the White Sea and Within Its Habitat, *Biologicheskie resursy Belogo morya* (Biological Resources of the White Sea), Moscow: Mosk. Gos. Univ., 1990, pp. 80–92.
20. Pertzova, N.M. and Kosobokova, K.N., Biology of the Arctic Copepod *Calanus glacialis* in the White Sea, *Biologicheskii monitoring pribrezhnykh vod Belogo morya* (Biological Monitoring of the Near-Shore Waters of the White Sea), Moscow: Inst. Okeanol. Ross. Akad. Nauk, 1990, pp. 57–71.
21. Pertzova, N.M. and Kosobokova, K.N., Interannual Changes in the Biomass and Distribution of Zooplankton in Kandalaksha Bay of the White Sea, *Okeanologiya*, 2002, vol. 42, no. 2, pp. 1–9.
22. Pertzova, N.M. and Prygunkova, R.V., Zooplankton, *Beloe more. Biologicheskie resursy i problemy ikh ratsional'nogo ispol'zovaniya. Chast' 1* (The White Sea: Biological Resources and Problems of Their Rational Use, Part 1), *Issledovaniya fauny morei*, St. Petersburg: ZIN RAN, 1995, vol. 42(50), pp. 115–141.
23. Pertzova, N.M. and Sakharova, M.I., Zooplankton of the Velikaya Salma Strait (White Sea) in Relation to the Features of the Hydrological Regime in 1966, *Okeanologiya*, 1967, vol. 7, no. 6, pp. 1068–1075.
24. Prygunkova, R.V., Some Features of the Zooplankton Distribution in Different Regions of Kandalaksha Bay (White Sea), *Biol. Morya*, 1977, no. 2, pp. 27–33.
25. Prygunkova, R.V., On the Reason for Interannual Changes in the Zooplankton Distribution in Kandalaksha Bay of the White Sea, *Biol. Morya*, 1985, no. 4, pp. 9–16.
26. Ronov, A.B. and Yaroshevskii, A.A., Chemical Structure of the Earth's Crust, *Geokhimiya*, 1967, no. 11, pp. 1285–1309.
27. Savenko, A.V., Hydrochemical Structure of the Mouth Areas of Minor Rivers Flowing into Kandalaksha Bay of the White Sea, *Okeanologiya*, 2001, vol. 41, no. 6, pp. 835–843.
28. Slonova, S.A., Feeding of the White-Sea Herring *Clupea harengus maris-albi* Berg, *Vopr. Ikhtiol.*, 1977, vol. 17, no. 6, pp. 1077–1082.
29. Shapiro, G.I. and Emel'yanov, M.V., Mesoscale Structure of the Hydrophysical Fields in the Region of Intensive Crill Fishery and Its Relation to the Hydrochemical and Hydrobiological Characteristics of the Waters, *Antarktika*, Moscow: Nauka, 1989, no. 28, pp. 121–136.
30. Berger, V., Dahle, S., Galaktionov, K., *et al.*, *White Sea. Ecology and Environment*, St. Petersburg–Tromso: Derzavets, 2001.
31. Dai, M. and Martin, J.-M., First Data on Trace Metal Level and Behaviour in Two Major Arctic River–Estuarine Systems (Ob and Yenisei) and in the Adjacent Kara Sea, Russia, *Earth Planet. Sci. Lett.*, 1995, vol. 131, pp. 127–141.
32. Hill, A.E., Souza, A.J., Jones, K., *et al.*, The Malin Cascade in Winter, 1996, *J. Marine Res.*, 1998, vol. 56, pp. 87–106.
33. Millward, G.E., Rowley, C., Sands, T.K., *et al.*, Metals in the Sediments and Mussels of the Chupa Bay Estuary (White Sea), Russia, *Estuarine, Coastal and Shelf Science*, 1999, vol. 48, pp. 13–25.
34. Kosobokova, K.N. and Pertzova, N.M., Seasonal Variations in the Zooplankton Community of the Deep Part of the White Sea in 1998 and 1999, *Sarsia*, 2002 (in press).
35. Pertzova, N.M. and Kosobokova, K.N., Zooplankton of the White Sea. History of Investigations and the Present State of Knowledge—A Review, *Berichte zur Polarforschung*, 2002, no. 359, pp. 30–41.
36. Redfield, A.C., Ketchum, B.H., and Richards, F.A., The Influence of Organisms on the Composition of Seawater, *The Sea*, Hill, M. N., Ed., London: Interscience, 1963, vol. 2, pp. 26–77.
37. Shevchenko, V.P., Lisitzin, A.P., and Zernova, V.V., Vertical Particle Fluxes in Seas of the Western Russian Arctic, *Humanity and the World Ocean. Interdependence on the Dawn of the New Millenium. PACON 99 Proceedings*, PACON International, 2000, pp. 239–249.
38. Sholkovitz, E.R., Flocculation of Dissolved Organic and Inorganic Matter during the Mixing of River Water and Seawater, *Geochim. Cosmochim. Acta*, 1976, vol. 40, pp. 831–845.
39. Wefer, G. and Fischer, G., Seasonal Patterns of Vertical Particle Flux in Equatorial and Coast Upwelling Areas of the Eastern Atlantic, *Deep-Sea Res.*, 1993, vol. 40, no. 8, pp. 1613–1645.

Oceanology, Vol. 43, Suppl. 1, 2003, pp. S26–S31.


MARINE PHYSICS

# Mixing Processes in the Gorlo Strait of the White Sea

**G. I. Shapiro[1,2], L. Latché[2], A. N. Pantiulin[3]**

[1] *P.P. Shirshov Institute of Oceanology, Moscow, Russia**

[2] *Institute of Marine Studies, Plymouth, UK*

[3] *Moscow State University, Russia*

Received February 27, 2003

**Abstract**—Mixing processes were studied in the southwest area of the Gorlo Strait, which has an important role in water mass exchange between the Barents Sea and the White Sea. A dense grid of CTD measurements in June 2000 revealed four contacting water masses: the well mixed Gorlo Strait Water (GSW), the warmer White Sea Surface Water (WSSW), the warm and fresher Dvina Bay Water (DBW), and the colder and more saline White Sea Intermediate Water (WSIW). The high vertical and horizontal resolution of temperature and salinity measurements showed the spatial structure of these water masses, different aspects of mixing, and the main characteristics of the resulting quasi-homogeneous mixed layers. A thermal front was evident in the southwest part of the Gorlo Strait that resulted in the formation of an intrusion of colder GSW into the White Sea basin. This intrusion was facilitated by Terskii Coastal Current and cyclonic Dvina Bay gyre. East of the front, a mesoscale "lens" of WSSW was observed in the near-surface layer. The intensity of mixing caused by bottom friction and/or intra-thermocline shear was judged by the degree of reduction of the core of the identified water masses. T-S diagrams and vertical profiles of temperature fluctuations have therefore clearly shown the relation between the nature of mixing between core water masses and the resultant quasi-homogeneous layers.

## INTRODUCTION

The White Sea is a semi-enclosed basin, which is connected to the adjacent Barents Sea via the Gorlo Strait and Voronka region. The Gorlo Strait is 50–60 km wide, 150 km long and typically 40 m deep. The surface area of the Gorlo Strait is about 10% of that of the White Sea. The Voronka region is known to have very strong tidal waves, which come from the Barents Sea and are enhanced by the funnel-like shape of the Voronka and Mezen' Bay. However, most of the tidal energy is reflected back at the entrance to the Gorlo Strait, so only 20% of the incoming tidal energy enters the Gorlo Strait, and only 6% enters the White Sea basin. Tidal currents in the Gorlo Strait are not strong and the maximum velocity is about 150–180 cm/s, which is mainly observed along the Terskii coast.

In the summer there are five water masses in the White Sea and Gorlo Strait which are involved in the mixing process. These are the well mixed Gorlo Strait Water (GSW), a thin layer (about 10 to 20 m) of White Sea Surface Water (WSSW), fresher Bay Waters, colder White Sea Intermediate Water (WSIW), which generally has the temperature $T = -0.2$ to $-0.9$°C, and the White Sea Deep Water (WSDW) below 100m.

Despite some progress achieved in previous studies, which analyzed the mixing process in the White Sea, this process is still not well understood due to its complex nature. Standard hydrographic sections have been carried out across the Voronka and Gorlo Strait [1], mainly obtained with Nansen bottles. The analysis of data from these sections at various seasons revealed the following features of the mixing processes. Traditionally, it has been thought [1] that the waters in the Voronka and the Gorlo Strait are well mixed from the bottom to the surface, excluding the period after the spring river flood, when low salinity waters enter the Gorlo from Dvina Bay. We will show below that this concept is not relevant to the southwestern part of the Gorlo Strait. A "belt" of maximum salinity gradients (i.e., the salinity front) was found to be located in the southern part of the Voronka [3], where salinity changes from 34 to 30 psu. Waters with a salinity of about 30 psu and a temperature of about $-1.5$° penetrate into the southern part of the Gorlo only during the second half of winter to renew bottom waters in the deep basin of the White Sea. The Gorlo Strait is the only route for water exchange between the Barents and White Seas. Derjugin [2] and later Timonov [4] suggested that there are two major steady currents: the outgoing current along the Winter coast, which removes the fresher White Sea waters, and the incoming current along the Terskii Coast, which maintains the salinity balance. Timonov [5] estimated the renewal time for the White Sea to be about two years, which is a rapid exchange rate compared to other semi-enclosed seas. However, there has been some concern about the accuracy of this estimate. This paper presents an analysis of mixing processes in the Gorlo Strait, based on recent observations using modern oceanographic technology.

*Corresponding author, e-mail: shapiro@sio.rssi.ru; gshapiro@plymouth.ac.uk

## MATERIALS AND METHODS

A CTD survey was carried out from June 17 to 21, 2000, over a rectangular area in the Gorlo Strait and adjacent shallow regions of the White Sea Basin and Dvina Bay (Fig. 1), in order to study water mass distribution and mixing. The measurements were taken in a region where water masses from the Basin, Dvina Bay, and the Gorlo Strait come into contact. The mixing process is intensified by strong tides and the shallow and ragged bottom topography. The survey consisted of 50 stations and it was part of a multidisciplinary EU-INTAS project, entitled Mesoscale Physical and Biogeochemical Processes in Coastal Waters of the Russian Arctic. Measurements were taken using the research vessel Kartesh, with typical distances between stations of 3–6 km. Vertical profiles of temperature and salinity were obtained with the CTD probe SBE–19 from Sea Bird Electronics, with a vertical resolution of about 0.3 m. Both down- and up-casts were recorded to monitor any changes in the water properties due to the ship drift caused by tidal currents during the period of measurements at a station (about 10 minutes). Throughout the survey, the weather was calm, with wind speeds never exceeding force 2 on the Beaufort scale. The study includes a comprehensive analysis of the 3D water mass structure, and it is based on horizontal charts of temperature and salinity distribution at various depths, vertical cross sections along and across the Gorlo Strait, temperature-salinity diagrams, vertical profiles at individual stations, and an analysis of temperature and salinity fluctuations in the areas of strong mixing. The results of the analysis are presented in the following section and are supported by a selection of plots, which reveal the mesoscale horizontal and small-scale vertical structure of water masses.

## RESULTS

Generally, the large-scale distribution of hydrographic parameters in the White Sea was typical for early summer conditions [1]. However, the dense grid of stations and the high vertical resolution of the newly obtained data allowed us to study the water mass distribution and mixing in greater detail. The chart of temperature distributions (Fig. 1) at a depth of 5 m clearly shows the spatial structure of water masses in the near-surface layer. The northern and northeastern parts of the study area are occupied by the modified Gorlo Strait

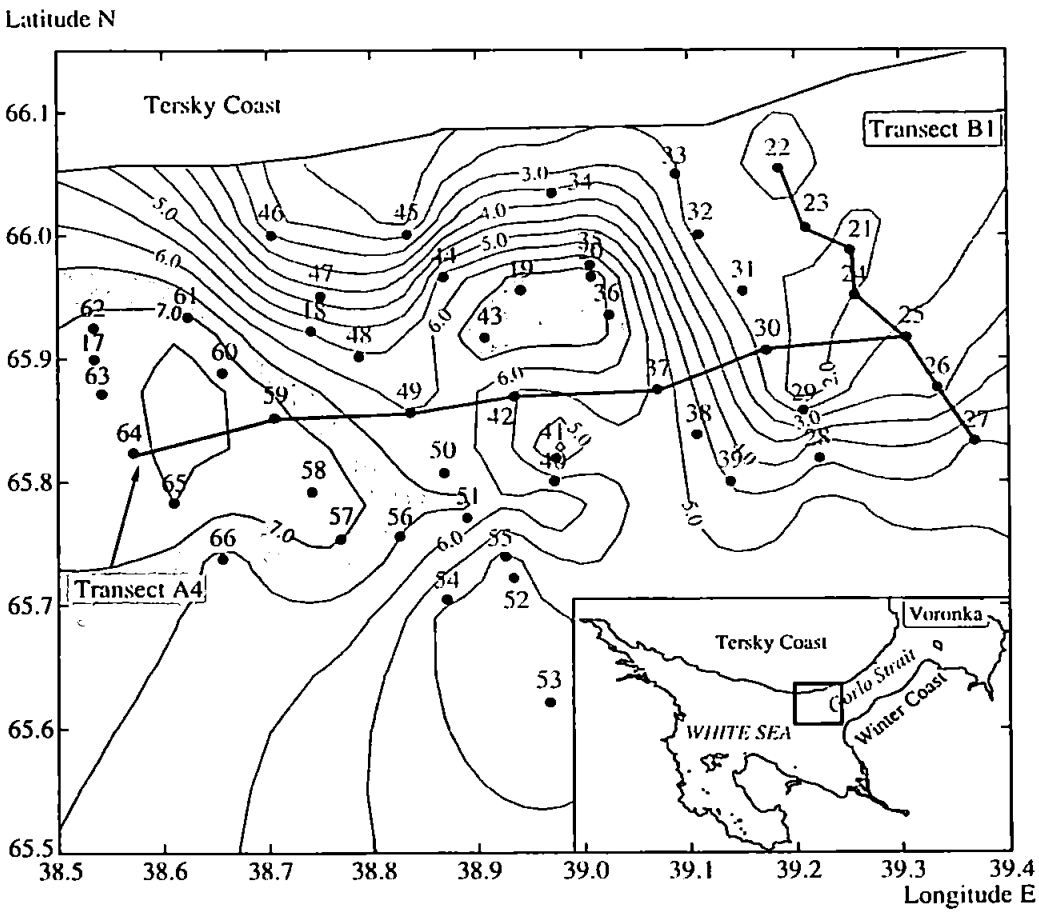


Fig. 1. Temperature distribution at a depth of 5 m in the mixing area at the southwestern end of the Gorlo Strait, June 2000.

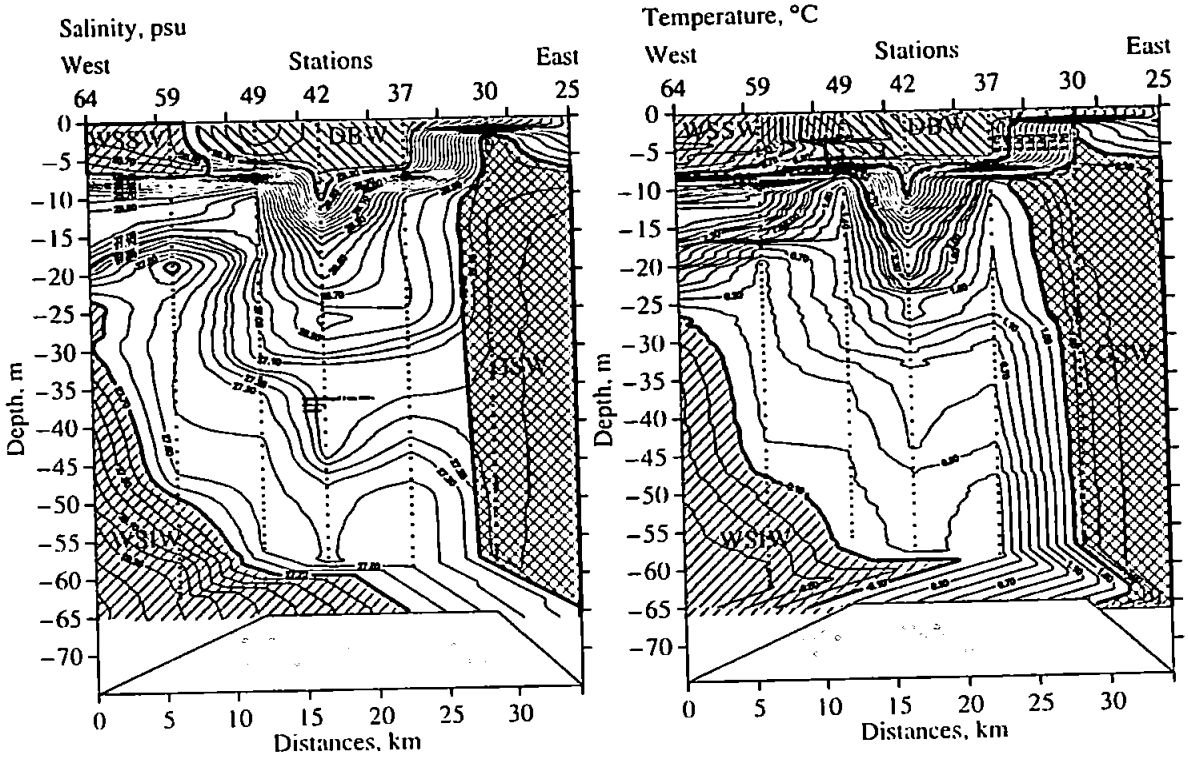


Fig. 2. Temperature and salinity on a cross-section (Transect A4) along the southwest end of the Gorlo Strait, June 2000.

Water (GSW, 1.9–2.4°C, 27.05–27.25 psu). The "source current" [1] brings waters from the Voronka into the Gorlo Strait, where it is well mixed due to intensive tidal mixing. The warmest was the White Sea Surface Water (WSSW; 6.7–8°C; 25.5–25.9 psu), which occupied the western side, whilst the fresher and slightly colder Dvina Bay Water (DBW, 4.8–6.1°C; 24.8–25.3 psu) was advected from the south, probably by the cyclonic Dvina Bay gyre [5, 8]. The influence of this gyre and the adjacent Terskii Coastal Current [1] is evident from the intrusion of colder GSW into the western end of the Gorlo Strait along the Tersky Coast in the north.

In the central part of the area studied, the measurements reveal a mesoscale patch (lens) of WSSW, which is surrounded by colder GSW from the north and a mixture of GSW and DBW in the south. Despite having a diameter of only 7–8 km and a thickness of 8–10 m, the lens core is well defined and occupied four adjacent CTD stations. The lens is separated by a sharp thermocline (a drop in temperature by 6°C at a 5-m depth) from the underlying water. This thermohaline feature is indicative of the initial stages of an anticyclonic mesoscale eddy formation, a process well observed in various parts of the World Ocean (e.g., [6, 7]) but which has not been reported in the White Sea before. Formation of the lens might be forced by the baroclinic instability of the thermohaline front and the associated current, or, alternatively, by the intensification of the Dvina Bay gyre due to the increase of fresh water discharge. South of this lens, there is a small patch of surface Dvina Bay Water; however, it was only evident at station 41, and we were not able to resolve its horizontal structure.

Contours of salinity and temperature in Transect B1 (see Fig. 1) clearly show the incoming Gorlo Sea Water. This water mass is present in Transect B1 (not shown here) through the entire water column and at the bottom, with the exception of fresh surface water—probably already mixed—from a depth of 10 m to the surface. The contours of salinity 27.05 and temperature 2.4°C show the parameters for the Gorlo Strait Water, which are separated from fresher and warmer water in the surface layers.

Moving closer to the White Sea Basin from the Gorlo Strait, the "core" of the Gorlo Strait Water is considerably reduced across the strait, due to mixing caused by the surrounding water masses. Here we note the presence at stations 28 and 29 (i.e., at the southernmost location) of the Dvina surface water, with a maximum salinity of 25.3 and minimum temperature of 4.8°C. In the thin surface layer (5–10, approximately 15 m below the surface) at stations 29–30, sharp gradients of temperature and salinity show a region of mixing between the Dvina surface water and the Gorlo Sea Water. In the shallow areas close to the Terskii shore (stations 32–33), the water is well mixed with water that is fresher compared to that of the Gorlo Strait Water. This probably implies topographic stirring near

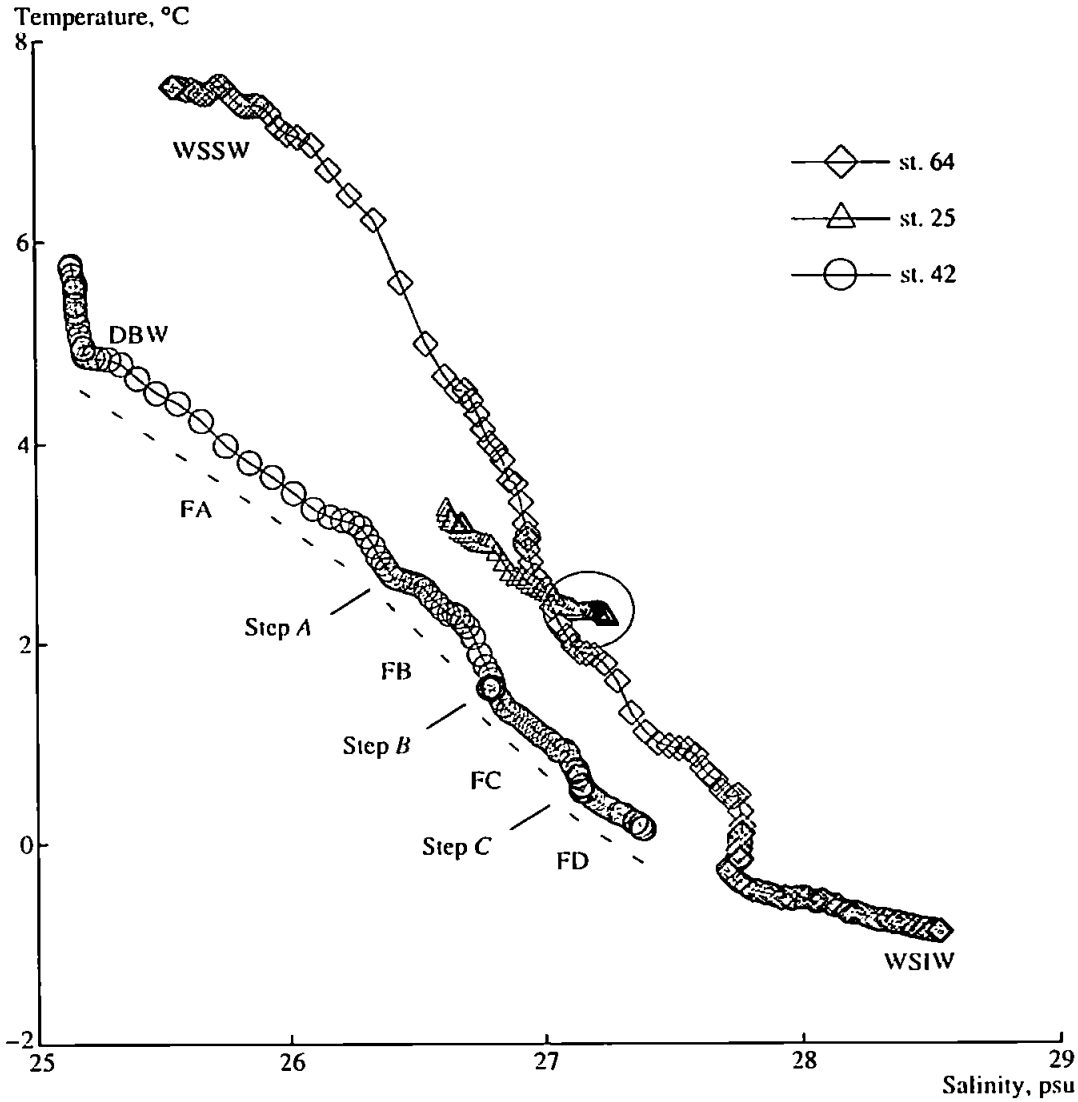


Fig. 3. TS Diagram of selected stations from Transect A4 showing the contacting water masses and different aspects of mixing in the southwestern part of the Gorlo Strait.

the bottom (25–30 m) and mixing with fresher and warmer WSSW coming from the basin with local circulation gyres.

Therefore, it is interesting to analyze along shore cross sections in order to identify the area where bottom mixing occurs more intensively. One could expect that areas of strong mixing should be separated from the source water masses by a sharp front. The temperature and salinity for transect A4, across the thermal front, is shown in Fig. 2. This transect avoids the warm mesoscale patch and it clearly shows four water masses and their interaction in the southwestern end of the Gorlo Strait. In addition to the three water masses described above, this transect reveals the cold and saline White Sea Intermediate Waters (WSIW, –0.1 to –1°C and below, 27.7 to 28.5 psu and more). This water mass occupies a depth range below 25 m, and it is believed to be formed by the previous winter's cooling and salinization due to the incoming current from the Gorlo Strait along the Terskii Coast. The current brings more saline Barents Sea waters, modified through stirring and mixing in Voronka Bay.

Gorlo Strait Water on the eastern side of the transect is well mixed below 5–7 m, and it is covered by a duvet of warmer surface water, which could be attributed to summer heating. Surface waters from the Basin (in the western end of the transect) and Dvina Bay (in the center) occupy a thin layer, penetrating no deeper than 8–10 m. The mixing area between WSSW and DBW is concentrated in a narrow band not exceeding 5 km. The temperature front between warmer GSW and colder WSIW occupies the water column from 15–25 m down

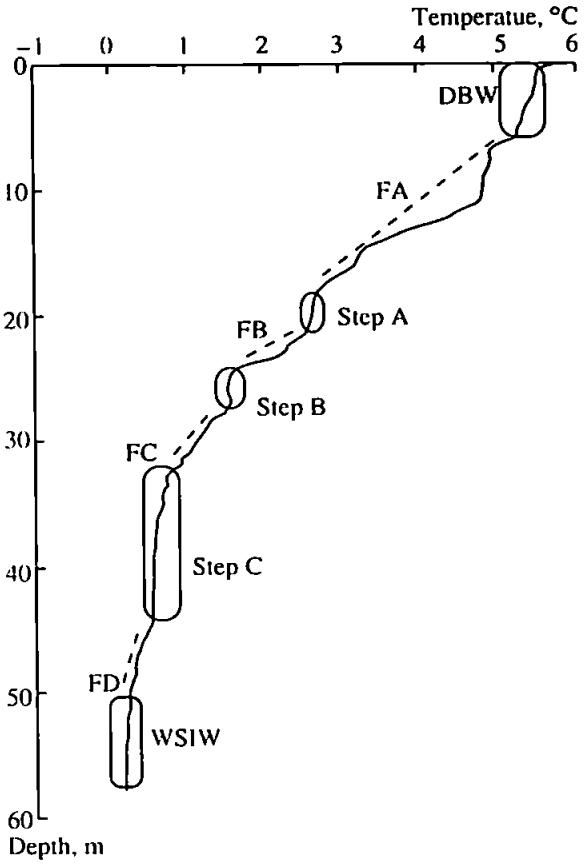


Fig. 4. Temperature profile at station 42, showing the mixing region marked as anomaly fluctuations FA, FB, FC, and FD, and identified water masses along with previously mixed water from observed quasi-homogeneous layers (Steps A, B, and C).

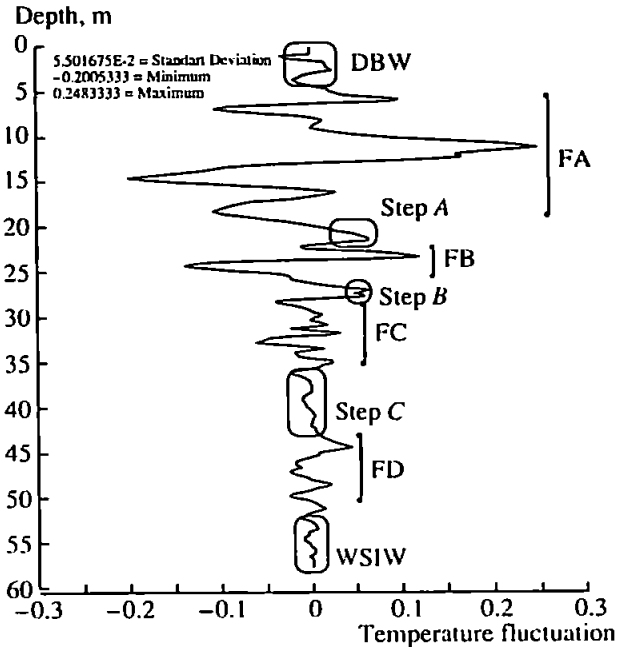


Fig. 5. Temperature fluctuation derived at station 42 using a running filter with a 15-point averaging window. Water masses and mixed layers (steps) are marked with the fluctuations FA, FB, FC, and FD, showing different aspects of mixing through the water columns.

to the seabed. Frontal mixing takes place in a strip between 20 and 25 km wide, coinciding with the shallowest area on the transect. The resultant water mass leaks into the White Sea as a thin intrusion at a depth of 15–25 m. Along its way, the water mixes with the overlying DBW and WSSW, producing well developed temperature and salinity inversions, as well as quasi-homogeneous layers (Steps).

Tidal currents occupy the whole water column from the bottom to the surface, although the shear stress caused by bottom friction is expected to be stronger than near the thermocline. Within the stratified layers, the intensity of mixing is controlled by the balance of production of turbulent energy by baroclinic shear currents, which facilitates mixing, and the hydrostatic stability of the water column, which suppresses mixing. We can also judge the intensity of mixing by the degree of reduction of the "core" of the identified water masses. Therefore, T-S diagrams are a useful tool to clearly determine the "core" of water masses, and to identify the mixed waters that result from these different mixing processes.

Core water masses and their mixtures are seen on the T-S diagrams shown in Fig. 3. In order to keep the figure clear, only three stations from the transect A4 are plotted, with stations 25, 42, and 64 representing the eastern end, the center and the western end of the transect, respectively. The diagram shows individual data records using nonconnected symbols, so that core waters and quasi-homogeneous layers are seen as the darker parts of the curve, while stratified waters are represented by lighter areas. Station 25 reveals the most uniform water, although two clusters—i.e., the colder GSW and warmer surface water—are easily identified. Station 64 incorporates the three main water masses—cold and saline WSIW, warm and less saline WSSW, and a small amount of GSW—penetrating into the Basin at a depth of 15–20 m in the form of a quasi-homogeneous layer.

The most complex picture of the mixing process was observed from station 42. This was obtained by subtracting the averaged profile from the original high-resolution profile. Smoothing was performed by a running mean method with an averaging window of 15 data points. There, the top of the water column is occupied by modified DBW from the sea surface down to 6 m, marked DBW in Fig. 4. Beneath it there is a sharply stratified pycnocline (marked FA), which ends at depth of 17 m. Further down we see a 4-m thick homogeneous layer (Step A), which contains the mixture of DBW, GSW, and WSIW. Beneath that, the strat-

ified layers FB and FC connect the temperature inversion (Step B, 24–28 m) and the deep homogeneous layer (Step C, 36–44 m). Mixed water with a strong contribution of WSIW occupies the near bottom layer.

Temperature fluctuations are shown in Fig. 4. The most intensive oscillations, up to 0.25°C, relate to the thermocline (marked as FA) that separates surface DBW from the modified waters of Step A. Strong fluctuations are evident near the bottom, despite the fact that the layer is already nearly homogeneous.

## CONCLUSION

The study area was located in the southwestern part of the Gorlo Strait, where four water masses come into contact. The measurements were carried out soon after the maximal intrusion of the Dvina Bay Waters into the Gorlo area. A high-resolution CTD survey revealed the mechanism of mixing of different water masses in the Gorlo Strait of the White Sea. Water masses in contact with each other were separated either by a sharp thermocline or by hydrographic fronts. At the time of measurements, the incoming waters from Voronka Bay were warmer and saltier than the home waters of the White Sea. Mixing processes included vertical stirring and horizontal exchanges through interleaving at the thermal and salinity fronts. The formation of mesoscale eddies, apparently due to baroclinic instability, extends the length of the boundary that separates differing water masses and hence facilitates horizontal mixing. Vertical mixing is highly enhanced by strong tides in the Gorlo Strait. The resultant mixed water is advected into the White Sea basin along the Terskii Coast.

## ACKNOWLEDGEMENTS

The study was partially supported by the EU through grant INTAS–97–1881 and by the Higher Education Funding Council for England (HEFCE) through QR funding. The authors wish to thank Prof. Geoff Millward for his helpful comments.

## REFERENCES

1. *Morya SSSR. Gidrometeorologiya i gidrokhimiya morei. T. II, Beloe more* (The Seas of the USSR. Hydrometeorology and Hydrochemistry of the Seas. Vol. II. The White Sea), Issue 1, Glukhovskoi, B.Kh. Ed., St. Petersburg: Gidrometeoizdat, 1991.
2. Deryugin, K.M., Fauna of the White Sea and Conditions of Its Dwelling, *Issledovaniya morei SSSR*, 1928, no. 7–8.
3. Pantyulin, A.N., On the Formation and Variability of the Water Structure in the White Sea, *Biologicheskie resursy Belogo morya* (Biological Resources of the White Sea), Matekin, P.V., Ed., Moscow: Moscow State University, 1990, pp. 9–16.
4. Timonov, V.V., Schematic of the General Water Circulation in the Basins of the White and the Barents Seas and Origin of Its Abyssal Waters, *Trudy GOIN*, 1947, no. 1 (13), pp. 118–131.
5. Timonov, V.V., Principal Features of the Hydrological Regime of the White Sea, *Pamyati Yu.M. Shokal'skogo*, (Yu.M. Shokal'skii in Memoriam), Moscow, 1950, pp. 206–235.
6. Filyushkin, B.N. and Plakhin, E.A., Experimental Study of the First Stage of Mediterranean Water Lens Formation, *Okeanologiya*, 1995, vol. 35, pp. 875–882.
7. Shapiro, G.I. and Meschanov, S.L., Spreading Pattern and Mesoscale Structure of Mediterranean Outflow in the Iberian Basin Estimated from Historical Data, *J. Mar. Sys.*, 1996, no. 7, pp. 337–348.
8. Latche, L., Shapiro, G.I., and Pantiulin, A.N., Thermohaline Intrusion in the White Sea in June 2000, *27th General Assembly of the European Geophysical Society*, Nice, France, 2002. http://www.cosis.net/abstracts/EGS02/03437/EGS02-A-03437.pdf